# La topographie comme marqueur de la déformation de la lithosphère

Julien Babault

**Mémoire d'Habilitation à Diriger des Recherches**

Université de Rennes 1

# La topographie comme marqueur de la déformation de la lithosphère


## Julien BABAULT

Professeur Lecteur

Universitat Autònoma de Barcelona


SOUTENANCE PREVUE LE 10 DECEMBRE 2015 DEVANT LE JURY COMPOSE DE :

| | |
|---|---|
| Guy SIMPSON | *Université de Genève, Genève* |
| Frédéric MOUTHEREAU | *Géosciences Environnement Toulouse, Toulouse* |
| Denis GAPAIS | *Géosciences Rennes, Rennes* |
| Dimitri LAGUE | *Géosciences Rennes, Rennes* |
| Rodolphe CATTIN | *Géosciences Montpellier, Montpellier* |

# *AVANT-PROPOS*

Ce mémoire dresse le bilan de mes activités de recherche depuis ma thèse de 3ème cycle afin d'obtenir l'Habilitation à Diriger des Recherches à l'Université de Rennes 1. J'ai effectuées ces recherches au département de Géologie de l'Université Autonome de Barcelone au cours d'un Post-doc financé par le ministère espagnol (Juan de la Cierva, 2005-2008) et par la suite comme professeur Lecteur de 2008 à 2015.

Il propose d'abord un curriculum vitae qui résume aussi mes activités de recherche et de formation, complétées par une liste de mes publications et communications.

Mon approche scientifique et mes activités de recherche sont ensuite détaillées, autour du thème principal de la compréhension des processus orogéniques à travers l'étude géomorphologique impliquant la modélisation expérimentale. Les développements futurs de l'activité de recherche que je souhaite mener sont ensuite présentés succinctement, en partie au travers de certains des projets chantier RGF (BRGM) et ANR auxquels j'émarge.

Une sélection des publications récentes auxquelles j'ai participé est présentée en annexes.

# *TABLE DES MATIÈRES*

# A. Curriculum vitæ

## *État Civil*

**Julien Babault**

Professeur Assistant (Lector)
Departament de Geologia
Établissement : Universitat Autònoma de Barcelona (Espagne)
Période 2008-2015
Docteur depuis le 2 juillet 2004
Qualification MCF 2012 CNU 35/36,
n° : 12235158742/12236158742

né le 10 février 1977 à Paris XII
38 ans Marié, trois enfants
Calle Solsona, 3B, bajos 1a, 08173
Sant Cugat del Vallès (ESPAGNE)
Tel : 0034 935 83 80 78
Email : julien.jbabault@gmail.com
Page Web avec les publications en pdf : https://sites.google.com/site/drbabault/home

## *Profil Scientifique*

Tectonique, Géomorphologie, Bassins, Modélisation expérimentale

18 Publications de Rang A, 1 direction et 4 Co-Encadrements de Thèses d'Université

## *Parcours Professionnel*

2008–2015 **Professeur Assistant** (7 contrats de 1 an, *Profesor Lector*), Dept. de Geologia, Àrea de Geodinàmica Externa – Universitat Autònoma de Barcelona (Espagne).

2005–2008 **Contrat Post-doctoral** (ministère espagnol), (3 ans, Investigador Juan de la Cierva), Departament de Geologia, Àrea de Gecodinàmica Interna – Universitat Autònoma de Barcelona (Spain).

2003–2005 **A**ttaché **T**emporaire d'**E**nseignement et de **R**echerche – Géosciences, Université de Nantes *(France)*.

2000–2004 **Thèse de Doctorat en Géologie** – Dynamique de l'érosion dans les chaînes de montagnes : Influence de la sédimentation de piedmont. L'exemple des Pyrénées – Géosciences, Université de Rennes1 *(France)*. ***Directeur et co-directeur:*** Prof. Jean Van Den Driessche et Dr. Stéphane Bonnet.

1999–2000 **DEA en Géologie** – Géosciences Université de Rennes (France). ***Co-directeurs:*** Dr. de Urreiztieta (*ELF-Exploration Production*), Dr. Delphine Rouby et Dr. Thierry Nalpas (*Université de Rennes1*) – Classement : 2/13.

## *Activités d'Enseignement*

J'ai enseigné pendant 14 ans à l'Université, d'abord en tant que moniteur (3 ans), par la suite comme ATER (2 ans), puis comme Post-Doc (2 ans) et jusqu'à septembre 2015 comme professeur Lecteur (Prof. Assistant, 7 contrats de 1 an : 2008-2015, cours : ~230h/an). J'ai dispensé des CM/TP/TD/sorties de terrain

en L1, L2, L3, M1, M2 et Doctorat. Je suis principalement intervenu dans les filières Sciences de la Terre mais également dans les filières de préparation au CAPES et à l'Agrégation en Sciences de la Vie et de la Terre.

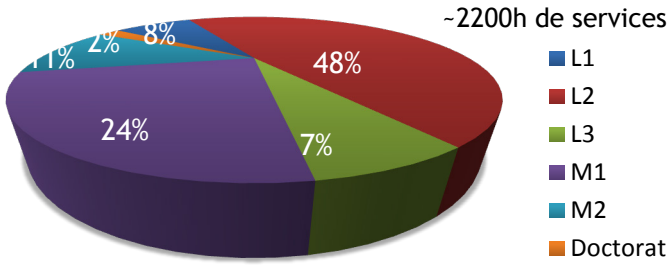


***Figure 1:*** *Distribution relative de mes enseignements par niveau.*

Mes enseignements ont été très variés, en ce qui concerne la matière enseignée, le niveau des étudiants et la pédagogie nécessaire. J'ai dispensé des enseignements très généraux en L1 (e.g., Tectonique des plaques) et L2 (e.g., Météorologie-Océanographie) et des enseignements plus spécialisés en L3 (e.g., Pétrologie, Géomorphologie), M1 (e.g., Analyse de la Déformation, Cartographie, Géodynamique Externe, Géologie de la France) et M2 (Interactions processus de surfaces et processus profonds). L'objectif de ces enseignements a été d'apporter aux étudiants des connaissances fondamentales en géologie, une vision générale des géosciences, ainsi qu'un sens critique à travers une compréhension intelligente des processus et la capacité de mener un raisonnement scientifique en s'appuyant sur l'analyse, l'interprétation et la synthèse.

## *Responsabilités et Gestion*

### *Responsable de projet de recherche et direction de thèse*

J'ai été responsable depuis 2011 d'un projet de recherche et de la direction d'une thèse (Marc Viaplana) soutenue en juillet 2015, tous deux financés par l'entreprise pétrolière Repsol (Madrid).

### *Responsable de modules d'enseignement*

J'ai été responsable depuis 2008 de 2 à 3 modules par an. Pour certains d'entre eux, nous avons été plusieurs professeurs impliqués dans les cours théoriques ainsi que pratiques. J'ai été le responsable en L1 année de *Planeta Tierra* (30h), en L2 année de *Procesos Geológicos Externos* (75h), de *Geomorfología II* (130h) et de SIG (110h), et en M1 année de *Geodinámica Externa* (60h) ainsi que de *Trabajo de campo Exogena II* (6 jours de terrains dans le sud pyrénéen). J'ai également supervisé pendant cinq ans un stage de terrain de 2 jours dans les Pyrénées Orientales pour les étudiants de M2.

*Gestion de Programmes Informatiques Destinés aux Salles de Cours*

J'ai introduit en 2008 l'utilisation de programmes utilisant des systèmes d'information géographique pour les étudiants de Géologie de l'Université Autonome de Barcelone. Cela m'a conduit à superviser l'achat puis l'installation dans les salles informatiques de programmes comme ArcMap (+ Spatial Analyst), Global Mapper et RiverTools.

## *Conférences Invitées*

| | |
|---|---|
| 2012-2014 | *Univ. Montpellier II* : Dynamique du réseau de drainage dans les chaînes de montagnes |
| 2008 | *Univ. Montpellier II* : Dynamique de l'érosion continentale à long terme |
| 2005 | *EGU Vienna* : « Origin of the highly elevated, dissected Pyrenean peneplain » in session GM5 « Late Cenozoic erosion and sedimentation: climate change or tectonics? » |
| 2005 | *Univ. Zaragoza* : Dynamique de l'érosion dans les chaînes de montagnes : Influence de la sédimentation de piedmont, l'exemple des Pyrénées |
| 2005 | *Univ. Lyon* : Dynamique de l'érosion dans les chaînes de montagnes : Influence de la sédimentation de piedmont, l'exemple des Pyrénées |

## *Encadrement et Co-Encadrements de thèses (Et Publications de Rang A associées)*

[5] **Gemma de Vicente i Bosh** (2013-2016) « Pénéplanation et dynamique profonde des Pyrénées », en co-encadrement avec Jean Van Den Driessche (U. Rennes 1) et Alexandra Robert (U. Toulouse)

Implication dans la direction : ***30%***

Financement: BRGM

1 publication de Rang A (CR. Géoscience)

[4] **Marc Viaplana** (2011-2015) « Dinámica de la red de drenaje en sistemas orogénicos-cuencas: implicaciones sobre los sistemas petroleros de los Atlas », **directeur de thèse**, en co-encadrement avec Stéphane Dominguez (U. Montpellier 2) et Jean Van Den Driessche (U. Rennes 1)

Implication dans la direction : ***70%***

Financement: Repsol, Espagne et Ministerio de Ciencia e Innovación

1 publication de Rang A (Tectonophysics)

[3] **Lucía Struth** (2011-2015) « Tectónica y evolución de la red de drenaje en la Cordillera Oriental de Colombia », en co-encadrement avec Antonio Teixell (UAB)

Implication dans la direction : ***50%***

Financement: Ministerio de Ciencia e Innovación

1 publication de Rang A (Geomorphology)

[2] **Mireia Domenech** (2010-2015) « Inversión tectónica y dinámica del relieve en orógenos de intraplaca: el caso del Alto Atlas occidental de Marruecos en co-encadrement avec María-Luisa Arboleya et Antonio Teixell

Implication dans la direction : ***20%***

Financement: Ministerio de Ciencia e Innovación

1 publications de Rang A (Tectonophysics)

[1] **Álvar Pastor** (2007-2013) « Evolución morfo-tectónica reciente en las cuencas de antepaís SubAtlásicas », en co-encadrement avec María-Luisa Arboleya et Antonio Teixell

Implication dans la direction : ***30%***

Financement: Ministerio de Ciencia e Innovación

2 publications de Rang A (Geomorphology et Tectonophysics)

### *Encadrements de Master 2*

[6] **Gerard Montardit** (2014) « Sedimentación en el surco de valencia como diagnóstico de la dinámica de la erosión de la Cordillera Catalana en el Neógeno», en co-encadrement avec Nicolas Loget et moi-même

[5] **Antoni Capó** (2012) « Dinámica de la red de drenaje en el Himalaya: factores que la controlan e implicaciones en la arquitectura sedimentaria »

[4] **Lucía Struth** (2011) « Tectónica y evolución de la red de drenaje en la Cordillera Oriental de Colombia », en co-encadrement avec Antonio Teixell et moi-même

[3] **Mireia Domenech** (2010) « Deformación alpina y dinámica del relieve en el macizo de Tizi-n-Test (Alto Atlas occidental, Marruecos) », en co-encadrement avec María-Luisa Arboleya et Antonio Teixell

[2] **Marc Alimbau** (2010) « Dinámica de la divisoria de aguas en el Pirineo »

[1] **Marc Viaplana** (2010) « Dinámica y evolución de la red de drenaje. Modelización experimental », en co-encadrement avec Stéphane Dominguez et Jean Van Den Driessche

### *Participation à des Programmes de Recherche*

2013-2016 Les Pyrénées: surface profond. chantier RGF Pyrénées du BRGM. Coordinateur : Pr. Van Den Driessche, J.

2012-2016 Le Nord des Pyrénées: évaluation intégrée de l'histoire de la Migration des fluides, l'Inversion du rift, le rôle des processus de surface et la Déformation dans un (rétro)prisme orogénique. ANR PYRAMID. Coordinateur : Dr. Ford, M.

2011-2014 Dinámica de la red de drenaje en sistemas orogénicos-cuencas: implicaciones sobre los sistemas petroleros. Repsol España, 100 k€. **Responsable : Dr. Babault, J.**

2011-2014 Inversión tectónica y dinámica de la erosión/sedimentación a largo plazo en cordilleras intracontinentales. Los casos del Atlas, la Cordillera Oriental de Colombia y los Pirineos. Ministerio de Ciencia e Innovación. CGL2010-15416. Coordinateur : Pr. Teixell, A.

2008–2011 La tectónica del Arco de Gibraltar y la Cordillera del Atlas: causas litosféricas y efectos topográficos (TOPOMED_SPAIN). MICINN-DGI. CGL2008-03474-E/BTE. Coordinateur : Dr. Fernández Ortiga, M. (CSIC).

2006–2010 Geociencias en Iberia: Estudios integrados de topografía y evolución 4D. “Topo-Iberia”. Ministerio de Educación y Ciencia. Proyecto CONSOLIDER INGENIO 2010. CSD2006-00041 Coordinateur : Pr Gallart Muset, J. (CSIC)

2007-2008 Tectónica, movimientos verticales y evolución del relieve del Atlas marroquí. Ministerio de Educación y Ciencia, Acción complementaria internacional PCI2006-A7-0577. Coordinateur : Pr. Teixell, A.

2007-2008 Estructura geológica del borde meridional de la cordillera del Atlas (Marruecos): implicaciones sobre la actividad tectónica reciente y la sismicidad. AECI, Ministerio de Asuntos Exteriores, BTE2003-00499. Coordinateur : Pr. Teixell, A. et Dr. Charroud, M.

2006–2008 Relaciones entre la tectónica y la evolución del relieve en el sistema atlásico de Marruecos. Un ejemplo de interacción entre procesos geodinámicos profundos y superficiales. Ministerio de Educación y Ciencia I. CGL2006-07226 Coordinateur : Pr. Arboleya, M.-L.

2006–2008 Datación de los abanicos aluviales y terrazas del Oued Madri (Alto Atlas, Marruecos) como marcadores de la actividad tectónica reciente. Ministerio de Educación y Ciencia Acción complementaria, CGL2005-25059-E Coordinateur : Pr. Arboleya, M.L.

2004-2006 Historia del levantamiento del Alto Atlas de Marruecos: implicaciones sobre la génesis de cadenas montañosas en el interior de los continentes. Ministerio de Ciencia y Tecnología (MCYT) BTE2003-00499 Coordinateur : Pr. Arboleya, M.-L.

2004-2005 Terrasse: Quantification et modélisation de la dynamique fluviale. CNRS-INSU Coordinateur : DR. Phlippe Davy.

2003-2004 ACI, Impacts des changements climatiques sur l'érosion et la géométrie des réseaux hydrographiques. CNRS-INSU Coordinateur : Dr. Stéphane Bonnet.

2001-2002 PNSE/ACI, Modélisation expérimentale de la dynamique des reliefs en érosion: rôle de la chenalisation. CNRS-INSU Coordinateur : Dr. Alain Crave.

1999-2002 Programme National Sol et Érosion: Développement et dynamique des systèmes fluviatiles. CNRS-INSU Coordinateur : Pr. Jean Van Den Driessche

### *Referee dans des Revues Etrangères d'Audience Internationale*

Par ordre alphabétique avec le nombre d'articles

[1] Basin Research
[2] Earth Surface Processes and Landforms
[2] Geology
[1] Geologica Acta
[3] Geomorphology
[1] Global Planetary and Change
[1] GSA Bulletin
[1] Journal of the Geological Society of London
[1] Tectonophysics

### *Publications De Rang A [18]*

Citation-index = 161 (ISI Web), 163 (SCOPUS); citations moy/public : 14 ; *h*-index = 7

*http://www.researcherid.com/rid/L-9748-2014*

* *Parues et Acceptées :*

[18] V. Bosch, G., Van Den Driessche, J., **Babault, J.**, Robert, A., Carballo, A., Le Carlier, C., Loget, N., Prognon, C., Wyns, R. and Baudin, T. Peneplanation and deep dynamics of the Pyrenees ***C.R. Géocience 2015**, accepté*

[17] Struth, L., **Babault, J.** and Teixell, A. Drainage reorganization during mountain building in the river system of the Eastern Cordillera of the Colombian Andes ***Geomorphology 2015**, accepté*

[16] Viaplana-Muzas, M., **Babault, J.**, Dominguez, S., Van Den Driessche J. and Legrand, X. Drainage network evolution and patterns of sedimentation in an experimental wedge ***Tectonophysics 2015**, sous presse*

[15] Pastor, A., **Babault, J.**, Owen L.A., Teixell A., Arboleya, M.-L., Extracting dynamic topography from river profiles and cosmogenic nuclide geochronology in the Middle Atlas and the High Plateaus of Morocco ***Tectonophysics 2015**, doi:10.1016/j.tecto.2015.06.007*

[14] Domenech, M., Teixell, A., **Babault, J.** and Arboleya, M.-L. The inverted Triassic rift of the Marrakech High Atlas: A reappraisal of basin geometries and faulting histories ***Tectonophysics 2015***, *doi:10.1016/j.tecto.2015.03.017*

[13] **Babault, J.**, Teixell, A., Struth, L., Van Den Driessche, J., Arboleya, M.L. and Teson, E. Shortening, structural relief and drainage evolution in thick-skinned thrust-fold belts: insights from the Atlas Mountains, the Eastern Cordillera of Colombia and the Pyrenees *In: Nemčok, M. Mora, A. & Cosgrove, J. W. (Eds), Thick-Skin-Dominated Orogens: From Initial Inversion to Full Accretion.* ***Journal of the Geological Society of London, Spec. Publ.****, 377, pp. 18. doi.org/10.1144/SP377.14* ***2013***

[12] **Babault, J.** and Van Den Driessche J. Plateau uplift, regional warping and subsidence *In: Shroder, J. (Editor in Chief), Owen L. (Ed.),* ***Treatise on Geomorphology 2013****, Academic Press, San Diego, CA, vol. 5, pp. 36.*

[11] Pastor A., **Babault, J.**, Teixell, A. and Arboleya M.L. Intrinsic stream-capture control of stepped fan-pediments in the High Atlas piedmont of Ouarzazate (Morocco). ***Geomorphology 2012***

[10] **Babault, J.** Van Den Driessche J. and Teixell, A. Longitudinal to transverse drainage network evolution in the High Atlas (Morocco): the role of tectonics ***Tectonics 2012***

[9] **Babault, J.**, Bonnet, S., Ruiz, G.M.H. and Van Den Driessche, J. A comment on 'Late- to post-orogenic exhumation of the Central Pyrenees revealed through combined thermochronological data and modelling' by M. Gibson, H. D. Sinclair, G. J. Lynn and F. M. Stuart ***Basin Research 2009****, 21, 139–141, doi: 10.1111/j.1365-2117.2008.00377.x*

[8] Arboleya, M.-L., **Babault, J.**, Owen L.A., Teixell, A. and Finkel R.C. Timing and nature of Quaternary fluvial incision in the Ouarzazate foreland basin, Morocco ***Journal of the Geological Society London 2008****, 165 (6), 1059-1073, doi: 10.1144/0016-76492007-151.*

[7] **Babault, J.**, Teixell, A., Arboleya, M.-L. and Charroud, M. A late Cenozoic age for the long-wavelength surface uplift of the Atlas Mountains of Morocco ***Terra Nova 2008****, 20 (2), 102–107, doi: 10.1111/j.1365-3121.2008.00794.x.*

[6] **Babault, J.**, Bonnet, S., Van Den Driessche J. & Crave, A. High elevation of low relief surfaces in mountain belts: Does it equate to post-orogenic surface uplift? ***Terra Nova 2007****, 19 (4), 272–277, doi:10.1111/j.1365-3121.2007.00746.x.*

[5] **Babault, J.**, Loget N., Van Den Driessche J., Castelltort S., Bonnet S. and Davy P. Did the Ebro basin connect to the Mediterranean before the Messinian Salinity Crisis? ***Geomorphology 2006****, 81, 155-165 doi:10.1016/j.geomorph.2006.04.004.*

[4] **Babault, J.**, Van Den Driessche J., Bonnet S., Castelltort S. and Crave, A. Reply to comment by Yanni Gunnel and Marc Calvet on 'Origin of the highly elevated Pyrenean peneplain' ***Tectonics 2006****, 25, TC3004, doi:10.1029/2005TC001922.*

[3] **Babault, J.**, Van Den Driessche J., Bonnet S., Castelltort S. and Crave, A. Origin of the highly elevated Pyrenean peneplain ***Tectonics 2005****, 24, TC2010, doi:10.1029/2004TC001697.*

[2] **Babault, J.**, Bonnet, S., Crave, A. and Van Den Driessche J. Influence of piedmont sedimentation on erosion dynamics of an uplifting landscape: an experimental approach ***Geology 2005****, 33 (4), 301-304, doi: 10.1130/G21095.1.*

[1] **Babault, J.**, Van Den Driessche J. Erosion of mountain belts: influence of piedmont sedimentation ***C.R. Géoscience 2005,*** *337 (16), 1431-1438 doi:10.1016/j.crte.2005.09.010.*

* *En préparation :*

**Babault, J.**, Viaplana-Muzas, M., Van Den Driessche, J., Legrand , X., González-Quijano, M., Predicted infill composition of the Cendrawasih Bay (Papua New Guinea): a source-to-sink approach

**Babault, J.**, Capò, T., Van Den Driessche, J., Owen L.A. and Caffee M. Rate of divide migration and switch from longitudinal to transverse drainage in the NW Himalaya

**Babault, J.**, Arboleya, M.-L., Owen L.A., Onset of the external drainage in the Ouarzazate Basin dated by cosmogenic nuclides ($Be^{10}$)

**Babault, J.** and Van Den Driessche J. Retro- to pro-side migration of the main drainage divide of a relaxing mountain belt: the case of the Pyrenees

Struth, L., **Babault, J.,** Owen L.A., Caffee M. and Teixell, A. Rate of drainage reorganization in the Eastern Cordillera of the Colombian Andes

Viaplana-Muzas, M., **Babault, J.**, Dominguez, S., Van Den Driessche J. and Legrand, X. Influence of drainage network reorganization on sedimentation in front of an experimental wedge

### *Publications De Rang B*

Pastor, A., **Babault, J.**, Teixell, A. and Arboleya, M.L. Evidencias del desequilibrio y la reorganización de la red fluvial en la cuenca de Ouarzazate (Marruecos) ***Geogaceta, 2010****, 20 (3-4), 119-135.*

**Babault, J.,** Van Den Driessche J. and Teixell, A. Tectonics from topography: two examples from the Pyrenees and the High Atlas ***Trabajos de Geología, 2009****, 29, 94-100*

Teixell, A., Ayarza, P., Tesón, E., **Babault, J.,** Alvarez-Lobato, F., Charroud, M., Julivert, M., Barbero, L., Amrhar, M. and Arboleya, M.L. Geodinámica de las cordilleras del Alto y Medio Atlas: Síntesis de los conocimientos actuales ***Revista de la Soc. Geol. de España, 2007****, 20 (3-4), 119-135.*

**Babault, J.** and Teixell, A. El relieve de los Pirineos ***Enseñanza de las Ciencias de la Tierra, 2007.***

**Babault, J.** Dynamique de l'érosion dans les chaînes de montagnes : Influence de la sédimentation de piedmont. L'exemple des Pyrénées ***Ph.D. Thesis,*** *University of Rennes1, Mémoires de Géosciences Rennes, Vol. 112, 218p, 2004.*

**Babault, J.** Nouvelle interprétation géométrique et quantification du champ de déplacement sur la rampe latérale Ouest du Montsec (Bassin de Graus-Tremp, Espagne) ***Mémoires de DEA*** *de Géosciences Rennes, 20p, 2000.*

### *Congrès Internationaux [26]*

*Communications Orales [15] (j'ai souligné celles que j'ai présenté)*

**V. Bosch**, G., Van Den Driessche, J., **Babault, J.**, Robert, A., Carballo, A., and Loget, N. Peneplanation and deep dynamics in the Pyrenees *Talk*. EGU: Vienna - Austria European Geosciences Union *April 2015*

**Babault, J**., Antoni Capó; Jean Van Den Driessche; Lewis A. Owen and Marc W. Caffee. Switch from longitudinal to transverse drainage during mountain building: as case study from the Himalaya. *Talk*. AGU: San Francisco – USA *December 2013*

Domenech, M., A. Teixell, M.-L. Arboleya, **J. Babault.** Opening and inversion of the Tizi-n-Test Triassic graben (Western High Atlas, Morocco). *Talk*. ILP MAAPG: Marrakech - Morocco *October 2011*

**Babault, J**., J. Van Den Driessche and A. Teixell. Retro- to pro-side migration of the main drainage divide in the Pyrenees: geologic and geomorphological evidence. *Talk*. EGU: Vienna - Austria European Geosciences Union *April 2011*

Pastor, À., **J. Babault**, A. Teixell y M.L. Arboleya. Systematic stream piracy controlling the evolution of transverse rivers in the Ouarzazate foreland basin (Morocco). *Talk*. EGU: Vienna - Austria European Geosciences Union *April 2011*

Ruiz, G., F. Negro, **J. Babault**, J. Foeken, F. Stuart, F. Kober, and S. Ivy-Ochs. Tectono-thermal evolution of the Atlas system - SW Morocco. *Talk*. EGU: Vienna - Austria European Geosciences Union *April 2009*

Ruiz, G., F. Negro, J. Foeken, F. Stuart, **J. Babault**, D. Frizon de Lamotte, and D. Stockli. The Atlas Mountains: why there? Why now? *Talk*. EGU: Vienna - Austria European Geosciences Union *April 2009*

Teixell, A., Arboleya, M.-L., **Babault, J.**, Teson, E., Owen, L. Tectonics, uplift and surface processes in the Moroccan Atlas Mountains. AGU fall meeting, San Francisco, USA *2008*

**Babault, J.**, Van Den Driessche J. and Teixell, A. Tectonics from topography: two examples from the Pyrenees and the High Atlas *YORSGET meeting*, Oviedo - Spain 2008

**Babault, J.**, J. Van Den Driessche, A. Crave and A. Teixell. High Atlas morphology: insight from the drainage pattern. *Talk*. Join MAPG ILP meeting Marrakech (Morocco), *October 28-31, 2007*

Arboleya, M.-L., **Babault, J.,** *Owen, L.*, Teixell, A. and Finkel, R.C. Rates of Quaternary landscape evolution of an intracontinental mountain belt foreland basin, Atlas Mountains, Morocco: defined by terrestrial cosmogenic nuclides *Talk.* INQUA: Cains - Australia International Union for Quaternary Research *August 2007*

**Babault, J.**, Van Den Driessche, J., Bonnet, S., Castelltort, S. & Crave, A. On the origin of the highly elevated dissected Pyrenean peneplain. ***Talk.*** Joint Meeting EGU, Vienne, *April 2005*

**Babault, J.**, Bonnet, S., Crave, A & Van Den Driessche, J. Influence of piedmont sedimentation on erosion dynamics of an uplifting landscape: an experimental approach. ***Talk.*** Joint Meeting EGU, Vienne, *April 2005*

Bonnet, S., A. Crave, and J. Babault. Relationships between uplift, erosion and sediment flux; insights from experimental modeling GeoMod 2004

**Babault, J.**, de Urreiztieta, M., Rouby, D., Remacha, E., Oms, O. and Eichenseer, H. 3D Restoration of Eocene features across the central Pyrenees. AAPG Pacific Section June 2001

*Posters [11]*

Janowski, M., Loget, N., Gautheron, C., Meyer, B., Van Den Driessche, J., and **Babault, J.** Neogene uplift of the eastern Betic Cordillera (Spain) : new constraints from low-temperature thermochronology and stream profile analysis Poster. *EGU: Vienna - Austria European Geosciences Union April 2015*

**Babault, J.**, J. Van Den Driessche and A. Teixell. Longitudinal to transverse drainage network evolution in the High Atlas (Morocco). Poster. *EGU: Vienna - Austria European Geosciences Union April 2012*

**Babault, J.**, J. Van Den Driessche, A. Crave and A. Teixell. Drainage pattern evolution and propagation of incision in response to late-Cainozoic mantle-related uplift in the High Atlas of Morocco. Poster. *EGU: Vienna - Austria European Geosciences Union April 2008*

Jimmenez-Munt, I., Garcia-Castellanos, D. and **Babault, J.**, Numerical modelling of intracontinental mountain building and drainage evolution in the Atlas. *Poster.* Join MAPG ILP meeting Marrakech (Morocco), *October 28-31, 2007*

**Babault, J.**, A. Teixell, M.-L. Arboleya, M. Charroud and B. Charai. Geological evidence for the timing of long-wavelength surface uplift of the Atlas mountains of Morocco. *Poster.* The third workshop of the ILP Task force on Sedimentary Basins, In the frame of the MAPG International Convention, Conference and Exhibition Marrakech (Morocco), *October 28-31, 2007*

**Babault, J.**, Teixell, A., Arboleya, M.-L. and Charroud, M. Evidence for late Cenozoic surface uplift of the Atlas Mountains. *Poster.* EGU: Vienna - Austria European Geosciences Union *April 2007*

**Babault, J.**, Bonnet, S., Crave, A & Van Den Driessche, J. Influence of piedmont sedimentation on the erosion dynamics: an experimental approach and implications for the Andes. *Poster.* 6° Simposio Internacional de Geodinámica de los Andes (ISAG), Barcelone, *Septembre 2005*

**Babault, J.**, Van Den Driessche, J., Bonnet, S. & Crave, A. Peneplanation of an uplifting landscape by aggradation of products of erosion at its foot. *Poster.* Joint Meeting EGU, Nice, **April 2004.**

Loget, N., **Babault, J.**, Castelltort, S., Van den Driessche, J., Bonnet, S. & Davy, P. When does the Ebro river connect to the Mediterranean? *Poster*. Joint Meeting EGU, Nice, *April 2004.*

**Babault, J.**, Van Den Driessche, J., Bonnet, S. & Crave, A. Morphological evolution of the Pyrenees and Ebro drainage basin: effect of a capture on the erosion of a mountain chain. *Poster.* Joint Meeting AGU-EGS-AUG, Nice, ***April 2003***.

**Babault, J.**, Van Den Driessche, J., Bonnet, S. & Crave, A. Morphological evolution of the Pyrenees and Ebro drainage basin: effect of a capture on the erosion of a mountain chain. *Poster*. DRT, St Malo*, May 2003.*

### *Congrès Nationaux [9]*

#### *Communications Orales [7]*

Viaplana, M., **Babault, J.**, Van Den Driessche, J. et Dominguez, S., Modélisation analogique de la dynamique du réseau de drainage dans un prisme d'accrétion. ***Talk***. 14eme ASF, Paris, *Nov 2013*

Loget, N., Diot, X., Van Den Driessche, J., **Babault, J.**, Do Couto, D. et Gorini, C. Évolution post tortonienne du réseau de drainage dans le Sud Est des Bétiques. ***Talk***. 14eme ASF, Paris, *Nov 2013*

Pastor, À., J. **Babault, J.**, A. Teixell y M.L. Arboleya. Evidencias del desequilibrio y la reorganización de la red fluvial en la cuenca de Ouarzazate (Marruecos). 49ª Sesión Científica, Gandesa, November 2010

**Babault, J.**, E. Tesón, D. Gómez-Gras, M. Corbella, E. Gómez-Rivas, JD. Martín-Martín, Ll. Casas y L-M. Castaño. Experimental modelling: a powerful tool for teaching surface processes from erosion and transport to sedimentation. VII Congreso Geologico de España, Canarias 2008.

**Babault, J.**, Teixell, A., Arboleya, M.-L. and Charroud, M. A late Cenozoic age for the long-wavelength surface uplift of the Atlas Mountains of Morocco. VII Congreso Geologico de España, Canarias 2008.

**Babault, J.**, Teixell, A., Arboleya, M.-L. and Charroud, M. Late Cenozoic surface uplift of the Atlas of Morocco. *Talk.* RST Lugar: Dijon - France - Société Géologique de France, Société Française de Minéralogie et Cristallographie *December 2006*

**Babault, J.**, Van Den Driessche, J., Bonnet, S., Castelltort, S. & Crave, A. On the origin of the highly elevated Pyrenean peneplain. ***Talk***. Joint Earth Sciences Meeting RST, Strasbourg, *Septembre 2004*

## *Posters [2]*

Arboleya, M.-L., **Babault, J.**, Owen L.A., Teixell, A. and Finkel R.C Climate-controlled fluvial incision in the Ouarzazate foreland basin (High Atlas, Morocco) revealed by cosmogenic nuclide dating of fluvial terraces. VII Congreso Geologico de España, Canarias 2008.

Babault, J., Remacha, E., Rouby, D., Oms, O., de Urreiztieta, M., Dinarès-Turell, J., Eichenseer, H. & Nalpas, T. 3D Restoration of Ilerdian to Cuisian features across the Central Pyrenees (Campo-Ainsa area): implications on the Graus-Tremp basin tectono-stratigraphic evolution. *Poster*. 3° congreso del Terciario, Tremp, Catalunya (Spain). **Septembre 2000.**

## B. La topographie comme marqueur de la déformation de la lithosphère

### 1. Introduction

L'objectif de ma recherche est de contribuer à la compréhension des processus géodynamiques à l'origine des chaînes de montagnes par l'étude des mouvements tectoniques. Ces derniers se décomposent en déplacements horizontaux qui décalent les rivières, et en déplacements verticaux de la topographie en réponse à un amincissement ou un épaississement de la lithosphère, ou encore en raison des mouvements dans le manteau inférieur à l'origine de la topographie dynamique. Les déplacements verticaux de la topographie correspondent au *surface uplift* comme l'ont défini England et Molnar (1990), c'est-à-dire le *rock uplift* moins l'érosion. Dans les chaînes actives, le *rock uplift* est généré par la tectonique qui force les rivières à inciser. Même si l'érosion dépend également du flux d'eau et qu'elle est donc modulée par le climat, elle est surtout contrôlée par la tectonique. Je me suis jusqu'à présent intéressé à la dynamique du *surface uplift* dans les chaînes, et à son influence sur le réseau de drainage et le remplissage des bassins sédimentaires.

J'aborde ce problème par une étude couplée des processus géomorphologiques, des structures tectoniques et du remplissage des bassins sédimentaires. J'ai choisi d'orienter mes recherches vers l'étude de cas naturels, et ce dans plusieurs régions du monde afin de comprendre leur histoire tectonique mais aussi pour tester le caractère général ou non des interprétations faites à partir de l'étude de cas particuliers. Pour cela, je réalise une analyse géomorphologique de la topographie sur le terrain et par l'analyse des modèles numériques de terrain, et je replace ces résultats dans leur contexte géologique par une analyse de terrain tout en tenant compte de la structure profonde des chaînes. Je quantifie les vitesses d'érosion pour pouvoir quantifier les vitesses de soulèvement en utilisant les techniques de thermochronologie basse température et de nucléides cosmogéniques. L'acquisition de données me permet de contraster les modèles d'évolution existant et d'en proposer de nouveaux si besoin. Enfin, j'utilise la modélisation expérimentale pour démontrer la validité des interprétations faites à partir des études de cas naturels.

Montrer l'existence d'un soulèvement de la topographie (*surface uplift*) reste encore un défi car la plus part des études, qui se basent sur des estimations de paléoaltimétries dont les marges d'erreur dépassent souvent les gammes de soulèvement considérées, ou de vitesses d'érosion, permettent d'obtenir le plus souvent des estimations ponctuelles du *rock uplift*, encore aujourd'hui interprétées parfois de façon erronée comme du *surface uplift* **(cf. Babault and Van Den Driessche, 2013, pour une synthèse)**. Au cours des deux dernières décennies, il a été démontré théoriquement et empiriquement que certains paramètres morphologiques pouvaient également être utilisés pour cartographier le *rock uplift*. Alors que les pentes sur les versants sont sensibles au *rock uplift* pour des valeurs faibles allant jusqu'à ~0.2 mm/a (e.g., Burbank et al., 1996), passée cette valeur les pentes sur les versants atteignent une valeur critique (~30º) qui dépend de leur résistance moyenne à la fracturation. En revanche, les pentes des rivières s'adaptent au *rock uplift* (e.g., Mudd et al., 2014; Perron and Royden, 2013; Royden and Perron, 2013) pour des valeurs allant jusqu'à quelques mm/a, comme c'est le cas dans l'Himalaya (e.g., Godard et al., 2014). On peut par conséquent cartographier le *rock uplift* par l'analyse morphologique des pentes des rivières et leur calibration par des données géologiques (vitesses de soulèvement et d'érosion). Puisqu'à tout soulèvement de la topographie

correspond un mécanisme profond ayant pu modifier l'altitude moyenne, il convient de démontrer son existence pour valider les estimations de *surface uplift*.

C'est en tenant compte de ces considérations que, pour étudier la dynamique du *surface uplift*, je me suis intéressé à la dynamique de l'érosion dans les chaînes de montagnes, comme marqueur de la déformation et en particulier des mouvements verticaux, ainsi qu'aux mécanismes profonds permettant de les expliquer. En parallèle, je me suis intéressé aux relations entre le *surface uplift* dans les chaînes et la dynamique de leurs réseaux de drainage, ainsi qu'aux conséquences de leurs interactions sur les flux sédimentaires. Après avoir montré au cours de ma thèse à Géosciences Rennes que la sédimentation de piedmont inhibe l'érosion en altitude, en prenant comme exemple les Pyrénées et par une approche expérimentale, je me suis intéressé à la dynamique du *surface uplift*, de l'érosion, du réseau de drainage et des flux sédimentaires dans les Pyrénées, dans le Haut Atlas marocain, dans la Cordillère Orientale de Colombie, dans la partie NO de l'Himalaya et dans le Central Range de Papouasie Nouvelle Guinée, tout en continuant à utiliser la modélisation expérimentale, désormais à Géosciences Montpellier. Ces approches placent mes recherches à l'échelle de la chaîne de montagnes et de ses bassins d'avant-pays, sur des gammes de temps allant de plusieurs centaines de milliers d'années à plusieurs dizaines de millions d'années.

## 2. Quantification des Mouvements Verticaux d'Origine Mantélique

### 2.1. Dans les Pyrénées

Il existe toujours un débat sur l'existence ou non d'un soulèvement récent (depuis le Miocène Supérieur) dans la partie orientale des Pyrénées (Babault et al., 2009; Gunnell et al., 2008), et qui se base principalement sur l'existence de surfaces d'érosion d'âge Oligo-Miocène à faible relief et à haute altitude dans la zone axiale des Pyrénées (Figure 1, gauche). Ces surfaces ont été interprétées comme des surfaces d'érosion formées proches du niveau de la mer et par la suite soulevées jusqu'à leur altitude actuelle à plus de ~2000 m a.s.l. (e.g., Calvet, 1996). En particulier, il a été proposé qu'un amincissement de la lithosphère soit à l'origine de leur soulèvement ce qui impliquerait un soulèvement de la topographie (un *surface uplift*) de l'ordre de ~2000 m depuis le Miocène Supérieur (e.g., Gunnell et al., 2008).

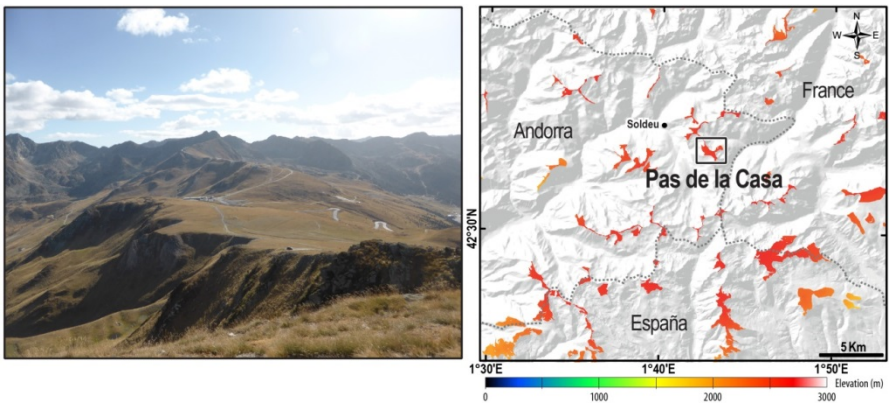


***Figure 1 :*** *(Gauche) Surface d'érosion à faible relief à plus de 2400 m d'altitude au Pas de la Casa (Andorre). (Droite) Cartographie automatisée qui permet de séparer les surfaces à faible relief qui correspondent aux fonds de cirques glaciaires des surfaces d'érosion à faible relief et situées au niveau des limites de bassins versants. Le cadre indique la localisation de la photographie de gauche* ***(V. Bosch, Van Den Driessche, Babault et al., accepted)****.*

Au cours de ma thèse, j'avais proposé comme alternative, à travers l'étude de la dynamique du relief, que l'aggradation des produits d'érosion sur les bordures de la Zone Axiale avait entraîné une inhibition du potentiel érosif des rivières qui drainent la Zone Axiale et une diminution, en altitude, du relief local au cours de l'Oligo-Miocène. Cette dynamique a été validée expérimentalement et les expériences montrent : (1) que les interactions entre les processus d'érosion et de sédimentation augmentent le temps de réponse du système en érosion lors de son adaptation aux conditions de soulèvement **(Babault et al., 2005a)** ; (2) un lissage en altitude de la topographie en soulèvement lorsqu'elle est bordée par une zone en sédimentation correspondant à une aggradation des produits d'érosion **(Babault et al., 2007)**. Comme dans le cas des Pyrénées, la construction d'une chaîne de montagnes s'accompagne généralement d'une aggradation de sédiments sur son piedmont. Ce fait suggère que le lissage en altitude du relief local est très probablement un processus intrinsèque à la destruction post-orogénique d'une chaîne de montagnes **(Babault et al., 2007; Babault et al., 2005b)**. Ce processus explique la formation en altitude d'une topographie à faible relief et, par conséquent, la préservation post-orogénique de la racine crustale d'une chaîne (Figure 2) **(Babault and Van Den Driessche, 2005; Babault et al., 2005b)**. Autrement dit, l'existence en altitude de surfaces d'érosion à faible relief n'est pas forcément un marqueur de mouvements verticaux, et encore moins s'il existe une racine crustale qui supporte la topographie comme c'est le cas dans les Pyrénées. Mes résultats de thèse allaient donc à l'encontre des modèles qui faisaient appel à un soulèvement depuis le Miocène Supérieur des Pyrénées.

Les travaux qui avancent un amincissement de la lithosphère comme moteur d'un *surface uplift* depuis le Miocène Supérieur sont basés sur des modèles de champs de potentiel (e.g., Gunnell et al., 2008). Or, dans ce type de modélisation (*foreward*), une faible augmentation de l'épaisseur de la croûte entraîne une très forte augmentation de l'épaisseur du manteau lithosphérique sous-jacent. Pour tester la sensibilité de ces modèles, nous avons, dans le cadre de la thèse de Gemma V. Bosch que je co-dirige, réalisé une nouvelle modélisation (*inverse*) à partir des champs de potentiel (topographie, anomalies du géoïde) et d'une analyse thermique en 1D. Nous avons par la suite comparé nos résultats aux nouvelles données qui imagent la base de la croûte et la lithosphère et qui ont été obtenues à partir de fonctions réceptrices et d'une tomographie locale (Chevrot et al., 2014). Le principal résultat est l'absence d'un amincissement anormal de la lithosphère qui aurait pu expliquer un *surface uplift* récent des Pyrénées (Figure 3). En revanche, l'altitude moyenne peut être simplement expliquée comme étant le résultat d'une compensation isostatique héritée de l'épaississement crustal d'âge Pyrénéen **(V. Bosch, Van Den Driessche, Babault et al., accepted)**. Nous avons également cartographié les surfaces d'érosion à faible relief par une méthode basée sur l'analyse de la topographie numérique (Figure 1, droite) et qui nous a permis de montrer de façon précise que des restes de ces surfaces d'érosion à faible relief existent dans l'ensemble de la zone axiale même si elles ont été en partie recoupées par les formes d'érosion glaciaire, et ce principalement dans les Pyrénées centrales (à l'Ouest de 1º30'E).

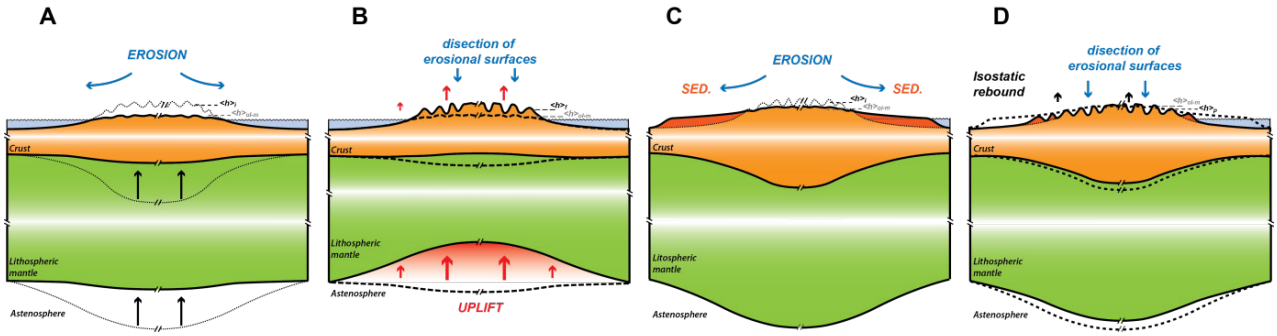


***Figure 2 :*** *(A-B) Modèle de pénéplaine formée au niveau de la mer au cours du Miocène puis soulevée et disséquée depuis moins de 10 Ma (e.g., Gunnell et al., 2008). (C-D) Modèle de lissage en altitude de la topographie au cours de l'Oligo-Miocène en réponse à un soulèvement du niveau de base, i.e., de l'apex de sédimentation* ***(Babault and Van Den Driessche, 2005; V. Bosch, Van Den Driessche, Babault et al., accepted)****. Dans ce modèle, l'incision postérieure n'est pas liée à un soulèvement de la topographie (surface uplift).*

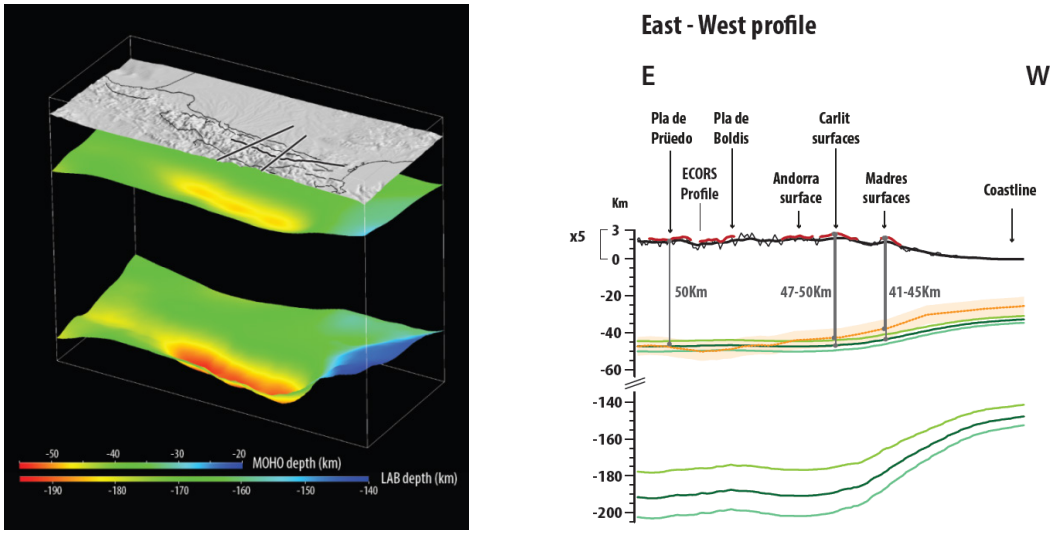


***Figure 3 :*** *(Gauche) Vue 3D de l'épaisseur de la croûte et de la lithosphère sous les Pyrénées, obtenues à partir d'une modélisation inverse des champs de potentiel. (Droite) Profil Est-Ouest passant par la zone axiale des Pyrénées montrant en nuances de verts 3 modèles obtenues en faisant varier les densités de croûte et du manteau. Les courbes rouges représentent les surfaces d'érosion à faibles relief projetées sur ce profil. Ces modèles qui considère une isostasie pure, reproduisent la profondeur du Moho (courbe orange foncé) obtenue par la tomographie (Chevrot et al., 2014) en tenant compte des margeurs d'erreur (bande orange clair) indiquant que l'altitude moyenne des Pyrénées peut être simplement expliquée comme étant le résultat d'une compensation isostatique héritée de l'épaississement crustal d'âge Pyrénéen* ***(V. Bosch, Van Den Driessche, Babault et al., accepted)****.*

## 2.2. Dans le Haut Atlas

Au cours de mon séjour post-doctoral à l'Université Autonome de Barcelone (UAB), j'ai étudié la dynamique de l'érosion du Haut Atlas marocain et des hauts plateaux qui l'entourent. Des études géologiques et géophysiques avaient mis en évidence un soulèvement de la topographie jusqu'à 1000 m des montagnes de l'Atlas et des hauts plateaux marocains. Ce soulèvement s'explique par un amincissement de la lithosphère mantellique dont l'origine est encore débattue. La détermination de l'histoire du soulèvement de la topographie est cruciale pour comprendre les processus tectonique en jeu. A partir de marqueurs géologiques, j'ai montré que ce soulèvement grande longueur d'onde de la topographie (*surface uplift*) a eu lieu au cours des derniers 5-7 Ma le long d'une ligne Nord-Sud qui s'étend depuis la bordure sud du Rif, qui traverse le Moyen Atlas et le Haut Atlas et qui atteint la bordure nord du Sahara (Figure 4). On y retrouve en

particulier des dépôts lacustres basculés d'âge pliocène et des sédiments marins peu profonds d'âge messinien culminant à plus de 1000 m a.s.l. ce qui implique une vitesse moyenne de soulèvement de la topographie de l'ordre de 0.2 mm/a **(Babault et al., 2008)**.

J'ai poursuivi ce travail dans le cadre de la thèse d'Alvar Pastor (2008-2013) que j'ai codirigé avec A. Teixell (UAB) et M. Arboleya (UAB) et qui s'inscrivait dans un projet financé par le ministère espagnol des sciences. Je venais d'être nommé Lecteur à l'Université Autonome de Barcelone (UAB) quand Alvar a commencé sa thèse. Dans sa thèse, Nous avons montré qu'en analysant les pentes des rivières il est possible de séparer l'incision et donc le soulèvement lié aux déformations crustales, du soulèvement lié à l'amincissement lithosphérique qui a affecté à la fois les zones déformés (le Moyen Atlas) et les zones non déformées (les Hauts Plateaux). Nous montrons que ce soulèvement grande longueur d'onde de la topographie (*surface uplift*) a affecté une zone de plusieurs centaines de kilomètres située à l'Est du profil Nord-Sud de la figure 4 et au Sud des Chaînes du Rif et du Tell, s'étalant depuis le Moyen Atlas jusqu'aux aux Hauts Plateaux de l'Est du Maroc (Figure 5). La datation à 50 Ka et 400 Ka, par la méthode des nucléides cosmogéniques ($^{10}$Be), de terrasses fluviatiles et de cônes alluviaux quaternaires incisés suggère que ce soulèvement d'origine mantellique a eu lieu au cours des deux derniers millions d'années, ce qui impliquerait des vitesses de soulèvement de l'ordre de 0.2 mm/a, équivalentes à la valeur moyenne proposée précédemment en nous basant seulement sur les marqueurs stratigraphiques **(Pastor, Babault et al., 2015)**.

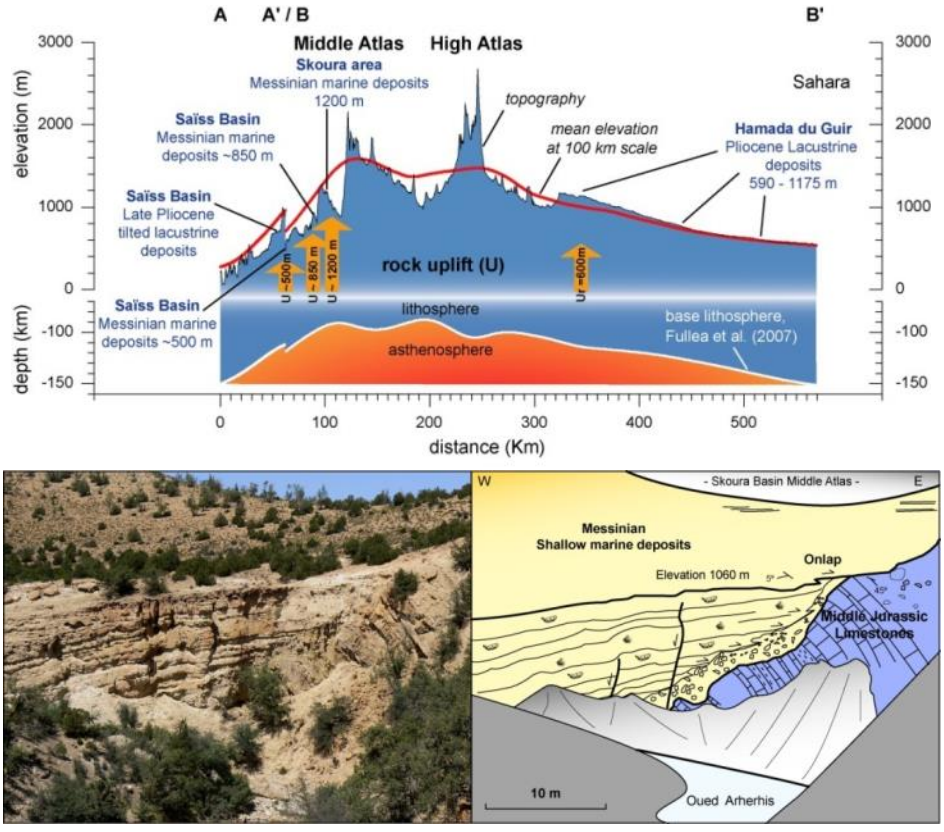


***Figure 4 :*** *(Haut) Profil topographique illustrant le soulèvement grande longueur d'onde des montagnes de l'Atlas et des plateaux marocains. (Bas) Photo des sédiments marins les plus récents préservés dans le Moyen Atlas. Ils sont d'âge messinien, peu déformés et indiquent un soulèvement de 1000 à 1200 m (rock uplift). Le faible degré d'érosion de ces sédiments indique un surface uplift de l'ordre de 1000 m* ***(Babault et al., 2008)****.*

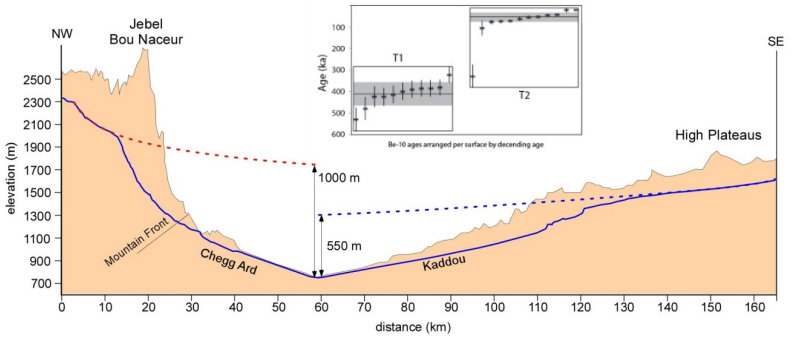


***Figure 5:*** *Profil topographique illustrant l'incision et le soulèvement différentiel entre le Moyen Atlas et les Hauts Plateaux.* ***(Pastor, Babault et al., 2015)****.*

# 3. Influence de la tectonique sur la dynamique du réseau de drainage

## 3.1. Réorganisation du réseau dans une chaîne en Construction

### *Le cas du Haut Atlas*

On sait que les rivières s'adaptent aux soulèvements en augmentant leurs pentes et parfois même en réduisant leur largeur. Dans les deux cas, ces modifications de la géométrie des lits des rivières permettent d'augmenter leur pouvoir d'incision. Il existe maintenant un nombre croissant d'études qui depuis plus d'une dizaine d'années ont montré que la pente des rivières est proportionnelle aux vitesses d'érosion et donc de soulèvement. Cependant, en étudiant la dynamique du soulèvement dans le Haut Atlas marocain, j'ai pris conscience qu'un système géomorphologique dans une chaîne en construction, tel que le Haut Atlas, avait une dynamique propre, qui potentiellement pouvait modifier les pentes des rivières, et par conséquent laisser un signal dans la topographie qui se superposerait alors au signal tectonique. Je me suis donc intéressé à l'organisation des bassins versants et à la dynamique du réseau de drainage. J'ai réalisé ce travail au cours de mon post-doctorat et par la suite comme professeur Lecteur à l'Université Autonome de Barcelone (UAB) en collaboration avec J. Van Den Driessche (Rennes), A. Teixell (UAB), M. Arboleya (UAB) dans le cadre d'un projet financé par le ministère espagnol des sciences.

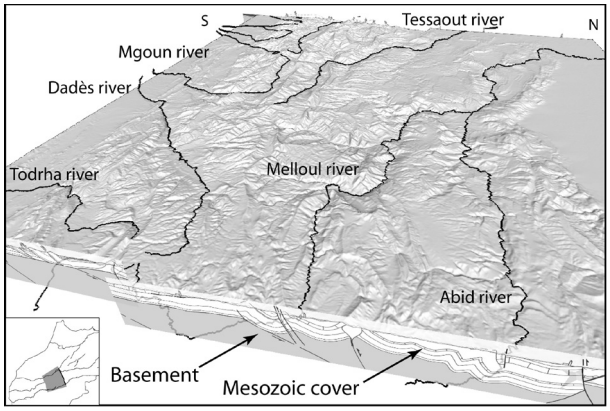


***Figure 6:*** *Vue d'ensemble vers l'Ouest de la topographie du Haut Atlas et d'une coupe géologique montrant la déformation de la couverture mésozoïque et la localisation des principales rivières dans les synclinaux qui s'écoulent en conséquence parallèlement à l'allongement de la chaîne (drains longitudinaux)* ***(Babault et al., 2012)****.*

La majeure partie du Haut Atlas marocain est dominé par des drains longitudinaux, parallèles aux structures tectoniques (Figure 6). Il s'agit d'une configuration surprenante puisque intuitivement on s'attendrait à ce que les rivières dans les chaînes de montagnes s'écoulent en suivant la pente régionale, depuis la principale ligne de partage des eaux jusqu'aux bassins d'avant-pays. C'est en général le cas dans la plus part des chaînes actives où les rivières sont généralement décrites comme étant transverses (Hovius, 1996), i.e., perpendiculaire au grain structural. A partir de l'étude du relief du Haut Atlas, nous avons proposé un modèle d'évolution du réseau de drainage qui permet de réconcilier l'observation faite dans le Haut Atlas avec l'organisation des réseaux dans les chaînes actives.

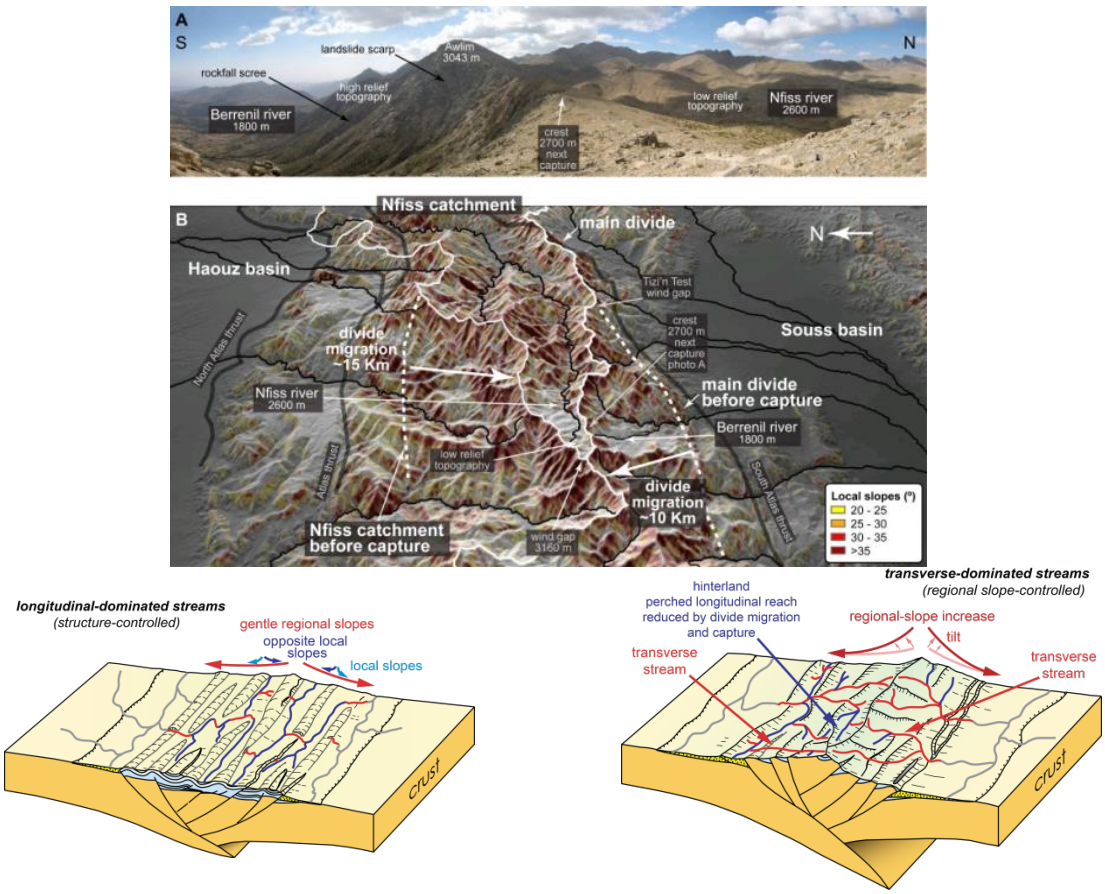


***Figure 7 :*** *(Haut) (A) Photo de la ligne de partage des eaux entre la rivière transverse Berrenil et la partie amont de la rivière longitudinal Nfiss. (B) Les pentes sont supérieures à 30° du côté du transverse, où on y observe des cicatrices de glissements de terrains. Par contre, les pentes sont inférieures à 20° du côté du longitudinal et on n'y observe pas d'activité érosive intense. Ces observations indiquent que le bassin versant du drain transverse est en expansion au dépend du bassin versant du drain longitudinal. (Bas) Schémas d'évolution du réseau de drainage au cours de la construction d'une chaîne de montagnes* ***(Babault et al., 2012)****.*

On observe dans le Haut Atlas une corrélation spatiale entre l'orientation des principales rivières et les quantités d'exhumation. Les rivières sont principalement transverse dans la partie occidentale (Figures 7A et 7B), là où les quantités d'exhumation et donc de soulèvement sont les plus élevées. Couplé à l'analyse géomorphologique de terrain et des modèles numériques de terrain, ce fait indique que l'épaississement tectonique et le soulèvement associé de la topographie ont augmenté l'énergie potentielle sur les deux flancs du Haut Atlas occidental et donc l'érosion fluviatile des cours d'eau transverses. L'augmentation des vitesses d'érosion dans les drains transverses est à l'origine d'une érosion différentielle entre les drains longitudinaux au centre de la chaîne et les drains transverses sur ses bords. Ce différentiel d'érosion a permis aux seconds de capturer des portions longitudinales et dans le même temps d'accroître leurs aires de

drainage. On en déduit que l'épaississement croissant et la réorganisation du réseau de drainage ont renforcé de façon continue la capacité érosive des drains transverses par l'augmentation des pentes et des aires drainées (Figure 7C) **(Babault et al., 2012)**. Ce processus entraînera à terme la destruction complète du réseau initialement longitudinal dans le Haut Atlas occidental mais également dans le reste du Haut Atlas si les vitesses actuelles de déformation et de soulèvement persistent dans le futur. Cette étude suggère que l'évolution depuis un drainage longitudinal vers un réseau transverse est un stade transitoire de l'évolution du réseau de drainage au cours de la construction d'une chaîne de montagnes.

Là où la capture d'un drain longitudinal par un drain transverse a lieu, le gain d'énergie potentiel engendre une augmentation des pentes locales et une vague d'érosion se propage dans la partie amont du drain capturé (e.g., Yanites et al., 2013). Si l'évolution du réseau de drainage, telle qu'on l'observe dans le Haut Atlas est un processus intrinsèque à la construction d'une chaine de montagne, il apparait raisonnable de réaliser une étude morphologique détaillée avant de pouvoir utiliser la topographie comme un enregistreur d'un quelconque soulèvement tectonique. Afin de vérifier qu'il s'agit d'un processus intrinsèque à une chaîne en construction, j'ai étudié la dynamique du réseau de drainage dans trois autres chaînes de montagnes en construction : la Cordillère Orientale de Colombie, le Central Range de Papouasie Nouvelle Guinée et la partie NO de l'Himalaya. Enfin, nous avons modélisé ce comportement expérimentalement pour valider nos interprétations.

### *Le cas de la Cordillère Orientale de Colombie*

La Cordillère Orientale de Colombie est une chaîne de montagne en construction, un rift de retro-arc ayant subi une inversion au cours du Cénozoïque. Elle est caractérisée par deux domaines topographiques (Figure 8) : (i) un haut plateau à 2500 m d'altitude, au centre (Sabana de Bogotá), avec un faible relief local et dominé par des rivières parallèles aux structures, longitudinales à la chaîne et (ii) des flancs abrupts et escarpés, dominés par des rivières transverses qui recoupent les structures tectoniques, et qui relient le haut plateau aux piedmonts situés à quelques centaines de mètres d'altitude. Comme dans le Haut Atlas marocain, on y observe un réseau de drainage précoce d'âge éocène-oligocène, dominé par des drains longitudinaux eux-mêmes contrôlés par les structures tectoniques, et qui est progressivement capturé par des drains transverses au cours de la construction de la chaîne **(Babault et al., 2013; Struth, Babault et al., accepted)**.

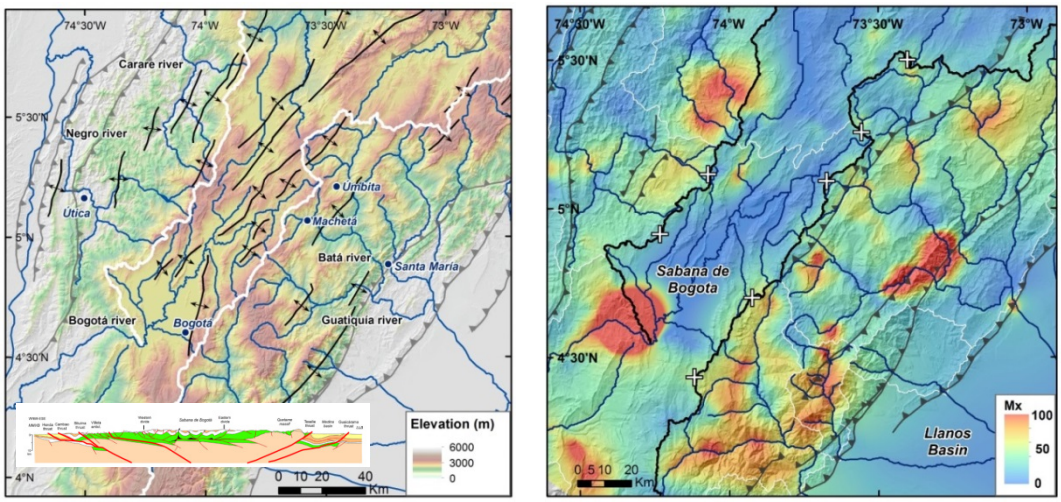


***Figure 8 :*** *(Gauche) Modèle numérique de terrain de la Cordillère Orientale de Colombie. Lignes blanches : positions des lignes de partage des eaux entre la Meseta de Bogotá et les flancs Est et Ouest. (Droite) Les indices de pentes normalisées des rivières (methode χ-plot) sont supérieurs du côté des drains transverses qui incisent à des vitesses de ~0.1 mm/a. Par contre, les pentes sont inférieures du côté des rivières longitudinales et on n'y observe pas d'activité érosive intense (~0.01 mm/a). Ces observations indiquent que les bassins versant des drains transverses sont en expansion au dépend des bassins versants des drains longitudinaux comme dans le Haut Atlas marocain.*

Nous montrons également que les vitesses d'érosion sur le cours terme (centaine de milliers d'années) à l'échelle des bassins versants ($^{10}$Be) des drains transverses incisent à des vitesses (~0.1 mm/a) d'un ordre de grandeur plus rapide comparées à celles des rivières longitudinales du haut plateau de Bogotá (~0.01 mm/a) (**Struth, Babault et al., en prep**.). Les analyses ont été réalisées en collaboration avec L. Owen (Univ. Cincinnati, US) qui nous donne accès à son laboratoire de nucléides cosmogéniques. Comme dans l'atlas marocain, l'épaississement croissant et la réorganisation du réseau de drainage ont renforcé de façon continue la capacité érosive des drains transverses par l'augmentation des pentes et des aires drainées transverses. Les résultats obtenus dans le cadre de la thèse de L. Struth montrent que le modèle d'évolution du réseau de drainage basé sur le cas naturel du Haut Atlas marocain explique également l'organisation du réseau de drainage de la Cordillère Orientale. J'ai codirigé avec A. Teixell la thèse de L. Struth dans le cadre d'un projet financé par le ministère espagnol des sciences et en collaboration avec A. Mora de l'Institut Colombien du Pétrole (EcoPétrole).

### *Le cas du Nord-Ouest de l'Himalaya*

De grandes rivières transverses incisent les montagnes himalayennes aux sommets dont l'altitude est beaucoup plus haute que leurs sources situées sur la bordure sud du plateau tibétain. L'âge de la formation de ces rivières trans-himalayennes est débattu. Dans la partie NO de l'Himalaya nous montrons qu'une rivière longitudinale, le Chenab (Figure 9), est bordée au Sud par un drain transverse, le Beas. Les indices de pente normalisés (Ksn), calibrés par les vitesses d'érosion issues de la littérature, indiquent une vitesse d'érosion différentielle sur le long terme entre les deux bassins de ~0.9 ±0.9 mm/a (Figure 12).

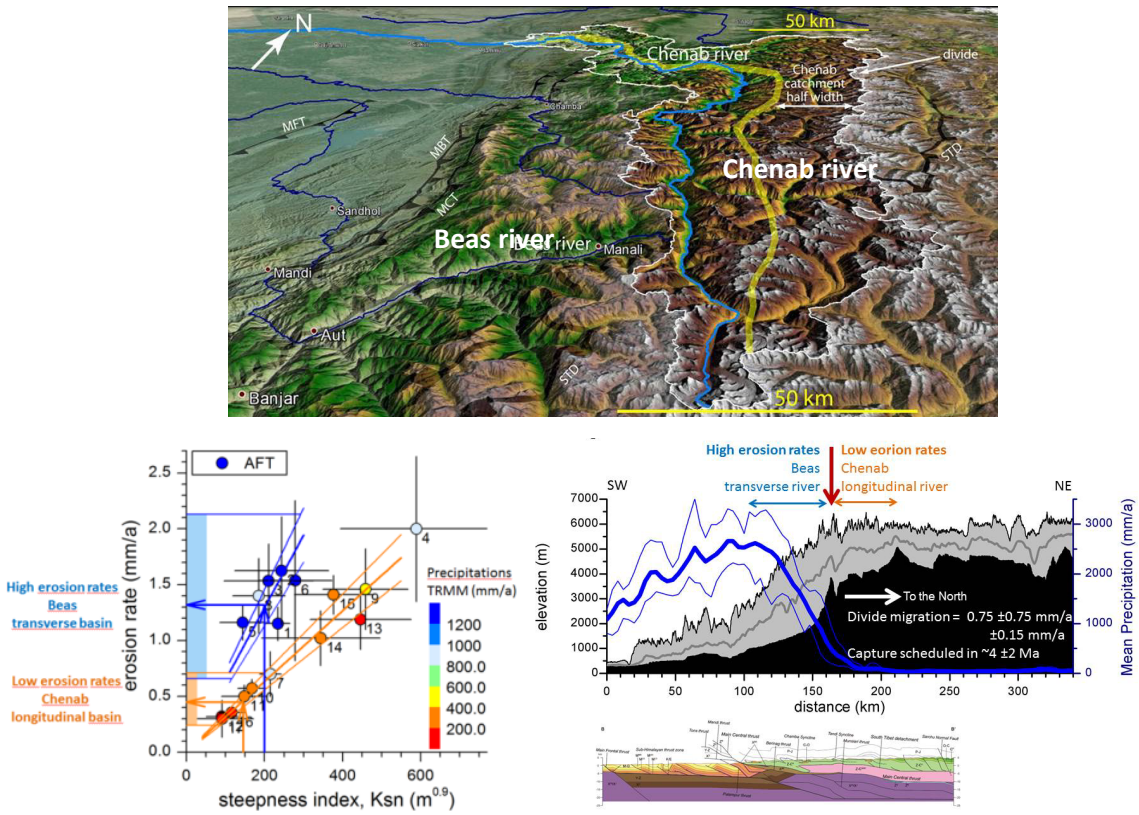


***Figure 9 :*** *(Haut) Vue 3D de la ligne de partage des eaux entre la rivière transverse Beas et la rivière longitudinale Chenab dans la partie NO de l'Himalaya. (Bas gauche) Calibrations des indices de pente des rivières (Ksn), utilisés comme proxy pour estimer les vitesses d'érosion sur le long terme dans les parties amont des bassins versants du Beas et du Chenab. (Bas droite) Profil topographique moyen de l'Himalaya montrant la position instable du drain longitudinal du Chenab situé à 3000 m d'altitude, menacé d'être capturé par le drain transverse du Beas, et coupe géologique (Webb et al., 2011).*

Des vitesses d'érosion obtenues par la méthode des nucléides cosmogéniques ($^{10}$Be) indiquent une vitesse d'érosion différentielle identique sur le cours terme (derniers milliers à centaines de milliers d'années). Ces résultats montrent que la ligne de partage des eaux migre vers le nord à une vitesse de ~0.75 mm/a et que la rivière Chenab sera capturée par le Beas au cours des prochains 4±2 Ma, aboutissant à la création d'une rivière trans-himalayenne. Considérées ensemble, les données géomorphologiques et les vitesses d'érosion conduisent également à un schéma d'évolution du réseau de drainage depuis un réseau longitudinal dans les stades précoces de la construction de la chaîne himalayenne vers un réseau dominé par des drains transverses (**Babault et al., en prep.**). J'ai réalisé ce travail (2011-2013) comme professeur Lecteur à l'Universitat Autonoma de Barcelona (UAB) en collaboration avec A. Capo (au cours d'un encadrement de M2), J. Van Den Driessche (Rennes) et L. Owen (Univ. Cincinnati) dans le cadre d'un projet financé par le ministère espagnol des sciences et par la National Science Foundation (US).

### *Le cas du Central Range de Papouasie Nouvelle Guinée*

Dans le Central Range, les résultats de l'analyse géomorphologique replacée dans leur contexte géologique montrent que le réseau de drainage est également en cours de réorganisation, depuis un réseau précoce dominé par des rivières longitudinales, elles-mêmes contrôlées par les structures tectoniques, dans les parties internes qui correspondent à un haut Plateau, vers un réseau dominé par des rivières transverses sur le flanc sud (Figure 10 gauche) (**Babault et al., en prep.**). Ce schéma confirme le modèle d'évolution du

réseau au cours de la construction d'une chaine de montagnes en réponse à une augmentation progressive des pentes et de l'épaississement comme nous l'avions proposé pour le Haut Atlas marocain et la Cordillère Orientale de Colombie.

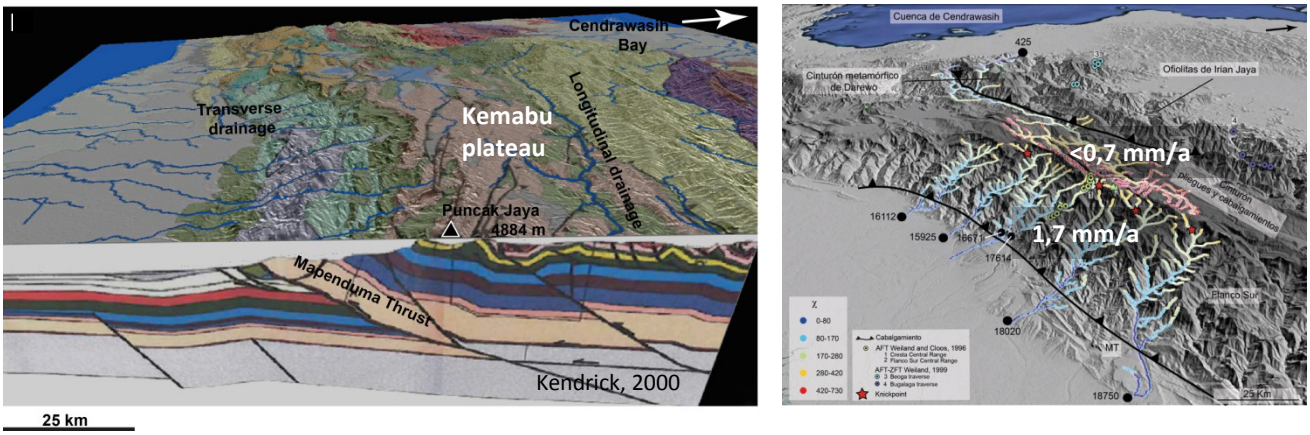


***Figure 10 :*** *(Gauche) Vue 3D vers l'Ouest du Central Range d'Irian Jaya (Papousie Nouvelle Guinée) qui correspond principalement à une ceinture de plis et chevauchements des sédiments de la marge passive australienne (Kendrick, 2000). Le flanc sud est drainé par des rivières transverses tandis que des rivières longitudinales erode le haut plateau de Kemabu. (Droite) Vue 3D des principales rivières et de leurs affluents qui drainent la ceinture de plis et chevauchement. Les couleurs indiques la valeur du paramètre $\chi$ qui indique un déséquilibre du réseau de drainage tel que l'ont démontré numériquement Willett et al. (2014). Les valeurs plus faibles du flanc sud indiquent une expansion des drains transverses vers le Nord que valident les vitesses d'érosion différentielles entre le plateau et le flanc sud.*

Les données de thermochronologie basse température disponibles dans la bibliographie suggèrent qu'il existe une érosion différentielle de l'ordre de 1 mm/a entre le flanc sud et le haut plateau. Cela valide l'interprétation géologique et se traduit par une expansion des bassins versants du flanc sud et une migration vers le Nord de la principale ligne de partage des eaux à une vitesse de ~1.7 mm/a et ce probablement depuis ~5 Ma (Pliocène). Cette réorganisation devrait avoir fortement influencé le remplissage du bassin d'avant pays situé au sud du Central Range. Ces travaux ont été réalisés dans le cadre de la thèse de M. Viaplana (2011-2014) que j'ai codirigé avec S. Dominguez (Univ. Montpellier2) et J. Van Den Driessche (Univ. Rennes1) dans le cadre d'un projet co-financé par le ministère espagnol des sciences et d'un projet que j'ai obtenu comme IP auprès de l'entreprise pétrolière Repsol (financement de thèse et financement de la recherche).

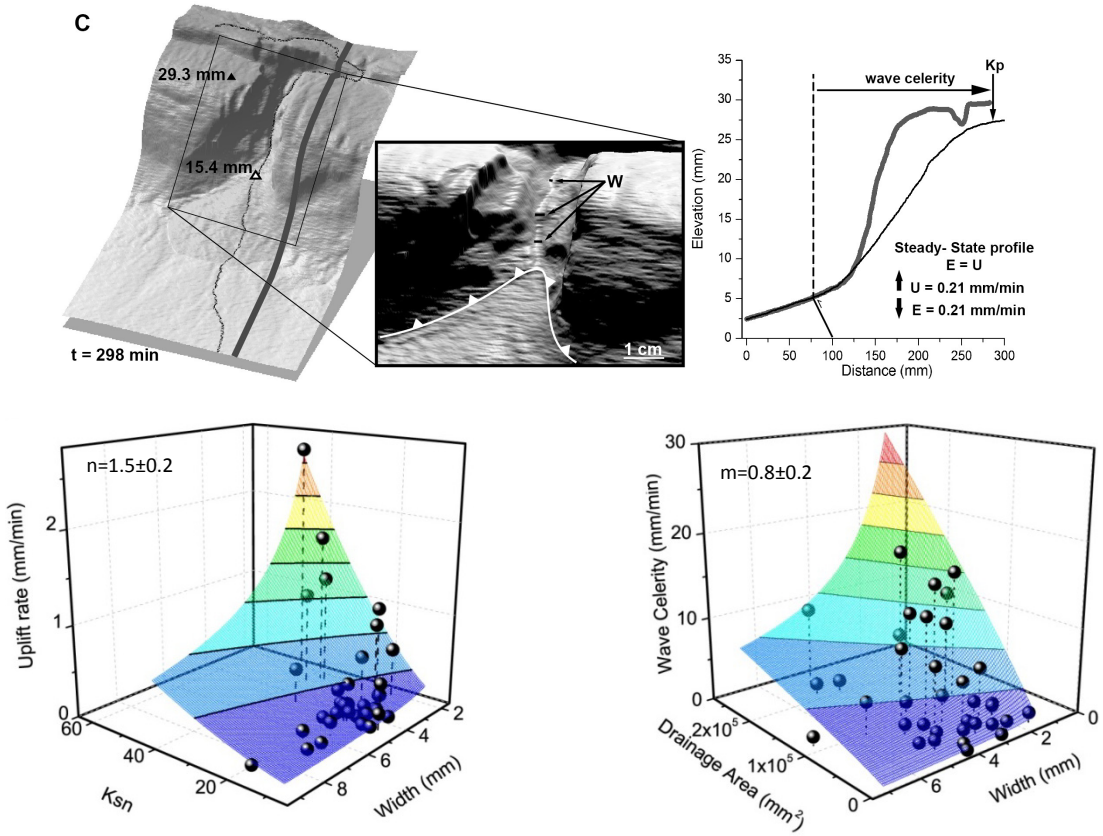


***Figure 11:*** *(Haut) Vue de détail 3D d'un chenal qui incise un chevauchement. Inséré en encadré un zoom du chenal et localisation des mesures de la largeur du chenal, W. La longueur du chenal dans cet encadré est 6 cm. Profil topographique de la crête et du chenal (les traces sont superposées sur la vue 3D) qui montre la localisation d'un knickpoint (Kp) qui s'est formé lorsque le chevauchement a commencé à émerger. (Bas) Calibration de la loi d'érosion dans les expériences à partir de la largeur et de la pente des chenaux et des vitesses de propagation des incisions dans les structures chevauchantes en soulèvement comme illustré ci-dessus* ***(Viaplana-Muzas, Babault et al., accepted)****.*

Toujours dans le cadre de la thèse de Marc Viaplana, nous avons étudié l'influence de la tectonique et de la pluviométrie sur la migration des lignes de partage des eaux dans des prismes d'accrétion expérimentaux. Une analyse détaillée des expériences nous a permis de montrer que les modèles expérimentaux ont des caractéristiques géométriques et cinématiques similaires à celles des rivières dans les chaines de montagnes. Les chenaux s'adaptent aux vitesses de soulèvement par une augmentation de leur pentes (*S*) et en réduisant leur largeur (*W)*, et les vitesses de propagation des incisions à l'intérieur des prismes sont proportionnelles à l'aire drainée (*A*) et inversement proportionnelles à la largeur des chenaux (Figure 11). Ces caractéristiques ont permis de proposer que la loi d'érosion qui gouverne les processus de surface dans les expériences est : $E = K\frac{A^{0.8\pm0.2}}{W}S^{1.5\pm0.2}$ **(Viaplana-Muzas, Babault et al., accepted).** Ce qui est très similaire à la loi d'érosion telle qu'elle est décrite dans la nature et justifie la comparaison entre les expériences et la nature même si un dimensionnement parfait des expériences est impossible.

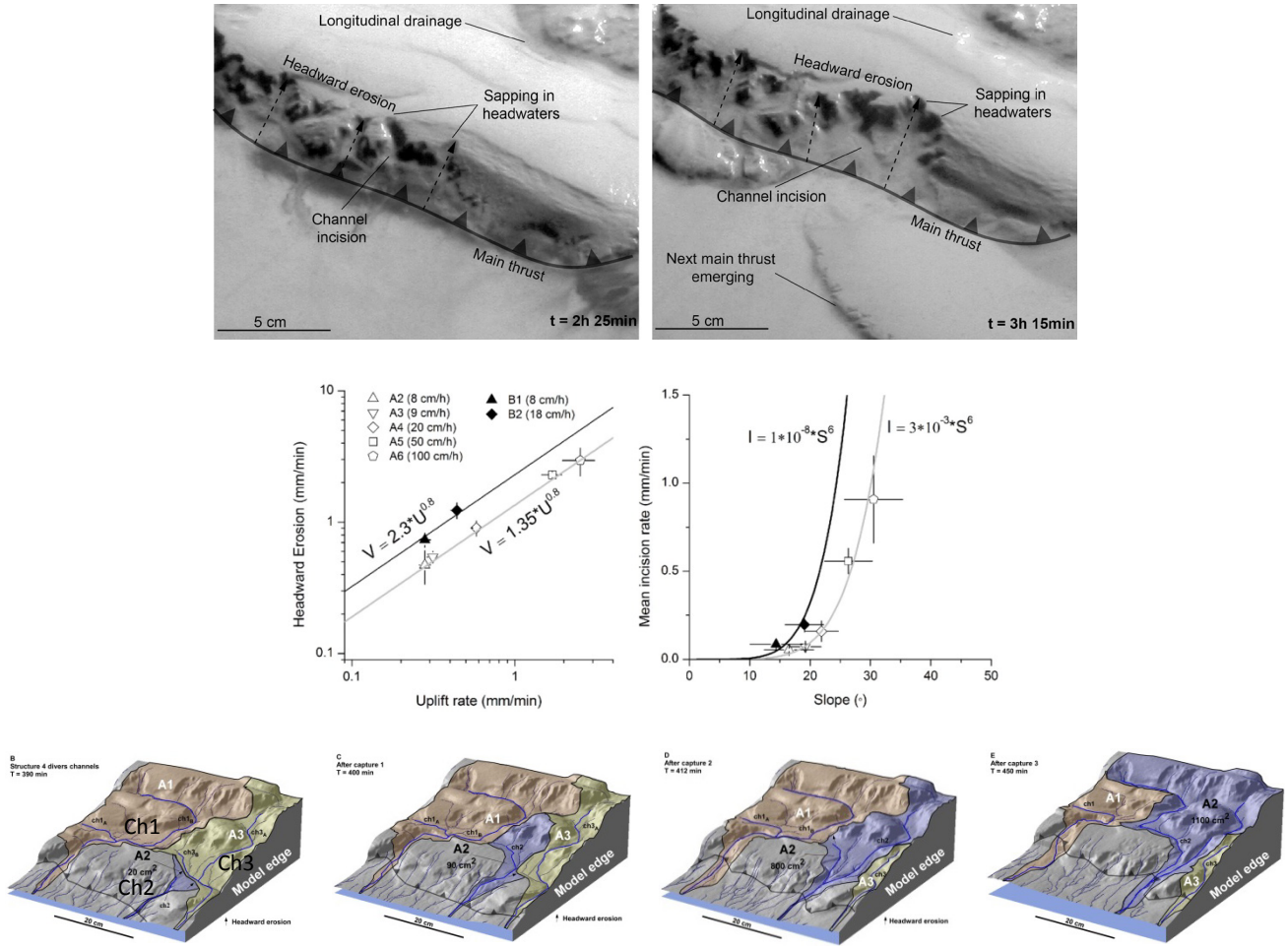


***Figure 12 :*** *(Haut) Photographies de détail de la partie extérieure d'un chevauchement. (Gauche) A t= 145 min on observe des têtes de réseau en forme d'amphithéâtre caractéristiques d'érosion par sapping qui affecte le premier millimètre d'érosion, le reste de l'érosion se fait par ruissellement. (Droite) 50 minutes plus tard, on observe que la topographie a été soulevée et que les têtes de réseau se sont propagées vers l'intérieur du prisme. (Milieu gauche) Vitesses moyennes de migration des têtes de réseau en fonction des vitesses de soulèvement. Les symboles en noir correspondent aux expériences ayant été soumise au double de pluviométrie par rapport aux expériences représentées par des symboles blancs. (Droite) Relation entre la vitesse d'incision moyenne des chenaux et leur pente pour les mêmes expériences. (Bas) Vue oblique des expériences montrant une structure chevauchante qui lors de sa formation a dévié les écoulements de surface et créé les chenaux longitudinaux $ch1_A$ et $ch3_B$ (parallèles à la trace du chevauchement). De gauche à droite, on observe les captures successives de ces chenaux longitudinaux par le chenal transverse $ch2_B$, qui s'est développé sur la structure émergente par érosion remontante* ***(Viaplana-Muzas, 2015)****.*

Au cours des expériences, l'incorporation des drains longitudinaux dans le prisme d'accrétion et l'augmentation de la pente dans la partie externe du prisme au cours de son élargissement permettent aux chenaux transverses d'inciser les parties frontales des structures chevauchantes et d'accroitre leur taille par érosion remontante (Figure 12 haut). Les expériences montrent que les vitesses de migration de la ligne de partage des eaux augmentent avec les vitesses de soulèvement de façon quasi-linéaire, à pluviométrie constante (Figure 12 milieu). On observe également que plus la pluviométrie est élevée plus la vitesse de migration de la ligne de partage des eaux est élevée. La relation entre vitesse de migrations des crêtes et vitesse de soulèvement reflète la corrélation positive qui existe entre la vitesse d'incision des chenaux transverses et leurs pentes, elles même contrôlées par la vitesse de soulèvement. Comme dans les cas naturels étudiés, l'érosion différentielle, entre les drains transverses qui incisent les parties externes des chevauchements et les portions longitudinales qu'ils transportent, aboutit à la capture des drains longitudinaux (Figure 12 bas), alors que les forçages externes (vitesse de raccourcissement et pluviométrie)

sont maintenus constants tout au long des expériences **(Viaplana-Muzas, 2015; Viaplana, Babault et al, en prep.)**.

### *Conclusion sur l'influence de la tectonique sur la dynamique du réseau de drainage*

Les cas naturels étudiés et les expériences montrent que la déformation précoce en plis et chevauchements de la couverture sédimentaire force les rivières à s'écouler parallèlement au grain structural avant d'être capturées par des drains transverses qui se propage depuis les bordures des zones en soulèvements, qu'il s'agisse de chaîne de montagnes formée par l'inversion d'un rift, comme c'est le cas du Haut Atlas et de la Cordillère Orientale de Colombie, ou qu'il s'agisse de chaînes de collision comme l'Himalaya et le Central Range. Ces études renforcent l'idée que l'évolution du réseau de drainage proposée pour le Haut Atlas correspond bien à un mécanisme intrinsèque à la construction d'une chaîne de montagnes. Comme corollaire, la réorganisation depuis un drainage longitudinal vers un drainage transverse dans une chaîne de montagnes est un indicateur du *surface uplift*. Enfin, la préservation de drainages précoces dans ces chaînes indique que la réorganisation du réseau est un processus lent qui opère sur une échelle de temps allant de la dizaine (cas du Central Range) à plusieurs dizaines de million d'années (cas du Haut Atlas et de la Cordillère Orientale de Colombie), ce que confirment les vitesses moyennes de migration de la ligne principale de partage des eaux, obtenus pour les derniers milliers d'années (méthode du $^{10}$Be), qui s'étendent sur des gammes allant de ~0.1 à ~1 mm/a. Comme le montrent les expériences, cette dynamique implique que les vitesses d'érosion obtenues sur des bassins versants appartenant à des chaînes dont le réseau de drainage est en cours de réorganisation sous estiment les vitesses de soulèvement (*rock uplift*).

## 3.2. Réorganisation du réseau de drainage en contexte stable

### *Dans une chaîne en relaxation : les Pyrénées*

Après m'être intéressé à la dynamique du réseau de drainage dans les chaînes actives, j'ai étudié sa dynamique dans les Pyrénées, une chaîne qui, d'après nos travaux récents (section 2.1.), peut être considérée comme une chaîne en relaxation. L'étude de la morphologie de ses flancs sud et nord le long de la ligne de partage des eaux montre que les bassins versants du flanc nord capturent ceux du flanc sud. Nous interprétons les grands cols de montagne comme d'anciennes vallées qui appartenaient au flanc sud. Dans le Val d'Aran, le Pla de Béret est un de ces cols qui culmine à 1900 m d'altitude et qui présente une forte asymétrie avec des pentes fortes face au flanc Nord. La présence de sédiments clastiques du Miocène supérieur dans le Val d'Aran indique que la Garonne a incisé de 1000 m récemment (post 11-7 Ma). Les profils longitudinaux de la Garonne et de ses affluents ainsi que la présence de sédiments clastiques miocènes dans le prolongement du Pla de Beret plaident en faveur d'une capture de la partie amont de la rivière Noguera Pallaresa, maintenant restreinte au Pla de Béret (Figure 13).

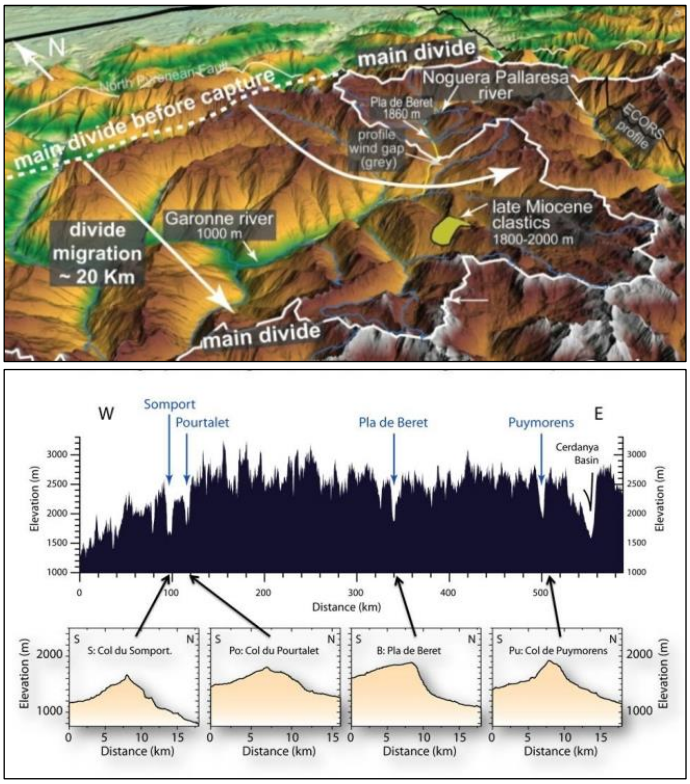


***Figure 13:*** *(Haut) Vue 3D du Val d'Aran (Pyrénées Centrales), la ligne de partage des eaux passe par le Pla de Béret à seulement 1900 m asl. (Bas) Profil topographique de la ligne de partage des eaux et profils longitudinaux des principaux cols.*

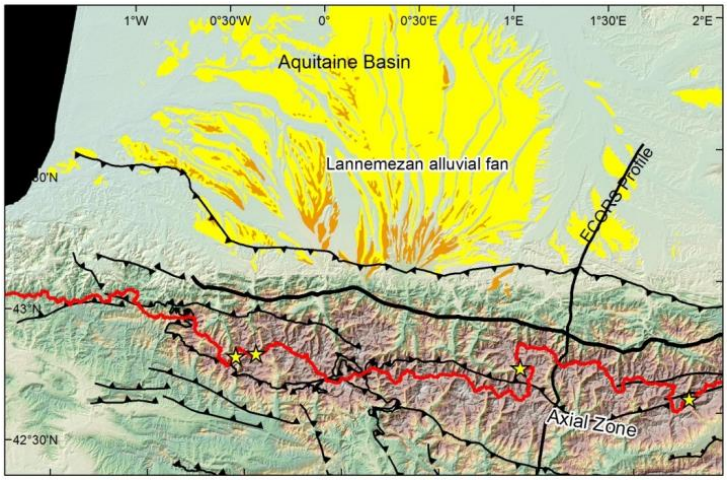


***Figure 14 :*** *Modèle numérique de terrain des Pyrénées. (Étoiles jaunes) Localisation des captures du réseau sud par le nord mises en évidence par l'analyse géomorphologique. (Ligne rouge) Position de la ligne de partage des eaux entre les flancs Nord et Sud. Les formations géologiques à l'affleurement du cône de Lannemezan sont également représentées en Jaune (Miocène supérieur) et en orange (pliocène).*

L'augmentation des aires drainées et des flux sédimentaires des grandes rivières du flanc nord pyrénéen à la fin du Cénozoïque est corroborée par l'histoire sédimentaire du cône de Lannemezan daté de la fin du Miocène et du Pliocène (Figure 14). Même s'il est difficile d'écarter une possible asymétrie dans les précipitations au cours des derniers millions d'années, la pente régionale, plus forte sur le flanc nord et héritée de la construction de la chaîne, apparaît être le principal facteur à l'origine de cette réorganisation du réseau de drainage. L'action des glaciers peut avoir favorisé cette évolution, par débordement là où les crêtes ont été partiellement érodées par érosion remontante lors des interglaciaires **(Babault et al. en**

**prep.)**. J'ai réalisé ce travail (2010-2011) comme professeur Lecteur à l'Universitat Autonoma de Barcelona (UAB) en collaboration avec J. Van Den Driessche (Rennes) dans le cadre d'un projet financé par le ministère espagnol des sciences et l'ANR Pyrénées (Pyramid).

### *Dans le Bassin d'Ouarzazate*

Au cours de mon post-doctorat à l'Université Autonome de Barcelona (UAB), et en collaboration avec A. Teixell (UAB), M.L. Arboleya (UAB) et L. Owen (Univ. Cincinnati, US) nous avons étudié la dynamique de l'érosion dans le bassin d'Ouarzazate, dans le cadre d'un projet financé par le ministère espagnol des sciences (2006-2008). Nous avions proposé que l'histoire de l'incision et de la sédimentation quaternaire dans le bassin de Ouarzazate (Maroc) avait été fortement modulé par le climat à l'échelle des périodes glaciaires–interglaciaires. Les âges d'abandon des cônes alluviaux et des terrasses fluviatiles obtenus par la méthode des nucléides cosmogéniques terrestres ($^{10}$Be) correspondent aux quatre derniers épisodes glaciaires (Figure 15). Les vitesses d'incision moyennes obtenues sont de l'ordre de 0.3 à 1.0 mm.a$^{-1}$ **(Arboleya, Babault et al., 2008)**.

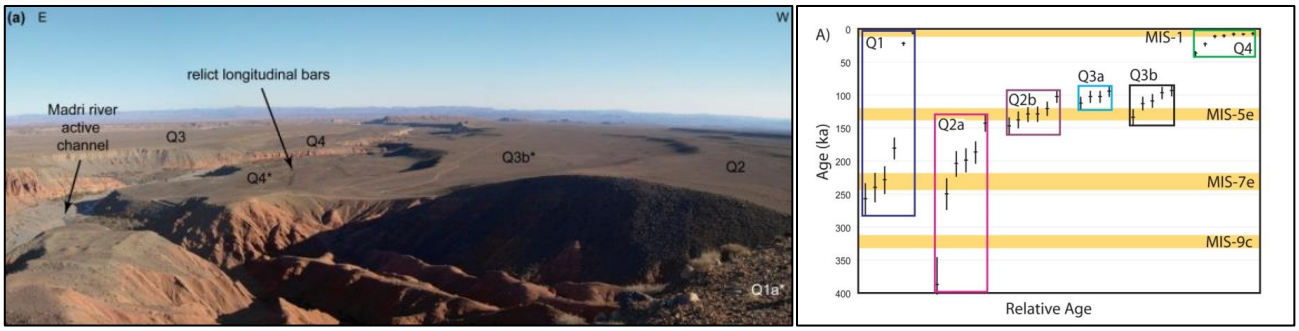


***Figure 15:*** *Séquence d'incision sur la rivière Madri (Bassin de Ouarzazate, Maroc) et âges d'abandon des glacis de sédimentation obtenu par la méthode des nucléides cosmogéniques terrestres ($^{10}$Be)* ***(Arboleya, Babault et al., 2008)***.

Dans le cadre de la thèse d'Alvar Pastor, nous avons mis en évidence la présence de captures systématiques au cours des dernières centaines de milliers d'années dans le bassin d'Ouarzazate. Les pentes des grandes rivières qui naissent dans le Haut Atlas sont supérieures à celles de leurs affluents qui naissent dans le bassin. La différence de pente est nécessaire au transport de la charge de fond plus importante et de plus grande granulométrie issue du Haut Atlas (« cover effect »). Par contre, les rivières naissant dans le bassin et qui ont une aire drainée plus petite incisent davantage, et avec des pentes plus faibles, le substratum facilement érodable. Sur les versants de ces affluents, des pédiments se forment par érosion remontante et capturent finalement les grandes rivières issues du Haut Atlas (Figure 16). Le « cover effect » est responsable de la réorganisation du réseau de drainage par capture dans le bassin d'Ouarzazate. Lorsqu'une capture a lieu, les faibles pentes des pédiments forcent le dépôt de la charge de fond et la formation d'un nouveau glacis de sédimentation. L'agencement des dépôts quaternaires indique que ce processus a modulé la réponse érosive aux changements climatiques quaternaires **(Pastor, Babault et al., 2012)**. Ce travail nous a permis de revoir l'interprétation que nous avions faite quelques années auparavant, et qui considérait que les terrasses dans le bassin d'Ouarzazate avaient toutes une origine climatique.

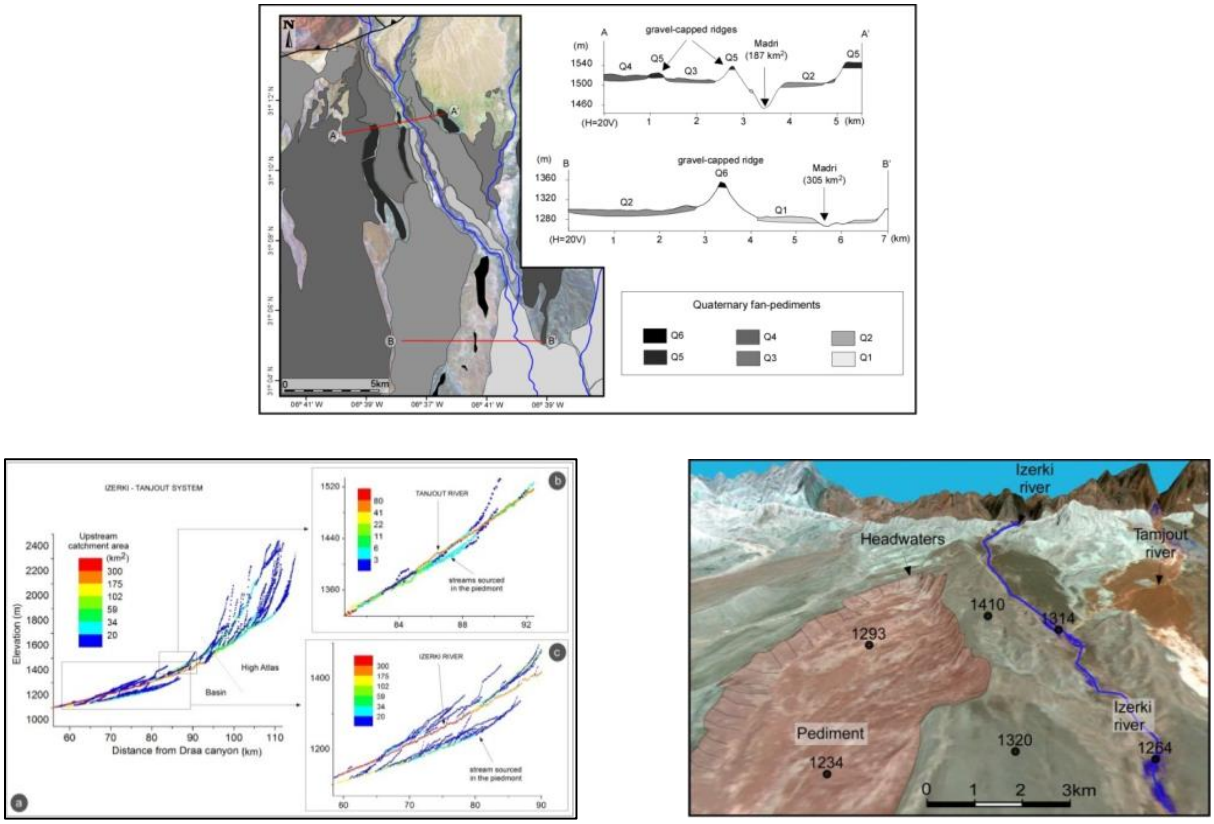


***Figure 16:*** *(Haut) Exemple de distribution des glacis de sédimentation dans le bassin d'Ouarzazate (Maroc). Les glacis Q2, Q3 et Q4 sont séparés par des crêtes qui correspondent elle-même à d'ancien glacis de sédimentation. L'érosion latérale ne peut expliquer la disposition des dépôts quaternaires et implique que des évènements de captures aient eu lieu. (Bas) Profil longitudinal et vue 3D de la rivière Izerki qui prend sa source dans le Haut Atlas. L'Izerki est bordé à l'ouest par un de ses affluents qui naît dans le bassin d'Ouarzazate et qui a une aire drainée d'un ordre de grandeur plus petite. Cet affluent a cependant incisé davantage (30 m) le substratum facilement érodable du bassin. Sur les versants de cet affluent, un pédiment est en cours de formation par érosion remontante* ***(Pastor, Babault et al., 2012)****.*

## 4. Influence de la tectonique sur le réseau de drainage et la distribution des flux sédimentaires : l'approche *source-to-sink*

Comprendre les processus qui contrôlent les flux de sédiments qui alimentent les bassins sédimentaires et donc la qualité des réservoirs intéresse directement l'industrie pétrolière. Cette thématique m'a permis d'obtenir un financement (100 k€) de recherche et de thèse auprès de l'entreprise pétrolière Repsol à Madrid (Espagne) pour étudier l'influence de la tectonique et de la dynamique de l'érosion et des rivières sur les flux sédimentaires dans un système *source-to-sink*. Dans le cadre de la thèse de M. Viaplana, nous avons exploré quelle était l'influence de la tectonique sur l'organisation des réseaux, et en conséquence sur la distribution des corps sédimentaires au front des prismes d'accrétion expérimentaux, réalisés à Géosciences Montpellier. En réponse à une réorganisation du réseau de drainage dans les zones sources, telles qu'elles existent dans les chaines que j'ai étudié (section 3.1.), on doit s'attendre à une modification du flux de sédiments qui alimentent un bassin sédimentaire. Nous avons montré, grâce aux modèles expérimentaux, quelle était l'influence de la dynamique intrinsèque du réseau de drainage telle sur les flux sédimentaires. Nous nous sommes également intéressés au système naturel Central Range-baie de Cendrawasih, où Repsol a des intérêts pétroliers. Par une approche géomorphologique couplée à l'étude des structures tectoniques et du remplissage de la baie de Cendrawasih, nous avons apporté des données nouvelles sur ce système

*source-to-sink* où l'exploration pétrolière et les études de terrains en sont encore à leur début du fait de la difficulté d'accès dans cette région très escarpée, la plus humide de la planète et qui est recouverte d'une épaisse couverture végétale (et qui plus est, instable politiquement).

## 4.1. Approche expérimentale

Les expériences confirment l'idée que les chenaux au front des prismes d'accrétions sont déviés par les chevauchements qui émergent dans leur partie frontale si leur flux d'eau est inférieur à un débit minimum nécessaire pour inciser les écailles chevauchantes. Ainsi, dans les ceintures de plis et chevauchements, la compétition entre le débit des rivières et le soulèvement tectonique contrôle les variations latérales des flux de sédiments qui alimentent les bassins sédimentaires, par un contrôle de l'organisation du réseau de drainage. A vitesses de soulèvement (raccourcissement) lentes, le réseau de drainage est dominé par des chenaux transverses et par une grande quantité de cônes coalescents dans la partie externe du prisme (Figure 17A et 17C). A vitesses de soulèvement (raccourcissement) rapides, le réseau de drainage est dominé par des chenaux longitudinaux et en faible proportion par des chenaux transverses qui alimentent en produits d'érosion de grands cônes sédimentaires séparés par des zones à faible sédimentation (Figure 17B et 17D) **(Viaplana, Babault et al., accepted)**.

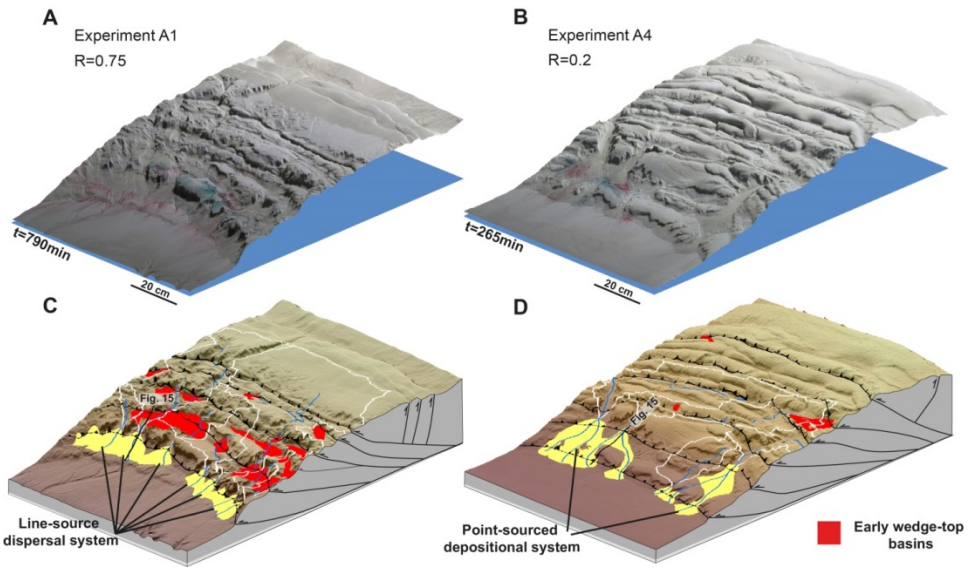


***Figure 17:*** *Vues 3D des expériences. À gauche une expérience à vitesse de raccourcissement lente (4 cm/h), à droite rapide (20 cm/h)* ***(Viaplana, Babault et al., accepted)****.*

Les variations des flux sédimentaires dans les bassins sont classiquement interprétées comme la marque de variations de l'activité tectonique, qui modifie les pentes et donc l'érosion dans les zones sources, ou bien comme une conséquence des variations climatiques qui modulent l'activité érosive des rivières. Après avoir montré, dans le cadre de la thèse de Marc Viaplana, que l'augmentation de la pente des prismes expérimentaux au cours de leur élargissement permet aux chenaux transverses de capturer les portions amont des drains longitudinaux (cf. section 3.1.) (Figures 12 et 18), nous montrons que la dynamique intrinsèque du réseau de drainage, par migration des lignes de partage de eaux et par captures, modifie la localisation des cônes sédimentaires et des flux (Figure 19) alors que les forçages externes, vitesse de raccourcissement et pluviométrie, sont maintenus constants tout au long des expériences **(Viaplana, Babault et al, en prep., Viaplana-Muzas, 2015)**. On voit sur la figure 19, qu'après la première capture qui a

lieu entre t2 et t3 (Figure 18), le flux de sédiments dans le cône de sédimentation F2 augmente considérablement au débouché du canal ch2 qui capture les parties amonts, d'abord du canal ch3, et par la suite du canal ch1 (cf. figure 12). Quant aux flux de sédiments aux débouchés des chenaux ch1 (F1) et ch3 (F3) privés progressivement de leurs aires amonts, ils diminuent dans le même temps (Figure 19).

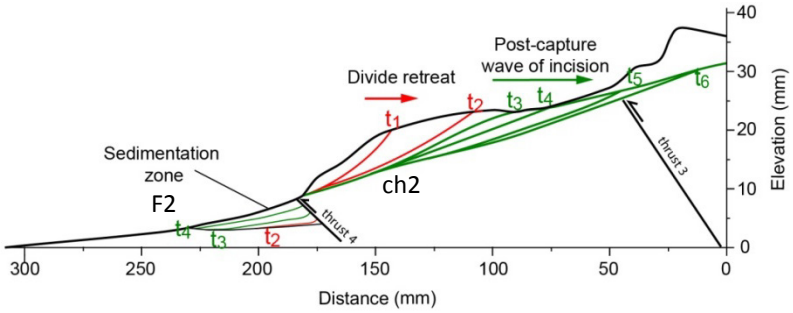


***Figura 18 :*** *Evolution du profil longitudinal du canal (ch2) qui a capturé la partie amont des chenaux ch1 et ch3 (en rouge, avant la première capture, et en vert après) et séquence de remplissage au débouché du ch2 dans le cône de sédimentation F2 (Viaplana-Muzas, 2015).*

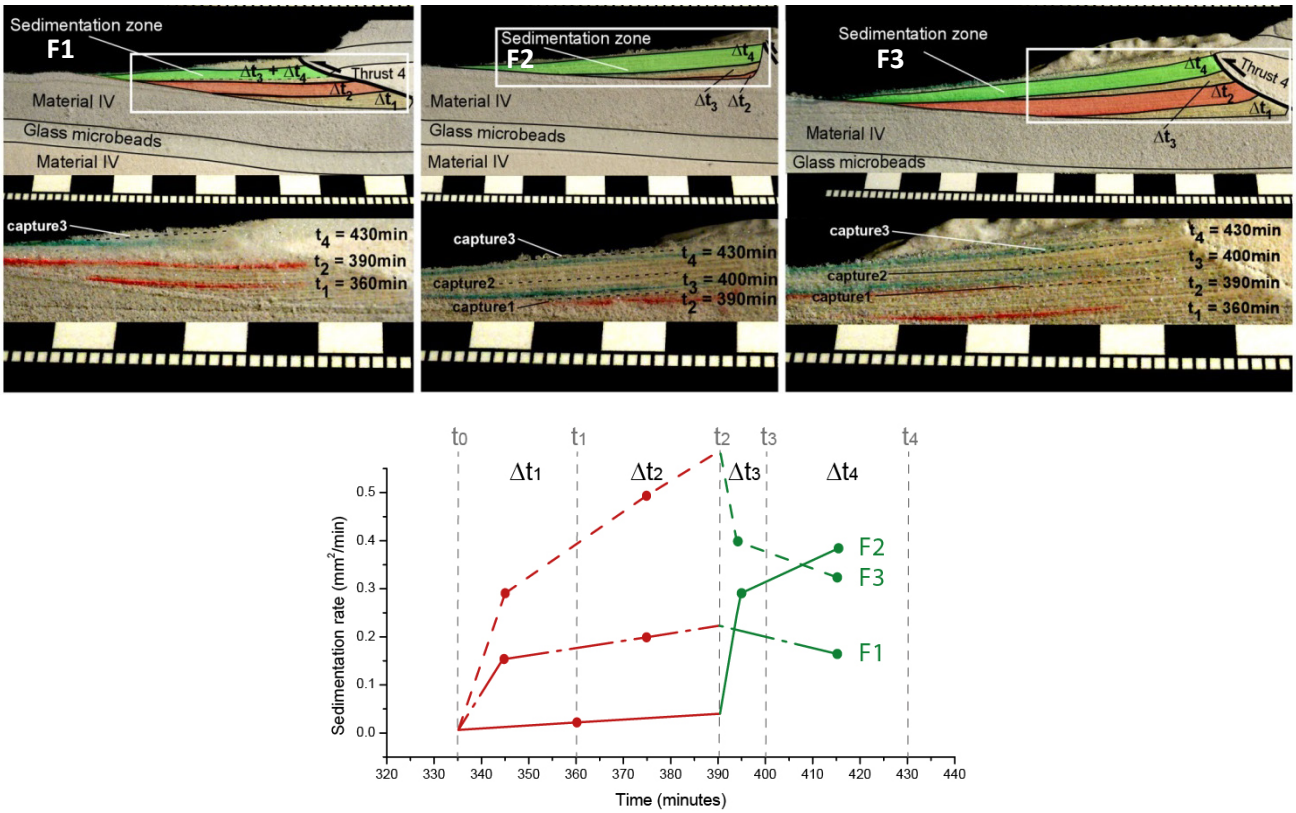


***Figure 19 :*** *(Haut) En réponse à l'augmentation de l'aire drainée par capture, l'enregistrement sédimentaire se traduit par une augmentation de la vitesse de sédimentation à l'embouchure du chenal 2 (surface B colorée en vert du cône F2). Par contre, au même moment à l'embouchure du chenal 3 (cône F3) la perte d'aire drainée se traduit par une diminution de la vitesse de sédimentation (surface B colorée en vert du cône F3). (Bas) Evolution des vitesses de sédimentation moyenne des cônes de sédimentation F1, F2 y F3 pendant les intervalles de temps marqués par les couches de couleur (en rouge avant les évènements de captures et vert après) (Viaplana-Muzas, 2015).*

## 4.2. Le système Central Range – baie de Cendrawasih (Papouasie-Nouvelle Guinée)

Toujours dans le cadre de la thèse de Marc Viaplana, nous avons réalisé un bilan des volumes érodés et sédimentés dans la partie Nord-Ouest de la Papouasie-Nouvelle Guinée en nous basant sur données de thermochronologie présentes dans la littérature et par une nouvelle interprétation des lignes sismiques. Cela nous a permis en retour de calculer la proportion des volumes de sédiments apportés par les différents bassins versant qui ont alimenté la baie de Cendrawasih ainsi que des différentes lithologies érodées depuis les premiers stades de développement de la chaîne au cours des derniers 12 Ma. La réorganisation du réseau de drainage dans le Central Range (section 3.1.) devrait avoir fortement influencé le remplissage du bassin d'avant pays situé au sud du Central Range. Nous montrons cependant que la dynamique intrinsèque du réseau n'a quant à elle pas influencé significativement la nature du remplissage sédimentaire de la baie de Cendrawasih, principalement contrôlé par les vitesses d'exhumation très rapides (1-6 mm/a) dans la ceinture métamorphique de Derewo (en jaune et rouge dans la figure 20). Cette approche qui nous a permis de prédire la composition des flux de sédiments détritiques et leur distribution dans le bassin sédimentaire de la baie de Cendrawasih ce qui permettra à l'entreprise Repsol d'améliorer la prédiction de la qualité du réservoir, et indirectement la gestion des risques liés à l'exploration pétrolière. Nous estimons que les sédiments silicoclastiques sont principalement composé de métapelites (~50%) qui contiennent des schistes sériciteux (phyllites) graphitiques (potentielles sources en matière organique), de diorites (~25%), de grès (~10%) et de calcaires (~10%) **(Babault et al, en prep., Viaplana-Muzas, 2015)**.

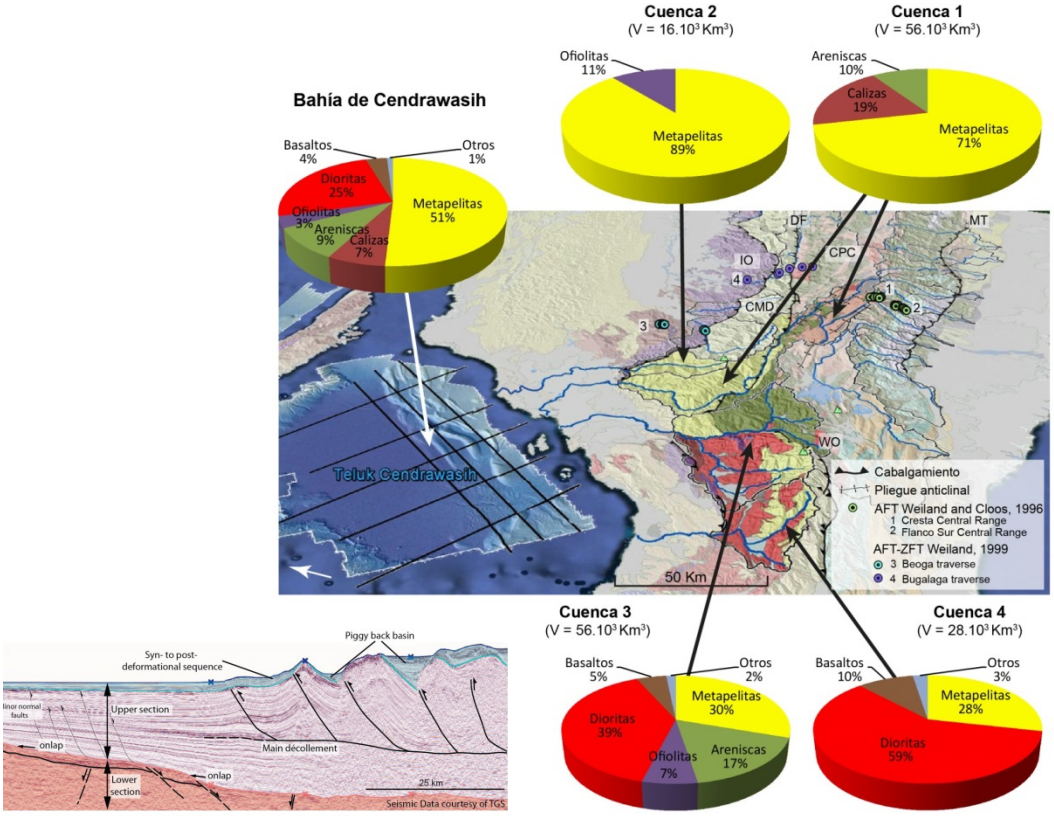


***Figure 20 :*** *(Gauche) Vue 3D vers l'Ouest du Central Range d'Irian Jaya qui correspond principalement à une ceinture de plis et chevauchements des sédiments de la marge passive australienne. (Haut) Schéma du différentiel d'érosion entre le flanc sud et le haut plateau composé des New Guinea Limestones (en rose). (Droite) Vue 3D vers l'Est de la partie Occidentale du Central Range et de la baie de Cendrawasih. Les quatre principaux bassins versants qui ont alimenté la baie de Cendrawasih et le réseau de drainage sont superposés à la carte géologique. Les diagrammes circulaires représentent la proportion des lithologies érodées par bassin versant et qui ont alimentées la baie de Cendrawasih* ***(Babault et al, en prep.)***.

# 5. Projet de recherche

## 5.1. Objectifs

Dans la droite ligne des recherches qui m'ont animé jusqu'ici, je souhaite continuer à m'intéresser à la dynamique de l'érosion et des réseaux de drainage dans chaînes de montagnes comme marqueurs de la déformation et en particulier des mouvements verticaux. Cette approche permet d'apporter des contraintes sur le mode de déformation des prismes orogéniques, et indirectement d'apporter des contraintes sur la rhéologie de la lithosphère. Je souhaite également continuer à m'intéresser à l'influence des interactions entre déformation et érosion sur le remplissage des bassins sédimentaires.

Le rôle fondamental des réseaux hydrographiques dans le façonnement des formes du relief terrestre, à commencer par celui des chaînes de montagnes, n'est plus à démontrer. Il est clair aujourd'hui que les rivières sont sensibles aux variables climatiques et tectoniques en termes de pente et de flux d'eau. Ce sont les rivières qui redistribuent les masses et définissent les conditions aux limites des versants. Les signaux tectoniques et climatiques sont en conséquence filtrés par le réseau fluviatile avant d'être transmis à l'ensemble de la topographie. Ceci signifie que la topographie est un enregistreur de l'activité de ces deux moteurs et peut donc être utilisée comme tel. Je suis persuadé qu'une analyse morphologique toujours plus sophistiquée permet une telle démarche, d'autant plus si elle est calibrée par des données géologiques (vitesses d'érosion, de déplacements verticaux et horizontaux) et si elle est couplée à la modélisation. Ceci demande à identifier (i) quels éléments du paysage sont les plus sensibles aux changements des conditions aux limites imposées par la tectonique, (ii) sur quelles échelles de temps les formes du relief terrestre répondent aux changements des conditions aux limites imposées par la tectonique et le climat, (iii) quelles sont les paramètres morphométriques qui enregistrent les signaux (climatiques et tectoniques) avec la plus grande acuité. Les études récentes sur les couplages entre déformation, érosion et climat dans les chaînes actives, ainsi que les derniers développements théoriques sur les lois qui gouvernent l'érosion continentale, suggèrent que l'enregistrement dans la topographie du signal tectonique domine sur le signal climatique qui apparaît comme un facteur de second ordre (e.g., Godard et al., 2014). En première approximation on peut par conséquent utiliser la topographie comme un enregistreur du forçage tectonique qu'il soit d'origine crustale ou mantellique. Ces résultats rejoignent ceux que j'ai obtenus par l'étude de la dynamique du réseau de drainage dans les chaînes actives qui montrent que la pente régionale est le facteur de contrôle principal dans les chaînes que j'ai étudié (l'Atlas, la Cordillère Orientale de Colombie, le Central Range de Papouasie Nouvelle Guinée et l'Himalaya) et dans les modèles expérimentaux.

Mes recherches actuelles visent à approfondir cette démarche en particulier en quantifiant les vitesses d'érosion et de soulèvement sur des périodes allant de plusieurs centaines de milliers d'années à plusieurs dizaines de millions d'années et couvrant trois états dynamiques des chaines de montagnes : en croissance, à l'équilibre dynamique et en relaxation. Plus concrètement, j'ai listé ci-dessous quatre activités (Terrain et Modélisation) supportées par une thèse en cours afin de mener à bien ce projet.

## 5.2. Quantification de la remontée du niveau de base sur le versant nord des Pyrénées et quantification de la migration de la ligne de partage des eaux

L'objectif de la thèse de Gemma V. Bosch, commencée en octobre 2013, est de résoudre le problème d'un hypothétique soulèvement récent dans les Pyrénées. Comme je l'ai présenté dans la section 2.1., elle confronte les données de surface et la structure profonde de la chaîne à partir de l'analyse de données morphologiques, géologiques et géophysiques. Elle réalise également une cartographie détaillée automatisée des surfaces d'érosion à haute altitude des Pyrénées et elle étudie le degré de corrélation entre leur altitude et la profondeur du Moho. Par ailleurs, les résultats de mes travaux sur l'évolution géomorphologique du réseau de drainage dans les Pyrénées montrent que la ligne de partage des eaux migre du nord au sud (Figure 13). Des données géologiques dans la partie centrale indiquent que cette migration est récente et qu'elle s'est amorcée depuis 7-11 Ma (Miocène supérieur).

Un objectif commun à ces deux problématiques, et qui devrait conforter mes travaux antérieurs, est d'obtenir de nouvelles données AHe dans les Pyrénées (flanc nord) et de modéliser les chemins de refroidissement (AHe et $^{4}He/^{3}He$ sur apatite) en collaboration avec P. Monié et Ph. Münch (Géosciences Montpellier), et Dani Stockli (Austin, USA). Il s'agit en particulier de quantifier le degré d'enfouissement du flanc nord au cours du Miocène qui comme sur le versant sud indiquerait une remontée du niveau de base et expliquerait la formation en altitude de surfaces d'érosion à faible relief. D'autre part, la modélisation des chemins de refroidissement des données d'He sur apatite permet de mettre en évidence la propagation d'incisions dans un réseau (e.g., Shuster et al., 2011). Les données de thermochronologie basse température permettront de quantifier la dynamique du réseau de drainage. Une comparaison entre les flux d'érosion et les flux sédimentaires dans le cône de Lannemezan s'imposera alors. Ce projet est financé par l'ANR Pyrénées (Pyramid) et par le chantier RGF Pyrénées du BRGM.

## 5.3. Le réseau de drainage dans la partie Est de l'Himalaya (Bhoutan), un marqueur passif de la déformation et un réseau dynamique

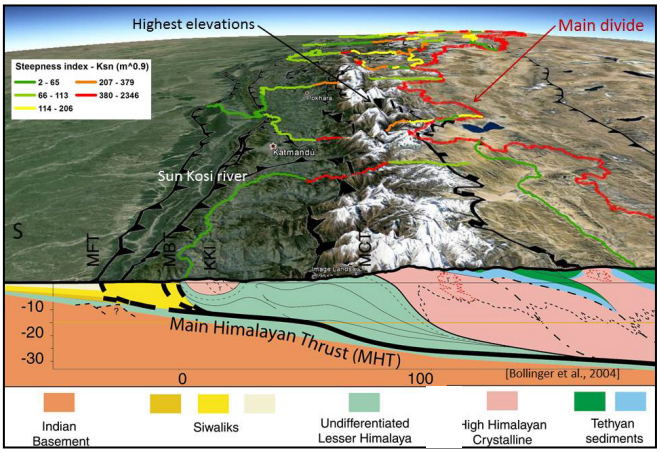


***Figure 21 :*** *Vue vers l'Ouest de la partie centrale de l'Himalaya. La ligne rouge correspond à la principale ligne de partage des eaux entre les rivières s'écoulant sur le flanc sud et les bassins versants de l'Indus et du Tsang Po s'écoulant sur le plateau tibétain avant de changer de direction au niveau des syntaxes Himalayennes. Le code de couleur représente les indices de pentes des principales rivières transverses. Les plus fortes pentes des rivières correspondent en profondeur a l'épaississement par un système de duplex situé en milieu de croûte (Bollinger et al., 2004).*

Contrairement à la plupart des chaînes actives et aux modèles couplant soulèvement et processus de surface, la ligne de partage des eaux principale dans l'Himalaya ne correspond pas aux zones internes les plus hautes, i.e. le Haute Himalaya, mais est décalée plus ou moins loin vers le nord où elle suit un parcours très sinueux (Figure 21). Il a été proposé que les rivières himalayennes avec leurs pentes plus fortes et leur plus courte distance au niveau de base (le bassin d'avant-pays du Ganges), recevant plus de précipitation, érodent plus vite que les affluents de l'Indus et du Tsangpo qui s'écoulent vers le nord sur le plateau tibétain. La migration de la ligne de partage des eaux vers le nord, par érosion remontante des rivières transhimalayennes, a été invoquée comme le processus responsable de sa localisation actuelle au-delà des hauts sommets himalayens (Brookfield, 1998; Hayden, 1907; Heron, 1922; Robl et al., 2008). Une alternative à ce modèle interprète la non coïncidence entre les hauts sommets et la ligne de partage des eaux comme une évidence de l'existence de grands drains transverses antérieure au soulèvement du Haut Himalaya (Gansser, 1964; Montgomery and Stolar, 2006; Oberlander, 1985; Seeber and Gornitz, 1983; Wager, 1937). Ce dernier modèle est en accord avec les fortes pentes des rivières transverses (ex : Sun Kosi, $K_{sn}$ > 380, figure 21) (e.g., Lavé and Avouac, 2001; Seeber and Gornitz, 1983; Wobus et al., 2003), localisées à l'aplomb d'un système de duplex à l'origine de l'épaississement de la croûte moyenne dans tout l'Himalaya (e.g., Adams et al., 2013; DeCelles et al., 2001; Molnar, 1984; Schelling and Arita, 1991; Webb et al., 2011; Yin et al., 2010).

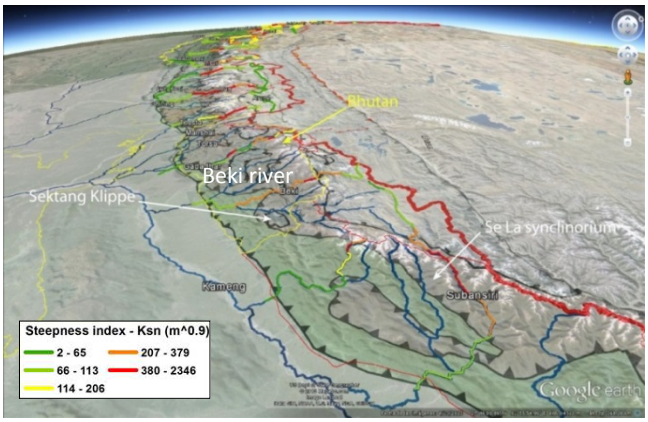


***Figure 22 :*** *Dans la partie Est de l'Himalaya, au Bhoutan, la principale ligne de partage des eaux se situe à plus de 20 km au nord des hauts sommets himalayens et du « South Tibetan Fault system ». On observe également des indices de pente non seulement élevés dans le Haut Himalaya cristallin (gneiss) mais également sur les séries téthysiennes au nord du « South Tibetan Fault system ».*

Les premiers résultats que nous avons obtenus montrent que dans la partie nord-ouest de l'Himalaya, la ligne de partage des eaux qui sépare un drain longitudinal d'un drain transverse (Figure 9), migre vers le nord (Babault et al., en prep.). Nous montrons en particulier que la rivière Chenab sera très probablement capturée par la rivière Beas au cours des prochains 4±2 Ma, aboutissant à la création d'une rivière transhimalayenne. Contrairement aux rivières népalaises comme le Sun Kosi (Figure 21), la rivière Beki (Figure 22) montre de très fortes pente non seulement à l'aplomb des duplex situés là où affleurent les séries cristallines du Haut Himalaya, mais également en amont, sur la bordure sud des séries téthysiennes. En l'absence de structure tectonique profonde pouvant rendre compte d'un soulèvement de la bordure sud du Tibet, ces fortes pentes pourraient être la preuve d'une érosion régressive de la bordure sud du plateau tibétain et de la migration vers le nord de la principale ligne de partage des eaux. Je tenterai de mettre en évidence l'érosion régressive de la rivière Beki par les méthodes de thermochronologie basse et très basse température (AHe et $^{4}He/^{3}He$ sur apatite) en collaboration avec P. Monié et Ph. Münch (Géosciences Montpellier), et Dani Stockli (Austin, USA). Dans l'hypothèse où le réseau est en cours de réorganisation,

celle-ci doit s'accompagner de la migration des lignes de partage des eaux. Il s'agit en conséquence de mettre en évidence des potentiels déséquilibres du réseau de drainage en utilisant le paramètre $\chi$ (e.g., Willett et al., 2014) et de quantifier la vitesse de migration de la ligne de partage des eaux en cartographiant les vitesses d'érosion différentielles entre bassins versants. Pour cela deux méthodes sont possibles, la première consiste à calibrer les paramètres morphologiques les plus sensibles aux soulèvements et à l'érosion ($M_\chi$ et $k_{sn}$) par des données ponctuelles de vitesses d'érosion (AHe, AFT, ZrHe, et leur modélisation dans Pecube), la seconde à quantifier les vitesses d'érosion à l'échelle des bassins versants ($^{10}$Be sur sables de rivières). L'acquisition de vitesses d'érosion par les méthodes de thermochronologie basse température et des cosmonucléides permettront de déterminer des vitesses d'érosion pour des périodes allant de quelques Ma à quelques ka respectivement.

Par ailleurs, la structure profonde au Bhoutan est mal connue et une des questions est de savoir quel est le degré de similitude entre la structure profonde dans la partie oriental de l'Himalaya et dans sa partie centrale, au Népal (Figure 21). Des études récentes ont mis en évidence une variation latérale de la rigidité flexurale de la plaque indienne entre le Népal et le Bhoutan (Berthet et al., 2013; Hammer et al., 2013). On peut se poser la question de savoir quelles sont les rétroactions entre l'évolution de la rhéologie de la plaque indienne lors de son enfoncement sous l'Himalaya, le style de déformation dans la chaîne et la dynamique de l'érosion en surface. En ce sens, il existe potentiellement une relation entre rhéologie, style de déformation et le degré d'érosion régressive de la bordure sud du Plateau du Tibet. L'intérêt d'aborder en premier la dynamique du réseau de drainage dans une étude géomorphologique c'est de pouvoir connaître la part dans les vitesses d'érosion attribuable aux processus intrinsèques au système géomorphologique (érosion différentielle entre bassins versants). Cette démarche permet par la suite une quantification fiable des vitesses d'érosion liées aux processus externes (tectonique). Les cartes de vitesses d'érosion doivent permettre de confirmer les variations latérales de la structure profonde de l'Himalaya. Une source potentielle de financement pourrait être le projet **ANR-2013** dont est responsable R. Cattin (Géosciences Montpellier).

## 5.4. Topographie dynamique et Deformations crustales dans le Rif et l'Atlas

Dans les parties ouest et est du Rif, des travaux récents ont montré l'existence de soulèvements récents associés à des déformations extensives qui affectent la bordure sud de la mer d'Alboran (Poujol et al., 2014; Romagny et al., 2014). Dans les montagnes de l'Atlas et les plateaux marocains (Figure 23), située au sud des Chaînes du Rif et du Tell, un soulèvement de la topographie (jusqu'à 1000 m de *surface uplift*) de grande longueur d'onde a été mis en évidence (e.g., Babault et al., 2008; Missenard et al., 2006; Teixell et al., 2003). Ce soulèvement s'explique par un amincissement de la lithosphère mantellique dont l'origine est encore débattue (e.g., Sun et al., 2014). Nous avons montré que ce *surface uplift* de grande longueur d'onde a eu lieu au cours des derniers 5-7 Ma (Figure 4), ce qui implique une vitesse moyenne de soulèvement de la topographie de l'ordre de 0.2 mm/a **(Babault et al., 2008; Pastor, Babault et al., 2015)**. Dans la chaîne des Bétiques un soulèvement Plio-Quaternaire grande longueur d'onde a également été mis en évidences (Braga et al., 2003) et attribué au déchirement d'un morceau de lithosphère océanique au cours de son retrait vers l'Ouest (Figure 23) (Garcia-Castellanos and Villasenor, 2011).

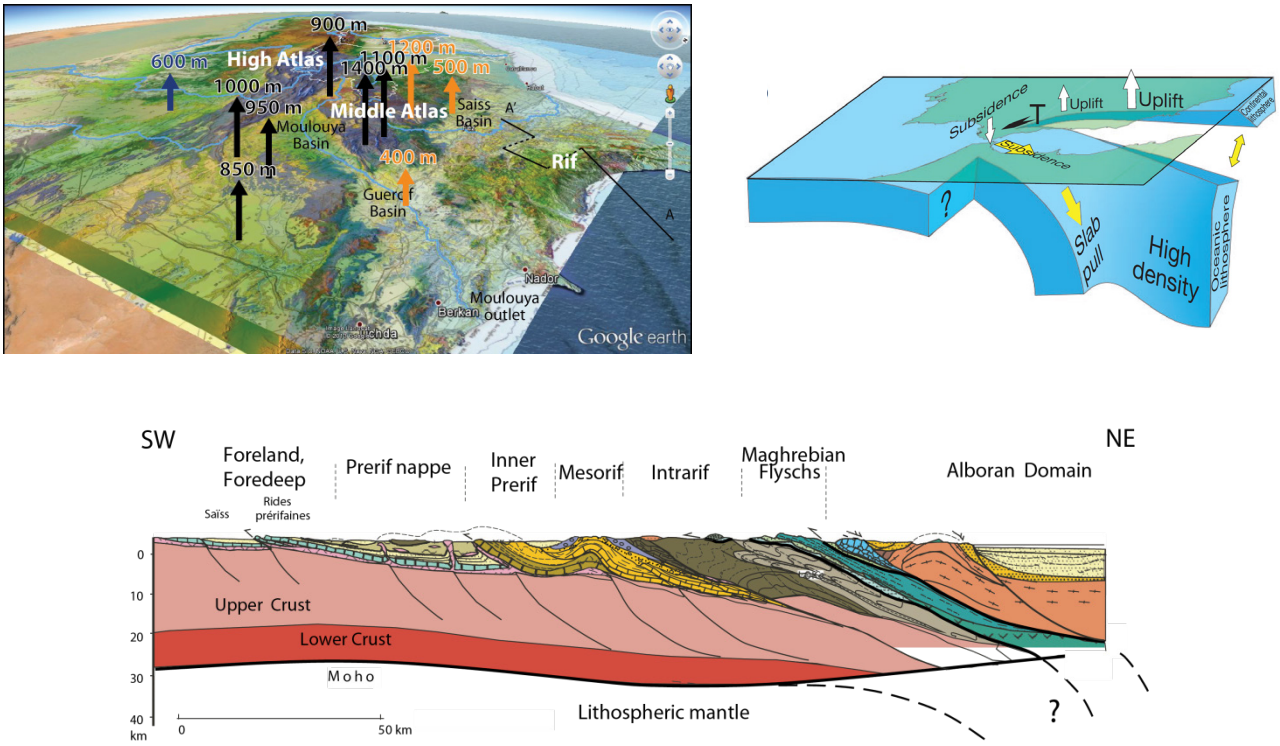


***Figure 23 :*** *(Haut gauche) Vue 3D vers le SW du Maroc septentrional sur laquelle sont indiquées les valeurs de rock uplift que nous avons déduits de la hauteur des knickpoints par rapport au niveau marin* ***(Pastor, Babault et al., 2015)****. Les flèches en orange et en bleu correspondent aux valeurs de « rock uplift » obtenues à partir des sédiments marins d'âge messinien et des sédiments lacustres pliocènes (Babault et al., 2008). (Haut droite) Vue 3D d'un modèle de retrait de slab et de déchirement sous les Betics (Garcia-Castellanos and Villasenor, 2011) et (Bas) coupe du Rif (Chalouan et al., 2008).*

Les études récentes n'ont pour l'instant pas mis en évidence de soulèvement grande longueur d'onde dans le rif. On peut se poser la question de savoir comment se fait la transition entre l'amincissement lithosphérique qui supporte le système atlasique et l'extension dans le Rif et la mer d'Alboran. Existe-t-il des évidences de mouvements verticaux associés à un déchirement de slab sous la côte marocaine comme c'est le cas dans les Bétiques ? Je tenterai de répondre à ces questions en m'intéressant à la dynamique du réseau de drainage dans le Rif et par une approche *source-to-sink*, l'objectif étant de mettre en évidence des mouvements verticaux de grande longueur d'onde d'origine mantellique dans la partie est du Rif et le prolongement du Moyen Atlas ainsi que de déterminer leur cinématique via la caractérisation des variations latérales d'exhumation et de taux d'érosion dans les unités externes du Rif oriental. Les données préliminaires semblent indiquer que le réseau de drainage a enregistré un basculement vers l'Est qui a permis aux principales rivières de s'écouler vers la Méditerranée alors que le réseau de drainage s'écoulait vers l'Atlantique depuis la fermeture du corridor sud rifain qui reliait l'Atlantique à la Méditerranée au Miocène. Cette hypothèse devrait pouvoir être confirmé par une estimation des volumes érodés dans le bassin versant de la Moulouya et sédimentés dans la Méditerranée au débouché de la rivière Moulouya. Ce projet s'appuie sur les données sismiques en mer accessibles dans le cadre du projet action marges (collaborations P. Münch, Géosciences Montpellier et E. d'Acremont, UPMC, Actions Marges chantier Méditerranée). Cette démarche devrait permettre de séparer le signal mantellique du signal tectonique lié aux déformations crustales dans le Rif.

### 5.5. Interactions tectonique, érosion et sédimentation dans une prisme expérimental soumis à l'érosion

Dans le cadre de la thèse de Marc Viaplana nous avons montré en utilisant le dispositif expérimental développé à Géosciences Montpellier (Graveleau et al., 2011) que la distribution des flux sédimentaires au front des prismes d'accrétion est contrôlée par l'influence de la tectonique sur l'organisation du réseau de drainage (Section 4.1.). Nous montrons également que la dynamique intrinsèque du système géomorphologique peut modifier la localisation des apports en produits d'érosion ainsi que les flux sédimentaires, et ce sans faire varier les forçages externes (vitesses de raccourcissement et pluviométrie). Cependant, les matériaux que nous avons utilisé dans le cadre de la thèse de Marc Viaplana ont un seuil d'érosion élevé et le matériel n'est érodé qu'à partir du moment où les pentes excèdent 3º. La conséquence d'une telle propriété est la préservation de surface non érodées dans les expériences et de quantités d'érosion faibles, quelques soient les conditions aux limites (vitesses de soulèvement et pluviométrie). Cette limite méthodologique restreint le mode de déformation à la croissance de prismes par l'accumulation de chevauchement en séquence. Jusqu'à présent, le dispositif expérimental ne permet pas de reproduire l'épaississement à l'intérieur d'un prisme par « *underplating* », alors que ce mécanisme qui est probablement à l'origine des déformations dans la Haute Himalaya a été mis en évidence dans des modèles sable/silicone en réponse à des vitesses d'érosion importantes (e.g., Konstantinovskaya and Malavieille, 2011). C'est pourquoi seule l'influence de la déformation sur l'érosion et la sédimentation peut être modélisée avec le matériau utilisé actuellement.

Je souhaite perfectionner le dispositif expérimental en collaboration avec Stéphane Dominguez (Géosciences Montpellier). Cela passe par une amélioration du matériau à éroder, notamment en sélectionnant des mélanges de poudres moins denses et ainsi favoriser à la fois l'érosion et le transport dans les modèles. Il s'agit également de faire évoluer le protocole expérimental en modifiant la rhéologie dans les modèles (épaisseur des couches, niveaux de décollement etc…) pour que le mode de déformation à l'intérieur du prisme d'accrétion puisse évoluer depuis une propagation des chevauchements en séquence vers un épaississement par « *underplating* ». Le but poursuivi est d'améliorer la compréhension des interactions tectonique/érosion/sédimentation/climat dans un prisme d'accrétion. Comme nous l'avons montré dans la thèse de Marc Viaplana, une approche *source-to-sink* expérimentale permet de mieux comprendre les relations entre la dynamique sédimentaire, les forçages externes et la dynamique du réseau de drainage (*routing system*). La prise en compte de la subsidence dans les modèles s'imposera alors pour reproduire les architectures sédimentaires telles qu'on les observe dans la nature. L'originalité de ces modèles est de reproduire des systèmes prisme d'accrétion/bassin en 3D qui permettent d'étudier les couplages tectonique/érosion/sédimentation avec un degré de résolution encore jamais atteint par les modèles numériques.

## 6. Conclusion

Ces exemples de mon activité récente de recherche montrent que mon travail est basé sur une analyse géomorphologique détaillée couplée à l'analyse des structures tectoniques et du remplissage des bassins sédimentaires, ainsi que sur la modélisation expérimentale des interactions déformation – érosion – transport – sédimentation. Cette approche couplée permet d'apporter des contraintes sur les processus orogéniques à l'origine des chaînes de montagnes. Elle permet également d'apporter une vision neuve des

relations entre la construction des chaînes de montagnes et les flux sédimentaires, avec potentiellement une application directe sur les systèmes pétroliers.

## Références bibliographiques


Adams, B. A., Hodges, K. V., van Soest, M. C., and Whipple, K. X., 2013, Evidence for Pliocene–Quaternary normal faulting in the hinterland of the Bhutan Himalaya: Lithosphere, v. 5, no. 4, p. 438-449.

Arboleya, M.-L., Babault, J., Owen, L. A., Teixell, A., and Finkel, R. C., 2008, Timing and nature of Quaternary fluvial incision in the Ouarzazate foreland basin, Morocco: Journal of the Geological Society, v. 165, no. 6, p. 1059-1073.

Babault, J., Bonnet, S., Crave, A., and Van Den Driessche, J., 2005a, Influence of piedmont sedimentation on erosion dynamics of an uplifting landscape: An experimental approach: Geology, v. 33, no. 4, p. 301-304, doi: 310.1130/G21095.21091.

Babault, J., Bonnet, S., Ruiz, G., and Van Den Driessche, J., 2009, A comment on 'Late- to post-orogenic exhumation of the Central Pyrenees revealed through combined thermochronological data and modelling' by M. Gibson, H. D. Sinclair, G. J. Lynn and F. M. Stuart: Basin Research, v. 21, no. 1, p. 139-141.

Babault, J., Bonnet, S., Van Den Driessche, J., and Crave, A., 2007, High elevation of low-relief surfaces in mountain belts: Does it equate to post-orogenic surface uplift?: Terra Nova, v. 19, no. 4, p. 272–277.

Babault, J., Teixell, A., Arboleya, M. L., and Charroud, M., 2008, A Late Cenozoic age for long-wavelength surface uplift of the Atlas Mountains of Morocco: Terra Nova, v. 20, no. 2, p. 102-107, doi:110.1111/j.1365-3121.2008.00794.x.

Babault, J., Teixell, A., Struth, L., Van Den Driessche, J., Arboleya, M. L., and Tesón, E., 2013, Shortening, structural relief and drainage evolution in inverted rifts: insights from the Atlas Mountains, the Eastern Cordillera of Colombia and the Pyrenees: Geological Society, London, Special Publications, v. 377.

Babault, J., and Van Den Driessche, J., 2005, L'érosion des chaînes de montagnes : influence de la sédimentation de piedmont: Comptes Rendus Geoscience, v. 337, no. 16, p. 1431-1438.

Babault, J., and Van Den Driessche, J., 2013, Plateau Uplift, Regional Warping, and Subsidence, *in* Shroder, J., F., ed., Treatise on Geomorphology, Volume 5, Tectonic Geomorphology: San Diego, Academic Press, p. 93-128.

Babault, J., Van Den Driessche, J., Bonnet, S., Castelltort, S., and Crave, A., 2005b, Origin of the highly elevated Pyrenean peneplain: Tectonics, v. 24, p. TC2010, doi:2010.1029/2004TC001697.

Babault, J., Van Den Driessche, J., and Teixell, A., 2012, Longitudinal to transverse drainage network evolution in the High Atlas (Morocco): The role of tectonics: Tectonics, v. 31, no. 4, p. TC4020.

Berthet, T., Hetényi, G., Cattin, R., Sapkota, S. N., Champollion, C., Kandel, T., Doerflinger, E., Drukpa, D., Lechmann, S., and Bonnin, M., 2013, Lateral uniformity of India Plate strength over central and eastern Nepal: Geophysical Journal International, v. 195, no. 3, p. 1481-1493.

Bollinger, L., Avouac, J. P., Beyssac, O., Catlos, E. J., Harrison, T. M., Grove, M., Goffé, B., and Sapkota, S., 2004, Thermal structure and exhumation history of the Lesser Himalaya in central Nepal: Tectonics, v. 23, no. 5, p. TC5015.

Braga, J. C., Martín, J. M., and Quesada, C., 2003, Patterns and average rates of late Neogene–Recent uplift of the Betic Cordillera, SE Spain: Cosmogenic isotopes in geomorphology, v. 50, no. 1–3, p. 3-26.

Brookfield, M. E., 1998, The evolution of the great river systems of southern Asia during the Cenozoic India-Asia collision: rivers draining southwards: Geomorphology, v. 22, no. 3-4, p. 285-312.

Burbank, D. W., Leland, J., Fielding, E., Anderson, R. S., Brozovic, N., Reid, M. R., and Duncan, C., 1996, Bedrock incision, rock uplift and threshold hillslopes in the northwestern Himalayas: Nature, v. 379, no. 6565, p. 505-510.

Calvet, M., 1996, Morphogénèse d'une montagne méditerranéenne : les Pyrénées orientales, Documents du BRGM, 1177 p.:

Chalouan, A., Michard, A., Kadiri, K. E., Negro, F., Lamotte, D. F. d., Soto, J. I., and Saddiqi, O., 2008, The Rif Belt, *in* Michard, A., Saddiqi, O., Chalouan, A., and Lamotte, D. d., eds., Continental Evolution: The Geology of Morocco, Volume 116, Springer Berlin Heidelberg, p. 203-302.

Chevrot, S., Villaseñor, A., Sylvander, M., Benahmed, S., Beucler, E., Cougoulat, G., Delmas, P., de Saint Blanquat, M., Diaz, J., Gallart, J., Grimaud, F., Lagabrielle, Y., Manatschal, G., Mocquet, A., Pauchet, H., Paul, A., Péquegnat, C., Quillard, O., Roussel, S., Ruiz, M., and Wolyniec, D., 2014, High-resolution imaging of the Pyrenees and Massif Central from the data of the PYROPE and IBERARRAY portable array deployments: Journal of Geophysical Research: Solid Earth, v. 119, no. 8, p. 6399-6420.

DeCelles, P. G., Robinson, D. M., Quade, J., Ojha, T. P., Garzione, C. N., Copeland, P., and Upreti, B. N., 2001, Stratigraphy, structure, and tectonic evolution of the Himalayan fold-thrust belt in western Nepal: Tectonics, v. 20, no. 4, p. 487-509.

Gansser, A., 1964, Geology of the Himalaya(s), London, Interscience Publishers (John Wiley and Sons, Ltd.), XV + 289 p.:

Garcia-Castellanos, D., and Villasenor, A., 2011, Messinian salinity crisis regulated by competing tectonics and erosion at the Gibraltar arc: Nature, v. 480, no. 7377, p. 359-363.

Godard, V., Bourlès, D. L., Spinabella, F., Burbank, D. W., Bookhagen, B., Fisher, G. B., Moulin, A., and Léanni, L., 2014, Dominance of tectonics over climate in Himalayan denudation: Geology.

Graveleau, F., Hurtrez, J. E., Dominguez, S., and Malavieille, J., 2011, A new experimental material for modeling relief dynamics and interactions between tectonics and surface processes: Tectonophysics, v. 513, no. 1-4, p. 68-87.

Gunnell, Y., Zeyen, H., and Calvet, M., 2008, Geophysical evidence of a missing lithospheric root beneath the Eastern Pyrenees: Consequences for post-orogenic uplift and associated geomorphic signatures: Earth and Planetary Science Letters, v. 276, no. 3-4, p. 302-313.

Hammer, P., Berthet, T., Hetényi, G., Cattin, R., Drukpa, D., Chophel, J., Lechmann, S., Moigne, N. L., Champollion, C., and Doerflinger, E., 2013, Flexure of the India plate underneath the Bhutan Himalaya: Geophysical Research Letters, v. 40, no. 16, p. 4225-4230.

Hayden, M. M., 1907, The geology of the provinces of Tsang and Ü in central Tibet: Mem. Geol. Surv. India, v. 36, no. 2, p. 122-201.

Heron, A. M., 1922, Geological Results of the Mount Everest Expedition, 1921: The Geographical Journal, v. 59, no. 6, p. 418-431.

Hovius, N., 1996, Regular spacing of drainage outlets from linear mountain belts: Basin Research, v. 8, no. 1, p. 29-44.

Kendrick, R. D., 2000, Structure, tectonics and thermochronology of the Irian Jaya Fold Belt, Irian Jaya, Indonesia: La Trobe University.

Konstantinovskaya, E., and Malavieille, J., 2011, Thrust wedges with décollement levels and syntectonic erosion: A view from analog models: Tectonophysics, v. 502, no. 3–4, p. 336-350.

Lavé, J., and Avouac, J. P., 2001, Fluvial incision and tectonic uplift across the Himalayas of central Nepal: Journal of Geophysical Research: Solid Earth, v. 106, no. B11, p. 26561-26591.

Missenard, Y., Zeyen, H., Frizon de Lamotte, D., Leturmy, P., Petit, C., Sébrier, M., and Saddiqi, O., 2006, Crustal versus asthenospheric origin of relief of the Atlas Mountains of Morocco: Journal of Geophysical Research, v. 111, p. B03401, doi:03410.01029/02005JB003708.

Molnar, P., 1984, Structure and Tectonics of the Himalaya: Constraints and Implications of Geophysical Data: Annual Review of Earth and Planetary Sciences, v. 12, no. 1, p. 489-516.

Molnar, P., and England, P., 1990, Late Cenozoic uplift of mountain ranges and global climate change: chicken or egg?: Nature, v. 346, no. 6279, p. 29-34.

Montgomery, D. R., and Stolar, D. B., 2006, Reconsidering Himalayan river anticlines: Geomorphology, v. 82, no. 1-2, p. 4-15.

Mudd, S. M., Attal, M., Milodowski, D. T., Grieve, S. W. D., and Valters, D. A., 2014, A statistical framework to quantify spatial variation in channel gradients using the integral method of channel profile analysis: Journal of Geophysical Research: Earth Surface, v. 119, no. 2, p. 2013JF002981.

Oberlander, T. M., 1985, Origin of drainage transverse to structures in orogens: Binghamton Symposia in Geomorphology: International Series, v. 15, p. 155-182.

Pastor, A., Babault, J., Owen, L. A., Teixell, A., and Arboleya, M.-L., 2015, Extracting dynamic topography from river profiles and cosmogenic nuclide geochronology in the Middle Atlas and the High Plateaus of Morocco: Tectonophysics.

Pastor, A., Babault, J., Teixell, A., and Arboleya, M. L., 2012, Intrinsic stream-capture control of stepped fan pediments in the High Atlas piedmont of Ouarzazate (Morocco): Cosmogenic isotopes in geomorphology, v. 173–174, no. 0, p. 88-103.

Perron, J. T., and Royden, L., 2013, An integral approach to bedrock river profile analysis: Earth Surface Processes and Landforms, v. 38, no. 6, p. 570-576.

Poujol, A., Ritz, J. F., Tahayt, A., Vernant, P., Condomines, M., Blard, P. H., Billant, J., Vacher, L., Tibari, B., Hni, L., and Idrissi, A. K., 2014, Active tectonics of the Northern Rif (Morocco) from geomorphic and geochronological data: Journal of Geodynamics, v. 77, no. 0, p. 70-88.

Robl, J., Stüwe, K., and Hergarten, S., 2008, Channel profiles around Himalayan river anticlines: Constraints on their formation from digital elevation model analysis: Tectonics, v. 27, no. 3, p. TC3010.

Romagny, A., Ph, M., Cornée, J. J., Corsini, M., Azdimousa, A., Melinte-Dobrinescu, M. C., Drinia, H., Bonno, M., Arnaud, N., Monié, P., Quillévéré, F., and Ben Moussa, A., 2014, Late Miocene to present-day exhumation and uplift of the Internal Zone of the Rif chain: Insights from low temperature thermochronometry and basin analysis: Journal of Geodynamics, v. 77, no. 0, p. 39-55.

Royden, L., and Perron, T. J., 2013, Solutions of the stream power equation and application to the evolution of river longitudinal profiles: Journal of Geophysical Research: Earth Surface, v. 118, no. 2, p. 497-518.

Schelling, D., and Arita, K., 1991, Thrust tectonics, crustal shortening, and the structure of the far-eastern Nepal Himalaya: Tectonics, v. 10, no. 5, p. 851-862.

Seeber, L., and Gornitz, V., 1983, River profiles along the Himalayan arc as indicators of active tectonics: Tectonophysics, v. 92, no. 4, p. 335-367.

Shuster, D. L., Cuffey, K. M., Sanders, J. W., and Balco, G., 2011, Thermochronometry Reveals Headward Propagation of Erosion in an Alpine Landscape: Science, v. 332, no. 6025, p. 84-88.

Struth, L., Babault, J., and Teixell, A., accepted, Present-day river system and drainage reorganization during mountain building in the Eastern Cordillera of the Colombian Andes: Geomorphology.

Sun, D., Miller, M. S., Holt, A. F., and Becker, T. W., 2014, Hot upwelling conduit beneath the Atlas Mountains, Morocco: Geophysical Research Letters, v. 41, no. 22, p. 2014GL061884.

Teixell, A., Arboleya, M. L., Julivert, M., and Charroud, M., 2003, Tectonic shortening and topography in the central High Atlas (Morocco): Tectonics, v. 22, no. 5, p. 1051, doi:1010.1029/2002TC001460.

V. Bosch, G., Van Den Driessche, J., Babault, J., Robert, A., Carballo, A., Le Carlier, C., Loget, N., Prognon, C., Wyns, R., and Baudin, T., accepted, Peneplanation and deep dynamics of the Pyrenees: Comptes Rendus Geoscience.

Viaplana-Muzas, M., 2015, Dinámica de la red de drenaje en sistemas orogénicos cuencas: implicaciones sobre los sistemas petroleros [PhD: Universitat Autònoma de Barcelona, 214 p.

Viaplana-Muzas, M., Babault, J., Dominguez, S., Van Den Driessche, J., and Legrand, X., accepted, Drainage network evolution and patterns of sedimentation in an experimental wedge: Tectonophysics.

Wager, L. R., 1937, The Arun river drainage pattern and the rise of the Himalaya: The Geographical Journal, v. 89, no. 3, p. 239-250.

Webb, A. A. G., Yin, A., Harrison, T. M., Célérier, J., Gehrels, G. E., Manning, C. E., and Grove, M., 2011, Cenozoic tectonic history of the Himachal Himalaya (northwestern India) and its constraints on the formation mechanism of the Himalayan orogen: Geosphere, v. 7, no. 4, p. 1013-1061.

Willett, S. D., McCoy, S. W., Perron, J. T., Goren, L., and Chen, C.-Y., 2014, Dynamic Reorganization of River Basins: Science, v. 343, no. 6175.

Wobus, C. W., Hodges, K. V., and Whipple, K. X., 2003, Has focused denudation sustained active thrusting at the Himalayan topographic front?: Geology, v. 31, no. 10, p. 861-864.

Yanites, B. J., Ehlers, T. A., Becker, J. K., Schnellmann, M., and Heuberger, S., 2013, High magnitude and rapid incision from river capture: Rhine River, Switzerland: Journal of Geophysical Research: Earth Surface, v. 118, no. 2, p. 1060-1084.

Yin, A., Dubey, C. S., Kelty, T. K., Webb, A. A. G., Harrison, T. M., Chou, C. Y., and Célérier, J., 2010, Geologic correlation of the Himalayan orogen and Indian craton: Part 2. Structural geology, geochronology, and tectonic evolution of the Eastern Himalaya: Geological Society of America Bulletin, v. 122, no. 3-4, p. 360-395.

**Mémoire d'Habilitation à Diriger des Recherches**

Université de Rennes 1

# La topographie comme marqueur de la déformation de la lithosphère

JULIEN BABAULT,

Professeur Lecteur

Universistat Autònoma de Barcelona

(VOLUME ANNEXE – Sélection d'articles)

# *SOMMAIRE*

Sélection des publications auxquelles j'ai participé et qui sont mentionnés afin d'illustrer mes propos pour ce mémoire d'habilitation à diriger des recherches. Les articles sont disponibles en ligne (cliquer sur les titres de la liste des publications p 11) :

Pastor, A., **Babault, J.,** Owen L.A., Teixell A., Arboleya, M.-L., Extracting dynamic topography from river profiles and cosmogenic nuclide geochronology in the Middle Atlas and the High Plateaus of Morocco Tectonophysics 2015, doi:10.1016/j.tecto.2015.06.007……p 201

Viaplana-Muzas, M., **Babault, J.,** Dominguez, S., Van Den Driessche J. and Legrand, X. Drainage network evolution and patterns of sedimentation in an experimental wedge Tectonophysics 2015, accepté……p 216

Struth, L., **Babault, J.** and Teixell, A. Present-day river system and drainage reorganization during mountain building in the Eastern Cordillera of the Colombian Andes Geomorphology 2015, accepté……p 250

V. Bosch, G., Van Den Driessche, J., **Babault, J.,** Robert, A., Carballo, A., Le Carlier, C., Loget, N., Prognon, C., Wyns, R. and Baudin, T. Peneplanation and deep dynamics of the Pyrenees C.R. Géocience 2015, accepté……p 291

Viaplana-Muzas, M., 2015, Dinámica de la red de drenaje en sistemas orogénicos cuencas: implicaciones sobre los sistemas petroleros [PhD: Universitat Autònoma de Barcelona, 214 p.
Disponible en ligne (cliquer sur le titre de la thèse).

Available online at www.sciencedirect.com
SCIENCE DIRECT
C. R. Geoscience 337 (2005) 1431–1438
COMPTES RENDUS GEOSCIENCE
http://france.elsevier.com/direct/CRAS2A/

Géomatériaux (Sédimentologie)

# L'érosion des chaînes de montagnes : influence de la sédimentation de piedmont

Julien Babault, Jean Van Den Driessche *

*Géosciences Rennes, UMR 6118, université Rennes-1, campus de Beaulieu, bât. 15, CS 74205, 35042 Rennes cedex, France*

Reçu le 12 octobre 2004 ; accepté après révision le 30 septembre 2005

Disponible sur Internet le 8 novembre 2005

Présenté par Jean Dercourt

**Résumé**

La pénéplanation des chaînes de montagnes est généralement considérée comme résultant de l'action de l'érosion à long terme, qui lisse le relief et diminue leur altitude jusqu'à tendre vers le niveau marin. Nous proposons un nouveau modèle, dans lequel la sédimentation de piedmont traduit une montée du niveau de base de la chaîne, entraînant son aplanissement en altitude. Ce modèle est illustré à travers l'évolution morphologique du versant sud des Pyrénées durant le Cénozoïque. ***Pour citer cet article : J. Babault, J. Van Den Driessche, C. R. Geoscience 337 (2005).***



**Abstract**

**Erosion of mountain belts: influence of piedmont sedimentation.** The applanation of mountain belts that results in peneplain is generally considered to be caused by the long-term activity of erosion. Peneplanation has been previously defined as the lowering of an elevated topography and the concomitant subduing of its relief. We propose a model following which piedmont sedimentation induces the base level rise, allowing applanation to develop at high elevation and resulting in an elevated 'peneplain'. This model is illustrated by the morphological evolution of the southern flank of the Pyrenees during the Cainozoic. ***To cite this article: J. Babault, J. Van Den Driessche, C. R. Geoscience 337 (2005).***



*Mots-clés :* Pénéplaine ; Aplanissement ; Surface d'érosion ; Érosion ; Sédimentation ; Piedmont ; Pyrénées

*Keywords:* Peneplain; Applanation; Erosional surfaces; Erosion; Sedimentation; Piedmont; Pyrenees

## Abridged English version

The word 'peneplain' classically refers to a low, nearly featureless, gently undulating land surface of considerable area, which presumably has been produced by the processes of long-continued subaerial erosion, almost to base level in the penultimate stage of a humid, fluvial geomorphic cycle [5,21,31]. Following such an interpretation, peneplanation is thus viewed as the lowering of the mean surface elevation and the concomitant relief subduing.

Surface uplift of mountain ranges results from thickening of the continental lithosphere and thus pene-

* Auteur correspondant.
*Adresses e-mail :* julien.babault@univ-rennes1.fr (J. Babault), jean.van-den-driessche@univ-rennes1.fr (J. Van Den Driessche).

1631-0713/$ – see front matter 
doi:10.1016/j.crte.2005.09.010

planation of mountain belts requires destroying their lithospheric roots. This can be achieved in three ways (Fig. 1). The model 1 considers that progressive exhumation and complete removal of lithospheric roots are due to superficial erosion through isostatic compensation. Since the 1980s, it has been demonstrated that thickening of large collisional orogens resulted in later gravity collapse, marked by the development of basins and ranges. Such a process, combined with erosion and long-term thermal cooling, allows the lithosphere to recover its initial thickness and the landscape elevation to decrease (model 2) (e.g., [11,25,34]). Alternatively, thermal cooling of the lithospheric root may induce its density increase so that the subsequent decrease of the lithospheric root buoyancy allows the lowering of land surface (model 3) [23]. These three models consider that peneplanation is always achieved near the sea level. In models 1 and 3, the final land surface is an erosional surface, whereas in model 2 the final topography alternately corresponds to an erosional or a depositional surface. Here we propose an alternative model in which peneplanation may develop at high altitude.

Indeed mountain ranges are usually bounded by sedimentary basins where eroded products accumulate. Foreland basins generally first fill up with marine sediments (underfilled stage) and evolve toward continental sedimentation (overfilled stage) (e.g., [20]). If sedimentation in front of a relief occurs above the sea level, it will increase the base level for erosion, defined as the limit between erosion and sedimentation [50]. We argue that, under certain conditions, the rise of the mountain range base-level due to massive alluvial sedimentation in foreland basins can considerably reduce the erosive efficiency of the drainage network in the mountain range [3,15], resulting in the development of a highly elevated ‘peneplain’ (Fig. 2) [4].

A striking feature of the Pyrenees morphology is the presence of highly elevated, low-relief, erosional surfaces, hereafter referred to as HE–LR surfaces (Fig. 3), which were extensively described since the beginning of the last century by numerous geomorphologists and geologists [2,6,8,14,22,27,32,36–39,46]. Late Miocene overlying continental deposits provide an upper limit age for these surfaces [6,43]. To explain the Pyrenean HE–LR surfaces, pioneering works have invoked a Pliocene upheaval contemporary with a phase of tangential compression, though it could not be documented [6,8,22,27]. Indeed, there is no evidence of tangential deformation during Pliocene times that could have produced the ca 12 km of crustal thickening necessary to induce the 2000 m of Pliocene uplift as invoked by De Sitter [22] and more recent works [9,10,13,14]. An alternative explanation [10] would have been to consider that the Palaeogene lithospheric root of the Pyrenees was removed from the Neogene, inducing Pliocene uplift. However, the tomographic study of [47] shows evidence for the still occurrence of a lithospheric root down to 100 km of depth beneath the Pyrenees.

Another striking feature of the Pyrenees is the occurrence along its southern flank of a huge accumulation of continental sediments that overlap the axial zone up to an elevation of about 2000 m [20,40,41,49]. This was favoured by the closure of the Ebro basin from the Late Eocene (e.g., [6,41,42,45]). Fig. 4 shows the reconstructed Miocene palaeo-piedmont along the southern flank of the Pyrenees based on the sedimentary remnants of the basin fill. The uppermost part of the profile merges into the HE–LR of the axial zone, strongly suggesting that the development of these erosional surfaces results from the rise of the base-level of the southern foreland basin.

Although the present elevation of the uppermost part of Aquitaine piedmont is only 650 m, the occurrence of similar HE–LR along the northern side of the axial zone also suggests that accumulation of detrital sediments [26] must have reached a high elevation during Cainozoic times.

By contrast with the classical models of mountain chains peneplanation, we suggest that relief subduing does not necessary equate surface elevation lowering, so that relief of mountain belts can be smoothed at high elevation. Such a process is allowed by the piedmont aggradation of the eroded products of mountain ranges, resulting in the increase of their base level. This explains to our opinion the paradox of the occurrence of post-tectonic HE–LR remnants of peneplain within the Pyrenees, the elevation of which has been previously misinterpreted as resulting from enigmatic Pliocene uplift.

## 1. Introduction

La morphologie des chaînes de montagnes résulte de la compétition entre les processus tectoniques, qui épaississent la lithosphère et soulèvent la surface des continents, et les processus d’érosion et de transport, qui soustraient la matière et l’exportent via le réseau de drainage vers les avant-pays des chaînes. Les chaînes jeunes sont élevées et disséquées, les chaînes anciennes sont de faible altitude et présentent un relief doux. Cette vision suppose que les chaînes s’aplanissent par « l’usure du temps », autrement dit par l’action de l’érosion à long terme. Suivant ce processus, que résume le modèle de Davis [21], l’aplanissement d’une chaîne sous l’effet de

l'érosion correspond à la chute de son altitude, en même temps qu'au lissage de sa topographie.

Dans les zones climatiques tempérées, les réseaux fluviatiles jouent un rôle primordial dans la dynamique des reliefs, en raison de leur potentiel érosif énorme et de leur fonction de transport des sédiments. La loi physique qui gouverne l'érosion fluviatile relie la quantité d'érosion ($E$) à la pente locale ($S$) et au flux d'eau des rivières, approché par la dimension de l'aire drainée amont ($A$) suivant une relation du type [28] :

$$E \propto A^m \times S^n$$

$m$ et $n$ étant des constantes positives.

Dans cette relation, l'effet de la tectonique est de modifier la pente régionale, donc les pentes locales [1,35]. Le climat influe, quant à lui, sur le flux d'eau et donc sur l'aire drainée amont. À climat constant et postérieurement à un soulèvement tectonique, l'érosion entraîne une diminution de l'altitude et donc de la pente régionale. À terme, les processus d'érosion des versants prennent le pas sur l'activité érosive décroissante des rivières, entraînant la pénéplanation d'un relief au sens de Davis [5,21,31]). Le modèle de Davis suppose que le niveau de base d'un relief reste constant au cours de son aplanissement. Dans le présent article, nous montrons qu'un effet identique peut être obtenu par une surrection du niveau de base, liée directement à l'accumulation des produits d'érosion au pied du relief, à la différence près que l'aplanissement se développe en altitude.

## 2. Processus classiques d'aplanissement d'une chaîne

Plusieurs processus sont à l'origine de la surrection de la surface terrestre, le plus « efficace » et spectaculaire étant l'épaississement de la lithosphère, consécutif à la tectonique des plaques, en particulier à la collision entre continents. Pour aplanir une chaîne de montagnes, il existe a priori deux possibilités : soit éliminer la racine de la chaîne, en d'autres termes ramener progressivement la lithosphère à son épaisseur initiale, soit augmenter la densité de cette racine, de telle sorte qu'elle tire vers le bas la chaîne.

En ce qui concerne la première hypothèse, deux modèles peuvent expliquer l'aplanissement d'une chaîne. Dans le premier modèle (modèle 1) (Fig. 1), l'exhumation progressive et l'élimination à terme de la racine lithosphérique provient uniquement de la compensation isostatique de l'érosion en surface.

Par ailleurs, on sait, depuis une vingtaine d'années, que les grandes chaînes de montagnes issues de la collision entre les continents finissent par s'effondrer sous

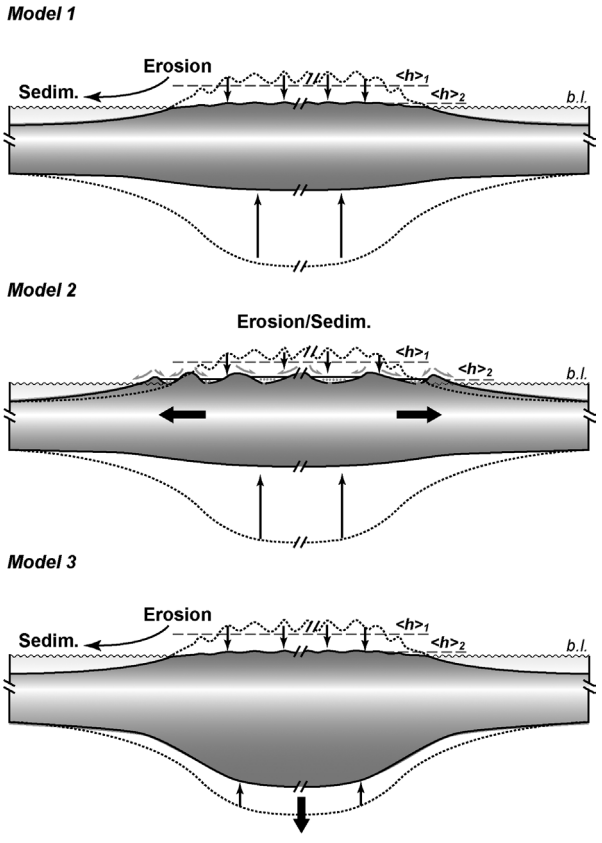


Fig. 1. Trois différents modèles d'aplanissement. Modèle 1 [21] : la pénéplanation résulte de la seule action de l'érosion qui entraîne l'exhumation par compensation isostatique et l'élimination à terme de la racine lithosphérique ; modèle 2 : la pénéplanation s'opère par l'effet combiné de processus tectonique (effondrement gravitaire) et thermique (refroidissement), et de l'érosion ; modèle 3 : l'augmentation de la densité de la racine lithosphérique refroidie entraîne l'enfoncement de la chaîne. Dans les modèles 1 et 3, la surface d'aplanissement est une surface d'érosion, dans le modèle 2, une surface mixte d'érosion et de dépôt. $\langle h \rangle_1$ : altitude moyenne initiale de la chaîne ; $\langle h \rangle_2$ : altitude moyenne finale ; b.l. : niveau de base (niveau marin).

Fig. 1. Three models of applanation. Model 1 [21]: peneplanation results from erosion that induces the progressive exhumation and the forward removing of the lithospheric root by isostatic compensation; model 2: peneplanation results from the combination of tectonic and thermal processes (gravity collapse and cooling, respectively), and erosion; model 3: the density increase of the cold lithospheric root causes the chain to sink. In models 1 and 3, the applanation surface is an erosional surface, in model 2 this surface is alternatively erosional and depositional. $\langle h \rangle_1$: initial mean elevation of the chain; $\langle h \rangle_2$: final mean elevation; b.l.: base level (sea level).

l'effet conjugué de leur poids et de l'amollissement thermique de leur racine crustale (par exemple, [11,25, 34]). L'épaississement crustal qui était à l'origine de leur haute altitude se trouve annihilé et cette dernière diminue drastiquement. Ainsi, la diminution de l'altitude des grandes chaînes ne peut être rapportée uni-

quement à l'action de l'érosion à long terme, mais est également due à un processus thermomécanique (modèle 2) (Fig. 1). Néanmoins, le fort flux de chaleur lié à l'épaississement initial persiste bien longtemps après l'effondrement, ce qui a pour effet, via la densité anormalement faible de la croûte et du manteau chauds, de maintenir ces chaînes « effondrées » à des altitudes anormalement élevées en regard de l'épaisseur de leur lithosphère (par exemple, [19]). La diminution de l'altitude sera liée, outre le retour à une épaisseur normale de la croûte, au refroidissement progressif du manteau.

Un autre effet de l'effondrement gravitaire est de modifier drastiquement la morphologie de la chaîne initiale. L'amincissement vertical de la lithosphère épaissie s'accompagne d'un étirement horizontal, qui se traduit par le développement d'une série de horsts et grabens. Leurs structures en « bassins et chaînons montagneux » (*basin and range*) et leurs grandes dimensions font que le drainage de ces domaines étirés est le plus souvent endoréique (par exemple, [19]), les produits de l'érosion des chaînons étant piégés dans les bassins immédiatement adjacents. Il en résulte un lissage progressif de leur topographie, les « hauts » s'érodant et s'abaissant, les « bas » se remplissant et s'élevant relativement. Un processus similaire a été invoqué en contexte compressif pour expliquer la formation de hauts plateaux, tel, le Tibet (par exemple, [33]). Ainsi, l'effondrement gravitaire des chaînes de collision, combiné à l'érosion, peut avoir un effet identique à celui de l'érosion seule à long terme, telle qu'elle est envisagée par le modèle de Davis. Dans le cas du processus d'effondrement gravitaire, le retour à une altitude proche du niveau de la mer reste néanmoins lié au refroidissement (lent) de la lithosphère.

La seconde hypothèse considère que le refroidissement de la racine crustale entraîne une augmentation de la densité des roches qui la composent à travers des transformations minéralogiques (modèle 3) (Fig. 1). Fischer [23] remarque que l'altitude moyenne d'une chaîne rapportée à l'épaisseur de sa racine crustale est plus faible pour les chaînes anciennes que pour les chaînes récentes. Elle en conclut que les racines des chaînes anciennes sont plus denses que celles des chaînes récentes, en raison du refroidissement avec le temps des premières. Suivant cette hypothèse, « l'enfoncement » de la chaîne entraîne une diminution du potentiel érosif des rivières qui la drainent et le lissage progressif de la topographie, de la même manière que dans le modèle de Davis.

Ainsi, la diminution de l'altitude des chaînes suivant les modèles considérés fait appel, soit à l'érosion seule à long terme (modèle 1), soit à la combinaison de l'érosion et d'un processus thermique à long terme (modèle 3), soit à une combinaison entre érosion, processus tectonique à cours terme et processus thermique à long terme (modèle 2). Dans les deux modèles 1 et 3, le lissage concomitant de la topographie des chaînes est directement lié à leur diminution d'altitude. Dans le cas de l'effondrement gravitaire (modèle 2), il faut y ajouter le piégeage des produits d'érosion à l'intérieur de la chaîne. Aussi la surface d'aplanissement d'une chaîne dans les modèles 1 et 3 correspondra à une surface d'érosion, alors qu'elle sera mixte, surface d'érosion et surface de dépôt dans le modèle 2. Quoi qu'il en soit, ces trois modèles supposent une diminution de l'altitude des chaînes et un lissage concomitant de leur topographie.

Cette notion d'aplanissement est toujours d'actualité, au point que l'observation de reliques d'une surface d'aplanissement en haute altitude est considérée comme symptomatique de la surrection ultérieure d'une pénéplaine initiale, ou encore du rajeunissement d'une chaîne érodée (par exemple, [7,22,30,44,48]. Dans ce dernier cas, la cause de ce nouveau soulèvement peut être complètement indépendante de la tectonique à l'origine de la chaîne.

## 3. Un modèle d'aplanissement en altitude

Les chaînes sont ou ont été bordées par des bassins d'avant-pays qui se développent ou se sont développés initialement, pour la plupart, sous l'eau avant d'émerger progressivement au fur et à mesure que les chaînes grandissent. Ainsi, le remplissage sédimentaire de ces bassins d'avant-pays correspond généralement à des séquences de comblement d'abord marines, puis continentales (par exemple, [24]), qui à terme aggradent en *onlap* jusque dans les zones internes des chaînes (par exemple, [20]). Si on définit le niveau de base d'un relief donné à un instant donné comme étant la limite entre la zone en érosion et la zone en dépôt (par exemple, [50]), le passage d'une sédimentation marine à une sédimentation continentale dans l'avant-pays traduit une surrection du niveau de base de la chaîne. Cette évolution est d'autant plus favorisée que ces bassins, pour une raison ou une autre, deviennent endoréiques. En fait, la présence d'une importante sédimentation de piedmont caractérise une chute drastique de la capacité des rivières à transporter les sédiments. Aussi, le niveau de base d'une chaîne de montagnes ne sera pas tant dépendant de la nature, endoréique ou exoréique, de son réseau de drainage que de la capacité des rivières à exporter les produits d'érosion [3,4,15].

Dans les trois modèles d'aplanissement des chaînes discutés précédemment, le niveau de base de la chaîne

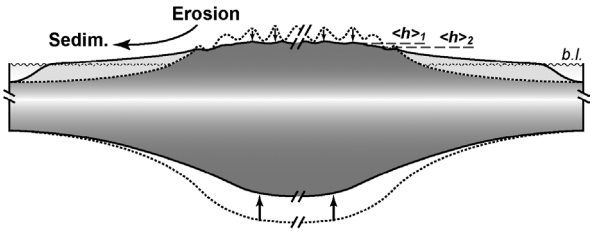


Fig. 2. Aplanissement en altitude. Le passage d'une sédimentation marine à continentale dans les bassins d'avant-pays des chaînes entraîne une élévation de leur niveau de base. À terme, la sédimentation de piedmont entraîne le développement d'une « pénéplaine » et la conservation de la racine crustale. $\langle h \rangle_1$ : altitude moyenne initiale de la chaîne ; $\langle h \rangle_2$ : altitude moyenne finale ; b.l. : niveau de base (niveau marin).

Fig. 2. Applanation at high elevation. The change from marine to continental sedimentation in foreland basins induces the rise of the base level of mountain belts. Eventually piedmont sedimentation causes a peneplain to develop at high elevation and a crustal root to be preserved. $\langle h \rangle_1$: initial mean elevation of the chain; $\langle h \rangle_2$: final mean elevation; b.l.: base level (sea level).

reste identique depuis sa surrection jusqu'à sa destruction, dans la mesure où il correspond au niveau de la mer (en faisant abstraction des variations eustatiques). L'hypothèse proposée ici est à l'inverse : elle considère que le niveau de base de la chaîne s'élève progressivement en raison de l'accumulation des produits de l'érosion au pied de la chaîne. Si la surrection de la chaîne s'arrête, alors le potentiel érosif des rivières diminue, entraînant le lissage de la topographie en altitude (Fig. 2). Ainsi, suivant cette hypothèse, le lissage de la topographie, s'il s'accompagne d'une certaine diminution de l'altitude de la chaîne, ne nécessite pas une chute de cette altitude jusqu'à un niveau proche de celui de la mer. Il est à noter qu'un tel modèle implique la conservation d'une racine crustale.

## 4. L'exemple des Pyrénées

L'une des caractéristiques majeures de la chaîne des Pyrénées, reconnue depuis longtemps, est la présence de reliques de surface d'aplanissement culminant à plus de 2000 m (par exemple, [2,4,6,14,22,27, 32,36–39,46] (Fig. 3). Ces surfaces ont toujours été interprétées comme la marque d'un soulèvement d'autant de cette chaîne depuis le Mio-Pliocène [9,10,13, 14,22], alors que la tectonique compressive pyrénéenne était finie (par exemple, [4,18,45]). Une telle interprétation suppose un aplanissement des Pyrénées au cours de l'Oligocène–Miocène, puis une nouvelle surrection dont la cause reste énigmatique, qu'elle soit tectonique ou thermique. Il est à noter qu'une surrection de 2000 m des Pyrénées nécessiterait, dans l'hypothèse tectonique, un épaississement crustal de l'ordre de 12 km. S'il existe bien une racine crustale actuellement sous les Pyrénées, le Moho s'enfonçant jusqu'environ 50 km, il est très peu probable que cette racine se soit constituée à partir du Mio-Pliocène, aucune trace de tectonique compressive d'ampleur n'ayant été enregistrée depuis cette époque. De même, aucune trace de processus de type délamination lithosphérique [47], entraînant une variation drastique de densité, n'est observée, telle que par exemple une augmentation du flux de chaleur (volcanisme, flux de chaleur élevé en surface...).

Le cas des Pyrénées n'est pas unique et le problème s'est également posé depuis très longtemps aux géographes, géomorphologues et géologues dans les Rocheuses américaines [7,30,44,48]. Aussi, l'existence de surfaces d'érosion planes en haute altitude dans les chaînes n'est pas un problème fortuit, mais pose celui, fondamental, de la dynamique de l'érosion des chaînes sur le long terme.

Une autre caractéristique remarquable de la chaîne des Pyrénées sur son flanc sud est l'accumulation très importante de dépôts détritiques, qui aggradent en *onlap* vers l'intérieur de la chaîne et dont la surface atteint actuellement près de 2000 m [20,40,41,49].

Le confinement du bassin de l'Èbre entre les chaînes Catalane, Ibérique et Celtibérique, à partir de l'Éocène supérieur, a entraîné le comblement de la topographie à relief élevé de l'Éocène moyen par des conglomérats de plusieurs centaines de mètres d'épaisseur sur la bordure sud de la zone axiale et par leurs équivalents distaux dans le centre du bassin lacustre [6,20,40–42, 45]. Les témoins du remplissage fini-Miocène culminent respectivement de 900 à 2000 m, dans le centre du bassin et sur la bordure sud de la zone axiale, respectivement. La reconstruction du paléopiedmont miocène des Pyrénées basé sur ces corps sédimentaires (Fig. 4) souligne la corrélation spatiale entre le piedmont miocène et les surfaces d'érosion de la zone axiale. Dans les Pyrénées orientales, ces surfaces d'érosion sont recouvertes par des dépôts continentaux détritiques d'âge Miocène supérieur (par exemple, [6,9,12,43]). Ainsi, les relations spatiales et temporelles entre le piedmont sud pyrénéen miocène et les hautes surfaces d'érosion miocènes à faible relief de la zone axiale supportent l'hypothèse suivant laquelle le développement d'une « haute pénéplaine » dans la zone axiale est contrôlé par l'altitude de son niveau de base, défini par la partie amont du piedmont de sédimentation miocène.

Sur le versant nord, le bassin d'Aquitaine montre une évolution similaire à celle du bassin de l'Ebre, c'est-à-dire caractérisée par le passage d'une sédimentation marine à continentale au cours de l'Éocène [26], bien

Fig. 3. Vue vers le nord-ouest d'une surface d'érosion dans les Pyrénées orientales. La surface subhorizontale au second plan correspond à une surface d'aplanissement dont l'altitude s'étage de 2500 à 2900 m (massif du Campcardos). La plaine au premier plan, située à une altitude de 1200 m, correspond au remplissage mio-pliocène du graben de la Cerdagne. La vallée sur la droite est celle de Carol.

Fig. 3. View looking toward the northwest of an erosional surface in the Eastern Pyrenees. The subhorizontal surface in the background is an erosional surface whose elevation ranges between 2500 and 2900 m (the Campcardos massif). The plain in the foreground, which lies at 1250 m asl, corresponds to the Miocene–Pliocene fill of the Cerdagne graben. The valley on the right side is the Carol Valley.

que le drainage soit resté connecté à l'Atlantique. Sur ce versant, on n'observe pas de reliques de corps sédimentaires aussi spectaculaires. Actuellement, le piedmont miocène du cône de Lannemezan atteint 600–700 m [27]. Suivant le modèle proposé ici, la présence de reliques de surfaces d'aplanissement implique que les dépôts détritiques sur le versant nord aient pu atteindre des altitudes plus élevées [4]. Dans ce sens, les « brèches » sédimentaires polygéniques post-métamorphiques et continentales observées le long de la bordure nord de la zone axiale (par exemple, [16,17,29]) sont probablement des témoins de la sédimentation de piedmont sur le versant nord.

## 5. Conclusion

Les mécanismes d'aplanissement des chaînes de montagnes généralement envisagés, qu'ils fassent appel à l'érosion seule ou combinée à des processus tectoniques et/ou thermiques, impliquent une diminution à terme de l'altitude des chaînes proche du niveau marin, qui est supposé correspondre à leur niveau de base tout au cours de leur évolution.

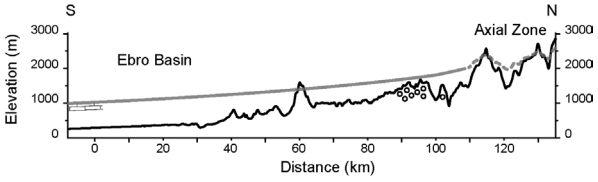


Fig. 4. Relation entre le piedmont miocène et les surfaces d'érosion de la zone axiale sur le versant sud des Pyrénées. Trait noir : Profil topographique transverse actuel ; trait gris : profil du piedmont miocène reconstitué ; tireté gris : surfaces d'érosion de la zone axiale. Figuré calcaire : calcaires lacustres miocènes du centre du bassin de l'Ebre ; cercles : conglomérats Eocène supérieur à Oligo-Miocène.

Fig. 4. Relation between the Miocene piedmont and the erosional surfaces of the axial zone in the southern flank of the Pyrenees. Black line: present transverse topographic profile; grey line: reconstructed profile of the Miocene piedmont, grey dashed line: erosional surfaces in the axial zone. Calcareous symbol: Miocene lacustrine calcareous within the Ebro basin; circles: Upper Eocene to Oligocene–Miocene conglomerates.

L'exemple des Pyrénées montre, à l'inverse, que le niveau de base d'une chaîne n'est pas tant constitué par le niveau de la mer que par l'altitude maximale

atteinte par les produits d'érosion constitutifs de son piedmont. Ce fait, finalement très simple, peut conférer aux chaînes de montagnes une évolution identique au modèle d'aplanissement classique de Davis, à la différence majeure près que cet aplanissement se développe à une altitude élevée dépendant de l'altitude maximale atteinte par le piedmont.

Finalement, la présence en altitude d'une surface d'aplanissement disséquée ne peut être utilisée de façon directe comme la marque d'un soulèvement tectonique.

## Références


[1] F. Ahnert, Functional relationships between denudation, relief, and uplift in large mid-latitude drainage basins, Am. J. Sci. 268 (1970) 243–263.

[2] G. Astre, Le bassin néogène de Bellver, Bull. Soc. Hist. nat. Toulouse L VI (1927) 231.

[3] J. Babault, S. Bonnet, A. Crave, J. Van Den Driessche, Influence of piedmont sedimentation on erosion dynamics of an uplifting landscape: An experimental approach, Geology 33 (2005) 301–304.

[4] J. Babault, J. Van Den Driessche, S. Bonnet, S. Castelltort, A. Crave, Origin of the highly elevated Pyrenean peneplain, Tectonics 24 (2005).

[5] R.L. Bates, J.A. Jackson, Glossary of Geology, Falls Church, VA, USA, 1980.

[6] P. Birot, Recherches sur la morphologie des Pyrénées orientales franco-espagnoles, thèse, Paris, 1937.

[7] D.L. Blackstone, Late Cretaceous and Cenozoic History of Laramie Basin Region, Southeast Wyoming, Geol. Soc. Am. Mem. 144 (1975) 249–279.

[8] H. Boissevain, Étude géologique et géomorphologique de la vallée de la haute Sègre, Bull. Soc. Hist. nat. Toulouse (1934).

[9] A. Briais, R. Armijo, T. Winter, P. Tapponnier, A. Herbecq, Morphological evidence for Quaternary normal faulting and seismic hazard in the Eastern Pyrenees, Ann. Tectonicae IV (1990) 19–42.

[10] M.-F. Brunet, The influence of the evolution of the Pyrenees on adjacent basins, Tectonophysics 129 (1986) 343–354.

[11] J.-P. Burg, J. Van Den Driessche, J.-P. Brun, Syn- to post-thickening extension: modes and consequences, C. R. Acad. Sci. Paris, Ser. II 319 (1994) 1019–1032.

[12] L. Cabrera, E. Roca, P. Santanach, Basin formation at the end of a strike-slip fault: the Cerdanya Basin (eastern Pyrenees), J. Geol. Soc. Lond. 145 (1988) 261–268.

[13] M. Calvet, Néotectonique et mise en place des reliefs dans l'Est des Pyrénées ; l'exemple du horst des Albères, Rev. Géol. Dyn. Géogr. Phys. 26 (1985) 119–130.

[14] M. Calvet, Morphogénèse d'une montagne méditerranéenne : les Pyrénées orientales, thèse d'État, université Paris-1 Panthéon–Sorbonne, 1994.

[15] S. Carretier, F. Lucazeau, How does alluvial sedimentation at range fronts modify the erosional dynamics of mountain catchments?, Basin Research 17 (2005) 361–381.

[16] P. Choukroune, La brèche de Lherz, dite « d'explosion liée à la mise en place des lherzolites » est une brèche sédimentaire d'âge Cénozoïque (Pyrénées ariégeoises), C. R. Acad. Sci. Paris, Ser. D 277 (1973) 2621–2624.

[17] P. Choukroune, Structure et évolution tectonique de la zone Nord-Pyrénéenne, analyse de la déformation dans une portion de chaîne à schistosité sub-verticale, Mém. Soc. géol. France LV (1976) 1–116.

[18] P. Choukroune, ECORS-Team, The ECORS Pyrenean deep seismic profile reflection data and the overall structure of an orogenic belt, Tectonics 8 (1989) 23–39.

[19] P.J. Coney, T.A. Harms, Cordilleran metamorphic core complexes: Cenozoic extensional relics of Mesozoic compression, Geology 12 (1984) 550–554.

[20] P.J. Coney, J.A. Muñoz, K.R. McClay, C.A. Evenchick, Syntectonic burial and post-tectonic exhumation of the southern Pyrenees foreland fold-thrust belt, J. Geol. Soc. Lond. 153 (1996) 9–16.

[21] W.M. Davis, The geographical cycle, Geogr. J. 14 (1989) 481–504.

[22] L.U. de Sitter, Pliocene uplift of Tertiary mountain chains, Am. J. Sci. 250 (1952) 297–307.

[23] K.M. Fischer, Waning buoyancy in the crustal roots of old mountains, Nature 417 (2002) 933–936.

[24] P.B. Flemings, T.E. Jordan, A synthetic stratigraphic model of foreland basin development, J. Geophys. Res. 94 (B4) (1989) 3851–3866.

[25] Y. Gaudemer, C. Jaupart, P. Tapponnier, Thermal control on post-orogenic extension in collision belts, Earth Planet. Sci. Lett. 89 (1988) 48–62.

[26] J.-P. Gély, K. Sztrakos, L'évolution paléogéographique et géodynamique du Bassin aquitain au Paléogène : enregistrement et datation de la tectonique pyrénéenne, Géol. France 2 (2000) 31–57.

[27] L. Goron, Les Pré-Pyrénées ariégeoises et garonnaises. Essai d'étude morphologique d'une lisière de montagne, thèse, faculté des lettres, université de Toulouse, 1941.

[28] A.D. Howard, G. Kerby, Channel changes in badlands, GSA Bull. 94 (1983) 739–752.

[29] M. Jaffrezo, D. Obert, Réunion extraordinaire de la Société géologique de France, Les Pyrénées (8–15 septembre 1977), Bull. Soc. géol. France XX (1978) 587–629.

[30] W.R. Keefer, Structural Geology of the Wind River Basin, Wyoming, Geol. Surv. Prof. Pap. US (1970) 495-D.

[31] H. Kooi, C. Beaumont, Large-scale geomorphology: classical concepts reconciled and integrated with contemporary ideas via a surface processes model, J. Geophys. Res. 101 (1996) 3361–3386.

[32] O. Mengel, À propos des paliers des vallées des Pyrénées orientales (réponse à M. de Martonne), Bull. Soc. géol. France, 4$^{e}$ série X (1910) 427.

[33] B. Meyer, P. Tapponnier, L. Bourjot, F. Métivier, Y. Gaudemer, G. Peltzer, S. Guo, Z. Chen, Crustal thickening in Gansu-Qinghai, lithospheric mantle subduction, and oblique, strike-slip controlled growth of the Tibet plateau, Geophys. J. Int. 135 (1998) 1–47.

[34] P. Molnar, P. Tapponnier, Active tectonics of Tibet, J. Geophys. Res. 83 (1978) 5361–5375.

[35] D.R. Montgomery, M.T. Brandon, Topographic controls on erosion rates in tectonically active mountain ranges, Earth Planet. Sci. Lett. 201 (2002) 481–489.

[36] F. Nussbaum, Sur les surfaces d'aplanissement d'âge Tertiaire dans les Pyrénées-Orientales et leurs transformations pendant l'époque quaternaire, C. R. Congr. int. Géogr., II Trav. de la Section II, Paris, 1931.

[37] A.J. Pannekoek, Évolution du bassin de la Têt dans les Pyrénées orientales pendant le Néogène, Utrecht, Pays-Bas, 1935.

[38] W. Panzer, Talentwicklung und Eiszeitklima in nord-östlichen Spanien, Abh. Senckenb. Naturforsch. Ges. 39 H. 3 (1926).

[39] A. Penck, Studien über das Klima Nordspaniens während der jungeren Terciärperiode und der diluvialperiode, Z. Ges. Erdkunde, Berlin, 1894.

[40] J.-L. Reille, Mise en évidence de paléoreliefs de 2000 m de dénivelée, fossilisés et enterrés par les formations continentales de l'Éocène supérieur, sur le versant sud des Pyrénées centrales (région de la Pobla de Segur, province de Lérida, Espagne), C. R. Acad. Sci. Paris, Ser. D 270 (1970) 1861–1864.

[41] J.-L. Reille, Les relations entre tectorogénèse et sédimentation sur le versant sud des Pyrénées centrales d'après l'étude des formations tertiaires essentiellement continentales, thèse, USTL, 1971.

[42] O. Riba, S. Reguant, J. Villena, Ensayo de síntesis estratigráfica y evolutiva de la cuenca terciaria del Ebro, in: J.A. Coumba (Ed.), Geologica España, vol. 2, Libro Jubilar J. M. Rios, 1983, pp. 131–159.

[43] E. Roca, The Neogene Cerdanya and Seu d'Urgell intramontane basins (Eastern Pyrenees), in: P.F. Friend, C.J. Dabrio (Eds.), Tertiary Basins of Spain, Cambridge University Press, 1996.

[44] G.R. Scott, Cenozoic Surfaces and Deposits in the Southern Rocky Mountains, Geol. Soc. Am. Mem. 144 (1975) 227–248.

[45] M. Seguret, Étude tectonique des nappes et séries décollées de la partie centrale du versant sud des Pyrénées. Caractère synsédimentaire, rôle de la compression et de la gravité, thèse, Montpellier, France, 1972.

[46] M. Sorre, Les Pyrénées méditerranéennes, thèse, 1913.

[47] A. Souriau, M. Granet, A tomographic study of the lithosphere beneath the Pyrenees from local and teleseismic data, J. Geophys. Res. 100 (1995) 18117–18134.

[48] O. Tweto, Laramide (Late Cretaceous–Early Tertiary) Orogeny in the Southern Rocky Mountains, Geol. Soc. Am. Mem. 144 (1975) 1–44.

[49] S.J. Vincent, The Sis paleovalley: a record of proximal fluvial sedimentation and drainage basin development in response to Pyrenean mountain building, Sedimentology 48 (2001) 1235–1276.

[50] H.E. Wheeler, Base level, lithosphere surface and time-stratigraphy, Geol. Soc. Am. Bull. 75 (1964) 599–610.

# Influence of piedmont sedimentation on erosion dynamics of an uplifting landscape: An experimental approach

Julien Babault*
Stéphane Bonnet
Alain Crave
Jean Van Den Driessche
Géosciences Rennes, Université de Rennes 1, UMR CNRS 6118, Campus de Beaulieu, 35042 Rennes cedex, France

**ABSTRACT**

**Models of relief development generally assume that eroded products are evacuated far from the landscape, whereas in nature they are often deposited at the foot of mountain belts, within continental environments. Because piedmont aggradation can modify the base level for erosion, we investigate the influence of piedmont sedimentation on the dynamics of an upstream relief. We developed an experimental study of relief dynamics using laboratory-scale models submitted to uplift under runoff-driven erosion. We compare the dynamics of topographies surrounded, or not, by a depositional belt made of eroded products coming from upstream. Piedmont aggradation acts on the dynamics of the upstream relief by modifying the relative uplift rate (applied uplift rate minus aggradation rate) that denudation tends to balance. Relief denudes at a lower rate than the applied uplift rate, so the mean elevation of the uplifting topography rises. When the time scale of aggradation is higher than the time scale of relief development, the topography cannot reach a steady state between denudation and the applied uplift rate as long as aggradation occurs. However, in this case denudation balances a continuously varying relative uplift rate during a dynamic equilibrium phase of the topography.**

**Keywords:** relief dynamics, uplift, erosion, sedimentation, denudation, experimental modeling.

## INTRODUCTION

The relief of mountain belts results from the competing action of tectonic processes that create topography and erosional processes that destroy it. Different models of relief dynamics have been proposed (Davis, 1889; Penck, 1953; Hack, 1960) following the time scale of these processes (Kooi and Beaumont, 1996). Hack (1960) argued that a steady state of the landscape may develop because of a balance between tectonic and erosional processes. The ability of a system to reach a steady state depends on its response time with regard to variation in the external forcing parameters such as tectonics and climate (Kooi and Beaumont, 1996; Tucker and Slingerland, 1997; Whipple, 2001). The steady state of a relief submitted to a constant uplift rate implies constant macroscale geometry of the relief, then constant denudation rates and outward sediment flux.

Mountain ranges are usually bounded by sedimentary basins where eroded products accumulate. Sediment flux to basins depends on the erosional dynamics of the upstream reliefs, and some works have tentatively used the sediment record as a proxy of relief dynamics (Pazzaglia and Brandon, 1996). Conceptual models of relief dynamics have been put forward independent of sedimentary processes within the basins. However, if sedimentation in front of a relief occurs above sea level (referred to in the following as piedmont aggradation), it will modify its dynamics because it will act as an increase of the base level for erosion, defined as the limit between erosion and sedimentation (Wheeler, 1964). The erosional dynamics of mountain belts will therefore be different, depending on the nature of the surrounded sedimentary basins: underfilled or overfilled (e.g., Flemings and Jordan, 1989). Moreover, as a foreland basin commonly evolves from underfilled to overfilled, changes in the base-level elevation control the denudation dynamics during mountain building. Here we investigate how sedimentation influences an upstream relief submitted to uplift by using an experimental approach of erosion dynamics.

## EXPERIMENTAL DESIGN AND PROCEDURE

We use an experimental device to simulate erosion of reliefs submitted to constant uplift and rainfall rates. The device is a modified version of a previous apparatus (Crave et al., 2000; Bonnet and Crave, 2003; Lague et al., 2003). The material eroded is a silica paste made of silica powder (D50 = 10 μm) mixed with water. The silica paste fills a rectangular box (erosion box, size 400 × 600 mm and 500 mm deep) with a moveable base, upward or downward within the box. These movements are driven by a screw and a computer-controlled stepping motor. During an experiment, the base moves upward at a constant rate and pushes the silica paste outside the top of the erosion box at a rate defined as the uplift rate ($U$). The erosion box is located in a rainfall simulator, where four industrial sprinklers deliver a high-pressure water-air mixture. All experiments were run under the same rainfall rate of 120 ± 5 mm/h. During an experimental run, every 30 to 60 min, we stop the uplift and rainfall devices to construct 0.5 mm square-grid digital elevation models. Topographic information is derived from optical stereo data acquired with the Advanced Topometric Sensor developed by the GOM Company.

We present results from three types of experiments (Table 1). Type 1 consists of four runs using different uplift rates. In these experiments the eroded products leave the erosion box (Fig. 1A). In type 2 the addition of a plateau surrounding the top of the erosion box allows the eroded products to deposit at the foot of the raising zone (Fig. 1B). Three

*Corresponding author e-mail: Julien.Babault@univ-rennes1.fr.

TABLE 1. EXPERIMENTAL CONDITIONS AND RESULTS

| Name | Uplift rate (mm/h) | Rainfall rate (mm/h) | Erosion box boundaries (mm) | $\langle h \rangle_{s.s.}$ (mm) | $\langle h \rangle_{s.s.-r}$ (mm) | $\langle h \rangle_{f-s.s.}$ (mm) | $\tau_{topo}$ (min) | $\tau_f$ (min) |
|---|---|---|---|---|---|---|---|---|
| Type 1 experiments | | | | | | | | |
| B4 | 5 | 120 | free | 11.3 | – | – | 95 ± 07 | – |
| B1 | 10 | 120 | free | 18 | – | – | 93 ± 06 | – |
| B6 | 15 | 120 | free | 19.5 | – | – | 98 ± 07 | – |
| B3 | 20 | 120 | free | 31 | – | – | 89 ± 06 | – |
| Type 2 experiments | | | | | | | | |
| P6 | 15 | 120 | plateau 125 | 33.1 | 19 | 14 | – | 107 ± 10 |
| P2 | 15 | 120 | plateau 150 | 44.8 | 19.6 | 25 | – | 247 ± 30 |
| P1 | 15 | 120 | plateau 500 | 55.8* | 18.2* | 52† | – | 513 ± 40 |
| Type 3 experiments | | | | | | | | |
| P5 | 15 | 120 | plateau 250 | 47.8 | 21 | 27 | – | 140 ± 08 |

*Note*: the $\tau_f$ is calculated from an exponential fit of the $\langle h \rangle_f$ curve as $\tau_{topo}$.
*$\langle h \rangle_{dyn.eq.}$ and $\langle h \rangle_{dyn.eq.-r}$ of dynamic equilibrium for $U_r$ = 13.6 mm/h at $t$ = 810 min.
†Estimated value from an exponential fit of the $\langle h \rangle_f$ curve.

experiments were run with the same uplift rate but with different sizes of surrounding plateau. The first phase of type 3 corresponds to type 1, followed by a second phase during which a plateau is added as in type 2 in order to simulate a change in the basin depositional system stage (underfilled to overfilled), a striking characteristic of foreland basins evolution around mountain belts (e.g., Flemings and Jordan, 1989).

## RELIEF DYNAMICS WITHOUT PIEDMONT SEDIMENTATION (TYPE 1 EXPERIMENTS)

When the experiments start, the top surface of the models is approximately flat. As uplift progresses, topographic incisions develop along the four borders of the model and propagate inward until the complete dissection of the initial surface is achieved. Figure 2A shows the typical evolution of the mean elevation $<h>$ during such an experiment. During a first stage, the mean elevation progressively increases, corresponding to the growth phase of the landscape (Lague et al., 2003). In a second stage, the mean elevation stabilizes around a constant value. It defines a macroscale steady state of the relief (Hack, 1960) and implies that the output eroded flux equals the input uplift flux (Fig. 2A). Hereafter we characterize the experiments by using two parameters (Table 1): $<h>_{s.s.}$, the mean elevation at steady state, and $\tau_{topo}$, the characteristic time scale to attain steady state. The value of $\tau_{topo}$ is derived from an exponential fit of the mean elevation data during the growth phase, of the form:

$$<h>_{s.s.} = a + b(1 - e^{-t/\tau}). \quad (1)$$

For four uplift rates we observe a positive threshold-linear relationship between $<h>_{s.s.}$ and $U$ (Fig. 3):

$$<h>_{s.s.} = <h_u> + \tau_u U, \quad (2)$$

with $<h_u>$ = 4.8 mm, and $\tau_u$ = 72 min. The value of $\tau_{topo}$ does not vary significantly with $U$ (Table 1) and is ~94 min. The steady state occurs after ~300 min of erosion (Fig. 2A). The erosional behavior of the models and their dependence with $U$ are similar to those obtained by Lague et al. (2003).

## RELIEF DYNAMICS ASSOCIATED WITH PIEDMONT SEDIMENTATION (TYPE 2 EXPERIMENTS)

### Dynamics of Sedimentation

Piedmont sedimentation of the eroded products does not change the sequence of the relief development with regard to the raising zone. At the outlet of the developing catchments small fans of sediments form that progressively coalesce into a unique larger one, as a natural bajada, surrounding the raising zone (Fig. 1B). As uplift and erosion progress, the fan progrades toward the plateau edge, keeping its mean slope constant (~4°), whereas its apex elevation ($<h>_f$) increases (e.g., Fig. 2B). These dynamics last until the fan reaches the plateau edge, where the particles can leave the system. Then no more aggradation occurs at the plateau edge, whereas sediments still aggrade upslope. This results in a progressive increase of the fan slope up to a threshold slope (~6.5°), for which the whole fan becomes a bypass zone. All the particles that are produced from now on by erosion within the raising zone leave the system, so that $<h>_f$ no longer increases. The $<h>_f$ curve then shows a progressive decrease of the aggradation rate ($U_f$). Three experiments were performed that differ in the size of the deposition zone and hence in the time over which the fan becomes a bypass zone ($\tau_f$, Table 1) and by the final elevation of the fan apexes ($<h>_{f-s.s.}$, Table 1) (Figs. 2B, 2C, 2D). The greater the plateau, the longer the time before $<h>_f$ stabilizes (Fig. 4).

### Relief Dynamics

Aggradation displaces upward the base level for the relief, which then rises at a relative uplift rate ($U_r$) such that $U_r = U - U_f$. Stabilization of $<h>$ is never achieved as long

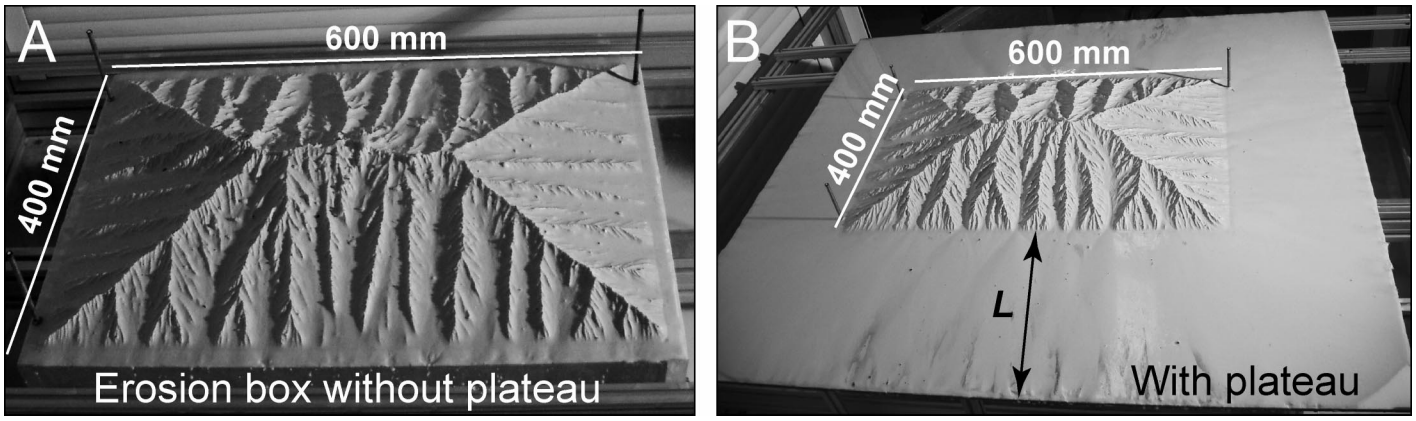


**Figure 1. A: Oblique view of experiment at steady state without piedmont deposition (type 1: experiment B6 at time, $t$ = 360 min). B: Oblique view of experiment at dynamic equilibrium associated with piedmont deposition (type 2: experiment P2 at $t$ = 380 min). Size $L$ of deposition zone is 250 mm.**

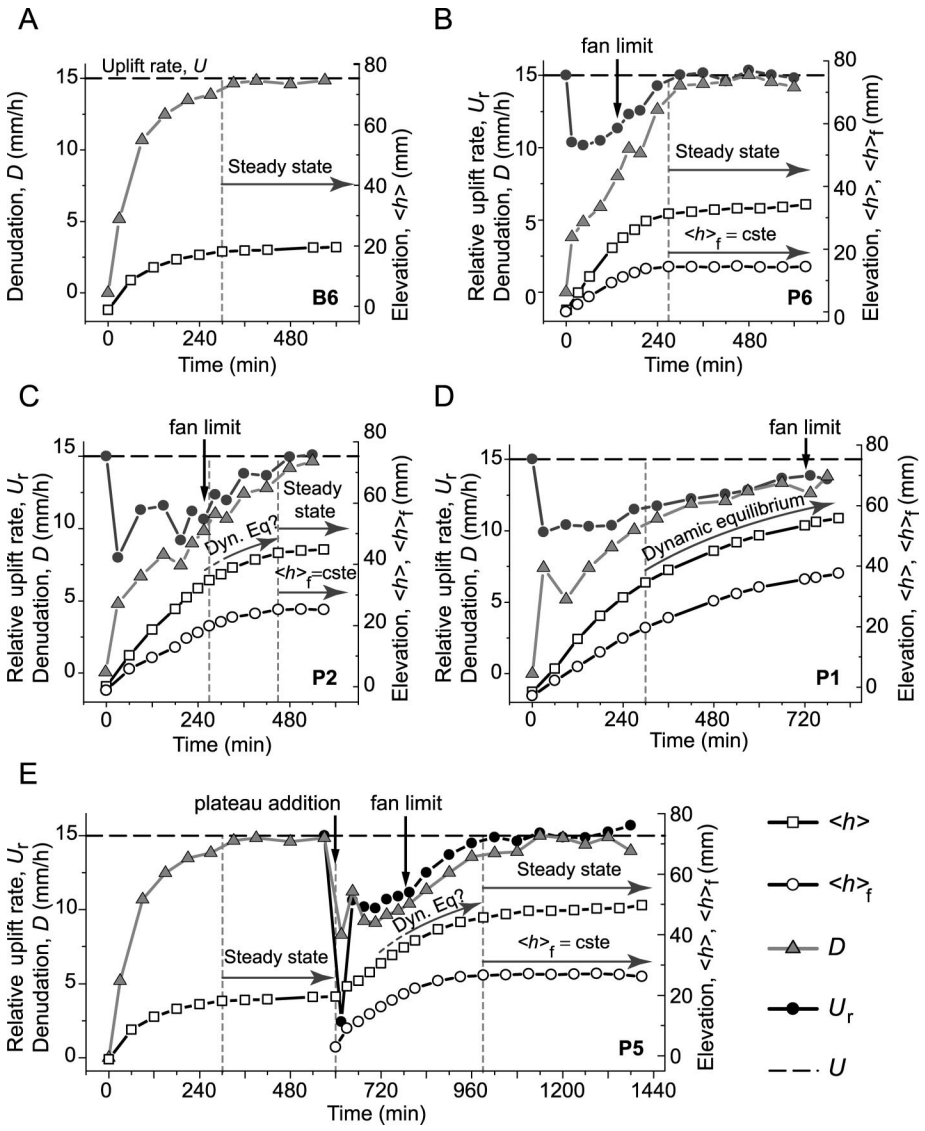


**Figure 2. Graphs showing mean elevation <*h*> of topography and mean fan apex elevation (<*h*>$_f$) evolutions of type 1 (A: B6), type 2 (B: P6; C: P2; D: P1), and type 3 (E: P5) experiments. Experiments evolved with same uplift rate (*U*) of 15 mm/h and rainfall rate of 120 mm/h (Table 1). Steady state is defined by constant mean elevation (cste) of relief through time and by denudation rate (*D*) that equals uplift rate. Dynamic equilibrium (Dyn. Eq.) is defined when denudation rate equals relative uplift rate ($U_r$). Fan limit refers to time fan reaches plateau edge.**

as piedmont aggradation occurs (Fig. 2D), i.e., no steady state is defined according to the mean elevation criteria. As $U_r$ varies depending on a time scale defined by $\tau_f$, and as $<h>_{s.s.}$ depends on the uplift rate (Fig. 3), the gradual change in $U_r$ prevents the development of any steady state. This is the case all along the experiment P1 (Fig. 2D). However, after 300 min the denudation rate balances $U_r$ indicating that the subsequent topographies are at equilibrium (Fig. 2D). From that point onward, denudation and the resulting topography adjust to a continuously changing uplift rate, with imperceptible response time. Such behavior is defined as dynamic equilibrium (Hack, 1960). Note that the time necessary to reach dynamic equilibrium in experiment P1 is nearly the same as the time required for experiments without sedimentation to attain steady state. This suggests that the presence of a sedimentation zone does not influence the drainage network growth, nor the time required for erosion to balance a varying uplift rate (dynamic equilibrium).

By contrast with experiment P1, the fans stop aggrading in experiments P2 and P6. The value of $U_r$ then approaches the uplift rate, and a steady-state topography develops (Figs. 2B, 2C). In these experiments the time to reach steady state depends on $\tau_f$. During experiment P6 this time is roughly the same as $\tau_{topo}$ for experiments without piedmont sedimentation (Figs. 2A, 2B; Table 1), preventing any dynamic equilibrium.

In experiment P2, steady state is reached later than in experiments without sedimentation (450 min compared to 300 min: Figs. 2C, 2A), because $\tau_f$ here exceeds $\tau_{topo}$ (Table 1). Between 300 and 450 min the topography probably evolves under a state close to dynamic equilibrium. Although the denudation rate does not strictly equal $U_r$ (Fig. 2C), both show a similar evolution. For experiment P1, the steady state has not been reached because the required time was too long for the initial volume of silica paste used. As the deposition zone is extensive, $\tau_f$ greatly exceeds $\tau_{topo}$ (Table 1), and the dynamic equilibrium phase lasts a long time, at least 510 min.

For experiments with piedmont sedimentation that reached steady state (P2 and P6), $<h>_{s.s.}$ is far above the $<h>_{s.s.}$ vs. *U* trend defined by equation 2 (Fig. 3). The fan apex elevation being constant, a relative steady state mean elevation ($<h>_{s.s.-r}$) can be defined, such that $<h>_{s.s.-r} = <h>_{s.s.} - <h>_f$. When considering $<h>_{s.s.-r}$, experiments P2 and P6 are close to the trend defined by equation 2. Similarly, the mean elevation of topographies at dynamic equilibrium ($<h>_{dyn.eq.}$) plotted against $U_r$ is far above the trend defined by equation 2 (Fig. 3). However, when considering the relative mean elevation at dynamic equilibrium, $<h>_{dyn.eq.-r} = <h>_{dyn.eq} - <h>_f$, it follows the trend defined by equation 2. Therefore, when denudation balances uplift, the relationship between $<h>_{s.s.-r}$ and *U*, or between $<h>_{dyn.eq.-r}$ and $U_r$ is not altered by the presence of a depositional zone or by the nature of the equilibrium (steady state or dynamic equilibrium).

## RELIEF DYNAMICS PERTURBATION BY EMERGENT PIEDMONT AGGRADATION (TYPE 3 EXPERIMENT)

The first phase of the type 3 experiment corresponds to the type 1 experiment (B6). As soon as a steady state is achieved, a plateau is added, as in type 2 experiments (Fig. 2E). In this case the <*h*> curve shows a two-stage evolution of the relief dynamics. The first stage (from 600 to 990 min) corresponds to the sudden increase of <*h*> just after the addition of the plateau and consequently to the break of the previous steady state. The <*h*> increase implies a decrease in the denudation rate. Topography dynamics during the second stage are similar to those of experiment P2, including a dynamic equilibrium phase. When the fan becomes a bypass zone at 990 min, topography enters a new steady state, for which <*h*> is much higher than for the previous steady state.

## DISCUSSION

A direct application to natural systems is not reliable, as perfect scaling of laboratory-

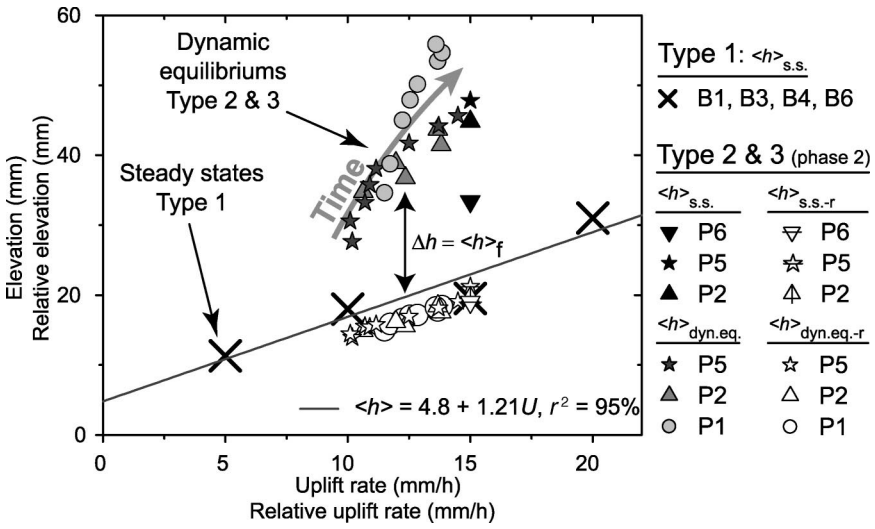


**Figure 3. Absolute (cross and solid symbols) or relative (open symbols) steady state (s.s.) and dynamic equilibrium (dyn. eq.) mean elevations of continuously uplifted zone against absolute (steady-state topographies) or relative uplift rate (dynamic equilibrium topographies). Solid line shows fit of mean elevation of type 1 experiments at steady state against imposed uplift rate.**

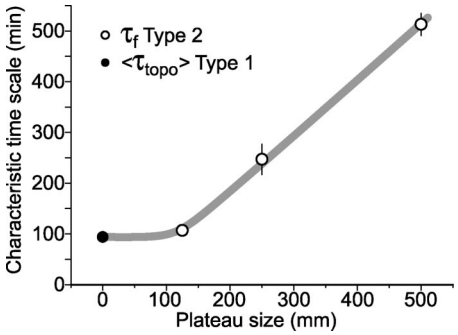


**Figure 4. Mean value of characteristic time scale to attain steady state for type 1 experiments that evolved without piedmont deposition (solid circle) and characteristic time scale of deposition zone to attain stabilization of $\langle h \rangle_f$ (open circle). Data are plotted against size of deposition zone. For plateau size larger than 125 mm, time scale of deposition zone is higher than time scale of relief development. In this case, deposition zone imprints its dynamics to relief, which then evolved under dynamic equilibrium after growth phase of drainage network. Thick gray line indicates general characteristic time scale for uplifted zone to reach steady state whether surrounded by deposit zone or not.**

scale reliefs is nearly impossible (Crave et al., 2000; Hasbargen and Paola, 2000; Lague et al., 2003). However, results from modeling can be used to emphasize general concepts of landscape behavior. The present experiments highlight the importance of the elevation dynamics of the piedmont at the catchment's outlets. The results from this study highlight that erosional dynamics are modified if the time scale of piedmont aggradation is higher than the time scale of relief development. In this case, after a period of drainage network growth, the relief enters a period of dynamic equilibrium. The transition from dynamic equilibrium to steady state occurs only if aggradation stops. Piedmont aggradation can consequently impose its dynamics to a relief submitted to uplift (Fig. 4). Whatever the time scale of processes, the second main effect of piedmont deposition is to shift the elevation of the drainage basins upward because relief denudates at a lower rate than the uplift rate. This results in the increase of the absolute elevation of the whole topography by an amount equal to the mean elevation of the fan apex (Fig. 3), which defines the base level of the upraising relief. The linear relation between the uplift rate and the mean elevation, as observed in experiments without piedmont sedimentation, also applies between the relative uplift rate and the relative mean elevation for experiments with piedmont sedimentation (Fig. 3).

The results of these experiments suggest that in nature piedmont sedimentation may contribute to the very high elevation of mountain peaks that surround high plateaus (e.g., Tibet, Altiplano), and that the transition from underfilled foreland basins to overfilled foreland basins will result in the lowering of the denudation rate of upraising mountain belts without involving any reduction of the tectonic uplift rate.


## ACKNOWLEDGMENTS

We thank Chris Paola and an anonymous reviewer for improving the paper. Special thanks to Jean-Jacques Kermarrec for his help in the development of the experimental apparatus. We also thank Laure and Polo for the all night-long duties during the experiments. Mimi Hill kindly improved the English. Financial support was provided by Centre National de la Recherche Scientifique–National Institute for the Sciences of the Universe (CNRS-INSU) research programs Programme National de Recherche Sol et Erosion and ATI. This study was also supported by the Ministère de l'Education Nationale, de la Recherche et de la Technologie, who funded Babault's Ph.D. thesis.


## REFERENCES CITED


Bonnet, S., and Crave, A., 2003, Landscape response to climate change: Insights from experimental modelling and implications for tectonic versus climatic uplift of topography: Geology, v. 31, p. 123–126.

Crave, A., Lague, D., Davy, P., Kermarrec, J., Sokoutis, S., Bodet, L., and Compagnon, R., 2000, Analogue modelling of relief dynamics: Physics and chemistry of the Earth, part A: Solid Earth and Geodesy, v. 25, p. 549–553.

Davis, W.M., 1889, The geographical cycle: Geographical Journal, v. 14, p. 481–504.

Flemings, P.B., and Jordan, T.E., 1989, A synthetic stratigraphic model of foreland basin development: Journal of Geophysical Research, v. 94, no. B4, p. 3851–3866.

Hack, J.T., 1960, Interpretation of erosional topography in humid temperate regions: American Journal of Science, v. 258, p. 80–97.

Hasbargen, L.E., and Paola, C., 2000, Landscape instability in an experimental drainage basin: Geology, v. 28, p. 1067–1070.

Kooi, H., and Beaumont, C., 1996, Large-scale geomorphology: Classical concepts reconciled and integrated with contemporary ideas via a surface processes model: Journal of Geophysical Research, v. 101, p. 3361–3386.

Lague, D., Crave, A., and Davy, P., 2003, Laboratory experiments simulating the geomorphic response to tectonic uplift: Journal of Geophysical Research, v. 108, p. ETG3.1–ETG3.2.

Pazzaglia, F.J., and Brandon, M.T., 1996, Macrogeomorphic evolution of the post-Triassic Appalachian mountains determined by deconvolution of the offshore basin sedimentary record: Basin Research, v. 8, p. 255–278.

Penck, W., 1953, Morphological analysis of landforms: London, Macmillan, 429 p.

Tucker, G.E., and Slingerland, R., 1997, Drainage basin responses to climate change: Water Resources Research, v. 33, p. 2031–2047.

Wheeler, H.E., 1964, Base level, lithosphere surface and time-stratigraphy: Geological Society of America Bulletin, v. 75, p. 599–610.

Whipple, K.X., 2001, Fluvial landscape response time: How plausible is steady-state denudation: American Journal of Science, v. 301, p. 313–325.



Manuscript received 5 August 2004
Revised manuscript received 17 December 2004
Manuscript accepted 26 December 2004

Printed in USA

# Origin of the highly elevated Pyrenean peneplain

Julien Babault, Jean Van Den Driessche, and Stéphane Bonnet

Géosciences Rennes, UMR CNRS 6118, Université de Rennes 1, Rennes, France

Sébastien Castelltort

Department of Earth Sciences, Eidgenossische Technische Hochschule-Zentrum, Zurich, Switzerland

Alain Crave

Géosciences Rennes, UMR CNRS 6118, Université de Rennes 1, Rennes, France

Received 9 June 2004; revised 5 December 2004; accepted 13 December 2004; published 19 April 2005.

[1] Peneplanation of mountain ranges is generally considered the result of long-term erosional processes that smooth relief and lower elevation near sea level. Therefore peneplain remnants at high elevation in mountain ranges are used to infer posttectonic surface uplift. Such an interpretation has been proposed for the Pyrenees where high-elevation, low-relief erosional surfaces rose up to more than 2000 m. Because the Pyrenean foreland basins are filled with very thick continental deposits, which have buried the early jagged landscape, we challenge this hypothesis by pointing out that relief applanation does not necessarily require elevation lowering. We propose an alternative interpretation in which piedmont aggradation of detrital sediment that comes from erosion of the high chain induces the rise of the base level of the range, therefore reducing strongly the erosive efficiency of the drainage system and resulting in the progressive smoothing of the relief. Such a process allows a high-elevation, low-relief erosional surface to develop at the scale of the range. In the Pyrenees, occurrence of high-elevation, low-relief erosional surface remnants does not imply a posttectonic uplift, but is instead due to the dissection of the initial Miocene high-elevation, low-relief surface by the recent drainage system, the erosive activity of which has been enhanced by global climate change from the late Pliocene onward. **Citation:** Babault, J., J. Van Den Driessche, S. Bonnet, S. Castelltort, and A. Crave (2005), Origin of the highly elevated Pyrenean peneplain, *Tectonics*, *24*, TC2010, doi:10.1029/2004TC001697.

## 1. Introduction

[2] Following the definition of *Davis* [1889], *Bates and Jackson* [1980] define the term "peneplain" as "a low, nearly featureless, gently undulating land surface of considerable area, which presumably has been produced by the processes of long-continued subaerial erosion, almost to base level in the penultimate stage of a humid, fluvial geomorphic cycle." They specify that "peneplain" also denotes "such a surface uplifted to form a plateau and subjected to dissection." This later definition derives from numerous works which have interpreted the occurrence of highly elevated, more or less flat, erosional surfaces in mountain ranges throughout the world as remnants of originally low peneplains, later uplifted and now dissected by the recent drainage network [*de Sitter*, 1952; *Keefer*, 1970; *Blackstone*, 1975; *Scott*, 1975; *Tweto*, 1975]. In this interpretation, peneplanation is thus viewed as a lowering of mean surface elevation and concomitant relief subduing. On the other hand, the occurrence of planation surfaces at high elevation in mountain belts is one of the criteria used to infer their surface uplift and is at the heart of the current debate between the late Cenozoic uplift of modern mountain belts through the world and global climate change [e.g., *England and Molnar*, 1990; *Molnar and England*, 1990; *Zhang et al.*, 2001].

[3] A striking feature of the Pyrenees morphology is the presence of highly elevated, low-relief, erosional surfaces which have been extensively described since the beginning of the last century by numerous geomorphologists and geologists [*Penck*, 1894; *Mengel*, 1910; *Sorres*, 1913; *Panzer*, 1926; *Astre*, 1927; *Nussbaum*, 1931; *Boissevain*, 1934; *Pannekoek*, 1935; *Birot*, 1937; *Goron*, 1941; *de Sitter*, 1952; *Calvet*, 1994]. Late Miocene overlying continental deposits provide an upper age limit for these surfaces [*Birot*, 1937; *Roca*, 1996]. Following previous works [*Boissevain*, 1934; *Birot*, 1937; *Goron*, 1941] *de Sitter* [1952] wrote that "admirably preserved posttectonic erosional leveling surfaces witness to the original low altitude of the folded chain and to later elevation." In other words, in *de Sitter*'s [1952] view, the present-day morphology (and elevation) of the Pyrenees is unrelated to the Palaeogene alpine tectonics that led to crustal thickening in the Pyrenees. To explain the Pyrenean high-elevation, low-relief surfaces, he invoked a Pliocene upheaval contemporary with a phase of tangential compression, though he could not document it. Indeed, there is no evidence of tangential deformation during Pliocene times that could have produced the ~12 km of crustal thickening necessary to induce the 2000 m of Pliocene uplift invoked by *de Sitter* [1952] and more recent works [*Calvet*, 1985; *Brunet*, 1986; *Briais et al.*, 1990;


0278-7407/05/2004TC001697$12.00

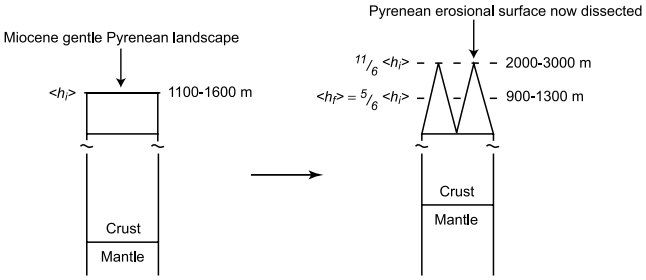


**Figure 1.** Effect of isostatically compensated erosion on the uplift of high-elevation, low-relief remnants. The $h_i$ is the initial mean elevation of a gentle Pyrenean Miocene landscape, and $h_f$ is the mean elevation of the resulting landscape after a post-Miocene dissection, that is, very heterogeneous erosion. Isostatically compensated erosion of *Molnar and England*'s model [1990] predicts a slight decrease of the final mean elevation by five sixths of the initial mean elevation $h_i$ and a rock and Moho uplift equal to $h_i$. Deep incision by streams near to sea level results in a peak elevation of $11/6 \times h_i$, that is, higher than the initial mean elevation. The model implies an already highly elevated, gentle landscape and river incision almost at sea level, which is not the case in the Pyrenees where downstream the course of rivers flow 300 m and 500 m asl on the northern and the southern flank, respectively. The present elevation of the high-elevation, low-relief surfaces (ranging from 2000 m to 3000 m) would require an initial Miocene mean elevation of 900 m to 1300 m, that is, in the same order as the current elevation, implying an unrealistic lack of erosion since the Miocene.

*Calvet*, 1994]. Moreover, Pliocene normal faulting in the eastern Axial Zone of the Pyrenees [*Cabrera et al.*, 1988; *Briais et al.*, 1990; *Carozza and Baize*, 2004] implies local horizontal extension, not compression. An alternative explanation [*Brunet*, 1986] is to consider that the Palaeogene lithospheric root of the Pyrenees was removed from the Neogene, inducing Pliocene uplift. However, the tomographic study of *Souriau and Granet* [1995] shows evidence of a lithospheric root down to 100 km depth beneath the Pyrenees. In addition, *Vacher and Souriau* [2001] have recently shown that the Pyrenean relief is currently overcompensated at crustal level, requiring the presence of a dense crustal root that could be achieved by the transformation of lower crust into the eclogite facies.

[4] *England and Molnar* [1990] observe that the 2000 m uplift of the Pyrenees, as inferred by *de Sitter* [1952] from the remnants elevation of the applanation surface, is overestimated. As this Miocene surface is currently highly dissected, the mean elevation of the chain has necessarily decreased since this epoch, whereas the remnants elevation increased due to isostatic compensation. Following *Molnar and England*'s model [1990], the current remnants elevation, between 2000 m and 3000 m, would require a mean elevation of the Pyrenees of 1100 m to 1600 m before post-Miocene dissection. This is of the same order as the current mean elevation of the chain (1500 m) implying that no erosion occurred since the Miocene, which is unrealistic (Figure 1). Besides the fact that the Miocene elevation of the applanation surface would be already high, isostatically compensated erosion as described by the Molnar and England model could not account for the whole elevation of the high-elevation, low-relief surfaces in the Pyrenees, even less so that it requires deep valley incision near sea level which is not the present case.

[5] In summary, we believe that the interpretation that the high-elevation, low-relief surfaces of the Pyrenees indicate that the chain was lowered and peneplaned before the Pliocene and that this peneplain was later uplifted from the Pliocene onward is wrong. The fundamental reason underlying this misinterpretation is the mistake of equating the destruction of relief with a lowering of the earth's surface, which is just the same mistake as equating the generation of relief with surface uplift as stressed by *England and Molnar* [1990].

[6] We will argue here that, under certain conditions, the rise of the mountain range base level due to massive alluvial sedimentation in foreland basins can considerably reduce the erosive efficiency of the drainage network in the mountain range, resulting in the development of a highly elevated "peneplain" (Figure 2).

[7] We first describe and analyze the present-day characteristics of the morphology of the Pyrenees. In a second step we review the morphologic evolution of the chain since the Eocene with regard to its southern flank, which allows us to propose a model for the development of the high-elevation, low-relief erosional surfaces. We then discuss the timing of the dissection of the high-elevation, low-relief surfaces with particular attention to the capture of the Ebro River by the Mediterranean as it has been assumed to have strongly influenced the present morphology of the southern flank. Finally, we extend the model developed for the southern flank to the entire chain. Our conclusions support the view

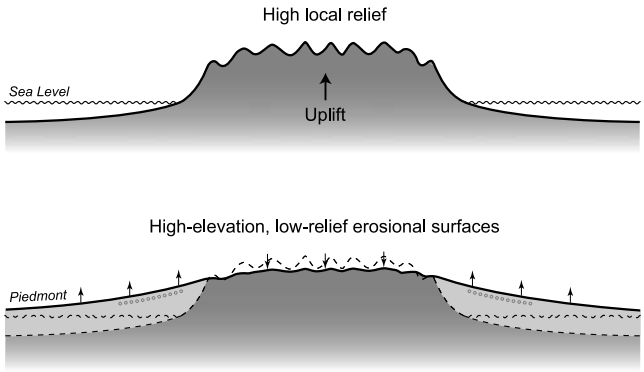


**Figure 2.** Sketch showing the effect of base level rise on the local relief of a mountain range. The change from marine sedimentation to continental sedimentation in foreland basins raises the initial base level of the chain that was corresponding to sea level. The base level rise reduces the local slopes and the erosive efficiency of the transverse rivers that drain the mountain range. By the end of tectonic uplift, the local relief is subdued almost as a peneplain but at an elevation well above sea level.

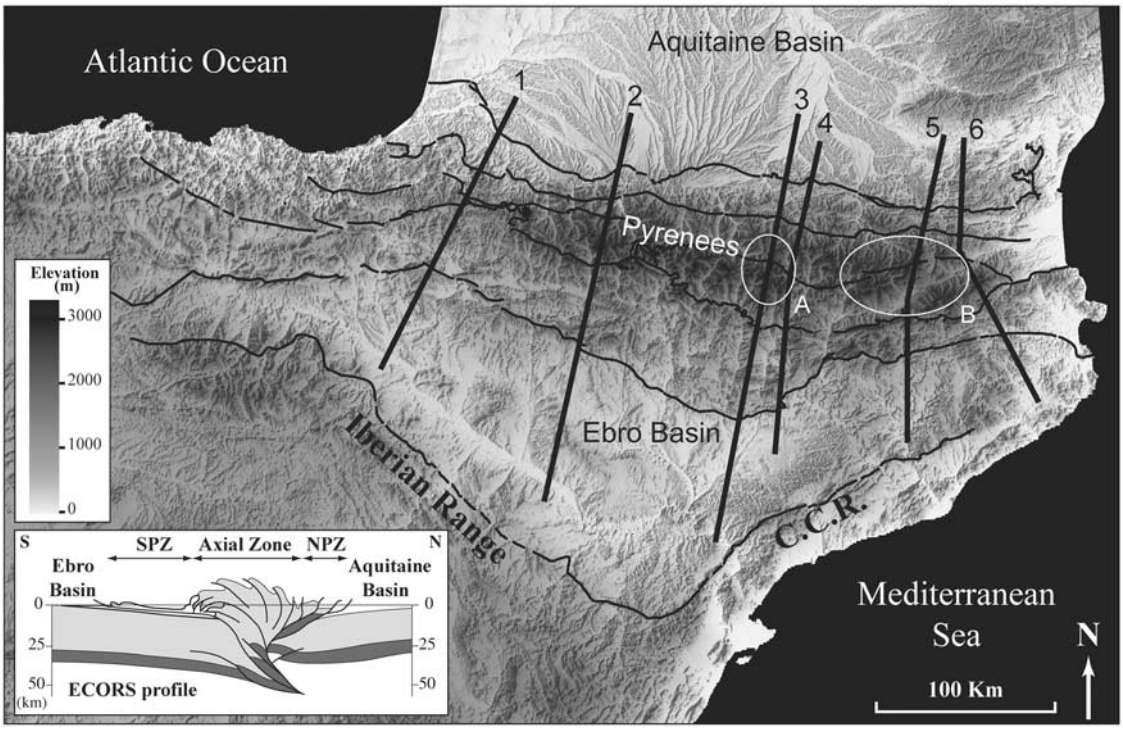


**Figure 3.** Digital elevation model (DEM) of the Pyrenees (from SRTM90 data), the Coastal Catalan Ranges (CCR), and the Iberian Range. The Pyrenees are flanked by the Aquitaine basin to the north and the Ebro basin to the south. The main faults are also represented. The topographic profiles of Figure 5 are distributed all over the Pyrenees and encompass parts of the Aquitaine and Ebro basins. Insert shows *Roure et al.*'s [1989] interpretation of the ECORS profile. NPZ is north Pyrenean zone; SPZ, south Pyrenean zone. Encircled areas are the two most extensive high-elevation, low-relief surfaces: A, Encantats massif; B, Aston, Andorra, and around the Cerdanya and Capcir basins (eastern Pyrenees).

that global climate exerts strong control on mountain morphology.

## 2. Geomorphology of the Pyrenees

### 2.1. General Characteristics

[8] The Pyrenees are a linear mountain range, around 450 km in length, orientated approximately east-west (Figure 3). Its width ranges from 100 km in both the eastern and western parts to 160 km in the central part. The mean elevation in the Axial Zone is about 2000 m in an area 200 km long and 20 km wide (Figure 4a). Elevation of the peaks is around 3000 m, with Pico de Aneto in Aragón (central Spanish Pyrenees) being the highest summit with an altitude of 3404 m. The Pyrenees are flanked by two low-elevation (300–500 m) foreland basins, the Aquitaine plain to the north and the Ebro basin to the south. The transverse

**Figure 4.** Analysis of the local relief of the Pyrenees derived from SRTM90 DEM data. Local relief is calculated by moving a 5 km wide circular search window over the DEM. At each point, the maximum range of elevation values within the window is determined and plotted at the center of the circle. The same method is used to perform the mean elevation by moving a 30 km wide window. (a) The mean elevation value is indicated and represented by lines superimposed on the local relief. The drainage divide between the northern and the southern flank is also reported. The map shows low values of local relief corresponding to low mean elevation and higher values of local relief corresponding to high mean elevation, except in the Encantats and the eastern Pyrenees. The low relief of Cerdanya and Capcir corresponds in part to Neogene and Quaternary depositional flat surfaces of extensional basins lying at 1000 m asl. (b) Rough contours of high-elevation, low-relief erosional surface remnants, such as described in the literature, superimposed on the local relief. Dissection of the initial erosional surface by the recent drainage system has resulted in small high-elevation, low-relief surface remnants of hundreds of square meters to several square kilometers which cannot be represented on the map, explaining the misfit between the contour lines and the local relief data. (c) The local slope map shows that high-elevation, low-relief surface remnants appear as small areas with a local slope less than 11°. See color version of this figure at back of this issue.

profiles (Figure 5) show a slight asymmetry: the southern flank is globally wider and has a lower slope than the northern flank. This asymmetry matches well the known structural asymmetry between the so-called north and south Pyrenean zones [e.g., *Mattauer*, 1968; *Choukroune et al.*, 1989]. The north Pyrenean zone is characterized by steeply dipping crustal thrusts which makes it narrow, whereas the south Pyrenean zone is recognized for its thin-skinned tectonics style that makes it very wide with shallow deformation (Figure 3). This structural and hence morphological asymmetry can eventually be related, at lithospheric scale, to the subduction of the Spanish lithosphere beneath

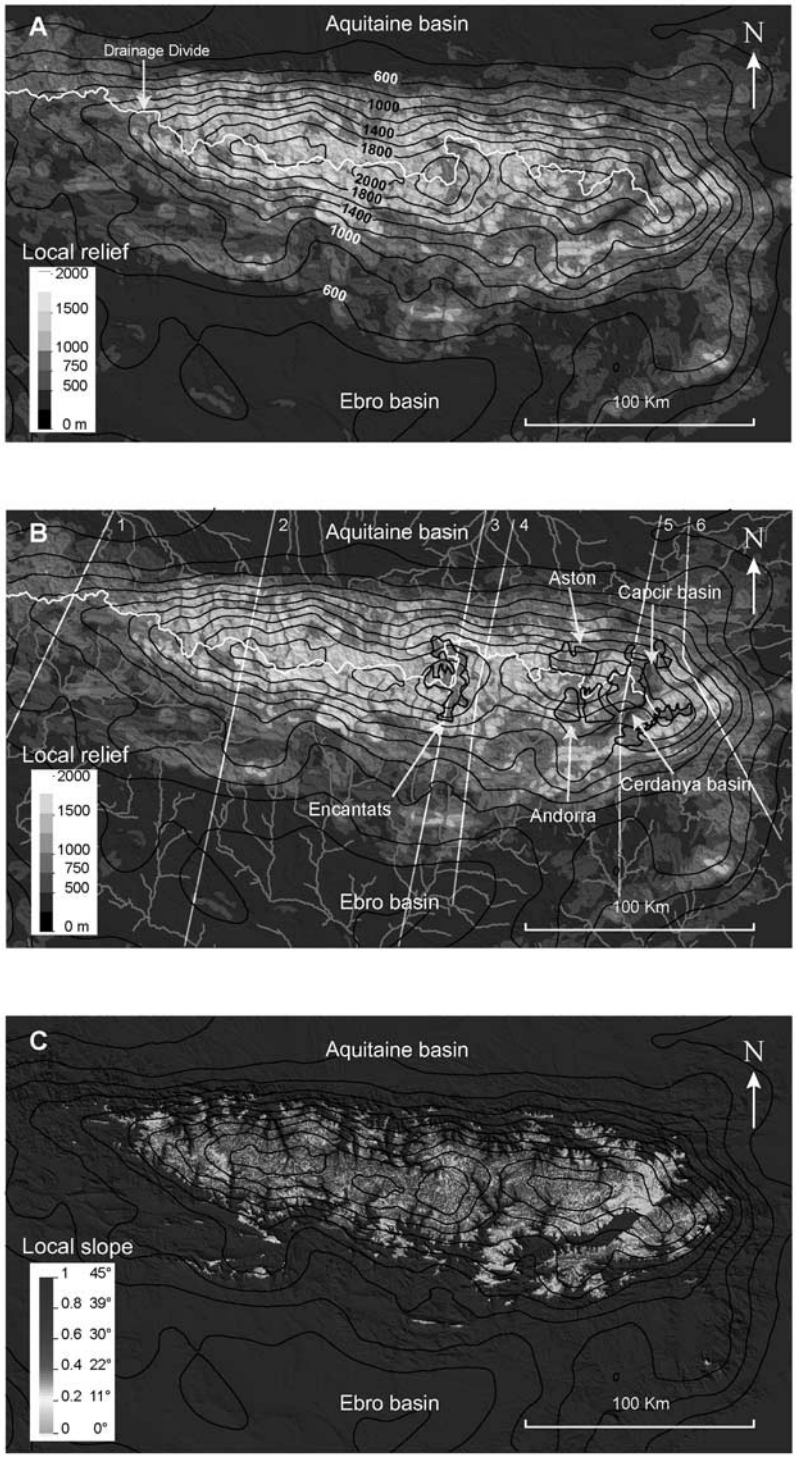


**Figure 4**

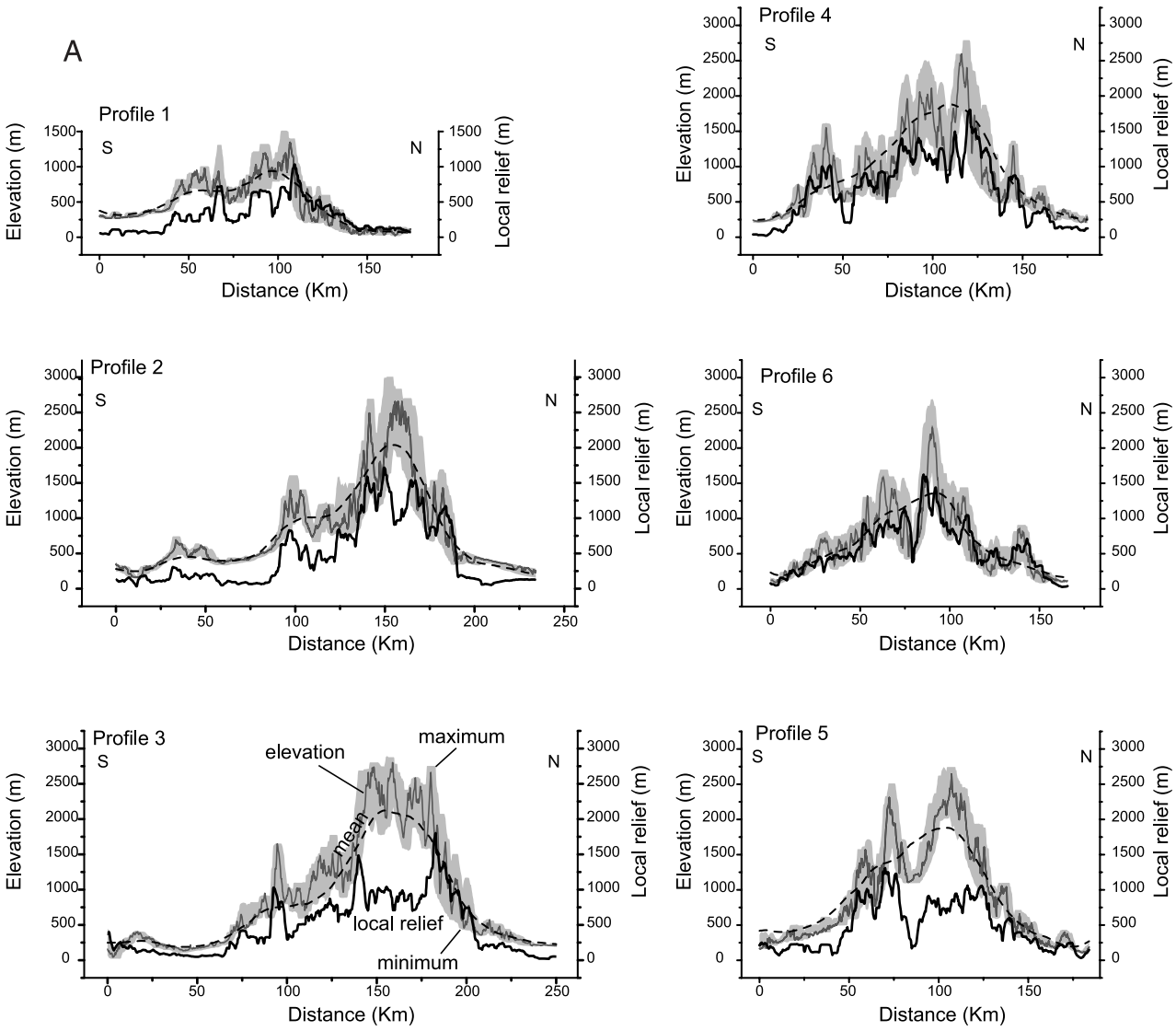


**Figure 5.** (a) Transverse topographic profiles across the Pyrenees (see location in Figure 3). On each profile are plotted the elevation, the maximum elevation, the minimum elevation, the mean elevation and the local relief. The local relief is computed over a 5 km moving window as in Figure 4. Profiles 1, 2, 4 and 6 show a gradual increase of the local relief with the mean elevation and vice versa. This configuration gives a bell-shaped geometry of the profiles. This is not the case for profiles 3 and 5 which cross the high-elevation, low-relief surfaces of the Encantats and the margin of the Cerdanya basin in the eastern Pyrenees. These profiles show a decrease of the local relief in the high chain. Each profile shows maximum and minimum elevations (shading). (b) Relationship between mean elevation and local relief. (left) Idealized sketch showing the relationship between mean elevation and local relief in mountain ranges including (or not including) a high plateau. (right) Where the transversal profiles cut across the high-elevation, low-relief surfaces, the local relief decreases as it does for high plateaus in mountain belts, arguing that the high-elevation, low-relief surfaces represent the remnants of an extensive smooth topography.

the European lithosphere [*Mattauer*, 1985; *Muñoz*, 1992; *Souriau and Granet*, 1995; *Teixell*, 1998].

### 2.2. Pyrenean Highly Elevated "Peneplain"

[9] A striking feature of the morphology of the Pyrenees is the occurrence of high-elevation, low-relief surfaces that have been previously interpreted as remnants of an uplifted peneplain surface [*Boissevain*, 1934; *Birot*, 1937; *Goron*, 1941; *de Sitter*, 1952; *Calvet*, 1985; *Brunet*, 1986; *Briais et al.*, 1990; *Calvet*, 1994]. By high-elevation flat surfaces, we mean a landscape with a smoothed morphology lying at about 2000 m above sea level (asl) (Figure 6), and which

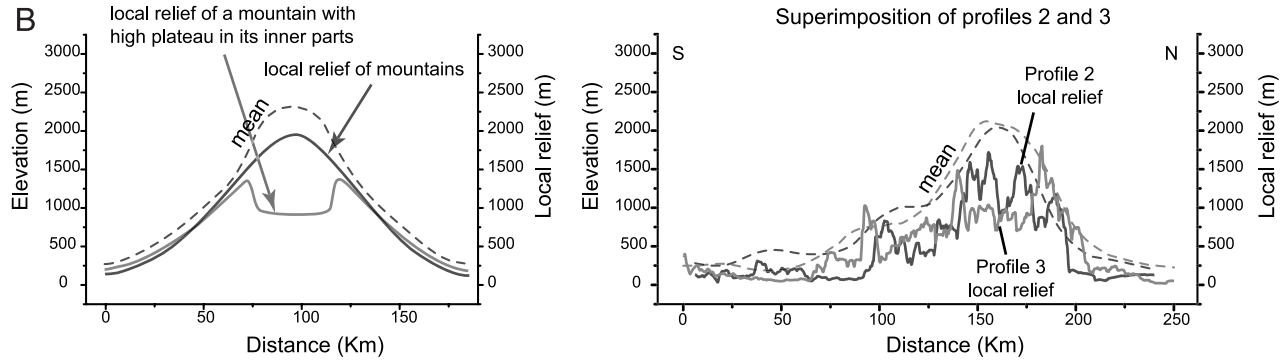


**Figure 5.** (continued)

contrasts with the surrounding jagged relief of peaks and deeply incised valleys.

[10] These remarkable erosional surfaces are located in two main areas, the central Pyrenees (Encantats) and the eastern Pyrenees (Aston, Andorra, around the Cerdanya and the Capcir basins, cf. Figures 3 and 4 and Table 1).

[11] On the basis of previous studies of the last century [*Penck*, 1894; *Mengel*, 1910; *Sorres*, 1913; *Panzer*, 1926; *Astre*, 1927; *Nussbaum*, 1931; *Boissevain*, 1934; *Pannekoek*, 1935; *Birot*, 1937; *de Sitter*, 1952; *Calvet*, 1994] and using GIS methods we mapped these high-elevation surfaces within the Axial Zone. Their extent ranges from tens to hundreds of square kilometers, which corresponds to 10% of the surface of the Axial Zone (Table 1).

#### 2.2.1. Identification of Highly Elevated, Low-Relief Surfaces

[12] Relief analysis has been performed within a moving circular search window over the SRTM 90 m resolution DEM. According to *Ahnert* [1984], the best result is obtained for a 5 km diameter window. At each point, the maximum range of elevation values within the window was determined and plotted at the centre of the window. The mean elevation of the chain has also been analyzed using a moving circular search window but with a larger diameter of 30 km as in the study of *England and Molnar* [1990].

[13] Figure 4a shows that maximum mean elevation is centered in the Axial Zone. The chain is not cylindrical, with its eastern part being larger than its western part as a result of more tectonic shortening in the former [*Roure et al.*, 1989; *Vergés et al.*, 1995; *Teixell*, 1998]. At the scale of the entire range, the local relief increases with the mean elevation, except in the most eastern part where a very low-relief, high-elevation, NE-SW to N-S narrow zone corresponds to the Tertiary grabens of Cerdanya, Capcir and Conflent basins. When reported on the map (Figures 4b), the high-elevation, low-relief surfaces described in the literature show a rather important local relief (750 m ± 250 m), yet contrasting with the rest of the high chain.

[14] In fact, by analyzing the local slopes, these surface remnants appear as small areas (hundreds of square meters to several square kilometers) with local slopes lower than 10° and situated above 1400 m of altitude (Figures 4c).

#### 2.2.2. Transverse Topographic Profiles

[15] Six topographic profiles perpendicular to the trend of the chain have been constructed from west to east (Figure 5a). Profiles 3 and 5 cut the main high-elevation,

**Figure 6.** Example of high-elevation, low-relief remnant: The Plan de Beret (view looking to the northeast). The Plan de Beret is located at the drainage divide between the Noguera Pallaresa flowing toward the Mediterranean via the Ebro River, and the Garonne River flowing toward the Atlantic. The Plan de Beret reaches 1900 m above sea level and is surrounded by peaks, the elevation of which range from 2600 m to 2900 m. The morphology of Plan de Beret looks like a gentle landscape despite its being located in the inner part of the chain.

**Table 1.** Topographic Characteristics of the High-Elevation, Low-Relief Erosional Surfaces[a]

| Region | Elevation Range, m | Mean Elevation, m | Extension, km$^2$ | Mean Local Slope, m/m | Mean Local Relief, m |
|---|---|---|---|---|---|
| Encantats | 1600–3000 | 2310 | 390 | 0.396 (21.5°) | 935 |
| Maladetta | 1960–3030 | 2485 | 26 | 0.416 (22.6°) | 1080 |
| North Cerdanya | 1091–2902 | 2150 | 623 | 0.321 (17.8°) | 875 |
| South Cerdanya | 1315–2902 | 2140 | 163 | 0.344 (19°) | 815 |
| East Capcir | 950–2450 | 1800 | 62 | 0.270 (15.1°) | 832 |
| Aston | 1030–2705 | 1950 | 233 | 0.270 (15.1°) | 1015 |

[a]The cumulated surface of these high-elevation surfaces (about 1500 km$^2$) corresponds to 10% of the surface of the Axial Zone.

low-relief surface remnants. Profile 4 corresponds to the surface profile of the ECORS deep seismic profile. All the profiles have the same characteristic bell-shaped geometry. As expected, the local relief values usually follow the topographic profiles, i.e., increase when elevation increases and vice versa. However, this is not true for profiles 3 and 5 (Figure 5a) where the local relief drastically decreases when the profile cuts the high-elevation, low-relief surfaces. Such a decrease of local relief with increase of mean elevation is also encountered when a high plateau develops in a mountain belt (Figure 5b). This suggests that the small high-elevation, low-relief surfaces encountered today in the Pyrenees may be the remnants of a much more extensive and more or less flat single surface.

### 2.3. Drainage Network

#### 2.3.1. Drainage Pattern

[16] The chain is deeply incised by transverse streams roughly orientated north-south and regularly spaced (20–30 km [*Hovius*, 1996]) as seen on the map in Figure 7.

[17] Most of the drainage on the northern flank is directed to the Atlantic Ocean. The streams situated in the western

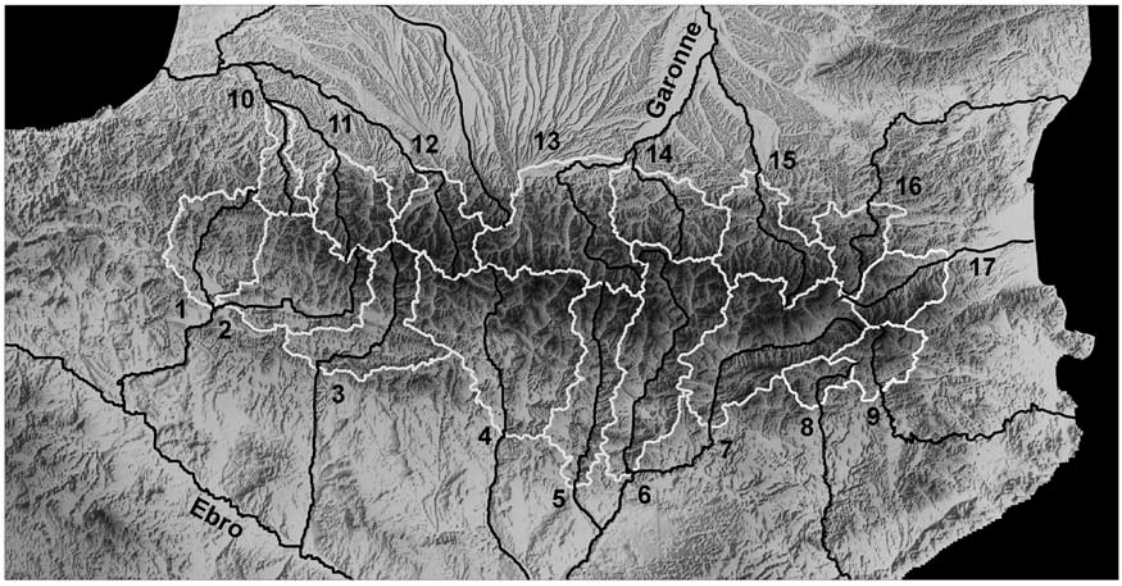


**Figure 7.** Present-day morphology and main catchments of the Pyrenees. The present-day morphology of the Pyrenees is characterized by transverse rivers that deeply incise the high-elevation, low-relief surfaces. The main transverse rivers on the southern flank and from west to east are as follows: Irati (1), Aragon (2), Gallego (3), Cinca (4), Noguera Ribagorzana (5), Noguera Pallaresa (6), Segre (7), Llobregat (8), and Ter (9). The main transverse rivers on the northern flank and from west to east are as follows: Saison (10), Gave d'Aspe herein referred as "Aspe" (11), Gave de Pau referred as "Gavarnie" (12) (because of the location of its spring in the famous Cirque de Gavarnie), Garonne (13), Salat (14), Ariege (15), and Aude (16). On the eastern part of the chain, although the Tet river (17) flows directly into the Mediterranean, we consider that it belongs to the northern flank. Longitudinal profiles of all these streams are performed using the SRTM90 DEM. White lines delimit the main catchments of the Pyrenees. The outlet of the drainage basins corresponds to the morphological outer limits of the north and south Pyrenean zones.

and eastern parts of the northern flank flow directly into the Atlantic Ocean and Mediterranean Sea (e.g., the Aude and Têt rivers, Figure 7) respectively. Drainage organization is different in the central part of the northern flank where transverse streams connect to the Garonne river which then runs a long distance northwestward across the Aquitaine basin before entering the Atlantic Ocean.

[18] The organization of the southern flank drainage is more classic with most of the transverse streams connecting to the longitudinal drainage of the NW-SE directed Ebro River which flows into the Mediterranean. Only in the most eastern part some streams flow directly toward the Mediterranean (e.g., the Llobregat River, Figure 7).

#### 2.3.2. Longitudinal Profiles of Transverse Rivers

[19] Figure 8 shows the longitudinal profiles of the transverse streams that rise near the topographic ridgepole and that flow either directly into the Atlantic Ocean and the Mediterranean Sea or into the Ebro and Garonne rivers. Accordingly with the morphologic and structural asymmetry of the range previously described, the profiles of rivers of the northern flank are systematically more concave and short than profiles of the southern flank (Figure 9a). This difference has to be related to the mean elevation asymmetry.

[20] *Hack* [1957], *Flint* [1974], and others have reported the following relationship between the slope $S$ and drainage area $A$ in channels:

$$S = kA^{-\theta},$$

where $k$ is the steepness index and $\theta$ is the concavity index. We use the concavity index as a measure of the concavity of rivers. This has been achieved for the main transverse rivers as defined above (drainage area $A > 10^8$ m$^2$) and for their tributaries ($1.10^6 < A < 2.10^8$ m$^2$) within the drainage basins delimited in Figure 7. Within each plot in log-diagrams, two linear fits were computed to encompass most of data.

[21] Plots of the concavity indexes measured in this way show that (1) the transverse rivers flowing on the northern flank are more concave than rivers of the southern flank (Figure 9a) as also shown on the longitudinal profiles of Figure 8, (2) tributaries of similar drainage areas show similar concavities irrespective of their location on the northern or the southern flank (Figures 9b and 9c), and (3) the concavity of tributaries increases with the elevation of the tributary (Figure 9c).

### 2.4. Present-Day Morphology of the Pyrenees: Discussion

[22] As mentioned before, morphological asymmetry at the scale of the entire chain, as revealed by mean elevation analysis, can be related to the northward subduction of the Iberian lithosphere beneath the European plate following *Willett and Brandon*'s [2002] model. Drainage network analysis also shows a slight difference in the concavity of the main transverse rivers between the two sides of the chain. Such a difference may be related to the regional slope between the two flanks of the chain just at the onset of the postorogenic decay. This will imply no significant difference in the incision rate of the main transverse rivers on both flanks, so that the initial asymmetry is preserved.

[23] In an alternative explanation to this general asymmetry, the influence of higher precipitation rates on the northern side to that on the southern one [e.g., *Hovius*, 2000] can be considered. Indeed, this contrast between a very humid northern side and an almost dry southern side is a well known characteristic of the Pyrenean climate of today, and is also well documented in the meteorological survey reports [*Météo-France*, 1987].

[24] However, the similarity of concavity indexes for the tributaries on both sides of the mountain range suggests no significant difference of erosional processes on both flanks and no link with particular climatic conditions specific to one or the other side. In summary, it is therefore more reasonable to attribute the large-scale asymmetry of the Pyrenees to the well known crustal and lithospheric structural asymmetry due to Pyrenean tectonics.

[25] One unexplained though striking feature of the Pyrenean morphology is the presence of high-elevation, low-relief erosional surfaces, mostly situated in the Axial Zone. These surfaces are highly dissected by Quaternary glacial and fluvial erosion. While several hypotheses have been proposed to explain the presence of such surfaces, their origin can still be debated. In the following, we present geological and geomorphologic constraints that allow us to draw an attempt to solve this problem by investigating the geological and morphological evolution of the southern flank of the Pyrenees since the Cenozoic.

## 3. Morphological Evolution of the Southern Pyrenees During the Cenozoic

[26] During early to middle Eocene times, the southern foreland basin of the Pyrenees was an E-W elongated narrow trough that was open toward the Atlantic Ocean allowing the dispersal of sediments supplied from the Axial Zone [e.g., *Puigdefàbregas and Souquet*, 1986; *Mutti et al.*, 1988; *Puigdefàbregas et al.*, 1992]. Further shortening and thickening afterward resulted in the southward and westward migration of the basin depocenter and the progressive deformation and exhumation of the basin northern margin. This period is characterized by both longitudinal and transverse inland drainage on the southern flank [*Nijman*, 1998; *Vincent*, 2001].

[27] Because of coeval southward migration of the deformation and sediment supply increase, the entire basin was rapidly filled from the late Eocene onward, thus entering a long period of continental sedimentation [e.g., *Birot*, 1937; *Reille*, 1971; *Séguret*, 1972; *Riba et al.*, 1983]. At the same time, the initial connection with the Atlantic Ocean closed and the basin drainage became internal [e.g., *Birot*, 1937; *Reille*, 1971; *Riba et al.*, 1983]. This resulted in the burying of the relief in the foreland fold and thrust belt developed during the Eocene period of external drainage which can be observed in a series of particularly well exposed Eocene transverse fluvial paleovalleys filled with Eocene alluvial sediments [e.g., *Birot*, 1937; *Reille*, 1971; *Vincent*, 2001] (e.g., Sierra de Sis paleovalley, Figure 10a).

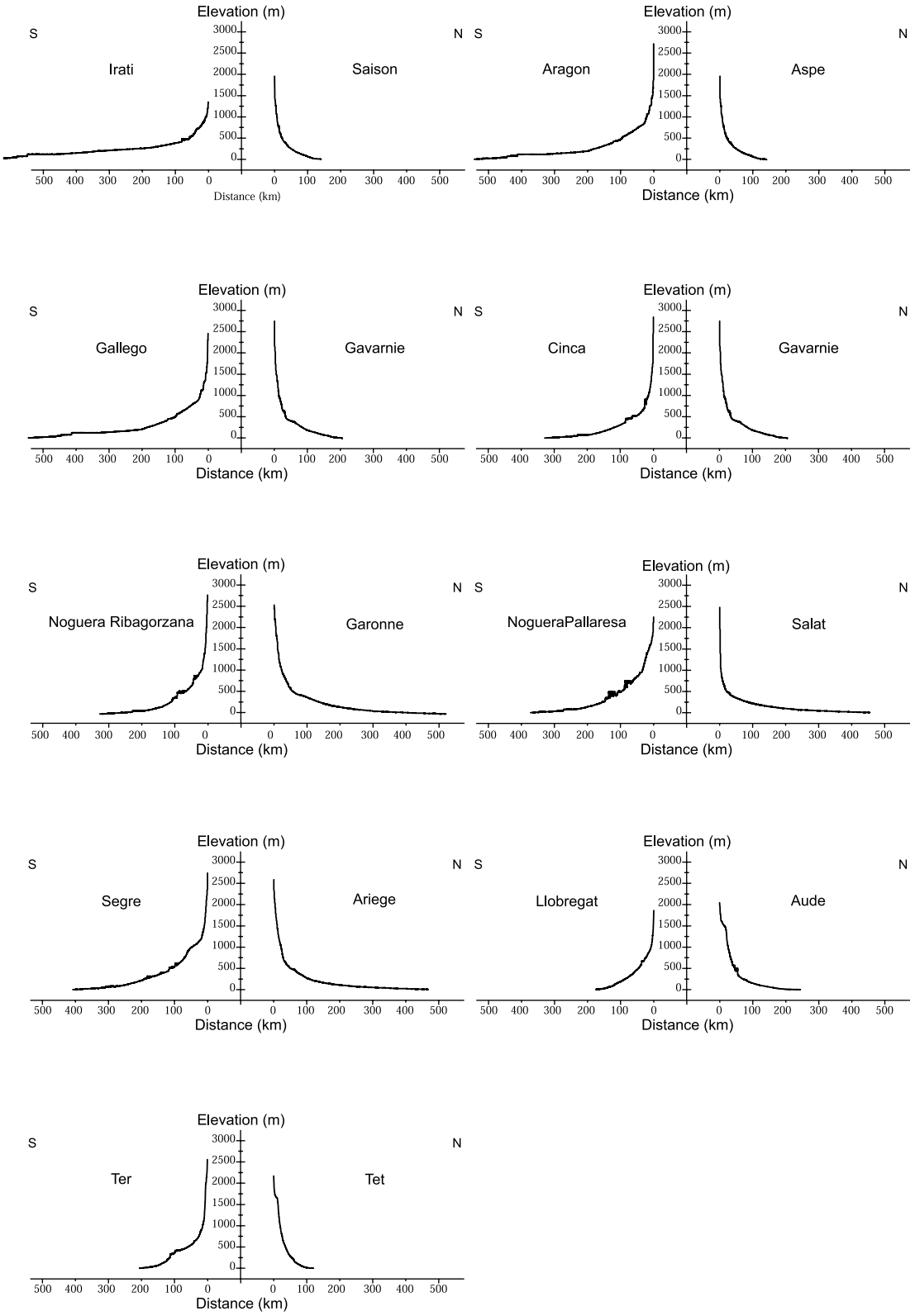


**Figure 8.** Longitudinal profiles of the main transverses rivers of the Pyrenees. For convenience we compare the northern and southern main transverse river profiles with ridgepole as the origin. The northern rivers are more concave than the southern ones matching the asymmetry of both the structure and the topographic profiles and of the chain, as described in Figures 3 and 5, respectively. See Figure 7 for location of the main transversal streams.

This phenomenon was probably amplified by the fact that this former foreland fold and thrust belt was then transported as piggyback subbasins on the top of southward propagating external thrust sheets, which enhanced subsidence and the trapping of sediments.

[28] *Coney et al.* [1996] summarize this story well as follows: the southern flank "was progressively buried, back to and overlapping the southern margin of the axial zone, in up to 3 km of massive continental fluvial-alluvial deposits." A fundamental observation is that at present, the remnants of subhorizontal uppermost top-wedge alluvial deposits outcrop at an elevation of up to 2000 m where they merge into the highly elevated, low-relief erosional surfaces of the Axial Zone [*Coney et al.*, 1996]. The maximum elevation of these deposits is about 1100 m asl along the frontal thrust of the south Pyrenean zone (Figure 10b) indicating the rise of the southern Pyrenees base level.

[29] After this burying, when and why the reexcavation of the southern flank started remains debated. For most authors [*Birot*, 1937; *Reille*, 1971; *Coney et al.*, 1996; *Garcia-Castellanos et al.*, 2003], reexcavation was induced by the capture of the Ebro River by the Mediterranean Sea, resulting in new external drainage of the Ebro foreland basin. Miocene extensional tectonics within the Catalan chain or dramatic sea level drop of the Mediterranean during the Messinian, or a combination of both, have been invoked to explain this capture [e.g., *Nelson and Maldonado*, 1990; *Coney et al.*, 1996]. Therefore, depending on which of these processes is considered to have been predominant, different ages have been proposed for the capture. Miocene or Quaternary climatic changes have also been considered to be of primary importance in the building of the present jagged relief [e.g., *Nelson*, 1990; *Coney et al.*, 1996; *Garcia-Castellanos et al.*, 2003]. In the following we will tentatively argue that the Ebro River was not connected to the Mediterranean before the Pliocene. In any case, the Ebro foreland basin and in particular the top-wedge basin, suffered strong erosion since the Pliocene, leaving remnants of Eocene to Miocene continental deposits all along the southern flank of the Pyrenees.

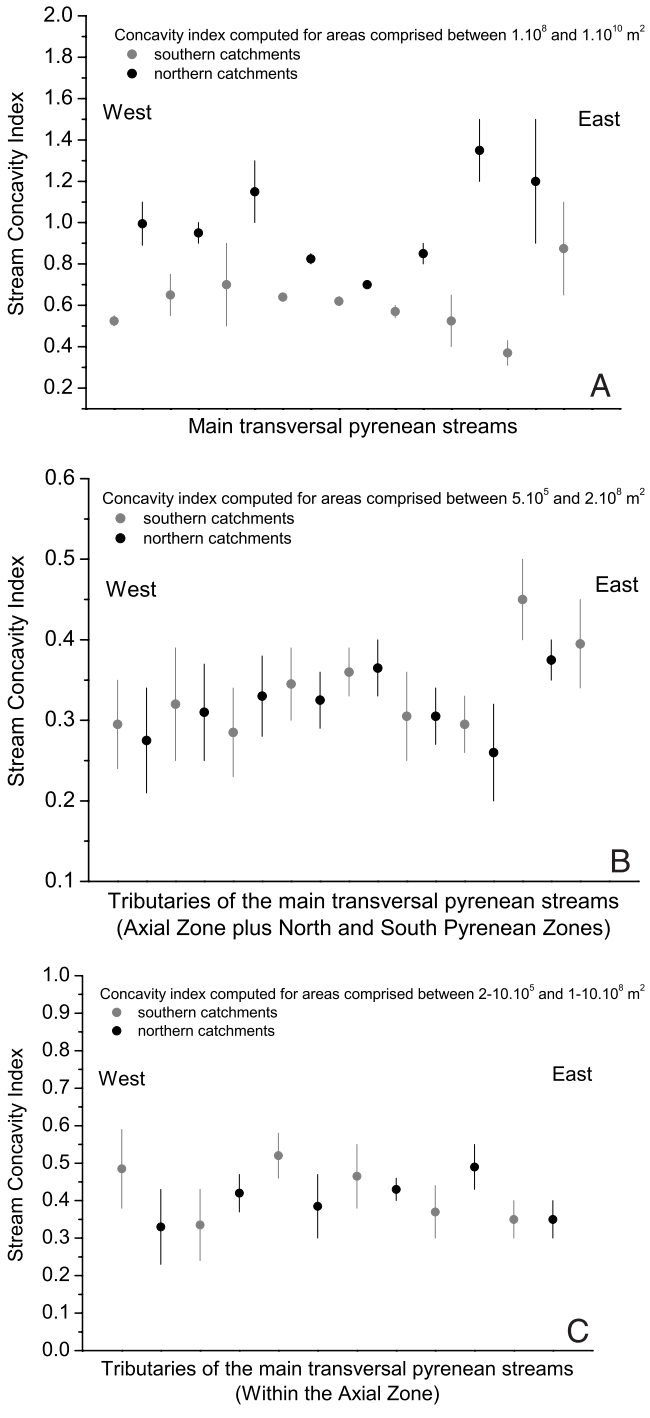


**Figure 9.** Concavity profiles of the main transverse rivers and their tributaries. Using the slope area relationship we computed the concavity indices for all the mainstreams and their tributaries. (a) The drainage area and local slope value along the main transversal streams were computed using the steepest-slope criteria. The concavity index analysis shows the higher concavity for the northern flank main rivers, that is, for drainage area values higher than $10^8$ m$^2$. (b) The concavity index of all the tributaries is determined by analyzing the slope variation for drainage areas ranging from $5 \times 10^5$ m$^2$ to $10^8$ m$^2$ within the whole area covered by the main drainage basins drawn in Figure 7. The main basin outlets correspond to the morphological fronts of the north and south Pyrenean zones. (c) Subbasins concavity indexes have been performed for parts of the main basins located within the Axial Zone. Whatever their location on the northern or on the southern flank of the Pyrenees, the tributaries have a similar concavity index. Figure 9c shows that the concavity indexes are higher in the high chain than in the rest of the range.

## 4. How Did the High-Elevation, Low-Relief Erosional Surfaces Develop?: A High-Elevation Peneplanation Model

[30] In the classical "geographical cycle" of *Davis* [1889], landscape maturity is reached after orogenic uplift

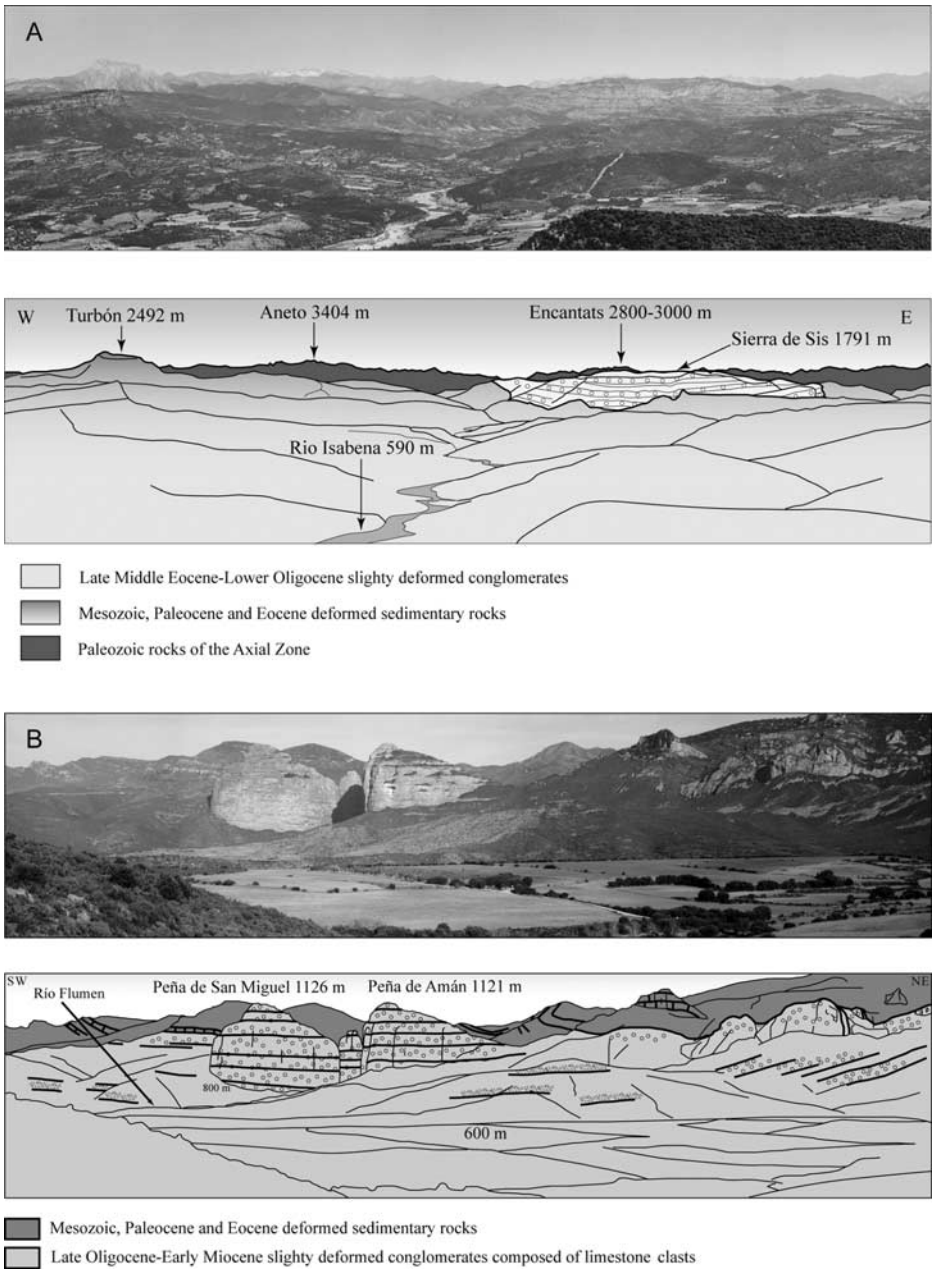


**Figure 10.** (a) Panorama looking to the north of the south Pyrenees showing N-S directed late Eocene-Oligocene paleovalley (Sierra de Sis). The late Eocene-Oligocene paleovalley is filled with alluvial conglomerates reaching nearly 1800 m asl. The Sierra de Sis conglomerate form a linear body extending up to 20 km long and 5 km wide. The picture is taken from a promontory made of the same undeformed conglomerates. Before dissection, the valley of the Rio Isabena was most probably looking like a bajada overlapping the southern margin of the Axial Zone up to 2000 m, or even higher, in the background and sloping down to 1000 m or more in the foreground. At the foot of the Sierra de Sis, the Rio Isabena reaches an elevation of 750 m implying about 1000 m of dissection. (b) View looking to the northwest of the early Miocene conglomerates of the Salto de Roldán (northern margin of the Ebro basin, north of Huesca). The conglomerates, which correspond to proximal fan delta and mass flow deposits, uncomformably overlie deformed Mesozoic, Paleocene and Eocene sedimentary rocks. They form spectacular high cliffs towering above the Ebro basin depression whose elevation ranges from around 300 – 500 m. The elevation of the conglomerates reaches 1120 m. (c) Eocene paleorelief buried by Oligocene conglomerates (Olvena, northeast of Barbastro). Oligocene conglomerates fill in a structural paleorelief that formed during folding of late Cretaceous limestones. Growth strata at the base show that folding was partly synsedimentary. See color version of this figure at back of this issue.

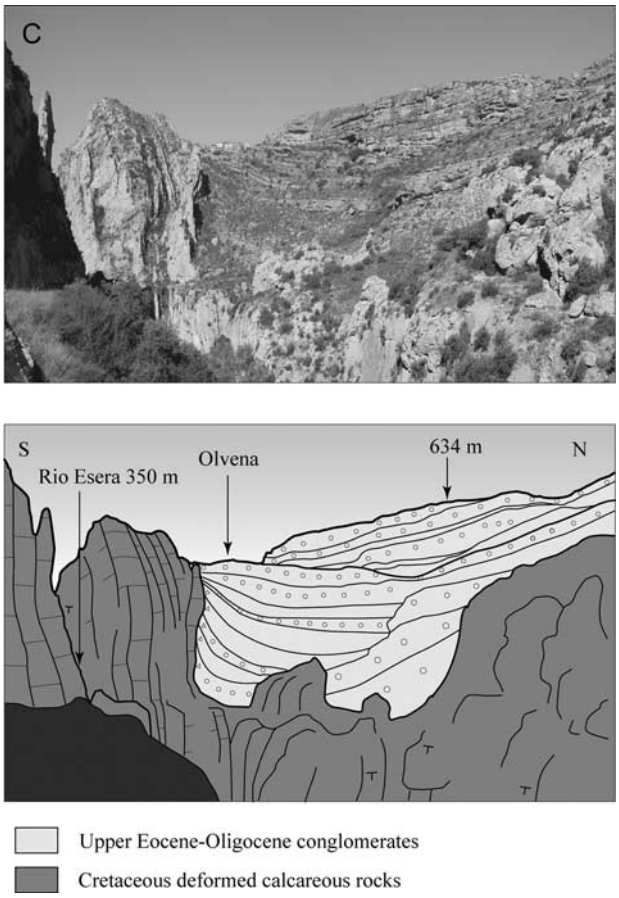


**Figure 10.** (continued)

when the valleys have reached maximum relief. Then, as degradation occurs, both relief and mean elevation are gradually reduced. At the end of the cycle, the landscape has been degraded to a surface of very low relief near base level called a "peneplain." In others words the decrease of the mean elevation toward sea level is accompanied by a progressive smoothing of the landscape. In this model, the sea level is viewed as the ultimate base level to which the landscape eventually grades. In this paper we further this idea by proposing that the same effect can result from a rise of base level (Figure 2). In particular, this can be expected at the front of mountain belts when foreland basins become closed and progressively filled with sediments. In such a case, internal drainage results in a general rise of the base level in the foreland basin and in considerable continental sedimentation. This is exactly what happened for the southern flank of the Pyrenees and the entire Ebro basin. The fluvial valleys developed on the southern flank of the Pyrenees during the period of external drainage were then rapidly filled when the Ebro foreland basin became internal, with the aggradation of sediments far inland the mountain range witnessing a large base level rise. We suggest here that before its recent excavation, the Pyrenean southern flank looked like a large-scale E-W elongated smoothed half-dome, at the top of which Paleozoic basement and minor Mesozoic sedimentary cover were outcropping, surrounded by Tertiary detrital sediments. We develop in the following two types of arguments that lead us to this conclusion.

### 4.1. Present Slight Difference in Elevation Between the Axial Zone and the Top of the Detrital Series is Inherited From the Internal Drainage Stage

[31] The unusual slight difference between the elevation of the Axial Zone summit and the Ebro foreland basin top-wedge at present cannot be entirely explained by the recent rejuvenation of the relief because this would assume much more erosion of the former. Indeed, the effect of recent rejuvenation can easily be distinguished when looking at the geomorphology of the Cerdanya region (Figure 11a). Cerdanya corresponds to a Miocene half-graben bounded to the south by a north dipping normal fault zone. The graben is filled by detrital continental sediments which overlap the basement to the north. Sedimentological analysis of the basin fill reveals the development of shallow ponds, swampy zones, and lacustrine paleoenvironment [*Cabrera et al.*, 1988; *Roca*, 1996]. All together, those observations suggest internal drainage of the graben. The fine-grained nature of most of the deposits also suggests that the surrounding summits were not very high with regard to the basin base level. At present, the erosional surface on top of the basement shows a gentle southward dipping slope of about 10° [*Briais et al.*, 1990] (0.17 m/m, Figure 11b) which was induced by Miocene tilting along the southern boundary fault. Therefore this surface was subhorizontal before the Miocene. This surface is now incised by the current drainage network (Figure 11c). It consists of a main longitudinal drain, the Segre River which is flowing southwestward, and several transverse tributaries on each side of the trough. In fact neither these tributaries nor the uppermost course of the Segre River do incise strongly the sedimentary basin fill and underlying basement. Both the

**Figure 11.** (a) Topography of the Eastern Pyrenees (SRTM90 DEM data) including the Cerdanya, Capcir, and Conflent intermontane basins. Black lines delimit the three main catchments drained respectively by the Segre, Aude and Têt rivers. Maximum elevation in the Miocene half graben of Cerdanya is about 1000 m. (b) The local slope map shows that north of Cerdanya and west of Capcir, extensive remnants of the Miocene erosional surface are preserved that show a slope of about 10° toward the S-SE. (c) Local geophysical relief highlighting the dissection of the high-elevation, low-relief surfaces and the margins of the Cerdanya Basin. It consists of the difference between two surfaces: a smooth surface that fits all the ridges and summits of tributaries of the Segre, Aude and Têt rivers and the current topography itself [e.g., *Abbott et al.*, 1997; *Small and Anderson*, 1998]. Deep incision develops on both southwestern and northeastern edges of the Cerdanya trough, contrasting with its rather gentle slopes (see text for further explanation).

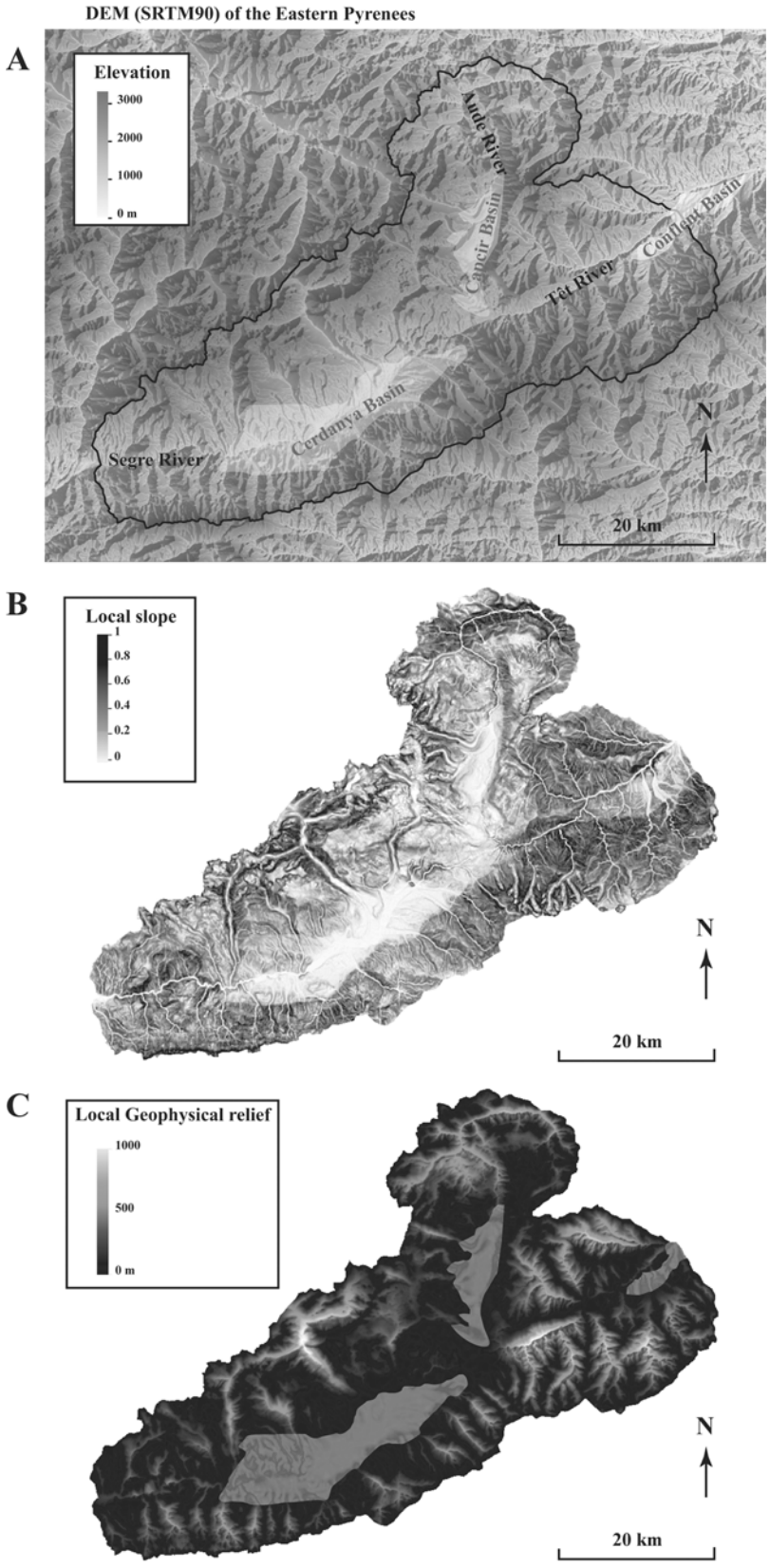
DEM (SRTM90) of the Eastern Pyrenees
A
Elevation
3000
2000
1000
0 m
Aude River
Capcir Basin
Têt River
Conflent Basin
Cerdanya Basin
Segre River
N
20 km
B
Local slope
1
0.8
0.6
0.4
0.2
0
N
20 km
C
Local Geophysical relief
1000
500
0 m
N
20 km

**Figure 11**

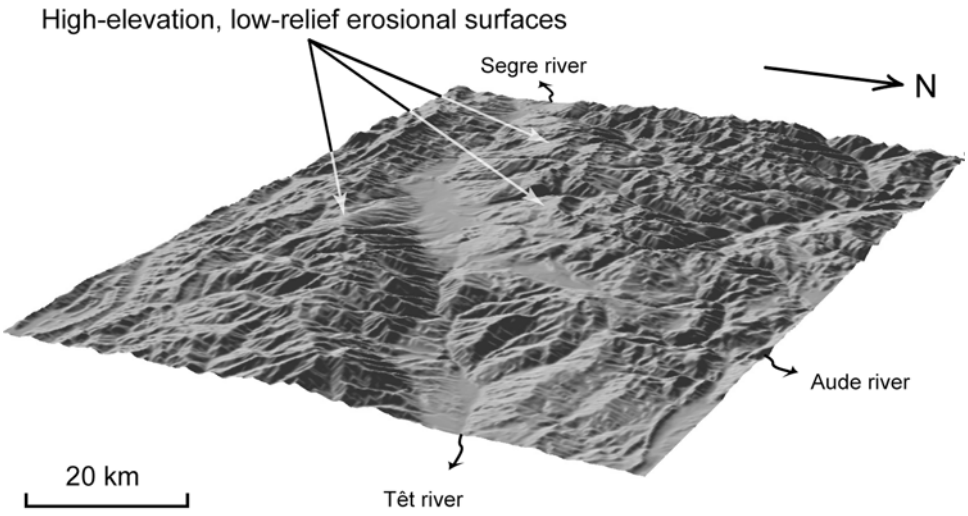


**Figure 12.** Three-dimensional view looking to the southwest of the Eastern Pyrenees showing high-elevation, low-relief surface remnants of the Miocene erosional surface. The remnants of the Miocene erosional surface are incised by the tributaries of the Segre. Note the knickpoint of the Têt river, at the northeastern edge of the Cerdanya Basin (similar knickpoint occurs along the Segre river, at the southwestern edge of the Cerdanya Basin, in the background. (No vertical exaggeration.)

Segre River and the Têt River begin to incise dramatically when they leave the Cerdanya trough at its southwestern and northeastern edges, respectively. In others words, the Cerdanya trough appears as an area mostly preserved from erosion by the current rivers, the Segre and the Têt rivers, whose longitudinal profiles display huge knick points when approaching the Cerdanya trough (Figures 8 and 12). A remarkable geomorphologic feature of this area is the contrast of relief and roughness of the valley sides observed between outside and within the Cerdanya area. Where the Segre and the Têt rivers leave the Cerdanya basin and begin to form deep valleys in the basement, the valley sides become strongly incised by their tributaries (Figures 11c and 12). This results from the fact that in this area the difference of local relief between the borders of the Cerdanya basin and valley sides of the Segre and Têt is directly related to the difference of base level position in both areas.

[32] This example can be viewed as a small-scale example of what happened at the scale of the Pyrenees (their southern flank at least) when the base level was much higher and Eocene valleys where filled with sediments. We therefore conclude that before the rejuvenation of the relief by the present drainage network, landscape in the Axial Zone was probably poorly incised and looking rather smooth because denudation was relative to a much higher base level. This implies (1) that the slight difference observed today between the mean elevation of the Axial zone and the top of the Tertiary detrital series cannot be attributed to the much more intense erosion of the Axial Zone during the recent period of relief rejuvenation, and (2) that high-elevation, low-relief surfaces were already present during Miocene times.

[33] In the Maladeta massif, *Fitzgerald et al.* [1999] have argued for a recent exhumation of about 2–3 km since the late Miocene. In this area, high-elevation, low-relief erosional surfaces lie between 2000 to 2600 m asl, whereas the uppermost Oligocene detrital series, located 20 km farther to the south, reaches an altitude of 1800 m. The maximum exhumation estimate was deduced from radiometric dating of samples located in a valley at an elevation of 1100 m. As quoted by *Fitzgerald et al.* [1999], "the present-day topographic form of the Pyrenees is largely a relict of the topography that formed in the Eocene and Oligocene." Hence their estimate only refers to exhumation in relation with recent valley incision. Their conclusions therefore do not hold for the whole area, and in particular for the area where high-elevation, low-relief surfaces are preserved. If their conclusions were valid for the whole area, this would imply that most of the detrital deposits of the Sis paleovalley would have been eroded. According to *Vincent* [2001], only 400 m were eroded on the top of the Sis paleovalley since the Oligocene-Miocene. Finally, *Fitzgerald et al.* [1999] also state that their exhumation model describes the recent rejuvenation of the southern flank, including the dissection of a previous highly elevated peneplain, which reinforces the idea we develop here.

### 4.2. Base Level Rise as a Cause for Relief Decrease Between the Axial Zone Summits (Mean of Peak Elevations) and the Top of the Detrital Series

[34] There is no doubt that the base level of the Pyrenean southern flank has dramatically risen since the closure of the Ebro basin. Huge discharge of continental detrital sediments, especially conglomerates, has back-stepped toward the chain, onlapping previously deformed basement. Conglomerates filled the paleovalleys which developed during the period of external drainage. Some of them, such as the

Sis valley, were up to 800 m deep, suggesting jagged relief on the southern flank during the period of external drainage. However the morphology of certain paleovalleys appears to have been controlled by large-scale folds so that the valley depth does not reflect vertical incision (Figure 10c). Moreover, the conglomerates that now fill these paleovalleys do not seem to have eroded the floor and walls much, they simply overlap them.

[35] However, the fact that the base level rose, does not imply that the relief between the Axial Zone summit and the top of the detrital series was decreasing, a requisite condition to smooth relief roughness. According to most authors [*Séguret*, 1972; *Choukroune et al.*, 1989] the main phase of tectonic shortening in the Pyrenees occurs during Eocene times and a second minor phase develops during the Oligocene in the most external parts of the chain. So, tectonic uplift was paroxysmal during Eocene times, and it can be reasonably expected that the chain reached its maximum elevation by the end of the Eocene. In a similar way, it can be expected that from the Oligocene onward, the mean elevation of the chain was progressively decreasing as tectonic uplift vanished. Continuation of continental sedimentation on the top of the previous Eocene top-wedge basin shows that the local base level of the Pyrenean southern flank was at least as high during the Oligocene and the Miocene as it was at the end of the Eocene. As the top of the detrital series overlaps the Axial Zone, if subsidence were to have occurred, inducing a decrease of the local base level elevation, it would have resulted in a similar effect for the elevation of the Axial Zone. Therefore, from the Oligocene onward, the relief between the Axial Zone summit and the top of the sediments was most probably decreasing, a process that will have strengthened during Miocene times as continental sedimentation still lasts. This results in the progressive smoothing of the relief roughness in the Axial Zone and the development of high-elevation, low-relief erosional surfaces.

[36] Finally, we cannot exclude the possibility that such a process initiated during Eocene times, when huge amount of conglomerates start to sediment. Indeed, as far as the surface elevation as defined by *England and Molnar* [1990], could be considered it was roughly constant during Eocene times, with the rapid filling of the initial marine foreland basin reflecting the rise of the southern flank base level as a whole. This relative relief decrease between the high chain and the sedimentary wedge could have therefore initiated the decrease of the local relief within the Axial Zone as soon as the mid-Eocene.

## 5. When Does the Dissection of the High-Elevation, Low-Relief Surfaces Begin?

[37] As discussed before, high-elevation, low-relief erosional surfaces in the Pyrenean southern flank are remnants of a smooth landscape that has been rejuvenated by a recent drainage network. Several explanations have been proposed to account for this rejuvenation (see above). Among them, the new connection of the Ebro River to the Mediterranean has been invoked, which is supposed to have occurred just after the dramatic sea level fall of the Mediterranean during the Messinian Salinity Crisis. Resulting strong regressive erosion along the eastern margin of the Catalan ranges would have broken the previous Catalan dam and finally induced the capture of the Ebro drainage network by the Mediterranean. It is well known that the sea level fall of around 1500 m in the Mediterranean induced strong incision of the continental surface by rivers and the creation of deep canyons all around the Mediterranean region [*Hsü et al.*, 1973; *Ryan*, 1976; *Clauzon*, 1978; *Clauzon et al.*, 1996; *Krijgsman et al.*, 1999]. The subsequent opening of the Strait of Gibraltar caused the catastrophic reflooding of the desiccated Mediterranean basin, stopping rivers incising and allowing the inland canyons to be preserved by early Pliocene marine deposits [*Denizot*, 1952; *Chumakov*, 1973].

[38] In the Rhone valley, fluvial incision propagated more than 300 km inland and canyons reached more than 1000 m depth in the downstream part. The present drainage area of the Ebro basin ($A = 0.9.10^5$ km$^2$) is similar to that of the Rhone ($A = 1.10^5$ Km$^2$). If the Ebro basin had been connected to the Mediterranean before or during the Messinian Salinity Crisis then similar canyons would have developed within the Ebro basin, but none has been identified at present. Messinian inland canyons that were identified do not cross through the Catalan coastal ranges [*Agustí et al.*, 1983; *Arasa Tuliesa*, 1990]. We therefore conclude that the Ebro River was not connected to the Mediterranean before the Pliocene. By analyzing the Valencia trough fill, where the Ebro enters the Mediterranean, *Field and Gardner* [1990] observe a major change in sedimentation style from clays to prograding sands. *Field and Gardner* [1990] link this change to the discharge of the Ebro River, suggesting that the Ebro River connected to the Mediterranean during the Quaternary. However a first order evaluation of the balance between the amount of eroded terranes within the Ebro basin and the amount of sediments deposited within the Valencia Trough, in which the Ebro River enters, since the Messinian Salinity Crisis shows that the Ebro River could have flowed into the Mediterranean as soon as the Pliocene (Figure 13). This means that the new base level of the Ebro basin has dropped at least since the Pliocene leading inevitably to regressive erosion within the entire Ebro catchment. In this way, relief rejuvenation in the Pyrenean southern flank could have started as soon as Pliocene times. Alternatively, major change in type of sedimentation from clays to sands recorded in the Valencia trough at the end of the Pliocene as well as the three times increase of sediment influx during late Pliocene, also suggests that relief rejuvenation could have been triggered by global climate change.

## 6. Discussion

### 6.1. Foreland Basin Overfilling and Base Level Rise

[39] We have tentatively demonstrated that the development of the high-elevation, low-relief erosional surfaces that are a striking feature of the Pyrenees morphology resulted from the rise of the base level of the southern foreland basin whereas surface uplift (i.e., uplift of rocks-exhumation) of

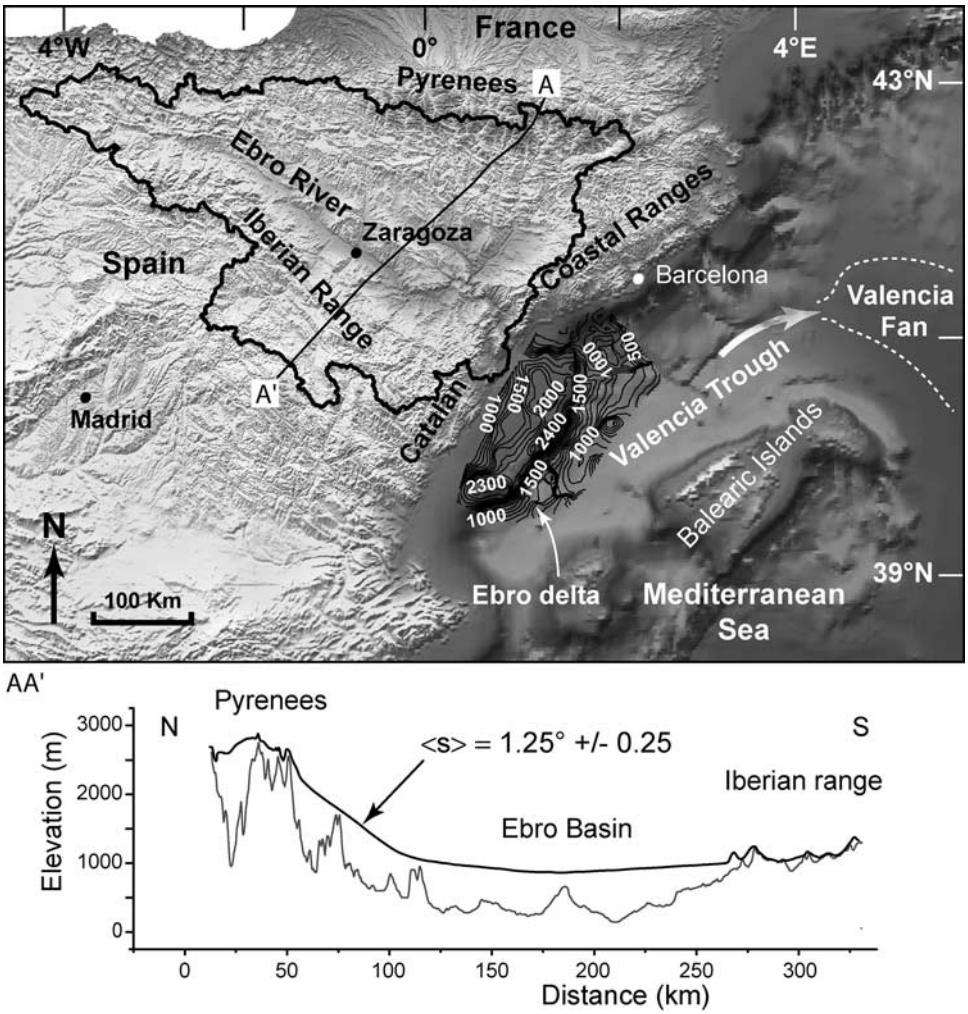


**Figure 13.** Estimate of the eroded volume in the Ebro basin since the Pliocene. (top) Topography of the Ebro drainage area (SRTM90 DEM data). Black line AA' marks location of the topographic profile shown below. The catchment contour of the Ebro River is also shown. The volume of post-Messinian detrital sediments within the Valencia trough has been determined as 25,700 km$^3$ from the difference between the Messinian top-surface and the current bathymetry (accurate reconstruction of the top-Messinian surface is from *Maillard* [1993]). *Nelson* [1990] estimated the volume of post-Messinian detrital sediments that are discharged by the Ebro River in the Valencia fan to be 6300 km$^3$. This provides a total amount of post-Messinian sediment of 32,000 km$^3$. (Black lines show isobaths of Pliocene and Quaternary deposits.) (bottom) Topographic profile of the reconstructed paleotopography and the current topography. The paleotopography has been computed by fitting a smooth surface between the Pyrenean summits, and the center of the Ebro basin within all the catchment of the Ebro river. The Ebro basin is a trough, the maximum elevation of which is 860 m [*Arenas*, 1993]. Elevation of the basin edges reaches 1000 m. From the southern limit of the Axial Zone to the limit of the south Pyrenean zone the paleosurface elevation decreases from 2000 m to 1000 m. The paleotopography is calculated with a mean slope $\langle s \rangle = 1.25°$. The eroded volume (37,800 km$^3$, computed from the difference between two surfaces: the paleotopography surface and the current topography) is comparable to that of post-Messinian deposits in the Valencia trough and Valencia fan.

the high chain was vanishing. We also suggest that this process of "high-altitude peneplanation" could have started during Eocene uplift, when the foreland basin became closed and started to overfill. From the Pliocene onward, excavation leads to the present morphology of the Pyrenean southern flank including the dissection of the high-elevation, low-relief erosional surfaces. Our interpretation disagrees with previous interpretations which consider that the high-elevation, low-relief surfaces were remnants of a low-elevation peneplain that resulted from long-term erosion of the Pyrenees and that was uplifted to 2000 m during the Pliocene. As shown by *Babault* [2004] and

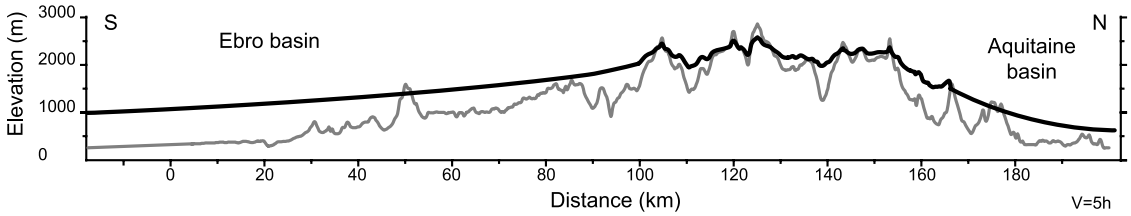


**Figure 14.** Idealized reconstruction of the paleotopography of the Pyrenees before post-Miocene landscape rejuvenation.

according to *England and Molnar*'s model [1990], removal by recent erosion accounts for a maximum of 400 m of isostatic rebound, which cannot explain the present-day high elevation of these low-relief surfaces.

[40] It has long been recognized that, at midlatitude, erosion is mainly governed by the potential energy of streams which depends on the difference in elevation between their source and base level. Whatever the process that will lower the potential energy, it will result in peneplanation but not necessarily near sea level. In the case of the southern flank of the Pyrenees the base level rose as sediments accumulated at the surface of the top-wedge foreland basin. Following tectonic uplift, ongoing sediment accumulation was obviously resulting in lowering such an elevation difference. Depending on the relative rates of both surface uplift and sedimentation, this difference may have decreased during tectonic uplift. This could be achieved if the difference between the surface uplift rate and the rate of the base level rise decreased. As discussed in section 4, it was probably the case from late Eocene to early Oligocene, in as far as one can consider that erosion was counterbalancing tectonic uplift when the chain was fully active (i.e., in steady state equilibrium [*Hack*, 1960]).

### 6.2. Internal/External Drainage and Sediment Length Transfer

[41] High-elevation, low-relief erosional surfaces also exist on the northern flank of the eastern Pyrenees. Their elevation reaches up to 1800–1900 m as in the Aston massif. They have been described as the continuation of the low-relief, erosional surfaces that occur at lower elevation, between 700–800 m. Both these erosional surfaces are supposed to belong to a posttectonic Miocene "gently undulating, very mature landscape, almost peneplain with low hills, which in the centre did not rise above 1000 m altitude" [*de Sitter*, 1952]. In others words, these surfaces would have been warped and uplifted up to 2000 m, long after Pyrenean tectonics [*Pannekoek*, 1935; *Birot*, 1937; *de Sitter*, 1952], an interpretation that is opposite with that proposed here for the high-elevation, low-relief surfaces of the southern flank.

[42] A major difference between the northern and southern Pyrenees is the fact that the drainage of the northern foreland basin (Aquitaine basin) remains external all along the building of the chain. However the sedimentation pattern, that is basin progressive overfilling, of the Aquitaine basin is rather similar to that of the Ebro basin [e.g., *Bureau de Recherches Géologiques et Minières* (*BRGM*), 1974; *Dubreuilh et al.*, 1995]. Indeed, from the mid-Eocene onward, previous marine sedimentation is replaced by continental sedimentation, including conglomerates. Moreover occurrence of extensive evaporites during the late Eocene in the western part of the basin [*BRGM*, 1974; *Crochet*, 1991] suggests a poorly drained area. However, coarse detrital deposits as observed today do not reach so high an elevation as they do on the southern flank. Miocene subhorizontal deposits reach 600 to 700 m asl at the top of Lannemezan fan in central part of the northern Pyrenees [*Goron*, 1941]. It is difficult to determine the maximum elevation pre-Miocene detrital deposits in the northern flank could have reached. Scarce continental coarse Eocene deposits occur up to 1700m asl in the Lers area (Central Pyrenees) [*Choukroune*, 1973, 1980]. Intercalation of conglomerates within extensive more fined-grained sediments, are also present all along the foothills. This suggests that coarse continental proximal deposits probably overlapped the northern flank during the Paleogene, and were later eroded. We therefore infer that the high-elevation, low-relief surfaces of the northern flank developed in the same way as the high-elevation, low-relief surfaces of the southern flank did (Figure 14).

[43] An important point to consider is the nature of the drainage with regard to the base level elevation. Although we mention that the northern flank was poorly drained, the drainage remains external all along the building of the chain contrary to the drainage of the southern flank which became internal from the late Eocene. This suggests that it is not so much the nature of drainage as the river capacity to transport sediments (sediment length transfer) that is the most influential factor in setting the base level of the chain. As a consequence, the limit of the most proximal, extensive detrital sedimentation can be considered as the "efficient" base level of a chain.

### 6.3. Rejuvenation of the Pyrenees Relief: Role of Climate

[44] It is clear that the present jagged relief of the Pyrenees has no relation with Palaeogene tectonic building of the chain insofar as the high elevation of the base level resulted in the high elevated applanation. By analyzing the characteristics of the present network on both flanks, we have concluded that the recent morphology of the Pyrenees results from rather uniform climatic conditions. Therefore the hypothesis where the Ebro River capture by the Mediterranean was merely the cause of the reexcavation of the buried southern flank needs to be revised. This is in

accordance with our remark about the relative relation of the drainage nature and the river capacity to transport sediments with the efficient base level of a chain.

[45] According to recent works [e.g., *Zhang et al.*, 2001], the marked increase, since the last 2 to 4 Ma, of both the sedimentation and erosion rates throughout the world has to be related to global climate change from rather equable climate during the Neogene to a period characterized by frequent and abrupt changes in temperature, rainfall and vegetation, from the late Pliocene. We suggest that in the case of the Pyrenees the climate shift from the Pliocene should have enhanced the transport capacity of rivers, resulting in the lowering of the Pyrenees efficient base level down to sea level. An alternative explanation is to consider late Pliocene and Quaternary oscillatory climate as much more efficient to erode and denude, than past equable climates, by combining different erosional processes such as chemical weathering, periglacial fracturing or other forms of mass wasting [*Zhang et al.*, 2001]. This would result in strong size reduction of eroded particles, hence favoring their discharge down to the sea.

[46] Finally we agree with *England and Molnar* [1990] when they wrote that "the marked climatic changes in the last few million years may be responsible for increased rates of denudation, and the creation of dramatic morphology, without any associated surface uplift."

## 7. Conclusion

[47] In contrast with the classical view of mountain chains peneplanation by long-term erosion as described by the "geographical cycle" of *Davis* [1889], we suggest that relief subduing does not necessarily equate to surface elevation lowering, so that relief of mountain belts can be smoothed at high elevation. Such a process is allowed by the piedmont aggradation of the eroded products of mountain ranges, resulting in the increase of their base level and the relative lowering of their mean elevation, and in the concomitant progressive decrease of the erosive power of their drainage system. This explains in our opinion the paradox of the occurrence of posttectonic high-elevation, low-relief surface remnants of peneplain within the Pyrenees, the elevation of which has been previously misinterpreted as resulting from enigmatic Pliocene uplift. The rejuvenation of the Pyrenean relief starts most probably during the Pliocene. As the current morphology of both sides of the chain present similar characteristics, we believe that rejuvenation is mostly due to the climate shift that occurs from the late Pliocene, rather than due to changing boundary conditions at the foreland basin margins such as the capture of the Ebro River by the Mediterranean sea. During Neogene times, most eroded products of the chain were trapped in the northern and southern Pyrenean foreland basins. Global climate change from the Pliocene might have enhanced the river capacity to transport the eroded products, so that the efficient base level of the Pyrenees was no longer their northern and southern piedmonts but the Atlantic Ocean and the Mediterranean Sea, respectively.

[48] Finally, the example of the Pyrenees is probably not a single case. Many ancient mountain chains show remaining elevation and relative jagged relief, as well as preserved crustal roots. The model of high peneplanation suggested for the Pyrenees and the role of recent global climate change in relief rejuvenation might also provide one explanation for such features.

[49] **Acknowledgments.** We are most grateful to Antonio Teixell and Peter Molnar for helpful reviews. Special thanks to P. Molnar for his warm encouragement to carry on this work. Mimi Hill kindly improved the English. Financial support was provided by CNRS-INSU research program PNSE and ATI. This study was also supported by the Ministère de l'Education Nationale, de la Recherche et de la Technologie, who funded Julien Babault's Ph.D. thesis.

## References

Abbott, L. D., E. A. Silver, R. S. Anderson, R. Smith, J. C. Ingle, S. A. King, D. Haig, E. Small, J. Galewsky, and W. Sliter (1997), Measurement of tectonic surface uplift rate in a young collisional mountain belt, *Nature*, *385*, 501–507.

Agustí, J., P. Anadón, and R. Julia (1983), Nuevos datos sobre el Plioceno del Baix Ebre: Aportación a la correlación entre las escalas marina y continental, *Acta Geol. Hisp.*, *18*, 123–130.

Ahnert, F. (1984), Local relief and the height limits of mountain ranges, *Am. J. Sci.*, *284*, 1035–1055.

Arasa Tuliesa, A. (1990), El terciario del Baix Ebre: Aportaciones estratigráficas y sedimentológicas, *Acta Geol. Hisp.*, *25*, 271–287.

Arenas, C. (1993), Sedimentología y paleogeografía del Terciario del margen pirenaico y sector central de la cuenca del Ebro (zona aragonesa occidental), Ph.D. thesis, 858 pp., Univ. de Zaragoza, Zaragoza, Spain.

Astre, G. (1927), Le bassin Néogène de Bellver, *Bull. Soc. Hist. Nat. Toulouse*, *LVI*, 231–258.

Babault, J. (2004), Dynamique de l'érosion dans une chaîne de montagnes: Influence de la sédimentation de piedmont: L'exemple des Pyrénées, Ph.D. thesis, 218 pp., Univ. de Rennes 1, Rennes, France.

Bates, R. L., and J. A. Jackson (1980), *Glossary of Geology*, Am. Geol. Inst., Falls Church, Va.

Birot, P. (1937), Recherches sur la morphologie des Pyrénées orientales franco-espagnoles, Doctorat ès Lettres thesis, 318 pp., Paris.

Blackstone, D. L. (1975), Late Cretaceous and Cenozoic history of Laramie Basin Region, southeast Wyoming, *Mem. Geol. Soc. Am.*, *144*, 249–279.

Boissevain, H. (1934), Etude géologique et géomorphologique de la vallée de la haute Sègre, *Bull. Soc. Hist. Nat. Toulouse*, *LXVI*, 33–170.

Briais, A., R. Armijo, T. Winter, P. Tapponnier, and A. Herbecq (1990), Morphological evidence for Quaternary normal faulting and seismic hazard in the eastern Pyrenees, *Ann. Tectonicae*, *IV*, 19–42.

Brunet, M. F. (1986), The influence of the evolution of the Pyrenees on adjacent basins, *Tectonophysics*, *129*, 343–354.

Bureau de Recherches Géologiques et Minières (BRGM) (1974), *Géologie du Bassin d'Aquitaine*, 26 pp., Ed. BRGM, Paris.

Cabrera, L., E. Roca, and P. Santanach (1988), Basin formation at the end of a strike-slip fault: The Cerdanya Basin (eastern Pyrenees), *J. Geol. Soc. London*, *145*, 261–268.

Calvet, M. (1985), Néotectonique et mise en place des reliefs dans l'Est des Pyrénées: L'exemple du horst des Albères, *Rev. Geol. Dyn. Geogr. Phys.*, *26*, 119–130.

Calvet, M. (1994), Morphogénèse d'une montagne méditerranéenne: Les Pyrénées orientales, Doctorat d'Etat thesis, 1177 pp., Univ. de Paris I Panthéon, Sorbonne, Paris.

Carozza, J. M., and S. Baize (2004), L'escarpement de la faille de la Têt est-il le résultat de la tectonique active Plio-Pléistocène ou d'une exhumation Pléistocène, *C. R. Geosci.*, *336*, 217–226.

Choukroune, P. (1973), La brèche de Lherz dite "d'explosion liée à la mise en place des lherzolites" est une brèche sédimentaire d'âge cénozoïque (Pyrénées Ariégeoises), *C. R. Acad. Sci. Paris*, *277*, 2621–2624.

Choukroune, P. (1980), Comment and Reply on "Quenching: An additional model for emplacement of the lherzolite at Lers (French Pyrenees)," *Geology*, *8*, 514–515.

Choukroune, P., et al. (1989), The ECORS Pyrenean deep seismic profile reflection data and the overall structure of an orogenic belt, *Tectonics*, *8*, 23–39.

Chumakov, I. S. (1973), Pliocene and Pleistocene deposits of the Nile valley in Nubia and upper Egypt, *Initial Rep. Deep Sea Drill. Proj.*, *13*, 1242–1243.

Clauzon, G. (1978), The Messinian Var canyon (Provence, southern France): Paleogeographic implications, *Mar. Geol.*, *27*, 231–246.

Clauzon, G., J.-P. Suc, F. Gautier, A. Berger, and M.-F. Loutre (1996), Alternate interpretation of the Messinian salinity crisis: Controversy resolved?, *Geology*, *24*, 363–366.

Coney, P. J., J. A. Muñoz, K. R. McClay, and C. A. Evenchick (1996), Syntectonic burial and posttectonic exhumation of the southern Pyrenees foreland fold-thrust belt, *J. Geol. Soc. London*, *153*, 9–16.

Crochet, B. (1991), Molasses syntectoniques du versant nord des Pyrénées: La série de Palassou, *Doc. B. R. G. M.*, *199*.

Davis, W. M. (1889), The geographical cycle, *Geogr. J.*, *14*, 481–504.

Denizot, G. (1952), Le Pliocène dans la vallée du Rhône, *Rev. Geogr. Lyon*, *27*, 327–357.

de Sitter, L. U. (1952), Pliocene uplift of Tertiary mountain chains, *Am. J. Sci.*, *250*, 297–307.

Dubreuilh, J., J. P. Capdeville, G. Farjanel, G. Karnay, J. P. Platel, and R. Simon-Coinçon (1995), Dynamique d'un comblement continental néogène et quaternaire: L'exemple du bassin d'Aquitaine, *Geol. Fr.*, *4*, 3–26.

England, P., and P. Molnar (1990), Surface uplift, uplift of rocks, and exhumation of rocks, *Geology*, *18*, 1173–1177.

Field, M. E., and J. V. Gardner (1990), Pliocene-Pleistocene growth of the Rio Ebro margin, northeast Spain: A prograding-slope model, *Geol. Soc. Am. Bull.*, *102*, 721–733.

Fitzgerald, P. G., J. A. Muñoz, P. J. Coney, and S. L. Baldwin (1999), Asymmetric exhumation across the Pyrenean orogen: Implications for the tectonic evolution of a collisional orogen, *Earth Planet. Sci. Lett.*, *173*, 157–170.

Flint, J. J. (1974), Stream gradient as a function of order, magnitude, and discharge, *Water Resour. Res.*, *10*, 969–973.

Garcia-Castellanos, D., J. Vergés, J. Gaspar-Escribano, and S. Cloetingh (2003), Interplay between tectonics, climate, and fluvial transport during the Cenozoic evolution of the Ebro Basin (NE Iberia), *J. Geophys. Res.*, *108*(B7), 2347, doi:10.1029/2002JB002073.

Goron, L. (1941), Les Pré-Pyrénées ariégeoises et garonnaises: Essai d'étude morphologique d'une lisière de montagne, Doctorat thesis, Fac. des Lettres, Univ. de Toulouse, Toulouse, France.

Hack, J. T. (1957), Studies of longitudinal stream profiles in Virginia and Maryland, *U.S. Geol. Surv. Prof. Pap.*, *294*, 45–94.

Hack, J. T. (1960), Interpretation of erosional topography in humid temperate regions, *Am. J. Sci.*, *258*, 80–97.

Hovius, N. (1996), Regular spacing of drainage outlets from linear mountain belts, *Basin Res.*, *8*, 29–44.

Hovius, N. (2000), Macroscale process systems of mountain belt erosion, in *Geomorphology and Global Tectonics*, edited by M. A. Summerfield, pp. 77–105, John Wiley, Hoboken, N. J.

Hsü, K. J., M. B. Cita, and W. B. F. Ryan (1973), The origin of the Mediterranean evaporites, in *Initial Rep. Deep Sea Drill. Proj.*, *13*, 1203–1231.

Keefer, W. R. (1970), Structural geology of the Wind River Basin, Wyoming, *U.S. Geol. Surv. Prof. Pap.*, *495–D*.

Krijgsman, W., F. J. Hiigeni, I. Raffi, F. J. Sierro, and D. S. Wilson (1999), Chronology, causes and progression of the Messinian salinity crisis, *Nature*, *400*, 652–655.

Maillard, A. (1993), Structure et riftogénèse du Golfe de Valence (Méditerranée Nord-Occidentale), Ph.D. thesis, 284 pp., Univ. Pierre et Marie Curie-Paris 6, Paris.

Mattauer, M. (1968), Les traits structuraux essentiels de la chaîne Pyrénéenne, *Rev. Geogr. Phys Geol. Dyn.*, *X*, 3–12.

Mattauer, M. (1985), Présentation d'un modèle lithosphérique de la chaîne des Pyrénées, *C. R. Acad. Sci. Paris, Ser. II*, *300*, 71–74.

Mengel, O. (1910), A propos des paliers des vallées des Pyrénées-Orientales (réponse à M. de Martonne), *Bull. Soc. Geol. Fr., Ser. 4*, *X*, 427.

Météo-France (1987), *Atlas Climatique de la France*, 30 pp., Paris.

Molnar, P., and P. England (1990), Late Cenozoic uplift of mountain ranges and global climate change: Chicken or egg?, *Nature*, *346*, 29–34.

Muñoz, J. A. (1992), Evolution of a continental collision belt: ECORS-Pyrenees crustal balanced cross section, in *Thrust Tectonics*, edited by K. R. McClay, pp. 235–246, CRC Press, Boca Raton, Fla.

Mutti, E., M. Séguret, and M. Sgavetti (1988), Sedimentation and deformation in the Tertiary sequences of the southern Pyrenees, *Field Trip Guide 7*, 153 pp., Am. Assoc. of Pet. Geol., Tulsa, Okla.

Nelson, C. H. (1990), Estimated post-Messinian supply and sedimentation rates on the Ebro continental margin, Spain, *Mar. Geol.*, *95*, 395–418.

Nelson, C. H., and A. Maldonado (1990), Factors controlling late Cenozoic continental margin growth from the Ebro Delta to the western Mediterranean deep sea, *Mar. Geol.*, *95*, 419–440.

Nijman, W. (1998), Cyclicity and basin axis shift in piggyback basin: Towards modelling of the Eocene Tremp-Ager Basin, south Pyrenees, Spain, in *Cenozoic Foreland Basin of Western Europe*, edited by A. Mascle et al., *Geol. Soc. Spec. Publ.*, *134*, 135–162.

Nussbaum, F. (1931), Sur les surfaces d'aplanissement d'âge tertiaire dans les Pyrénées-Orientales et leurs transformations pendant l'époque quaternaire, in *C. R. Congr. Int. Geogr.*, *II*, 529–534.

Pannekoek, A. J. (1935), *Evolution du Bassin de la Têt dans les Pyrénées Orientales Pendant le Néogène: Edtude de morphotectonique*, 72 pp., N. V. Ooshoek's, Utrecht.

Panzer, W. (1926), Talentwicklung und Eiszeitklima in nord-östlichen Spanien, *Abh. Senckenberg. Nat. Ges.*, *39*, 141–182.

Penck, A. (1894), Studien über das Klima Nordspaniens während der jungeren Terciärperiode und der diluvialperiode, *Z. Ges. Erdkunde Berlin*, *29*, 109–141.

Puigdefàbregas, C., and P. Souquet (1986), Tectono-sedimentary cycles and depositional sequences of the Mesozoic and Tertiary from the Pyrenees, *Tectonophysics*, *129*, 173–204.

Puigdefàbregas, C., J. A. Muñoz, and J. Vergés (1992), Thrusting and foreland basin evolution in the southern Pyrenees, in *Thrust Tectonics*, edited by K. R. McClay, pp. 247–254, CRC Press, Boca Raton, Fla.

Reille, J. L. (1971), Les relations entre tectorogénèse et sédimentation sur le versant sud des Pyrénées centrales d'après l'étude des formations terciaires essentiellement continentales, Doctorat d'Etat Science thesis, 330 pp., Univ. des Sci. et Technol. du Languedoc, Montpellier, France.

Riba, O., S. Reguant, and J. Villena (1983), Ensayo de síntesis estratigráfica y evolutiva de la cuenca terciaria del Ebro, in *Libro Jubilar de J. M. Ríos*, *Geol. Esp.*, vol. 2, edited by J. A. Comba, pp. 131–159, Inst. Geol. y Min. de Esp., Madrid.

Roca, E. (1996), The Neogene Cerdanya and Seu d'Urgell intramontane basins (eastern Pyrenees), in *Tertiary Basins of Spain: The Stratigraphic Record of Crustal Kinematics*, edited by P. F. Friend and C. J. Dabrio, pp. 114–119, Cambridge Univ. Press, New York.

Roure, F., P. Choukroune, X. Berastegui, J. A. Muñoz, A. Villien, P. Matheron, M. Bareyt, M. Séguret, P. Camara, and J. Deramond (1989), ECORS deep seismic data and balanced cross section: Geometric constraints on the evolution of the Pyrenees, *Tectonics*, *8*, 41–50.

Ryan, W. B. F. (1976), Quantitative evaluation of the depth of the western Mediterranean before, during and after the late Miocene salinity crisis, *Sedimentology*, *23*, 791–813.

Scott, G. R. (1975), Cenozoic Surfaces and Deposits in the Southern Rocky Mountains, *Mem. Geol. Soc. Am.*, *144*, 227–248.

Séguret, M. (1972), Etude tectonique des nappes et séries décollées de la partie centrale du versant sud des Pyrénées: Caractère synsédimentaire, rôle de la compression et de la gravité, Ph.D. thesis, Univ. Montpellier, Montpellier, France.

Small, E. E., and R. S. Anderson (1998), Pleistocene relief production in Laramide mountain ranges, western United States, *Geology*, *26*, 123–126.

Sorres, M. (1913), *Les Pyrénées Méditerranéennes: Étude de Géographie Biologique*, 508 pp., A. Collin, Paris.

Souriau, A., and M. Granet (1995), A tomographic study of the lithosphere beneath the Pyrenees from local and teleseismic data, *J. Geophys. Res.*, *100*, 18,117–18,134.

Teixell, A. (1998), Crustal structure and orogenic material budget in the west central Pyrenees, *Tectonics*, *17*, 395–406.

Tweto, O. (1975), Laramide (Late Cretaceous-early Tertiary) orogeny in the southern Rocky Mountains, *Mem. Geol. Soc. Am.*, *144*, 1–44.

Vacher, P., and A. Souriau (2001), A three-dimensional model of the Pyrenean deep structure based on the gravity modelling, seismic images and petrological constraints, *Geophys. J. Int.*, *145*, 460–470.

Vergés, J., H. Millán, E. Roca, J. A. Muõz, M. Marzo, J. Cirés, T. Den Bezemer, R. Zoetemeijer, and S. Cloetingh (1995), Eastern Pyrenees and related foreland basins: Pre-, syn- and post-collisional crustal-scale cross-section, *Mar. Pet. Geol.*, *12*, 893–915.

Vincent, S. J. (2001), The Sis paleovalley: A record of proximal fluvial sedimentation and drainage basin development in response to Pyrenean mountain building, *Sedimentology*, *48*, 1235–1276.

Willett, S. D., and M. T. Brandon (2002), On steady states in mountain belts, *Geology*, *30*, 175–178.

Zhang, P., P. Molnar, and W. R. Downs (2001), Increased sedimentation rates and grain sizes 2–4 Myr ago due to the influence of climate change on erosion rates, *Nature*, *410*, 891–897.

J. Babault, S. Bonnet, A. Crave, and J. Van Den Driessche, Géosciences Rennes, UMR CNRS 6118, Université de Rennes 1, 35 av. du General Leclerc, F-35042, Rennes Cedex, France. (julien.babault@univ-rennes1.fr)

S. Castelltort, Department of Earth Sciences, ETH-Zentrum, Sonneggstrasse 5, CH-8092 Zürich, Switzerland.

**Figure 4.** Analysis of the local relief of the Pyrenees derived from SRTM90 DEM data. Local relief is calculated by moving a 5 km wide circular search window over the DEM. At each point, the maximum range of elevation values within the window is determined and plotted at the center of the circle. The same method is used to perform the mean elevation by moving a 30 km wide window. (a) The mean elevation value is indicated and represented by lines superimposed on the local relief. The drainage divide between the northern and the southern flank is also reported. The map shows low values of local relief corresponding to low mean elevation and higher values of local relief corresponding to high mean elevation, except in the Encantats and the eastern Pyrenees. The low relief of Cerdanya and Capcir corresponds in part to Neogene and Quaternary depositional flat surfaces of extensional basins lying at 1000 m asl. (b) Rough contours of high-elevation, low-relief erosional surface remnants, such as described in the literature, superimposed on the local relief. Dissection of the initial erosional surface by the recent drainage system has resulted in small high-elevation, low-relief surface remnants of hundreds of square meters to several square kilometers which cannot be represented on the map, explaining the misfit between the contour lines and the local relief data. (c) The local slope map shows that high-elevation, low-relief surface remnants appear as small areas with a local slope less than 11°.

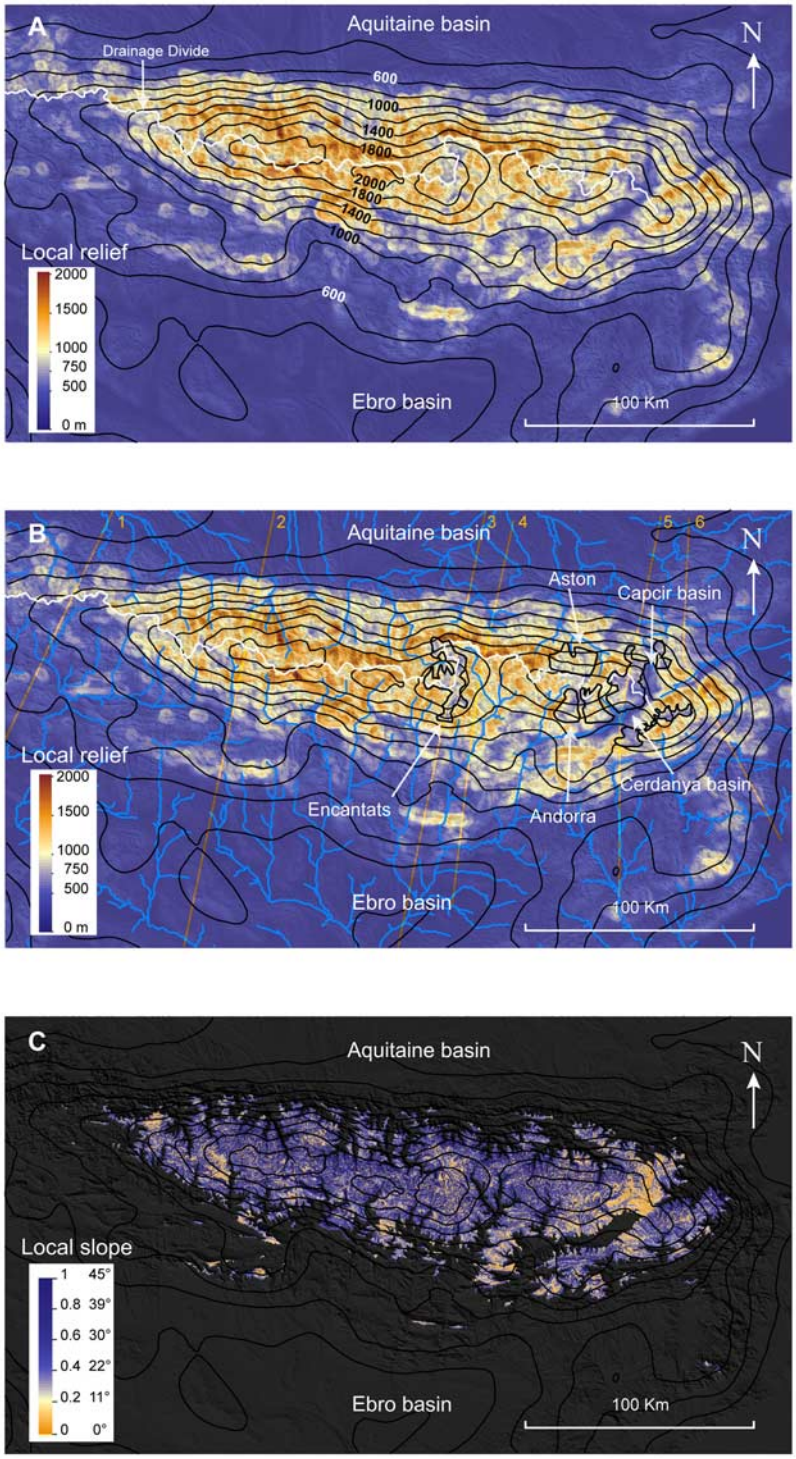
A
Aquitaine basin
Drainage Divide
N
600
1000
1400
1800
2000
1800
1400
1000
600
Local relief
2000
1500
1000
750
500
0 m
Ebro basin
100 Km
B
1
2
Aquitaine basin
3
4
5
6
N
Aston
Capcir basin
Local relief
2000
1500
1000
750
500
0 m
Encantats
Andorra
Cerdanya basin
Ebro basin
100 Km
C
Aquitaine basin
N
Local slope
1 45°
0.8 39°
0.6 30°
0.4 22°
0.2 11°
0 0°
Ebro basin
100 Km

**Figure 4**

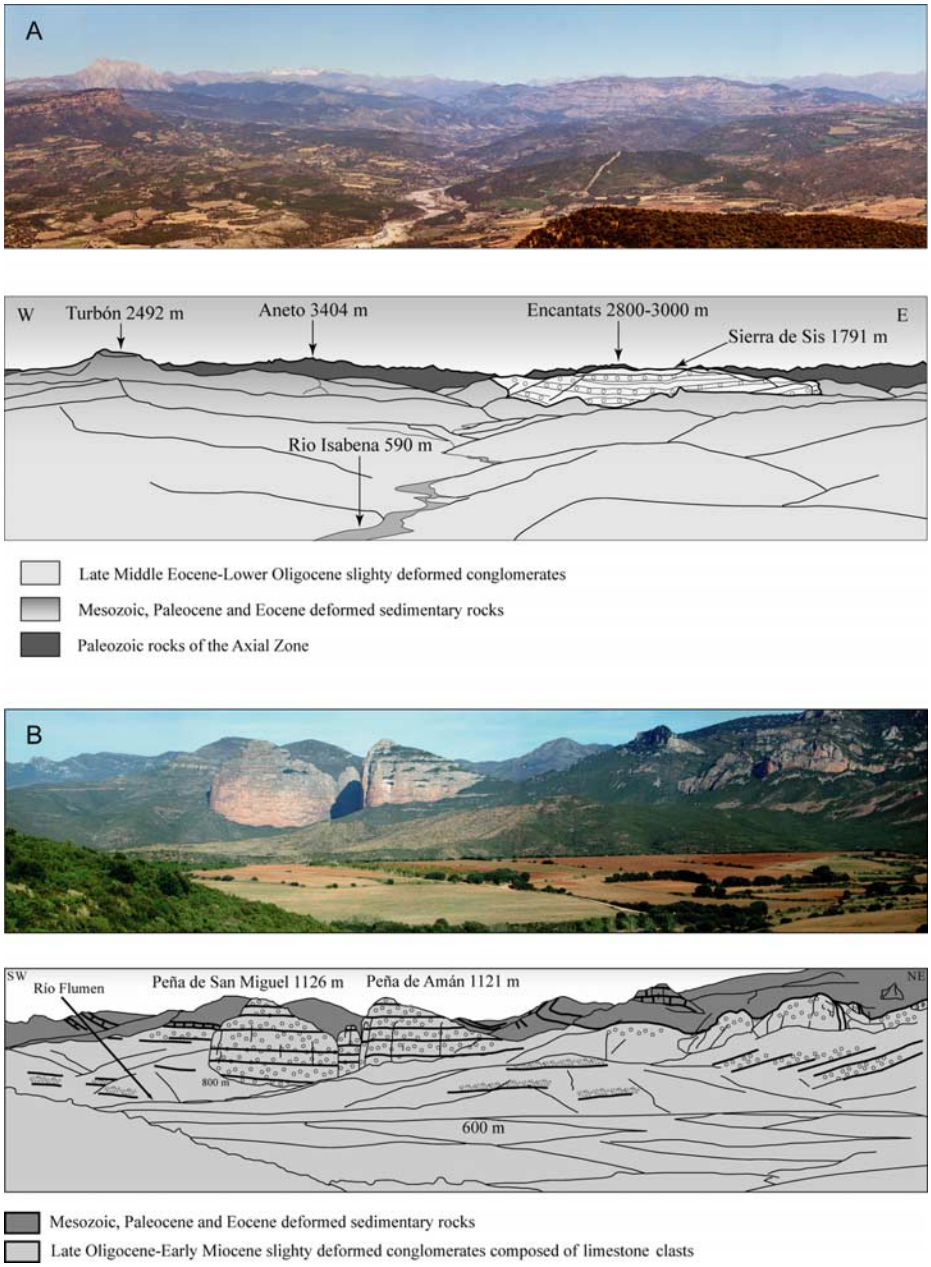


**Figure 10.** (a) Panorama looking to the north of the south Pyrenees showing N-S directed late Eocene-Oligocene paleovalley (Sierra de Sis). The late Eocene-Oligocene paleovalley is filled with alluvial conglomerates reaching nearly 1800 m asl. The Sierra de Sis conglomerate form a linear body extending up to 20 km long and 5 km wide. The picture is taken from a promontory made of the same undeformed conglomerates. Before dissection, the valley of the Rio Isabena was most probably looking like a bajada overlapping the southern margin of the Axial Zone up to 2000 m, or even higher, in the background and sloping down to 1000 m or more in the foreground. At the foot of the Sierra de Sis, the Rio Isabena reaches an elevation of 750 m implying about 1000 m of dissection. (b) View looking to the northwest of the early Miocene conglomerates of the Salto de Roldán (northern margin of the Ebro basin, north of Huesca). The conglomerates, which correspond to proximal fan delta and mass flow deposits, uncomformably overlie deformed Mesozoic, Paleocene and Eocene sedimentary rocks. They form spectacular high cliffs towering above the Ebro basin depression whose elevation ranges from around 300 – 500 m. The elevation of the conglomerates reaches 1120 m. (c) Eocene paleorelief buried by Oligocene conglomerates (Olvena, northeast of Barbastro). Oligocene conglomerates fill in a structural paleorelief that formed during folding of late Cretaceous limestones. Growth strata at the base show that folding was partly synsedimentary.

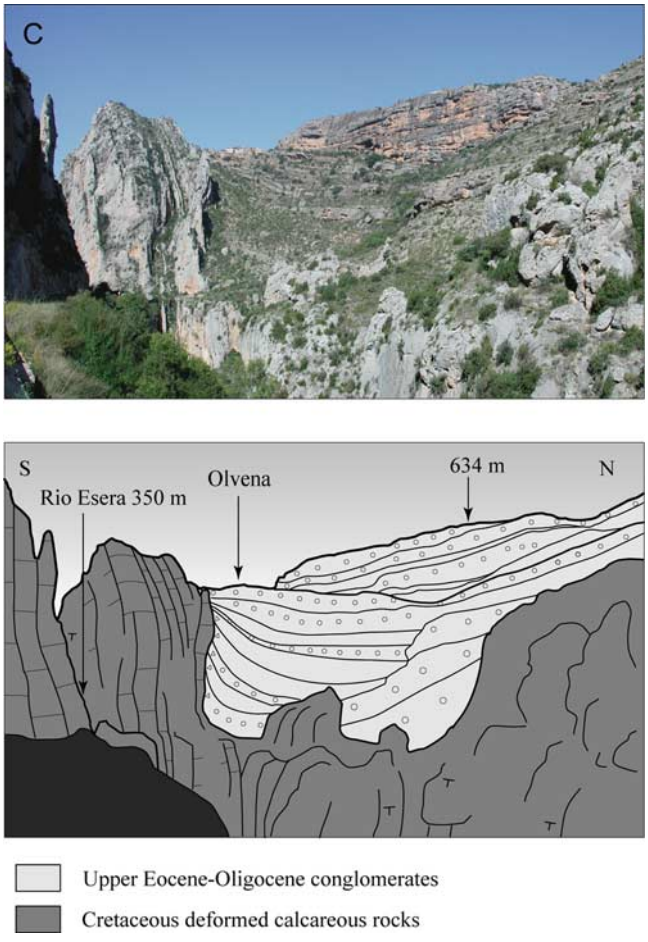


**Figure 10.** (continued)

doi: 10.1111/j.1365-3121.2007.00746.x

# High elevation of low-relief surfaces in mountain belts: does it equate to post-orogenic surface uplift?

Julien Babault,[1,2] Stéphane Bonnet,[1] Jean Van Den Driessche[1] and Alain Crave[1]

[1]*Géosciences Rennes, Université de Rennes 1, UMR CNRS 6118, Campus de Beaulieu, 35042 Rennes cedex, France;* [2]*Present address: Departament de Geologia, Àrea de Geodinàmica Interna, Campus de la Universitat Autònoma de Barcelona, 08193 Bellaterra (Cerdanyola del Vallès), Spain*

## ABSTRACT

**We present experiments of upraising and relaxing topographies showing that peneplanation can occur above the ultimate base level (sea level). After active uplift, the erosion of a topography bounded by a piedmont generates a final smooth and highly elevated topography. Smoothing at high elevation is even possible during active uplift if the evolution of topography is disrupted by the deposition of the products of erosion on its piedmont which is the case at the transition from underfilled to overfilled conditions in foreland basins.**

Terra Nova, 19, 272–277, 2007

## Introduction

The origin of low relief erosion surfaces lying at high elevation in mountain belts throughout the world has been long debated (e.g. Davis, 1911; de Sitter, 1952; England and Molnar, 1990; Molnar and England, 1990; Gregory and Chase, 1994; Leonard, 2002; McMillan *et al*., 2002; Molnar, 2004). Most previous interpretations considered that those were remnants of peneplain worn near to sea level, which was later uplifted by post-orogenic tectonics, then dissected by recent streams (e.g., Davis, 1911; Tweto, 1975; Epis *et al*., 1980). An implicit concept to those interpretations is that relief subduing is concomitant with surface elevation lowering near sea level, and thus remnants of peneplain at high elevation require tectonic uplift to occur. On the other hand, Molnar and England (1990) proposed that uplift of the peneplain remnants was the isostatic consequence of Pliocene-Quaternary climate-driven dissection, not the cause. But erosion-driven isostatic uplift appears to have a limited effect and cannot account for overall assumed uplift of peneplain remnants from near sea-level to their present elevation (e.g., Gilchrist *et al*., 1994; Montgomery, 1994; Small and Anderson, 1998; Leonard, 2002). Alternatively, other works have appealed for deep mantle processes to account for large scale uplift of such low-relief surfaces (e.g. Leonard, 2002; McMillan *et al*., 2002).

Several works have recently suggested that piedmont sedimentation in foreland basins corresponds to the rise in the base level for mountain belts erosion, resulting in reducing erosion rate (Baldwin *et al*., 2003; Babault, 2004; Pelletier, 2004; Babault *et al*., 2005a; Carretier and Lucazeau, 2005). In particular, from the relation between piedmont sedimentation and erosion pattern in the Pyrenees during the Cenozoic, Babault *et al*. (2005b) reached the conclusion that relief subduing does not necessarily equate to surface elevation lowering, so that relief of mountain chains can be smoothed at high elevation. We used a similar experimental approach as Babault *et al*. (2005a) who investigated the influence of piedmont sedimentation on the relation between denudation rate and uplift rate of upraising mountain belts. In this study, we investigated the effect of piedmont sedimentation on local relief, and we described the mechanisms by which a relief is subdued at high elevation.

Correspondence: Julien Babault, Departament de Geologia, Àrea de Geodinàmica Interna, Campus de la Universitat Autònoma de Barcelona, 08193 Bellaterra (Cerdanyola del Vallès), Spain. Tel.: +34 935 811 035; fax: +34 935 811 263; e-mail: Julien.Babault@uab.es

## Experimental models

The experimental design we used is the same as described in Babault *et al*. (2005a). It is made of an erosion box (600 × 400 mm and 500-mm deep) filled by a material to erode, a silica paste, which consists of silica powder (D50 = 10 μm) mixed with water (20%). The silica paste is uplifted within the erosion box by moving the base of the erosion box, the movements being driven by a screw and a computer controlled stepping motor. In some experiments, a plateau is added at the top of the erosion box, allowing deposition of the eroded products from upstream (herein referred to as 'piedmont sedimentation'). The erosion box is located in a rainfall simulator, where four sprinklers deliver a high-pressure water–air mixture (Figs S1 and S2). All experiments were run under the same rainfall rate of 120 ± 5 mm/h, as in experiments in Babault *et al*. (2005a). To construct 0.5-mm square-grid digital elevation models, we stopped the uplift and rainfall devices every 30–60 min. Topographic information is derived from optical stereo data acquired with the Advanced Topometric Sensor developed by the GOM Company.

At first, we used the experiments previously performed by Babault *et al*. (2005a) to analyse the evolution of local relief within a rising zone, without piedmont sedimentation. We also referred to experiment where piedmont sedimentation is allowed after a first phase of erosion of an experimental landscape submitted to constant uplift but without deposition (Babault *et al*., 2005a). Subsequently, we performed new experiments that investigated the effect of piedmont sedimentation on the relationship between the local relief and the mean

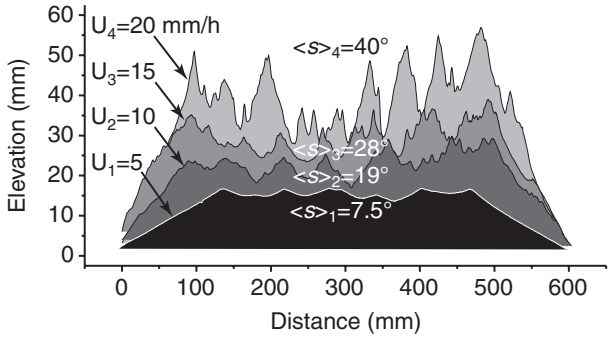


**Fig. 1** Effect of uplift on the local slopes and the local relief of steady-state topographies. The transversal topographic profiles are parallel to the length of the models, at a distance of 110 mm from the border of the uplifted zone. The mean local slope and the local relief increase with the uplift rate. $U$: uplift rate; $< s >$: mean local slope.

elevation during a post-uplift decay of the topography. The dynamics of the local relief was studied by analysing the variation of the mean local slope of the experimental landscapes (within the erosion box), the local slopes being computed over two adjacent pixels of the DEMs in the steepest direction.

### Effect of an emergent piedmont on the local relief of an uplifting topography

The first set of experiments (Babault *et al.*, 2005a) runs under constant uplift and rainfall rates, without piedmont deposition. Different uplift rate values have been applied (5, 10, 15 and 20 mm/h). In each experiment, rills first develop from the borders towards the centre of the erosion box when the mean elevation of the experimental landscapes increases, defining a growth stage of the topography. After 300 min, the mean elevation reaches a constant value defining a macroscale steady state stage for the relief dynamics (Hack, 1960) where the output eroded flux balances the input uplifted flux. The mean elevation ($< h >$) of the steady-state topography increases linearly with the uplift rate ($U$) (Lague *et al.*, 2003; Babault *et al.*, 2005a). As for the mean elevation vs. uplift rate relationship, the mean local slope $< s >$ increases with $U$ (Fig. 1).

In the second step, we added a plateau around the steady-state topography (for $U$ = 15 mm/h) at $t$ = 600 min, and we carried out the experiment at the same uplift and rainfall rates (Fig. 2b). The piedmont sedimentation that starts to surround the uplifted topography induces the onset of the mean elevation growth and the disruption of the previous macroscale equilibrium. Although the uplift and rainfall rates remain continuous, the end of the steady-state at $t$ = 600 min and the revival of surface uplift mean that the mean denudation does no longer balance the input flux (Fig. 2b) (Babault *et al.*, 2005a). At the local scale, the inhibition of erosion goes with a modification of the local relief. The transversal topographic profiles evolution (Fig. 2a,c and d) shows an increase in the elevations with time, concomitant with a decrease in the local relief. The smoothing of the upraising topography starts downstream and propagates upwards. At $t$ = 630 min, the topography is only smoothed in the downstream parts (Fig. 2c) whereas the local relief of the upstream parts is not modified until $t$ = 660 min (Fig. 2d).

The piedmont deposition raises the limit between the erosion zone and the deposition zone, i.e. the base level for erosion. As a result, the uplifted zone rises at a relative uplift rate ($U_r$) that depends on the aggradation rate ($U_f$) (Babault *et al.*, 2005a). Since the onset of the piedmont sedimentation, the relative uplift rate decreases from the initial value of $U$ = 15 mm/h down

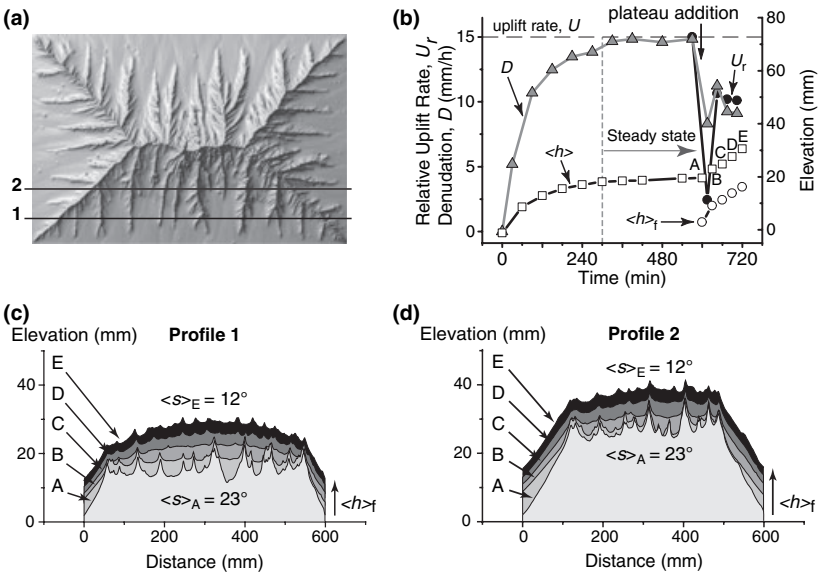


**Fig. 2** Effect of an emergent piedmont on the local relief of an uplifting topography. (a) DEM of a laboratory experiment. The view corresponds to the topography at $t$ = 630 min (point 'B' in b). The two series of transversal topographic profiles (black lines 1 and 2) on C and D are located at a distance of 55 mm and 110 mm, respectively, from the border of the uplifted zone. (b) Macroscale evolution of the experiments with free borders ($0 < t < 600$ min) and with a surrounding plateau ($600 < t < 720$ min). Open squares: mean elevation ($< h >$); open circles: mean fan apex elevation ($< h >_f$); grey triangles: mean denudation rate ($D$); black circles: relative uplift rate ($U_r$). (c) and (d) series of topographic profiles located in downstream and upstream parts respectively. It shows the progressive increase of the elevation and the concomitant smoothing of the topography (from $< s > = 23°$ at $t$ = 600 min to $< s > = 12°$ at $t$ = 720 min) from the onset of piedmont sedimentation.

 

to $U$ = 10 mm/h (Fig. 2b). As the local slopes depend on the uplift rate (Fig. 1), the decrease in the relative uplift rate then induces the smoothing of topography (Fig. S3 is given in supplementary material). It is also responsible for the decrease of the local denudation rates (Fig. 3 and Fig. S4), before and after the onset of the piedmont sedimentation. Figure 3 also shows that the subdued topographies are erosional surfaces, i.e. smoothing does not result from the infill of the depressions by erosion products but from lowering of valley slopes by erosion (except between 600 and 630 min and only for the channelized downstream parts). It is to note that the ongoing uplift leads eventually to a dynamic equilibrium of the topography, characterized by a progressive reincrease in the local relief as the piedmont aggradation rate decreases (see Babault *et al.*, 2005a).

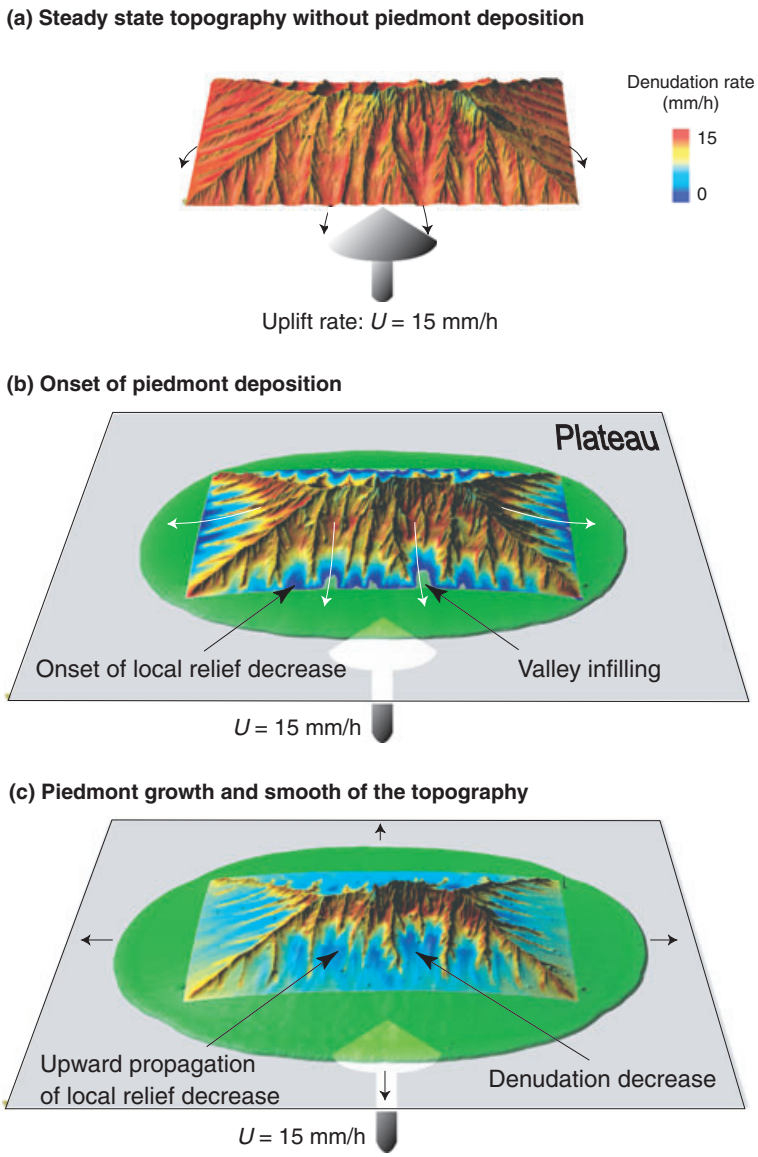


**Fig. 3** Effect of an emergent piedmont on the local denudation of an uplifting topography. Local denudation rates are superimposed on the DEM of the topographies of experiments a, b and c at $t$ = 600 min, at $t$ = 630 min and at $t$ = 660 min respectively (points 'A', 'B' and 'C' in Fig. 2b). Coloured topography, from blue to red, corresponds to increasing denudation rate, green corresponding to sedimentation. It shows the decrease in both the local erosion and local relief that is induced by the piedmont deposition although the uplift and rainfall rates (15 mm/h and 120 mm/h respectively) are kept constant during the experiment. The plateau is 250-mm large (measured from the border of the uplifting zone). Note that except for the topography B, the smoothed topography is an erosional surface, i.e. smoothing is not achieved by the infilling of depressions with the products of erosion.

### Effect of piedmont deposition on mean elevation dynamics following the cessation of active uplift

In this new set of experiments, we first looked at the evolution of the topographic decay of a previous steady-state topography with free borders (Fig. 4). At $t$ = 0, the denudation was at equilibrium with $U$ = 15 mm/h and afterwards the experiment was run without uplift. Figure 4 shows the decay of both the mean elevation $<h>$ and the mean local slope $<s>$ from the initial steady state topography to the final relaxed one. The mean elevation evolves following an exponential decay of the form:

$$y = y_0 + Ce^{-x/\tau} \qquad (1)$$

with $y_{0\text{free}}$ = 6.4 mm, $C_{\text{free}}$ = 15.4 and $\tau_{\text{free}}$ = 90 yr$^{-1}$ ($r^2$ = 99.5%).

We performed another relaxation experiment but we added a plateau just after uplift was stopped, allowing piedmont sedimentation to develop. The pattern of the decay of topography was similar to that in the previous experiment with free borders, the respective value of the terms of Eq. (1) being: $y_{0\text{piedmont}}$ = 11.8 mm, $C_{\text{piedmont}}$ = 8.2 and $\tau_{\text{piedmont}}$ = 100 yr$^{-1}$ ($r^2$ = 98%).

The value of the mean local slope at infinite time is similar in both experiments (Fig. 4, $<s>_{\text{final}}$ ~3.5°), but a main difference that exists is the much higher final mean elevation reached in the experiment with piedmont ($y_{0\text{piedmont}}$ = 11.8 mm) compared with the experiment with free borders ($y_{0\text{free}}$ = 6.4 mm). This difference in elevation (5.4 mm) almost corresponds to the elevation of the fan apex at $t$ = 425 min ($<h>_{\text{f}}$ = 6.5 mm).

## Discussion

Numerical modeling and laboratory experiments have already stressed the

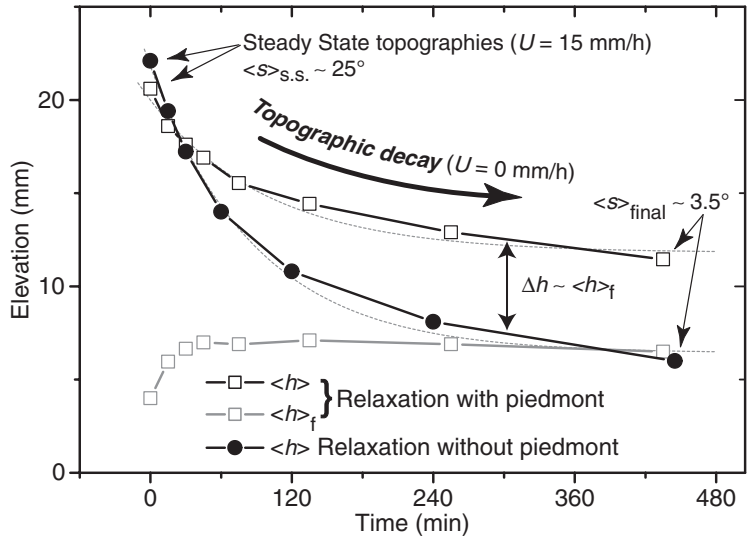


**Fig. 4** Effect of piedmont deposition on the mean elevation in relaxation experiments. Open squares and black circles: mean elevations ($< h >$) of relaxation experiments with and without piedmont sedimentation respectively. Grey open squares: mean fan apex elevation ($< h >_f$). Relaxation experiments start from steady-state topography. $< s >_{s.s.}$ is the mean local slope of the steady-state topographies for similar uplift and rainfall rates, and $< s >_{final}$ is the mean local slope of the final topographies. The greater elevation of the smoothed topography surrounded by piedmont almost correlates with the final elevation of the fan apex.

effect of piedmont deposition, on time scale of mountain denudation and erosion dynamics in mountain catchments, as corresponding to the rise in the efficient base level of mountain belts (Pelletier, 2004; Babault *et al.*, 2005a; Carretier and Lucazeau, 2005). In the present work, we focussed on this effect with regard to the local relief in mountain belts.

The experiments showed that relief subduing, which corresponds to local slope decrease, may develop during the new growth stage of an uplifting topography initially at steady state in response to the development of an aggrading piedmont. They also showed that the development of a piedmont during relief decay induces relief subduing at high elevation, the value of which is a function of the final elevation reached by the piedmont apex. In both types of experiments, relief subduing results from the rise of the efficient base level of the uplifting topography.

The dominating process by which the peneplanation develops is most probably a hybrid process between detachment-limited and transported-limited models. Indeed, in this type of experiments, local slopes and mean elevation decrease with increasing precipitation rates. A detachment-limited process predicts an inverse correlation suggesting that the rate-limiting process governing the evolution of the experimental channels is the transport of sediments rather than the rate of bed incision (Turowski *et al.*, 2006). However, the upward migration of the topography smoothing argues for a rather advective process, not a diffusive one as predicted by a transported-limited model. Note that hybrid-type numerical model encompasses these two-end members of landscape evolution model by introducing a varying transfer distance. This suggests that the transfer distance may vary during experimental peneplanation but this remains to investigate. More importantly, in both transport-limited model and detachment-limited model, slope depends on the uplift rate. Hence, the decrease in the relative uplift rate triggered by piedmont aggradation should allow the development of a peneplain as well in both end-members.

The direct application of the experimental results to natural systems is not reliable, as perfect scaling of laboratory-scale reliefs is nearly impossible (Crave *et al.*, 2000; Hasbargen and Paola, 2000; Lague *et al.*, 2003; Bonnet and Crave, 2006). However, results from modeling can be used to emphasize general concepts of landscape behaviour (Bonnet and Crave, 2006). Here, the experimental results provide an alternative explanation in the long-standing debate on the origin of high-elevation, low-relief surface remnants observed in several mountain belts throughout the world, including the Southern Rocky Mountains, the Pyrenees, the Atlas (e.g. Davis, 1911; Birot, 1937; Choubert, 1945; de Sitter, 1952; Scott, 1975; Molnar and England, 1990). Most interpretations consider that uplift, whatever its origin is, is required to explain the high elevation of low-relief surface remnants that are supposed to have developed near sea-level. Isostatic rebound resulting from heterogeneous erosion or thermal mantle anomaly may also account for post-orogenic uplift (e.g. Molnar and England, 1990; Leonard, 2002; McMillan *et al.*, 2002; Molnar, 2004; Teixell *et al.*, 2005), but not for the whole elevation in most cases. For example, paleobotanical data show that the present-day elevation of the low-relief surfaces in the Southern Rocky Mountains was nearly the same as during the Late Eocene, suggesting that these surfaces formed at high elevation (Gregory and Chase, 1994; Wolfe *et al.*, 1998). On the other hand, according to Babault *et al.* (2005b), the example of the Pyrenees strongly argues for relief subduing at high elevation during post-orogenic decay as shown by the second set of experiments. Indeed, neither post-Pyrenean tectonics nor mantle thermal anomaly exists that can explain the uplift of low-relief surfaces in this example (Babault *et al.*, 2006). As well, Pliocene-Quaternary, erosionally driven isostatic rebound does not account either for most of the present-day elevation of these surfaces (Babault, 2004; Babault *et al.*, 2005b).

As mountain belt building is generally accompanied by piedmont aggradation, this suggests that relief subduing at high elevation is most likely an intrinsic erosional process to post-orogenic decay of mountain belts.

 

## Acknowledgements

We thank Jean-Jacques Kermarrec and Jean-Pierre Caudal-Robin for making the experimental apparatus in working order; Philippe Davy for providing the GridVisual soft for experimental topographies display. The manuscript benefited from thorough comments by Sierd Cloetingh and an anonymous reviewer. This research was funded by the CNRS-INSU research programme PNSE and ATI. The Ministère de l'Éducation Nationale, de la Recherche et de la Technologie funded Julien Babault's Ph.D. thesis.

## References

Babault, J., 2004. Dynamique de l'érosion dans une chaîne de montagnes: Influence de la sédimentation de piedmont. L'exemple des Pyrénées. PhD, Université de Rennes1, Rennes (France), 218 pp.

Babault, J., Bonnet, S., Crave, A. and Van Den Driessche, J., 2005a. Influence of piedmont sedimentation on erosion dynamics of an uplifting landscape: An experimental approach. *Geology*, **33**, 301–304. doi: 10.1130/G21095.1.

Babault, J., Van Den Driessche, J., Bonnet, S., Castelltort, S. and Crave, A., 2005b. Origin of the highly elevated Pyrenean peneplain. *Tectonics*, **24**, TC2010. doi: 10.1029/2004TC001697.

Babault, J., Van Den Driessche, J., Bonnet, S., Castelltort, S. and Crave, A., 2006. Reply to comment by Yanni Gunnell and Marc Calvet on "Origin of the highly elevated Pyrenean peneplain". *Tectonics*, **25**, TC3004. doi: 10.1029/2005TC001922.

Baldwin, J.A., Whipple, K.X. and Tucker, G.E. 2003. *Implications of the shear stress river incision model for the timescale of postorogenic decay of topography*. *J. Geophys. Res.*, **108**, doi: 10:1029/2001JB000550.

Birot, P. 1937. *Recherches sur la morphologie des Pyrénées orientales franco-espagnoles*. Doctorat Ès Lettres, Faculté des Lettres de l'Université de Paris, Paris, 318 pp.

Bonnet, S. and Crave, A., 2006. Macroscale dynamics of experimental landscapes. In: *Analogue and Numerical Modelling of Crustal-Scale Processes* (S.J.H. Buiter and G. Schreurs, eds) *J. Geol. Soc. London, Spec. Publ.*, **253**. pp. 327–339. The Geological Society of London, London.

Carretier, S. and Lucazeau, F., 2005. How does alluvial sedimentation at range fronts modify the erosional dynamics of mountain catchments? *Basin Res.*, **17**, 361–381.

Choubert, G., 1945. Note Préliminaire sur le Pontien au Maroc (Essai de synthèse orogénique du Maroc Atlasique). *Bull. Soc. géol. France*, **5**, 677–764.

Crave, A., Lague, D., Davy, P., Kermarrec, J., Sokoutis, S., Bodet, L. and Compagnon, R., 2000. Analogue modelling of relief dynamics. *Phys. Chem. Earth, Part A: Solid Earth Geodesy*, **25**, 549–553.

Davis, W.M., 1911. The Colorado Front Range, a study on physiographic presentation. *Ann. Assoc. Am. Geogr.*, **1**, 21–83.

England, P. and Molnar, P., 1990. Surface uplift, uplift of rocks, and exhumation of rocks. *Geology*, **18**, 1173–1177.

Epis, R.C., Scott, G.R., Taylor, R.B. and Chapin, C.E., 1980. Summary of Cenozoic geomorphic, volcanic and tectonic features of central Colorado and adjoining areas. In: *Colorado Geology* (H.C. Kent and K.W. Porter, eds) pp. 135–156. Association of Geologists, Denver, Colorado, USA.

Gilchrist, A.R., Summerfield, M.A. and Cockburn, H.A.P., 1994. Landscape dissection, isostatic uplift and the morphologic development of orogens. *Geology*, **22**, 963–966.

Gregory, K.M. and Chase, C.G., 1994. Tectonic and climatic significance of a late Eocene lo-relief, high-level geomorphic surface, Colorado. *J. Geophys. Res.*, **99**, 20,141–20,160.

Hack, J.T., 1960. Interpretation of erosional topography in humid temperate regions. *American Journal of Science*, **258**, 80–97.

Hasbargen, L.E. and Paola, C., 2000. Landscape instability in an experimental drainage basin. *Geology*, **28**, 1067–1070.

Lague, D., Crave, A. and Davy, P., 2003. Laboratory experiments simulating the geomorphic response to tectonic uplift. *J. Geophys. Res.*, **108**, doi: 10:1029/2002JB001785.

Leonard, E.M., 2002. Geomorphic and tectonic forcing of late Cenozoic warping of the Colorado piedmont. *Geology*, **30**, 595–598.

McMillan, M.E., Angevine, C.L. and Heller, P.L., 2002. Postdepositional tilt of the Miocene-Pliocene Ogallala Group on the western Great Plains: Evidence of late Cenozoic uplift of the Rocky Mountains. *Geology*, **30**, 63–66.

Molnar, P., 2004. Late cenozoic increase in accumulation rates of terrestrial sediment: How might climate change have affected erosion rates? *Ann. Rev. Earth Planet. Sci.*, **32**, 67–89.

Molnar, P. and England, P., 1990. Late Cenozoic uplift of mountain ranges and global climate change: chicken or egg? *Nature*, **346**, 29–34.

Montgomery, D.R., 1994. Valley incision and the uplift of mountain peaks. *J. Geophys. Res.*, **99**, 13,913–13,921.

Pelletier, J.D., 2004. Influence of piedmont deposition on the time scale of mountain-belt denudation. *Geophys. Res. Lett.*, **31**, L15502. doi:10.1029/2004GL020052.

Scott, G.R., 1975. Cenozoic surfaces and deposits in the Southern Rocky Mountains. *Geol. Soc. Am. Mem.*, **144**, 227–248.

de Sitter, L.U., 1952. Pliocene uplift of Tertiary mountain chains. *Am. J. Sci.*, **250**, 297–307.

Small, E.E. and Anderson, R.S., 1998. Pleistocene relief production in Laramide mountain ranges, western United States. *Geology*, **26**, 123–126.

Teixell, A., Ayarza, P., Zeyen, H., Fernandez, M. and Arboleya, M.-L., 2005. Effects of mantle upwelling in a compressional setting: the Atlas Mountains of Morocco. *Terra Nova*, **17**, 456–461.

Turowski, J.M., Lague, D., Crave, A. and Hovius, N., 2006. Experimental channel response to tectonic uplift. *J. Geophys. Res.*, **111**, F03008. doi:10.1029/2005JF000306.

Tweto, O., 1975. Laramide (late cretaceous-early tertiary) orogeny in the Southern Rocky Mountains. *Geol. Soc. Am. Mem.*, **144**, 1–44.

Wolfe, J.A., Forest, C.E. and Molnar, P., 1998. Paleobotanical evidence of Eocene and Oligocene paleoaltitudes in midlatitude western North America. *Geol. Soc. Am. Bull.*, **110**, 664–678. doi:10.1130/0016-7606.

*Received 1 June 2006; revised version accepted 25 May 2007*

## Supplementary material

The following material is available at http://www.blackwell.synergy.com:

**Figure S1** Drawing of the experimental apparatus that shows the erosion box filled by silica paste and the moveable bottom used to simulate uplift. The erosion box is located within a rainfall simulator where four sprinklers deliver a high-pressure water–air mixture.

**Figure S2** Detailed picture of the erosion box at the end of an experiment. The uplifted landscape is surrounded by a piedmont that formed by the aggradation of the products of erosion. Lower left corner: detailed picture of a sprinkler.

**Figure S3** Perturbation of a steady-state topography by piedmont deposition. Photos of the experiment and evolution of its mean elevation ($< h >$), mean fan apex elevation

 

($< h >_f$), mean denudation ($D$), relative uplift rate ($U_r$) and uplift rate ($U$). The piedmont sedimentation that starts to surround the uplifted topography (photo and point 'D') induces the onset of the mean elevation growth and then the disruption of the previous macroscale equilibrium. At the local scale, the inhibition of erosion goes with a modification of the local relief. A smoothing of the upraising topography starts downstream and it propagates upwards.

**Figure S4** Perturbation of a steady-state topography by piedmont deposition. DEMs movie of the experiment and evolution of its mean elevation ($< h >$; blue squares), mean fan apex elevation ($< h >_f$; yellow circles), mean denudation ($D$; green triangles), relative uplift rate ($U_r$; red circles) and uplift rate ($U$).

Please note: Blackwell Publishing are not responsible for the content or functionality of any supplementary materials supplied by the authors. Any queries (other than missing material) should be directed to the corresponding author for the article.

doi: 10.1111/j.1365-3121.2008.00794.x

# A Late Cenozoic age for long-wavelength surface uplift of the Atlas Mountains of Morocco

Julien Babault,[1] Antonio Teixell,[1] Maria Luisa Arboleya[1] and Mohammed Charroud[2]

[1]*Departament de Geologia, Unitat de Geotectònica, Universitat Autònoma de Barcelona, 08193 Bellaterra, Spain;* [2]*Département de Géologie, Faculté des Sciences et Techniques Fès-Saïss, Université Sidi Mohammed Ben Abdellah, Fès, Morocco*

## ABSTRACT

**The Atlas Mountains have been uplifted by two mechanisms: Cenozoic thickening of the crust and thinning of the mantle lithosphere due to a buoyant thermal anomaly, previously inferred by indirect criteria to have started some 15 Ma. Because crustal shortening-related uplift and mantle-related uplift affect the topography at different spatial scales, we use scattered direct surface evidence to clarify the palaeoelevation dynamics. Uplifted Messinian shallow marine sediments in the southern margin of the Saïss Basin and in the northern Middle Atlas, tilted Pliocene lacustrine deposits in the Saïss Basin and in the piedmont of the southern High Atlas and drainage-network reorganization in the Saïss Basin underscore the long-wavelength rock uplift of the Atlas domain of mantle origin. The low erosion of the aforementioned deposits indicates that such uplift is a true surface uplift that occurred in post-Miocene times at a minimum rate ranging from 0.17 to 0.22 mm yr$^{-1}$.**

Terra Nova, 20, 102–107, 2008

## Introduction

The timing of the rise of mountains is important in understanding the relationship between tectonics and erosion. It plays a critical role in determining the degree to which various mechanisms – crustal thickening, thinning of the mantle lithosphere – contribute to the elevation of topography. Uplift of mountains has also profound effects on the moisture distribution at continental scale and consequently, the potential generation of orographically controlled rain shadows and aridification (e.g. Sepulchre *et al*., 2006). One of the main difficulties in establishing uplift histories lies particularly in defining palaeoaltitudes (e.g. Ghosh *et al*., 2006). This is why the occurrence at elevation of marine sediments or of deformed palaeohorizontal markers can provide powerful geological evidence in unravelling the complex uplift history of mountainous regions, such as the Atlas of Morocco, where mountain-building processes have received great attention in recent years.

The High, Middle and Anti-Atlas of Morocco are mountain belts that reach high elevations in the foreland of the Rif-Tell orogen, built at the Iberia-Europe plate boundary in the Western Mediterranean (Fig. 1). The High and Middle Atlas are 100 km wide, intracontinental fold-thrust belts (Mattauer *et al*., 1977) in which mean elevation locally exceeds 2600 and 2000 m respectively (Fig. 1a). Cenozoic inversion of a system of Mesozoic rifts led to crustal thickening that uplifted these mountain belts with respect to the adjoining plains. However, the Atlas mountain belts are surrounded by peripheral plateaux and plains in which the mean elevation is above ~1200 m.

Cenozoic tectonic shortening in the Atlas mountains is small, ranging from 15% to 24% in the central High Atlas (Teixell *et al*., 2003), < 10% in the Middle Atlas (Gomez *et al*., 1998; Arboleya *et al*., 2004), and even less in the Anti-Atlas. Accordingly, crustal thickening is insufficient in accounting for the high topography, and the system is isostatically undercompensated at crustal level (Van Den Bosch, 1971; Makris *et al*., 1985; Ayarza *et al*., 2005). Sub-crustal phenomena, such as a hot, thinned or delaminated lithosphere, have been proposed as an alternative reason for the elevated topography (Seber *et al*., 1996; Ramdani, 1998; Teixell *et al*., 2003). Recent modelling of the lithospheric structure based on potential fields has argued for a thinned lithospheric mantle beneath the Atlas mountains of Morocco (Fig. 1), implying that 1000 m of the topography is supported by mantle processes in the Atlas (Teixell *et al*., 2005; Zeyen *et al*., 2005; Missenard *et al*., 2006; Fullea *et al*., 2007). Based on indirect evidence, such as the age of the alkaline volcanism related to the thinned structure, Teixell *et al*. (2005) and Missenard *et al*. (2006) inferred that the main episode of long-wavelength, mantle-related uplift started some 15 Ma.

In this paper, we present a new model, based on robust geological arguments, for the timing of large-scale topographic doming in the Moroccan Atlas system. We combine new and published scattered observations, such as elevated marine sediments, tilted palaeohorizontal markers and drainage-network reorganization, that taken as a whole indicate a Late Cenozoic (post-Miocene to post-Late Pliocene) surface uplift, more recent than hitherto inferred, and locally exceeding 1000 m.

## Geological evidence for Late Cenozoic uplift in Morocco

### Uplifted Messinian-age marine deposits on the northern flank of the Middle Atlas

Neogene marine deposits crop out in the northern flank of the folded Middle Atlas, in the Skoura area (Fig. 1b). These correspond to shallow marine sandstone, mudstone and coral reef formations, up to 200 m thick, that accumulated on a gulf south of the

Correspondence: Dr Julien Babault, Departament de Geologia, nº116, Edifici CB, Universitat Autònoma de Barcelona, 08193 Bellaterra (Cerdanyola del Vallès), Spain. Tel.: +34 935 811 035; fax: +34 935 811 263; e-mail: julien.babault@uab.es

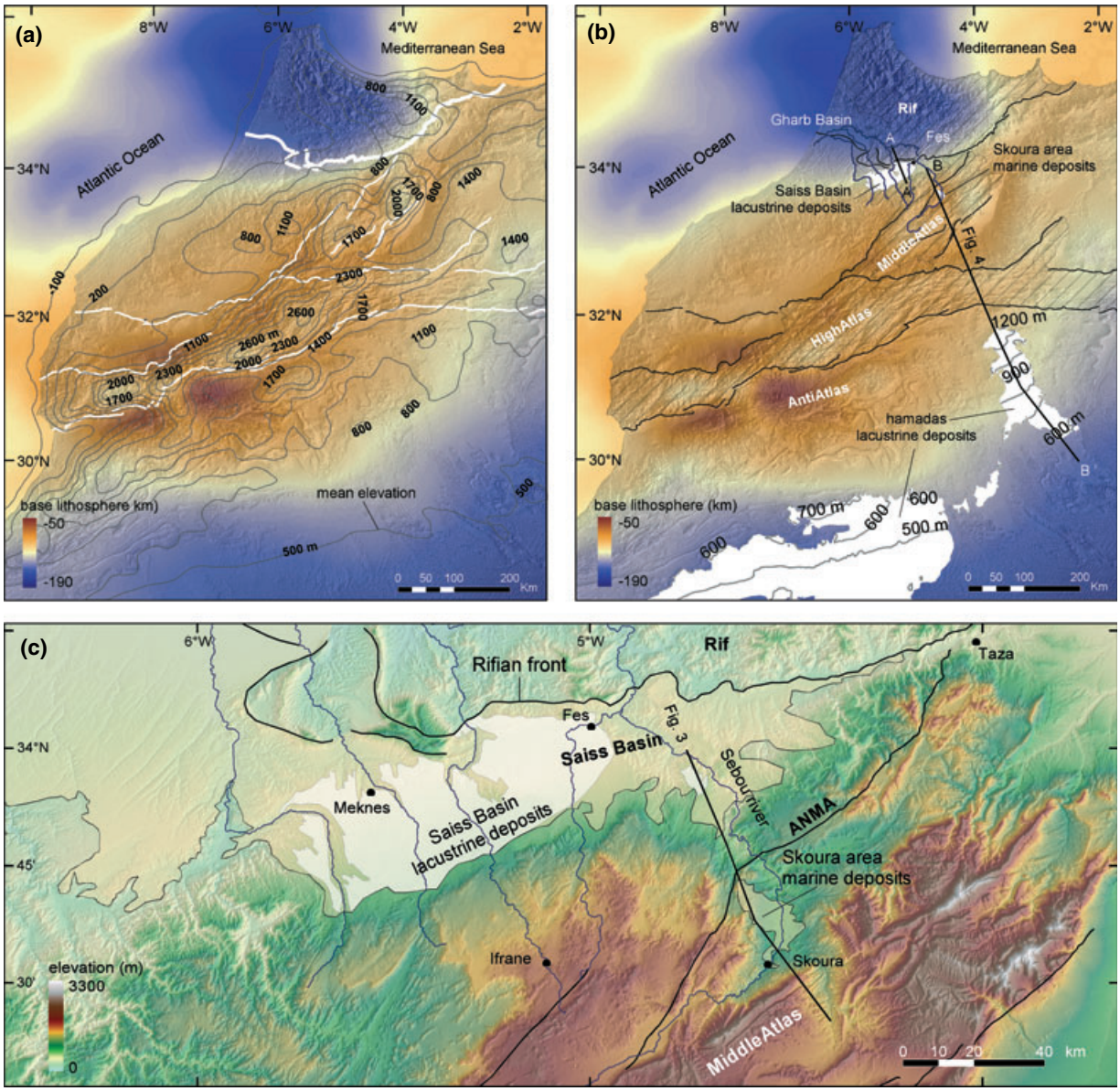


**Fig. 1** (a) Map of Morocco indicating: white, the boundaries of the deformed chains and colours, the depth of the base of the lithosphere (after Fullea *et al.*, 2007). Contour lines (grey) show the mean elevation calculated by a 30-km diameter moving window. (b) Location of the palaeoelevation criteria. Plotted is the drainage pattern of the northern flank of the Middle Atlas, where rivers cut through the ENE-trending Saïss Basin filled with lacustrine deposits during the Late Pliocene; thick line represents the Sebou River. Contour lines (grey) of the Lower Pliocene lacustrine deposits in the Sahara region show an overall large-scale tilting to the SSE. Black line corresponds to the transect in Fig. 4. (c) Topographic map (SRTM90) showing contours of the Saïss Basin, and of the Late Pliocene lacustrine deposits of the Saïss Basin. The Sebou River and its tributaries (blue lines) that drain the northern flank of the Middle Atlas flow to the north, and incise the Late Pliocene age lacustrine limestone of the Saïss Basin before entering the Rifian thrust front. Such drainage pattern indicates a post-Pliocene tilting of the Saïss Basin to the north.

margin of the Rifian foreland basin (Saïss Basin) during the Tortonian and Messinian (Martin, 1968; Charrière, 1984, 1989; Charrière and Saint-Martin, 1989). Almost undeformed Messinian deposits unconformably overlap folded Mesozoic strata (Figs 2 and 3). In the Skoura area, the Messinian marine deposits reach 1200 m asl, whereas, in the southern margin of the Saïss Basin, they reach an elevation of ~850 m (at 4º42′52″W, 33º48′53″N). This implies a rock uplift of ~850 and ~1200 m respectively. The reverse offset of the base of these deposits on both sides of the deformed zone comprising the Northern Middle Atlas Fault zone (ANMA) and the two thrust faults to the north (Fig. 3) is at most 250 m, which is their actual difference in elevation. This, together with the unconformable nature of the deposits, indicates that they postdate the main

 

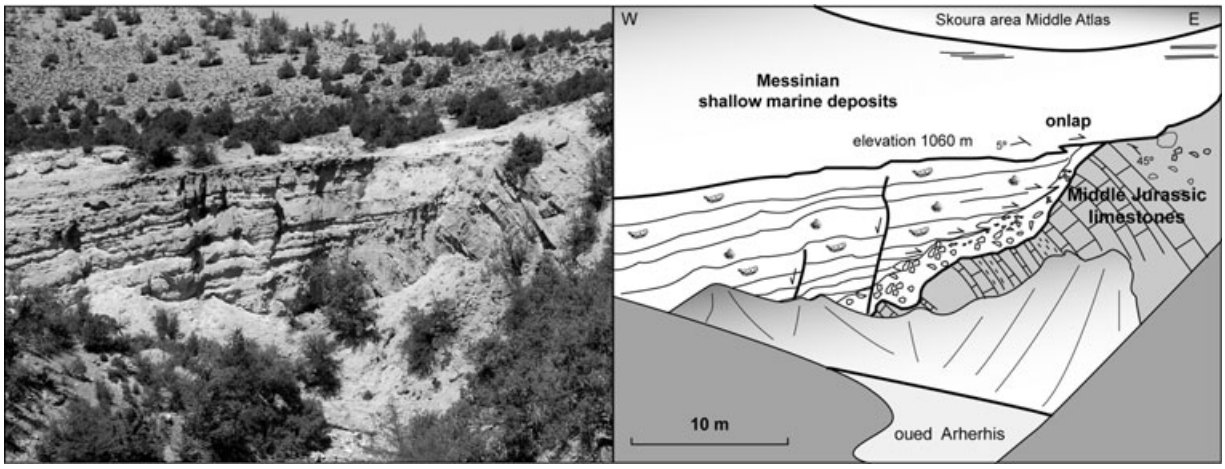


**Fig. 2** Photograph of the youngest marine deposits preserved in the Skoura area (Middle Atlas). These shallow marine deposits are Messinian in age and they are almost not affected by contractional deformation. The Messinian marine deposits have been uplifted 1000–1200 m since their deposition between 7.1 and 5.3 Ma.

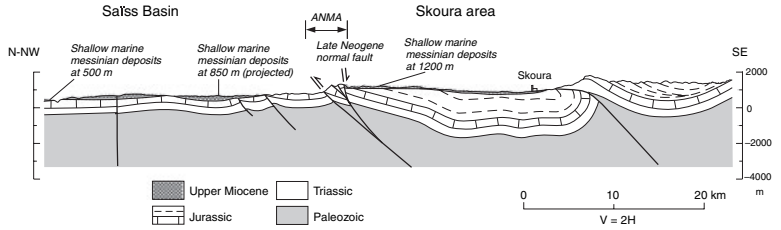


**Fig. 3** Cross-section of the northern flank of the Middle Atlas across the Skoura area (location in Fig. 1c). The Miocene sediments lie unconformably upon the Mesozoic-deformed rocks. Messinian marine shallow deposits reach an elevation of 850 and 1200 m in the southern margin of the Saïss Basin and in the Skoura area respectively. ANMA, North Middle Atlas Fault zone.

finite crustal shortening and thickening of the northern sector of the Middle Atlas. Further north (20 km) in the Saïss Basin, the Messinian shallow marine deposits reach 500 m (4º45′W, 33º59′30″N), implying a northward tilt of about ~1º of the northern flank of the Middle Atlas (north of the ANMA, Fig. 3) over 20 km, at the very most since the end of the Miocene (Fig. 3).

### Orogen-directed drainage network in the southern Rifian front and tilted Late Pliocene lacustrine deposits in the Saïss Basin

The Saïss Basin constitutes a foreland depression between the Rifian orogenic front and the Middle Atlas. Striking ENE, it projects as a corridor of low lands from the East of the city of Fes to the Atlantic coast, linking with the Gharb coastal basin. The rivers draining from the northern slopes of the Middle Atlas (the Sebou River being the most prominent amongst these) enter the Saïss Basin flowing north to north-westward (Fig. 1b). Once in the basin, the rivers do not deviate to follow the basin axis, as would be usual in foreland basins, but keep their flow direction to cross the Rifian front and enter the Rif orogenic belt. Further north, rivers eventually turn towards the West to reach the Atlantic Ocean (Fig. 1b).

Only a superimposed large-scale northward tilt of the surface, dominating over the topographic building of the Rif wedge, can explain the paradoxal drainage pattern in the Saïss Basin in which rivers flow opposite to the transport direction (Bargach *et al.*, 2004) of the external Rif thrust sheets. Chronological constraints on the development of this anomalous northward flow are provided by (1) up to 20 m thick Late Pliocene age lacustrine limestones in the Saïss Basin (Taltasse, 1953; Martin, 1981; Feinberg, 1986) and (2) by volcanic activity developed in the Middle Atlas during the Quaternary (0.5–1.8 Ma, cf. Harmand and Cantagrel, 1984; El Azzouzi *et al.*, 1999). Cross-sections of the Saïss Basin (Margat and Taltasse, 1953; Martin, 1981) show a tilt of the lacustrine strata to the North (segment A–A′ on Fig. 4). These lacustrine deposits are incised by the northward-flowing tributaries of the Sebou River (Fig. 1c) and are covered by northward flowing Quaternary lavas from the Middle Atlas. The geological record and drainage pattern both indicate a recent tilting of the Saïss Basin to the north that postdated the Late Pliocene and took place prior to 0.5 Ma, which is the age of the youngest dated lavas. Moreover, as discussed above, elevated Messinian shallow marine deposits imply an uplift of ~850 m for the southern margin of the Saïss Basin (Fig. 4).

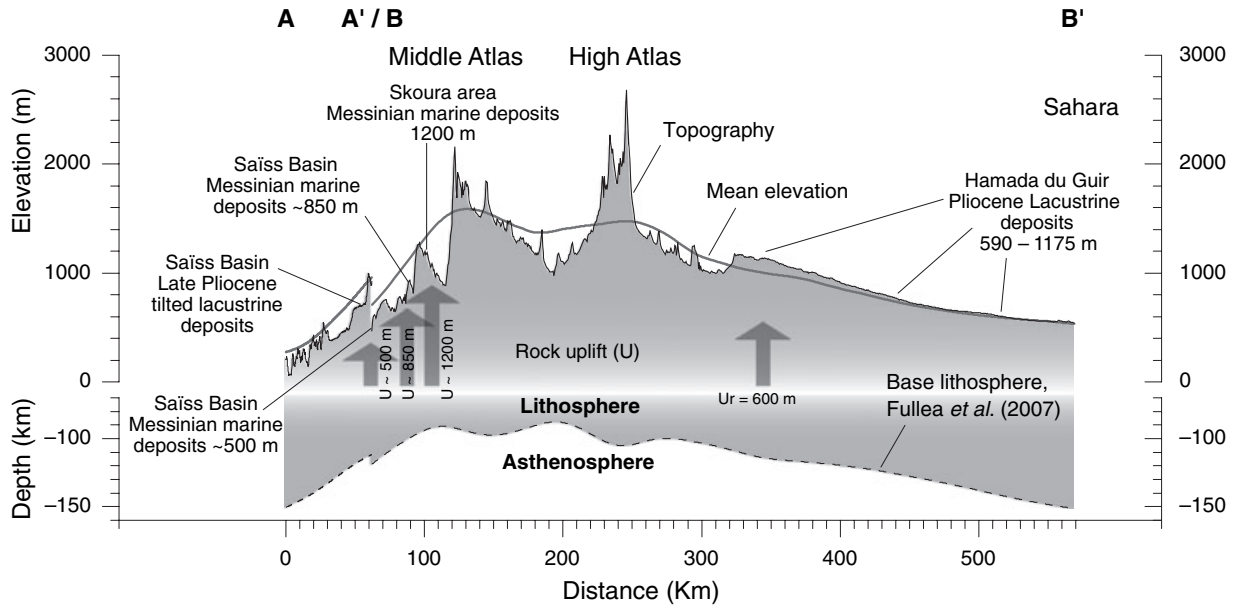


**Fig. 4** Topographic transect illustrating the post-Miocene doming of the Atlas Mountains and plateaux of Morocco (location in Fig. 1b). Indicated are the rock uplift criteria used in this work. Mean elevation is calculated by a moving window of 100 km diameter. The position of the lithosphere/astenosphere boundary modelled by Fullea *et al.* (2007) shows a good correlation with the long-wavelength doming.

### Tilted Early Pliocene lacustrine deposits south of the High Atlas

South of the Atlas thrust front, in the northern Sahara craton, Neogene terrestrial carbonates form large tablelands (called 'hamadas' in the Sahara region) over hundreds of kilometres. In Morocco, these carbonate deposits are preserved SE of the High Atlas and S of the Anti-Atlas (the Hamadas of Guir and Draa respectively; Fig. 1b), where they were attributed to the end of the Early Pliocene on the basis of gastropod fauna (Lavocat, 1954). The hamada carbonate deposits are several metres thick and lie unconformably on folded Palaeozoic-to-Cretaceous rocks of the Anti-Atlas, being only slightly dissected (≤350 m) by current drainage. They have been interpreted as lacustrine deposits (Lavocat, 1954; Thiry and Ben Brahim, 1997), thus defining a palaeohorizontal surface. However, they are presently tilted towards the SSE with a difference in elevation of more than 600 m over 200 km (Figs 1b and 4), again indicating a Late Cenozoic, broad surface deformation that is unrelated to tectonic shortening and loading in the area, which would have tilted the foreland lacustrine strata northwards.

## Discussion and conclusions

When calculated at lithospheric scale, i.e. in a 100-km diameter moving window, mean elevation in the Atlas Mountains and plateaux of Morocco describes a broad topographic swell on which the High and Middle Atlas are superimposed (Fig. 4). Pliocene lacustrine deposits in Morocco have been tilted, and Late Miocene marine deposits have been uplifted, both defining a dome-like shape over 500 km wide that mimics the pattern of the mean elevation (Fig. 4). Such broad-scale surface deformation coincides with the NE-trending imaged thinning of the lithosphere in this region (Figs 1 and 4), the buoyant mantle anomaly giving a simple geodynamic explanation for recent rock uplift.

Although flexural subsidence and isostatic rebound due to erosional unloading could have triggered a similar pattern of deformation, such processes are not realistic explanations, neither in the Sahara region nor in the northern flank of the Middle Atlas. The propagation of the Rif thrust wedge initiated the subsidence and deepening of the Rifian corridor during the Late Miocene (Chalouan *et al.*, 2001). Shallow marine Messinian deposits lie at 850 m in the Saïss Basin and at 1200 m in the Skoura area, indicating that large-scale uplift exceeded the tectonic loading associated to the building of the Rif wedge. At Skoura, the marine deposits lie in a wide palaeodepression surrounded by pre-existing mountains of the Middle Atlas, and the incision of these deposits by the present-day fluvial network is minor ($< 200$ m). This suggests a small contribution by erosionally driven isostatic rebound to their present high elevation. Moreover, the widespread preservation of Mesozoic series in the High and Middle Atlas and the old ages of apatite-fission tracks recorded (Barbero *et al.*, 2007) imply a low amount of erosion since the onset of mountain building in the Atlas. In the southern part of the hamadas, Quaternary deposits correspond only to a thin veneer; hence, sedimentary loading as a mechanism to tilt the Pliocene lacustrine deposits can be ruled out. The southern piedmont of the High Atlas is incised by rivers, such as the Ziz, between the Hamada du Guir and the Anti Atlas. In the highest section of the Hamada du Guir tableland, the amount of incision is maximum and reaches 350 m. Therefore, a

 

part of the whole tilt of the Hamada du Guir is attributed to erosionally driven flexural isostatic uplift. In the Colorado piedmont, at the North Platte-South Platte interfluve, where the same magnitude of erosion between piedmont deposits and current rivers has been reported, estimation of erosionally driven isostatic uplift is about 200 m (Leonard, 2002). Similarly, in the case of the Hamada du Guir a positive feedback between mantle-related uplift and erosionally induced uplift probably did take place, and erosion may also be responsible for some 200 m (1/3) of the total relative rock uplift. Given the low values of erosion in the transect studied (Fig. 4), the described values of rock uplift tend to equate to true values of surface uplift.

A widespread stage of alkaline volcanism in the Atlas domain started in mid-Miocene times. Teixell *et al.* (2005) attributed this to the change in the mantle thermal structure that led to the thinning of the lithosphere. Consequently, the mantle-driven uplift was thought to be contemporaneous (Teixell *et al.*, 2003, 2005; Missenard *et al.*, 2006). The present study argues for an uplift associated to the mantle thermal anomaly that is mostly younger than the Miocene volcanic activity, and probably contemporary with that of the Plio-Quaternary. The amount of this post-Miocene uplift as recorded at Skoura (*ca.* 1000 m), is a large fraction of the total thermal uplift estimated by Missenard *et al.* (2006) for the Atlas domain.

The Guercif Basin lies in the continuation of the Rifian corridor, East of the Saïss Basin. Progressive emergence of deep marine sediments was dated by Krijgsman *et al.* (1999b), who interpreted it mainly as a result of uplift, initiated some 7.1 Ma, attributed to tectonic deformation associated to the Rifian orogen. Missenard *et al.* (2006) hypothesized that this uplift could be related to the mantle thermal anomaly, although a part of it is due to post-Tortonian tectonic shortening as documented by Gomez *et al.* (2000). The Messinian Salinity Crisis resulted from the closure of the Rifian corridor and the Betic Strait that connected the Atlantic to the Mediterranean (Hsü *et al.*, 1973; Krijgsman *et al.*, 1999a). Therefore the large-scale, mantle-driven uplift of the northern Atlas domain we document might have been a process initiated immediately after the Miocene marine sedimentation, not before, and it probably enhanced closure of one of the marine passageways, thus contributing to the Messinian Salinity Crisis.

In summary, we infer that the doming of the Atlas Mountains and plateaux of Morocco, which is mainly a consequence of the mantle thermal anomaly, mostly occurred after the Miocene. Based on new and published scattered surface data, our study gives the first direct evidence for the geophysically inferred ~1000 m of surface uplift generated by the SW-NE lithospheric thinning of north-western Africa, the mean rate of which reaches at least 0.17 to 0.22 mm $yr^{-1}$ (1200 m of uplift since the Messinian, 7.1–5.3 Ma, at the Skoura area, where lithospheric thinning is maximum). It should also be emphasized that the current mean elevation of the Atlas system of mountains and plateaux is young in comparison with the Cenozoic crustal thickening that built the deformed belts of the High and Middle Atlas (mostly Oligocene and Miocene, Görler *et al.*, 1988; Tesón and Teixell, 2006 and references therein). This gives an explanation to the enigmatic Late Cenozoic uplift inferred by de Sitter (1952) to account for renewed erosion and incision of river canyons in the Ziz valley. It remains to be ascertained what the influence of the Late Cenozoic climatic change was, and to what extent this amplified the erosional response (e.g. Molnar and England, 1990) to the new boundary conditions.

## Acknowledgements

This work was supported by the Ministerio de Educación y Ciencia projects BTE2003-00499 and CGL2006-07226, the Ministerio de Asuntos Exteriores AECI grant A/2921/05 and the CONSOLIDER-INGENIO 2010 project CDS2006-00041. We acknowledge constructive discussion with Jean Van Den Driessche, especially about the link between the mantle-related surface uplift and the Messinian Salinity Crisis. We thank P. Molnar for his encouragements and constructive comments. Comments of an anonymous reviewer and the associate editor also enhanced the quality of this paper. We thank B. Charai from the University of Fes for a preliminary discussion on the Saïss Basin, Mabrock for the 'aspirines marocaines', Ivone Jimenez-Munt and Daniel Garcia-Castellanos for their company and discussion along the field study, Mabrock again and his chauffeur for their escort to the boundary between Morocco and Algeria.

## References

Arboleya, M.L., Teixell, A., Charroud, M. and Julivert, M., 2004. A structural transect through the High and Middle Atlas of Morocco. *J. Afr. Earth Sci.*, **39**, 319–327.

Ayarza, P., Alvarez-Lobato, F., Teixell, A., Arboleya, M.L., Teson, E., Julivert, M. and Charroud, M., 2005. Crustal structure under the central High Atlas Mountains (Morocco) from geological and gravity data. *Tectonophysics*, **400**, 67–84.

Barbero, L., Teixell, A., Arboleya, M.-L., Rio, P.D., Reiners, P.W. and Bougadir, B., 2007. Jurassic-to-present thermal history of the central High Atlas (Morocco) assessed by low-temperature thermochronology. *Terra Nova*, **19**, 58–64, doi: 10.1111/j.1365-3121.2006.00715.x.

Bargach, K., Ruano, P., Chabli, A., Galindo-Zaldívar, J., Chalouan, A., Jabaloy, A., Akil, M., Ahmamou, M., Sanz de Galdeano, C. and Benmakhlouf, M., 2004. Recent tectonic deformations and stresses in the frontal part of the Rif Cordillera and the Saïss Basin (Fes and Rabat regions, Morocco). *Pure Appl. Geophys.*, **161**, 521–540, doi: 10.1007/s00024-003-2461-6.

Chalouan, A., Michard, A., Feinberg, H., Montigny, R. and Saddiqi, O., 2001. The Rif mountain building (Morocco); a new tectonic scenario. *Bull. Soc. Géol. Fr.*, **172**, 603–616, doi: 10.2113/172.5.603.

Charrière, A., 1984. Evolution néogène des bassins continentaux et marins dans le moyen Atlas central (Maroc). *Bull. Soc. Géol. Fr.*, **26**, 1127–1136.

Charrière, A., 1989. *Carte géologique du Maroc, Scale 1:100000, sheet NI-30-VII-3: Sefrou*. Service Géologique du Maroc Notes et Mémoires, 354, Ministère de l'Énergie et des Mines Direction de la Géologie, Rabat.

Charrière, A. and Saint-Martin, J.P., 1989. Relations entre les formations récifales du Miocène supérieur et la dynamique d'ouverture et de fermeture des communications marines a la bordure méridionale du sillon sud-rifain (Maroc). *C. R. Acad. Sci. II*, **309**, 611–614.

El Azzouzi, M., Bernard-Griffiths, J., Bellon, H., Maury, R.C., Piqué, A., Fourcade, S., Cotten, J. and Hernandez, J., 1999. Evolution des sources du volcanisme marocain au cours du Néogène. *C. R. Acad. Sci. II*, **329**, 95–102.

 

Feinberg, H., 1986. Les séries tertiaires des Zones Externes du Rif (Maroc). Biostratigraphie, Paléoécologie et aperçu tectonique. Notes et Mémoires du Service Géologique du Maroc, 315, Rabat.

Fullea, J., Fernandez, M., Zeyen, H. and Vergés, J., 2007. A rapid method to map the crustal and lithospheric thickness using elevation, geoid anomaly and thermal analysis. Application to the Gibraltar Arc System, Atlas Mountains and adjacent zones. *Tectonophysics*, **430**, 97–117.

Ghosh, P., Garzione, C.N. and Eiler, J.M., 2006. Rapid uplift of the Altiplano revealed through $^{13}C$-$^{18}O$ bonds in paleosol carbonates. *Science*, **311**, 511–515.

Gomez, F., Allmendinger, R.W., Barazangi, M., Er-Raji, A. and Dahmani, M., 1998. Crustal shortening and vertical strain partitioning in the Middle Atlas Mountains of Morocco. *Tectonics*, **17**, 520–533.

Gomez, F., Barazangi, M. and Demnati, A., 2000. Structure and Evolution of the Neogene Guercif Basin at the Junction of the Middle Atlas and the Rif Thrust Belt, Morocco. *AAPG Bulletin*, **84**, 340–1364, doi: 10.1306/A9673EAO-1738-11D7-8645000102C1865D.

Görler, K., Helmdach, F.-F., Gaemers, P., Heißig, K., Hinsch, W., Mädler, K., Schwarzhans, W. and Zucht, M., 1988. The uplift of the central High Atlas as deduced from Neogene continental sediments of the Ouarzazate province, Morocco. In: *The Atlas System of Morocco* (V. Jacobshagen, ed.), pp. 361–404. Springer-Verlag, New York.

Harmand, C. and Cantagrel, J.M., 1984. Le volcanisme alcalin Tertiaire et Quaternaire du Moyen Atlas (Maroc); chronologie K/Ar et cadre geodynamique. *J. Afr. Earth Sci.*, **2**, 51–55.

Hsü, K.J., Cita, M.B. and Ryan, W.B.F., 1973. The origin of the Mediterranean evaporites. In: *Initial Reports of the Deep Sea Drilling Project* (A.G. Kaneps, ed.), pp. 1203–1231. U. S. Government Printing Office, Washington, DC.

Krijgsman, W., Hilgen, F.J., Raffi, I., Sierro, F.J. and Wilson, D.S., 1999a. Chronology, causes and progression of the Messinian salinity crisis. *Nature*, **400**, 652–655.

Krijgsman, W., Langereis, C.G., Zachariasse, W.J., Boccaletti, M., Moratti, G., Gelati, R., Iaccarino, S., Papani, G. and Villa, G., 1999b. Late Neogene evolution of the Taza-Guercif Basin (Rifian Corridor, Morocco) and implications for the Messinian salinity crisis. *Mar. Geol.*, **153**, 147–160.

Lavocat, R., 1954. Reconnaissance géologique dans les hammadas des confins algero-marocains du sud. Notes et Mémoires du Service Géologique du Maroc, 116, Rabat.

Leonard, E.M., 2002. Geomorphic and tectonic forcing of late Cenozoic warping of the Colorado piedmont. *Geology*, **30**, 595–598.

Makris, J., Demnati, A. and Klussmann, J., 1985. Deep seismic soundings in Morocco and a crust and upper mantle model deduced from seismic and gravity data. *Ann. Geophys.*, **3**, 369–380.

Margat, J. and Taltasse, P., 1953. Structure et extension du Lias sous la couverture néogène du bassin lacustre de Fès-Meknès. *Notes Mémo. Serv. Géol. Maroc*, **117**, 95–107.

Martin, J., 1968. L'évolution du bassin de Skoura (Moyen Atlas) au cours du Néogène. *Rev. Géogr. Maroc*, **14**, 117–132.

Martin, J., 1981. Le Moyen Atlas central, étude géomorphologique. Notes et Mémoires du Service Géologique du Maroc, 258, Rabat.

Mattauer, M., Tapponier, P. and Proust, F., 1977. Sur les mécanismes de formation des chaines intracontinentales. L'exemple des chaines atlasiques du Maroc. *Bull. Soc. Géol. Fr.*, **7**, 521–536.

Missenard, Y., Zeyen, H., Frizon de Lamotte, D., Leturmy, P., Petit, C., Sébrier, M. and Saddiqi, O., 2006. Crustal versus asthenospheric origin of relief of the Atlas Mountains of Morocco. *J. Geophys. Res.*, **111**, B03401, doi: 10.1029/2005JB003708.

Molnar, P. and England, P., 1990. Late Cenozoic uplift of mountain ranges and global climate change: chicken or egg? *Nature*, **346**, 29–34.

Ramdani, F., 1998. Geodynamic implications of intermediate-depth earthquakes and volcanism in the intraplate Atlas mountains (Morocco). *Physics Earth Planet. Int.*, **108**, 245–260.

Seber, D., Barazangi, M., Tadili, B.A., Ramdani, M., Ibenbrahim, A. and Ben Sari, D., 1996. Three dimensional upper mantle structure beneath intraplate Atlas and interplate Rif mountains of Morocco. *J. Geophys. Res.*, **101**, 3125–3138.

Sepulchre, P., Ramstein, G., Fluteau, F., Schuster, M., Tiercelin, J.-J. and Brunet, M., 2006. Tectonic uplift and Eastern Africa aridification. *Science*, **313**, 1419–1423.

de Sitter, L.U., 1952. Pliocene uplift of Tertiary mountain chains. *Am. J. Sci.*, **250**, 297–307.

Taltasse, P., 1953. Recherches géologiques et hydrogéologiques dans le bassin lacustre de Fès-Meknès. Notes et Mémoires du Service Géologique du Maroc, 115, Rabat.

Teixell, A., Arboleya, M.L., Julivert, M. and Charroud, M., 2003. Tectonic shortening and topography in the central High Atlas (Morocco). *Tectonics*, **22**, 1051, doi: 10.1029/2002TC001460.

Teixell, A., Ayarza, P., Zeyen, H., Fernandez, M. and Arboleya, M.-L., 2005. Effects of mantle upwelling in a compressional setting: the Atlas Mountains of Morocco. *Terra Nova*, **17**, 456–461.

Tesón, E. and Teixell, A., 2006. Sequence of thrusting and syntectonic sedimentation in the eastern Sub-Atlas thrust belt (Dadès and Mgoun valleys, Morocco). *Int. J. Earth Sci.*, doi: 10.1007/s00531-006-0151-1.

Thiry, M. and Ben Brahim, M., 1997. Silifications de nappe dans les formations carbonatees tertiaires du piedmont atlasique (Hamada du Guir, Maroc). *Geodyn. Acta*, **10**, 12–29.

Van Den Bosch, J.W.H., 1971. Mémoire explicatif de la carte gravimétrique du Maroc (provinces du Nord) au 1/500000. Notes et Mémoires du Service Géologique du Maroc, 234, Rabat.

Zeyen, H., Ayarza, P., Fernàndez, M. and Rimi, A., 2005. Lithospheric structure under the western African-European plate boundary: a transect across the Atlas Mountains and the Gulf of Cadiz. *Tectonics*, **24**, TC2001, doi: 10.1029/2004TC001639.

*Received 2 October 2007; revised version accepted 14 December 2007*

 

*Journal of the Geological Society, London*, Vol. **165**, 2008, pp. 1059–1073. Printed in Great Britain.

# Timing and nature of Quaternary fluvial incision in the Ouarzazate foreland basin, Morocco

MARIA-LUISA ARBOLEYA[1], JULIEN BABAULT[1], LEWIS A. OWEN[2], ANTONIO TEIXELL[1] & ROBERT C. FINKEL[3]

[1]*Departament de Geologia, Universitat Autònoma de Barcelona, E-08193, Bellaterra, Spain (e-mail: MariaLuisa.Arboleya@uab.es)*

[2]*Department of Geology, University of Cincinnati, Cincinnati, OH 45221, USA*

[3]*Center for Accelerator Mass Spectrometry, Lawrence Livermore National Laboratory, Livermore, CA 92521, USA*

**Abstract:** The history of alluvial fan and terrace formation within a stretch of the Ouarzazate basin along the southern margin of the Central High Atlas is reconstructed using geomorphological and $^{10}$Be terrestrial cosmogenic nuclide (TCN) methods. Alluvial fan and terrace incision was controlled partially by a drop in base level during the Pliocene or early Pleistocene as the outlet channel, the Draa river, progressively cut through the Anti-Atlas to the south of the Ouarzazate foreland basin, the drainage of which started to become external after a long period of internal drained conditions. The alluvial fans and terrace surfaces have abandonment ages that date to at least the past four glacial cycles. Their formation was strongly modulated by climate on glacial–interglacial time scales as base level dropped. This demonstrates a strong climatic control on sediment transfer and landscape denudation during the Quaternary and provides a model for understanding sediment transfer in other intracontinental mountain belts. Furthermore, these data show that mean rates of fluvial incision in this region range between 0.3 and 1.0 mm $a^{-1}$ for the latter part of the Quaternary. This study provides the first comprehensive TCN chronology for the Atlas Mountains, and it illustrates the applicability and limitations of TCN methods.

Understanding the nature of denudation, sediment transfer and deposition, and landscape evolution in foreland basins is important for defining and quantifying tectonic and geomorphological models for orogenesis. Numerous studies have shown that sedimentation during foreland basin development may progressively advance away from the mountain belt as deformation propagates into the foreland and as proximal basins overfill with sediment (Flemings & Jordan 1989; Sinclair *et al*. 1991; DeCelles & Giles 1996). These studies have broadly defined the rates of sedimentary and geomorphological processes on million year time scales, generally spanning the Cenozoic and/or Mesozoic. There are few studies, however, that provide data on millennial time scales that span the Quaternary. Given the high frequency and the large magnitudes of climatic change throughout the Quaternary, it is likely that there has been a strong climatic control on geomorphological and sedimentary processes in general during this time span and that these climatic controls have ultimately controlled the nature of the landscape evolution of foreland basins. We therefore undertook a study of the Ouarzazate basin in Morocco to examine the nature of Quaternary landscape evolution of a foreland basin in the context of Quaternary climate change.

The Ouarzazate basin is sandwiched between the High Atlas and the Anti-Atlas Mountains to the north and south, respectively (Fig. 1). The Atlas mountain system is considered as a type example of an intracontinental mountain belt (Mattauer *et al*. 1977; Rodgers 1987; Ziegler *et al*. 1995). This active mountain system formed during the Cenozoic in the interior of the African plate ahead of the Rif–Tell plate boundary orogen.

Impressive alluvial fans and terraces rising more than 100 m above active rivers flowing from the High Atlas are present within the Ouarzazate basin. These fans and terraces record a history of sedimentation and denudation that allows rates of denudation to be determined. Using geomorphological mapping, sedimentology, and the $^{10}$Be terrestrial cosmogenic radionuclide (TCN) method, the recent history of sedimentation and erosion within a stretch of the Ouarzazate basin was reconstructed to provide one of the first studies of the geomorphological evolution of an intracontinental mountain belt foreland basin that is defined by Quaternary geochronology, representing one of the first chronological datasets for continental NW Africa.

Significant work has been undertaken on alluvial fans and terraces around the Mediterranean, notably by Harvey & Wells (1987), Macklin *et al*. (1995, 2002), Fuller *et al*. (1998), Rose *et al*. (1999), Kelly *et al*. (2000), Mather (2000), Santisteban & Schulte (2007) and Schulte *et al*. (2008). These studies argue for strong links between climate, the fluvial system and landscape evolution. However, no studies of the geomorphology of alluvial fan and terraces have been undertaken in the forelands of the Atlas Mountains. Our paper therefore presents the first quantitative chronologies on terraces for the region, which begin to test key questions about the role of tectonics, climate and autocyclicity in landscape evolution in the Atlas Mountains and adjacent regions.

## Research area

The Ouarzazate basin is situated within the Alpine foreland of the Rif–Tell orogen, which comprises several intracontinental mountain belts and plateaux. The Atlas chains developed as a consequence of continental convergence between Africa and Europe, from the inversion of Jurassic rift or transtensional basins during the Cenozoic (Choubert & Faure-Muret 1962; Mattauer *et al*. 1977; Schaer 1987; Jacobshagen 1988; Laville &

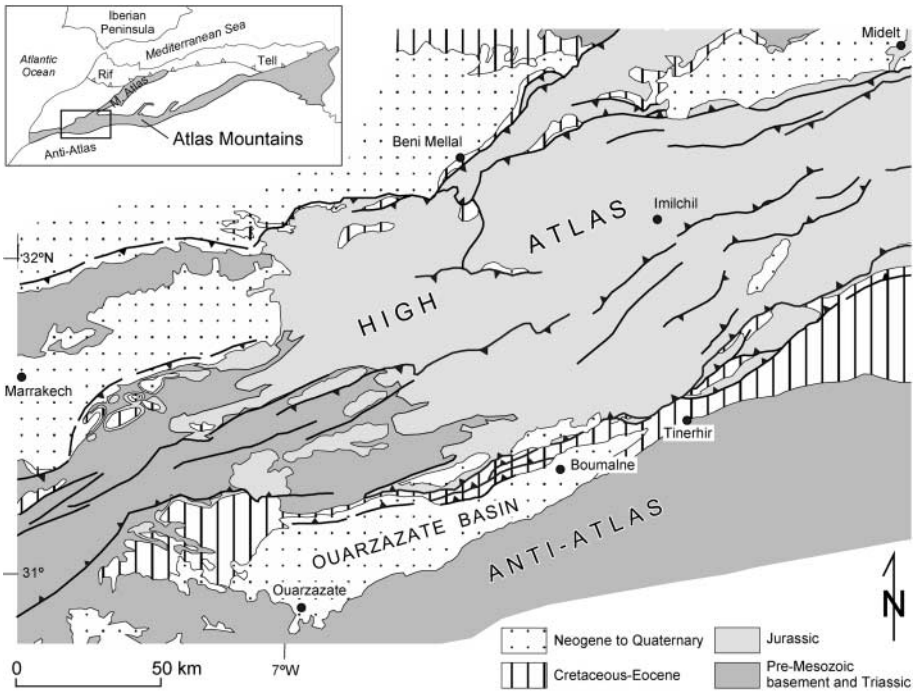


**Fig. 1.** Simplified geological map of the western part of the Central High Atlas Mountains, the Ouarzazate basin, and the Anti-Atlas Mountains. Inset shows the location of the map region in the Atlas mountain system of NW Africa.

Piqué 1992; Beauchamp *et al*. 1996; Frizon de Lamotte *et al*. 2000; Gomez *et al*. 2000; Teixell *et al*. 2003; Arboleya *et al*. 2004). The High Atlas forms the most prominent mountain chain, rising to 4000 m above sea level (a.s.l.); it is *c*. 100 km wide, and extends roughly east–west for 2000 km from Morocco into Algeria and Tunisia (Fig. 1, inset), where the range is known as the Saharan Atlas and the Tunisian Atlas, respectively. The High Atlas is composed at the surface of deformed Precambrian, Palaeozoic and Mesozoic rocks (mostly Jurassic) (Fig. 1). Flanking the High Atlas to the south, the Anti-Atlas Precambrian–Palaeozoic massif is a zone of wide domal uplift with much weaker Alpine deformation, but still reaches altitudes of more than 2000 m a.s.l. Part of the highly elevated topography of the Atlas system is due to crustal shortening and thickening, but a fraction of it is related to mantle upwelling (Teixell *et al*. 2003; Ayarza *et al*. 2005), expressed by 100 km scale lithospheric thinning (Teixell *et al*. 2005; Zeyen *et al*. 2005; Missenard *et al*. 2006).

The Ouarzazate basin is located between the High Atlas and Anti-Atlas Mountains; it has an elevation of 1200–1800 m a.s.l., extends more than 150 km roughly east–west and reaches a width of 40 km near its western end (Fig. 2a). The basin is filled with a thin (<1 km) succession of Cenozoic molasse that comprises alluvial, fluvial and lacustrine sediments (Fraissinet *et al*. 1988; Görler *et al*. 1988; El Harfi *et al*. 2001; Tesón & Teixell 2008). The Cenozoic sediments onlap the Precambrian to Palaeozoic rocks of the Anti-Atlas to the south and are overthrust by the High Atlas to the north (Fig. 2b). Basin rocks of Tertiary age are deformed by a series of southward verging folds and blind thrusts that propagate from the High Atlas Mountains (Fig. 2b). The Quaternary deposits are less deformed (Couvreur 1973; Sébrier *et al*. 2006) and comprise essentially fanglomerates, which radiate southward and cap the older rocks (Fig. 2a).

Streams drain southward and northward into the Ouarzazate basin from the High Atlas and Anti-Atlas Mountains, respectively. Most of these are ephemeral and experience flash floods during heavy rainstorm events. These ephemeral streams ultimately drain into the Draa river (Fig. 2a), which was perennial until the recent construction of a dam south of Ouarzazate. The Draa river traverses the Anti-Atlas and has cut a deep box-shaped gorge, which is >300 m deep (Figs 2b and 3). Impressive successions of terraces are present along the streams that drain the High Atlas Mountains. These terraces comprise straths in Cenozoic rocks and are capped with Quaternary fanglomerates. At least six well-defined surfaces comprising alluvial fans, terraces and an active stream (Q1–Q6) can be recognized along most of the main drainages. These are well illustrated in the Madri and Izerki valleys (Figs 2a, 4 and 5). The Madri river drains the High Atlas, in an area where the rocks that crop out are mostly Precambrian to Palaeozoic in age, consisting primarily of slate, greywacke and rhyolite. The mountainous headwaters of the Madri river drains an area of *c*. 66 $km^2$ before joining its main tributary, the Tagragra river, located to the west (Fig. 2), which drains an area of *c*. 84 $km^2$. The mean elevation of the entire Madri–Tagragra catchment is 2275 m a.s.l., and the fraction of the catchment lying above 3300 m a.s.l. is negligible (0.15%, i.e. *c*. 0.2 $km^2$). The Madri basin, therefore, lies below the snowline (3300 m a.s.l.) for the coldest stages of the Pleistocene (Dresch 1941; see also references given by Hughes *et al*. 2004, 2006).

The climate of the Ouarzazate basin is sub-Saharan, situated within the subtopical high-pressure system. Precipitation ranges from 1 to 20 mm per month, with the heaviest rainfall occurring between December and March, and totals *c*. 100 mm $a^{-1}$ (Knippertz *et al*. 2003). Temperature in the region ranges from 1 to 37 °C (Allmetsat 2007). Vegetation within the Ouarzazate basin is sparse, comprising small xerophytic shrubs.

## Field methods

Field work was undertaken throughout the Ouarzazate basin. The Madri valley was chosen for detailed study because it contains some of the best-formed and most well-preserved terraces (Figs 4 and 5). Furthermore, the valley is one of the major drainage

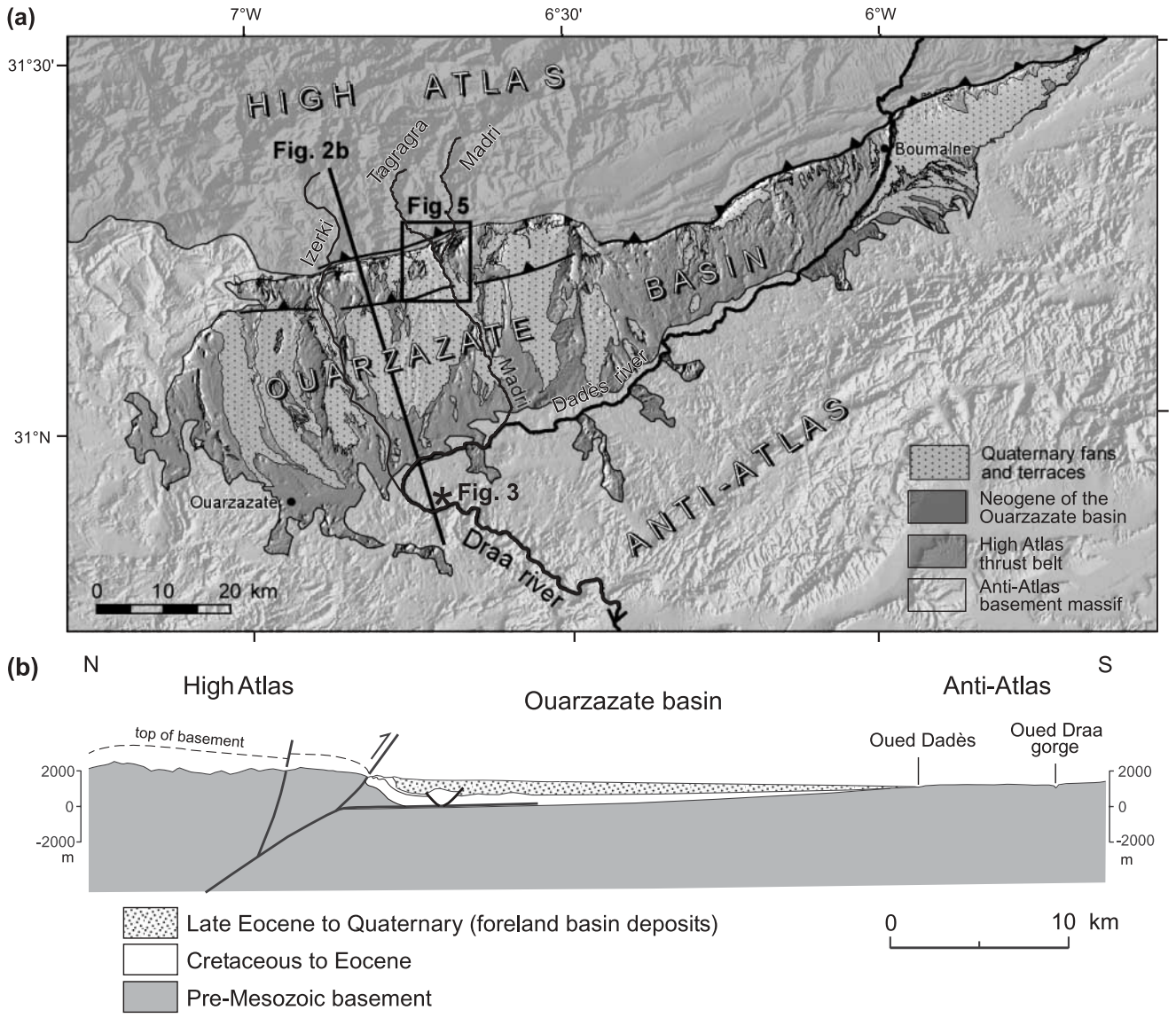


**Fig. 2.** (**a**) Map of the distribution of Quaternary fans and terraces in the Ouarzazate basin. (**b**) Cross-section of the Ouarzazate basin located between the High Atlas and the Anti-Atlas Mountains. This shows the wedge geometry of the basin and the low thickness of sediments accumulated in it (<1000 m). Deformation in the High Atlas propagates to the south, leading to Neogene and Quaternary thrusts and folds within the basin.

systems along the southern margin of the High Atlas Mountains (Fig. 2a). In addition, the catchment area is composed mostly of rhyolite and other rocks that have high quartz contents, which is essential for $^{10}$Be TCN surface exposure dating. A tectonically deformed terrace west of the Madri valley was also studied and dated to examine the possible effect of surface erosion during its deformation (Fig. 4c). An extensive surface that extends for about 15–20 km to the west of the Madri valley was also sampled at a location *c*. 11 km from the river (31.17°N, 6.80°W), where there was no evidence of surface deformation or erosion.

Geomorphological mapping aided by remote sensing using ASTER images (http://asterweb.jpl.nasa.gov/) and cross-valley profiles were used to determine the sizes and relative ages of the terraces and fan surfaces within the study areas (Figs 5 and 6). The terraces, alluvial fan and active channel surfaces were numbered Q1 (oldest) to Q6 (youngest). Sedimentary sections were studied at natural exposures to examine the terrace and fan deposits. Where fan surfaces were not contiguous, correlations were based on relative elevations and surface characteristics. These surface characteristics are listed in Table 1 and are shown in Figure 7.

The development of TCN methods in recent years has allowed alluvial fan surfaces in drylands to be successfully dated; studies using these methods include those by Zehfuss *et al*. (2001), Matmon *et al*. (2005), Benn *et al*. (2006), Akçar *et al*. (2007), Frankel *et al*. (2007*a*, *b*) and Le *et al*. (2007). We build on the methods used in these studies for sampling and interpretation of the age data.

Samples for TCN surface exposure dating were collected by chiselling off *c*. 500 g of rock from the upper surfaces of quartz-rich boulders on high areas of terrace surfaces. Locations were chosen where there was no apparent evidence of exhumation or slope instability. The largest boulders were chosen to help reduce the possibility that boulders were previously covered with

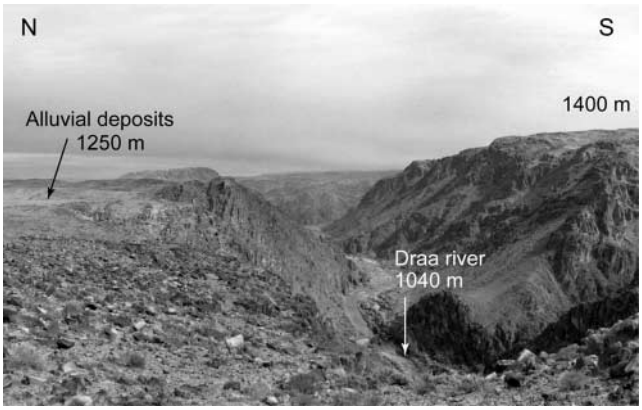


**Fig. 3.** The Draa canyon in the Anti-Atlas (location shown in Fig. 2a). South of the Ouarzazate basin margin, in the Anti-Atlas Precambrian rocks, the Draa river incision is more than 300 m deep. The view also shows light-coloured, flat-lying conglomerate deposits of Anti-Atlas origin resting on the crystalline basement (arrow). The aggradation of these Mio-Pliocene alluvial deposits near the ridge of the Anti-Atlas suggests that overfilling of the Ouarzazate basin is a possible cause for the change from internal to external drainage.

sediment. The typical boulder diameter was 70 cm; the dimensions of all sampled boulders are listed in Table 2. Several (four to seven) boulders were sampled from each alluvial fan or terrace surface (Q1–Q5). Two boulders within the active stream surface (Q6, boulders Maroc-50 and 51) were also collected. The degree of weathering and the site conditions for each boulder were recorded. In all cases, no topographic shielding correction was necessary.

## Laboratory methods

All the samples for TCN surface exposure dating were prepared in the geochronology laboratories at the University of Cincinnati. First, the samples were crushed and sieved. Quartz was separated from the 250–500 μm fractions using the methods of Kohl & Nishiizumi (1992). After addition of $^{9}$Be carrier, Be was separated and purified by ion exchange chromatography and precipitated at pH >7. Be-bearing hydroxides were oxidized by ignition in quartz crucibles. BeO was then mixed with Nb metal and loaded onto targets for the determination of $^{10}$Be/$^{9}$Be ratios by accelerator mass spectrometry (AMS) at the Center for Accelerator Mass Spectrometry at the Lawrence Livermore National Laboratory (USA). Isotope ratios were compared with ICN Pharmaceutical Incorporated $^{10}$Be and NIST (National Institute Standard of Technology) standards prepared by K. Nishiizumi (pers. comm.) and using a $^{10}$Be half-life of $1.35 \times 10^{6}$ years. The measured isotope ratios were converted to TCN concentrations in quartz using the total $^{10}$Be in the samples and the sample weights. TCN $^{10}$Be concentrations were then converted to zero-erosion exposure ages using a sea-level high-latitude (SLHL) $^{10}$Be production rate of 4.98 atoms g$^{-1}$ of quartz per year (Stone 2000). There is currently much debate regarding the appropriate scaling models and geomagnetic corrections for TCN production to calculate surface exposure ages (e.g. Pigati & Lifton 2004; Staiger *et al*. 2007; Balco *et al*. 2008). We chose to use $^{10}$Be production rates scaled to the latitude and elevation of the sampling sites, applying the time-independent scaling factors of Lal (1991) and Stone (2000) with 3% SLHL muon contribution, using the CRONUS Earth 2 calculator (Balco *et al*. 2008; http://hess.ess.washington.edu/math/). However, we recognize that other scaling models would produce ages that may differ by up to 20% (see Balco *et al*. 2008). We also calculated the TCN ages for an erosion rate of 3 m Ma$^{-1}$, which we believe is the maximum possible erosion in this environment (see discussion below). Several sample ages (the oldest samples) could not be calculated for 3 m Ma$^{-1}$ erosion because they were incompatible with this erosion rate.

## Age determination methods: accuracy and limits

Several problems are commonly recognized with TCN surface exposure dating and it is important to discuss these before assigning ages to each terrace. The first is that sampled boulders may retain a signal of prior exposure inherited from their previous location, sometimes referred to as 'derived' boulders (Anderson *et al*. 1996; Hancock *et al*. 1999). Collecting multiple samples from each terrace and looking for potential outliers, that is, exposure ages that fall significantly outside (>2σ) the weighted mean value for all the ages obtained for a given landform, can help us to recognize the potential problem of derived boulders. Furthermore, a second check on prior exposure can be made by dating boulders from the modern floodplain (Anderson *et al*. 1996). Young ages from the floodplain suggest little inheritance whereas old ages highlight a potential inheritance problem. A second problem is that boulders can produce erroneously young TCN surface exposure ages. This is usually caused by boulders that have been exhumed or toppled. The potential of exhumation can be reduced by choosing the largest boulders on a surface, sampling on ridges (not depressions) on a landform surface, choosing boulders with maximum relief above the surface (Table 2), and sampling the highest point on each boulder surface. The potential for sampling toppled boulders is reduced by choosing boulders on the distal edges of a landform to avoid toppling from higher surfaces and by sampling boulders that appear well embedded in the landform surface.

Disregarding problems of inheritance, TCN concentrations can be interpreted as either minimum exposure ages (assuming zero erosion) or maximum erosion rates (erosional equilibrium). For estimating steady-state erosion rates, samples with older apparent exposure ages provide limits on erosion rates. For many of the samples collected in the study area, maximum erosion rates of 1–3 m Ma$^{-1}$ were calculated using the oldest boulders by applying the methods of Lal (1991). Given that these are maximum erosion rates and that it is unlikely that they are in erosional equilibrium because the preserved fluvial forms (rounded smooth surfaces) on many of the boulders suggest moderate to little erosion, a reasonable estimation of erosion for boulders in the study area is *c*. 1 m Ma$^{-1}$. Furthermore, the absence of notable weathering features, such as exfoliated surfaces, suggests that erosion of boulders is <1 m Ma$^{-1}$. Assuming that all boulders weather at this rate, we can assess the impact of this amount of erosion on our chronologies. For samples having a 1 m Ma$^{-1}$ erosion rate, an age of 10 ka would increase uncertainty by 1%; an age of 50 ka, by 4%; an age of 100 ka, by 10%; an age of 200 ka, by 22%; and an age of 300 ka, by 42%. An erosion rate of 1 m Ma$^{-1}$ is consistent with the TCN data from studies in other dryland regions (Small *et al*. 1997; Zehfuss *et al*. 2001; Owen *et al*. 2006). Given the uncertainties in defining the erosion rate, we plot all our data with zero erosion, but also present the ages in Table 2 for an erosion rate of 3 m Ma$^{-1}$, which places an upper limit on the possible ages when considering erosion in this region.

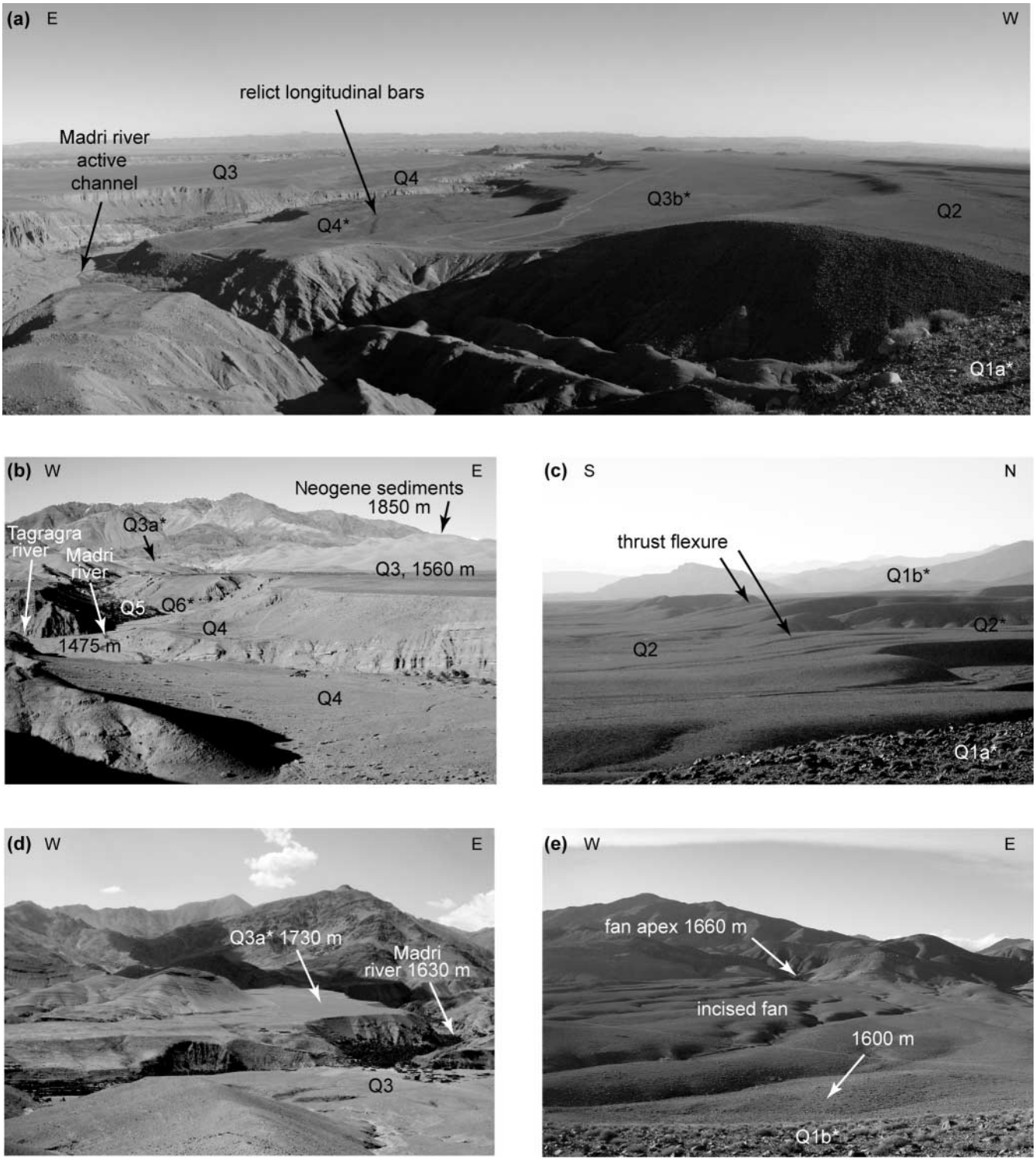


**Fig. 4.** Succession of terraces in the Madri (**a**, **b** and **d**) and Tagragra (**c** and **e**) valleys (terrace locations shown in Fig. 5) The asterisks indicate the sampled terraces. (**a**) Madri river viewed to the south towards the Anti-Atlas (ridge line in the background). Terraces Q2 and Q3 are very extensive and merge to the south of the study area. Longitudinal bars are preserved on terrace Q4. In the foreground, the badlands are Neogene deposits tilted to the south and cut by the strath terraces. (**b**) Madri river viewed northwards towards the High Atlas showing four fill-terraces (Q3–Q6). Terraces Q2 to Q5 lie at elevations ranging from 1585 m to 1510 m a.s.l., respectively (see topographic profile 2, Fig. 6). In the background the sampled terrace Q3a reaches an elevation of 1740 m a.s.l. (see topographic profile 3, Fig. 6). The terraces are inset into the Neogene basin fill, which reaches an elevation of around 1850 m a.s.l. on the northern border of the Ouarzazate basin. (**c**) Folding is active in this part of the Ouarzazate basin: in the area shown, flexure of terrace Q2 generated an offset of 20 m. (**d**) Abandoned and deeply incised fan Q3a viewed to the north near the High Atlas Mountains front. (**e**) Poorly incised fan located west of the Tagragra river viewed to the north; distance from the foreground to the fan apex is 1500 m. Foreground is the sampled surface Q1b.

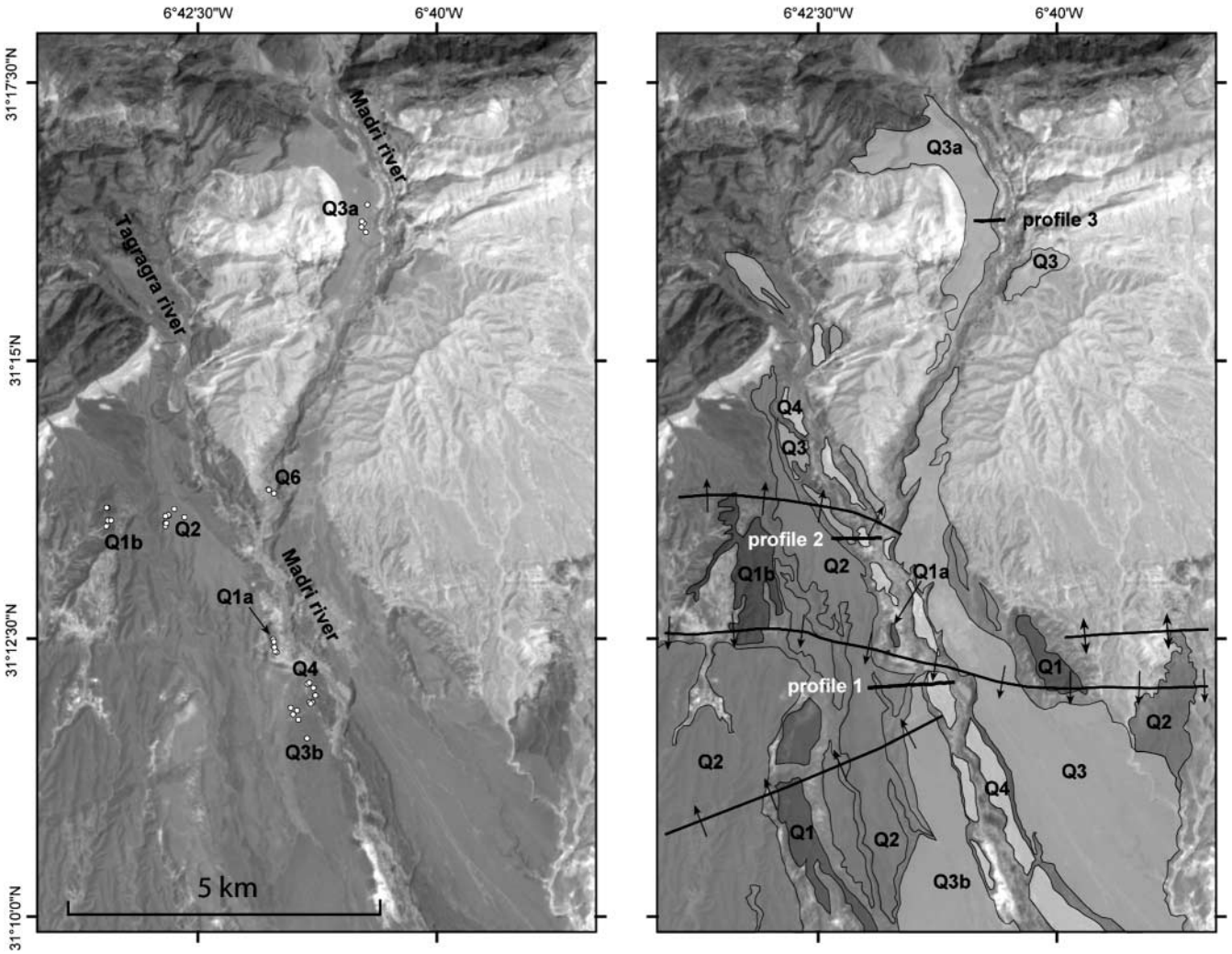


**Fig. 5.** ASTER image of the study area showing the location of samples (left) and the mapped terraces (right). Also shown are the flexure and folding axes of the Neogene and Quaternary deposits. Sample Q3c is not shown in this figure but is located *c*. 10 km to the west of the mapped area (Table 2 provides detailed locations). The trend of the Amekchoud anticline is highlighted in the right hand panel by the black line and dip arrows.

## Results

The geomorphology of the terraces within the study area is illustrated in Figures 4–6. The terraces are more incised near the mountain front, where the sedimentary deposits are thickest (see terrace Q3a in Fig. 4d and inset in Fig. 6). The thickness of the Quaternary sediments varies considerably along the length of each valley, reflecting infilling of large channels many tens of metres across and more than 10 m deep. The sediments comprise well-rounded clast-supported cobbles and metre-size boulders in a sandy matrix, and show crude downvalley, low-angle cross-stratification. Over most of the length of each terrace the capping Quaternary sediments are 3–5 m thick.

Given the caveats discussed in the previous section, we assign modelled ages to each of the dated surfaces. These modelled ages represent the time when the terrace surface was abandoned, leaving the boulders exposed to cosmic rays. Tables 1 and 2 list the results of the TCN surface exposure dating, and in Figure 8 these data are plotted as scatter graphs and probability distributions. The range of ages for each surface varies considerably (third column in Table 1). This probably reflects the variability of geomorphological processes on terrace surfaces as discussed above and the range is greatest for the oldest surfaces. However, for many of the surfaces there is a clustering of ages (fourth column in Table 1), notably Q3 and Q4 surfaces. Given the clustering of ages and identification of possible inherited, exhumed, toppled and weathered boulders, an age is assigned to each surface (fifth column in Table 1). Table 2 also provides details on the lithology and size of the boulders dated and their weathering characteristics. The more resistant lithologies, and larger and less weathered boulders would be expected to give the oldest age on any given surface. However, there is no clear relationship in the dataset between boulder size and/or weathering characteristic and the age of the boulder for a particular surface, so it is difficult to explain anomalously young ages as a direct consequence of weathering.

Surface Q6 is the active channel of the Madri river and two dated boulders in this channel give ages of 0.5 ka and 19 ka. The first sample indicates that there is almost no inheritance in the active channel and the second one indicates that there may be some inheritance in some boulders but this is probably not important given the very old ages for most terraces (see below).

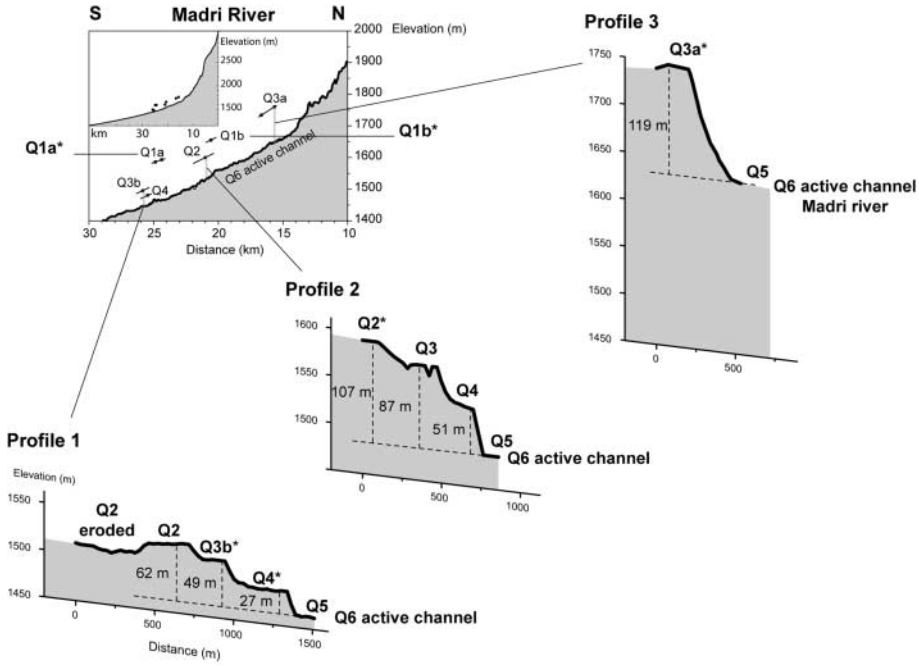


**Fig. 6.** Site location of abandoned filled terraces on transverse and longitudinal profiles. Along the Madri river, three transverse topographic profiles (numbered 1, 2 and 3 from downstream to upstream) have been performed where terraces have been sampled except for terraces Q1a, Q1b and Q2. Samples Q1a are located between profiles 1 and 2. Samples Q2 and Q1b are located 600 m NW and 1600 m west of profile 2, respectively (see Fig. 5). The asterisks indicate the sampled terraces. Graph in the upper left corner shows the sampled terraces projected (dots) onto the longitudinal profile of the Madri river extracted from SRTM90 DEM. Inset shows the longitudinal profile from the source to the confluence of the Madri river with the Dades river.

Surface Q5 is less than a few metres above the present channel. This terrace is used for agriculture and sampling was not possible, although it is likely that surface Q5 is historical.

Surface Q4 has ages that range from 7 to 36 ka, but the ages cluster between 7 and 11 ka. The pristine nature of the surface (well-preserved bar and swale forms and imbricated boulders) support the view that boulders Maroc-20 (36 ka) and Maroc-21 (23 ka) have inherited TCN. Therefore it is likely that this surface formed during the early Holocene or at the end of the Late-glacial.

Surface Q3 is very extensive in the southern part of the Ouarzazate basin. This surface was dated at three locations, which are named Q3a, Q3b and Q3c (see Table 2 for sampling locations). Ages span 85–105 ka, 87–121 ka and 84–93 ka, and cluster at 85–95 ka, 87–100 ka and 84–93 ka, respectively. An age range of 87–93 ka is favoured given that the surfaces are contemporaneous. Given some weathering (1 m $Ma^{-1}$), these ages become *c*. 10% older (*c*. 96–102 ka) and a maximum value of 3 m $Ma^{-1}$ yields ages of 113–125 ka. The abandonment age for the Q3 surface corresponds broadly to marine oxygen isotope stage 5c. The age of the Q3 surface could straddle marine isotope stage 5e, however, given the uncertainty associated with the different scaling models and geomagnetic corrections that may be applied to calculate TCN ages (see discussion above). We favour the view that incision and abandonment of the sediments that form the Q3 surface occurred during the wetter last interglacial, but recognize the possibility that the surface may have formed during marine isotope stage 5c or earlier.

Surface Q2 is an extensive surface that can be traced in the upstream parts of the Ouarzazate basin. Near our sampling location, this surface has been gently deformed into a 2 m high broad flexure, as a result of the foreland propagation of thrust faulting. The ages on this surface range between 129 and 295 ka, but cluster between 163 and 174 ka. Samples Maroc-16 (129 ka) and Maroc-15 (295 ka) are probably from weathered–exhumed and derived boulders, respectively. Given a weathering rate of 1 m $Ma^{-1}$, the remaining ages should be *c*. 22% older (*c*. 196–211 ka), which suggests terrace deposition during the penultimate interglacial (marine oxygen isotope stage 7e) with incision and abandonment during post- or late-penultimate interglacial time.

The oldest surface, Q1, occurs on the top of mesas within several kilometres of the mountain front throughout the basin. These mesas have been deformed (Fig. 4c) and are intensely eroded. To test the stability of deformed surfaces, samples were collected from two relicts of the deformed surface Q1: the first along the Madri river (Q1a) and the second several kilometres west of the Tagragra river (Q1b). Both sample sites are between two flexures that merge to the east into the flanks of the east–west-trending Amekchoud anticline (Fig. 5).

Ages on surface Q1a range from 7 to 214 ka, but cluster around 193–214 ka. This wide range of ages probably reflects strong erosion, particularly for sample Maroc-8 (7 ka), which probably was recently exhumed. Given the 1 m $Ma^{-1}$ erosion rate, the ages on this surface are likely to be at least 30% older and fall in the range 250–278 ka. The oldest boulder is most probably closest to the true age of the surface given that the surface has been eroded. Therefore surface Q1 is older than marine isotope stage 7e. Given the glacial–interglacial temporal spacing of the other terraces and the strong carbonate development (stage IV–V of Gile *et al*. 1981) in the terrace sediments for Q1, we assign Q1 to the interglacial of marine oxygen isotope stage 9c. However, this is tentative as the ages are widely scattered, probably because the surface has been deformed and eroded.

North of the Q1a area, surface Q1b is deformed into a steep monocline that rises between 5 and 7 m. This represents a ramping thrust that is related to foreland-propagating deformation from the High Atlas. Although this surface morphostratigraphically correlates with Q1a, the boulder ages range from 94 to 131 ka and they cluster between 109 and 124 ka. These are significantly younger ages compared with those of surface Q1a, and suggest that the Q1b surface has experienced considerable erosion.

Rates of fluvial incision (determined by dividing the elevation between surfaces by their ages) can be estimated using the depth of incision of terraces Q2–Q4 from profiles measured in the field

**Table 1.** *Descriptions and TCN ages for terraces in the Madri valley and the adjacent region*

| Surface name | Sample numbers | Age range using 0 m $Ma^{-1}$ erosion (ka) | Age cluster using 0 m $Ma^{-1}$ erosion (ka) | Favoured age (ka) | Surface altitude (m asl) | Description of surface |
|---|---|---|---|---|---|---|
| Q1a | Maroc-4, and 6 to 10 | 7–214 | 193–214 | 250–278; MIS-9c | 1590 | This is the highest surface and occurs on top of small mesas. It is present within several kilometres of the mountain front throughout the basin. The surfaces undulate and have well-developed desert pavements. Most surfaces may have experienced considerable deflation and erosion prior to desert pavement formation. The surface sediments have a well-developed carbonate cement (carbonate morphology stage IV–V of Gile *et al*. 1981) |
| Q1b | Maroc-35 to 38, 40 and 41 | 94–131 | 109–124 | MIS-9c | 1660 | This surface has the same general characteristics as Q1, but it is warped, deformed by a growth fold. It has areas of pronounced erosion |
| Q2 | Maroc-11, and 13 to 17 | 129–295 | 163–174 | MIS-7e | 1600 | This surface is planar and can be traced for many tens of kilometres across the basin. It has a well-developed desert pavement, but few boulders larger than 1 m in diameter. In places this surface is subtly deformed by growth folds and faults. A 10–15 cm thick calcrete layer is present across part of this surface and the clasts within the first few metres of this surface are densely cemented with carbonate (carbonate morphology stage IV–V of Gile *et al*. 1981) |
| Q3a | Maroc-27, 29, 30, 31, 33 and 34 | 85–105 | 85–95 | MIS-5e | 1730 | Apex of fan near Imin Tazarhgt village. Contains many boulders, with abundant bars and swale forms (carbonate morphology stage III of Gile *et al*. 1981) |
| Q3b | Maroc-42, 43, 46, 47 and 49 | 87–121 | 97–100 | MIS-5e | 1495 | This is an extensive surface that can be traced many kilometres along and down the basin. The surface is a flat surface with occasional metre-size boulders. The surface is deformed by a growth fold. The upper 2 m of sediment has porous carbonate cement (carbonate morphology stage III of Gile *et al*. 1981) |
| Q3c | Maroc-112, 113, 115 to117 | 84–93 | 84–93 | MIS-5e | 1450 | This is an extensive surface that can be traced for several tens of kilometres. The surface is very flat, but faulted and warped in place, and it has occasional metre-size boulders. The upper 2 m of sediment has porous carbonate cement (carbonate morphology stage III of Gile *et al*. 1981) |
| Q4 | Maroc-20 to 26 | 7–36 | 7–11 | Early Holocene | 1482 | Surface with many large boulders (>1 m in diameter). The boulders are commonly imbricated and form longitudinal bars. Desert pavement is present between these bars. Millimetre-thick carbonate rims are present around clasts within the top few metres of the surface sediment (carbonate morphology stage II of Gile *et al*. 1981) |
| Q5 | Maroc-52 | Not dated | | | | Historical terrace; many boulders on agricultural terrace. No carbonate development |
| Q6 | Maroc-50 and 51 | 0.5–19 | Not applicable | recent | recent | Active channel; abundant large boulders. No carbonate development |

MIS, marine oxygen isotope stage.

(Fig. 6) and the assigned ages. Assuming that incision and abandonment occurred during each interglacial, we use Winograd *et al*. (1997) interglacial termination ages for the interglacials that are assigned to the surfaces to provide maximum incision rates. Incision rates based on surface Q2 are 0.28 mm $a^{-1}$ and 0.49 mm $a^{-1}$ for profiles 1 and 2, respectively. For surface Q3, calculated incision rates are 0.39 mm $a^{-1}$, 0.70 mm $a^{-1}$ and 0.95 mm $a^{-1}$ for profiles 1, 2, and 3, respectively. If we assign the Q3 surface to marine isotope stage 5c, the incision ranges from 0.51 to 1.24 mm $a^{-1}$. The rates of incision for the Q4 surface are less than 2.45 mm $a^{-1}$ and less than 5.18 mm $a^{-1}$ for profiles 1 and 2, respectively. The higher incision rates for Q4 probably reflect the fact that the present interglacial cycle is not yet complete, and given more time the rates are likely to be

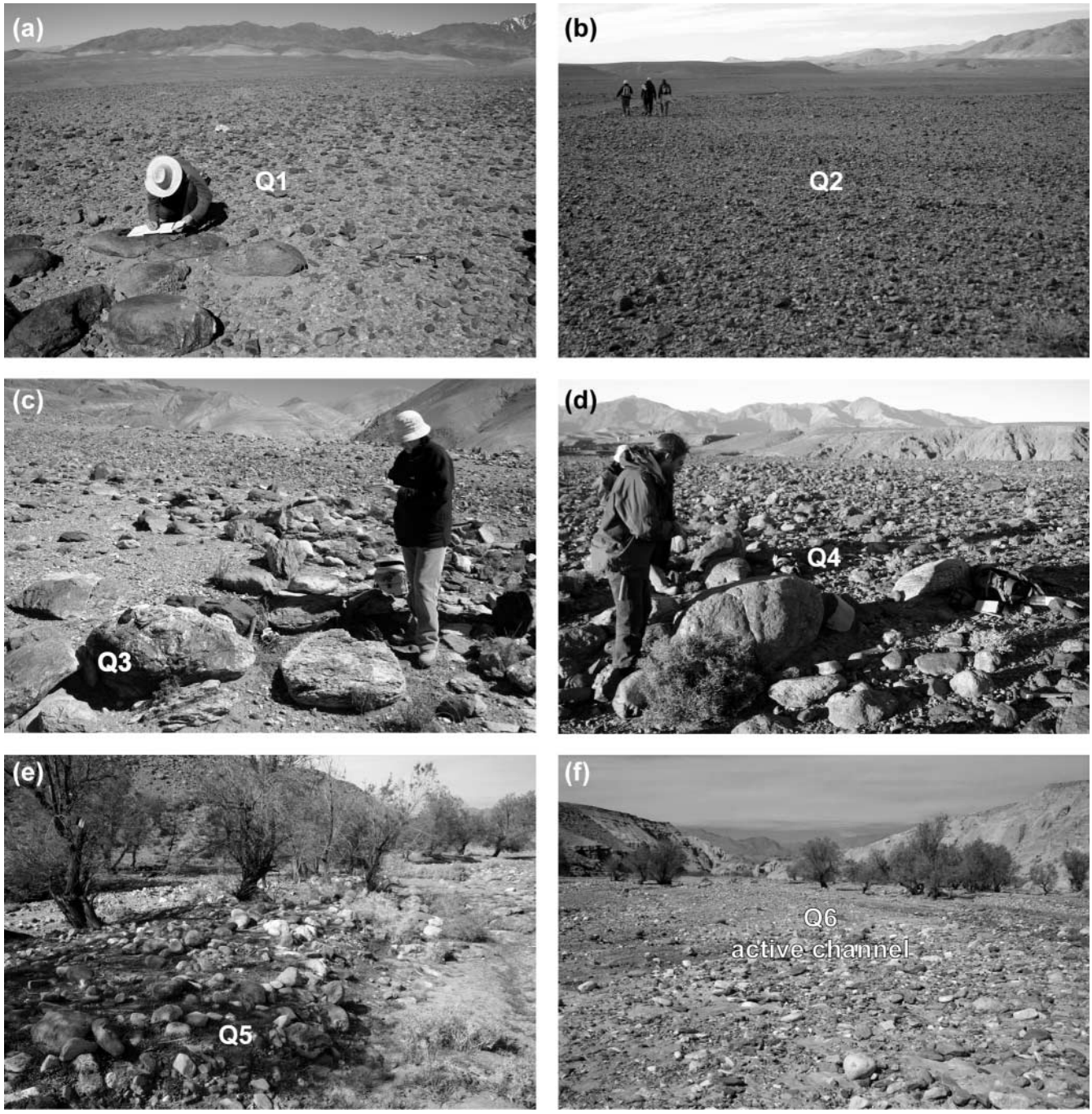


**Fig. 7.** Detail views of terrace surface characteristics. (**a**) Q1; (**b**) Q2; (**c**) Q3; (**d**) Q4; (**e**) Q5; (**f**) Q6. Terrace characteristics are described in Table 1.

substantially reduced. The fluvial incision rate calculations based on the terraces in our study area is in accordance with rates of fluvial incision for other semi-arid environments (e.g. Anders *et al*. 2005).

## Discussion

The history of the Ouarzazate foreland basin can be broadly divided into two periods. Its early record is dominated by net sedimentation as Tertiary fluvial and lacustrine sediments were deposited within an internally drained basin confined between the Atlas and Anti-Atlas Mountains (e.g. Görler *et al*. 1988; Fig. 9a). In contrast, its later history is dominated by erosion and began when the Draa river cut through the Anti-Atlas Mountains and the basin became externally drained (Fig. 9b–g). Stäblein (1988) suggested that the Draa river captured the Ouarzazate basin by regressive erosion. Alternatively, the piracy may have been induced when sediments overfilled the Ouarzazate basin and overtopped ridges of the Anti-Atlas, which allowed the southward drainage of streams from the basin via what is now the Draa river canyon (Fig. 3). In any case, the timing of the development of this superimposed drainage has yet to be defined,

**Table 2.** *Sample locations, descriptions, and terrestrial cosmogenic nuclide surface exposure data and ages*

| Sample number | Surface | Latitude (°N) | Longitude (°W) | Altitude (m) | Lithology | Height/width/ breadth of sampled clast (cm) | Buried* | Weathering† | Sample thickness (cm) | $^{10}$Be atoms g$^{-1}$ $SiO_2$ ($10^5$) | TCN age (no erosion)‖ | | | TCN age (3 m Ma$^{-1}$ erosion)‖ | | |
|---|---|---|---|---|---|---|---|---|---|---|---|---|---|---|---|---|
| | | | | | | | | | | | Age (ka) | Internal error (ka) | External error (ka) | Age (ka) | Internal error (ka) | External error (ka) |
| Maroc-4 | Q1a | 31.208 | 6.694 | 1590 | Quartzite breccia | 13/90/56 | d | n | 2.5 | 2.71 ± 0.11 | 21.8 | 0.9 | 2.2 | 23.1 | 1.0 | 2.5 |
| Maroc-6 | Q1a | 31.209 | 6.695 | 1593 | Unknown‡ | 17/15/6 | s | n | 6 | 18.40 ± 0.46 | 157.7 | 4.1 | 15.6 | 315.5 | 21.7 | 81.6 |
| Maroc-7 | Q1a | 31.210 | 6.695 | 1595 | Quartzite‡ | 11/7/4 | s | s | 4 | 23.65 ± 0.48 | 201.7 | 4.3 | 19.9 | § | § | § |
| Maroc-8 | Q1a | 31.209 | 6.695 | 1594 | Metaconglomerate‡ | 21/11/6 | d | s | 6 | 0.80 ± 0.07 | 6.6 | 0.6 | 0.8 | 6.7 | 0.6 | 0.8 |
| Maroc-9 | Q1a | 31.209 | 6.695 | 1599 | Red sandstone‡ | 15/11/8 | s | n | 8 | 24.27 ± 0.49 | 213.7 | 4.6 | 21.1 | § | § | § |
| Maroc-10 | Q1a | 31.208 | 6.695 | 1592 | Red sandstone‡ | 14/15/5 | s | s | 5 | 22.55 ± 0.46 | 193.1 | 4.1 | 19.0 | 706.2 | 183.2 | 842.1 |
| Maroc-35 | Q1b | 31.227 | 6.724 | 1662 | Quartzite | 26/68/56 | d | e | 5 | 11.85 ± 0.31 | 94.1 | 2.5 | 9.2 | 127.3 | 4.9 | 17.6 |
| Maroc-36 | Q1b | 31.226 | 6.724 | 1660 | Quartzite | 15/61/4 | d | s | 5 | 15.39 ± 0.50 | 123.9 | 4.2 | 12.4 | 194.3 | 11.5 | 34.0 |
| Maroc-37 | Q1b | 31.226 | 6.724 | 1661 | Quartzite | 15/51/42 | d | n | 5 | 14.58 ± 0.32 | 117.1 | 2.6 | 11.3 | 177.0 | 6.6 | 28.3 |
| Maroc-38 | Q1b | 31.227 | 6.723 | 1660 | Quartzite | 19/58/40 | d | n | 5 | 14.52 ± 0.36 | 117.2 | 3.0 | 11.4 | 177.2 | 7.5 | 28.6 |
| Maroc-40 | Q1b | 31.229 | 6.724 | 1654 | Quartzite | 22/54/41 | d | s | 3 | 13.86 ± 0.35 | 109.2 | 2.8 | 10.6 | 158.5 | 6.4 | 24.1 |
| Maroc-41 | Q1b | 31.229 | 6.724 | 1655 | Quartzite | 43/92/59 | d | f | 3 | 16.52 ± 0.41 | 131.2 | 3.4 | 12.8 | 215.1 | 10.4 | 39.3 |
| Maroc-11 | Q2 | 31.212 | 6.712 | 1603 | Quartzite | 26/46/40 | d | s | 4 | 19.40 ± 0.46 | 162.6 | 4.0 | 16.0 | 342.0 | 24.5 | 96.9 |
| Maroc-13 | Q2 | 31.228 | 6.713 | 1599 | Rhyolite | 18/48/34 | d | n | 4 | 20.38 ± 0.50 | 170.9 | 4.4 | 16.9 | 395.7 | 35.8 | 137.0 |
| Maroc-14 | Q2 | 31.228 | 6.714 | 1600 | Siliceous volcanic rocks | 20/49/40 | d | n | 4 | 20.84 ± 0.61 | 176.1 | 5.4 | 17.7 | 438.1 | 54.9 | 180.4 |
| Maroc-15 | Q2 | 31.227 | 6.714 | 1600 | Rhyolite | 35/71/37 | m | n | 3 | 34.24 ± 0.82 | 295.2 | 7.6 | 30.1 | § | § | § |
| Maroc-16 | Q2 | 31.225 | 6.713 | 1602 | Siliceous volcanic rocks | 18/65/36 | m | n | 3 | 15.53 ± 0.39 | 128.6 | 3.3 | 12.6 | 207.4 | 9.8 | 37.0 |
| Maroc-17 | Q2 | 31.226 | 6.714 | 1595 | Quartzite | 36/54/46 | d | s | 2 | 24.85 ± 0.63 | 208.8 | 5.6 | 20.9 | § | § | § |
| Maroc-27 | Q3a | 31.271 | 6.680 | 1729 | Rhyolite | 37/114/120 | d | n | 3 | 11.42 ± 0.28 | 85.1 | 2.2 | 8.2 | 111.0 | 3.8 | 14.5 |
| Maroc-29 | Q3a | 31.271 | 6.679 | 1735 | Rhyolite | 26/80/49 | d | n | 2 | 14.16 ± 0.34 | 105.2 | 2.6 | 10.2 | 149.9 | 5.6 | 22.1 |
| Maroc-30 | Q3a | 31.272 | 6.679 | 1736 | Rhyolite | 47/106/75 | d | f | 3 | 12.73 ± 0.31 | 94.6 | 2.4 | 9.2 | 128.3 | 4.6 | 17.7 |
| Maroc-31 | Q3a | 31.272 | 6.679 | 1737 | Rhyolite | 23/97/55 | d | n | 3 | 13.84 ± 0.35 | 102.9 | 2.7 | 10.0 | 145.0 | 5.7 | 21.1 |
| Maroc-33 | Q3a | 31.270 | 6.679 | 1734 | Rhyolite | 39/87/53 | d | n | 3 | 12.65 ± 0.31 | 94.7 | 2.3 | 9.2 | 128.6 | 4.5 | 17.8 |
| Maroc-34 | Q3a | 31.254 | 6.680 | 1738 | Rhyolite | 35/71/69 | d | f | 3 | 11.80 ± 0.29 | 87.6 | 2.2 | 8.5 | 115.5 | 3.9 | 15.3 |
| Maroc-42 | Q3b | 31.199 | 6.691 | 1494 | Rhyolite | 15/58/34 | d | s | 2 | 11.41 ± 0.45 | 99.8 | 4.1 | 10.2 | 138.5 | 8.3 | 20.8 |
| Maroc-43 | Q3b | 31.199 | 6.691 | 1494 | Conglomerate | 21/66/42 | d | s | 3 | 11.71 ± 0.37 | 104.3 | 3.4 | 10.3 | 147.7 | 7.2 | 22.1 |
| Maroc-46 | Q3b | 31.199 | 6.692 | 1498 | Rhyolite | 20/61/44 | d | n | 2 | 9.97 ± 0.28 | 86.6 | 2.5 | 8.5 | 113.5 | 4.5 | 15.1 |
| Maroc-47 | Q3b | 31.198 | 6.691 | 1496 | Rhyolite | 33/65/92 | d | s | 3 | 10.16 ± 0.35 | 88.8 | 3.2 | 8.9 | 117.5 | 5.8 | 16.2 |
| Maroc-49 | Q3b | 31.195 | 6.689 | 1494 | Sandstone | 16/45/56 | d | e | 1 | 13.79 ± 0.33 | 120.5 | 3.0 | 11.7 | 185.2 | 7.8 | 30.6 |
| Maroc-112 | Q3c | 31.166 | 6.802 | 1449 | Psammite | 26/42/70 | d | n | 5 | 98.11 ± 0.30 | 84.2 | 2.3 | 7.8 | 109.2 | 3.9 | 13.6 |
| Maroc-113 | Q3c | 31.166 | 6.802 | 1449 | Phyllite | 20/30/75 | d | n | 5 | 10.83 ± 0.26 | 93.1 | 2.2 | 8.6 | 125.3 | 4.2 | 16.2 |
| Maroc-115 | Q3c | 31.166 | 6.802 | 1448 | Phyllite | 22/25/55 | d | s | 6 | 10.26 ± 0.30 | 88.9 | 2.3 | 8.2 | 117.6 | 4.2 | 15.0 |
| Maroc-116 | Q3c | 31.166 | 6.802 | 1450 | Psammite | 10/36/40 | d | s | 4 | 10.27 ± 0.24 | 87.4 | 2.2 | 8.0 | 114.9 | 3.9 | 14.4 |
| Maroc-117 | Q3c | 31.165 | 6.803 | 1446 | Psammite | 18/25/52 | m | n | 4 | 10.38 ± 0.20 | 88.6 | 1.8 | 8.0 | 117.1 | 3.2 | 14.6 |
| Maroc-20 | Q4 | 31.203 | 6.689 | 1481 | Rhyolite | 60/151/81 | d | n | 2.5 | 4.11 ± 0.15 | 35.9 | 1.4 | 3.6 | 39.5 | 1.7 | 4.4 |
| Maroc-21 | Q4 | 31.202 | 6.688 | 1480 | Rhyolite | 70/165/125 | d | n | 2 | 2.60 ± 0.11 | 22.5 | 1.0 | 2.3 | 23.9 | 1.1 | 2.6 |
| Maroc-22 | Q4 | 31.201 | 6.688 | 1482 | Rhyolite | 63/120/80 | d | n | 2 | 0.97 ± 0.18 | 8.3 | 1.6 | 1.8 | 8.5 | 1.7 | 1.8 |
| Maroc-23 | Q4 | 31.201 | 6.688 | 1485 | Gneiss | 41/88/45 | d | n | 2 | 0.95 ± 0.06 | 8.2 | 0.5 | 0.9 | 8.4 | 0.6 | 1.0 |
| Maroc-24 | Q4 | 31.200 | 6.688 | 1482 | Rhyolite | /88/52 | m | f | 5 | 0.80 ± 0.16 | 7.1 | 1.4 | 1.5 | 7.2 | 1.4 | 1.6 |
| Maroc-25 | Q4 | 31.200 | 6.689 | 1484 | Rhyolite | 66/147/84 | m | n | 3 | 1.21 ± 0.16 | 10.5 | 1.4 | 1.7 | 10.8 | 1.4 | 1.8 |
| Maroc-26 | Q4 | 31.200 | 6.688 | 1484 | Siliceous volcanic rocks | 46/76/66 | m | n | 2 | 1.27 ± 0.17 | 10.9 | 1.4 | 1.7 | 11.3 | 1.5 | 1.8 |
| Maroc-50 | Q6 | 31.231 | 6.695 | 1503 | Rhyolite | 23/38/66 | d | n | 2 | 2.17 ± 0.18 | 18.5 | 1.6 | 2.3 | 19.4 | 1.7 | 2.6 |
| Maroc-51 | Q6 | 31.231 | 6.695 | 1503 | Rhyolite | 30/30/50 | d | n | 3 | 0.06 ± 0.06 | 0.5 | 0.5 | 0.5 | 0.5 | 0.5 | 0.5 |

*d, deeply buried; m, moderate burial; s, slight burial.
†n, no noticeable weathering; s, slight weathering; f, fractures; e, exfoliation.
‡Cobble.
§Cannot calculate.
‖Internal error incorporates only analytical uncertainty, while external error incorporates both analytical and production rate uncertainty.

but it probably occurred during the late Pliocene or early Pleistocene, as there is little evidence of large cut–fill sequences within Tertiary red beds within the basin.

The extensive and deep incision developed throughout the Ouarzazate basin as the Draa river cut its way through the Anti-Atlas and essentially lowered the local base level has resulted in the succession of terraces we have described (Fig. 9b–g). The TCN ages for the terrace Q4 argue for climate and vegetation cover control of the fluvial behaviour at least for the last interglacial. Q4 TCN dates cluster between 7 and 11 ka (Table 2). These ages correspond to the abandonment and the start of incision of this terrace, now lying at 27 m above the active Madri channel. In the northern margin of the Sahara, south of the Atlas mountains of Algeria, after an arid glacial time, permanent lacustrine conditions prevailed during the early to mid-Holocene (from *c*. 11–10 to 5.7–3.3 ka; Gasse *et al*. 1987, 1990; Gasse 2000). Consistently, fluctuations in terrigenous supply to the continental margin off southern Morocco indicate an abrupt increase in humidity at 11.5–11 ka (Holz *et al*. 2007). This humid period correlates with the replacement of the Last Glacial Maximum (centred on *c*. 22 ka) cool grass–shrub steppe vegetation in north Africa (Lamb *et al*. 1989; Jolly *et al*. 1998; Elenga *et al*. 2000) by wooded biomes (temperate xerophytic wood or warm mixed forest in mountain catchments) that were present at elevations between 1200 and 2200 m a.s.l. by at least 6 ka (Reille 1979; Lamb *et al*. 1989, 1995; Salamani 1991, 1993; Jolly *et al*. 1998). Such a change in the vegetation cover suggest that vegetation-controlled slope stabilization in the beginning of the present interglacial reduced hillslope sediment supply to trunk streams, causing the end of fluvial aggradation in the Madri valley and, consequently, offering a mechanism for abandonment and incision of Q4.

Correlation with climatic cycles is not so straightforward for the older terraces (Q3 to Q1) because of uncertainties in the TCN ages (see Table 2). With regard to the Q3 surface, correcting for an erosion rate of 1 m Ma$^{-1}$ places the most probable age of this terrace at 96–102 ka. If the same relationship to climate applies (i.e. incision during wet interglacial stages as for Q4), the abandonment of Q3 can be attributed to interglacial marine isotope stage 5e or the humid stadials of marine isotope stage 5 (specifically stage 5c).

Although direct palaeoclimate data for this epoch in Morocco

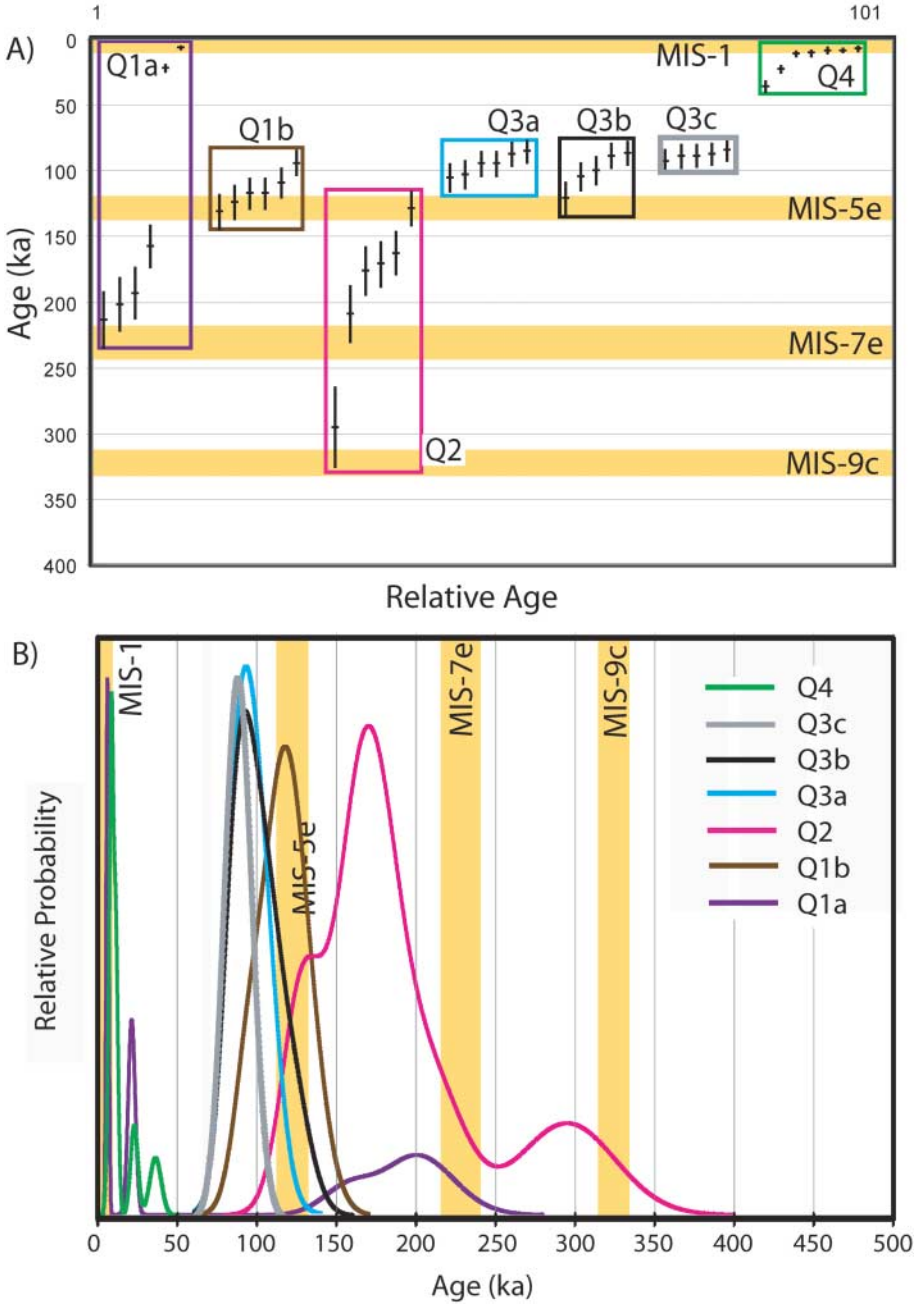


**Fig. 8.** TCN results plotted as (**a**) scatter graphs and (**b**) summed probability distributions for each surface. The duration of the interglacials MIS 1, 5e, 7e, and 9c (MIS, marine oxygen isotope stage) are based on the Devil's Hole $\delta^{18}O$ record (after Winograd *et al*. 1997).

are lacking, marine palaeoclimate records are available for the western Mediterranean (see, e.g. Cacho *et al*. 1999; Magri & Parra 2002; Hoogakker *et al*. 2004), but correlation with the terrestrial record across the Atlas Mountains is very tentative. Some of these issues have been discussed by Tzedakis (2007). However, previous studies on the Pleistocene fluvial behaviour of the Mediterranean region (e.g. Lewin *et al*. 1995; Fuller *et al*. 1998; Harvey *et al*. 1999*a*; Macklin *et al*. 2002; Santisteban & Schulte 2007; and references herein) provide important insights and have emphasized the sensitivity of fluvial systems to climate change, with sediment pulses in cold glacials or stadials and incision in warmer interglacials or interstadials. Climatic controls on alluvial fan and terrace development have long been recognized in other semi-arid settings, such as in the Basin and Range province and the Mojave Desert of the Western USA (Bull 1991; Harvey *et al*. 1999*b*). Moreover, Macklin *et al*. (2002) described a major river aggradation stage occurring at 109–111 ka (marine oxygen isotope stage 5d) in many Mediterranean catchments, a result that is broadly compatible with the age of aggradation that can be inferred for Q3.

We postulate that Q2 and Q1 correlate with the previous two interglacials. To our knowledge, independent data on humidity and vegetation cover in North Africa around these events are not available for either interglacial, but we may speculate that the same processes inferred for Q4 incision apply also for these cases.

Macklin *et al*. (2002) argued that, over the last 200 ka, fluvial aggradation phases generally occur during cool, dry glacials or

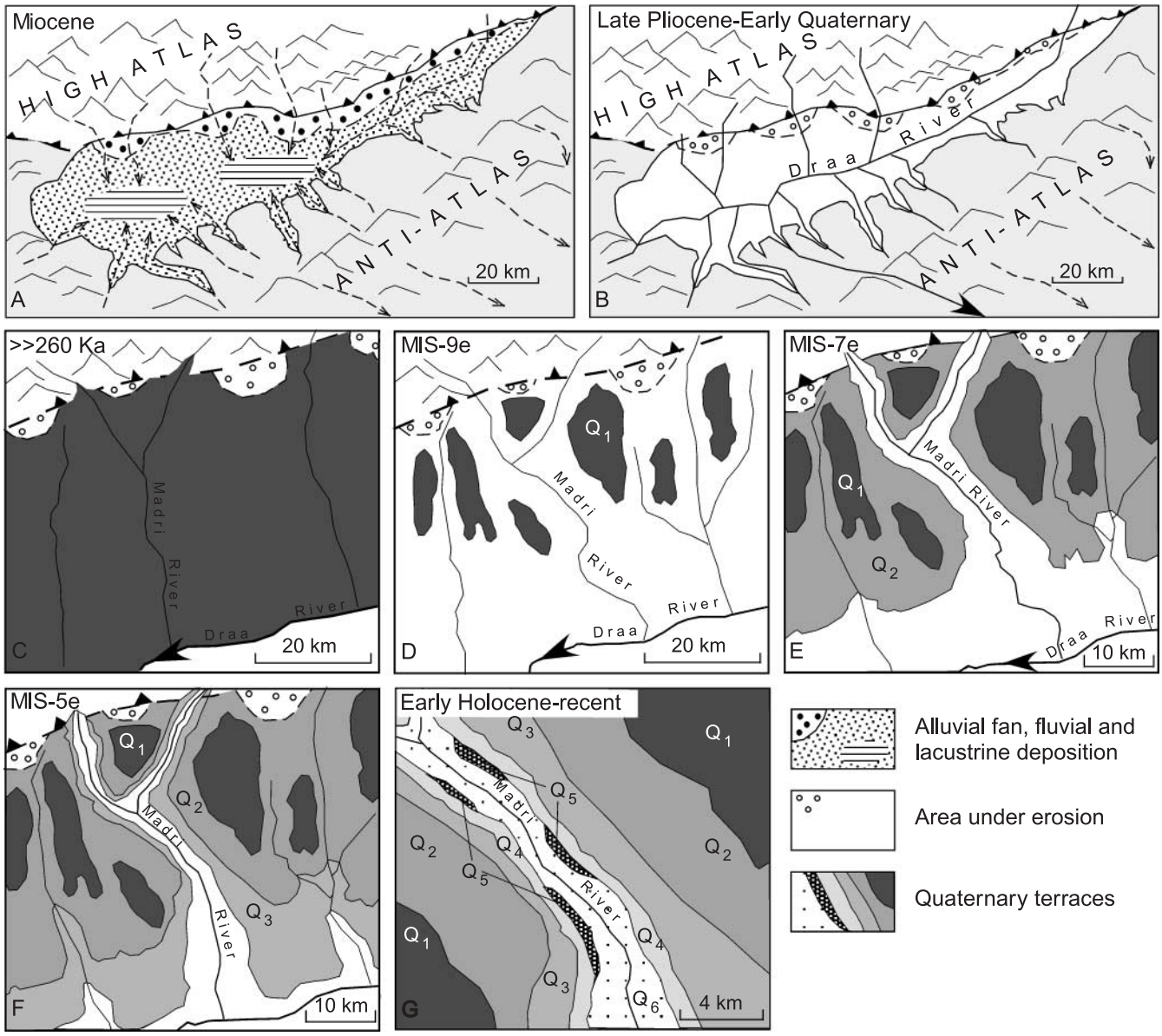


**Fig. 9.** Schematic diagrams showing the evolution of the Ouarzazate basin highlighting the formation of terraces along the Madri River.

stadials because catchment erosion is most active and associated rates of sediment supply are high. In consonance with what we can deduce for the Holocene, they suggested that this process is induced by changes in hydrology and vegetation cover: in periods of cool and dry climate, steppe vegetation replaces forest or wooded steppe biomes, the development of which occurs during warm and wet interglacials or interstadials. Conversely, Macklin *et al*. (2002) suggested that the inverse modification of vegetation cover at the transition between glacial and interglacial stages results in a decrease of the catchment erosion and associated sediment supply, in response to an increase in slope stability. Such processes together with an increase in humidity would be responsible for the incisions in the trunk streams that are documented around the Mediterranean for the interglacial stages. Climate change throughout glacial and interglacial cycles is complex and the relationship between precipitation changes may not be simple (see Cacho *et al*. 1999; McManus *et al*. 1999). Statements regarding precipitation changes between glacial and interglacials must therefore be regarded as somewhat tentative until independent proxies are available to quantify precipitation changes on Milankovitch and sub-Milankovitch time scales.

Glacial landforms have been described from the highest massifs of the High Atlas. These have been reviewed by Hughes *et al*. (2004, 2006). The timing of glaciation, however, is unknown, and thus this prevents any correlation of our fluvial aggradation–incision history with glaciation. The deduced snow-line for the coldest stages of the Pleistocene is >3300 m a.s.l. (see references given by Hughes *et al*. 2004, 2006). Hence, the extent of glaciation in the High Atlas was very limited, and it did not affect the Oued Madri catchment, most of which lies at an elevation below 3300 m a.s.l. Furthermore, the headwaters of our study area are about 10 km to the SSW of the glaciated catchments of the Central High Atlas (Mgoun massif) and would not have been directly affected by glacially controlled hydro-

logical changes. Glacial erosion processes, therefore, did not control sediment supply in the study area.

We can conclude that the TCN dates of the terraces within our study area provide evidence that abandonment of each terrace and fan occurred at intervals of *c*. 100 ka, that is, at glacial–interglacial time scales. Strong climatic control on fan development and sedimentation has been recognized for Quaternary fans and terraces in the foreland basins of other intracontinental mountain belts, notably the Gobi Altai Mountains (Owen *et al*. 1997). Our study provides one of the most comprehensive datasets for foreland basin landforms and it supports earlier speculation on the climatic control of landscape evolution in Morocco (e.g. Choubert 1965).

Surfaces Q1, Q2 and Q3 are tectonically deformed, with progressively more deformation on the older surfaces. The absence of notable deformation on surfaces Q4 and Q5 suggests that deformation progresses too slowly to deform Holocene surfaces to a noticeable extent, and that there has been no significant earthquake event during the last 10 ka that would have produced significant deformation. The newly dated surfaces now provide a framework for defining the magnitude of deformation throughout the Ouarzazate basin. In addition, the young ages on the deformed surface Q1b highlight the need to be careful when applying TCN surface exposure methods to deforming surfaces that may be progressively eroding.

The deformation of the fluvial terraces demonstrates that the transition from aggradation to erosion in the Ouarzazate basin occurred while thrust loading was still active along the High Atlas margin. The modification of the drainage pattern from internal to external and oscillations of the Quaternary climate are the dominant factors controlling erosion in the Ouarzazate basin at least during the past 300 ka. In addition, mantle-related uplift of the entire system of mountains and basins with respect to base level in the Late Cenozoic (Babault *et al*. 2008) provided additional potential for erosion to overtake subsidence and accumulation within the Ouarzazate basin.

## Conclusions

The terrace and pediment incision in the active Ouarzazate foreland basin was primarily induced by a drop in base level as the main outlet channel of the basin, the Draa river, progressively cut through the Anti-Atlas Mountains to the south. Geomorphological analysis and TCN surface exposure dating show, however, that the development of Quaternary alluvial fans and terraces along the northern margin of the Ouarzazate basin is strongly controlled by climate oscillations on glacial–interglacial time scales. Surface abandonment ages for four terraces define their ages to the present and broadly last three interglacials. This suggests that incision occurs during interglacial times, when the region is wetter with hillslopes stabilized by wooded vegetation cover in mountainous catchments and streams are more pervasive, albeit still ephemeral. In contrast, during the more arid glacial times aggradation dominates, as increased hillslope erosion enhances sediment supply and the hydrological regime is less effective at transporting sediment. These data clearly demonstrate that knowledge of the character of climate change is essential to understand the nature of sediment transfer and landscape denudation in foreland basins. Surface exposure dating of abandoned fill-terraces suggests that rates of fluvial incision in this region range between 0.3 and 1.0 mm $a^{-1}$ for the later part of the Quaternary. Furthermore, this study provides the first comprehensive TCN chronology for alluvial surfaces in Morocco and illustrates the problems associated with dating surfaces in this region that are significantly older than 100 ka.

We should like to thank J. Woodward, P. Hughes, D. Maddy and an anonymous reviewer for their very constructive and useful reviews of our manuscript. This work was supported by the Ministerio de Educación y Ciencia (Spain) projects CLG2005-25059 and CGL2006-07226, the Ministerio de Asuntos Exteriores AECI grant A/2921/05 and the CONSOLIDER-INGENIO 2010 project CDS2006-00041 (TOPOIBERIA). The TCN AMS analytical work was undertaken at the Lawrence Livermore National Laboratory (under DOE contract W-7405-ENG-48). M.L.A. benefited from a grant from the Salvador de Madariaga Program (MEC, Spain) during her sabbatical leave at the University of Cincinnati. She also thanks C. Dietsch and E. Ward for their hospitality during her stay. We thank C. Dietsch for his comments on an early version of this manuscript.

## References

Akçar, N., Yavuz, V., Ivy-Ochs, S., Kubik, P.W., Vardar, M. & Schlüchter, C. 2007. Paleoglacial records from Kavron Valley, NE Turkey: Field and cosmogenic exposure dating evidence. *Quaternary International*, **164-165**, 170–183.

Allmetsat 2007. Climate of Ouarzazate, Morocco. World Wide Web Address: http://en.allmetsat.com/climate/morocco.php?code=60265.

Anders, M.D., Pederson, J.L. & Rittenour, T.M. *et al*. 2005. Pleistocene geomorphology and geochronology of eastern Grand Canyon; linkages of landscape components during climate changes. *Quaternary Science Reviews*, **24**, 2428–2448.

Anderson, R.S., Repka, J.L. & Dick, G.S. 1996. Explicit treatment of inheritance in dating depositional surfaces using *in situ* 10 Be and 26 Al. *Geology*, **24**, 47–51.

Arboleya, M.L., Teixell, A., Charroud, M. & Julivert, M. 2004. A structural transect through the High and Middle Atlas of Morocco. *Journal of African Earth Sciences*, **39**, 319–327.

Ayarza, P., Alvarez-Lobato, F., Teixell, A., Arboleya, M.L., Teson, E., Julivert, M. & Charroud, M. 2005. Crustal structure under the central High Atlas Mountains (Morocco) from geological and gravity data. *Tectonophysics*, **400**, 67–84.

Babault, J., Teixell, A., Arboleya, M.L. & Charroud, M. 2008. A Late Cenozoic age for long-wavelength surface uplift of the Atlas Mountains of Morocco. *Terra Nova*, **20**, 102–107, doi:10.1111/j.1365-3121.2008.00794.x.

Balco, G., Stone, J.O., Lifton, N.A. & Dunai, T.J. 2008. A complete and easily accessible means of calculating surface exposure ages or erosion rates from $^{10}$Be and $^{26}$Al measurements. *Quaternary Geochronology*, **3**, 174–195.

Beauchamp, W., Barazangi, M., Demnati, A. & El Alji, M. 1996. Intracontinental rifting and inversion: Missour Basin and Atlas Mountains, Morocco. *AAPG Bulletin*, **80**, 1459–1482.

Benn, D.I., Owen, L.A., Finkel, R.C. & Clemmens, S. 2006. Pleistocene Lake outburst floods and fan formation along the eastern Sierra Nevada: implications for the interpretation of intermontane lacustrine records. *Quaternary Science Reviews*, **25**, 2729–2748.

Bull, W.B. 1991. *Geomorphic Responses to Climatic Change*. Oxford University Press, New York.

Cacho, I., Grimalt, J.O., Pelejero, C., Canals, M., Sierro, F.J., Flores, J.A. & Shackleton, N.J. 1999. Dansgaard–Oeschger and Heinrich event imprints in Alboran Sea palaeotemperatures. *Palaeoceanography*, **14**, 698–705.

Choubert, G. 1965. Evolution de la connaissance du Quaternaire au Maroc. *Notes et Mémoires du Service Géologique du Maroc*, **25**, 9–27.

Choubert, G. & Faure-Muret, A. 1962. Evolution du domaine atlasique marocain depuis les temps paleozoïques. *In:* Choubert, G. & Faure-Muret, A. (eds) *Livre à la Mémoire du Professeur Paul Fallot*. Société Géologique de France, Mémoire hors série, **1**, 447–527.

Couvreur, G. 1973. Etagement de formes et néotectonique sur le versant sud du Haut Atlas. *Revue de Géomorphologie Dynamique*, **22**, 109–124.

DeCelles, P.G. & Giles, K.A. 1996. Foreland basin systems. *Basin Research*, **8**, 105–123.

Dresch, J. 1941. *Recherches sur l'évolution du relief dans le Massif Central du Grand Atlas, le Haouz et la Souss*. Arrault, Tours.

El Harfi, A., Lang, J., Salomon, J. & Chellai, E.H. 2001. Cenozoic sedimentary dynamics of the Ouarzazate foreland basin (Central High Atlas Mountains, Morocco). *International Journal of Earth Sciences*, **90**, 393–411.

Elenga, H., Peyron, O., Bonnefille, R., *et al*. 2000. Pollen-based biome reconstruction for southern Europe and Africa 18,000 yr BP. *Journal of Biogeography*, **27**, 621–634, doi:10.1046/j.1365-2699.2000.00430.x.

Flemings, P.B. & Jordan, T.E. 1989. A synthetic stratigraphic model of foreland basin development. *Journal of Geophysical Research*, **94**, 3851–3866.

Fraissinet, C., Zouine, E.M., Morel, J.L., Poisson, A., Andrieux, J. & Faure-Muret, A. 1988. Structural evolution of the southern and northern central High Atlas in Paleogene and Mio-Pliocene times. *In:* Jacobshagen, V.H. (ed.) *The Atlas System of Morocco*. Springer, New York, 272–291.

Frankel, K.L., Brantley, K.S., Dolan, J.F., *et al.* 2007a. Cosmogenic $^{10}$Be and $^{36}$Cl geochronology of offset alluvial fans along the northern Death Valley fault zone: Implications for transient strain in the eastern California shear zone. *Journal of Geophysical Research—Solid Earth*, **112**, B06407, doi:10.1029/2006JB004350.

Frankel, K.L., Dolan, J.F., Finkel, R.C., Owen, L.A. & Hoeft, J.S. 2007b. Spatial variations in slip rate along the Death Valley–Fish Lake Valley fault system determined from LiDAR topographic data and cosmogenic $^{10}$Be geochronology. *Geophysical Research Letters*, **34**, LI8303, doi:10.1029/2007GL030549.

Frizon de Lamotte, D., Saint Bezar, B., Bracène, R. & Mercier, E. 2000. The two main steps of the Atlas building and geodynamics of the western Mediterranean. *Tectonics*, **19**, 740–761.

Fuller, I.C., Macklin, M.G., Lewin, J., Passmore, D.G. & Wintle, A.G. 1998. River response to high-frequency climate oscillations in Southern Europe over the past 200 k.y. *Geology*, **26**, 275–278.

Gasse, F. 2000. Hydrological changes in the African tropics since the last glacial maximum. *Quaternary Science Reviews*, **19**, 189–211.

Gasse, F., Fontes, J.C. & Plaziat, J.C. *et al.* 1987. Biological remains, geochemistry and stable isotopes for the reconstruction of environmental and hydrological changes in the Holocene lakes from North Sahara. *Palaeogeography, Palaeoclimatology, Palaeoecology*, **60**, 1–46.

Gasse, F., Tehet, R., Durand, A., Gilbert, E. & Fontes, J.-C. 1990. The arid–humid transition in the Sahara and the Sahel during the last deglaciation. *Nature*, **346**, 141–146.

Gile, L.H., Hawley, J.W. & Grossman, R.B. 1981. *Soils and geomorphology in the Basin and Range area of southern New Mexico; guidebook to the Desert Project*. New Mexico Bureau of Mines and Mineral Resources, Memoir, **39**.

Gomez, F., Beauchamp, W. & Barazangi, M. 2000. Role of the Atlas Mountains (northwest Africa) within the African–Eurasian plate-boundary zone. *Geology*, **28**, 775–778.

Görler, K., Helmdach, F.-F. & Gaemers, P. *et al.* 1988. The uplift of the central High Atlas as deduced from Neogene continental sediments of the Ouarzazate province, Morocco. *In:* Jacobshagen, V.H. (ed.) *The Atlas System of Morocco*. Springer, New York, 361–404.

Hancock, G.S., Anderson, R.S., Chadwick, O.A. & Finkel, R.C. 1999. Dating fluvial terraces with $^{10}$Be and $^{26}$Al profiles; application to the Wind River, Wyoming. *Geomorphology*, **27**, 41–60.

Harvey, A.M. & Wells, S.G. 1987. Response of Quaternary fluvial systems to differential epeirogenic uplift: Aguas and Feos River systems, south-east Spain. *Geology*, **15**, 689–693.

Harvey, A.M., Silva, P.G., Mather, A.E., Goy, J.L., Stokes, M. & Zazo, C. 1999a. The impact of Quaternary sea-level and climatic change on coastal alluvial fans in the Cabo de Gata Ranges, Southeast Spain. *Geomorphology*, **28**, 1–22.

Harvey, A.M., Wigand, P.E. & Wells, S.G. 1999b. Response of alluvial fan systems to the late Pleistocene to Holocene climatic transition; contrasts between the margins of pluvial lakes Lahontan and Mojave, Nevada and California, USA. *Catena*, **36**, 255–281.

Holz, C., Stuut, J.-B.W., Henrich, R. & Meggers, H. 2007. Variability in terrigenous sedimentation processes off Northwest Africa and its relation to climate changes; inferences from grain-size distributions of a Holocene marine sediment record. *Sedimentary Geology*, **202**, 499–508.

Hoogakker, B.A.A., Rothwell, R.G., Rohling, E.J., Paterne, M., Stow, D.A.V., Herrle, J.O. & Clayton, T. 2004. Aridity episodes during the last glacial cycle recorded in calcium carbonate records from the western Mediterranean Sea. *Marine Geology*, **211**, 21–43.

Hughes, P.D., Gibbard, P.L. & Woodward, J.C. 2004. Quaternary glaciation in the Atlas Mountains, North Africa. *In:* Ehlers, J. & Gibbard, P.L. (eds) *Quaternary Glaciation—Extent and Chronology. Volume 3: Asia, Latin America, Africa, Australia, Antarctica Elsevier, Amsterdam*. 255–260.

Hughes, P.D., Woodward, J.C. & Gibbard, P.L. 2006. Quaternary glacial history of the Mediterranean mountains. *Progress in Physical Geography*, **30**, 334–364, doi:10.1191/0309133306pp481ra.

Jacobshagen, V.H. 1988. Geodynamic evolution of the Atlas system, Morocco; an introduction. *In:* Jacobshagen, V.H. (ed.) *The Atlas System of Morocco*. Springer, New York, 3–9.

Jolly, D., Harrison, S.P., Damnati, B. & Bonnefille, R. 1998. Simulated climate and biomes of Africa during the late Quaternary; comparison with pollen and lake status data, Late Quaternary climates; data synthesis and model experiments. *Quaternary Science Reviews*, **17**, 629–657.

Kelly, M., Black, S. & Rowan, J.S. 2000. A calcrete-based U/Th chronology for landform evolution in the Sorbas basin, Southeast Spain. *Quaternary Science Reviews*, **19**, 995–1010.

Knippertz, P., Christoph, M. & Speth, P. 2003. Long-term precipitation variability in Morocco and the link to the large-scale circulation in recent and future climates. *Meteorology and Atmospheric Physics*, **83**, 67–88.

Kohl, C.P. & Nishiizumi, K. 1992. Chemical isolation of quartz for measurement of *in-situ*-produced cosmogenic nuclides. *Geochimica et Cosmochimica Acta*, **56**, 3583–3587.

Lal, D. 1991. Cosmic ray labeling of erosion surfaces; *in situ* nuclide production rates and erosion models. *Earth and Planetary Science Letters*, **104**, 424–439.

Lamb, H.F., Eicher, U. & Switsur, V.R. 1989. An 18,000-year record of vegetation, lake-level and climatic change from Tigalmamine, Middle Atlas, Morocco. *Journal of Biogeography*, **16**, 65–74.

Lamb, H.F., Gasse, F. & Benkaddour, A. *et al.* 1995. Relation between century-scale Holocene arid intervals in tropical and temperate zones. *Nature*, **373**, 134–137.

Laville, E. & Piqué, A. 1992. Jurassic penetrative deformation and Cenozoic uplift in the central High Atlas (Morocco); a tectonic model; structural and orogenic inversions. *Geologische Rundschau*, **81**, 157–170.

Le, K., Lee, J., Owen, L.A. & Finkel, R.C. 2007. Late Quaternary slip rates along the Sierra Nevada frontal fault zone, California: slip partitioning across the western margin of the Eastern California Shear Zone/Basin and Range Province. *Geological Society of America Bulletin*, **119**, 240–256.

Lewin, J., Macklin, M.G. & Woodward, J.C. (eds) 1995. *Mediterranean Quaternary River Environments*. Balkema, Rotterdam.

Macklin, M.G., Lewin, J. & Woodward, J.C. 1995. Quaternary fluvial systems in the Mediterranean Basin. *In:* Lewin, J., Macklin, M.G. & Woodward, J.C. (eds) *Mediterranean Quaternary River Environments*. Balkema, Rotterdam, 1–25.

Macklin, M.G., Fuller, I.C. & Lewin, J. *et al.* 2002. Correlation of fluvial sequences in the Mediterranean basin over the last 200 ka and their relationship to climate change. *Quaternary Science Reviews*, **21**, 1633–1641.

Magri, D. & Parra, I. 2002. Late Quaternary western Mediterranean pollen records and African wind. *Earth and Planetary Science Letters*, **200**, 401–408.

Mather, A.E. 2000. Adjustment of a drainage network to capture induced base-level change. *Geomorphology*, **34**, 271–289.

Matmon, A., Schwartz, D.P., Finkel, R., Clemmens, S. & Hanks, T. 2005. Dating offset fans along the Mojave section of the San Andreas fault using cosmogenic $^{26}$Al and $^{10}$Be. *Geological Society of America Bulletin*, **117**, 795–807.

Mattauer, M., Tapponier, P. & Proust, F. 1977. Sur les mécanismes de formation des chaînes intracontinentales. L'exemple des chaînes atlasiques du Maroc. *Bulletin de la Société Géologique de France*, **7**, 521–536.

McManus, J.F., Oppo, D.W. & Cullen, J.L. 1999. A 0.5 million-year record of millennial-scale climate variability in the North Atlantic. *Science*, **283**, 971–975.

Missenard, Y., Zeyen, H., Frizon de Lamotte, D., Leturmy, P., Petit, C., Sébrier, M. & Saddiqi, O. 2006. Crustal versus asthenospheric origin of relief of the Atlas Mountains of Morocco. *Journal of Geophysical Research*, **111**, B03401, doi:10.1029/2005JB003708.

Owen, L.A., Caffee, M.W., Bovard, K.R., Finkel, R.C. & Sharma, M.C. 2006. Terrestrial cosmogenic nuclide surface exposure dating of the oldest glacial successions in the Himalayan orogen: Ladakh Range, northern India. *Geological Society of America Bulletin*, **118**, 383–392.

Owen, L.A., Windley, B.F., Cunningham, W.D., Badamgarav, J. & Dorjnamjaa, D. 1997. Quaternary alluvial fans in the Gobi, southern Mongolia; evidence for neotectonics and climate change. *Journal of Quaternary Science*, **12**, 239–252.

Pigati, J.S. & Lifton, N.A. 2004. Geomagnetic effects on time-integrated cosmogenic nuclide production with emphasis on *in situ* $^{14}$C and $^{10}$Be. *Earth and Planetary Science Letters*, **226**, 193–205.

Reille, M. 1979. Analyse pollinique du lac de Sidi Bou Rhaba, littoral atlantique (Maroc). *Ecologia Mediterranea*, **4**, 61–65.

Rodgers, J. 1987. Chains of basement uplifts within cratons marginal to orogenic belts. *American Journal of Science*, **287**, 661–692.

Rose, J., Meng, X. & Watson, C. 1999. Palaeoclimate and palaeoenvironment responses in the western Mediterranean over the last 140,000 ka: evidence from Mallorca, Spain. *Journal of the Geological Society, London*, **156**, 435–448.

Salamani, M. 1991. Premières données palynologiques sur l'histoire Holocene du massif de l'Akfadou (Grande-Kabylie, Algérie). *Ecologia Mediterranea*, **17**, 145–159.

Salamani, M. 1993. Premières données paléophytogéographiques du Cèdre de l'Atlas (*Cedrus atlantica*) dans la région de grande Kabilie (NE Algérie). *Palynosciences*, **2**, 147–155.

Santisteban, J.I. & Schulte, L. 2007. Fluvial networks of the Iberian Peninsula: a chronological framework. *Quaternary Science Reviews*, **26**, 2738–2757.

Schaer, J.-P. 1987. Evolution and structure of the High Atlas of Morocco. *In:*

Schaer, J.-P. & Rodgers, J. (eds) *The Anatomy of Mountain Ranges*. Princeton University Press, Princeton, NJ, 107–127.

Schulte, L., Julià, R.J., Burjachs, F. & Hilgers, A. 2008. Middle Pleistocene to Holocene geochronology of the River Aguas terrace sequence (Iberian Peninsula): Fluvial response to Mediterranean environmental change. *Geomorphology*, **98**, 13–33.

Sébrier, M., Siame, L., Zouine, E.M., Winter, T., Missenard, Y. & Leturmy, P. 2006. Active tectonics in the Moroccan High Atlas. *Comptes Rendus Géosciences*, **338**, 65–79.

Sinclair, H.D., Coakley, B.J., Allen, P.A. & Watts, A.B. 1991. Simulation of foreland basin stratigraphy using a diffusion model of mountain belt uplift and erosion; an example from the Central Alps, Switzerland. *Tectonics*, **10**, 599–620.

Small, E.E., Anderson, R.S., Repka, J.L. & Finkel, R. 1997. Erosion rates of alpine bedrock summit surfaces deduced from *in situ* $^{10}$Be and $^{26}$Al. *Earth and Planetary Science Letters*, **150**, 413–425.

Stäblein, G. 1988. Geomorphological aspects of the Quaternary evolution of the Ourzazate basin, southern Morocco. *In:* Jacobshagen, V.H. (ed.) *The Atlas System of Morocco*. Springer, New York, 433–444.

Staiger, J., Gosse, J., Toracinta, R., Oglesby, B., Fastook, J. & Johnson, J.V. 2007. Atmospheric scaling of cosmogenic nuclide production: Climate effect. *Journal of Geophysical Research*, **112**, B02205, doi:10.1029/2005JB003811.

Stone, J.O. 2000. Air pressure and cosmogenic isotope production. *Journal of Geophysical Research*, **105**, 23753–23759.

Teixell, A., Arboleya, M.L., Julivert, M. & Charroud, M. 2003. Tectonic shortening and topography in the central High Atlas (Morocco). *Tectonics*, **22**, 1051, doi:10.1029/2002TC001460.

Teixell, A., Ayarza, P., Zeyen, H., Fernandez, M. & Arboleya, M.-L. 2005. Effects of mantle upwelling in a compressional setting: the Atlas Mountains of Morocco. *Terra Nova*, **17**, 456–461.

Tesón, E. & Teixell, A. 2008. Sequence of thrusting and syntectonic sedimentation in the eastern Sub-Atlas thrust belt (Dadès and Mgoun valleys, Morocco). *International Journal of Earth Sciences*, **97**, 103–113, doi:10.1007/s00531-006-0151-1.

Tzedakis, P.C. 2007. Seven ambiguities in the Mediterranean palaeoenvironmental narrative. *Quaternary Science Reviews*, **26**, 2042–2066.

Winograd, I.J., Landwehr, J.M., Ludwig, K.R., Coplen, T.B. & Riggs, A.C. 1997. Duration and structure of the past four interglaciations. *Quaternary Research*, **48**, 141–154.

Zehfuss, P.H., Bierman, P.R., Gillespie, A.R., Burke, R.M. & Caffee, M.W. 2001. Slip rates on the Fish Springs fault, Owens Valley, California, deduced from cosmogenic $^{10}$Be and $^{26}$Al and soil development on fan surfaces. *Geological Society of America Bulletin*, **113**, 241–255.

Zeyen, H., Ayarza, P., Fernàndez, M. & Rimi, A. 2005. Lithospheric structure under the western African–European plate boundary: A transect across the Atlas Mountains and the Gulf of Cadiz. *Tectonics*, **24**, TC2001, doi:10.1029/2004TC001639.

Ziegler, P.A., Cloetingh, S. & van Wees, J.-D. 1995. Dynamics of intra-plate compressional deformation; the Alpine Foreland and other examples. *Tectonophysics*, **252**, 7–59.

Received 24 October 2007; revised typescript accepted 1 May 2008.
Scientific editing by Jamie Woodward

*Basin Research* (2008) doi: 10.1111/j.1365-2117.2008.00377.x

# A comment on 'Late- to post-orogenic exhumation of the Central Pyrenees revealed through combined thermochronological data and modelling' by M. Gibson, H. D. Sinclair, G. J. Lynn and F. M. Stuart

J. Babault,* S. Bonnet,†§ G. Ruiz‡ and J. Van Den Driessche†§

**Department of Geology, Universitat Autònoma de Barcelona, Bellaterra, Spain*
*†Géosciences Rennes, Université de Rennes 1, Campus de Beaulieu, Rennes, France*
*‡IGH, University of Neuchatel, Neuchatel, Switzerland*
*§CNRS/INSU, UMR 6118, Campus de Beaulieu, Rennes, France*

In a recent contribution to Basin Research, Gibson *et al.* (2007) advanced new thermochronological data from different massifs in the Pyrenees to argue for a 2 km of continuous post-orogenic exhumation since ~30 Ma. Gibson *et al*'s model (2007) is based on low-temperature thermochronometry from different sub-vertical profiles. This included apatite fission-track (AFT, most of them being previously published in Sinclair *et al.*, 2005) and the first apatite U-Th/He (AHe) data from the Pyrenees. Using Pecube software (Braun, 2003) they interpret their data as revealing a dramatic change in exhumation at about 30 Ma from rapid ($\sim$1.5 mm yr$^{-1}$) to very low rates ($\sim$0.03 mm yr$^{-1}$) as earlier suggested by Fitzgerald *et al.* (1999) using the sole AFT thermochronometer from the same plutons. They considered such a decrease in exhumation rate to reflect the transition into a post-orogenic state for the mountain belt. In addition, the presence of Oligocene to early Miocene AHe ages at the surface today is used by Gibson *et al.* (2007) to negate a possible reactivation of erosion during late Neogene as it has been inferred by geological and geomorphological data (Coney *et al.*, 1996; Babault *et al.*, 2005, 2006), and AFT data (Fitzgerald *et al.*, 1999). Moreover Gibson *et al.* (2007) state that the preservation of peneplain surfaces at high altitude, as inferred by Babault *et al.* (2005), could not be possible.

Our major concern with the study by Gibson *et al.* (2007) is that they implicitly consider that the rocks they sampled were exposed at the Earth's surface only in the very recent past, that is at 0 Ma. Gibson *et al.* (2007) recognize that their data do not allow determining the exhumation history since 30 Ma. They cannot, therefore, rule out the possibility that the sampled rocks rose to the surface, or very near to the surface, in the late Miocene. Most of exhumation since 30–20 Ma should be included in the process of peneplanation at high elevation that develops before the late Miocene as proposed by Babault *et al.* (2005). AFT and AHe data are in agreement with such a scenario and cannot therefore be used as evidence to discard the well documented preservation of erosional surfaces in altitude in the Pyrenees. Finally, it is not surprising that Gibson *et al.* (2007) were not been able to determine a Plio-Quaternary increase of erosion, which corresponds mainly to a deep dissection of the former smoothed topography by fluvial network. Indeed, the amplitude of the fluvial incision, which never exceed 1000 m, was not sufficient to alter the shape of the isotherms below the Pyrenean topography during the Plio-Pleistocene in a manner it imprints the AHe thermochronological data (see Braun, 2003).

Firstly, contradictions in the estimates of rock exhumation by Gibson *et al.* (2007) question the robustness of their conclusions. The authors state that (p. 331) '*Since 29 Ma, the amount of exhumation cannot have exceeded 2 km, at an average rate of* $< 0.03$ *mm yr*$^{-1}$', which they followed by the opposite assertion: '*The requirement of at least 2 km of rock exhumation . . . since 30–20 Ma means . . .*'. Whatever the geothermal gradient they used to calculate the 2 km of crustal material removed since 30 Ma, 0.03 mm yr$^{-1}$ of exhumation during 30 Ma correspond definitely to 900 m of erosion, not 2 km as stated!

In essence, the thermochronological data documents the patterns of exhumation and rates up to a depth corresponding to a closure temperature, taken in Gibson *et al.* (2007) at 70 °C for AHe and near 100 °C for AFT data. Gibson *et al.* (2007) used geothermal gradients that vary from 20 to 35 °C km$^{-1}$. Therefore these temperatures correspond to a range of crustal depths between 2 and 5 km. When the rocks are sampled at the Earth's surface, as in the study by Gibson *et al.* (2007), there is a gap in the exhumation history of the rocks (between the closure depth and the surface) that does not imprint on AFT nor AHe data. Consequently, the details of the exhumation between the closure depth and the surface (defined here as the post-orogenic exhumation) cannot be documented solely by thermochronological data.

(1) Gibson *et al.* (2007) used Pecube software (Braun, 2003) to model the exhumation history of the Axial Zone (see their Fig. 4). There is an important assumption in their modelling of exhumation histories that is not clearly stated: the authors assumed that the final exhumation of

Correspondence: J. Babault, Department of Geology, Universitat Autònoma de Barcelona, Bellaterra, Spain. E-mail: Julien.Babault@uab.es

the samples (final exposure to the surface) occurred in the very recent past, that is at 0 Ma in their simulations (Fig. 1a). Given this assumption, the modelled exhumation rates they obtained for the '. . . *time-averaged, post-orogenic history of the Pyrenees* [are] *at least an order of magnitude slower than during the last phases of syn-orogenic exhumation*' (Gibson *et al.*, 2007, p. 333). Their results would consequently imply a sudden 50-folds decrease in the pattern of the mountain belt exhumation. These conclusions are therefore derived from the assumption that the samples were recently brought to the surface. Unfortunately, there is no evidence to support this assumption.

(2) AFT and AHe results discussed by Gibson *et al.* (2007) show an impressive similarity of ages whatever the thermochronological system considered. Given the range of temperatures involved for the partial annealing/retention zones of AFT (120–60 °C) and AHe (80–35 °C), the mountain range must have experienced several kilometres of exhumation in a very short time interval (only a very few million of years), up to a temperature lower or in the order of 35 °C. The simplest interpretation of the data would suggest that the final exhumation history of the Central Pyrenees, from the isotherm 35 °C to the very near surface, occurred in the continuity of the syn-orogenic exhumation as defined by Gibson *et al.* (2007) (Fig. 1b). If a geothermal gradient of 35 °C km$^{-1}$ and a surface temperature of 0 °C, and, rates of 1.0–1.5 mm yr$^{-1}$ (Gibson *et al.*, 2007) are assumed, then the time necessary to remove the final 2 km of crustal material between the AHe closure temperature (70 °C) and the surface would only represent $\leq$ 2 Ma of Pyrenean exhumation.

(3) Geological and geomorphological data support the idea that the main final exhumation history of the Pyrenees did not take place during all the Cenozoic. A striking feature of the Pyrenees is the presence of highly elevated, low-relief, erosional surfaces. These surfaces truncate both the Palaeozoic basement rocks of the Axial Zone and Mesozoic sedimentary cover (Babault *et al.*, 2005 and references herein). In the southern flank of the Pyrenees, sub-horizontal uppermost top-wedge alluvial deposits outcrop at an elevation of up to 2000 m asl where they merge into the highly elevated, low-relief erosional surfaces of the Axial Zone (e.g. Coney *et al.*, 1996). In the eastern Pyrenees, Late Miocene sediments [Vallesian in age references in Roca, 1996 (11.1–8.7 Ma, e.g. Garcés *et al.*, 1996)] onlap these surfaces in the Cerdanya area allowing these surfaces to be dated as pre-late Miocene in age (Babault *et al.*, 2005 and references herein). These pre-Late Miocene erosional surfaces are presently preserved on the hillcrests. Their presence indicates that bedrock erosion has been negligible in this region (at the scale of the Pyrenean exhumation) since the Late Miocene (after $\sim$11 Ma). This implies that the post-orogenic exhumation of the Pyrenees occurred before the Late Miocene (minimum age for cessation of bedrock exhumation; Fig. 1c) and not up to the present-day as argued by Gibson *et al.* (2007). The use of these geological data in the modelling undertaken by Gibson *et al.* (2007), would

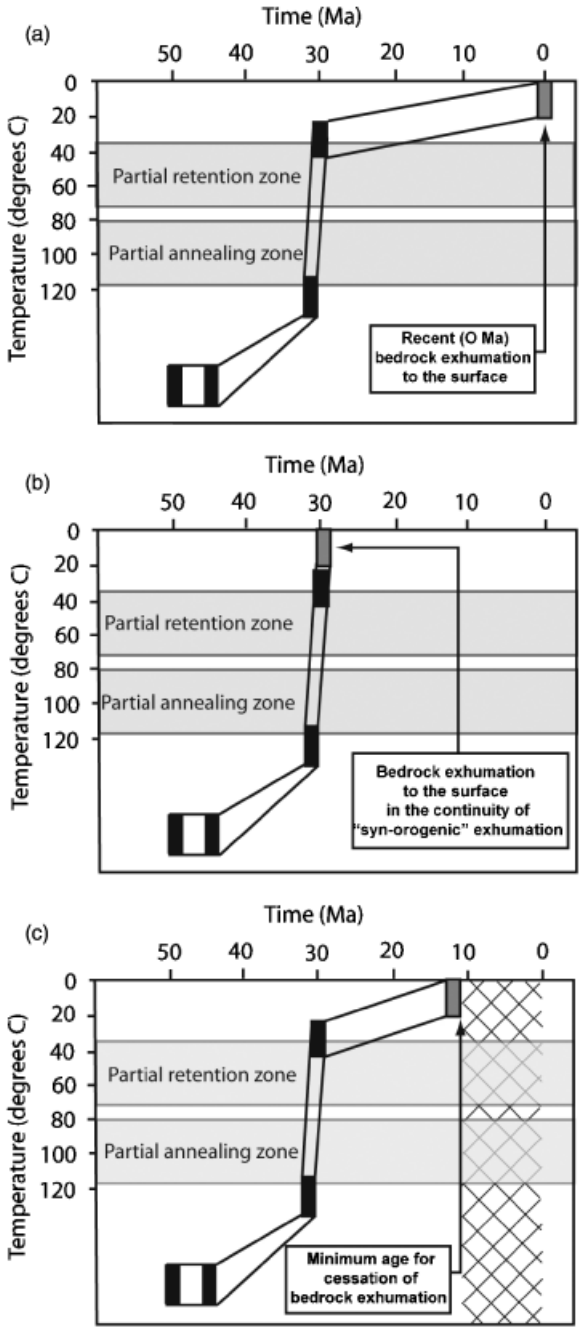


**Fig. 1.** (a) Best modelled cooling history for the Maladeta thermochronological data, modified form Fig. 1c of Gibson *et al.* (2007). This modelling assumes a recent (0 Ma) final bedrock exhumation up to the surface (grey box) and then implies a continuous post-orogenic exhumation for the last 30 Ma. (b) Hypothetical cooling history assuming a bedrock exhumation to the surface in the direct continuity of the 'syn-orogenic' exhumation (grey box). (c) Hypothetical cooling history, taking into account geomorphological and geological data (Coney *et al.*, 1996; Babault *et al.*, 2005, 2006) which indicates that bedrock exhumation to the surface occurred before the Late Miocene (grey box). Such a scenario considers the minimum conceivable rate of 'post-orogenic' exhumation. Pyrenean exhumation probably lies between cases (b) and (c).


 *Basin Research*, 10.1111/j.1365-2117.2008.00377.x

have allowed a much more realistic determination of the exhumation history of the Pyrenean orogen.

(4) Babault *et al*. (2005) presented a model for the generation of the highly elevated, low-relief, erosional surfaces of the Pyrenees that has been successfully tested experimentally (Babault *et al*., 2007). This model supports the view that piedmont sedimentation elevated the base level of the chain and lowered the potential energy for erosion, allowing high-elevation and low-relief erosional surfaces to develop. The post-orogenic, low-relief erosional surfaces formed primarily at high-elevation, resulting into a Late Miocene Pyrenean plateau.

## REFERENCES


Babault, J., Bonnet, S., Van Den Driessche, J. & Crave, A. (2007) High elevation of low relief surfaces in mountain belts: does it equate to post-orogenic surface uplift? *Terra Nova*, **19**(4), 272–277, doi: 10.1111/j.1365-3121.2007.00746.x.

Babault, J., Loget, N., Van Den Driessche, J., Castelltort, S., Bonnet, S. & Davy, P. (2006) Did the Ebro basin connect to the Mediterranean before the Messinian Salinity Crisis? *Geomorphol ogy*, **81**, 155–165, doi: 10.1016/j.geomorph.2006.04.004.

Babault, J., Van Den Driessche, J., Bonnet, S., Castelltort, S. & Crave, A. (2005) Origin of the highly elevated Pyrenean peneplain. *Tectonics*, **24**, TC2010, doi: 10.1029/2004TC001697.

Braun, J. (2003) Pecube; a new finite-element code to solve the 3D heat transport equation including the effects of a time-varying, finite amplitude surface topography. *Comput Geosci*, **29**(6), 787–794.

Coney, P.J., Munoz, J.A., Mcclay, K.R. & Evenchick, C.A. (1996) Syntectonic burial and post-tectonic exhumation of the southern Pyrenees foreland fold-thrust belt. *J Geol Soc*, **153**, 9–16.

Fitzgerald, P.G., Munoz, J.A., Coney, P.J. & Baldwin, S.L. (1999) Asymmetric exhumation across the Pyrenean orogen: implications for the tectonic evolution of a collisional orogen. *Earth Planet Sci Lett*, **173**(3), 157–170.

Garcés, M., Agusti, J., Cabrera, L. & Pares, J.M. (1996) Magnetostratigraphy of the Vallesian (late Miocene) in the Valles-Penedes Basin (Northeast Spain). *Earth Planet Sci Lett*, **142**(3–4), 381–396.

Gibson, M., Sinclair, H.D., Lynnn, G.J. & Stuart, F.M. (2007) Late- to post-orogenic exhumation of the Central Pyrenees revealed through combined thermochronological data and modelling. *Basin Res*, **19**, 323–334, doi: 10.1111/j.1365-2117.2007.00333.x.

Roca, E. (1996) The Neogene Cerdanya and Seu d'Urgell intramontane basins (eastern Pyrenees). In: *Tertiary Basins of Spain: The Stratigraphic Record of Crustal Kinematics* (Ed. by P.F. Friend & C.J. Dabrio), pp. 114–119. Cambridge University Press, New York.

Sinclair, H.D., Gibson, M., Naylor, M. & Morris, R.G. (2005) Asymmetric growth of the Pyrenees revealed through measurement and modeling of orogenic fluxes. *Am J Sci*, **305**(5), 369–406.


*Manuscript received 23 April 2008; Manuscript accepted 23 June 2008.*

 

Geomorphology 173–174 (2012) 88–103

Contents lists available at SciVerse ScienceDirect

Geomorphology

journal homepage: www.elsevier.com/locate/geomorph

# Intrinsic stream-capture control of stepped fan pediments in the High Atlas piedmont of Ouarzazate (Morocco)

A. Pastor *, J. Babault, A. Teixell, M.L. Arboleya

*Departament de Geologia, Universitat Autònoma de Barcelona, 08193 Bellaterra, Spain*

ARTICLE INFO

*Article history:*
Received 29 December 2011
Received in revised form 25 May 2012
Accepted 31 May 2012
Available online 9 June 2012

*Keywords:*
Drainage network
Cover effect
Fan pediment
Piedmont-stream capture
Intrinsic process
Ouarzazate basin

ABSTRACT

The Ouarzazate basin is a Cenozoic foreland basin located to the south of the High Atlas Mountains. The basin has been externally drained during the Quaternary, with fluvial dynamics dominated by erosive processes from a progressive base level drop. The current drainage network is composed of rivers draining the mountain and carrying large amounts of coarse sediments and by piedmont streams with smaller catchments eroding the soft Cenozoic rocks of the Ouarzazate basin. The coarse-grained sediments covering the channel beds of main rivers cause the steepening of the channel gradient and act as a shield inhibiting bedrock incision. Under such circumstances, piedmont streams that incise to lower gradients evolve to large, depressed pediments at lower elevations and threaten to capture rivers originating in the mountain. Much of the current surface of the Ouarzazate basin is covered by coarse sediments forming large systems of stepped fan pediments that developed by the filling of low elevation pediments after a capture event. We identified 14 capture events, and previously published geochronology support an ~100 ka frequency for fan pediment formation. Our study indicates that the reorganization of the fluvial network in the Ouarzazate basin during the late Pleistocene and Holocene has been controlled by the piedmont-stream piracy process, a process ultimately controlled by the cover effect. The stream capture is influenced by erosion, sediment supply and transport, and therefore may not be entirely decoupled from tectonic and climatic forcing. Indeed, we show that at least two capture events may have occurred during climate changes, and local tectonic structures control at most the spatial localization of capture events.



## 1. Introduction

Piedmonts of active mountain ranges are usually dominated by sediment transport and deposition. However, changes of drainage conditions, e.g., a transition to externally drained conditions, can lower the local base level of a piedmont and may cause erosion to dominate over the long term even if mountain building is still active. As a consequence, low relief, gently inclined bedrock erosional surfaces may be formed, and products of erosion coming from the mountains are transported across them. These surfaces of erosion and/or transportation are termed 'pediments'. Pediments have been reported in all climatic zones, mostly in piedmonts of decaying mountains (e.g., Dresch, 1957; Whitaker, 1979; see references in Pelletier, 2010). Two types of pediment exist depending on the contrast in rock strength between the pediment surface and the adjacent upland area. If a pediment develops on the same lithology as its adjacent mountain range, it is called a 'rock pediment' (e.g., Oberlander, 1989). In this study, we consider the other type of pediments that develop on soft basin rocks in contrast with a more resistant adjacent upland. In semi arid environments, hydrologic networks made of ephemeral streams develop on this second class of pediments, locally veneered by thin and discontinuous coarse debris deposits. Sediments accumulate on alluvial fans close to the mountain front or, in distal areas, on the bed of streams originating in the mountains. The thickness of covering deposits on pediment erosional surfaces is usually <20 m, decreasing downstream where fluvial terraces and erosional surfaces merge. Both erosional and buried pediments are landforms that have a fan shape and that are called fan terraces, or fan pediments (Mills, 1983). They are common in the flanks of the Atlas Mountains of North Africa, where they were called 'glacis d'érosion' by French researchers (e.g., Gauthier, 1957).

The occurrence of ephemeral streams, fans, or fluvial terraces on pediments carved in weak lithologies indicates that they result from fluvial erosion. Multiple levels of fan pediments are usually reported in piedmont areas, and they are considered to be the equivalent in the piedmont of mountain river terraces, the highest level being the oldest.

Periods of lateral channel migration in rivers occur if sediment load tends to equal transport capacity, inhibiting vertical erosion and allowing lateral planation to produce erosional surfaces like strath terraces or pediments (e.g., Gilbert, 1877; Mackin, 1936; Bull, 1991; Merritts et al., 1994; Pazzaglia et al., 1998; Hancock and

* Corresponding author. Tel.: +34 93868364; fax: +34 935811263.
*E-mail address:* alvar.pastor@uab.cat (A. Pastor).

0169-555X/$ – see front matter © 2012 Elsevier B.V. All rights reserved.
doi:10.1016/j.geomorph.2012.05.032

Anderson, 2002; Wegmann and Pazzaglia, 2002; Montgomery, 2004). The deposition of an alluvial mantle is thought to be concomitant with lateral planation, and its abandonment may be caused by effective discharge increase and a resulting increase in incision. As for the formation and abandonment of fluvial terraces, stepped fan pediments are usually interpreted as a consequence of lateral planation owing to hydrological regime changes related to climatic oscillations or tectonic activity, i.e., controlled by external changes (e.g., Bryan, 1926; Johnson, 1932; Coque, 1962; Hadley and Goldsmith, 1963; Oberlander, 1989; White et al., 1996; Cook et al., 2009).

On the other hand, landform changes or variations in the rate of depositional or erosional processes can also be inherent to the erosional development of a landscape without variations in climate or tectonic forcing. This old concept (e.g., Schumm, 1973, 1979, and references therein) has been used to explain the development of stepped fan pediments in the soft piedmonts of the Book Cliffs, Utah (Rich, 1935); of the Absaroka Mountains, Wyoming (Mackin, 1936); of the Henry Mountains, Utah (Hunt et al., 1953); of the Shadow Mountain, California (Denny, 1967); of the Shenandoah Valley, Virginia (Hack, 1965); of the Beartooth Mountains, southern Montana (Ritter, 1972); and of the Roan Mountains, North Carolina (Mills, 1983). These works showed that relatively small piedmont streams incise more deeply to lower average slopes than the parallel-flowing main rivers originating in the mountain and transporting coarse sediments. This is so because fluvial erosion is not only proportional to the catchment area and channel longitudinal slope, but it is also modulated by the sediment flux (e.g., Gilbert, 1877). Rich (1935) and Mackin (1936) interpreted that the steeper slopes of the main rivers in the piedmont were those needed to transport their high content of coarse sediments and that the coarse bedload in main rivers inhibits the erosion by covering the channel bed (the cover effect) (e.g., Gilbert, 1877; Rich, 1935; Mackin, 1936; Hunt et al., 1953; Sklar and Dietrich, 1998, 2001, 2006; Whipple and Tucker, 2002; Cowie et al., 2008; Johnson et al., 2009; Yanites et al., 2011). As a consequence, piedmont streams and their tributaries excavate piedmont valleys or pediments in soft rocks at a level below the adjacent main rivers.

Low elevation pediments developed in soft rocks, elongated in the piedmont slope direction and parallel to the mountain streams, are separated from their trunk valleys by remnants of old fan pediments, sometimes a few tens of meters above them. The lower elevation of piedmont valleys or pediments gives them the potential to capture the larger streams that originated in the mountains and are situated a few meters up to tens of meters above them. Captures occur by erosional retreat of the divide and expansion of the pediments (Rich, 1935; Mackin, 1936; Hunt et al., 1953; Denny, 1967; Ritter, 1972; Mills, 1983). Following a capture, a main stream is forced to flow on the gently sloping surface of a pediment, losing transport capacity. In order to recover the slope needed to transport its sediment load, coarse sediments are aggraded and a new fan pediment is formed (Fig. 1). In summary, the intrinsic process of stream captures is the consequence of coarse sedimentary flux, steep longitudinal slope of transportation, and cover effect in the main rivers. The stream-capture process has been emphasized as an important mechanism for development of stepped fan terraces in piedmont settings without any change in external forcing. To date the only natural cases where the stream-capture process has been identified are located in the USA, the most recent account having been published in the early 1980s (Mills, 1983).

Stepped fan pediments in soft rocks in the flanks of the Atlas Mountains of North Africa are thought to result from lateral fluvial erosion by channels sourced in the adjacent and more resistant upland (e.g., Dresch, 1957; Gauthier, 1957; Coque, 1960; Choubert, 1965; Coque and Jauzein, 1967; White, 1991; Arboleya et al., 2008). These studies suggested that lateral erosion and terrace abandonment could be a response to hydrological changes induced by oscillating climate, but none of them considered the potential effect of intrinsic processes.

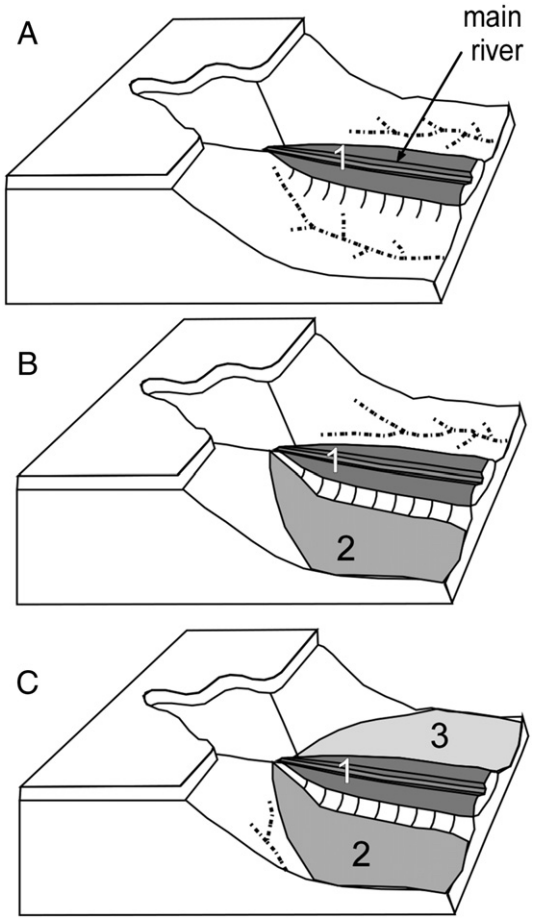


**Fig. 1.** Development of stepped fan terraces by stream capture (modified after Rich, 1935; Schumm, 1979). Stream piracy occurs when one parallel flowing piedmont stream erodes headward and laterally into the channel of a stream originating in the mountain (1) and diverts (pirates) its water. In this case, the main channel is diverted first to one side and then to the other, and will eventually form stage fan terraces (2 and 3). (A) The main trunk with steep longitudinal slope is entrenched in its own coarse sediments, whereas the minor adjacent streams incise to a lower gradient and at a lower level on either side leading to the formation of pediments. (B) The main trunk (located at a higher level) is captured by a piedmont tributary resulting in a new fan-terrace. (C) The main trunk is diverted again by another parallel-flowing tributary resulting in a third level of fan-terrace.

In this study, we evaluate the potential of intrinsic origins versus external forcing factors for fan pediments in the Ouarzazate foreland basin, located in the southern flank of the High Atlas Mountains of Morocco (Fig. 2). The study is based on an analysis of longitudinal profiles of rivers originating in the mountains, piedmont streams and the geomorphological analysis of Quaternary stepped fan pediments in the piedmont. We base our interpretation on terrestrial cosmogenic nuclide (TCN) ages previously obtained on fan terraces by Arboleya et al. (2008), as well as on the spatial relationship between fan terraces and Quaternary tectonic structures mapped by Pastor et al. (2010). Our study suggests that the stream-capture process, neglected during the past three decades as an origin for stepped landforms, explains the formation of the majority of fan pediments in the eroding Ouarzazate foreland basin.

## 2. Geological setting

The High Atlas chain is an ENE–WSW trending mountain belt that represents the highest topographic relief of North Africa. Mean elevation of the central High Atlas well exceeds 2000 m (Babault et al., 2008), and the highest peaks reach up to 4000 m. The tectonic style

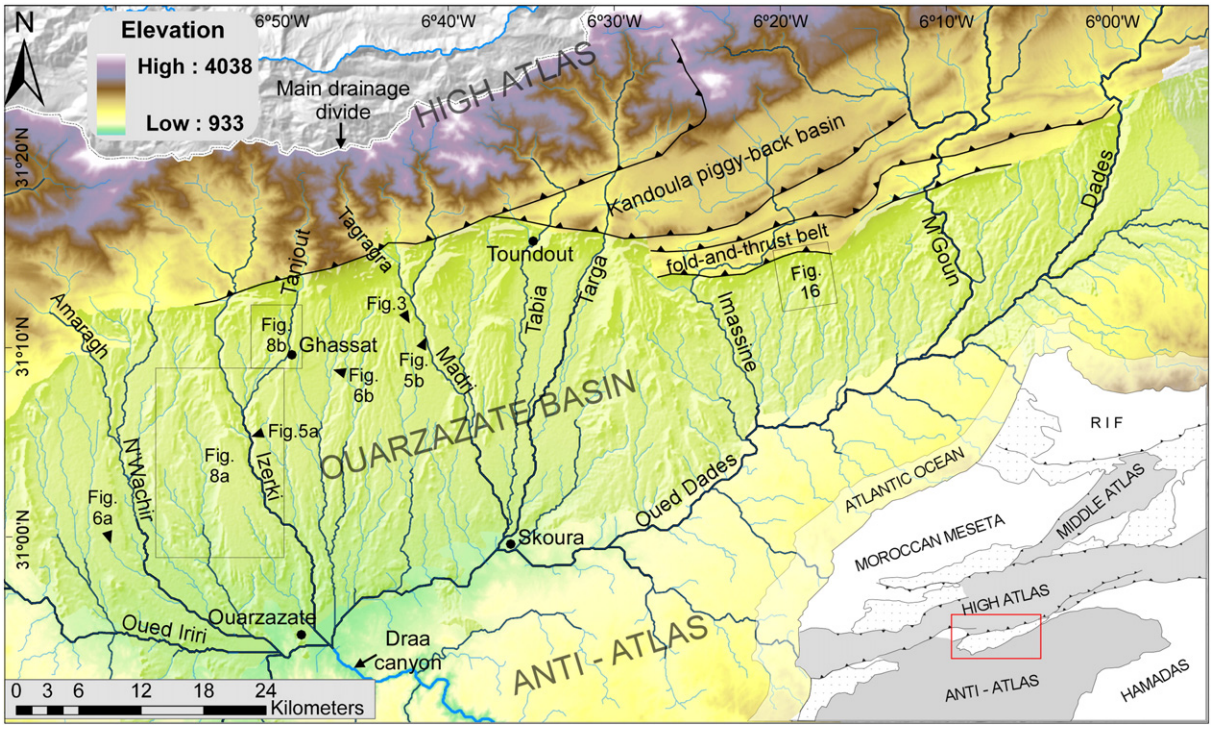


**Fig. 2.** Digital elevation model of the Ouarzazate basin, with its drainage network represented. The network features the nine main rivers with headwaters at the main drainage divide of the High Atlas Mountains (thick white line) and crossing the Ouarzazate basin in an N–S direction. Inset: structural map of Morocco showing the location of the Ouarzazate basin within the Atlas Mountain belts (grayed).

of the High Atlas range conforms to an intracontinental, thick-skinned, thrust-fold belt formed by the Cenozoic inversion of a Triassic to Jurassic rift (e.g., Mattauer et al., 1977; Arboleya et al., 2004, and references therein). The discrepancy between topographic mean elevation and magnitude of shortening across the Moroccan High Atlas (Teixell et al., 2003) suggests that crustal thickening does not fully explain the observed topography and suggests a mantle-sourced, thermal contribution to large-scale surface uplift (Teixell et al., 2003)—corroborated by geophysical (Seber et al., 1996; Ayarza et al., 2005; Teixell et al., 2005; Zeyen et al., 2005; Missenard et al., 2006; Fullea et al., 2007) and geomorphic-stratigraphic data (Babault et al., 2008).

The Ouarzazate foreland basin is located between the High Atlas frontal thrust belt and the domal uplift of the Anti-Atlas Mountains (Fig. 2). It stands at an elevation of 1200–1800 m asl, extending more than 150 km in an east–west direction with a maximum width of 40 km. The north-bordering High Atlas fold-and-thrust belt presents structural and topographic differences between the west and the east of the basin (e.g., Fraissinet et al., 1988; Tesón, 2009). The wider western half of the basin (about 40 km), coincides in the north with the narrower segment of the south-draining flank of the central High Atlas (Fig. 2). The frontal structures of the High Atlas system are located well within the basin, deforming dated Quaternary pediments (Sébrier et al., 2006; Pastor et al., 2010). Neogene shortening rates are about 0.5 mm/a (Tesón, 2009) for the entire south Atlas frontal thrust belt. Recent shortening rates for individual structures within the basin obtained from deformed Quaternary deposits are 0.03–0.1 mm/a (Pastor et al., 2010).

The Ouarzazate basin is infilled by up to 1 km of Cenozoic (mainly Miocene) continental sediments, which are overthrust by the High Atlas to the north and onlap the Anti-Atlas to the south. The Neogene to Quaternary history of the basin can be broadly divided into two periods. The early record is dominated by net aggradation of alluvial, and lacustrine sediments within an internally drained basin (e.g., Görler et al., 1988; El Harfi et al., 2001), mostly during the mid and late Miocene (Tesón et al., 2010). A hiatus of 5–6 Ma in the sedimentary record separates the aggradation period from the recent erosional period, which is characterized by episodic fluvial aggradation within an incised drainage network created after the basin became externally drained via the Draa River canyon (Fig. 2). The timing of the basin aperture and the inception of the superimposed drainage within the basin remains undefined, but it probably occurred during the late Pliocene or early Pleistocene (Stäblein, 1988; Arboleya et al., 2008).

The basin surface is partially covered by coarse-grained sediments derived from the erosion of the High Atlas Mountains and aggraded during the late Quaternary (see Arboleya et al., 2008, for detailed description). These deposits form systems of stepped fan pediments (e.g., Fig. 3) covering a range of areas (reaching several square kilometers in the west half of the basin) and up to 30 m thick. Arboleya et al. (2008) argued that the base level for all the streams of the basin, and therefore their incision rates, may have kept pace with the progressive cutting of the Draa canyon, the basin outlet. The Draa River drains about 13,000 square kilometers of the High Atlas southern flank and the Ouarzazate basin through the Anti-Atlas Mountains. Arboleya et al. (2008) found average incision rates of 0.3–2 mm/a over the last 250 ka, which are slightly higher than the tectonic uplift rates, estimated for the same period on the basis of fault throws (0.1–0.2 mm/a; Pastor et al., 2010).

The drainage network of the Ouarzazate basin is composed by N–S transverse channels with great variability of catchment size ($1–10^3$ km$^2$). All the transverse channels join to the south in longitudinal, E–W oriented collectors: the Dades trunk River to the east and the Iriri trunk river to the west, fixed to the edge of the Anti-Atlas Mountains (Fig. 2). These perennial collecting rivers act as local base levels for the rest of the N–S drainage network.

Climate changes in the Atlas Mountains during the Quaternary are evidenced only for the late Pleistocene to the present. A change from arid to more humid conditions occurred at the transition from the last

**Fig. 3.** Field view to the south of the Madri valley where different levels of coarse gravel sediments form a system of stepped glacis covering the Miocene basin bedrock, composed of soft sediments (red shale and sandstone).

glacial maximum (22 ka) to the early to mid-Holocene (11–5 ka) (Reille, 1979; Gasse et al., 1987, 1990; Lamb et al., 1989, 1995; Salamani, 1991, 1993; Jolly et al., 1998; Elenga et al., 2000; Gasse, 2000; Holz et al., 2007). Older palaeoclimate records are available for the western Mediterranean but their correlation with the Atlas region is very tentative. The current climate of the study area is semi-arid. Precipitations are infrequent but intense, being concentrated in a few episodes of heavy rainfall occurring between December and March, accumulating 100 mm/a of precipitation for the period 1931–2000 (Knippertz et al., 2003). Vegetation within the Ouarzazate basin is sparse, comprising small xerophytic shrubs.

## 3. Methods

Piedmont tributary valley floor elevation must be lower than the adjacent river for a capture to occur (Mackin, 1936). We searched for low elevation valleys or pediments adjacent to perched main rivers originating in the mountain and evidence of past captures. Our analysis was based on longitudinal profiles of trunk rivers as well as piedmont streams and on the geomorphological analysis of Quaternary stepped fan terraces on the piedmont.

### *3.1. Mapping of low elevation piedmont valleys and low elevation pediments*

The drainage network of the south Atlas piedmont has been studied using the 90-m-resolution SRTM90v4 DEM. We mapped the network with the D8 flow routing (O'Callaghan and Mark, 1984) available in the Spatial Analyst tool (ArcMap). We further extracted elevations, distances from headwater and outlets, and drainage areas to derive longitudinal river profiles.

In similar studies, Hunt et al. (1953) and, later, Johnson et al. (2009) showed reaches of longitudinal profiles where piedmont tributary streams with gentler gradients lay at lower elevations than their adjacent main river. Similarly, we compared the longitudinal profile of a river originating in the mountains with that of its piedmont tributary valleys. The long of all channels with a drainage area above 5 $km^2$ were plotted as elevation against upstream distance graph, measured from the Draa canyon, the local base level of the Ouarzazate basin. Information on the variation of the contributing catchment area along the river profile allowed the discrimination of the rivers with large mountain catchments from the smaller piedmont streams. The N–S flowing channels share tributary junctions or merge into one of the main longitudinal streams (Iriri or Dadès), so they have experienced the same base level history.

We mapped the spatial extent of differences in elevation between piedmont streams and their adjacent main rivers for all the N–S fluvial systems of the Ouarzazate basin. Higher order tributaries that join before reaching the Iriri or Dadès trunk rivers, were measured from their shared tributary junction. Where piedmont streams and adjacent mountain rivers do not share a tributary junction, we measured the upstream distance from the longitudinal trunk stream. In these cases, we selected piedmont streams that join the longitudinal river upstream from the main river junction with the same trunk stream. In this way, we compared piedmont streams that have experienced no advantage in distance to base level, that is to say, piedmont streams that have an outlet at a level close to, or slightly higher than, the adjacent main rivers. The elevation versus distance from a common base level allowed us to perform second-order polynomial fits (with $<1\%$ error) of the longitudinal profiles of the streams originating in the mountain. The obtained equations were used to map the differences in elevation between main rivers and their adjacent piedmont streams with drainage areas $>5$ $km^2$.

The analysis revealed that after stream capture the depressed pediments are the erosional surfaces onto which sediments eroded from the uplands aggrade to form a new fan pediment. The spatial extent of the low elevation pediments and the differences in elevation between the pediment surfaces and adjacent main streams were mapped by projecting the main stream elevation in an E-W direction. This assessed the relationship between the occurrence of deeply incised piedmont streams and depressed pediment surfaces.

### *3.2. Evidence used to infer Quaternary captures*

The second aim of the study was to identify stepped fan pediments that resulted from stream captures and not from lateral planation. For a single river, fan terraces produced by climatic changes should consist of a sequence of progressively younger terraces inset within older ones. On the other hand, stepped fan pediments produced by the stream-capture process should consist of sequences of terraces separated by remains of older deposits. Moreover, the piedmont-stream capture process occurs randomly, and it is unlikely that a similar number and arrangement of fan pediments are formed in two adjacent fluvial systems.

In the following we summarize the indicators of past captures that have been described by Rich (1935), Mackin (1936), and Mills (1983). First, fan pediments at different levels, but with a lithologically similar

clast content, flanking of a gravel-capped ridge (Figs. 1 and 4), that is, a divide composed by higher gravel deposits. This arrangement indicates that the old course of a river originated in the mountain was diverted to one side and then to another, most probably by capture. Second, the presence of abandoned valleys, which leave wind gaps in the landscape (Fig. 4). Third, sharp stream bends in plant view or elbows of capture (Bishop, 1995) (Fig. 4). And fourth, some extension of gravel-free pediment in piedmont valleys upstream of the apex of a fan pediment (Fig. 4).

We based our mapping of fan pediments on field surveys, DEM analysis, and enhanced satellite imagery. Topographic profiles were constructed using the SRTM90v4 DEM. Color contrasts between fan pediments of the Landsat imagery 4–5 TM were enhanced with a color composition based on bands 70, 30, and 10, as red, green, and blue channels, respectively. Based upon their topographic position above main rivers, fan surfaces and terraces were mapped and classified as young, intermediate, or old, the lower being the younger.

## 4. Analysis and results

### 4.1. Drainage network

We observe two types of channels that compose the N–S transverse drainage crossing the Ouarzazate basin, both sharing tributary junctions and thus subjected to the same base level variations: (i) main rivers originating in the High Atlas Mountains, whose channel beds are draped by coarse sediments; and (ii) parallel-flowing piedmont streams sourced within the basin domain or in the mountain front, with no significant supply of coarse sediments.

A common feature of all the mountain rivers in the Ouarzazate basin is the braided channels blanketed by a layer of coarse-grained sediments of variable thickness, covering the Miocene basin bedrock (Fig. 5A and B). Their mountainous headwaters reach maximum elevations > 3000 m, whereas the average altitude of the valley floor at the mountain front is ca. 1500 m, so their fluvial relief is high (~ 1500 m). Mountain rivers have catchments mainly composed by mechanically strong rocks exposed in moderate to steep hillslopes, with average local slope of about 18°. Because of the semiarid climate, such main rivers are ephemeral or have a moderate flow during most of the year. However, during heavy rainstorm events main rivers drastically increase their discharge and transport capacity. Field evidence show that main rivers are capable of moving coarse sediments accumulated in their upland channels to the gently inclined basin reach, where the transport capacity is lessened. In the basin, mountain rivers are separated by minor piedmont streams sourced within the basin domain or on the mountain front hillslopes, with catchment areas ranging between 1 and 100 km$^2$. They

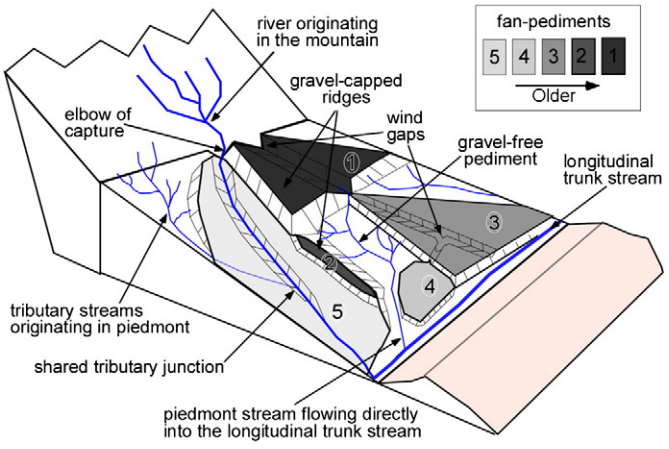


**Fig. 4.** Sketch showing the geomorphic elements used to infer piedmont stream captures (see text for explanation).

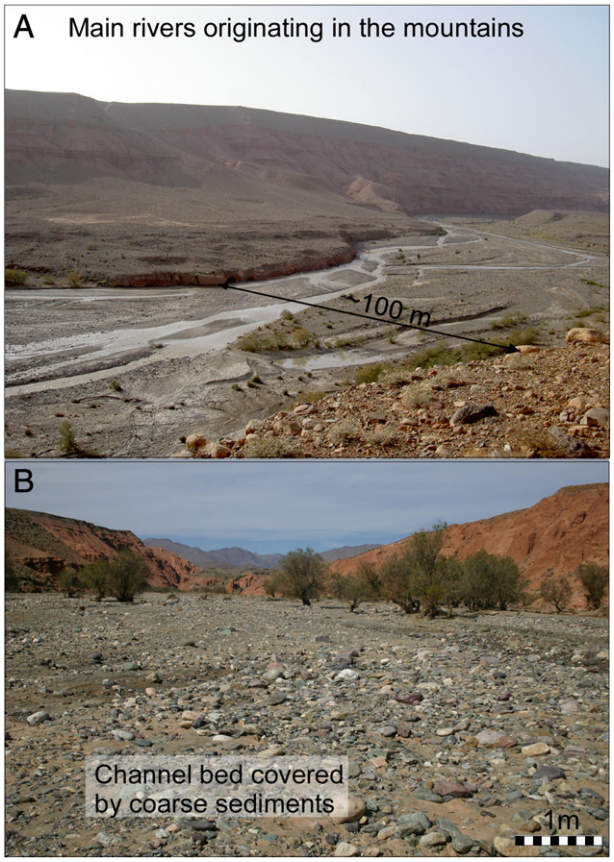


**Fig. 5.** Field images showing representative examples of mountain rivers. (A) General view of the Izerki River located in the central part of the basin. The Izerki shows braided channels entrenched in older fan terraces and Miocene strata outcrop in the banks above the coarse deposits. (B) The channel of the Madri River in the central part of the basin is blanketed by coarse gravels (10–30 cm) coming from the uplands.

have no coarse sediment supply and commonly expose the Miocene bedrock in their channel beds and banks (Fig. 6A and B). Bedload material is essentially composed of fine-grained sediment (silt, sand) derived from local lithologies (mostly sandstones and shales); their channels, however, usually contain gravels derived from the colluvial denudation of the surrounding fan terraces.

Two scenarios can be differentiated east and west of the basin as a consequence of the structural differences of the High Atlas southern flank and the basin morphology. The western part of the Ouarzazate basin is about 40 km wide. To the north, the short distance (15 km in average) between the main drainage divide of the High Atlas hinterland and the southern mountain front defines relatively small mountain river catchment areas (between 50 and 280 km$^2$) where they emerge onto the Ouarzazate basin, and the spacing between outlets at the mountain front is only 5–10 km. In contrast, the eastern half of the Ouarzazate basin (east of Targa River) is only 10 km wide on average. A more northern position of the main High Atlas divide and the presence of a well-developed fold-and-thrust belt at the basin margin, increase the distance between the drainage divide and the mountain front to more than 35 km. In the narrow eastern half of the basin, mountain rivers emerge onto the basin with outlets spaced by 20 km apart (Fig. 2); and most of the basin surface is drained by small piedmont streams (catchments < 50 km$^2$). There, main rivers exhibit larger catchment areas and perennial flow (the rivers M'Goun and Dades emerge onto the basin with catchments of 1245 and 1535 km$^2$, respectively).

The fluvial systems flowing through the western, widest part (40 km) of the Ouarzazate basin (from the N'Wachir River to the Targa River) have the best developed steeped fan pediments

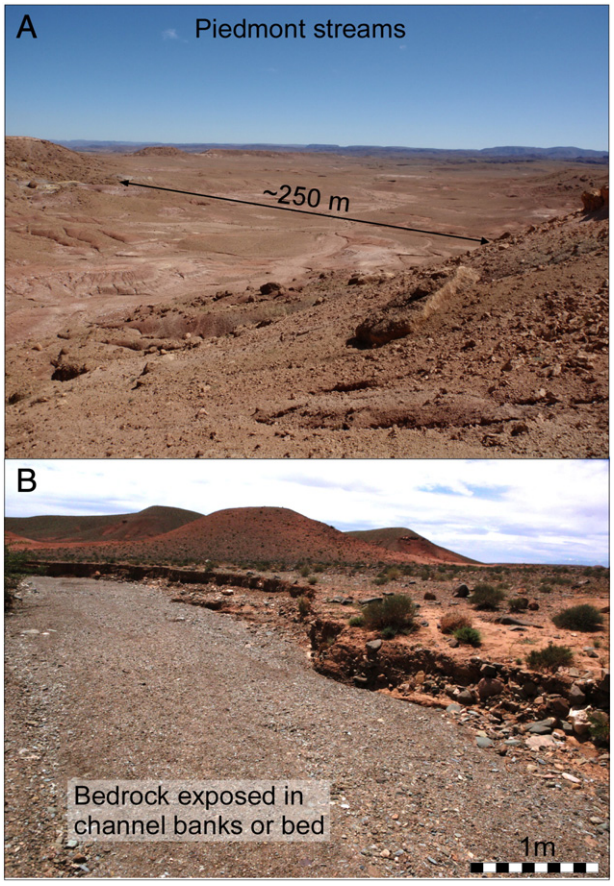


**Fig. 6.** Field images showing representative examples of piedmont streams. (A) General view of a piedmont stream located west of the Izerki River. The channel bed and most of its catchment expose Miocene bedrock strata. (B) Example of a piedmont stream sourced in the mountain front hillslopes located east of the Tanjout River. In this case, the channel bed is covered by a thin layer of sand and fine gravel.

(Fig. 3). There, some piedmont streams are locally more deeply incised than main rivers, which have larger catchment areas and steeper slopes.

### 4.2. Piedmont valleys adjacent to the Izerki and Tanjout Rivers

Fig. 7A plots the longitudinal profiles of the main rivers Izerki and Tanjout originating in the mountain, including their adjacent piedmont streams located westward and other small tributaries, all with drainage areas > 5 km$^2$. We note that most of the small tributaries are at a higher level than their trunk river. However, some larger piedmont streams present gentler slopes than the main rivers rising in the mountain and therefore are lying at lower elevations than the main rivers. A few kilometers west of the Izerki valley, a parallel-flowing piedmont stream is largely below the Izerki River level in most of the N–S path of the Izerki River, and the difference in elevation locally reaches 40 m (Figs. 7B and 8A). This piedmont stream reaches 100 km$^2$ of watershed close to the southern edge of the basin, whereas the catchment size of the Izerki river across the basin ranges from 180 to more than 300 km$^2$ (Fig. 7B).

West of the Tanjout River, a small piedmont stream sourced within the basin has deeply incised the Miocene substrate. This low piedmont stream has a catchment area of 5–10 km$^2$ and incises 30 m below the elevation of the adjacent Tanjout River, which drains a catchment of 70 km$^2$ (Figs. 7C and 8B).

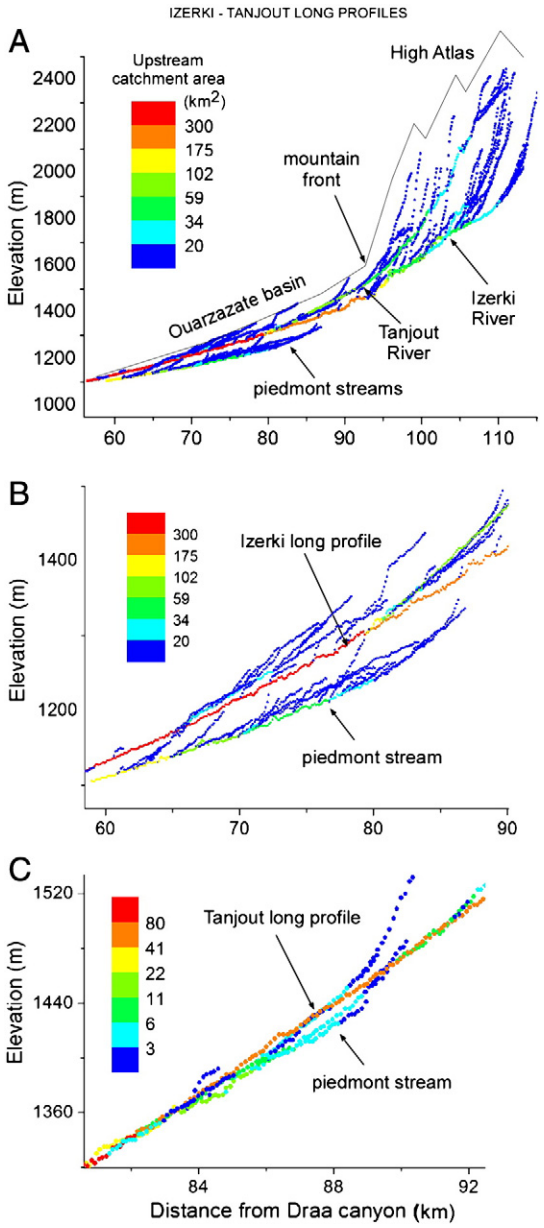


**Fig. 7.** Longitudinal profiles of different channels (with drainage area > 5 km$^2$) in graphs with elevation versus upstream distance. We added a grey scale that gives information about the variation of the contributing catchment area along the river profile. (A) Longitudinal profiles of the Izerki and Tanjout rivers (see location in Fig. 2), including the secondary stream located to the west. (B) Subset of the Izerki River profile at the southern half of the basin where a secondary stream has a gentler slope and lies at a lower elevation than the main river. (C) Subset of the Tanjout River profile where some secondary streams present gentler slopes.

### 4.3. Low elevation valleys and pediments in the Ouarzazate basin

The analysis included the 11 main mountain rivers of the Ouarzazate basin (Amaragh, N'Watchir, Izerki, Tanjout, Tagragra, Madri, Tabia, Targa, Imassine, M'Goun, and Dadès Rivers; Fig. 2). Five of the main mountain rivers (the Izerki, Tanjout, Tabia, Targa, and Imasine Rivers) are flanked by low elevation piedmont stream valleys (Fig. 9). The depth of incision of the piedmont valleys relative to their adjacent main rivers is randomly distributed and attains maximum values ranging from 10 to more than 40 m. The relative deeper incision of the piedmont streams indicates that they have greater incision power than their adjacent trunk rivers, in spite of their lower gradient and smaller catchment. Only the N'Wachir, Madri, M'Goun, and Dades Rivers are not bordered by low elevation piedmont

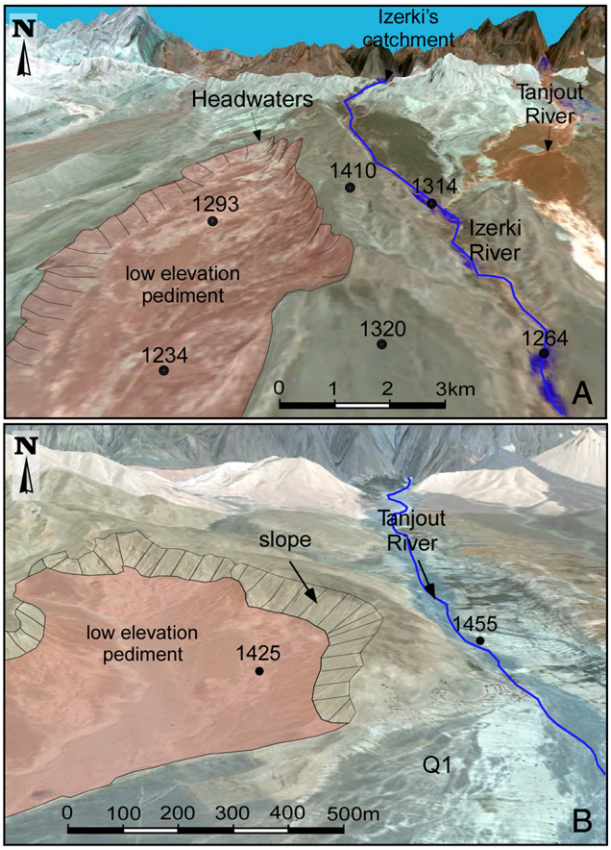


**Fig. 8.** (A) Oblique image (obtained from Google™ Earth) of a depressed valley (pediment) located westward and trending parallel to the Izerki valley in the western part of the Ouarzazate basin. This area currently represents one of the larger accommodation spaces for sediments in the entire basin, being up to 0.4 km$^3$ lying below the level of the Izerki main river (view to the north). (B) Oblique image (obtained from Google Earth) of a depressed valley (pediment) located westward and trending parallel to the Tanjout River (view to the north).

streams. However, their adjacent piedmont streams are situated at a similar level despite the great contrast in catchment areas. This indicates that in these cases small piedmont streams incise at a similar rate as the main rivers. Alternatively, it may indicate that these piedmont streams are at a different (earlier) stage in their evolution, perhaps because they have been filled by alluvium from the main channel more recently.

Interestingly, the low elevation piedmont streams are not confined by narrow valleys, their width corresponds to the low relief and gently inclined pediment erosional surfaces. Fig. 10 shows the depth of these pediments below their adjacent rivers originating in the mountain, and it also underlines the large extent of this kind of pediment, with N–S length > 10 km and area ranging from 5 to more than 100 km$^2$ in the southern edge of the basin. Light greenish colors in the Landsat imagery 4–5 TM correspond to the pediments where the basin bedrock is exposed. The pediments have almost everywhere a thin alluvial cover (<1 m), giving them the same spectral colors in the Landsat imagery, as the adjacent fan pediments (Fig. 11).

### 4.4. Quaternary stepped pediments

As pointed out above, the Ouarzazate foreland basin has been subjected to erosion and contains stepped pediments veneered by coarse debris, here referred to as 'fan pediments'. The base of the fan pediments is composed of coarse-grained sediments (including boulder size) indicating that deposition occurred suddenly, being not a progressive change in transport conditions.

The generalized occurrence of fractured and exfoliated clasts at the surface of fan pediments indicates that mechanical weathering reduces the grain size. Consequently, the mean grain size at the surface of older deposits is usually smaller than the grain size of the bedload in the younger ones. The different levels of stepped fan pediments were mapped using topographic elevation, field observations, and color contrasts on Landsat imagery (Fig. 11). The number of fan pediments preserved in the different fluvial systems across the basin varies from three to six. For a given fluvial system, we labeled the fan pediments and terraces beginning numbering with the oldest deposits. The most recent fan pediments merge distally in the basin, and accordingly, we have assigned them the same label (Q6 in Fig. 11). As a result of this, the label of the highest fan pediment for a fluvial system may vary, i.e. from Q1 to Q4, depending on the specific number of fan pediments preserved. Implicitly, the numbering does not correspond to a temporal/altitudinal correlation across different fluvial systems, except for the most recent fan pediments Q6 that coalesce. In Fig. 11 we have indicated the boundaries of the rivers systems for which a particular numbering sequence is valid.

The morphology of the well-developed stepped fan pediments of the Tanjout, Madri, Tabia, Targa, Amaragh, Talat-n-Ouznag, and N'Wachir fluvial systems originating in the mountain (see Fig. 2 for location) are analyzed in detail below.

#### 4.4.1. The stepped fan pediments of the Tanjout River

The Tanjout River (72 km$^2$) enters the Ouarzazate basin 7 km to the west of the Izerki River and becomes its tributary at the middle of the basin (Fig. 11). The old channel of the Tanjout River donwstream of the junction is recognizable forming a wind gap (Fig. 12), suggesting that it was recently captured by the Izerki River channel. Towards the north, about 5 km south of the High Atlas mountain front, three lobes of coarse debris deposits show fan shape morphology (Q6, Q5, and Q4; Fig. 12). The current course of the Tanjout River is flanked by two levels of these coarse debris deposits 1 km wide and several kilometers long each one. These deposits rise 1–5 and 20–40 m above the Tanjout River (Q6 and Q4, respectively; in Figs. 11 and 12). The third level of coarse debris deposits is developed in the low elevation pediment catchment east of the Tanjout River, and it is situated 20 m above the Tanjout River bed (Q5, profile B–B' in Fig. 12). In this study, Q5 corresponds to Q3c in Arboleya et al. (2008). Basement exposures at the base of these coarse debris deposits indicate that they are 5 to 20 m thick and that they rest on smooth erosional surfaces planed into Miocene bedrock, that is, on pediments. Because these coarse debris deposits rest on pediments, we refer to them as 'fan pediments'. The coarse material of the fan pediments is predominantly composed of Mesozoic and Paleozoic clasts, indicating the same High Atlas provenance for the three fan pediments and implying that the Tanjout River deposited all three fan pediments.

The highest and oldest fan pediment (Q4) is located at the divide between the Q6 in the Tanjout catchment and Q5 in its adjacent piedmont catchment. Lateral channel migration of the Tanjout River between Q5 and Q6 would have implied the erosion of the ridge formed by Q4 fan pediment. Therefore, the observed arrangement cannot be explained by lateral migration and successive abandonments of terraces. The preservation of the high level fan pediment Q4 argues for stream diversion upstream. Whatever the mechanism that produced the deviation of the Tanjout course upstream of Q4, the river must have been bordered by a low elevation pediment in expansion, for fan pediment Q6 to be formed below Q5. Finally, the divide between the Tanjout River and the western pediment must have been breached either by lateral erosion of the Tanjout River leading to an avulsion, by the headward erosion of the captor, or by a combination of both processes.

Another plausible explanation for the shift of the Tanjout River path from Q5 to Q6 would be the aggradation of the Q5 valley to

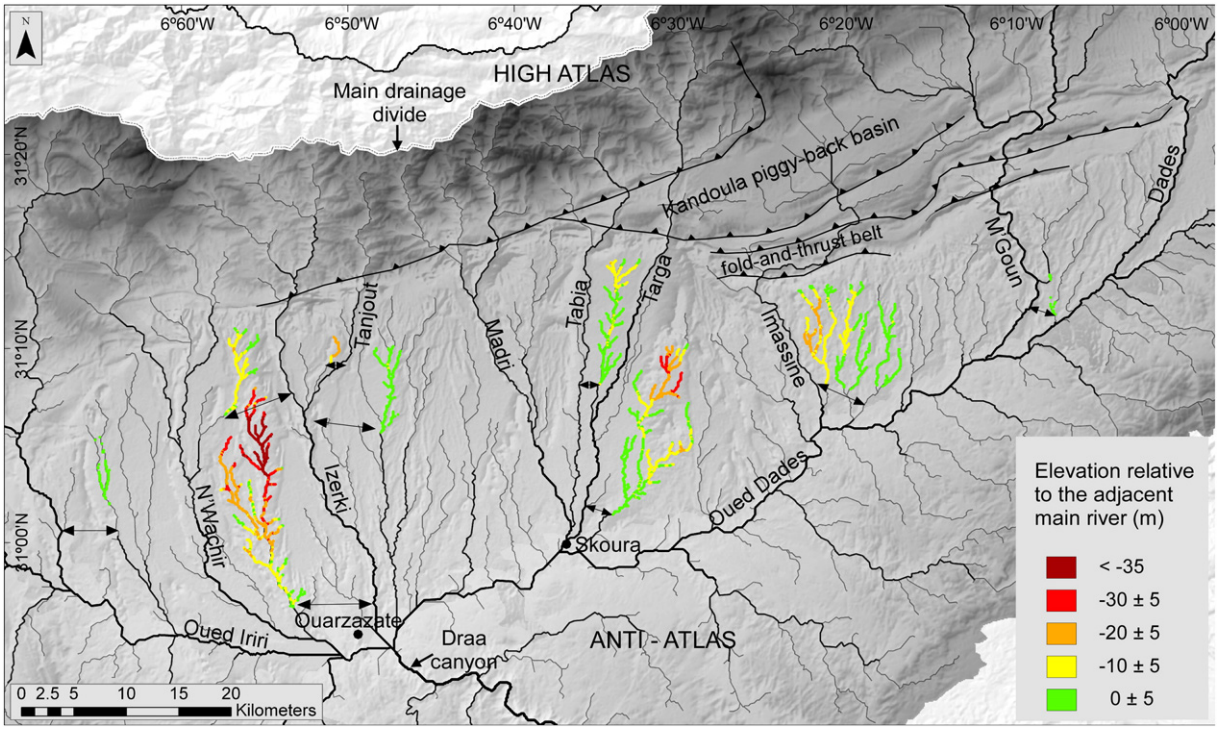


**Fig. 9.** Hillshade DEM of the Ouarzazate basin where colors represent the difference in elevation of the piedmont streams located below their adjacent main rivers originating in the mountains. The range (0 ± 5) corresponds to the zone of no detectable difference. Arrows indicate the exact points of the long profiles where rivers were compared (maintaining the same distance from their common base level).

the level of the Q4, followed by the lateral shift of the Tanjout River toward the west and its subsequent entrenchment. In this case, remnants of Q5 should be found at both sides of the valley. No evidence of valley infill suggests a piedmont-stream capture for the shift to Q6.

The sediments of the Q5 fan pediment have been deposited on a lower pediment that is still preserved as a gravel-free pediment in the piedmont valley north of Q5 (Fig. 12). The base of Q5 also dips to the east indicating that it filled the western flank of a large valley.

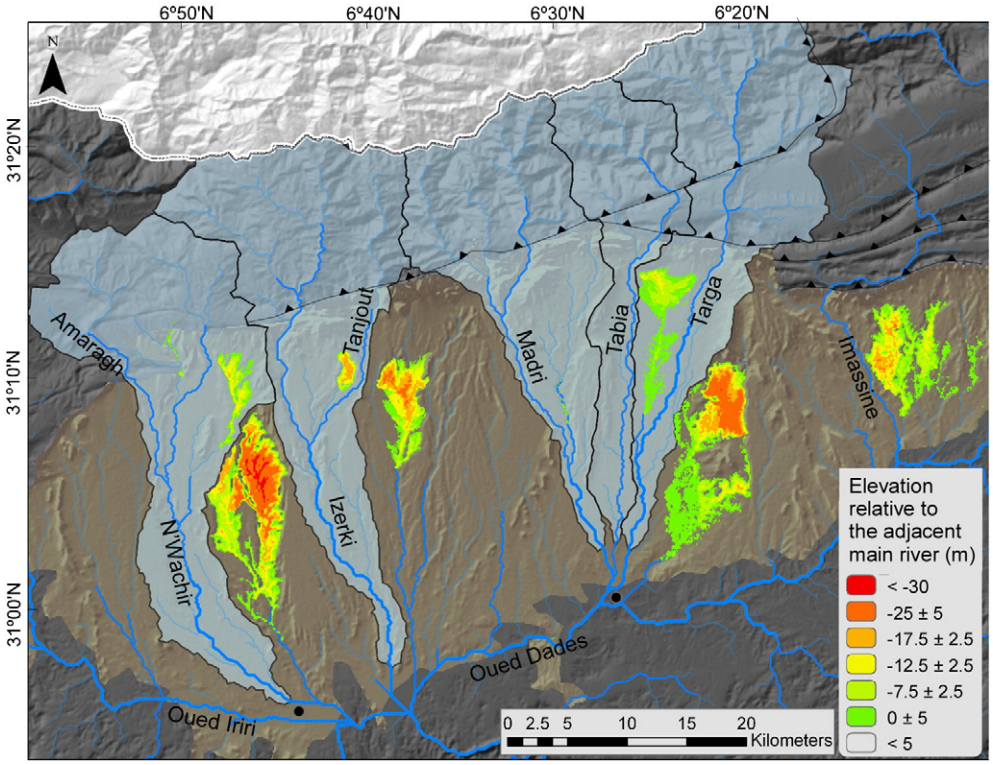


**Fig. 10.** Hillshade DEM of the Ouarzazate basin where colors represent areas of piedmont stream catchments (forming low elevation pediments), which are below their adjacent main rivers. The range (0 ± 5) corresponds to the zone of no detectable difference.

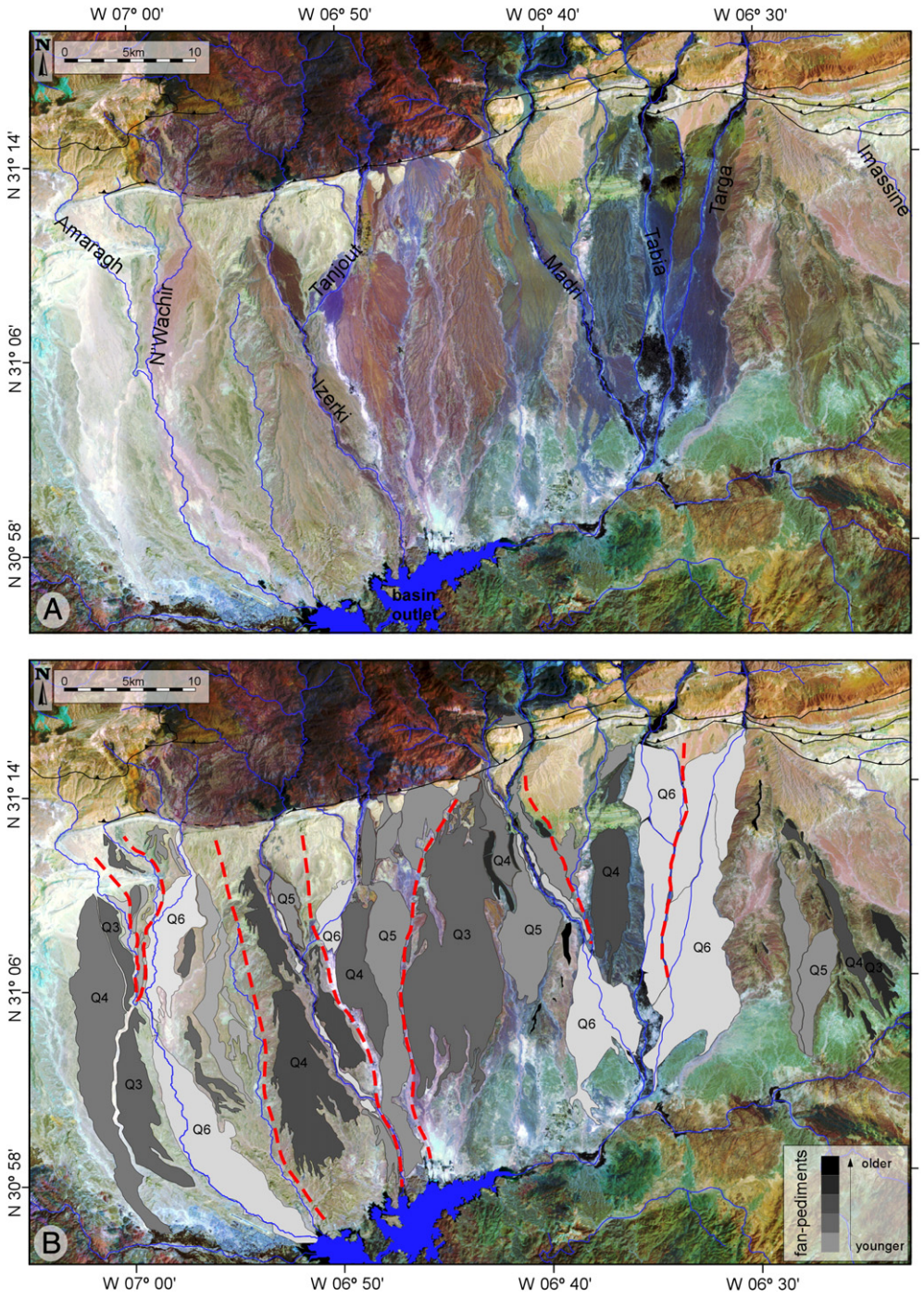


**Fig. 11.** Cartography of the Quaternary stepped pediments of the western Ouarzatate basin. (A) Landsat 4–5 TM color composition. (B) Mapping of the Quaternary fan pediments based on Landsat imagery, topographic elevation, and field reconnaissance. The red dashed lines correspond to the boundaries of fluvial systems with a particular sequence of terraces.

In fact, fan pediment Q5 might also have resulted from a capture event. Its apex is located in the NW corner of the deposit, with a sediment transport direction eastward; whereas upstream, the Tanjout River flows southward. This abrupt shift of the Tanjout course may represent an elbow of capture.

A topographic profile in the northern part of the system (A–A' in Fig. 12) shows low elevation pediments drained by piedmont streams and located at both sides of the current Tanjout River. The low elevation pediments threaten the Tanjout River to be captured, a potential event that would produce the same pattern as the one observed for Q5 and Q6. In summary, all these evidence argue that Q6, and likely Q5, formed by capture events.

*4.4.2. The stepped fan pediments of the Madri River*

The Madri River flows 10 km east of the Tanjout valley (Fig. 2). The river is flanked by six levels of coarse debris deposits ranging from 1 to 5 km wide and up to 25 km long (Figs. 11 and 13; see also Arboleya et al., 2008). Based on their morphology of large extent, thin sedimentary cover and flat basement exposure, we refer to these coarse debris deposits as 'fan pediments'. However, Q6 in the northern half of the basin is confined to the Madri valley, and it forms a paired terrace. The Q2 and Q1 are poorly preserved remnants in narrow ridges. Fan pediments and terraces Q6, Q5, Q4 and Q2 of the Madri valley in this study correspond to Q4, Q3, Q2 and Q1 in Arboleya et al. (2008), respectively. The Q3 corresponds to the

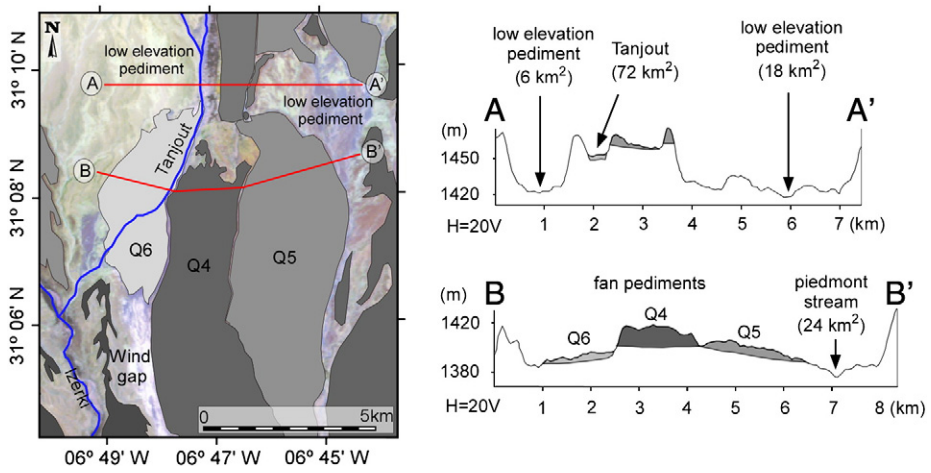


**Fig. 12.** Interpreted Landsat image of the Ghassat alluvial fan, showing the mapping of the Quaternary stepped fan pediments associated with the Tanjout River. Labels of the rivers in the topographic profiles to the right include the catchment area size in square kilometers. The topographic profiles are perpendicular to the transport direction and present an exaggerated vertical scale. The upper profile shows that the Tanjout main river has depressed areas at both sides. The lower profile show the Q4 as a relief preserved between age-successive levels Q5 and Q6. Such arrangement suggests that the shift from deposits Q4 to Q6 did not occur by channel lateral migration.

western part of Q2 and the Q1b in Arboleya et al. (2008), whereas the Q1 was not recognized by Arboleya et al. (2008).

The westernmost deposit in the area is a large Q3 fan pediment reaching 25 km long and up to 8 km wide, situated 80–100 m above the Madri River bed (profile A–A' in Fig. 13). This fan pediment shows an apex located close to the mountain front where the Madri River emerges onto the Ouarzazate basin (Fig. 11). The lithology of the coarse material indicates a High Atlas provenance for all terraces (from Q6 to Q1), even the Q3, which belongs to a piedmont catchment now draining only a few square kilometers of the southern edge of the High Atlas. This fan pediment contains Cambro-Ordovician clasts derived from outcrops situated in the uplands of the Madri River catchment. Clast content and the position of its apex indicate that Q3 is an old Madri river bed now abandoned.

In the Madri's fluvial system, successively younger fan pediments are separated by older (higher) deposits forming gravel-capped ridges between them. This is the case of Q2, forming ridges between Q3 and Q4 and between Q4 and Q5. Similarly, the higher level Q1 forms a 40–50 m high ridge between Q5 and Q6 (Fig. 13). The classic mechanism of lateral river erosion and deposition of a terrace, followed by its abandonment and entrenchment, would have implied erosion of the high level ridges and would have produced sequences of younger terraces inset within older ones. Here again, the stream-capture process gives a simple explanation to an arrangement of fan pediments deposited by the same river and separated by gravel-capped ridges. The aggradation to the level of the gravel-capped ridges followed by the lateral shift of the Madri River toward the east is unlikely because no evidence is found of thick aggradational sequences in Q3, Q4, and Q5 up to the gravel-capped ridges Q2 and Q1.

In any case, the Madri River must have been flanked by large open valleys successively at lower elevations for stepped fan pediments to develop. The arrangement of gravel-capped ridges and abandoned fan pediments strongly argue for three captures to have resulted in

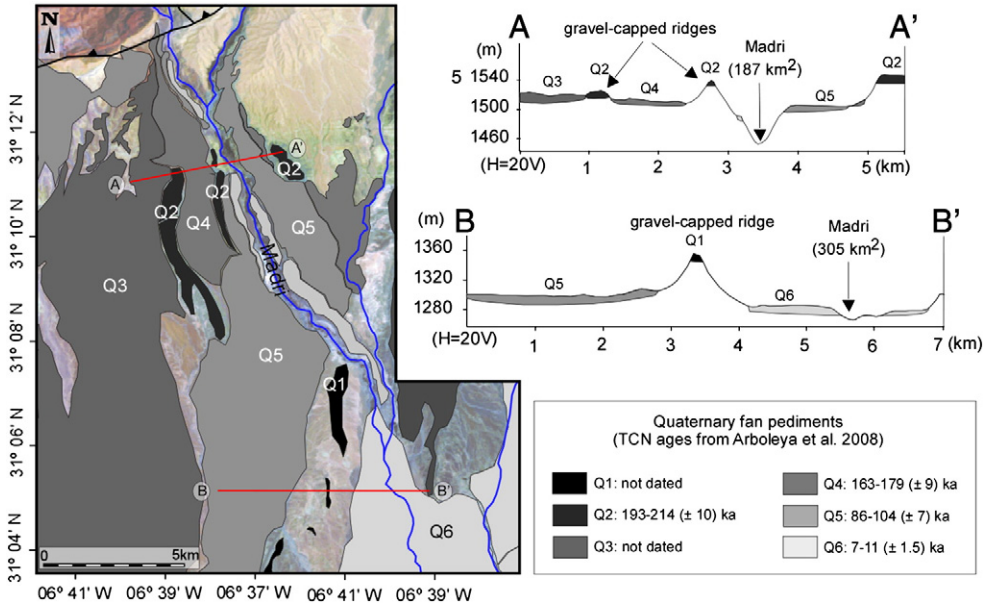


**Fig. 13.** Interpreted Landsat image showing the mapping of the Quaternary stepped fan pediments and terraces of the Madri valley, which are numbered from lowest to highest (note the different nomenclature from Arboleya et al., 2008). Topographic profiles are perpendicular to the transport direction with exaggerated vertical scale. They show the existence of relict reliefs (gravel-capped ridges) preserved between age-successive levels. In profile AA', the difference in elevation between different ridges labeled Q2 is caused by tectonic deformation. The legend includes the abandon ages of the fan pediments dated by Arboleya et al. (2008).

the successive formation of the stepped fan pediments Q4, Q5, and Q6.

*4.4.3. The stepped fan pediments of the Tabia River*

The Tabia River is located ~10 km east of the Madri valley (Fig. 2) and has a mountain catchment area of 125 km$^2$. The river is flanked by three levels of coarse debris deposits: Q6, Q5, and Q4 at 4, 80, and 140 m above the Tabia River, respectively. They are 1 to 3 km wide, 4 to 17 km long, and 5 to 20 m thick (Figs. 11 and 14). The large extent in width and length of the coarse deposits and the occurrence of basement exposures at their base indicate that they have been deposited on pediments. Fan pediments Q6, Q5, and Q4 are made of coarse material coming from the uplands of the Tabia River catchment, indicating that they were old Tabia River beds now abandoned. Fan pediments Q6 and Q5 also have their apex located close to the mountain front where the Tabia River emerges onto the Ouarzazate basin. Most of fan pediment Q5 now belongs to a piedmont catchment currently draining only a very small area in the southernmost edge of the High Atlas. Although Q6 has a large extent, its eastern part has an elevation lower than the Tabia River. We described this low elevation area as an erosional pediment in Section 4.3.

The Tabia River is separated from its fan pediment Q5 by the fan pediment ridge Q4. As in the other cases, lateral erosion of the Tabia River from Q5 to Q6 would have eroded the ridge, arguing against a mechanism of lateral erosion and terrace abandonment. The stream-capture process is, as in the Tanjout and Madri valleys, more likely to have produced such geometries. In this case again, we find no evidence for aggradation of the Tabia River up to the fan pediment ridge Q4. Moreover, differences in spectral colors of fan pediments Q5 and Q4 argue for fan pediments of distinct ages, which would not be the case if aggradation would have filled the Tabia valley during stage Q5 up to the Q4 level.

*4.4.4. The stepped fan pediments of the Targa River*

The Targa River emerges to the basin 5 km east of the Tabia River (Fig. 2). Six coarse debris deposits east of the Targa River, labeled Q6 to Q1, are lying at 10 to 190 m above the river channel. Except for Q6, all these deposits belong to piedmont catchments. All these deposits are made of coarse material coming from the uplands of the Targa River catchment, indicating that they were old Targa River beds now abandoned. The large extent in width and length of the 5- to 15-m-thick alluvial deposits, and the basement exposures indicate that Q6, Q5, and Q3 have been deposited on pediments, so they are fan pediments. Similarly, as in the case of the Tabia River, part of Q6 is located below the present-day Targa River. We described these low elevations of Q6 as erosional pediments in Section 4.3. On the one hand, Q4 is not a fan pediment, but rather it is a terrace inset in older ones. The Q2 and Q1 are poorly preserved gravel-capped ridges and they do not match the large extent in width and length defining fan pediments. The Q6 is the largest coarse debris deposit, with up to 4 km width and up to 23 km length; and it is the only one with its apex situated close to the mountain front where the Targa River emerges onto the Ouarzazate basin (Figs. 11 and 14). By contrast, Q5, Q4, and Q3 have their apex located several kilometers to the south of the mountain front. A perched valley separates the uplands from deposits Q5, Q4, and Q3 (perched valley 1 in Fig. 14).

The fan pediment Q5 merges with the longitudinal profile of perched valley 1. The upstream part of this perched valley is a scarp facing the current valley of the Targa River, which means that the old Tagra River has been beheaded when diversion occurred toward its current valley between stages Q5 and Q6. The upstream part of this perched valley now forms a wind gap (WG1 in Fig. 14). Perched valley 1 is separated from the current Targa River valley by the gravel-capped ridge Q1. Fan pediment Q5 is also separated from the current Targa River and fan pediment Q6 by gravel-capped ridges of Q3 (Fig. 14). Lateral erosion of the Targa River from Q5 to Q6 would have eroded ridges Q3 and Q1.

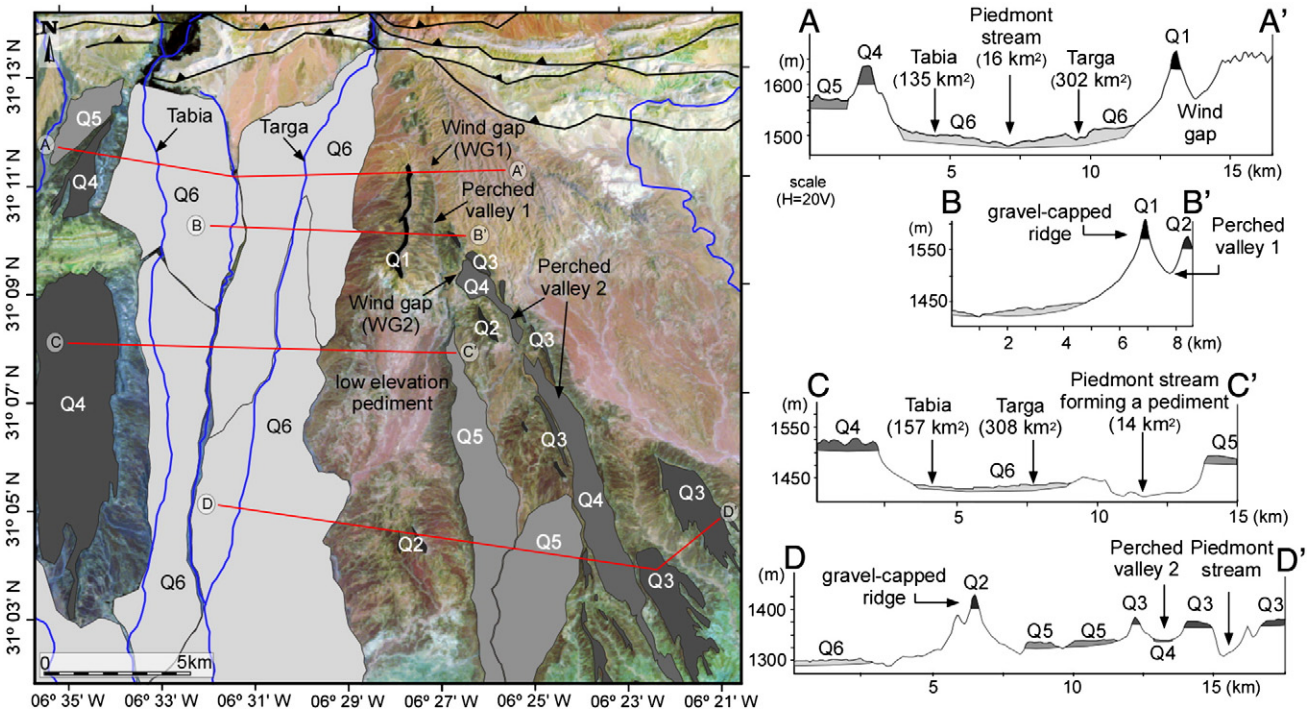


**Fig. 14.** Interpreted Landsat image showing the mapping of the Quaternary stepped fan pediments and terraces associated to the Tabia and Targa Rivers. The topographic profiles perpendicular to the transport direction show relict reliefs (gravel-capped ridges) preserved between age-successive levels, as well as wind gaps and low elevation pediments. The labels of the rivers in the topographic profiles include the catchment area size in square kilometers.

The Q4 is confined to an ~1-km-wide and 17-km-long perched valley reaching the longitudinal Dades River (perched valley 2 in Fig. 14). The upstream part of Q4 is limited by a scarp facing Q5. It means that between stages Q4 and Q5, the Targa River has been beheaded. The upstream part of perched valley 2 now forms a wind gap (WG2 in Fig. 14). Gravel-capped ridges Q3 and Q2 separate terrace Q4 from fan pediments Q5 (Fig. 14), arguing again against lateral erosion. The stream-capture process is—as in the Tanjout, Madri, and Tabia valleys—more likely to have produced the observed pattern. In this case again, no evidence for aggradation of the Targa River up to the different gravel-capped ridges is found, and the presence of wind gaps strongly argue for diversion of the Targa River by captures.

*4.4.5. Stepped fan pediments in the western Ouarzazate basin*

Three rivers originating in the mountains emerge onto the Ouarzazate basin close to its western edge: the Amaragh, Talat-n-Ouznag, and N'Wachir Rivers. These rivers do not reach the High Atlas main divide (Fig. 2), and consequently, they present smaller catchments than other main rivers analyzed in this study. The Amaragh and N'Wachir have catchment areas of 80 km$^2$ at the mountain front, whereas the catchment of the Talat-n-Ouznag (located between them) is only 35 km$^2$. The headwaters of these catchments are higher than 2000 m. The tributary junction of the N'Wachir and Talat-n-Ouznag Rivers is located close to the mountain front, and the Amaragh River joins with the N'Wachir in the centre of the basin. Deposits related to the Amaragh River, Talat-n-Ouznag and N'Wachir Rivers have been labeled with the subindex 'a', 'b' and 'c', respectively. The areal extension of these coarse deposits shows a high variability of width (0.5 to 4 km) and length (~1 to 20 km). They are a few meters thick (rarely reach thicknesses up to 5 m), and they fill flat erosional surfaces (pediments)—so they are fan pediments.

The Amaragh fluvial system contains four deposits: Q6a, Q5a, Q4a, and Q3a (Fig. 15). The westernmost deposit (Q4a) is up to 20 km long and 4 km wide. Its apex is located close to the mountain front where the Amaragh River emerges onto the Ouarzazate basin, but its surface now drains to the south by little piedmont streams. The Q4a is mainly composed by Cretaceous clasts coming from outcrops situated in the uplands of the current Amaragh River catchment. Clast content and the position of its apex indicate that Q4a is an old Amaragh River bed, now abandoned. The Q4a is separated from a younger fan pediment (Q5a) and from the active channel by an older fan pediment (Q3a, profile A–A' in Fig. 15), which is easily identifiable because its spectral response in the Landsat composition is different from its nearby deposits. The mechanism of lateral erosion, followed by the abandonment of Q4a and river entrenchment, would have implied the erosion of Q3a. No field evidence is found of aggradation of Q4a up to the level of the gravel-capped ridge (Q3a) followed by the lateral shift of the Amaragh River toward the east. Consequently, the abandonment of Q4a is the result of a capture. Southward, the presence of an abandoned channel and an elbow of capture (Fig. 15) indicates that the Amaragh River have been captured by the N'Wachir River. A small fan pediment (Q6a) has been developed where the Amaragh River emerges into the N'Wachir valley.

The coarse debris related to the Talat-n-Ouznag River (Q6b, Q5b, and Q4b in Fig. 15) are restricted to the northern half of the basin, with limited extension (~1 km$^2$). In this case, their arrangement follows the normal pattern, with the younger deposits inset within older ones. However, a perched valley incised in the Q5b surface suggests that the diversion to Q6b also occurred after a capture event.

The N'Wachir fluvial system is composed by three deposits: Q6c, Q5c, and Q4c (Fig. 15). Profiles B–B' and C–C' (Fig. 15) show that the older fan pediment (Q4c) separates the two younger and age-successive fan pediments (Q5c and Q6c). This arrangement indicates that the course of the N'Wachir River shifted westward to a lower elevation valley.

The captures responsible for the formation of the gravel deposits Q6a, Q6b, and Q6c are all related to the previous development of a low elevation piedmont valley in this area.

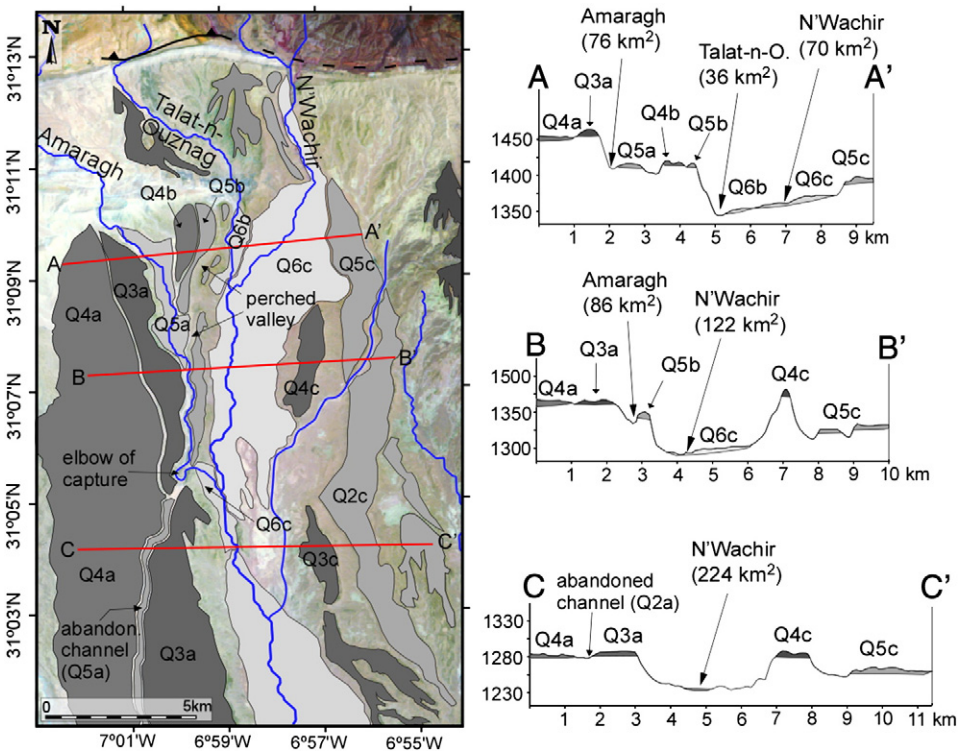


**Fig. 15.** Interpreted Landsat image showing the mapping of the Quaternary stepped fan pediments and terraces associated with the rivers of the western basin. The topographic profiles perpendicular to the transport direction show relict reliefs (gravel-capped ridges) preserved between age-successive levels, as well as wind gaps and low elevation pediments. The labels of the rivers in the topographic profiles include the catchment area size in square kilometers.

## 5. Discussion

Five rivers (Izerki, Tanjout, Madri, Tabia, Targa, and Imassine Rivers) of the 11 main fluvial systems originating in the mountain and crossing the Ouarzazate basin are bordered by low elevation, parallel-flowing piedmont streams. The most important difference between the main rivers and the piedmont streams is that the former carry coarse sediments whereas piedmont streams transport fine-grained bedload. The low elevation piedmont valleys, mostly developed in the western half of the basin (Fig. 9), constitute almost flat erosional surfaces that can be considered as low elevation pediments (Fig. 10). Drainage networks of ephemeral streams are well developed in these pediments indicating that they result from fluvial erosion.

Because they share tributary junctions, the higher position of main rivers originating in the mountain indicates that smaller piedmont tributaries incise at higher rates despite their lower longitudinal slope and smaller drainage area. This shows that fluvial erosion is not only a function of catchment area size but also channel longitudinal slope and bedrock erodability. Channel bedload is also an important factor that controls the fluvial regimes, especially in areas adjacent to the mountains where channels receiving abundant supply of coarse sediments flow into weak bedrock of sedimentary basins (Sklar and Dietrich, 2006). The occurrence of coarse sediments in the main rivers and their absence in piedmont streams strongly argues that fluvial erosion is also modulated by the sediment flux, a relationship first proposed by Gilbert (1877). Following Sklar and Dietrich (2006), the total channel longitudinal slope can be divided into three components: the first one corresponds to the slope needed to exceed the sediment threshold of motion, the second is the slope needed to transport the sediments coming from upstream, and the third corresponds to the slope needed for erosion at a rate equal to the base level lowering rate. Rich (1935) and Mackin (1936) recognized that the steeper slopes of the main rivers in the piedmont were those needed to transport their high content of coarse sediments. Rich (1935) added that the coarse bedload in main rivers serves as an effective blanket to protect the underlying rocks from erosion". In the case of the Utah's Henry Mountain piedmont, Hunt et al. (1953) considered the main streams as agents of aggradation, although the long term state of erosion in the Colorado canyon and its tributaries indicates that the main streams in the piedmont of the Henry Mountains incise their bedrock on the long-term. Indeed, Johnson et al. (2009) showed that incision dominates on the long term even in the main channels carrying coarse bedload: they preferred to call them 'sediment-load-dominated bedrock channels' instead of 'transport-limited channels'. Recent studies support the old view (e.g., Gilbert, 1877; Rich, 1935; Hunt et al., 1953) that an optimum content of transported clasts may enhance the erosion by the process of impact abrasion (the tool effect) and that a too high content of bedload may inhibit the erosion in rivers by covering the channel bed (the cover effect) (e.g., Sklar and Dietrich, 1998, 2001, 2006; Whipple and Tucker, 2002; Cowie et al., 2008; Johnson et al., 2009; Lague, 2010; Yanites et al., 2011). The lesser incision efficiency in main rivers in the Ouarzazate basin is best explained by a high content of coarse bedload, which inhibits the incision (the cover effect).

A divide between a main river and a piedmont stream or pediment must be breached either by headward erosion of the captor, by lateral erosion of the captured river, or by a combination of both processes. Field evidence from the Ouarzazate basin shows that active gullying is eroding the soft Miocene basement at the piedmont catchments' boundaries, which are usually composed by the easily erodible bedrock at the base and by the more resistant Quaternary gravels on top (Fig. 16). Such gullying activity in the catchment boundaries produces the retreat of the slopes by basal sapping of the higher levels, resulting in the expansion of the low elevation areas drained by piedmont streams. Piedmont stream valleys are much wider than the main river valleys. If large low elevation pediments exist in the Ouarzazate basin, it means that erosion rates must be higher in piedmont catchments—not only in the incising valley floors but also at their divides as well. The higher erosion rates in the boundaries of the low elevation pediments are likely owing to the higher potential energy at the divides. Hence, the greater incision efficiency of piedmont streams over the weak basin bedrock combined with the retreat of their catchment boundaries in the Ouarzazate basin cause the development of large depressed valleys lying below the level of the main rivers. Indeed, in many places within the basin, headward-eroding streams (developed at boundaries of low elevation pediments) threaten to capture the adjacent and higher main rivers (Figs. 8, 17).

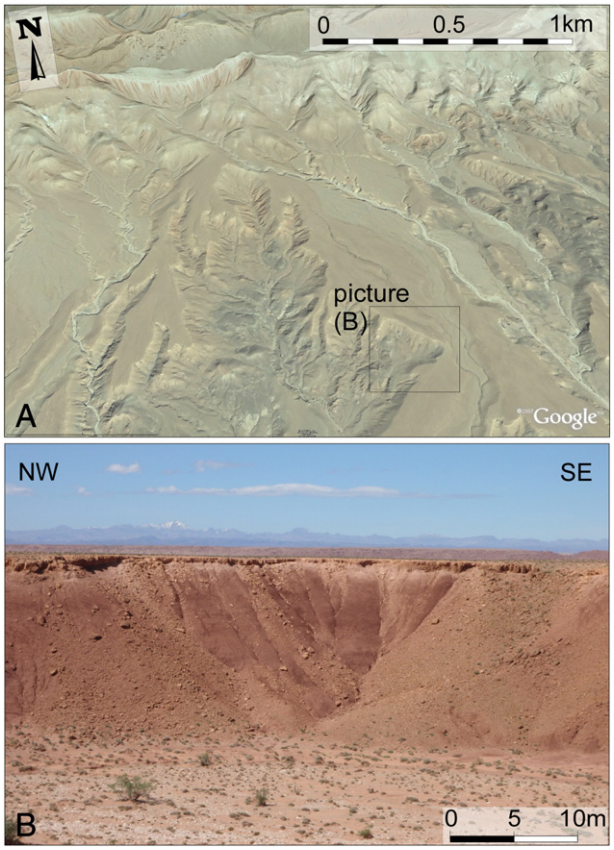


**Fig. 16.** (A) Oblique view (obtained from Google Earth) showing the intensive gullying that takes place in hillslopes of the Ouarzazate basin. (B) Gullies developed in the lateral slopes of the incised secondary streams, usually composed by easily erodible bedrock and resistant alluvial gravels on top, favoring the erosion by basal sapping.

Once divides separating piedmont catchments from main rivers are breached, main rivers are forced to flow across the gentler slopes of pediments. As a consequence, the flow is retarded and forced to leave part of its sediment load, leading to the formation of a fan pediment downstream of the capture point. The temporal aggradation of sediments continues until the new channel reaches slopes large enough to recover its transport capacity.

Younger terraces inset in older ones constitute the common arrangement associated with lateral erosion, abandonment, and entrenchment of rivers. Only terraces Q6 in the Izerki, Q6 in the Madri, and Q4 in the Targa valley are inset in their adjacent older terraces. By contrast, we identified 14 Quaternary captures of 7 rivers originated in the mountains (from west to east: Amaragh, Talat-n-Ouznag, N'Watchir, Tanjout, Madri, Tabia, and Targa Rivers). Like in previous studies in the United States (Rich, 1935; Mackin, 1936; Hunt et al., 1953; Hack, 1965; Denny, 1967; Ritter, 1972; Mills, 1983), we show that the stream-capture process controlled the formation of the

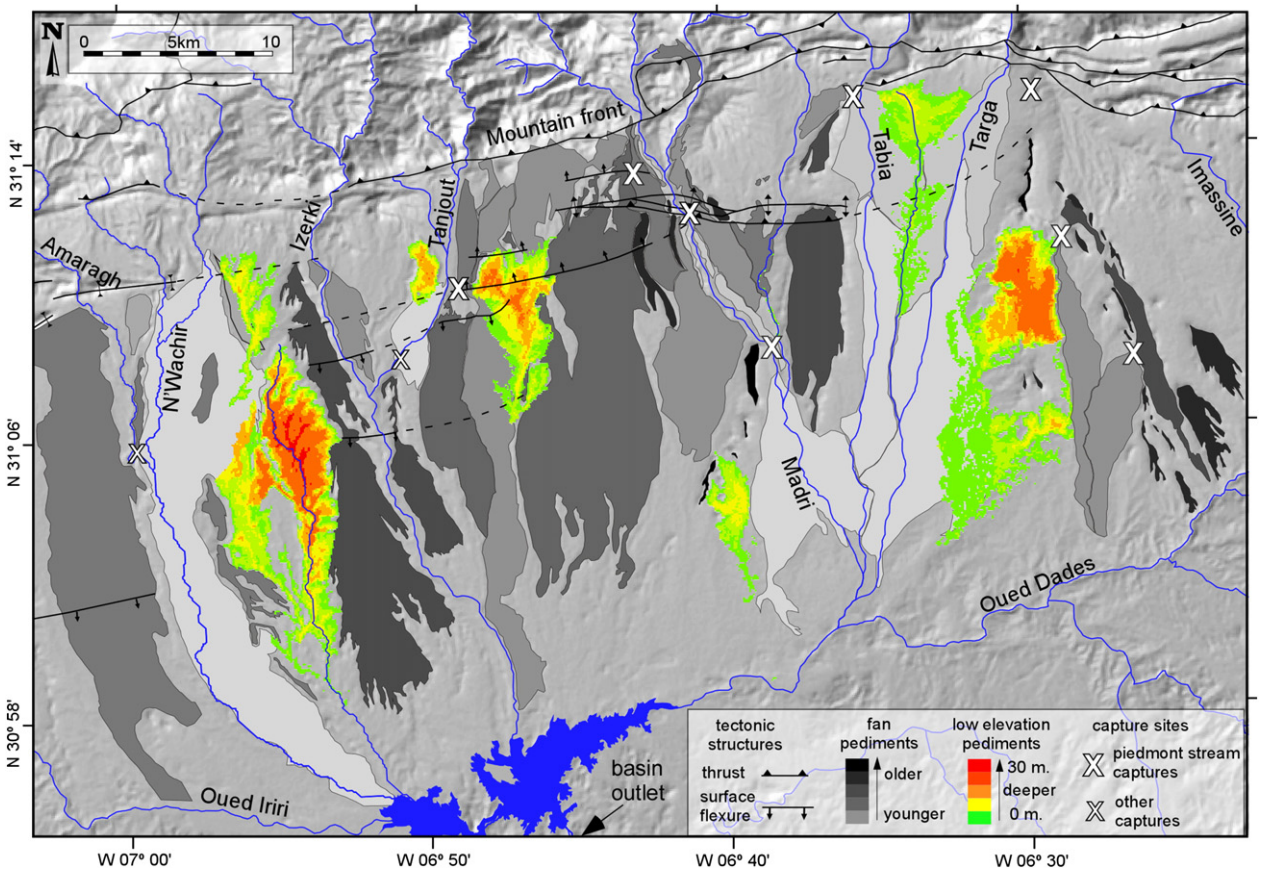


**Fig. 17.** Interpreted hillshade DEM showing the location of the 14 piedmont stream captures (crosses) that occurred in the western Ouarzazate basin. Red crosses indicate captures that occurred over active tectonic structures. The intrabasin tectonic structures, the current low elevation pediments, and the Quaternary fan pediments and terraces are also represented.

majority of fan pediments in the western half of the Ouarzazate basin. As for the Ouarzazate basin case, the process of stream capture in the origin of stepped fan pediments may have been neglected in other settings. The stream-capture model does not conflict with explanations based on external controls, rather it supplements them. However, because fluvial erosion responsible for pediment growth also depends on climate, we cannot discard a combined effect of climate change and stream capture on the development of fan pediments.

In order to explain the formation of fan pediments as a result of external factors or the intrinsic process of stream capture alone, dating of fan pediments and terraces in all the considered fluvial systems is needed. Similar ages are expected in all the different catchments if abandonment of deposits is related to the influence of an extrinsic control alone (Mills, 1983) or even combined with the process of stream capture. Arboleya et al. (2008) dated the abandonment of all the fluvial terraces and fan pediments in the Madri River basin using the $^{10}$Be terrestrial cosmogenic radionuclide method. They also dated Q5 in the Tanjout fluvial system (Q3c in Arboleya et al., 2008). The Madri River is entrenched into terrace Q6 with abandonment age of 7–11 ±1.5 ka (Q4 age cluster in Arboleya et al., 2008) that can be attributed with confidence to a climate change alone toward more humid conditions from a glacial to an interglacial stage (Arboleya et al., 2008). Based on Q6 abandonment ages, Arboleya et al. (2008) extended this interpretation for the last 250 ka and they argued that aggradation and incision result from changes in hydrology and vegetation cover. This interpretation is supported by the fact that in the Mediterranean region the Pleistocene fluvial behavior is thought to respond to climate changes (e.g., Macklin et al., 2002 and references herein). Although the fan pediment Q6 preserved in the lower part of the Madri River is related to a capture and the abandonment of Q5 (Figs. 13, 17), it can be traced back upstream forming a river terrace inset in the older ones. The Q5 abandonment ages in the Madri and Tanjout fluvial system range from 86±5 ka to 104±7 ka (four samples, labeled Q3b in Arboleya et al., 2008) and from 84±5 ka to 94±5 ka (five samples, labeled Q3c in Arboleya et al., 2008), respectively. The very similar minimum ages for the abandonment of Q5 in two different fluvial systems where the stream capture process demonstrably occurred to form Q6 fan pediments, and the fact that terrace Q6 is inset in Q5 in the upstream reaches of the Madri River, would argue for a climatic control of these two captures. The occurrence of a stream capture depends on the expansion of a piedmont catchment by headward erosion. Because the timing of climate conditions and changes in vegetation cover, as well as their influence on headward erosion, is poorly known in the Ouarzazate basin, any attempt to relate events of stream capture and fan pediment development to a specific climate stage or climate change is speculative. Palaeoclimatic data and more dating of fan pediments formed by the stream-capture process are needed to demonstrate if the intrinsic stream capture process is systematically enhanced by climatic changes.

Tectonics is the other major external factor influencing sedimentary flux. An increase of shortening or rock uplift rates in the uplands can increase erosion rates and bedload in mountain rivers. For steady climate conditions, tectonic variations could therefore modify the transport capacity of rivers toward transport-limited conditions and theoretically account for the steep longitudinal slopes of the main rivers, and then for the formation of fan pediments by the piedmont-stream capture process. Low shortening rates (mean value 0.5 mm/a since the Oligo-Miocene) have been calculated in the southern High Atlas fold-and-thrust belt (Tesón and Teixell, 2008; Tesón, 2009).

Similarly, the tectonic uplift rates measured for individual structures within the Ouarzazate basin for the last 250 ka (ranging between 0.1 and 0.2 mm/a; Pastor et al., 2010) are also mean rates, and there is not enough resolution to correlate the formation of fan pediments with accelerations of shortening, rock uplift, and subsequent erosion increase in the uplands.

The Quaternary tectonic structures of the Ouarzazate basin trend E–W and affect both the N–S piedmont streams and the mountain rivers, rendering it unlikely that recent tectonics induced a relative inhibition of erosion in main rivers only. However, we must point out that six piedmont stream captures are localized close to the mountain front, where the difference in elevation between a piedmont stream and its adjacent main river is maximum and the distance from the shared base level (tributary junction) is also the maximum. There, low elevation pediments cannot expand farther north because they encounter the northern limit of the soft Miocene sediments. Captures are expected to occur at the mountain front where the potential energy is maximum and where pediments can only expand laterally. On the other hand, three piedmont stream captures occurred, and fan pediments are sourced, where active tectonic structures reach the surface within the Ouarzazate basin (red crosses in Fig. 17). This coincidence suggests that active tectonics within the basin did influence the spatial location of these captures. We speculate that the local degradation of the alluvial cover caused by tectonic structures would favor the gullying activity in pediments and therefore, the lateral expansion of pediments needed for captures to occur. However, the spatial coincidence of Quaternary captures and recent tectonic features is not systematic. Moreover, the low elevation valleys and pediments that are threatening to capture the main rivers are currently located all along the N–S divides, not just where tectonic structures emerge (Fig. 17).

In summary, most of the extensive gravel deposits in the Ouarzazate basin have been formed by the piedmont stream capture process. During the erosional history of low elevation valleys and pediments, climate changes may have enhanced erosion and entailed the process of stream capture. Although systematic dating by $^{10}$Be terrestrial cosmogenic radionuclides across different valleys is necessary to fully support this conclusion, at least two fan pediments resulted from a combined effect of climate change and stream capture. It follows that if the occurrence of piedmont stream captures is not always enhanced by climate changes, any attempt of altitude correlations of extensive gravel deposits across different fluvial systems should be discarded.

In the Madri valley, the capture-related abandonments of fan pediments Q4 and Q5 date 163–174 ka and 86–104 ka, respectively, and in the Tanjout valley the age of capture-related abandonments of fan pediment Q5 is 84–94 ka. Hence, in these fluvial systems the temporal scale for these captures to occur is of the order of 100 ka. The space carved below a main trunk increases with pediment expansion. Consequently, the capacity of storage in low elevation valleys and pediments increases with time. Hence, as a broad approximation, the frequency of captures in a given system should be inversely correlated to the size of their related deposits.

## 6. Conclusions

The presence of piedmont streams lying at lower topographic elevations than the main rivers strongly supports the cover effect in the main rivers of the Ouarzazate basin. We are led to the conclusion that the main rivers present steeper slopes in order to transport the large amounts of coarse sediments supplied from the erosion of High Atlas hillslopes across the basin, whereas piedmont streams with no significant supply adjust their channel geometry to the basin bedrock properties, and the slope required is remarkably lower.

River longitudinal profiles, low elevation pediments, and the stepping pattern of Quaternary fan pediments (gravel deposits mantling extensive pediments) point to an intrinsic origin for the stepped fan pediments of the Ouarzazate basin in the High Atlas foreland. Five piedmont rivers originating within the Ouarzazate basin are at lower topographic elevations than their adjacent main rivers originating in the mountain. Consequently, piedmont streams currently threaten to capture 5 of the 11 rivers that originated in the mountains. We identified 14 capture sites that occurred during the late Pleistocene and Holocene in 7 of the 11 rivers that originated in the mountains. After a capture event, the diverted flow of the main mountain river to the depressed pediment results in the formation of a new fan pediment (glacis d'acumulation). Unlike filled strath terraces, fan pediments result from the erosion and transport dynamics of two distinct streams. Terrestrial cosmogenic radionuclide ages provided in an earlier work suggest that the stream capture process occurs on timescales of about 100 ka.

The chronological frame for fan pediments associated with two of the main streams suggests that two of the capture events may have occurred during climate changes. More dating of fan pediments formed by the stream-capture process are needed to demonstrate if the intrinsic stream capture process is systematically enhanced by external climatic changes. The spatial coincidence between three captures and local tectonic structures suggests a possible tectonic control on the spatial localization. In any case, recent tectonics cannot explain a relative inhibition of erosion in main rivers only.

This study suggests that the piedmont stream capture process is responsible for the formation of levels of extensive gravel deposits in an eroding sedimentary basin.

## Acknowledgements

This research was supported by projects CLG2006-07226, CGL2010-15416, CGL2007-66431-CO2-01 (TOPOMED), and Consolider-Ingenio 2010 CSD2006-00041 (TOPOIBERIA) of the Ministerio de Ciencia e Innovación of Spain. The comments of three anonymous reviewers that served to considerably improve the manuscript are much appreciated.

## References

Arboleya, M.L., Teixell, A., Charroud, M., Julivert, M., 2004. A structural transect through the High and Middle Atlas of Morocco. Journal of African Earth Sciences 39 (3–5), 319–327.
Arboleya, M.-L., Babault, J., Owen, L.A., Teixell, A., Finkel, R.C., 2008. Timing and nature of Quaternary fluvial incision in the Ouarzazate foreland basin, Morocco. Journal of the Geological Society 165 (6), 1059–1073.
Ayarza, P., Alvarez-Lobato, F., Teixell, A., Arboleya, M.L., Teson, E., Julivert, M., Charroud, M., 2005. Crustal structure under the central High Atlas Mountains (Morocco) from geological and gravity data. Tectonophysics 400 (1–4), 67–84.
Babault, J., Teixell, A., Arboleya, M.L., Charroud, M., 2008. A Late Cenozoic age for long-wavelength surface uplift of the Atlas Mountains of Morocco. Terra Nova 20 (2), 102–107.
Bishop, P., 1995. Drainage rearrangement by river capture, beheading and diversion. Progress in Physical Geography 19 (4), 449–473.
Bryan, K., 1926. The San Pedro valley, Arizona, and the geographical cycle. Geological Society of America Bulletin 37, 169–170.
Bull, W.B., 1991. Geomorphic Responses to Climatic Change. Oxford Univ. Press, New York, NY.
Choubert, G., 1965. Evolution de la connaissance du Quaternaire au Maroc. Notes et Mémoires du Service Géologique du Maroc 25 (185), 9–27.
Cook, K.L., Whipple, K.X., Heimsath, A.M., Hanks, T.C., 2009. Rapid incision of the Colorado River in Glen Canyon—insights from channel profiles, local incision rates, and modeling of lithologic controls. Earth Surface Processes and Landforms 34 (7), 994–1010.
Coque, R., 1960. L'evolution des versants en Tunisie présaharienne. Zeitschrift für Geomorphologie Supplementband 1, 172–177.
Coque, R., 1962. La Tunisie Présaharienne. Etude Géomorphologique. Armand Colin, Paris.
Coque, R., Jauzein, A., 1967. The geomorphology and Quaternary geology of Tunisia. In: Martin, L. (Ed.), Guidebook to the Geology and History of Tunisia. Petroleum Exploration Society of Libya, Tripoli, pp. 127–257.
Cowie, P.A., Whittaker, A.C., Attal, M.I, Roberts, G., Tucker, G.E., Ganas, A., 2008. New constraints on sediment-flux dependent river incision: implications for extracting tectonic signals from river profiles. Geology 36 (7), 535–538.
Denny, C.S., 1967. Fans and pediments. American Journal of Science 265 (2), 81–105.
Dresch, J., 1957. Pediments et glacis d'érosion, pédiplains et inselbergs. Information Géographique 22, 183–196.

El Harfi, A., Lang, J., Salomon, J., Chellai, E.H., 2001. Cenozoic sedimentary dynamics of the Ouarzazate foreland basin (central High Atlas Mountains, Morocco). International Journal of Earth Sciences 90 (2), 393–411.
Elenga, H., Peyron, O., Bonnefille, R., Jolly, D., Cheddadi, R., Guiot, J., Andrieu, V., Bottema, S., Buchet, G., de Beaulieu, J.L., Hamilton, A.C., Maley, J., Marchant, R., Perez-Obiol, R., Reille, M., Riollet, G., Scott, L., Straka, H., Taylor, D., Van Campo, D., Vincens, A., Laarif, F., Jonson, H., 2000. Pollen-based biome reconstruction for southern Europe and Africa 18,000 yr BP. Journal of Biogeography 27, 621–634.
Fraissinet, C., Zouine, E.M., Morel, J.L., Poisson, A., Andrieux, J., Faure-Muret, A., 1988. Structural evolution of the southern and northern central High Atlas in Paleogene and Mio-Pliocene times. In: Jacobshagen, V. (Ed.), The Atlas System of Morocco. Springer-Verlag, New York, pp. 272–291.
Fullea, J., Fernandez, M., Zeyen, H., Vergés, J., 2007. A rapid method to map the crustal and lithospheric thickness using elevation, geoid anomaly and thermal analysis. Application to the Gibraltar Arc System, Atlas Mountains and adjacent zones. Tectonophysics 430 (1-4), 97–117.
Gasse, F., 2000. Hydrological changes in the African tropics since the last glacial maximum. Quaternary Science Reviews 19, 189–211.
Gasse, F., Fontes, J.C., Plaziat, J.C., et al., 1987. Biological remains, geochemistry and stable isotopes for the reconstruction of environmental and hydrological changes in the Holocene lakes from North Sahara. Palaeogeography, Palaeoclimatology, Palaeoecology 60, 1–46.
Gasse, F., Tehet, R., Durand, A., Gilbert, E., Fontes, J.-C., 1990. The arid–humid transition in the Sahara and the Sahel during the last deglaciation. Nature 346, 141–146.
Gauthier, H., 1957. Contribution à l'étude géologique des formations post-liasiques des bassins du Dadès et du Haut-Todra (Maroc méridional). Notes et Mémoires du Service Géologique du Maroc 119, 1–212.
Gilbert, G.K. (Ed.), 1877. Report on the Geology of the Henry Mountains: Geographical and Geological Survey of the Rocky Mountain Region. Publication of the Powell Survey. U.S. Gov. Print. Off, Washington, DC. 160 pp.
Görler, K., Helmdach, F.-F., Gaemers, P., Heißig, K., Hinsch, W., Mädler, K., Schwarzhans, W., Zucht, M., 1988. The uplift of the central High Atlas as deduced from Neogene continental sediments of the Ouarzazate province, Morocco. In: Jacobshagen, V. (Ed.), The Atlas System of Morocco. Springer-Verlag, New York, pp. 361–404.
Hack, J.T., 1965. Geomorphology of the Shenandoah Valley, Virginia and West Virginia, and Origin of the Residual Ore Deposits. Professional Paper 484. U.S. Geological Survey, Washington, D.C. 84 pp.
Hadley, J.B., Goldsmith, R., 1963. Geology of the Eastern Great Smoky Mountains, North Carolina and Tennessee. Professional Paper 349b. U.S. Geological Survey, Washington, D.C. 118 pp.
Hancock, G.S., Anderson, R.S., 2002. Numerical modeling of fluvial strath-terrace formation in response to oscillating climate. Geological Society of America Bulletin 114 (9), 1131–1142.
Holz, C., Stuut, J.B.W., Henrich, R., Meggers, H., 2007. Variability in terrigenous sedimentation processes off Northwest Africa and its relation to climate changes; inferences from grain-size distributions of a Holocene marine sediment record. Sedimentary Geology 202, 499–508.
Hunt, C.B., Averitt, P., Miller, R.L., 1953. Geology and Geography of the Henry Mountains Region, Utah. Professional Paper 228. U.S. Geological Survey, Washington, D.C. 239 pp.
Johnson, D., 1932. Rock planes of arid regions. Geographical Review 22 (4), 656–665.
Johnson, J.P.L., Whipple, K.X., Sklar, L.S., Hanks, T.C., 2009. Transport slopes, sediment cover and bedrock channel incision in the Henry Mountains, Utah. Journal of Geophysical Research 114, F02014.
Jolly, D., Harrison, S.P., Damnati, B., Bonnefille, R., 1998. Simulated climate and biomes of Africa during the late Quaternary; comparison with pollen and lake status data, Late Quaternary climates; data synthesis and model experiments. Quaternary Science Reviews 17, 629–657.
Knippertz, P., Christoph, M., Speth, P., 2003. Long-term precipitation variability in Morocco and the link to the large-scale circulation in recent and future climates. Meteorology and Atmospheric Physics 83 (1), 67–88.
Lague, D., 2010. Reduction of long-term bedrock incision efficiency by short-term alluvial cover intermittency. Journal of Geophysical Research 115, F02011.
Lamb, H.F., Eicher, U., Switsur, V.R., 1989. An 18,000-year record of vegetation, lake-level and climatic change from Tigalmamine, Middle Atlas, Morocco. Journal of Biogeography 16, 65–74.
Lamb, H.F., Gasse, F., Benkaddour, A., El, Hamouti N., Van der Kaars, S., Perkins, W.T., Pearce, N.J., Roberts, C.N., 1995. Relation between century scale Holocene arid intervals in tropical and temperate zones. Nature 373, 134–137.
Mackin, J.H., 1936. The capture of the Greybull River. American Journal of Science Series 5 31 (185), 373–385.
Macklin, M.G., Lewin, J., Woodward, J.C., 1995. Quaternary fluvial systems in the Mediterranean Basin. In: Lewin, J., Macklin, M.G., Woodward, J.C. (Eds.), Mediterranean Quaternary River Environments. Balkema, Rotterdam, pp. 1–25.
Mattauer, M., Tapponier, P., Proust, F., 1977. Sur les mécanismes de formation des chaines intracontinentales. L'exemple des chaines atlasiques du Maroc. Bulletin de la Société Géologique de France 7 (3), 521–536.
Merritts, D.J., Vincent, K.R., Wohl, E.E., 1994. Long river profiles, tectonism, and eustasy: a guide to interpreting fluvial terraces. Journal of Geophysical Research 99 (B7), 14031–14050.
Mills, H.H., 1983. Pediment evolution at Roan Mountain, North Carolina, USA. Geografiska Annaler 65 (Series A, Physical Geography) 111–126.
Missenard, Y., Zeyen, H., Frizon de Lamotte, D., Leturmy, P., Petit, C., Sébrier, M., Saddiqi, O., 2006. Crustal versus asthenospheric origin of relief of the Atlas Mountains of Morocco. Journal of Geophysical Research 111, B03401.
Montgomery, D.R., 2004. Observations on the role of lithology in strath terrace formation and bedrock channel width. American Journal of Science 304 (5), 454–476.
Oberlander, T.M., 1989. Slope and pediment systems. In: Thomas, D.S.G. (Ed.), Arid Zone Geomorphology. Belhaven, London, pp. 58–59.
O'Callaghan, J.F., Mark, D.M., 1984. The extraction of drainage networks from digital elevation data. Computer Vision, Graphics, and Image Processing 28 (3), 323–344.
Pastor, A., Teixell, A., Arboleya, M.L., 2010. Tectónica reciente en la cuenca de Ouarzazate (Atlas Marroquí): Tasas de acortamiento y levantamiento tectónico a partir de los marcadores cuaternarios. Geogaceta 48, 195–198.
Pazzaglia, F.J., Gardner, T.W., Merrits, D.J., 1998. Bedrock fluvial incision and longitudinal profile development over geologic time scales determined by fluvial terraces. In: Tinkler, K.J., Wohl, E.E. (Eds.), Rivers Over Rock: Fluvial Processes in Bedrock Channels. AGU, Washington, DC, pp. 207–235.
Pelletier, J.D., 2010. How do pediments form? A numerical modeling investigation with comparison to pediments in southern Arizona, USA. Bulletin of the Geological Society of America 122, 1815–1829.
Reille, M., 1979. Analyse pollinique du lac de Sidi Bou Rhaba, littoral atlantique (Maroc). Ecologia Mediterranea 4, 61–65.
Rich, J.L., 1935. Origin and evolution of rock fans and pediments. Geological Society of America Bulletin 46, 999–1024.
Ritter, F.D., 1972. The significance of stream capture in the evolution of a piedmont region. Annals of Geomorphology 16, 83–92.
Salamani, M., 1991. Premières données palynologiques sur l'histoire Holocene du massif de l'Akfadou (Grande-Kabylie, Algérie). Ecologia Mediterranea 17, 145–159.
Salamani, M., 1993. Premières données paléophytogéographiques du Cèdre de l'Atlas (Cedrus atlantica) dans la région de grande Kabilie (NE Algérie). Palynosciences 2, 147–155.
Schumm, S.A., 1973. Geomorphic thresholds and complex response of drainage systems. In: Morisawa, M. (Ed.), Fluvial Geomorphology. New York State University, Publications in Geomorphology, Binghamton, NY, pp. 299–309.
Schumm, S.A., 1979. Geomorphic thresholds: the concept and its applications. Transactions of the Institute of British Geographers 4 (4), 31.
Seber, D., Barazangi, M., Tadili, B.A., Ramdani, M., Ibenbrahim, A., Ben Sari, D., 1996. Three-dimensional upper mantle structure beneath intraplate Atlas and interplate Rif Mountains of Morocco. Journal of Geophysical Research 101, 3125–3138.
Sébrier, M., Siame, L., Zouine, E.M., Winter, T., Missenard, Y., Leturmy, P., 2006. Active tectonics in the Moroccan High Atlas. Comptes Rendus Geosciences 338 (1–2), 65–79.
Sklar, L., Dietrich, W.E., 1998. River longitudinal profiles and bedrock incision models: stream power and the influence of sediment supply. In: Tinkler, K.J., Wohl, E.E. (Eds.), Rivers Over Rock: Fluvial Processes in Bedrock Channels. AGU, Washington, DC, pp. 237–260.
Sklar, L.S., Dietrich, W.E., 2001. Sediment and rock strength controls on river incision into bedrock. Geology 29 (12), 1087–1090.
Sklar, L.S., Dietrich, W.E., 2006. The role of sediment in controlling steady-state bedrock channel slope: implications of the saltation-abrasion incision model. Geomorphology 82 (1–2), 58–83.
Stäblein, G., 1988. Geomorphological aspects of the Quaternary evolution of the Ourzazate basin, southern Morocco. In: Jacobshagen, V. (Ed.), The Atlas System of Morocco. Springer-Verlag, New York, pp. 433–444.
Teixell, A., Arboleya, M.L., Julivert, M., Charroud, M., 2003. Tectonic shortening and topography in the central High Atlas (Morocco). Tectonics 22 (5), 1051.
Teixell, A., Ayarza, P., Zeyen, H., Fernandez, M., Arboleya, M.-L., 2005. Effects of mantle upwelling in a compressional setting: the Atlas Mountains of Morocco. Terra Nova 17 (5), 456–461.
Tesón, E., 2009. Estructura y cronología de la deformación en el borde Sur del Alto Atlas de Marruecos a partir del registro tectono-sedimentario de la cuenca de antepaís de Ouarzazate. Univ. Autònoma de Barcelona, Spain. 221 pp.
Tesón, E., Teixell, A., 2008. Sequence of thrusting and syntectonic sedimentation in the eastern sub-Atlas thrust belt (Dadès and Mgoun valleys, Morocco). International Journal of Earth Sciences 97 (1), 103–113.
Tesón, E., Pueyo, E.L., Teixell, A., Barnolas, A., Agustí, J., Furió, M., 2010. Magnetostratigraphy of the Ouarzazate basin: implications for the timing of deformation and mountain building in the High Atlas Mountains of Morocco. Geodinamica Acta 26 (4), 15.
Wegmann, K.W., Pazzaglia, F.J., 2002. Holocene strath terraces, climate change, and active tectonics: the Clearwater River basin, Olympic Peninsula, Washington State. Geological Society of America Bulletin 114 (6), 731–744.
Whipple, K.X., Tucker, G.E., 2002. Implications of sediment-flux-dependent river incision models for landscape evolution. Journal of Geophysical Research 107 (B2), ETG3.1–ETG3.20.
Whitaker, C.R., 1979. The use of the term 'pediment' and related terminology. Zeitschrift für Geomorphologie 23, 427–439.
White, K., 1991. Geomorphological analysis of piedmont landforms in the Tunisian southern Atlas using ground data and satellite imagery. The Geographical Journal 157 (3), 279–294.
White, K., Drake, N., Millington, A., Stokes, S., 1996. Constraining the timing of alluvial fan response to late Quaternary climatic changes, southern Tunisia. Geomorphology 17 (4), 295–304.
Yanites, B.J., Tucker, G.E., Hsu, H.-L., Chen, C.-C., Chen, Y.-G., Mueller, K.J., 2011. The influence of sediment cover variability on long-term river incision rates: an example from the Peikang River, central Taiwan. Journal of Geophysical Research 116 (F3), F03016.
Zeyen, H., Ayarza, P., Fernàndez, M., Rimi, A., 2005. Lithospheric structure under the western African-European plate boundary: a transect across the Atlas Mountains and the Gulf of Cadiz. Tectonics 24, TC2001.

# Longitudinal to transverse drainage network evolution in the High Atlas (Morocco): The role of tectonics

Julien Babault,[1] Jean Van Den Driessche,[2] and Antonio Teixell[1]

Received 31 August 2011; revised 26 May 2012; accepted 1 June 2012; published 14 August 2012.

[1] The High Atlas of Morocco is a still-active, linear intracontinental mountain chain in the NW African plate, which results from weak crustal thickening associated with rift inversion during the Cenozoic and from uplift related to mantle thermal doming. A striking morphological feature of the High Atlas is the occurrence of both transverse and longitudinal (i.e., strike-parallel) drainage characterized by deep fluvial incision of more than 1000 m in low-relief topography of the axial zone of the chain. Most of the transverse component of the drainage appears to postdate the longitudinal component as indicated by recent or incipient captures and wind gaps. The longitudinal drainage is inherited from an early stage of fluvial organization controlled by the tectonic structures developed during upper crustal folding and thrusting in the post-Paleozoic cover. Amplification of N-S regional slope in the western High Atlas by continued crustal shortening and thickening triggered: (i) higher erosion rates in transverse than in longitudinal catchments and (ii) captures of longitudinal streams by transverse ones, creating a new organization of the drainage system toward the regional slope. Such evolution from a longitudinal to a transverse-dominated drainage may represent a common mechanism of fluvial network development in mountain belts where the amplification of the regional slope results from long-lived lithospheric convergence.

**Citation:** Babault, J., J. Van Den Driessche, and A. Teixell (2012), Longitudinal to transverse drainage network evolution in the High Atlas (Morocco): The role of tectonics, *Tectonics*, *31*, TC4020, doi:10.1029/2011TC003015.

## 1. Introduction

[2] Rivers draining mountain belts follow paths influenced by both mean topographic gradient (or "regional slope") and local surface roughness (or "local slope"). Both tectonics (uplift, crustal thickening, structural deformation) and erosion patterns influence regional and local slopes and drainage patterns can be expected to evolve over orogenic timescales. Incipient orogenic shortening in the upper crust is accommodated by gentle folding and thrusting. These induce local slopes, both parallel and opposite to the regional slope of the mountain belt, which eventually force streams to follow fold axes and thrust faults, i.e., perpendicular to the regional slope [e.g., *Koons*, 1995]. Ongoing crustal shortening and thickening will cause the amplification of the regional slope and the progressive tilt of the folds and faults developed in the upper crust, decreasing the downstream slopes parallel and opposite to the regional slope. Such evolution of regional and local slopes should favor the progressive capture by transverse streams (via headward erosion) of the longitudinal drains initially controlled by folds and thrust faults.

[3] Authors have long observed the occurrence of both longitudinal and transverse rivers in mountain belts [e.g., *Birot*, 1970; *Bordet*, 1955; *Davis*, 1889; *Hovius*, 1996; *Koons*, 1995; *Lugeon*, 1901; *Oberlander*, 1965, 1985; *Ramsey et al.*, 2008; *van der Beek et al.*, 2002]. While to *Oberlander* [1985] the transverse orientation of rivers appeared anomalous, *Hovius* [1996] remarked that many actively uplifting mountain belts around the world have simple drainage patterns transverse to their main structural trend. A simple explanation to these apparent contradictory views is that they concern orogens that differ in the amount of erosion they suffered, which can be directly related to the regional slope. *Oberlander* [1985] addressed the Zagros fold and thrust belt, with low shortening (20%) [*McQuarrie*, 2004] and regional slope (about 1°) [*Oberlander*, 1965], but relatively strong local slopes, whereas *Hovius* [1996] is concerned with orogens with much greater crustal shortening and exhumation, involving steeper regional slopes and only weak topographic expression of individual folds and thrusts (e.g., Himalaya, Andes, Southern Alps of New Zealand; etc.). Hence, the pattern in the Zagros can be taken as representative of an early stage of the mountain building process when compared for example to the Himalayas [e.g., *Hatzfeld and Molnar*, 2010].

[4] We test here the roles of regional and local slopes in controlling the drainage pattern of mountain belts by analyzing the evolution of the main rivers that drain the High

[1]Departament de Geologia, Universitat Autònoma de Barcelona, Barcelona, Spain.
[2]Géosciences Rennes, Université de Rennes 1, Campus de Beaulieu, Rennes, France.

Corresponding author: J. Babault, Departament de Geologia, Universitat Autònoma de Barcelona, Despatx C2 124, Barcelona ES-08193, Spain. (julien.babault@uab.es)

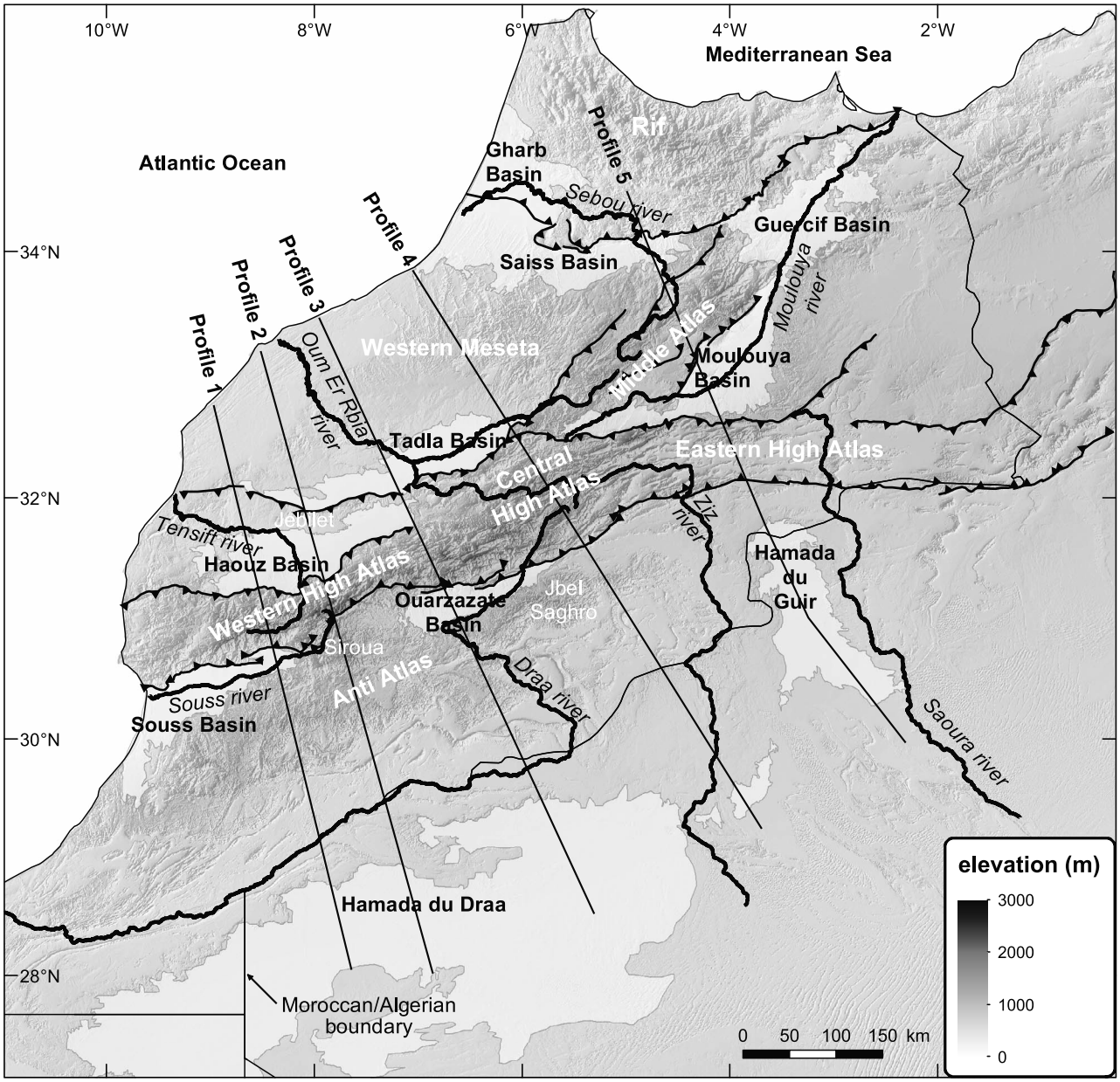


**Figure 1.** Sketch map showing the main tectonic and topographic features of Morocco. Barbed lines represent the boundaries of the deformed thrust-fold belts of the High Atlas, the Middle Atlas and the Rif. Light gray areas indicate the Cenozoic basins. Profile lines refer to Figure 3.

Atlas mountain belt of Morocco. Variations of structural relief (i.e., the uplift of rock units above their regional, undeformed elevation) and regional surface slope are observed along the strike of the High Atlas, which have favored the selective development of a transverse drainage at the expense of an early longitudinal drainage. Having escaped the effect of glacial erosion due to its low latitudinal position, this mountain belt is particularly appealing for the investigation of the relationships between fluvial drainage networks and tectonics.

## 2. Tectonics of the High Atlas

[5] The ENE-trending High Atlas and the NE-trending Middle Atlas (Figure 1) are Cenozoic intracontinental thrust-fold belts composed at the surface essentially by Mesozoic rocks (mostly carbonate and shale), with sparse Paleozoic and Precambrian basement occurrences (slate, greywacke, rhyolite and granite). The internal structure of the High Atlas is relatively simple, consisting of doubly verging systems of folds and thrust faults, where most of the shortening is concentrated in the orogen margins [*Teixell et al.*, 2003]. No internal crystalline zones developed; on the contrary, the inner parts of the mountain belt are often constituted by tabular sedimentary strata (dominantly Jurassic in age), disrupted by spaced thrusts and folds.

[6] The High Atlas formed after a Triassic-Jurassic rift [*Mattauer et al.*, 1977; *Laville and Piqué*, 1992; *Frizon de Lamotte et al.*, 2000; *Teixell et al.*, 2003; *Arboleya et al.*,

2004]. Internal thrusts and folds of the High Atlas trend NE-SW to ENE-WSW, commonly associated to the inversion of former extensional faults. The western High Atlas, south of Marrakech, is dominated by basement exposure, which not only results from differential Atlasic shortening and exhumation, but to the fact the area was originally covered by relatively thin Mesozoic rocks [*Balestrieri et al.*, 2009; *Choubert and Faure-Muret*, 1962].

[7] Orogenic shortening across the High Atlas is modest (15–25%) [*Teixell et al.*, 2003]. Crustal thickening is also moderate, and cannot account for its high elevation [*Ayarza et al.*, 2005; *Makris et al.*, 1985; *Wigger et al.*, 1992]. The occurrence of Cenozoic alkaline magmatism and a geophysical modeling suggested that the elevation is partly supported by an abnormally thin lithosphere [*Missenard et al.*, 2006; *Teixell et al.*, 2003; *Teixell et al.*, 2005; *Zeyen et al.*, 2005], probably as a result of deep thermal upwelling.

[8] Based on syntectonic sediments, the age of crustal shortening in the High Atlas is placed from mid Eocene to Quaternary times [see a recent review in *Tesón et al.*, 2010, and references therein], while geomorphic evidence suggests that much of the mantle-related surface uplift (∼1000 m) occurred in post-Miocene times [*Babault et al.*, 2008].

## 3. Analysis of Topography and Sources of Uplift

[9] We describe the topography of the Atlas mountains and surroundings by their mean elevation at crustal and lithospheric scale, calculated in moving windows of 30 or 100 km of diameter, respectively. The elevation data used for the analysis is the SRTM90v4 DEM (A. Jarvis et al., 2008, Hole-filled SRTM for the globe, version 4, available at http://srtm.csi.cgiar.org). In temperate regions and under slow to moderate erosion rates (∼<0.2 mm/yr), hillslope erosion rates have been shown to be dependent on mean basin slopes and local relief [e.g., *Montgomery and Brandon*, 2002; *Ouimet et al.*, 2009]. Indeed, local relief measured at 5 km scales is more a reflection of channel steepness than hillslope gradient and correlates with erosion rate up to 1 mm/yr [*DiBiase et al.*, 2010]. Accordingly, we calculated the local relief (maximum minus minimum elevation) in a 5-km-moving window (Figure 3), and we used it as a proxy to identify regions of probable high and low erosion rates.

[10] The High Atlas of Morocco is 700 km long and 50 to 120 km wide. In 26% of the chain the mean elevation at 30 km scale is higher than 2000 m asl (Figure 2a). This high land is ∼440 km long and >20 km wide in the western part of the High Atlas (SW of Marrakech) and up to >70 km wide around Imilchil, at 6°W (Figures 2a and 3, profiles 2 and 4). Only 2.6% of the Moroccan High Atlas is at a mean elevation that exceeds 2600 m.

[11] The foreland basins flanking the High Atlas lie at low elevation in the west (≤500 m, Haouz, Souss and Tadla basins, Figures 1 and 2a), whereas in the south-central part and the east they correspond to plateaux at 1200–1400 m asl (Ouarzazate, Moulouya and Hamada du Guir, Figures 1 and 2a). These elevated plains have not been shortened during the Cenozoic. The mean elevation at 100 km scale shows a 400-km-long swell higher than 1500 m asl and reaching values above ∼2100 m asl that extends from the Anti-Atlas to the Middle Atlas. These high elevations are slightly oblique to the mean tectonic trend of the High Atlas (Figure 2b).

[12] The highest values of mean elevation at 30 km scale coincide with the areas affected by crustal shortening during the Cenozoic (Figures 2a and 3). In the absence of systematic estimates of the depth to the Mohorovicic discontinuity, the negative Bouguer gravity anomaly in these areas reveals that shortening is accommodated at depth by crustal thickening (Figures 2a and 3).

[13] The superposition of the mean elevation contour lines at 100 km scale fit well the NE-trending asthenospheric doming (Figures 2b and 3). Mantle-related surface uplift has affected the High and Middle Atlas deformed belts, and is responsible for the high elevation above 1200 m a.s.l. of the Anti-Atlas and the Ouarzazate and Moulouya basins as well (Figure 2a). The crustal shortening [*Teixell et al.*, 2003] and lithospheric thinning [*Fullea et al.*, 2007; *Missenard et al.*, 2006; *Teixell et al.*, 2005; *Zeyen et al.*, 2005] explain well the distribution of the mean elevation in the central and eastern High Atlas. However, the western High Atlas and the low-elevation Haouz and Souss foreland basins lie outside the maximum lithospheric thinning [*Missenard et al.*, 2006]. Therefore, much of the high mean elevations in the western High Atlas must be sustained by crustal thickening.

## 4. Analysis of the Drainage Pattern of the High Atlas

### 4.1. Drainage Network Organization

[14] The northern flank of the High Atlas is drained to the Atlantic by the Tensift and the Oum Er Rbia rivers in the west, and to the Mediterranean by the Moulouya river in the east (Figure 1). Along the southern flank, the main rivers from west to east are the Souss, the Draa and the Ziz (Figure 1). The Ziz river ends in the Sahara desert while the outlets of the Souss and the Draa rivers reach the Atlantic (although the Draa river is actually not perennial and water often evaporates or infiltrates before reaching the ocean).

[15] Along much of the northern flank from 5°W to 8°30′W and along the southern flank from 5°W to 6°30′W, trunk streams are dominated by reaches parallel to the trend of the chain (Figure 4a), termed here "longitudinal" reaches. The length of these main rivers ranges between 30 km to more than 150 km. On the northern flank of the western High Atlas, longitudinal reaches are principally located in the highest part of the chain (Nfiss, Ourika and Zate rivers, Figure 4a) and they flow to the ENE. A marked change occurs east of 7°W (Figure 4a); the longitudinal reaches of the Tessaout, Guemez and Melloul rivers, localized also in the interior of the chain, flow to the WNW, opposite to the flow of the Nfiss, Ourika and Zate longitudinal reaches. The Abid river, a tributary of the Melloul, has also a large longitudinal reach that in this case appears localized close to the mountain front.

[16] On the southern flank of the High Atlas, from the western termination of the chain to the longitude of Ouarzazate, most rivers are transverse (Figure 4a). Although drainage is mainly transverse north of the Ouarzazate basin, the course of the main rivers, i.e., the Dadès and the upper reaches of the Mgoun river, are almost parallel or slightly oblique to the trend of the orogen (Figure 4a). Some rivers of the smaller catchments localized north of Ouarzazate are

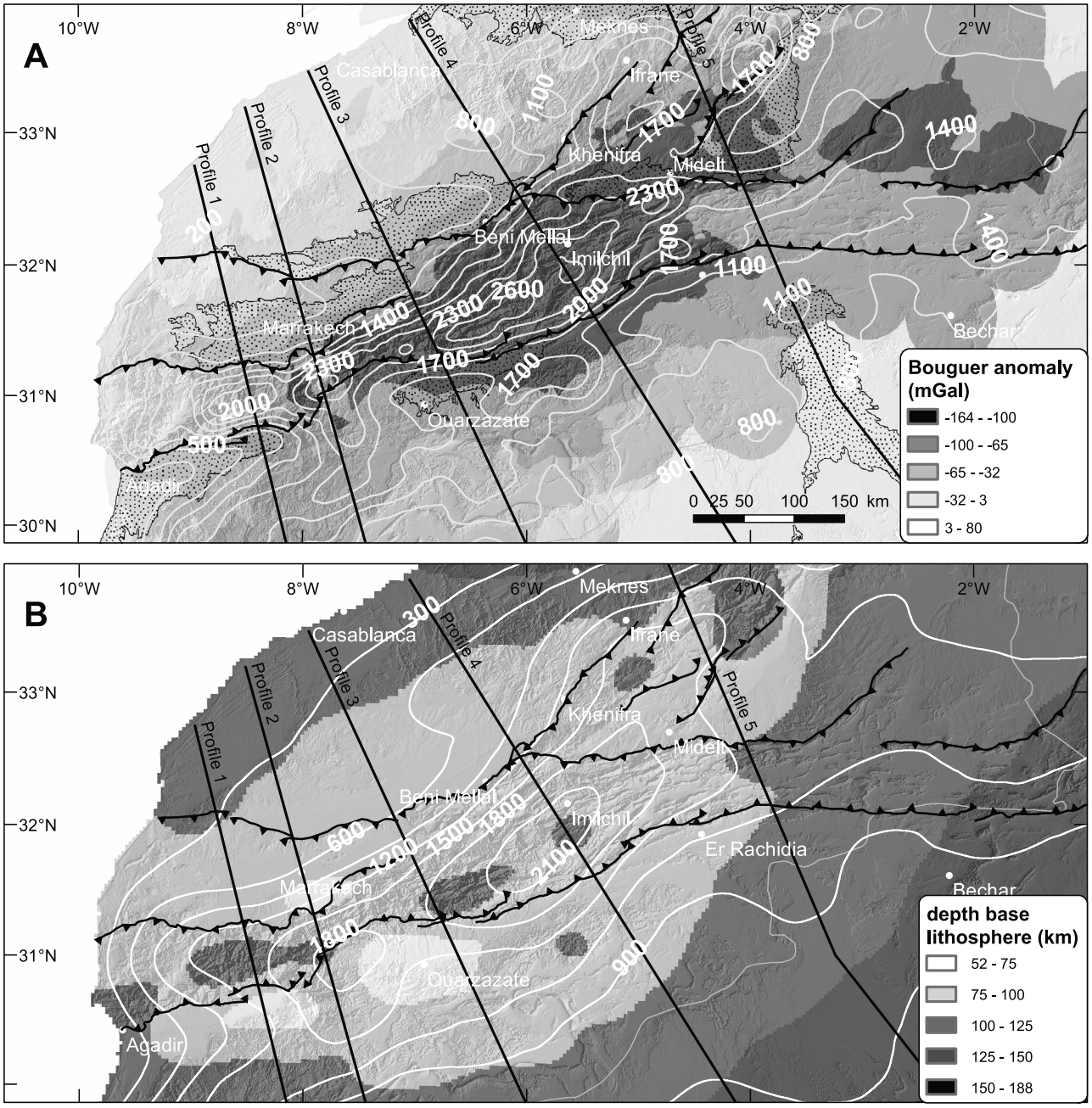


**Figure 2.** Shaded relief maps of the High Atlas region indicating the main tectonic features (thrust fronts bounding the deformed belts) and (a) the Bouguer gravity anomaly and contours of mean elevation calculated at crustal scale, i.e., in a 30 km moving window, (b) the depth to the lithosphere/asthenosphere boundary [after *Fullea et al.*, 2007] and contours of the mean elevation calculated at lithospheric scale, i.e., in a 100 km moving window.

also characterized by longitudinal reaches (Figure 4a). The Ziz river and its main tributaries (Figure 4a) are also characterized by long reaches parallel to the trend of the chain.

### 4.2. Relationship Between Drainage Pattern, Structure, Lithology, and Regional Slope Values

[17] In the central and eastern High Atlas, the previously described longitudinal reaches are all parallel to the structural grain, as defined by map-scale folds and thrust fronts (Figure 4b). Most of the transverse reaches connecting the longitudinal streams correspond to fold terminations or transfer faults. In Figures 5a and 5b, we project the main rivers on 3-D diagrams constructed with geologic cross-sections of the High Atlas and the shaded topography. These diagrams illustrate that in most of the High Atlas, longitudinal rivers flow along the axis of large synclines of the folded and faulted Mesozoic cover. There are strong contrasts of erodability; the most resistant layers generally form the crest of the narrow anticlines, while wide synclines are frequently occupied by weak shale formations.

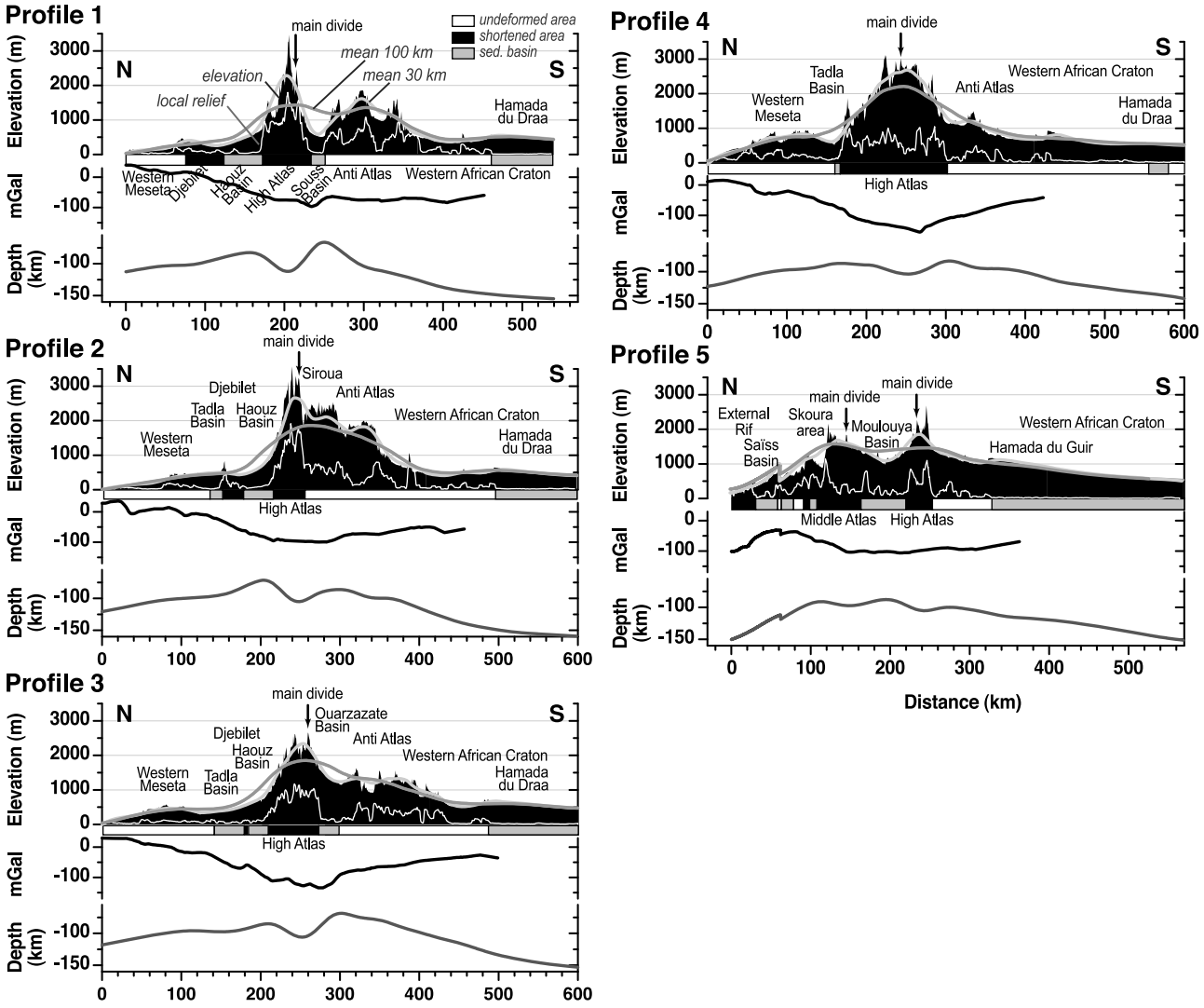


**Figure 3.** Profiles transverse to the Atlas chains indicating the actual topography (black area), the mean elevation calculated in a 30 km moving window (light gray line), the mean elevation calculated in a 100 km moving window (dark gray line), the local relief (thin white line), and, below the topographic profiles, the Bouger gravity anomaly (in mGal) and the depth to the lithosphere/asthenosphere boundary as indicated in Figure 2b (see Figure 2 for profile location).

[18] In the western High Atlas (Toubkal Massif), the Ourika and Zate rivers follow the structural grain of the chain in the axial zone in spite of being made of Precambrian to Paleozoic magmatic and metamorphic rocks. The longitudinal segment of the Ourika river coincides with the trace of a main fault parallel to the general trend of the chain, suggesting a structural control of the river orientation. Similarly, it is plausible that the longitudinal reaches of the Ourika and Zate rivers formed originally in synclines of a now eroded Mesozoic cover. More to the west, the Nfiss river flows parallel to the trend of the chain in granitic basement and in a syncline of Triassic sedimentary rocks. These Triassic rocks are the remnants of an inverted graben now preserved only in the lower part of the longitudinal reach of the Nfiss river (Figure 5b). This suggests that sediments covered the western High Atlas and that their folding controlled the development of a longitudinal drainage in same way as it does to the east where the folded and faulted sedimentary cover is preserved.

[19] Where the main rivers cut through the outer parts of the western High Atlas, they follow the regional slope across structures. This is the case for the transverse reaches of the Ourika and Zate rivers in the northern flank of the chain. Regional slope values were calculated using the grid of mean elevation at 30 km scale. The correlation between slope angles and the drainage network is shown in Figure 4c; this map shows that rivers are transverse at least in 4 specific areas where the regional slope value is greater than 3°. By contrast, longitudinal rivers flow where the regional slope is less than 2.5°.

### 4.3. Azimuth Distribution of Main Rivers Versus Regional Slope Direction Distribution

[20] In order to evaluate to what degree rivers follow the regional slope, we plotted the azimuth of flow for each main river (and for each set of neighboring rivers with a similar planform geometry) and the regional slope in polar diagrams

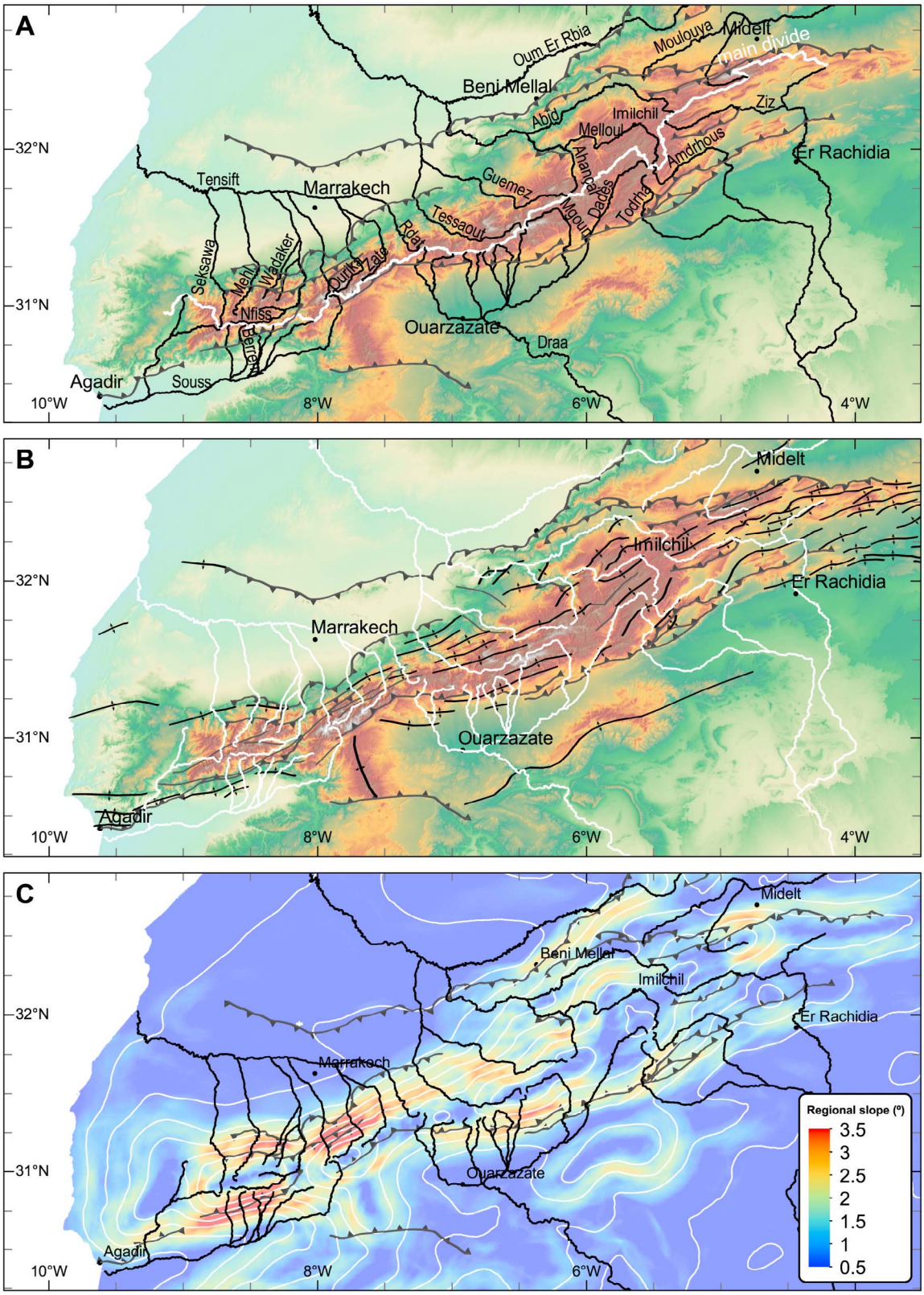


**Figure 4.** (a) Shaded relief map of the High Atlas region including the projection of the principal rivers and the trace of the main divide. (b) Tectonic sketch map representing the main folds and thrust fronts. (c) Map of the drainage network superimposed to the regional slope, calculated using the grid of mean elevation at 30 km scale. Contours indicate the mean elevation calculated in a 30 km moving window.

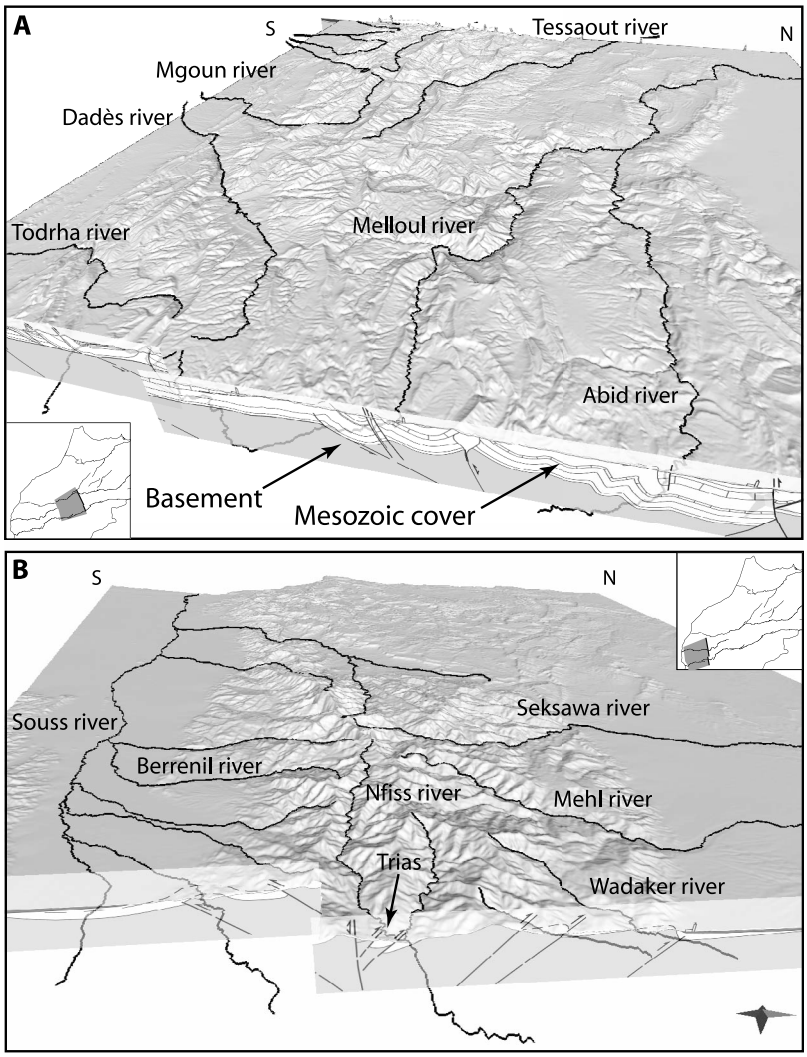


**Figure 5.** 3-D along-strike views of the topography and the cross-sectional structure of the (a) central and (b) western High Atlas. The longitudinal reaches of the main rivers are preferentially located in between anticlinal or thrust ridges. Figure 5a represents a view west of the Imiclchil section of *Teixell et al.* [2003], whereas Figure 5b represents a view west of a transect through the Tizi n'Test area. Transverse rivers become more prominent in Figure 5b, which exhibits higher structural relief and extensive exposure of exhumed basement.

(black histograms in Figure 6). River flow azimuths were extracted using the D8 flow routing [*O'Callaghan and Mark*, 1984] in RiverTools (L. L. C. Rivix, Rivertools 3.0, 2003, available at http://www.rivertools.com), and each pixel (90 m × 90 m) of the main river paths has been sampled ("n" in Figure 6 is the number of sampled pixels). Because DEM grids are usually north-south, east-west oriented rectangles, D8 flow routing only allows the computation of eight azimuths ranging from 0° to 315° and spaced by intervals of 45°. Circular mean directions [*Fisher*, 1993] have also been calculated (black dots in polar diagrams).

[21] We computed the azimuth distribution of the main regional slope where those rivers flow by extracting the flow angles of the smoothed topography, i.e., the mean elevation at 30 km scale. Accordingly, we used the Mass Flux Method of RiverTools (L. L. C. Rivix, Rivertools 3.0, 2003, available at http://www.rivertools.com), because the smoothed topography, which has a dome-like shape, is convex up. We sampled the azimuths of the smoothed topography along the main river paths. The continuous flow angle of the regional steepest slope directions have been binned at intervals of 15° following *Fisher* [1993], starting at −7.5° and ending at 352.5° (gray histograms in Figure 6). The circular mean direction has also been calculated for each sample (gray dots in polar diagrams). The resulting composite diagrams of Figure 6 allow determining three types of catchments in the High Atlas with regard to the percentage of reaches (of pixel size) of the main rivers that flow in the regional slope: longitudinal-dominated, transverse-dominated and mixed.

[22] Within a given catchment, the proportion of streams that flow in the main regional slope direction may vary from 11% to 58%. In the sub-catchments in white in Figure 6, the proportion of river reaches that flow parallel to the regional slope is high (40%, 41%, 47% and 58%, for Tensift west, Ouarzazate west, Tensift Ighighayene-Rdat,

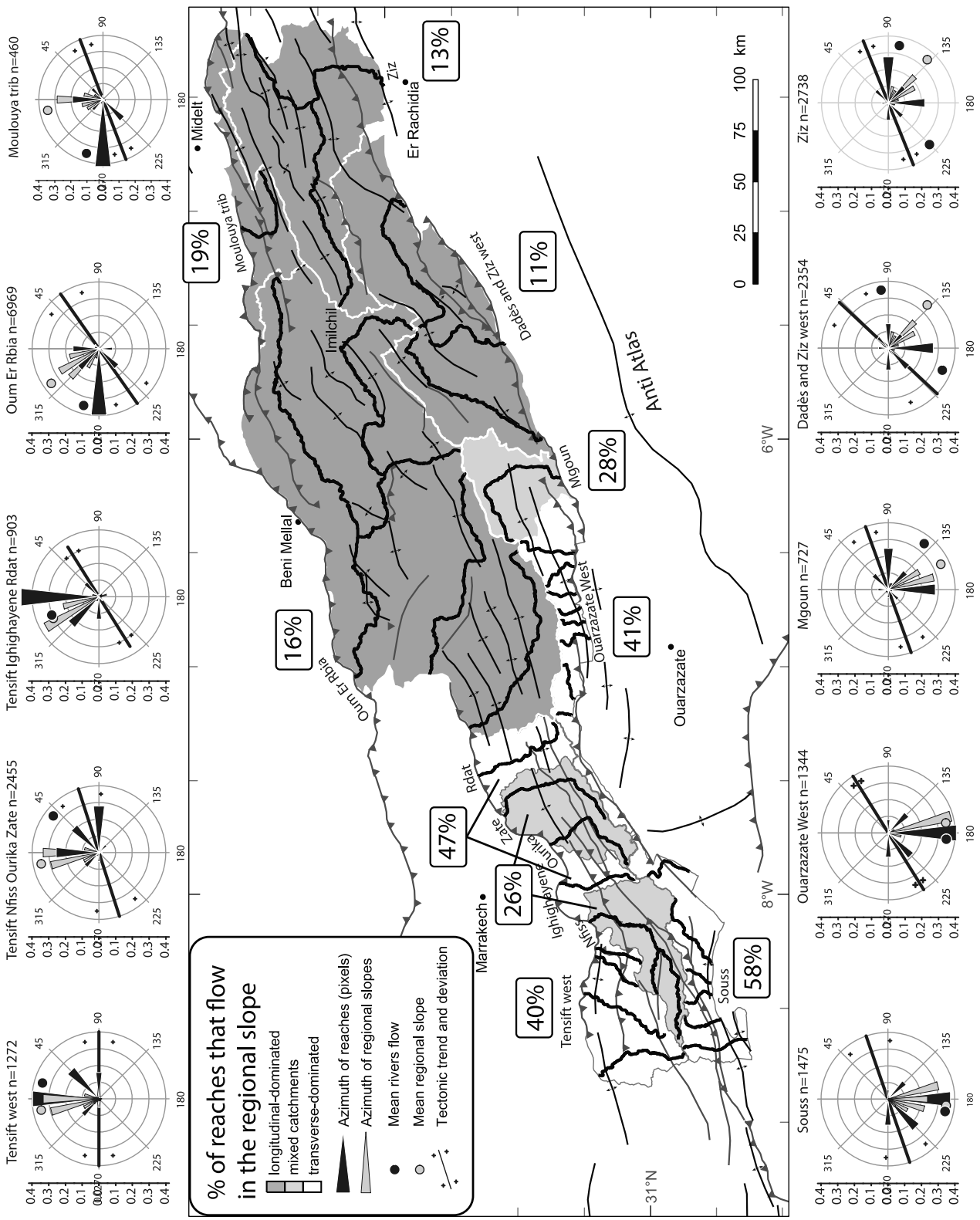
% of reaches that flow in the regional slope
longitudinal-dominated
mixed catchments
transverse-dominated
Azimuth of reaches (pixels)
Azimuth of regional slopes
Mean rivers flow
Mean regional slope
Tectonic trend and deviation
Tensift west n=1272
Tensift Nfiss Ourika Zate n=2455
Tensift Ighighayene Rdat n=903
Oum Er Rbia n=6969
Moulouya trib n=460
Souss n=1475
Ouarzazate West n=1344
Mgoun n=727
Dadès and Ziz west n=2354
Ziz n=2738
Midelt
Er Rachidia
Ziz
Beni Mellal
Marrakech
Ouarzazate
Imilchil
Moulouya trib
Dadès and Ziz west
Anti Atlas
Mgoun
Ouarzazate West
Rdat
Zate
Ourika
Ighighayene
Nfiss
Tensift west
Souss
Oum Er Rbia
19%
16%
47%
26%
40%
58%
41%
28%
11%
13%
0 25 50 75 100 km
8°W
6°W
31°N

**Figure 6**

and Souss subcathments, respectively). These catchments are mainly characterized by transverse streams. By contrast, in the sub-catchments in dark gray in Figure 6, the proportion of reaches that follow the regional slope is low (11%, 13%, 16% and 19%, for Dadès and Ziz west, Ziz, Oum Er Rbia, and Moulouya tributary sub-catchments, respectively). We classify these catchments as longitudinal-dominated. The difference between the mean river flow direction and the mean regional slope in these is at least 45°.

[23] In the sub-catchments in light gray in Figure 6, the proportion of reaches that follow the regional slope is between 26% and 28% (Tensift-Nfiss-Ourika-Zate, and Mgoun subcatchments). Longitudinal and transverse reaches develop respectively in the upstream and downstream parts of these mixed catchments.

[24] For each subcatchment, the polar diagrams of Figure 6 report the main trend of the tectonic structures (faults and folds), and the deviation from the main tectonic trend of the High Atlas. The orientation of the structures is almost everywhere perpendicular to the main regional slope, and the longitudinal-dominated catchments have a high percentage of reaches (of pixels) that flow subparallel to the main folds and faults.

[25] In summary, most of the catchments of the central and eastern High Atlas are longitudinal-dominated, whereas transverse-dominated catchments prevail in the western High Atlas south of Marrakech, with mixed catchments to a lesser extent.

## 5. Drainage Reorganization

[26] The western High Atlas shows impressive jagged relief where the drainage is transverse, with steep slopes and a mean local relief at 5 km scale of more than 1100 m (profiles 1 and 2, Figure 3). Hillslope processes are dominated by landslides (shallow and deep) and rockfalls (e.g., in the southern flank in Figure 7a). On the other hand, the central and eastern High Atlas has a mean local relief of 900 m, and of only 600 m at profiles 4 and 5 (Figure 3). The landscape of the latter is smooth with a few canyons (e.g., Melloul river, 30 km west of profile 4, and Dadès, Todhra and Ziz rivers at the southern flank).

[27] In spite of the jagged relief that characterizes the western High Atlas in general, the longitudinal reaches close to the headwaters of the Nfiss, Ourika and Zate rivers exhibit a remarkably smooth landscape. In these upstream reaches, local relief ranges from 100 to 600 m (Figures 7b and 8). The low-relief, upstream reaches of the longitudinal catchments are surrounded by local slopes of more than 30° in the high-relief, transverse catchments. Landslides in the upstream areas of the transverse valleys cut the smooth topographies producing a retreat of the divide and reducing the width of the longitudinal catchments in both flanks (Figures 7 and 8). The longitudinal drainage basins of the Nfiss, Ourika and Zate rivers become narrower in their upstream reaches (to the west) and beyond the western divide of the Nfiss and Ourika catchments streams are transverse.

[28] The presence of a longitudinal catchment along the main divide area and of transverse catchments on each side causes the occurrence of triple-junctions of divides (Figure 7b and 8). In those places the remnants of longitudinal streams are preserved as wind gaps indicating they previously extended upstream before having been captured. Such wind gaps are very common along the divides bordering the longitudinal rivers. They are characterized by strong slope asymmetry, the lower slope being always directed toward the longitudinal catchment, and the greater slope toward the transverse one. This indicates that the upstream parts of the tributaries of the main longitudinal trunks have also been captured by the transverse catchments (Figures 7a, 9a, and 9b). Ongoing captures of the narrow, low-relief, longitudinal upstream reaches will lead to the disappearance of the old divides and the creation of a new main divide separating transverse catchments.

[29] Applying this scheme to the parts of the main divide that separate transverse catchments, it follows that originally a longitudinal catchment was probably separating the northern and southern flanks of the mountain chain.

[30] From this drainage evolutionary pattern we infer a shift toward the center of the High Atlas of ~10–15 km of the divides that lie between the transverse rivers of both flanks and the Nfiss axial longitudinal catchment (Figure 7b). Values of divide shifts are lower (~7–8 km) in the upper Ourika river and in the upper Zate river (<3 km) (Figure 8).

## 6. Discussion

### 6.1. Mechanisms Causing a Fluvial Drainage Reorganization in the High Atlas

[31] Fluvial captures all over the western High Atlas indicate that the drainage network systematically evolves from longitudinal-dominated to transverse-dominated. In what follows we discuss potential mechanisms that may be causing this process of fluvial drainage reorganization at the scale of the mountain chain.

[32] Differences in erodibility due to spatial variations in rock strength can explain differential erosion rates between catchments and local changes in drainage organization, as it happens in some areas of the Zagros fold and thrust belt [*Oberlander*, 1985] though not everywhere [*Ramsey et al.*, 2008]. However, the upper reaches of the longitudinal Nfiss and transverse Berrenil rivers of the High Atlas (Figure 7a) are both located within a granitic massif without lithological changes (Tichka granite), indicating that rock strength is not influencing the process of divide retreat and capture. Diverse lithologies compose the western High Atlas, the main being Precambrian rhyolite and granite, and Paleozoic slate, greywacke and granite. Major variations of lithology are perpendicular to the main trend of the chain. However, we systematically observe captures of longitudinal

**Figure 6.** Polar diagrams of the flow direction of main river reaches in the High Atlas and of the regional slope direction within the same catchments. The subcatchments Tensift west, Ouarzazate west, Tensift Ighighayene-Rdat, and Souss are mainly characterized by transverse streams. The Dadès and Ziz west, Ziz, Oum Er Rbia and Moulouya tributary subcatchments are classified as longitudinal-dominated. In the Tensift-Nfiss-Ourika-Zate and Mgoun subcatchments, longitudinal and transverse reaches develop respectively in the upstream and downstream parts of these mixed catchments. The polar diagrams also report the main trend of the tectonic structures (faults and folds), and the deviation from the mean.

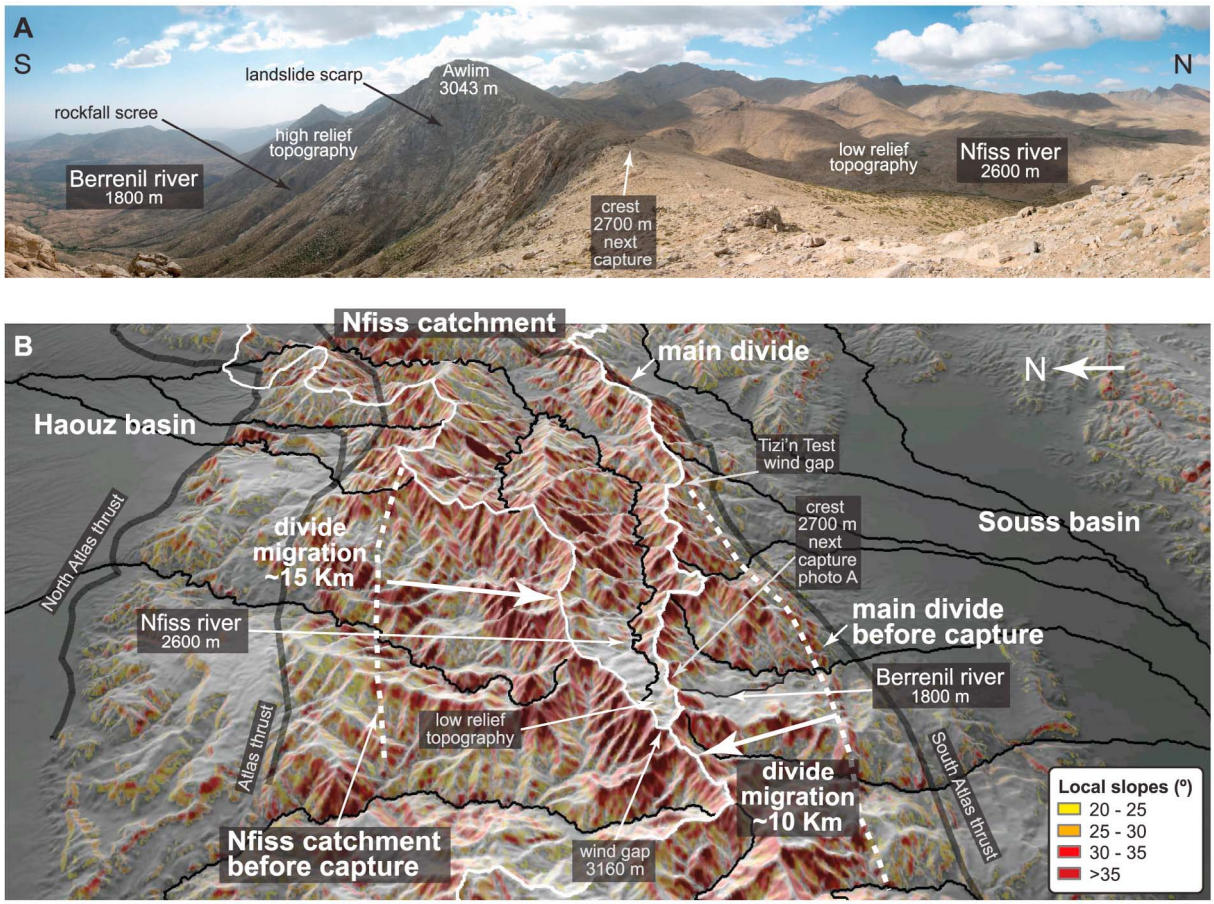


**Figure 7.** (a) Field image of the upstream parts of the Nfiss longitudinal river and the Berenil transverse river, in the western High Atlas (see location of rivers in Figure 4a). The southern slope of the divide is very steep with local relief of 1000 m, whereas local relief is only 150 m on the northern side. Landslides and rockfalls are common in the steep hillslopes. (b) 3-D view to the east of the upstream reach of the Nfiss longitudinal river, which is characterized by high elevation (above 2600 m) and low local relief (300 m). The color scale indicates local slopes. Landslides in the upstream areas of the transverse valleys cut the smooth topographies producing a retreat of the divide and reducing the width of the longitudinal catchments in both flanks. Remnants of longitudinal streams are preserved as wind gaps indicating they previously extended upstream before having been captured.

reaches by transverse streams over ~200 km of the higher part of the western High Atlas, which indicates that lithology is not the dominant control on drainage reorganization in the western High Atlas.

[33] Erosion is proportional to water flux, and earlier studies proposed that precipitation gradients perpendicular to an orogen may lead to the migration of the main divide toward the drier flank [e.g., *Bonnet*, 2009; *Willett*, 1999]. The only gradients of precipitation that occur in the western High Atlas at the scale of the orogen are from east to west, due to the westerlies that supply moisture laterally from the Atlantic Ocean, and from the lowlands to the uplands, i.e., orographic rainfall enhancement [*MADRPM*, 2000]. On the assumption that these modern patterns of moisture and precipitation held in the recent past, and since captures occur on both flanks, the systematic drainage network evolution from longitudinal-dominated to transverse-dominated is not controlled by asymmetric precipitation.

[34] In mountain belts in the northern hemisphere, glacial headwall retreat of the glaciated north-facing sides of valleys during the Pleistocene have induced a migration of east-west trending ridgelines toward the unglaciated, south-facing side [e.g., *Naylor and Gabet*, 2007]. However, glacial erosion in the Toubkal massif could not explain the observed captures facing south. Moreover, the equilibrium line altitude (ELA) in the coldest stages of the Pleistocene was at 3300 m asl [*Dresch*, 1941; see also references in *Hughes et al.*, 2011, 2006], leaving only 0.6% of the High Atlas above the ELA and hence under glacial conditions for erosion. Consequently, drainage reorganization cannot either be a consequence of glacial erosion in the High Atlas, which is dominated by fluvial erosion.

[35] The position of the longitudinal network correlates with the structural grain of the Mesozoic cover in the central and eastern High Atlas (Figures 4b, 5, and 6) with longitudinal reaches that are mainly confined in wide synclines or in front of anticline-related thrusts. In these segments of the chain the regional slope is low, mostly below 2.5° (Figure 4c). In contrast, transverse-dominated rivers spatially correlate with regional slopes ranging from 3° to 5° (Figure 4c), with high

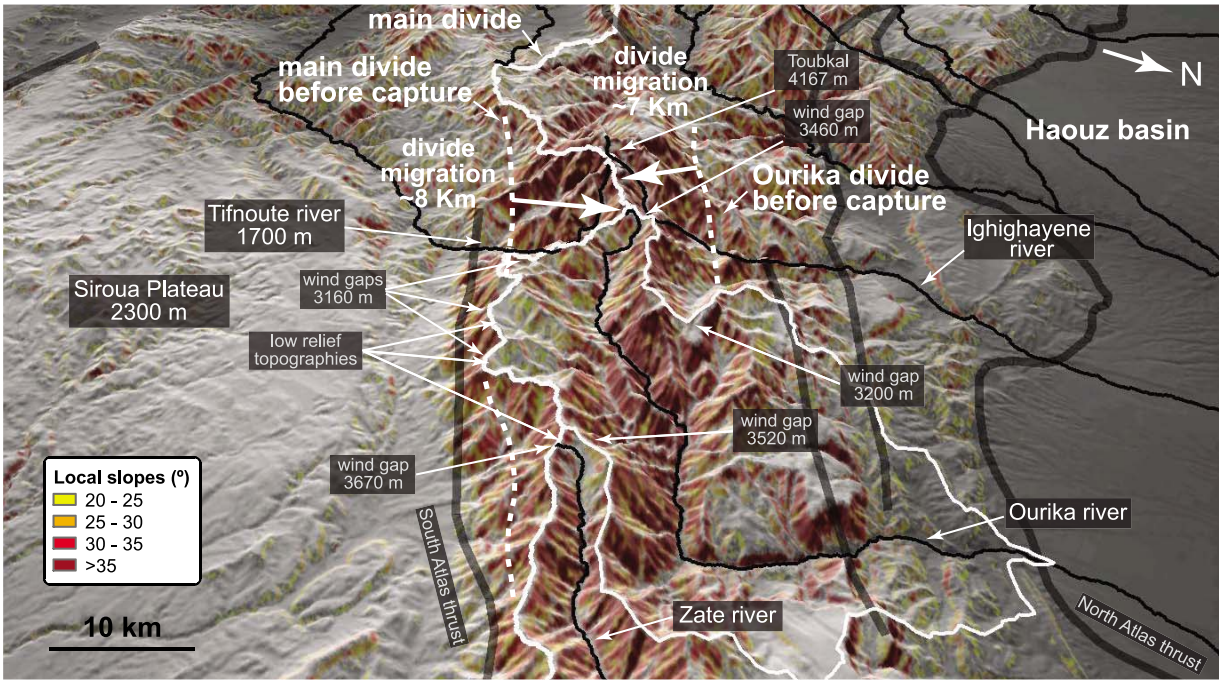


**Figure 8.** Shaded relief view to the east of the upstream reach of the Ourika longitudinal valley (western High Atlas), characterized by high elevation (above 2600 m) and low local relief (300 m). Landslides in the upstream parts of the transverse valleys cut the smooth topographies producing a retreat of the divide and reducing the width of the longitudinal catchments in both flanks. Remnants of longitudinal streams are preserved as wind gaps indicating they previously extended upstream before having been captured.

local valley slopes (high local relief at 5 km scale, Figure 3), and with very active hillslope erosion evidenced by landslides (Figure 7), suggesting a threshold for aggressive headward migration and drainage capture by transverse systems. Greater erosion during the Cenozoic in the western High Atlas is also evidenced by Miocene apatite fission track ages with respect to preorogenic Cretaceous and older ages in the central and eastern High Atlas [*Balestrieri et al.*, 2009; *Barbero et al.*, 2007; *Missenard et al.*, 2008]. Hence, the western High Atlas can be seen as an equivalent of the eastern High Atlas but with more structural relief of basement units, greater regional slope, and deeper exhumation that has largely removed the Mesozoic cover, all these specific features resulting from more rock uplift. We conclude that the mean regional slope is left as the main factor that can explain the drainage reorganization from longitudinal to transverse-dominated rivers in the High Atlas mountains.

[36] Modeling based on potential fields [*Missenard et al.*, 2006] and surface data [*Babault et al.*, 2008] argue for a maximum 1000 m of mantle-related surface uplift of the Atlas system, decreasing on both sides of the elongated thermal lithospheric anomaly (Figure 2b). The wavelength of this uplift (hundreds of km) is far too large, compared to the width of the western High Atlas, to have triggered the drainage reorganization in this narrow segment of the chain.

### 6.2. A Model for Landscape Evolution in the High Atlas Inversion Orogen

[37] The study of the Atlas system shows that the drainage network in an intracontinental mountain belt resulting from the inversion of a rift may experience an evolutionary trend from longitudinal to transverse. In the early stages of inversion, shortening produced folds and thrusts in the sedimentary cover more or less decoupled from basement which kept a low and homogeneous structural elevation. The previously stretched nature of the crust prevented its rapid overthickening and the establishment of high mean elevations and regional slopes. Under these circumstances, local structures produced sufficient local relief to deflect the rivers and make them flow parallel to the structural grain (Figure 10a). Ongoing shortening increased crustal thickening to exceed values acquired during the rifting phase. Flexural isostatic response to thickening increased the mean elevation of the orogen and the regional slopes on both flanks. Consequently, increased potential energy on both sides of the deformed belt enhanced fluvial erosion in short transverse rivers. Progressively, the differential erosion rates between the longitudinal rivers in the center of the chain and the transverse rivers made the latter capture longitudinal reaches and at the same time increase their contributing area. Ongoing thickening and drainage reorganization continuously reinforced transverse rivers' capacity of erosion by increasing slopes and drainage areas. This process should eventually lead to the complete destruction of the early longitudinal drainage (Figure 10b). Hence, the incision rates in the main rivers ultimately control drainage evolution. If incision equals rock uplift rates then surface uplift stops (provided that hillslope erosion rates equal fluvial erosion) and the regional slopes no longer increase. In such conditions, the drainage reorganization can be expected to freeze even if longitudinal reaches are still preserved in the core of the orogen.

[38] This model of drainage evolution agrees with the observation that most of rivers in evolved mountain belts are

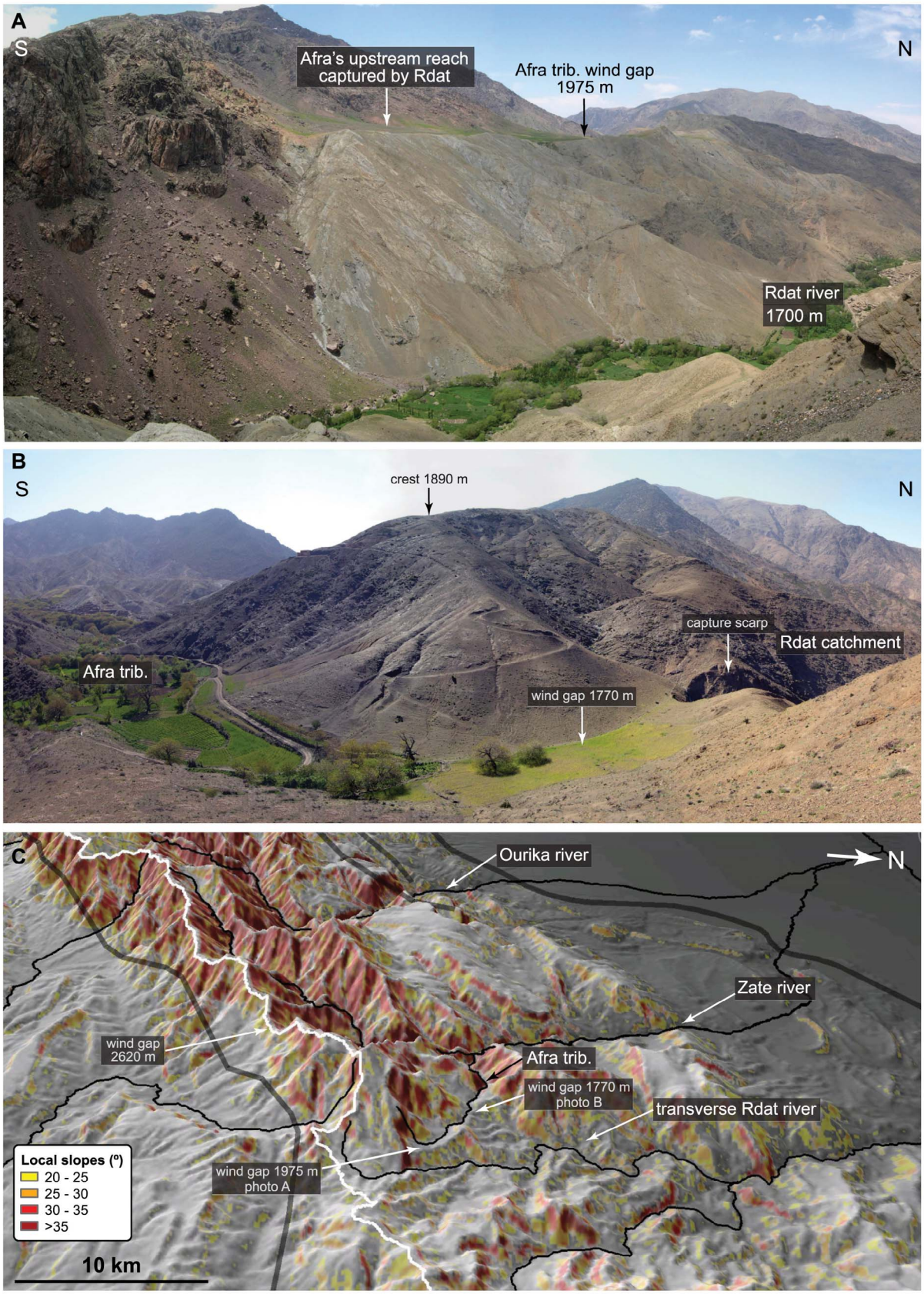


**Figure 9.** (a and b) Field images and (c) shaded relief view of the piracy of a longitudinal tributary of the Zate river by the Rdat (transverse) river near the Tichka pass (western High Atlas). Color in Figure 9c indicates the local slopes as in Figure 8.

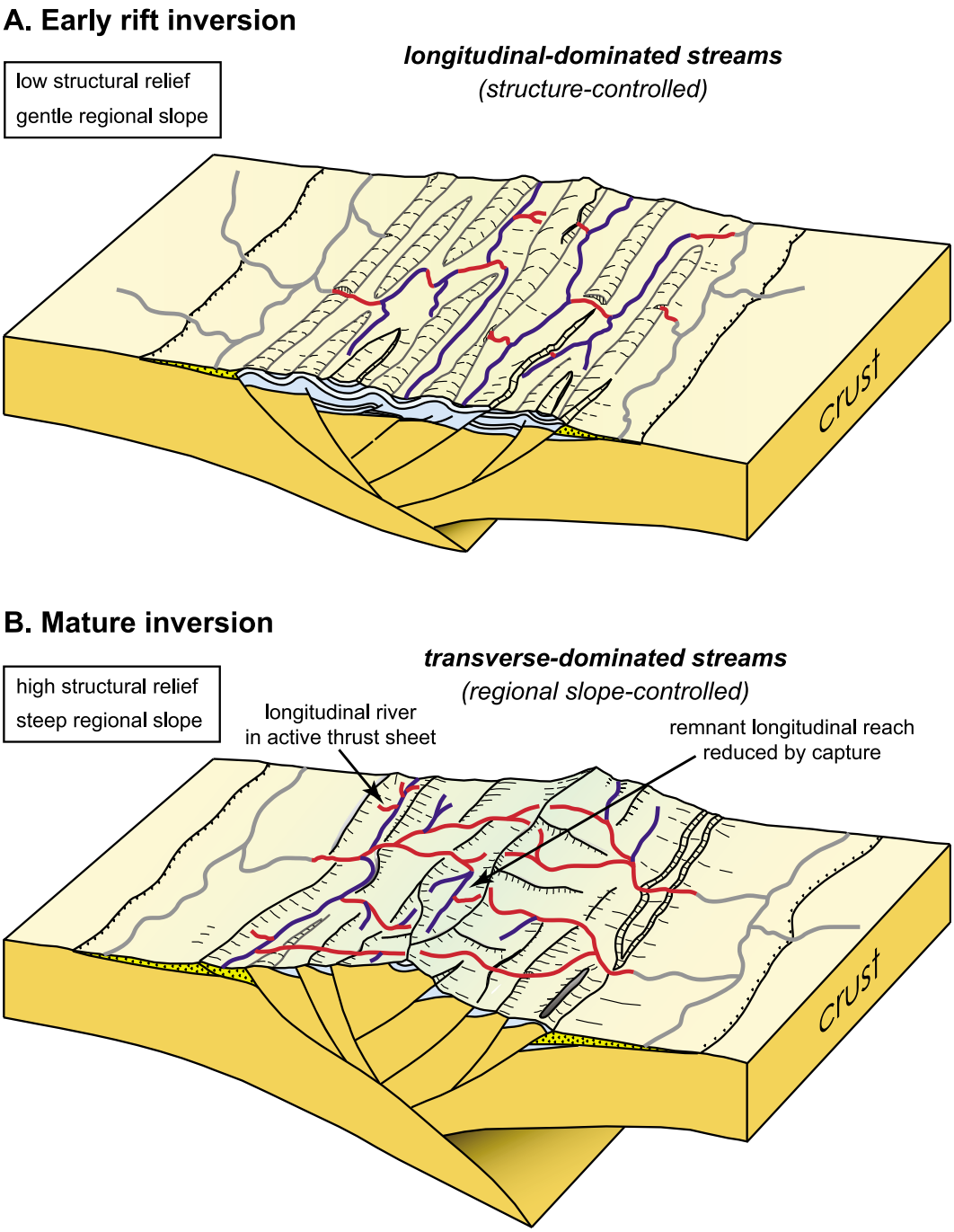


**Figure 10.** Block diagrams illustrating two stages of fluvial drainage versus tectonic structure and regional slope in orogens formed by rift inversion. The evolution from longitudinal to transverse drainage is characteristic of the transient stage of drainage systems in growing mountain belts. Longitudinal streams are shown in blue, whereas transverse streams are indicated in red.

transverse whatever the climatic conditions [*Hovius*, 1996]. The evolution from a longitudinal to a transverse drainage can be considered as a transient stage of drainage evolution during mountain building.

## 7. Conclusion

[39] While the eastern and central High Atlas, with lower elevation and regional slopes, are dominated by longitudinal (i.e., strike-parallel) drainage, fluvial captures all over the western High Atlas of Morocco indicate that the drainage network systematically evolves from longitudinal-dominated to transverse-dominated. Lithology and climate are not the dominant control on drainage reorganization in the High Atlas, leaving the mean regional slope as the dominant factor.

[40] We propose that increased tectonic thickening and surface uplift enhanced potential energy on both sides of the deformed western High Atlas and enhanced the fluvial

erosion in short transverse rivers. The differential erosion rates between the longitudinal rivers in the center of the chain and the transverse rivers in the margins made the latter capture longitudinal reaches and at the same time increase their contributing area. Ongoing thickening and drainage reorganization continuously reinforced transverse rivers capacity of erosion by increasing slopes and drainage areas. This process will inevitably lead to the complete destruction of the early longitudinal drainage in the western High Atlas and also in the eastern High Atlas if deformation and uplift continue at the present rates.

[41] Our study suggests that the evolution from a longitudinal to a transverse drainage in orogenic belts is a transient stage of drainage evolution during mountain building.

[42] **Acknowledgments.** This work was supported by the Ministerio de Educación y Ciencia projects (CGL2006-07226 and CGL2010-15416), the Consolider Ingenio 2006 TOPOIBERIA (CSD2006-00041), and the TOPOMED project (CGL2007-66431-CO2-01). We thank two anonymous reviewers, the associate editor and the editor, Onno Oncken, for their constructive comments and suggestions that have contributed to the improvement of the manuscript. We thank Alain Crave, Geoffrey Ruiz, and François Negro for help and discussion during field campaigns and María Luisa Arboleya for discussion and support.

## References

Arboleya, M. L., A. Teixell, M. Charroud, and M. Julivert (2004), A structural transect through the High and Middle Atlas of Morocco, *J. Afr. Earth Sci.*, *39*(3–5), 319–327, doi:10.1016/j.jafrearsci.2004.07.036.

Ayarza, P., F. Alvarez-Lobato, A. Teixell, M. L. Arboleya, E. Tesón, M. Julivert, and M. Charroud (2005), Crustal structure under the central High Atlas Mountains (Morocco) from geological and gravity data, *Tectonophysics*, *400*(1–4), 67–84, doi:10.1016/j.tecto.2005.02.009.

Babault, J., A. Teixell, M. L. Arboleya, and M. Charroud (2008), A Late Cenozoic age for long-wavelength surface uplift of the Atlas Mountains of Morocco, *Terra Nova*, *20*(2), 102–107, doi:10.1111/j.1365-3121.2008.00794.x.

Balestrieri, M. L., G. Moratti, G. Bigazzi, and A. Algouti (2009), Neogene exhumation of the Marrakech High Atlas (Morocco) recorded by apatite fission-track analysis, *Terra Nova*, *21*(2), 75–82, doi:10.1111/j.1365-3121.2008.00857.x.

Barbero, L., A. Teixell, M.-L. Arboleya, P. del Rio, P. W. Reiners, and B. Bougadir (2007), Jurassic-to-present thermal history of the central High Atlas (Morocco) assessed by low-temperature thermochronology, *Terra Nova*, *19*(1), 58–64, doi:10.1111/j.1365-3121.2006.00715.x.

Birot, P. (1970), *Les Régions Naturelles du Globe*, 380 pp., Masson, Paris.

Bonnet, S. (2009), Shrinking and splitting of drainage basins in orogenic landscapes from the migration of the main drainage divide, *Nat. Geosci.*, *2*(12), 766–771, doi:10.1038/ngeo666.

Bordet, P. (1955), Les éléments structuraux de l'Himalaya de l'Arun et de la région de l'Everest (Nepal oriental), *C. R. Hebd. Seances Acad. Sci.*, *240*(1), 102–104.

Choubert, G., and A. Faure-Muret (1962), Evolution du domaine atlasique marocain depuis les temps paleozoïques, in *Livre à la Mémoire du Professeur Paul Fallot*, pp. 447–514, Soc. Géol. de Fr., Paris.

Davis, W. M. (1889), *The Rivers and Valleys of Pennsylvania*, pp. 183–253, Nat. Geogr. Soc., Washington, D. C.

DiBiase, R. A., K. X. Whipple, A. M. Heimsath, and W. B. Ouimet (2010), Landscape form and millennial erosion rates in the San Gabriel Mountains, CA, *Earth Planet. Sci. Lett.*, *289*(1–2), 134–144, doi:10.1016/j.epsl.2009.10.036.

Dresch, J. (1941), *Recherches sur l'Évolution du Relief dans le Massif Central du Grand Atlas, le Haouz et la Souss*, 712 pp., Imprim. Arrault, Tours, France.

Fisher, N. I. (1993), *Statistical Analysis of Circular Data*, 277 pp., Cambridge Univ. Press, Cambridge, U. K., doi:10.1017/CBO9780511564345.

Frizon de Lamotte, D., B. Saint Bezar, R. Bracène, and E. Mercier (2000), The two main steps of the Atlas building and geodynamics of the western Mediterranean, *Tectonics*, *19*(4), 740–761, doi:10.1029/2000TC900003.

Fullea, J., M. Fernandez, H. Zeyen, and J. Verges (2007), A rapid method to map the crustal and lithospheric thickness using elevation, geoid anomaly and thermal analysis. Application to the Gibraltar Arc system, Atlas Mountains and adjacent zones, *Tectonophysics*, *430*(1–4), 97–117.

Hatzfeld, D., and P. Molnar (2010), Comparisons of the kinematics and deep structures of the Zagros and Himalaya and of the Iranian and Tibetan plateaus and geodynamic implications, *Rev. Geophys.*, *48*(2), RG2005, doi:10.1029/2009RG000304.

Hovius, N. (1996), Regular spacing of drainage outlets from linear mountain belts, *Basin Res.*, *8*(1), 29–44, doi:10.1111/j.1365-2117.1996.tb00113.x.

Hughes, P. D., J. C. Woodward, and P. L. Gibbard (2006), Quaternary glacial history of the Mediterranean mountains, *Prog. Phys. Geogr.*, *30*(3), 334–364, doi:10.1191/0309133306pp0309133481ra.

Hughes, P. D., P. L. Gibbard, and J. C. Woodward (2011), Quaternary glaciation in the Atlas Mountains, North Africa, *Dev. Quat. Sci.*, *15*, 255–260, doi:10.1016/B978-0-444-53447-7.00076-3.

Koons, P. O. (1995), Modeling the topographic evolution of collisional belts, *Annu. Rev. Earth Planet. Sci.*, *23*, 375–408, doi:10.1146/annurev.ea.23.050195.002111.

Laville, E., and A. Piqué (1992), Jurassic penetrative deformation and Cenozoic uplift in the central High Atlas (Morocco); a tectonic model; structural and orogenic inversions, *Geol. Rundsch.*, *81*(1), 157–170, doi:10.1007/BF01764546.

Lugeon, M. (1901), Recherches sur l'origine des vallées des Alpes occidentales, *Ann. Georgr.*, *10*(54), 401–428, doi:10.3406/geo.1901.2148.

MADRPM (2000), *Atlas de l'Agriculture, Colloque National de l'Agriculture et du Développement Rural*, Minist. de l'Agric. du Dév. Rural et de Pêches Mar., Rabat, Morocco.

Makris, J., A. Demnati, and J. Klussmann (1985), Deep seismic soundings in Morocco and a crust and upper mantle model deduced from seismic and gravity data, *Ann. Geophys.*, *3*(3), 369–380.

Mattauer, M., P. Tapponier, and F. Proust (1977), Sur les mécanismes de formation des chaines intracontinentales. L'exemple des chaines atlasiques du Maroc, *Bull. Soc. Geol. Fr.*, *7*(3), 521–536.

McQuarrie, N. (2004), Crustal scale geometry of the Zagros fold-thrust belt, Iran, *J. Struct. Geol.*, *26*(3), 519–535, doi:10.1016/j.jsg.2003.08.009.

Missenard, Y., H. Zeyen, D. Frizon de Lamotte, P. Leturmy, C. Petit, M. Sébrier, and O. Saddiqi (2006), Crustal versus asthenospheric origin of relief of the Atlas Mountains of Morocco, *J. Geophys. Res.*, *111*, B03401, doi:10.1029/2005JB003708.

Missenard, Y., O. Saddiqi, J. Barbarand, P. Leturmy, G. Ruiz, F.-Z. El Haimer, and D. Frizon de Lamotte (2008), Cenozoic denudation in the Marrakech High Atlas, Morocco: Insight from apatite fission-track thermochronology, *Terra Nova*, *20*, 221–228, doi:10.1111/j.1365-3121.2008.00810.x.

Montgomery, D. R., and M. T. Brandon (2002), Topographic controls on erosion rates in tectonically active mountain ranges, *Earth Planet. Sci. Lett.*, *201*(3–4), 481–489, doi:10.1016/S0012-821X(02)00725-2.

Naylor, S., and E. J. Gabet (2007), Valley asymmetry and glacial versus nonglacial erosion in the Bitterroot Range, Montana, USA, *Geology*, *35*(4), 375–378, doi:10.1130/G23283A.1.

Oberlander, T. M. (1965), *The Zagros Streams: A New Interpretation of Transverse Drainage in an Orogenic Zone*, 168 pp., Syracuse Univ. Press, Syracuse, N.Y.

Oberlander, T. M. (1985), Origin of drainage transverse to structures in orogens, *Binghamton Symp. Geomorphol. Int. Ser.*, *15*, 155–182.

O'Callaghan, J. F., and D. M. Mark (1984), The extraction of drainage networks from digital elevation data, *Comput. Vis. Graph. Image Process.*, *28*(3), 323–344, doi:10.1016/S0734-189X(84)80011-0.

Ouimet, W. B., K. X. Whipple, and D. E. Granger (2009), Beyond threshold hillslopes: Channel adjustment to base-level fall in tectonically active mountain ranges, *Geology*, *37*(7), 579–582, doi:10.1130/G30013A.1.

Ramsey, L. A., R. T. Walker, and J. Jackson (2008), Fold evolution and drainage development in the Zagros Mountains of Fars Province, SE Iran, *Basin Res.*, *20*(1), 23–48, doi:10.1111/j.1365-2117.2007.00342.x.

Teixell, A., M. L. Arboleya, M. Julivert, and M. Charroud (2003), Tectonic shortening and topography in the central High Atlas (Morocco), *Tectonics*, *22*(5), 1051, doi:10.1029/2002TC001460.

Teixell, A., P. Ayarza, H. Zeyen, M. Fernandez, and M.-L. Arboleya (2005), Effects of mantle upwelling in a compressional setting: The Atlas Mountains of Morocco, *Terra Nova*, *17*(5), 456–461, doi:10.1111/j.1365-3121.2005.00633.x.

Tesón, E., E. L. Pueyo, A. Teixell, A. Barnolas, J. Agusti, and M. Furió (2010), Magnetostratigraphy of the Ouarzazate Basin: Implications for the timing of deformation and mountain building in the High Atlas Mountains of Morocco, *Geodin. Acta*, *23*, 151–165, doi:10.3166/ga.23.151-165.

van der Beek, P., B. Champel, and J.-L. Mugnier (2002), Control of detachment dip on drainage development in regions of active fault-propagation folding, *Geology*, *30*(5), 471–474, doi:10.1130/0091-7613(2002)030<0471:CODDOD>2.0.CO;2.

Wigger, P., G. Asch, P. Giese, W. D. Heinsohn, S. O. El Alami, and F. Ramdani (1992), Crustal structure along a traverse across the Middle

and High Atlas mountains derived from seismic refraction studies, *Geol. Rundsch.*, *81*(1), 237–248, doi:10.1007/BF01764552.

Willett, S. D. (1999), Orogeny and orography: The effects of erosion on the structure of mountain belts, *J. Geophys. Res.*, *104*, 28,957–28,981, doi:10.1029/1999JB900248.

Zeyen, H., P. Ayarza, M. Fernàndez, and A. Rimi (2005), Lithospheric structure under the western African-European plate boundary: A transect across the Atlas Mountains and the Gulf of Cadiz, *Tectonics*, *24*, TC2001, doi:10.1029/2004TC001639.

# 5.6 Plateau Uplift, Regional Warping, and Subsidence

**J Babault,** Universitat Autònoma de Barcelona, Barcelona, Spain
**J Van Den Driessche,** Université Rennes 1, Rennes, France





Babault, J., Van Den Driessche, J., 2013. Plateau uplift, regional warping, and subsidence. In: Shroder, J. (Editor in Chief), Owen, L.A. (Ed.), Treatise on Geomorphology. Academic Press, San Diego, CA, vol. 5, Tectonic Geomorphology, pp. 93–128.

## Glossary

**$\delta^2$H** Indicates the hydrogen isotopic composition of a sample. It is the difference between the isotope ratio of $^2$H to $^1$H in a sample and that in a standard, divided by the ratio in the standard, and expressed as parts per thousand per million.

**$\delta^{18}$O** Indicates the oxygen isotopic composition of a sample. It is the difference between the isotope ratio of $^{18}$O to $^{16}$O in a sample and that in a standard, divided by the ratio in the standard, and expressed as parts per thousand per million.

**Convective instability** Also potential instability, a condition in which a stable fluid forced to rise or fall becomes unstable thereby triggering its later vertical motion.

**Cosmogenic nuclides** Rare isotopes within minerals induced by nuclear reactions induced by cosmic rays (mostly neutrons and muons). The length of surface exposure, or alternatively, the rate of surface erosion, is computed from the concentration of cosmogenic nuclides in a landform.

**Delamination** Separation of the dense lower part of the continental or oceanic lithosphere replaced by warmer, less dense mantle rock.

**Endorheic basin** Said of a basin characterized by internal drainage, a condition in which no surface drainage reaches the ocean.

**Hypsometry** The distribution of topographic surface area with respect to altitude.

**Knickpoints** (Nickpoint) refers to a substantially steepened reach of a stream long profile.

**Laramide orogeny** Also Columbian orogeny, was an ocean–continent collision orogen like the Andes now. The subducting plate, the Farallon oceanic plate caused thrusting and orogen building from what are now the south-western USA to northern South America.

**Local relief** Generally calculated in 5 or 10 km, a moving window, depending on the scale at which the topography has to be analyzed. It is the difference between the maximum elevation and the minimum elevation. It can also be calculated along a swath profile.

**Magnetotelluric sounding** The use of changing components of the geomagnetic field to study the electrical conductivity of the rocks within the Earth. It is generally applied to studies of the lower crust and upper mantle.

**Mean elevation** The critical variable that measures the force balance in orogens and reflects the isostatic balance of the lithospheric column. It is generally calculated in a 30 km moving window on a digital elevation model (DEM, a raster of altitudes), that is, at the scale of the crust thickness. It can also be calculated along a swath profile of at least 30 km wide.

**Paleosurface** A relict landscape more or less preserved, often a low-relief landscape deeply incised by the current drainage network. Its local characteristics may vary as a function of bedrock lithology, deformation, elevation, and latitude.

**Stable isotope paleoaltimetry** Determination of past elevations based on naturally occurring stable isotopes of an element.

**Stream power** The rate at which a stream can work for erosion and transport of its load, and measured over a specific length.


### Abstract

The authors present the physiognomic and deep characteristics of the seven largest plateaus on Earth. In the second part, the evidence used by the Earth science's community to infer rock and/or surface uplifts of plateaus are reviewed. Finally, the authors briefly present the debate between the feedbacks between plateaus uplift and global climate change. Some of the results contained in this chapter are still under debate and ongoing research is still needed to confirm them because different studies invoke for a same object contradictory processes, in that they result in conflicting uplift history.


## 5.6.1 An Introduction to Surface and Deep Features of High Plateaus

### 5.6.1.1 Components and Scales of Landscape Dynamics

Earth's surface results from the competition between deep processes induced by the tectonic system that deforms, raises, or lowers the topography, and, from surface processes controlled by the erosion-transport system that destroy the highs and fill the lows. The former deep processes are a combination of the motion of lithospheric plates and/or mantle convection, the vertical component of which moves rocks with respect to the geoid, the sea level, or a reference ellipsoid. This vertical movement is generally referred to as "rock uplift" following England and Molnar's (1990) definition. Surface processes rely on erosion, transport capacity, and sedimentation, processes that are at least dependant on potential energy, hence, on vertical motions.

Taking into account the duration of tectonics and geomorphic events, it is evident that the interactions between deep-Earth and surface-Earth systems depend on the relative rates and response times of one system with respect to the other. For that reason the relative rates and response times act on the resulting topographic evolution. For example, erosion

tends to compensate rock uplift, but by definition a delay exists between both rock uplift and removal of rocks, otherwise no mountains would form.

Large-scale tectonic processes act on the whole thickness of the crust (~30 km) or the entire lithosphere (~100 km thick). Large-scale tectonics breaks, folds, tilts, raises, and lowers the landscape over a very large expanse of land, by more than $10^3 - 10^4$ km$^2$ (England and Molnar, 1990), defining in this way, the regional-scale of tectonic geomorphology. Consequently, the study of plateau uplift, regional warping and subsidence focus on extensive landmasses. More, in the understanding of plateau generation, rock uplift data only may not be a pertinent measure of plateau uplift since the surface uplift equals the rock uplift minus the erosion (or tectonic denudation) (England and Molnar, 1990; Molnar and England, 1990). Evidence of plateau uplift will be discussed in Section 5.6.2 of this chapter.

Driving mechanisms that produce plateaus uplift have received considerable attention in the literature over the past four decades, since the broad acceptance of plate tectonics are still under debate. Timing and rates of vertical movements are critical to understand which processes are the causes of the vertical forces acting on topography. Low rates of surface uplift ($<0.5$ mm yr$^{-1}$) can be explained by crustal shortening, thickening and consequent isostatic compensation, whereas high rates of surface uplift ($>0.5$ mm yr$^{-1}$) during one or several millions of years have their origin in mantle dynamics (Garzione et al., 2006). Mantle processes responsible for high rates of surface uplift are (among others): mantle lithosphere delamination following intracontinental subduction (Bird, 1978); convective instability of cold, dense thickened-lithospheric mantle in orogens; and, its replacement by relatively hotter and lighter mantle asthenosphere (England and Houseman, 1989; Houseman et al., 1981). This point will be elaborated in Section 5.6.3 of this chapter. The elevation history of plateaus, and how long high elevations of plateaus last, is also of great interest in order to understand the interaction between asthenospheric, lithospheric and climatic processes. Since paleoelevations can only be obtained using proxies, the way the inferred estimates of vertical motions occur are greatly interpreted and debated (e.g., Molnar, 2005).

Paleoelevation data are, in general, sparse in continental regions; generally they cover only a very small part of a plateau, preventing them being used as representative of the whole plateau (e.g., Molnar et al., 2006). Recently, new tools for paleoelevation's determination based on stable isotope paleoaltimetry ($^{13}$C-$^{18}$O bonds) provide new evidence for the dynamics of surface uplift and the nature of its driving mechanism in the Andes (Garzione et al., 2008; Ghosh et al., 2006b; Hoke et al., 2009) and in Tibet (Garzione, 2008). However, doubts have been shed on the reliability of this new method (Poulsen et al., 2010).

### 5.6.1.2 Definition and Types of Plateaus at Earth's Surface

As defined in the Glossary of Geology (Neuendorf et al., 2005), a plateau is, "broadly, any comparatively flat area of great extent and elevation, specifically an extensive land region considerably elevated (>150 m in altitude) above the adjacent country or above sea level. It is commonly limited on at least one side by an abrupt descent; has a flat or nearly smooth surface but is often dissected by deep valleys and surmounted by high hills or mountains; and has a large part of its total surface at or near the summit level." Although the term tableland also applies to a "broad, elevated region with a nearly level or undulating surface of considerable extent" (Glossary of Geology, Neuendorf et al., 2005), it might be

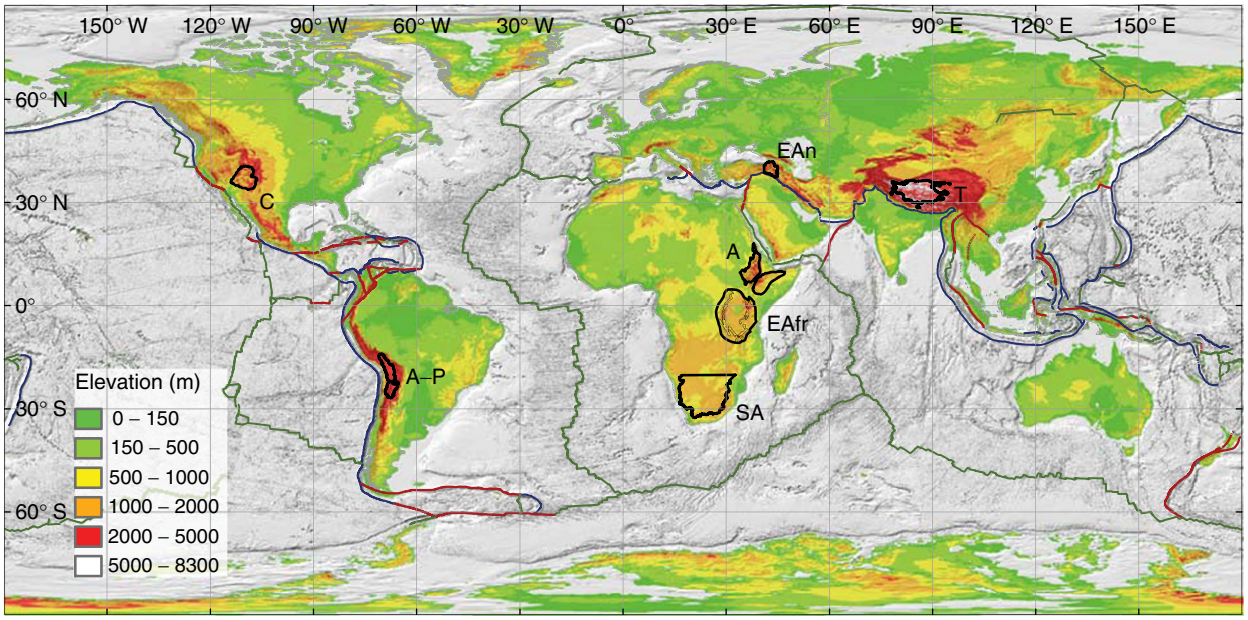


**Figure 1** Location of the main studied uplifted-plateaus (black outlined areas) on the ETOPO1 DEM. T: Tibetan Plateau, A-P: Altiplano–Puna plateau, C: Colorado Plateau, EAn: Eastern Anatolian, A: Afar (or Ethiopian) Plateau, SA: southern African plateau, EAfr: East African plateau. Green, Red, and Blue curves correspond to divergent, transform-fault and convergent plate boundaries, respectively.

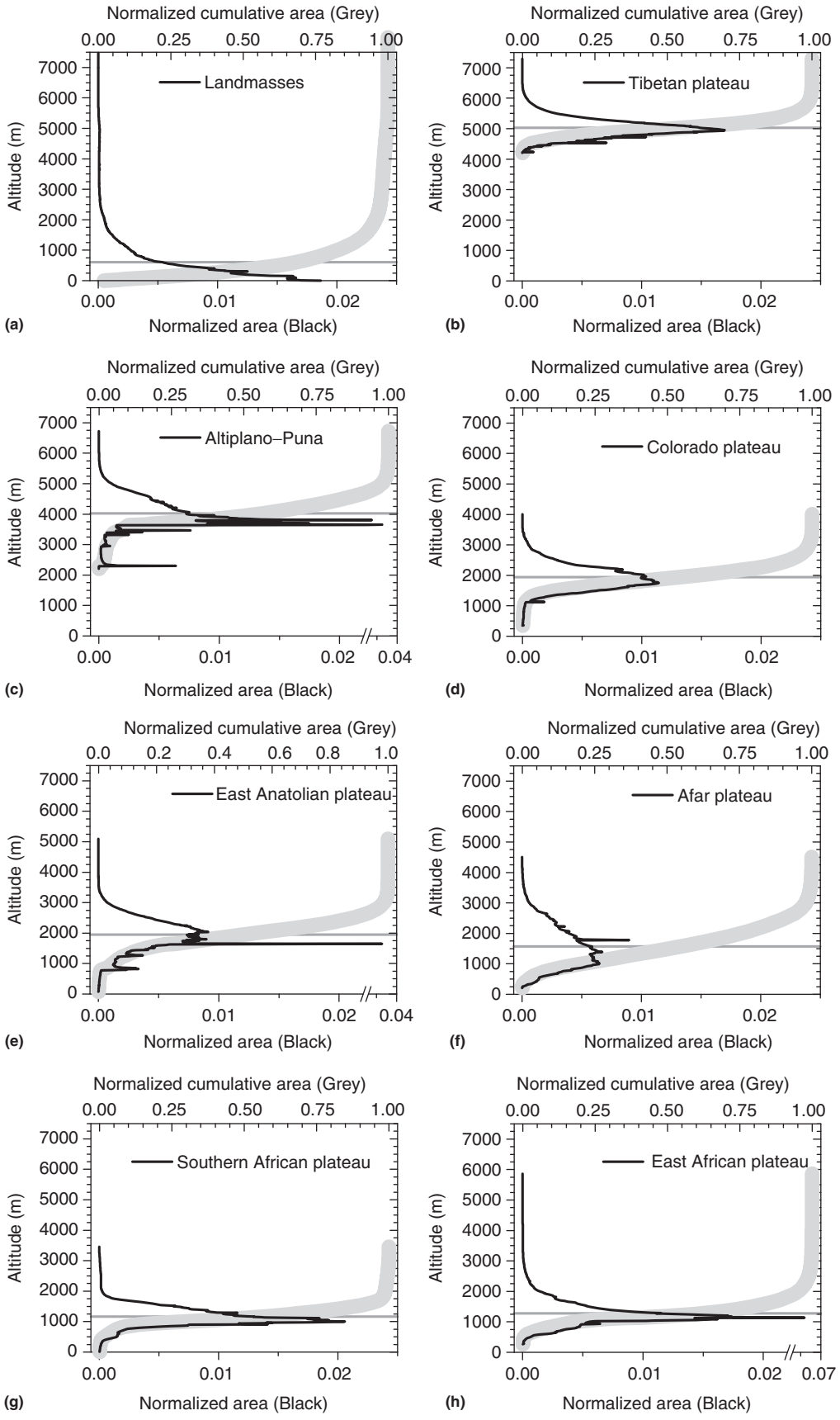

used for smaller plateau-like features (Press et al., 2004) such as the Cheyenne Tablelands, a preserved interfluve between the North and South Platte Rivers located in western Nebraska and southeastern Wyoming, USA (e.g., Leonard, 2002).

From the theory of plate tectonics, the authors know that continental collision produces orogens and, in some cases, high plateaus such as the Tibetan Plateau in central Asia or the Altiplano–Puna plateau in southern America, for the largest and highest plateaus on Earth. However, plateaus can also develop in plate-interior regions, such as the Colorado Plateau in the western US, the Ordos block in China or the southern African plateau. Plateaus also exist in the oceans and they have been extensively studied since the onset of oceanographic campaigns and, sediments and rocks sampling of the seafloor since 1968 when the Deep Sea Drilling Project started, then during the Ocean Drilling Program and now within the Integrated Ocean Drilling Program. The authors center this chapter on landmass plateaus and leave out any synthesis of studies concerned with the oceanic plateaus. Broadly, oceanic plateaus are believed to be formed by extensive basaltic floods induced by rising mantle plumes. The thickening of the oceanic crust and the replacement of cold mantle lithosphere by a hot mantle plume produces significant surface uplift (Olson and Nam, 1986) and generates a plateau that is usually, at least in part, subaerial. After the onset of magmatic activity, the relative plate motion from the plume source forces the plateau to subside below sea level (Coffin, 1992; Detrick et al., 1977). Although the origin of oceanic plateaus is still under debate as it is the case for the Ontong-Java plateau, the largest basaltic plateau on Earth (e.g., Roberge et al., 2005), most studies agree that mantle convection affects subsidence and bathymetry of oceanic sea floor (e.g., Sutherland et al., 2010).

Continental high plateaus stand on almost every continent (**Figure 1**), and if not, they may have formed in the past and they may have then subsided as has occurred in Australia (e.g., Gurnis et al., 1998), or collapsed and eroded as in the Eastern US (Coney and Harms, 1984). The mean elevation of most of the studied high-plateaus lies above 1000 m above sea level (asl) contrasting with the 600 m mean elevation of the continental areas (**Figure 2**). This chapter will summarize the main geomorphologic characteristics of the most carefully studied high plateaus.

#### 5.6.1.3 The Main High Plateaus

To compare the topography of the Tibetan Plateau, the Altiplano–Puna plateau, the Colorado Plateau, the Eastern Anatolian plateau, the East African and Ethiopian plateaus, and the southern African plateau (**Figure 1**) the authors performed a new analysis of elevation and slope frequencies (**Figures 2** and **3**) using the digital elevation model (DEM, SRTM90v4) published by Jarvis et al. (2008).

##### *5.6.1.3.1 The Tibetan plateau*

The internally drained area of Tibet (**Figure 1**) is situated on the average at 5023 m ($\pm$200 m) asl, it is characterized by mean slopes of 5° over 250 m windows (Fielding et al., 1994). At longer wavelengths of 100-km-wide swaths crossing Tibet at its greatest width and length, Fielding et al. (1994) obtained relief (maximum minus minimum elevations) estimates of $\sim$1 km or less for most of Tibet. The authors performed an analysis using the SRTM90v4 DEM published by Jarvis et al. (2008) and they obtained a similar mean elevation (5028 m, **Figure 2**) to Fielding et al. (1994) for the internally drained Tibetan Plateau ($\sim$700 000 km$^2$). Tibet is an almost flat and high area of great extent (**Figure 4**).

Almost 60% of the local slopes are less than 5° (**Figure 3**). Recent and active tectonic structures such as compressional mountain ranges, strike–slip fault-related uplifts and normal fault-related escarpments within the plateau (e.g., Liu-Zeng et al., 2008; Molnar and Tapponnier, 1978) explain the other 40% of slopes that are greater than 5°. The narrow Kunlun Mountains define the northern edge of the Tibetan Plateau, its steepest boundary. To the south it is bounded by the 2500-km-long Himalaya which, mostly in its central part, defines a steep boundary (Duncan et al., 2003). To the east the Tibetan Plateau slopes gently over 1000 km at a mean elevation of 3500 m asl up to the abrupt Longmen Shan topographic front.

**Figure 2** Elevation frequencies (black lines) and hypsometries (heavy grey lines) computed at 10 m bins for the main-studied uplifted-plateaus of the world (see **Figure 1** for locations). (a) Histogram of the global landmasses used as a reference plot. Elevation values are derived from the SRTMv4 DEM (Jarvis, A., Reuter, H.I., Nelson, A., Guevara, E., 2008. Hole-filled SRTM for the globe Version 4. Available from the CGIAR-CSI SRTM 90 m: http://srtm.csi.cgiar.org) excepted for the global landmasses analysis (a) for which elevations have been extracted from ETOPO1 bedrock (Amante, C., Eakins, B.W., 2009. ETOPO1 1 Arc-minute global relief model: procedures, data sources and analysis. In: Memorandum, N.T. (Ed.), National Geophysical Data Center, Marine Geology and Geophysics Division, Boulder, CO, p. 19). Hypsometries of Tibet (b) and Altiplano–Puna (c) are computed for the internal drainage areas. The boundaries of the Colorado Plateau (d) used in this study are that used in Roy, M., Jordan, T.H., Pederson, J., 2009. Colorado Plateau magmatism and uplift by warming of heterogeneous lithosphere. Nature (London) 459, 978–982. The boundaries of the Eastern Anatolian Plateau (e) are from that defined by Şengör, A.M.C., Ozeren, M.S., Keskin, M., Sakinc, M., Ozbakir, A.D., Kayan, I., 2008. Eastern Turkish high plateau as a small turkic-type orogen; implications for postcollisional crust-forming processes in turkic-type orogens. Earth-Science Reviews 90, 1–48. The boundaries of the Afar plateau (f) and the East African plateau (h) are from the boundaries published by Ebinger, C.J., Bechtel, T.D., Forsyth, D.W., Bowin, C.O., 1989. Effective elastic plate thickness beneath the East African and Afar plateaus and dynamic compensation of the uplifts. Journal of Geophysical Research 94, 2883–2901; the narrow rift valleys of the Main Ethiopian Rift, the Kenyan and Western rift systems, which correspond to flat and depressed areas superimposed on the plateaus, have been removed for the topographic analysis. Elevations for the southern African plateau (g) correspond to the landmasses south of 20° S and in the hinterland of southern Africa behind the Great Escarpment as defined by Ollier, C.D., Marker, M.E., 1985. The great escarpment of southern Africa. Zeitschrift für Geomorphologie. Supplementband 54, 37–56. Reproduced from Gurnis, M., Mitrovica, J.X., Ritsema, J., van Heijst, H.-J., 2000. Constraining mantle density structure using geological evidence of surface uplift rates; the case of the African Superplume. Geochemistry, Geophysics, Geosystems 1(7), 1020. doi:10.1029/1999GC000035.

To the west, the Tibetan Plateau merges with the jagged relief of the Karakoram and Pamir ranges.

#### 5.6.1.3.2 The Altiplano–Puna plateau

The Altiplano–Puna plateau is the second highest on Earth (~4000 m mean elevation, Isacks, 1988) with much of the plateau (a 250–300 km wide area) being internally drained (Vandervoort et al., 1995) (**Figure 5**). Isacks (1988) defined the plateau as the area of landmasses lying above the 3-km elevation contour which is considerably broader than the internally drained areas of the Altiplano and Puna. The authors analyzed the distribution of elevations and slopes within the internally drained areas, using the SRTM90v4 DEM published by Jarvis et al. (2008), in order to discard the deep incisions of the Andean plateau margins and to get a mean elevation closer to the definition of surface uplift following the definition of England and Molnar (1990). They obtained from the SRTM90v4 (Jarvis et al., 2008) a 4020 m asl mean elevation (**Figure 2(c)**) for the internally drained areas (~330 000 km$^2$, **Figure 1**), a value a little higher than the 3660 m asl mode value (**Figure 2(c)**) that corresponds to the Salar de Uyuni, in Bolivia. Other spikes in the histogram (**Figure 2(c)**) correspond to other major endorheic basins like the Salar de Atacama basin at 2300 m asl in northern Chile (**Figure 2(c)**). On the Altiplano–Puna plateau, the mean elevation is higher than the mode value and, than all the spikes in the histogram (**Figure 2(c)**) that are due to the mountains that surmount the main sedimentary basins. The mean elevation of the Puna is approximately 1000 m higher than that of the Altiplano (Allmendinger et al., 1997; Isacks, 1988; Wdowinski and Bock, 1994; Whitman et al., 1996). The cumulative hypsometric curve (**Figure 2(c)**) shows that 80% of the internally drained Andes lie between 2270 m and 4400 m asl. The Altiplano–Puna plateau is one of the flattest plateaus on Earth, 84% of local slopes are less than 5° (**Figure 2**) and ~70% are less than 0.6° (1%). The great number and extent of sedimentary basins, combined with the lack of major active tectonics in the Altiplano–Puna plateau, explains the smooth Andean landscape. The Altiplano–Puna plateau is flanked to the West by the Western Cordillera, a smooth edge sloping gently toward the Pacific trench (Farías et al., 2005; Isacks, 1988; Lamb et al., 1997), whereas the Eastern flank, the Eastern Cordillera, consist of a rough topography (Horton, 1999; Isacks, 1988; Lamb and Hoke, 1997; Lamb et al., 1997; Masek et al., 1994) containing smooth, highly elevated, topographic remnants of low-relief paleosurfaces (Kennan, 2000; Kennan et al., 1997; Servant et al., 1989).

#### 5.6.1.3.3 The Colorado Plateau

The Colorado Plateau (**Figure 1**) in the southern United States of America has a mean elevation of 1941 m asl (**Figure 2**). This is the third highest plateau on Earth. The physiographic extent of the Colorado Plateau used here is the same as defined by Hunt (1956) and also used recently by Pederson et al. (2002) and by Roy et al. (2009). The plateau is surrounded to the northwest and to the south by the Basin and Range Province, to the northeast by the Rocky Mountains, to the east by the Rio Grande Rift. Mostly in its southwestern part, the plateau is deeply dissected by the Colorado River and its tributaries (Rigby, 1977). The western and central parts consist of high plateaus separated from each other by faults or more or less incised by canyons (Rigby, 1977). The southeastern part of the plateau is extensively covered by volcanic rocks whereas the northern part consists of the Uinta Basin (Rigby, 1977). Only 63% of the local slopes are less than 5° (**Figure 3**). The relative roughness of the Colorado Plateau is mostly a consequence of its deep dissection by the Colorado River and its tributaries (Pederson et al., 2002).

#### 5.6.1.3.4 The Eastern Anatolian plateau

The East Anatolian plateau in Turkey (**Figure 1**) is bounded to the north by the Caucasus and to the southeast by the Zagros Mountains, and it extends from longitudes 41° E to 45° E (e.g., Şengör et al., 2008) and has a mean elevation of 1947 m asl (**Figure 2**). Two depressions at elevations above 1500 m asl compose the plateau: the Erzurum-Kars plateau in the north (Atalay and Koçman, 1979) and the Murat region in the south. They are separated by the Central Range with crest above 3000 m asl (e.g., Şengör et al., 2008). The Murat region is an internally drained region of 12 000 km$^2$ restricted to the surrounding of the Saline, 450-m-deep and 4406 km$^2$ of extent, Lake Van, perched at 1643 m (Spike in **Figure 2**(e)). Elsewhere, the Murat plateaus are dissected by permanent powerful streams including: the Euphrates; the Tigris; the Greater Zap; the Araxes; and their tributaries (e.g., Şengör et al., 2008). Only 38% of the local slopes are less than 5° (**Figure 3**), making the East Anatolian plateau the most rugged of all the plateaus described in this chapter. Recent deformation and deep incisions easily explain such a rough topography.

#### 5.6.1.3.5 The East African and Ethiopian plateaus

A striking feature of the almost 3000 km of the East African Rift System is the presence of high plateaus surrounding the axial rift valley (**Figure 1**). These highly elevated topographies are distributed in two broad domes: the 1500-km-wide East African (or Kenyan) dome, or plateau, and the 1000-km-wide Ethiopian (or Afar) dome, or plateau. Such plateaus are characterized by elevations mainly above 800 m asl (Ebinger et al., 1989). Analysis of the topography of the high plateaus only, using the SRTM90v4 DEM, yields a mean elevation 1572 m asl and 1274 m asl for the Afar and East African plateaus, respectively (**Figure 2**). The frequency of local slopes (**Figure 3**) highlights the highest degree of dissection of the Afar plateau, by the Blue Nile among other streams (Ayalew and Yamagishi, 2004; Gani et al., 2007; Pik et al., 2003), with only 55% of slopes less than 5° compared to 77% for the less incised East African plateau. The spike in the histogram of elevations (**Figure 2**, Afar plateau) is approximately 2000 m asl, corresponding to the Tana basin, which resulted from the junction of three grabens during the late Cenozoic (Chorowicz et al., 1998).

#### 5.6.1.3.6 The southern African plateau

The authors used the SRTM90v4 DEM published by Jarvis et al. (2008) to analyze the region south of latitude 20° S and enclosed by the Great Escarpment that bound the plateau on the coast of South Africa. The South African plateau has a mean elevation of 1166 m asl (**Figure 2**), the lowest value of the seven plateaus we analyzed. Local slope frequency reveals

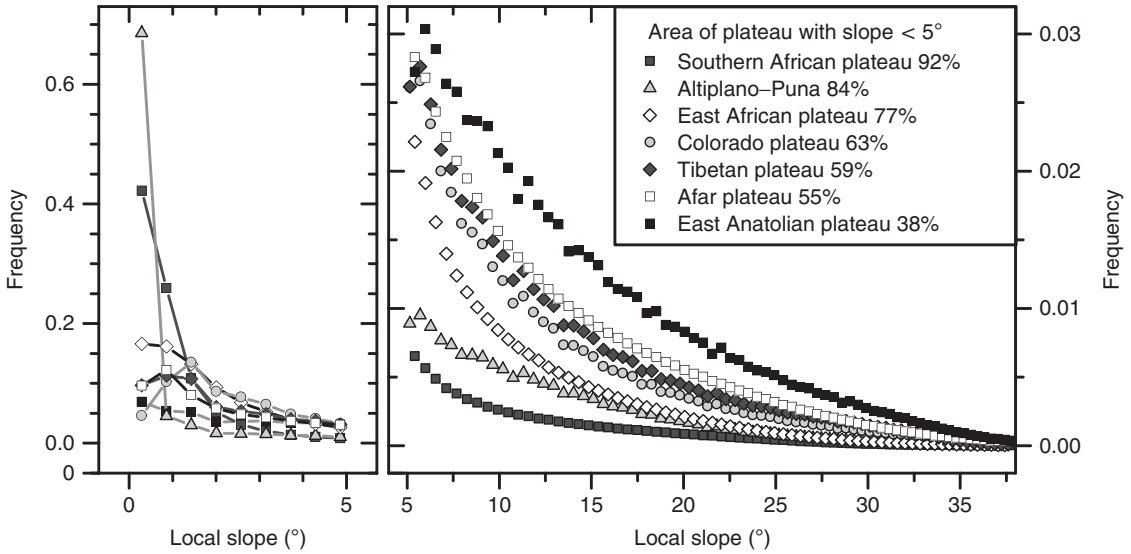


**Figure 3** Relative occurrence (frequency) of local slopes binned at 0.01 (m m$^{-1}$); (left) lower than 5°, and (right) higher than 5°. Data are derived from the SRTMv4 DEM. Reproduced from Jarvis, A., Reuter, H.I., Nelson, A., Guevara, E., 2008. Hole-filled SRTM for the globe Version 4. Available from the CGIAR-CSI SRTM 90m: http://srtm.csi.cgiar.org.

**Figure 4** View of the Tibetan Plateau between the Tanggula Shan and the Nyainqentangulha Shan. In the foreground the elevation is ~4500 m asl, and the summits in the background are at 5000–5200 m asl. Photo taken by Lewis Owen on the Golmud and Lhasa highway.

**Figure 5** View to the south-east of the Puna plateau. The Salar in the background (white area close to the center of the picture) is at 4200 m asl and the highest summits in the right part of the picture are the Cordón de Puntas Negras, a chain of volcanoes reaching 5850 m asl. Photo taken by Dominique Savanier at 5400 m asl, from the Lascar volcano located on the eastern margin of the Salar de Atacama (Chile) and west of the Aguas Calientes Volcano.

that the southern African plateau is also the flattest with 92% of its area with slopes lower than 5° (**Figure 3**). The southern African plateau, the East African plateau and the southeastern Atlantic Ocean basin to the southwest form together a region of anomalous topography and bathymetry called the African Superswell (Nyblade and Robinson, 1994).

### 5.6.1.4 Deep Structures of the Main High Plateaus

The crust and upper mantle structures for these high plateaus are important constraints for evaluating possible surface uplift mechanisms. The following is an up-to-date summary of our knowledge of their physical and thermal structures; most of these results and interpretations are still under debate and will probably be improved in the near future.

#### *5.6.1.4.1 Continent–continent collision plateaus (Tibet and Anatolian plateaus)*

##### *5.6.1.4.1.1 The Tibetan Plateau*

Located within a broad zone of N–S continent–continent collision (**Figure 1**), compression is active on the borders of the Tibetan Plateau, whereas extension is active in its center and orientated E–W (e.g., Armijo et al., 1986; Molnar and Tapponnier, 1978; Chapters 5.3 and 5.15).

The Tibetan Plateau is underlain by 60-up to 80-km-thick crust (**Figure 6**), with the maximum thickness being just beneath the Zangbo (Tsangpo) suture at ~30° N (Hirn et al., 1984a, b; Holt and Wallace, 1990; Li and Mooney, 1998). A widespread low-velocity zone is evidenced from seismic studies in the midcrust and lower crust, and is interpreted as

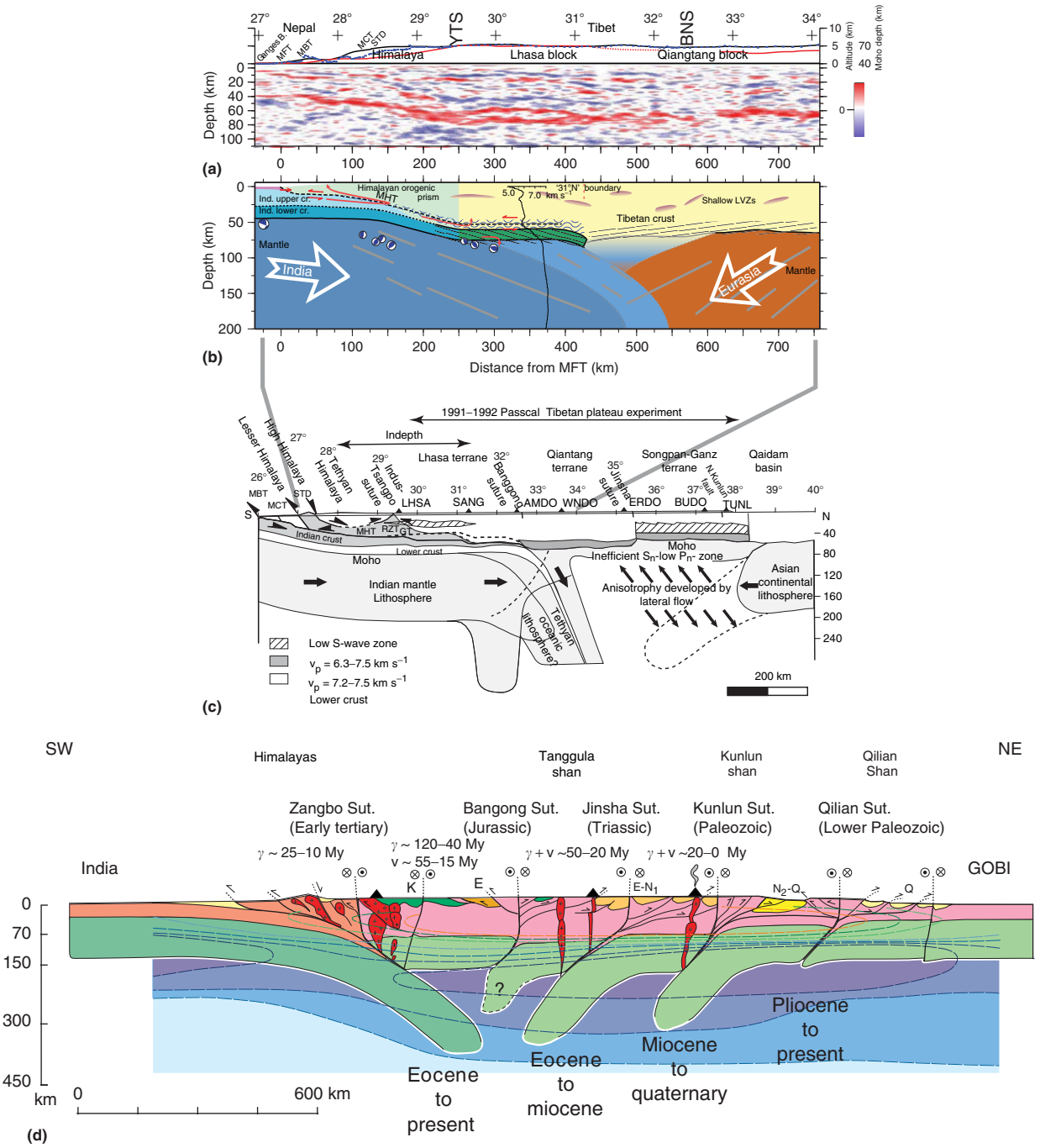


**Figure 6** Deep structure of the Himalaya-Tibetan Plateau. (a) Receiver function image along the main profile showing the principal contrasts within the lithosphere (red and blue colors represent interfaces with increasing and decreasing impedance with depth, respectively. Reproduced from Nábělek, J., Hetenyi, G., Vergne, J., et al., 2009. Underplating in the Himalaya-Tibet Collision Zone Revealed by the Hi-CLIMB Experiment. Science 325, 1371–1374. (b) Interpretative cross section of the India–Euria collision zone. Reproduced from Nábělek, J., Hetenyi, G., Vergne, J., et al., 2009. Underplating in the Himalaya-Tibet Collision Zone Revealed by the Hi-CLIMB Experiment. Science 325, 1371–1374. (c) Representative cross-section of the Tibetan Plateau modified from the work of Owens, T.J., Zandt, G., 1997. Implications of crustal property variations for models of Tibetan plateau evolution. Nature 387, 37–43; Beaumont, C., Jamieson, R.A., Nguyen, M.H., Medvedev, S., 2004. Crustal channel flows: 1. Numerical models with applications to the tectonics of the Himalayan-Tibetan orogen. Journal of Geophysical Research 109, B06406; using information compiled by DeCelles, P.G., Robinson, D.M., Zandt, G., 2002. Implications of shortening in the Himalayan fold-thrust belt for uplift of the Tibetan Plateau. Tectonics 21, 1062; Johnson, M.R.W., 2002. Shortening budgets and the role of continental subduction during the India–Asia collision. Earth-Science Reviews 59, 101–123; Tilmann, F., Ni, J., Team, I.I.S., 2003. Seismic imaging of the downwelling Indian lithosphere beneath Central Tibet. Science 300, 1424–1427; Haines, S.S., Klemperer, S.L., Brown, L., et al. , 2003. INDEPTH III seismic data: from surface observations to deep crustal processes in Tibet. Tectonics 22, 1001. (d) Representative cross-section of the Tibetan Plateau by Tapponnier, P., Zhiqin, X., Roger, F., Meyer, B., Arnaud, N., Wittlinger, G., Jingsui, Y., 2001. Oblique stepwise rise and growth of the Tibet Plateau. Science 294, 1671–1677, in which the Asian continental lithospheric manlte is preserved, decoupled from the Asian thickened crust and subducted. Note that cross-sections (a) and (b) correspond only to the left hand half part of the cross-sections (c) and (d) that share the same horizontal scale.

partly molten crust or a layer of aqueous fluids (Xu et al., 2007; Yao et al., 2008). Magnetotelluric data show that this low-velocity zone is consistent with a weak crust at depth of 20–40 km distributed in two main zones that extend from the Tibetan Plateau as far as 800 km into southwest China (Bai et al., 2010).

At lithospheric scale, some seismological studies of the central Tibetan Plateau (at 92° E to 93° E) argue for the Indian plate underthrusting southern Tibet (Figures **6(a)** and **6(b)**) at least up to the south Lhasa block, ~29° N (Hirn et al., 1984b; Li et al., 2008; Nelson et al., 1996; Schulte-Pelkum et al., 2005) but with a northern boundary uncertain. Beneath northern Tibet, north of ~34° N (McNamara et al., 1995, 1997; Ni and Barazangi, 1983), and south of the Kunlun range, south of ~36° N (Wittlinger et al., 1996), studies argue for a low-velocity body in the mantle (**Figure 6(c)**). Together with the mechanical properties of the crust of northern Tibet (Owens and Zandt, 1997) and the volcanic activity of northern Tibet (Turner et al., 1993), such seismic properties have been interpreted as a portion of crust and mantle of higher temperature, that is, a thinned lithosphere and a hot and partially molten crust (Molnar et al., 1993; Owens and Zandt, 1997; Zhu et al., 1995). Such a 250–300 km dome-like structure of hot mantle lies between two cold lithospheres characterized by relatively high seismic velocities (Wittlinger et al., 1996). These deep physical and thermal structures have been interpreted as the evidence for the underthrusting of the cold Indian lithospheric mantle beneath the Asian crust up to the Bangong–Nujiang suture at ~33° N (**Figure 6(c)**) (Owens and Zandt, 1997). Later, Kosarev et al. (1999) reexamined these data and suggested that the Indian lithosphere has underthrust the entire Asian lithosphere (not only the crust) from the base of the Moho (80 km depth), 50 km north of ~29.5° N, where the Indus–Tsangpo suture is located, as far as the Bangong–Nujiang suture at ~33° N, up to a depth of 200 km where it is inferred to be cut by a mostly vertical subducting structure. From 33° N to 36.5° N, Kosarev et al. (1999) also showed a discontinuous Asian lithospheric mantle made of fragments interpreted as a process of destruction and subduction of the sinking Asian lithosphere. Alternatively, Tapponnier et al. (2001) proposed the origin of the low velocity zone between the Tanggula and the Kunlun ranges (between 34° N and 36° N) to lie in the thick crust of the plateau. Their interpretation is based on the seismic work of Griot et al. (1998) and it implies that the Asian lithosphere has not been thinned (**Figure 6(d)**). Recently, Nábělek et al. (2009) have shown with a continuous seismic image that the Indian lithosphere has underthrust the Asian crust only, and that the Indian lower crust extends horizontally beneath the Tibetan Plateau up to approximately 31° N (**Figures 6(a)** and **6(b)**), as it is present in eastern and western Tibet (Kind et al., 2002; Wittlinger et al., 2004). The Asian and Indian crust are shown to be separated by the main Himalayan thrust (MHT) from Nepal (~27.5° N) into a midcrustal low velocity zone observed across the southern Lhasa Block (~29.5° N–31° N). Based on the differences in the seismic characteristics of the lower crust and uppermost mantle, Nábělek et al. (2009) proposed that the zone located around 31° N–32° N, and south of the Bangong–Nujiang suture (~33° N), is a boundary between the Eurasian plate and the Indian plate that is underthrusting the Tibetan upper crust. The Nábělek et al. (2009) interpretation shifts to the south the plate boundary inferred to be at ~33° N by Kosarev et al. (1999). South and north of 31° N–32° N Nábělek et al.'s (2009) boundary, mantle lineations dip north and south, respectively, suggesting a mantle downwelling along this plate boundary (**Figures 6(a)** and **6(b)**), a continental subduction also put in evidence east of Nábělek et al.'s profile (Shi et al., 2004; Tilmann et al., 2003). Such continental subduction of the Indian and Eurasian plates beneath and south of the Bongong–Nujiang suture (southern Tibet) mainly agrees with the lithospheric-scale cross-section proposed by Tapponnier et al. (2001) (**Figure 6(d)**) and based on compiled surface and subsurface data (see references in Tapponnier et al., 2001). One of the main differences between the two models of the deep structure of the Tibetan Plateau is the preservation, or not, of the Asian lithosphere (**Figures 6(c)** and **6(d)**). In Tapponnier et al.'s (2001) model, the crust thickened since the collision of Indian and Asian plates, whereas the mantle did not. Such a model implies that the lithospheric mantle is decoupled from the weak lower crust, and subducted into the hot asthenospheric mantle.

#### 5.6.1.4.1.2 *The Eastern Anatolian and Iranian plateaus*

Like the Tibetan Plateau, the Eastern Anatolian plateau corresponds to a zone of north–south continental collision (**Figure 1**). Folding is confined to the southwestern part of the plateau (as defined by Şengör et al., 2008) and thrusting is confined to east–west depressions in the southwestern, central, and northeastern parts of the plateau (for a compilation of neotectonic data see Şengör et al., 2008). However, the plateau is dominated by strike–slip faults: a sinistral northeast–southwest orientated set and a dextral northwest–southeast striking set (Şengör et al., 2008 and references herein).

Seismic data show a mean crustal thickness of 45 km beneath the eastern Anatolian plateau (**Figure 7**) with 42 km near the southern part of the Biltis suture zone (the southern edge of the plateau) and 50 km along the northern edge of the Anatolian plateau, whereas in the southeastern part of the plateau the crust is thinner than 40 km (Zor et al., 2003).

Furthermore, seismic data argue for a thinned or totally removed lithospheric mantle beneath the plateau (Al-Lazki et al., 2004; Gök et al., 2003, 2007) which is consistent with the high heat flow and the late Cenozoic volcanic activity (Keskin, 2003; Pearce et al., 1990; Yilmaz et al., 1998). Tomography indicates that it is not only the Turkish plateau but all the Turkish–Iranian plateau, the Middle East region north of the Bitlis–Zagros suture, that is affected by a lithospheric mantle thinning and its replacement by a warm or perhaps partially molten uppermost mantle (Maggi and Priestley, 2005; Tabatabai Mir et al., 2008) to a depth of ~200 km (Zor, 2008). The region also lacks subcrustal earthquakes, which is evidence for the absence of the subducting Arabian Plate beneath the Anatolian plateau (Turkelli et al., 2003).

### 5.6.1.4.2 *Ocean–continent collision plateau (The Andes)*

The Andes result from oceanic-continent convergent margin processes. The Nazca oceanic plate is subducted on a 30°-east-dipping direction beneath the Altiplano–Puna plateau,

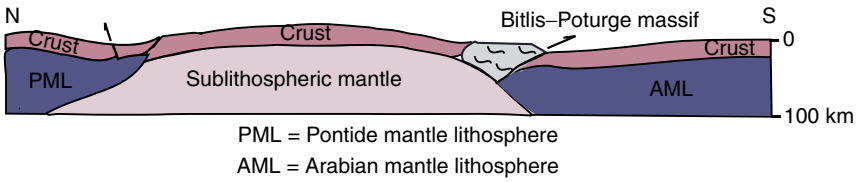


**Figure 7** Lithospheric structure beneath eastern Anatolia from Gögüs, O.H., Pysklywec, R.N., 2008. Mantle lithosphere delamination driving plateau uplift and synconvergent extension in eastern Anatolia. Geology 36, 723–726, originally modified from Şengör, A.M.C., Özeren, S., Genç, T., Zor, E., 2003. East Anatolian high plateau as a mantle-supported, north-south shortened domal structure. Geophysical Research Letters 30, 8045; Dhont, D., Chorowicz, J., 2006. Review of the neotectonics of the Eastern Turkish–Armenian Plateau by geomorphic analysis of digital elevation model imagery. International Journal of Earth Sciences 95, 34–49; Gök, R., Michael, E.P., Ekrem, Z., 2007. Lithospheric structure of the continent–continent collision zone: eastern Turkey. Geophysical Journal International 169, 1079–1088, and Keskin, M., 2003. Magma generation by slab steepening and breakoff beneath a subduction-accretion complex: an alternative model for collision-related volcanism in Eastern Anatolia, Turkey. Geophysical Research Letters 30, 8046.

whereas in the narrower northern and southern Andes the plate shallows and becomes nearly flat (Cahill and Isacks, 1992, and references herein). Gephart (1994) showed that the central Andean orogen as well as the underlying Wadati–Benioff zone exhibit a high symmetry with the axis of symmetry for the two surfaces nearly coincident. More, Gephart (1994) showed that these axes were coincident with the Nazca/South America finite relative rotation pole for the period 36–20 Ma, that is, coincident with plate kinematics, which has been stable since the mid-Tertiary. Such geometric and kinematics evidence suggest that the tectonic forces that built the Andean topography are strongly related to the subduction process, or plate tectonics, in this noncollisional orogen (Gephart, 1994) whatever the significant along-strike geological variations.

Crustal thicknesses in the Andes vary strongly on the region considered, and, also depending on the kind of methods used to estimate it (see Allmendinger et al., 1997). From north to south, seismic studies show that they range from 59 to 70 km in southern Peru (**Figure 8**), from 49–60 to 80 km beneath the Central Andes and from 40–50 to 60–70 km above the Pampean flat slab of the Southern Andes (Beck et al., 1996; Fromm et al., 2004; Heit et al., 2008; McGlashan et al., 2008; Yuan et al., 2002). Crust maximum thickness is beneath the Western and Eastern Cordilleras where it reaches ~70 km (Beck and Zandt, 2002; Beck et al., 1996; Swenson et al., 2000). Now considering the Altiplano–Puna plateau alone, depending on different studies, crustal thicknesses vary beneath the Puna–Altiplano from 60 to 65 km (Beck and Zandt, 2002; Beck et al., 1996) or they range between 57 and 82 km beneath the Altiplano, and they thin to 40–45 km beneath the 1000 m higher Puna (McGlashan et al., 2008; Yuan et al., 2002). Alternatively, the crust under the Altiplano and Puna plateau has been deduced to be 60 and 67 km thick, respectively, in correlation with the higher 1000 m asl mean elevation of the Puna (Baumont et al., 2002). Gravity studies also yield the conclusion that the crust beneath the Altiplano and Puna is less than 70-km thick (Fukao et al., 1989; Götze et al., 1994; Kono et al., 1989). Beneath the Altiplano, a low-velocity zone has been inferred for the midcrust to lower crust to be felsic (quartz-rich) composition and it may correspond to a weak layer decoupled from the brittle upper crust (Beck and Zandt, 2002; Koulakov et al., 2006; Yuan et al., 2000). Mafic lower crust is inferred by seismic velocities to be in the eclogite facies or to be absent in the Central Andes (Beck and Zandt, 2002).

Lithospheric thickness has been estimated to reach 150 km beneath the Altiplano, to thin under the Western Cordillera and to thin by 50 km beneath the Puna plateau (Whitman et al., 1992; Whitman et al., 1996). Seismic velocities under the Altiplano–Eastern Cordillera transition also suggest that the asthenosphere reaches near the base of the crust (Dorbath and Granet, 1996; Koulakov et al., 2006; Myers et al., 1998; Wigger et al., 1994). Geochemistry of hydrothermal fluids and gases of the Altiplano and the Eastern Cordillera also supports the views that the lithosphere has been thinned (Hoke et al., 1994). The upper part of the subducted Nazca plate is topped by a low-velocity zone interpretated as magma generation zone induced by dehydratation of subducted material dragged along the slab (Baumont et al., 2002). To the East of the Altiplano, numerous studies suggest that the mechanically strong Brazilian lithosphere has underthrust the Sub Andes and the Eastern Cordillera but not the Altiplano (Beck and Zandt, 2002, and references herein).

#### 5.6.1.4.3 Intraplate plateaus (Colorado and African plateaus)

##### 5.6.1.4.3.1 The Colorado Plateau

A Mesozoic ocean–continent collision started at 150 Ma in the western coast of North America. Consequently, the east dipping Farallon plate subduction, and the associated compression triggered compressional deformation and the formation of the Sevier orogen. During the late Cretaceous and early Tertiary, the shallowing of the Farralon plate subduction (e.g., Dickinson and Snyder, 1978) propagated the deformation into the interior of the North American plate leading to the formation of the Laramide orogen. These orogenies lead to an overthickened crust up to 60 km thick (Coney and Harms, 1984). The Colorado Plateau was located close to the eastern front of the Laramide orogen but it experienced only a very small amount of crustal shortening, less than a few percent (Spencer, 1996). The Colorado Plateau is now bordered by the Basin and Range Province to the west and south and the Rio Grande Rift to the east; both are thinned regions (e.g., Bird, 1988; Sonder and Jones, 1999; Wernicke et al., 1987) where extension is still active. However, no significant extension is reported on the Colorado Plateau.

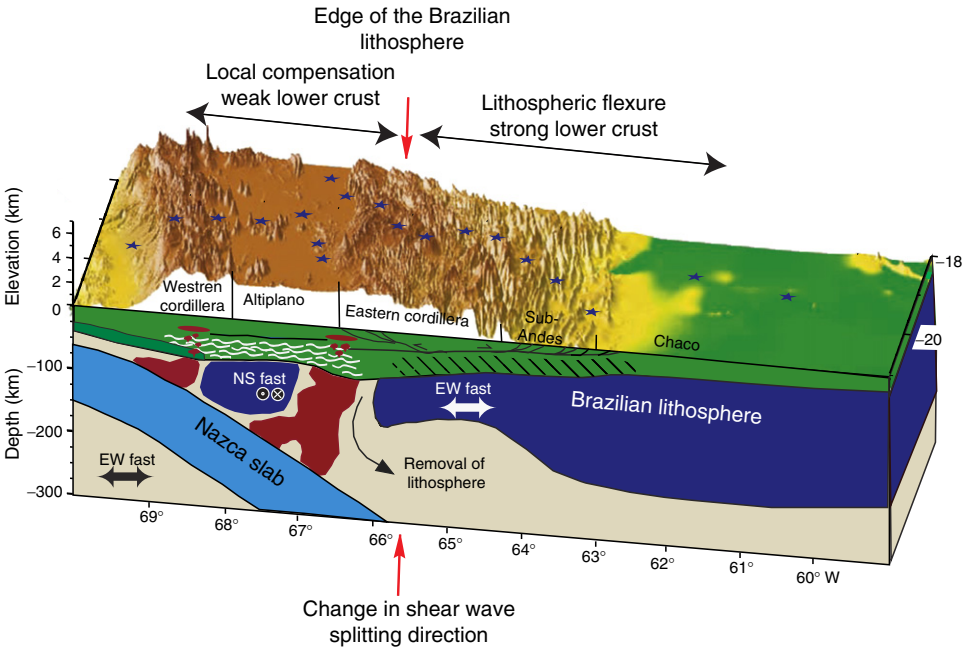


**Figure 8** Schematic cross-section from Beck, S.L., Zandt, G., 2002. The nature of orogenic crust in the central Andes. Journal of Geophysical Research 107, 2230 showing their interpretation of the lithospheric structure of the central Andes from geophysical and geological studies. Red and blue indicate upper mantle P wave velocities that are slower and faster, respectively, than the reference IASPEI-91 model. Reproduced from Myers, S.C., Beck, S., Zandt, G., Wallace, T., 1998. Lithospheric-scale structure across the Bolivian Andes from tomographic images of velocity and attenuation for P and S wavesJournal of Geophysical Research 103, 21233–21252.

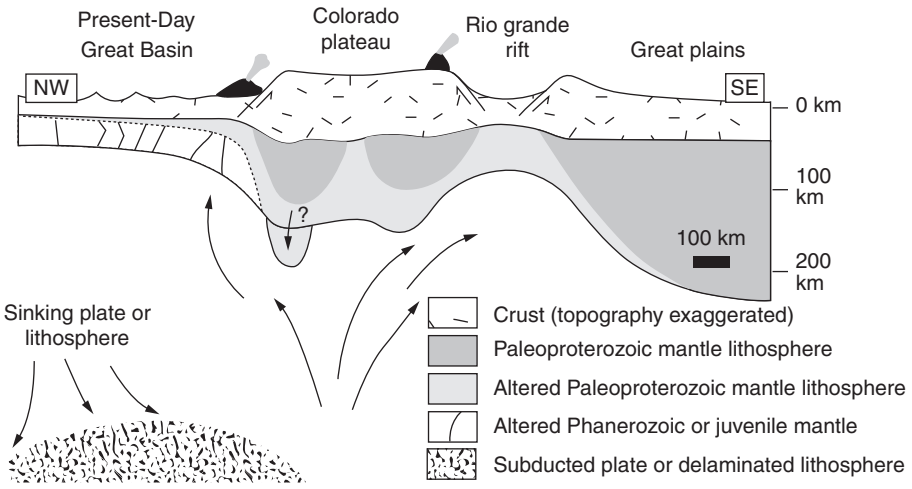


**Figure 9** Deep structure beneath the Colorado Plateau and the Basin and Ranges, Rio Grande Rift and Great Plains neighboring regions, from Sine, C.R., Wilson, D., Gao, W., Grand, S.P., Aster, R., Ni, J., Baldridge, W.S., 2008. Mantle structure beneath the western edge of the Colorado Plateau. Geophysical Research Letters 35, L10303.

The crust beneath the Colorado Plateau is inferred by seismic studies to be 44- to 47-km-thick (**Figure 9**) (Das and Nolet, 1998; Wilson et al., 2005). Crustal thickness is almost similar, 42–46 km, in the Great Plains, whereas the crust underwent thinning to 35 km centered on the Rio Grande Rift (Wilson et al., 2005). The Basin and Range Province underwent thinning of the crust up to 20–30 km thick (Coney and Harms, 1984), seismic studies suggest that the crust thins from 30 to 25 km eastward (Das and Nolet, 1998, and references therein). The crust of the Rocky Mountains to the north is inferred to be 50-km-thick (Das and Nolet, 1998, and references therein).

Seismic data argue for a 120- to 150-km-thick lithosphere beneath the Colorado Plateau and ~200 km beneath the Great Plains to the east (West et al., 2004). In between, thinned lithosphere, 45- to 55-km-thick, is inferred to exist

beneath the Rio Grande Rift (West et al., 2004). To the west, the lithosphere is also thin at 60-km-thick beneath the Basin and Range (Zandt et al., 1995).

A thick low-velocity zone is inferred beneath the Colorado Plateau lithosphere (West et al., 2004) from a depth of 150 to 300 km. Based on seismic studies Wang et al. (2008) and Sine et al. (2008) inferred mantle regional flow at the southeastern edge and at the western edge of the Colorado Plateau.

#### 5.6.1.4.3.2 The East African (Kenyan) and Ethiopian plateaus

The East African and Ethiopian plateaus are located in the African plate along the East African Rift System. The Ethiopian plateau is covered by extensive basalts dated at 31–29 Ma (e.g., Hofmann et al., 1997). Sedimentary and volcanic sequences are modeled to reach 2 to 5 km of thickness on the Ethiopian plateau (Mackenzie et al., 2005) with 1 to 2 km of flood basalts and volcanoes on top of the western Ethiopian plateau (Pik et al., 2003). Depending on the studies carried out, the crust is inferred to be 42- to 50-km-thick west of the Ethiopian rift and 37- to 40-km-thick to the east (Mackenzie et al., 2005) or is inferred to be 33- to 44-km-thick on either side of the Main Ethiopian rift (Dugda et al., 2005). Beneath the western Ethiopian plateau, a 15-km-thick layer composing the base of the lower crust is characterized by seismic high-velocities. Crustal thicknesses vary from 37 to 38 km west and from 39 and 42 km east of the Kenyan rift (Dugda et al., 2005). These studies indicate that crust away from the rifts has not been significantly modified by the Cenozoic rifting and magmatism, and the Cenozoic flood basalts on the Ethiopian plateau do not appear to be thick enough to alter the depth of the base of the crust (Dugda et al., 2005). Only a slight thinning of the crust is observed below the Main Ethiopian Rift (Mackenzie et al., 2005) and crustal thickness is inferred to vary from 27 to 38 km (Dugda et al., 2005).

Beneath the Ethiopian plateau, the lithosphere-asthenosphere boundary is imaged at 90 km depth (Ayele et al., 2004). Almost similar values are obtained by Dugda et al. (2007) who inferred the base of the lithosphere at 70–80 km beneath the Ethiopian plateau and at 50 km beneath the Main Ethiopian Rift and the Afar. By contrast, the lithosphere of the Tanzanian craton beneath the East African plateau reaches deeper levels up to approximately 170–200 km (Ritsema and van Heijst, 2000) (**Figure 10(b)**), though 50–80 km shallower than the lithosphere of the thicker Congo craton to the west.

In the Afar and surrounding regions a deep low-velocity anomaly in the upper mantle (Debayle et al., 2001; Ritsema et al., 1999; Ritsema and van Heijst, 2000) is interpreted as hot mantle extending to at least 660-km-depth (e.g., Debayle et al., 2001). Beneath the East African plateau a low-velocity anomaly is present in the upper mantle that is ~500 km wide and extends from the eastern edge of the Main Ethiopian Rift westward (Bastow et al., 2008). A low velocity zone also extends up to a depth of ~400 km and to at least 300 km beneath the eastern branch in Tanzania and in Kenya, respectively (Park and Nyblade, 2006; Ritsema et al., 1998; Weeraratne et al., 2003). The top and bottom of the transition zone (410–660 km) beneath the Eastern Plateau is depressed and it could be related to a thermal anomaly in the lower mantle (**Figure 10(a)**) (Huerta et al., 2009) (see Section 5.6.1.4.3.3).

Following the pioneer work of Dziewonski (1984), Ritsema et al. (1999) presented a global tomographic model inferring (like Dziewonski) a broad low-velocity zone in the lower mantle and initiating at the core mantle boundary beneath southern Africa and propagating up to the upper mantle beneath the Afar Plateau (**Figure 10(a)**). Such anomalous low seismic velocity is interpreted as hot and less dense lower mantle material combined with a chemical anomaly (Ritsema et al., 1999; Simmons et al., 2007) and referred to as the deep-mantle African Superplume.

#### 5.6.1.4.3.3 The Southern African plateau

The southern African plateau is located within a stable continent and bordered by Mesozoic passive margins (**Figure 1**). The southern African plateau is bounded on the coast by rift shoulders, the Great Escarpment and the Drakensburg Mountains, characterized by a warping down of the topography from 1000 m asl toward the margin (Ollier, 1985; Ollier and Marker, 1985; ten Brink and Stern, 1992).

Crustal thickness beneath the southern African plateau varies between 33 and 45 km beneath the Archean cratons and 45 and 50 km beneath the Proterozoic orogenic belts (Nguuri et al., 2001).

A 250 to 300 km thick lithosphere has been inferred by Ritsema and van Heijst (2000) and James and Fouch (2002), respectively. High lithospheric thickness and low heat flow, $<45\ \mathrm{mW\ m^{-2}}$ (Nyblade et al., 1990), are considered to mark a strong upper mantle which is corroborated by high estimates of effective lithospheric thicknesses (Stark et al., 2003).

Beneath southern Africa and the southern Atlantic Ocean, global tomography suggests that there is a low-velocity zone in the lower mantle and initiating at the core mantle boundary (Ritsema et al., 1999) (**Figure 10(a)**).

### 5.6.1.5 High Plateaus: Uplifted Peneplains, Growing Plateau or Applanation at High Elevation?

Davis (1899) interpreted elevated and smooth landscape as a step in a sequence or a cycle in which ongoing erosion of a previous landscape eventually leads to the complete destruction of the relief and the formation of a low-relief erosional surface at almost sea level: the peneplain. Davis's cycle of erosion (1899) was based on the idea that after a rapid surface uplift of the peneplain, the increase in potential energy enhances erosion that in turn increases significantly the local relief and local slopes. A wave of fluvial and hillslope erosion then propagates inside the plateau from the borders. Ongoing erosion eventually leads to the complete destruction of the topography and the formation of another low-relief erosional surface at almost sea level. A new uplift of such peneplain means a wave of erosion starts afresh: a new cycle of erosion began (see Chapter 5.16 for more discussion).

In contrast, several models have been proposed for the non instantaneous development of topography as it has been the case for the Tibetan Plateau. They argue for the progressive surface uplift of the whole plateau (Fielding et al., 1994), or for progressive surface uplift of the whole followed by rapid surface uplift events (England and Houseman, 1989;

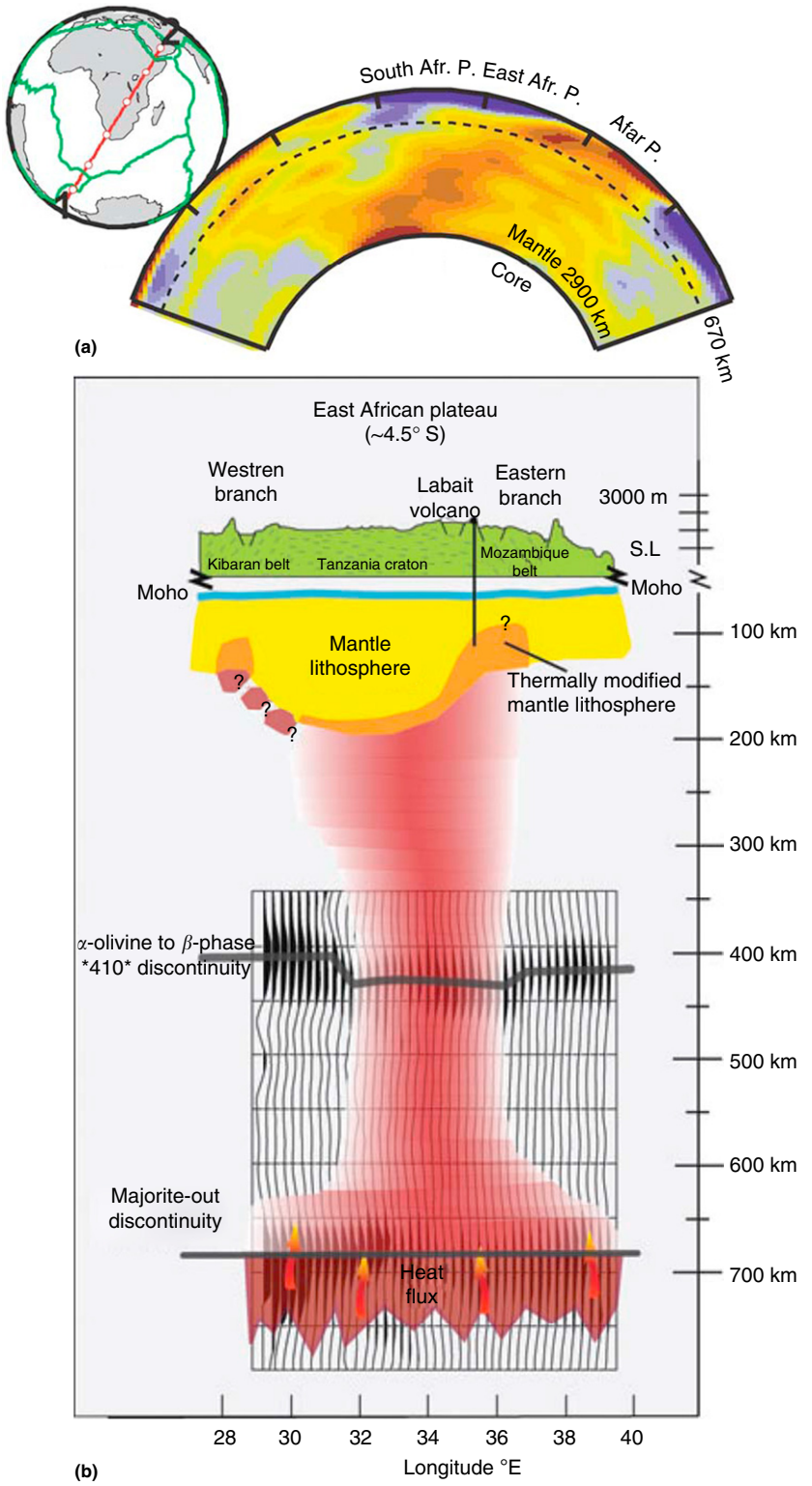


**Figure 10** (a) Cross-sections through the South and eastern African plateaus, and across the Afar plateau, obtained from a tomographic model extending up to the core-mantle boundary along a 140° wide great circle arcs (inset). Relatively high velocity and low velocity regions are indicated by blue and red colors, respectively. The dashed line represents the 670-km seismic discontinuity. Reproduced from Ritsema, J., Heijst, H.J.V., Woodhouse, J.H., 1999. Complex shear wave velocity structure imaged beneath Africa and Iceland. Science 286, 1925–1928. (b) Schematic cross-section of the East African plateau at ~4.5° S showing receiver function stacks of mantle transition zone and cartoon of the associated thermal upwelling from Huerta, A.D., Nyblade, A.A., Reusch, A.M., 2009. Mantle transition zone structure beneath Kenya and Tanzania: more evidence for a deep-seated thermal upwelling in the mantle. Geophysical Journal International 177, 1249–1255, which is an updated version from Nyblade, A.A., Owens, T.J., Gurrola, H., Ritsema, J., Langston, C.A., 2000. Seismic evidence for a deep upper mantle thermal anomaly beneath east Africa. Geology 28, 599–602.

Harrison et al., 1992; Molnar et al., 1993) or for the successive surface uplift of external parts of the plateau incorporated into the plateau to produce its present shape (Tapponnier et al., 2001).

Plateaus in compressional settings, such as Tibet and the Andes, are associated with erosion, transport and sedimentation in now highly elevated endorheic sedimentary basins. Forward propagation of the deformation has been proposed as a mechanism for the progressive incorporation of endorheic basins in Tibet (Tapponnier et al., 2001) and in the Altiplano–Puna plateau (Sobel et al., 2003; Strecker et al., 2007). Based on the study of the Pyrenean landscape evolution and experimental modeling of surface processes interaction between rock uplift, erosion, and sedimentation it has been shown that the accumulation of sediments at the foot of mountain ranges produces a rise of the apex of sedimentation, that is, the effective base level for erosion, which in turn inhibits the erosion at high elevation (Babault et al., 2005a, b, 2007). Such processes, combined with the progressive incorporation of internally drained basins, allowed the formation of a low-relief topography in the Tibetan Plateau and in the Altiplano–Puna plateau during and after their rise (Babault et al., 2005a; Liu-Zeng et al., 2008).

#### 5.6.1.6 On the Existence of Past High Plateaus in the Earth History

The demonstration of the existence of past high plateaus requires determining both the paleoelevation and the flatness of large continental areas. This is less easy for past high plateaus that have, by definition, disappeared. Paradoxically, the way they have been destroyed suggests their past existence. Indeed, currently very large areas of continental extension such as the Basin and Range Province are viewed as resulting from the collapse of overthickened crustal welts resembling high plateaus (Coney and Harms, 1984). The intense bimodal magmatism that accompanies extension in such areas is considered as indicative of the partial melting of the thermally relaxed crust and the underlying upper mantle (e.g., Buck, 1991; Dewey and Burke, 1973; Sonder and England, 1989), attesting to crustal thickening and therefore past high elevation of Earth's surface in those areas. But the main reason why this problem is so difficult to resolve relates to the problems of deciphering the paleoelevation of continents.

Paleoelevation is commonly deduced from reconstruction of crustal thickness assuming isostatic compensation, or from paleotemperature estimates through paleoenvironment and stable isotopes studies (see Section 5.6.2). Methods to determine paleoatmospheric pressures allowing the determination of paleoelevation, such as the use of basalt vesicularity are rare (e.g., Sahagian and Proussevitch, 2007; Sahagian et al., 2002a, see Section 5.6.2.5 of this chapter). Whatever the methods used, the results are subjected to debate, mostly because of the great margins of error associated with the methods used in providing paleoelevation estimates.

Coney and Harms (1984) estimated the amount of Tertiary extension in the Basin and Range to be between 40 and 75%. They concluded that the initial crustal thickness could have reached 60 km over a several hundred kilometers width and they suggested that, during the Late Mesozoic–Early Cenozoic times, this area resembled the present-day Tibetan Plateau. However, Coney and Harms (1984) did not provide any information regarding the flatness of this area so that they could not definitively argue the existence of a high plateau. Best et al. (2009) used the compositions of contemporaneous calc-alkaline lava flows as well as the configurations of the ignimbrite sheets to show that the Basin and Range Province during the middle Cenozoic was a relatively smooth plateau underlain by unusually thick crust. In particular, Best et al. (2009) observed that the generally small between-site variations in the palaeomagnetic directions of individual sheets lend further support for a relatively smooth landscape over which the sheets were draped and they conclude that during the middle Cenozoic this area was a relatively flat plateau.

Wolfe et al. (1998) compared the physiognomy of leaves from modern vegetation of known climates with that of Eocene and Oligocene fossil leaf assemblages from middle latitudes of western North America and they concluded that most of the western US and southern Canada was higher in elevation in early Cenozoic time than today. Moreover, where normal faulting has been intense, paleoelevations commonly suggest a subsidence of the region.

Menard and Molnar (1988) have suggested that the Variscan belt of Europe was a 'Hercynian Tibetan plateau' that collapsed into a 'late Paleozoic European Basin and Range Province.' Although most studies on the Variscan belt have concluded that the crust was significantly thickened during the Late Paleozoic, Menard and Molnar (1988) observed that Late Paleozoic sedimentary basins are presently juxtaposed with metamorphic basement rocks. Erosion cannot therefore explain the present-day crust thickness of 30 km. As no pervasive extensional tectonics occurred during the Mesozoic and the Cenozoic, Menard and Molnar (1988) concluded that the thickened crust returned to normal thickness by collapse during the Late Paleozoic, resulting in the exhumation of the deep crust and the concomitant development of sedimentary basins at the surface in a similar way to that of the North American Cordillera, in the western US, during the Cenozoic. Becq-Giraudon and Van Den Driessche (1994) and Becq-Giraudon et al. (1996) have tentatively argued the paleoaltitude of this Variscan belt and its morphology resembled that of a high plateau by looking at the characteristics of the late Carboniferous-early Permian continental sedimentation. In addition, Becq-Giraudon et al. (1996) remarked that the presence of many sedimentary futures such as stratified slope deposits, diamictites, water escape craters and ghosts of ice crystals are related to periglacial effects. The clay mineral assemblage, dominated by the association illite-chlorite-interlayed clays and the absence of significant weathering of feldspathic clasts and granitic pebbles favor the prevalence of a cold to temperate climate during sedimentation. The flora and entomofauna also indicate a seasonally varying climate with cold winters. Furthermore, the extreme homogeneity of the flora composition from one basin to another indicate a lack of appreciable altitude zoning and a plateau-like morphology (Becq-Giraudon et al., 1996). In view of the paleoequatorial position of the Variscan belt during the late Caboniferous-early Permian, Becq-Giraudon et al. (1996) concluded that the

morphology of the chain was that of a near 4500 m asl high plateau.

## 5.6.2 Evidence for Plateau Uplift, Regional Warping, and Subsidence

### 5.6.2.1 Geomorphic Markers

#### *5.6.2.1.1 Low-relief, high-elevation erosional surfaces*

A striking feature of high plateaus' margins is the occurrence of deeply dissected, almost flat topographic remnants at high elevation. As mentioned above (Section 5.6.1.5) and following Davis's cycle of erosion (1899), a smooth landscape generates from the destruction of a previous smooth landscape uplifted and then progressively more dissected and characterized by steeper slopes. This is followed by successive stages, with a decrease in slope gradients associated with the decrease of the elevations near to sea level. Based on these views, rock uplift is usually deduced from the elevation of more or less localized changes in the local slopes that separate a subdued relief above, also called a relict landscape (for a summary see Widdowson, 1997), from a steeper one below (e.g., Clark et al., 2006; Epis and Chapin, 1975; Gregory and Chase, 1994; Kennan et al., 1997).

Following Powell (1875), a stream cannot erode below its base level, which is the lower limit in the landscape and is ultimately represented by sea level. If the process of formation of low-relief erosional surfaces follows Davis' model, the key point to infer rock uplift from highly elevated remnants of low-relief erosional surfaces lies in the assumption that they formed close to sea level. Such assumption is however almost never demonstrated in orogens and plateaus because of the destructive nature of erosion or the lack of marine sedimentation on the low-relief erosional surfaces. Consequently, where it cannot be demonstrated that low-relief erosional surfaces developed close to sea level, it cannot be ruled out that a smooth landscape may have developed well above sea level. Within continents, if an erosional smooth landscape is 1000 km away from its base level and that the formational regional slope is 0.0057° ($10^{-4}$) or 0.057° ($10^{-3}$) then a low-relief erosional surface can develop 100 to 1000 m above its base level.

An alternative model of planation is that of parallel scarp retreat by backwearing of slopes (King, 1953). As that of Davis, in King's model a discontinuous surface uplift is responsible for the high elevation of a smooth landscape that starts to develop near the sea level. The plateau successively expands just above sea level by river incision, scarp retreat, and the formation of pediments at its base. Ongoing erosion creates pediments that coalesce to form a pediplain. A next surface uplift will promote a new planation surface near to sea level. However, ongoing lateral erosion of the first pediplain occurs above sea level and is disconnected from the younger pediplain by an escarpment. Pediments are broad, concave-up and sloping at an angle of 6–7° at the base of the retreating escarpment, whereas pediplains are inclined gently (commonly thought to be less than 1° although never demonstrated) toward the sea level. As a consequence, low-relief erosional surfaces developed in this way form near to sea level only close to the coast line. Such considerations imply that rock uplift cannot be deduced from their elevation alone, a correcting factor must take into account for the regional slope of erosion down to the coast.

Drainages of mountains and plateaus are not always open to the sea. Where streams flow into closed basins (endorheic basins), their base level is considered to be the basin floor or the terminal lake. In the Andes or in Tibet, for example, highly elevated endorheic basins cover extensive areas setting the base level for their streams at high elevation. But long-term landscape evolution of mountain belts argues for the apex of sedimentation in foreland basins to be the effective base level for erosion below which no erosion occurs on the long-term (Babault et al., 2005a, b; Carretier and Lucazeau, 2005), instead of a coastline or a lake's shoreline where drainages are opened or closed, respectively. Babault et al. (2005a, b) and Carretier and Lucazeau (2005) considered that it is not so much the ultimate base level of stream waters but the transport capacity of rivers, in controlling the long-term limit between the erosion and deposition, that sets the effective base level for erosion. In such a case, slopes and concavity of the rivers, of the alluvial and of the fluvial fans, control how high the elevation of the apex of sedimentation stands above the coastline or the terminal lake. Gradually over time, the aggradation of the products of erosion raises the base level when a sedimentary basin is overfilled, whether its nature is endorheic or not (Babault et al., 2005a). However, the apex of sedimentation, the effective base level in an endorheic basin can be expected to be always higher than that of a basin opened to the sea.

Davis' cycle of erosion in which a landscape is smoothed close to sea level can therefore be valid at high elevation whether drainage is endorheic or not, at least but not necessarily provided that tectonic uplift has ended (Babault et al., 2007). The same is true for the formation of stepped pediments in continental and internally drained areas like those of the Iberian range in Spain (e.g., Casas-Sainz and Cortes-Gracia, 2002). The corollary of this conclusion is that where remnants of low-relief erosional surfaces are bounded by overfilled sedimentary basins, smoothing might have occurred well above sea level. In such geological settings, rock uplift cannot be inferred from the elevation of remnants of low-relief erosional surfaces alone (Babault et al., 2005b, 2007). The paleoelevation of the apex of sedimentation as well as the distance from it and the fluvial paleogradient must be taken into account to infer rock uplift from smooth relict landscapes. Another requisite to infer rock uplift from relict landscapes is the slow long-term erosion rates of the remnant surfaces (e.g., Clark et al., 2006). High erosion rates of the remnant surfaces would lead to an underestimation of the rock uplift.

It is important to note that the above considerations of landscape evolution allow the inferring of rock uplift, but in most cases not surface uplift. When a high-elevation, low-relief landscape is incised by the modern fluvial system, surface uplift is always lower than rock uplift (Molnar and England, 1990). Another important point to underline is that the erosionally driven unloading of the crust induces a flexural isostatic rebound at the regional scale. Consequently, a fraction of the measured rock uplift has to be attributed to the isostatic response of the missing masses, whereas the

remaining fraction has to be linked to one or more deep processes in the crust or in the mantle (e.g., Abbott et al., 1997; Leonard, 2002; Roy et al., 2009).

In the Andes, ~2000 m of rock uplift have been deduced from the study of channel longitudinal profiles and in particular the reconstruction of past longitudinal profiles in the eastern Cordillera of Bolivia based on low-relief paleosurface remnants (Kennan et al., 1997). As defined above, uplift of low-relief paleosurface remnants, now incised by the current drainage network, is rock uplift and not surface uplift. In their topographic reconstruction at ~10 Ma, Kennan et al. (1997) obtained a downstream profile ranging from 500 to mostly 1500 m in elevation. Such results argue for the low-relief erosional surfaces of Bolivia to have developed above 500 to 1500 m depending on their distance from the coastline, ~25 to 325 km, respectively. Barke and Lamb (2006) reconstructed the paleoprofiles of the Eastern Cordillera using values of concavity and steepness (see Section 5.6.2.1.4) and they obtained a more accurate estimate of rock uplift at $1705 \pm 695$ m.

In the eastern Tibetan Plateau, Clark et al. (2006) deduced a minimum of 3000 to 4000 m surface uplift of the highest parts of the southeastern Plateau from the elevation of remnants of a high elevation, low-relief surface. Clark et al. (2006) based their reasoning on the low values of erosion (0.01–0.02 mm $yr^{-1}$) of remnant surfaces to argue that rock uplift can be deduced from relict landscape elevations, assuming a paleoslope to the east ranging between 0.0057° ($10^{-4}$) and 0.057° ($10^{-3}$).

#### 5.6.2.1.2 Drainage network development and reorganization on a plateau

Although drainage development and reorganization might be complex in some cases it can be used to unravel the tectonic evolution of a region. Uplift influences drainages via baselevel changes, drainage reversals, and capture processes. The dictum 'Drainage systems have a heritage rather than an origin' (in Summerfield, 1991, Chapter 16) summarizes well the constant interaction between tectonics, erosion, and deposition. This view is opposed to an old and unrealistic one that considers that a drainage network originally grows on an initial slope before channels adapt their course to structure. Although drainage does not generally start to develop on a flat, gently sloping topography, overfilling of landscapes by lava flows or sediments can lead to a smoothing of the local relief and to the resetting of a previous channel network. The incorporation in an orogen of a drainage network newly formed in an overfilled foreland basin could, however, explain the similarity of network geometry in orogens (Castelltort and Simpson, 2006).

Where the local relief is low, a trunk of a gently sloping river can be reversed by only a slight regional tilt of the topography. This occurs only if the rate of incision downstream of that trunk cannot balance the rate of rock uplift. Plumes generate dome-like plateaus and consequently they can trigger a modification of the drainage network associated with drainage reversals and captures that eventually lead to a radial drainage (Cox, 1989). Later, such drainage can be more or less captured by a structurally controlled drainage that develops in a rift valley superimposed on the domal plateau like that of the East African plateau (Cox, 1989; Moore and Blenkinsop, 2002). The result of the channel network reorganization is a barbed drainage pattern with junction angles greater than 90°, see Figures 12.7 and 16.9 in Ollier (1981) and in Summerfield (1991), respectively.

Rock uplifts of plateaus induce a gain in potential energy that enhances the stream power (e.g., Whipple and Tucker, 1999) of the surrounding channels. Consequently, internally drained areas with higher local base level are expected to be captured by external transverse drainages with lower base level and located on rims of plateaus. If so, stream piracies can provide evidence of plateau uplift. Captures can be identified by a series of drainage patterns and deposits that indicate poorly–integrated drainage. These include the occurrence of hanging valleys with wind gaps in the drainage divide, and wind gap sediments (if preserved) in the headwaters of a beheaded river, elbows of capture, and a river paleoflow direction different than present flow direction (see Douglass et al., 2009, for a compilation of the various criteria). Drainage reorganization by captures have been used to indicate surface uplift in the southeastern Tibetan Plateau margin (Clark et al., 2004) and in the Anatolian plateau (Nicoll, 2010).

#### 5.6.2.1.3 River longitudinal profiles: Steepness indices

Rock uplift increases the potential energy and triggers an increase in the stream power (e.g., Whipple and Tucker, 1999). Consequently, the increase in incision modifies the streams' morphologies, first at the rims of a plateau and eventually inside the plateau. The downstream slopes of rivers increase and in most cases knickpoints develop (Whipple and Tucker, 1999). Local slopes are not the only variable in bed morphology that rock uplift can potentially modify; channel width, (e.g., Whittaker et al., 2007) and sinuosity (among others) can also be affected and in turn they can change the relationship between local slopes and rock uplift (See Wobus et al., 2006, for a review). However, a relation between rock uplift and downstream slopes has been highlighted in many different natural landscapes. In the following the authors summarize the methodology developed to derive rock uplift from digital elevation models, which is based on the empirical power-law that relates the downstream slope in a river bed to the contributing drainage area (Flint, 1974; Howard and Kerby, 1983):

$$S = k_s A^{-\theta}$$

where $S$ is the local downstream slope, $A$ is the upstream drainage area, $\theta$ is the concavity index and $k_s$ is the steepness index. Studies in California (Snyder et al., 2000) and in the Siwalik Hills in front of the Himalaya (Wobus et al., 2006) demonstrated a positive correlation between the steepness indices of a set of channels with comparable morphologies (normalized to a common concavity index), and spatially uniform rock uplift rates encompassing each drainage basin. In these studies, steady-state conditions are assumed, that is, rock uplift is everywhere balanced by erosion. Inference of rock uplift rates using steepness indices derived from digital elevation data requires first a calibration area with known uplift rates and similar channel morphologies. If not, the spatial variability of steepness indices provides at least a high spatial resolution estimate of the rock uplift pattern

(Hodges et al., 2004; Wobus et al., 2003). Special care must be taken in the interpretation of steepness indices as a proxy for rock uplift rates. Rock uplift rates not only modify the local slopes leading to a simple relation between steepness indices and uplift rates. Steepness index depends also on other factors (e.g., Whipple, 2004; Whipple and Tucker, 1999) including rock strength (erosivity), sediment flux (tools for erosion or cover of the bedrock that inhibits erosion), channel width, drainage basin hydrology, river incision process(es) (plucking, abrasion, and weathering) and critical shear stress for incision. For example, where the pattern of the channel width, $W$, with respect to the cumulative drainage area, $A$, varies downstream in a different fashion from that commonly assumed, $W = 0.35A^{0.5}$ (Montgomery and Gran, 2001), steepness indices may not reflect rock uplift rates. Fluvial erosion is commonly understood to scale with bed shear stress and water flow velocity. Both variables depend on the local slope and on the channel cross-sectional geometry. Consequently, local channel width and water depth modifications can strongly alter the relationship between steepness indices and rock uplift rates (e.g., Whittaker et al., 2007). That some of the parameters listed above might be expected to vary with tectonic rates and consequently alter the significance of the steepness index, it is not the only limitation to use it as a proxy for rock uplift rates. It is important to note that some of the parameters listed above vary with lithology and climate. However, local significant variations of steepness indices values are thought to reflect changes in rock uplift rates, where the spatial variations of the factors listed above are negligible (Wobus et al., 2003).

In the eastern Tibetan Plateau, this method has been used to infer the distribution of active rock uplift (Kirby et al., 2003). However, since the obtained steepness indices are assumed to relate to the rates of rock uplift, no total amount of rock uplift can be derived from this method alone until the duration of the considered tectonic event is known.

#### 5.6.2.1.4 Longitudinal paleoprofile reconstruction of rivers

The total amount of rock uplift can be deduced from the reconstruction of a river's paleoprofile. Two methods can be used based on the longitudinal profile equation and paleomarkers of the river longitudinal profile such as river terraces.

The first method relies on the study of a series of rivers characterized by segments bounded by a knickpoint. First, it is assumed that an increase in fluvial incision in response with a sudden base level fall, or an increase in the rate of a base level fall (conceptually equivalent to an increase in rock uplift), propagates upward along a channel and is associated with a knickpoint that separates an unmodified upstream part from a downstream segment that adapts its slopes to the new boundary conditions imposed by the new rock uplift rate (e.g., Whipple and Tucker, 1999). Second, it is assumed that the upstream part corresponds to a river profile that is adjusting or adjusted to a prior state of base level fall. Third, incision rates in the upstream part above the knickpoint must be slow, a condition matched under dominated semiarid to hyperarid climate conditions as indicated by the preservation of transient landscape, such that profile lowering is negligible and the inferred rock uplift is not underestimated. Under those assumptions an empirical power-law gradient–area relationship can be used (Flint, 1974; Howard and Kerby, 1983) along with the well-known relationship between downstream distance, $x$, and cumulative drainage area (Hack, 1957) to reconstruct a river paleoprofile from the equation of a longitudinal river profile elevation, $z(x)$, in two dimensions (Whipple, 2001; Whipple and Tucker, 1999):

$$z(x) = k_s k_a^{-\theta}(1 - h\theta)^{-1}(L^{1-h\theta} - x^{1-h\theta}) + z(L); \quad h\theta \neq 1; \quad x_c \leq x \leq L$$

where $z$ is the elevation, $x_c$ is the distance from the division to the channel head, $L$ is the distance of outlet from source, $k_s$ is the steepness index, $\theta$ concavity index, $k_a$ is Hack's coefficient, and $h$ Hack's exponent. The river paleoprofile is obtained from a fit of the longitudinal river profile elevation equation, $z(x)$, to the preserved paleoprofile in the upstream parts. The difference in elevation between the reconstructed profile set high up and the modern downstream segment at the outlet elevation provides an estimate of the rock uplift even if it is not spatially uniform (e.g., Hoke et al., 2007).

In the Andes, at least 1000 m of relative rock uplift of the Western Cordillera and adjacent central Andean plateau with respect to the Central Depression, located between the Pacific coast and the Western Cordillera, has been deduced using this method (Hoke et al., 2007). Based on perched paleoprofiles near to the Pacific Coast, Hoke et al. (2007) also proposed that the Central Depression could have undergone a rock uplift of 1000 m. If this interpretation can be confirmed by another proxy, and if the Central Depression is not tectonically decoupled from the Altiplano, then ~2000 m of rock uplift of the Western Cordillera and adjacent central Andean plateau can be deduced from the paleoprofiles reconstruction. Using a similar approach, 2000–2700 m of rock uplift have been estimated for the Eastern Cordillera at the eastern edge of the paleodrainage systems that drained the Eastern Cordillera as indicated by the paleosurface remnants and the associated fluvial deposits (Barke and Lamb, 2006). Barke and Lamb (2006) also inferred rock uplift from upstream propagation of the modern river profile and its difference in elevation with respect to the paleosurface remnants, and the heights above the foreland basin of the knickpoints that separate the paleodrainage system from the modern downstream profiles. From the combination of all these measures they obtained a value of $1705 \pm 695$ m for rock uplift for the eastern edge of the Eastern Cordillera.

In the eastern margin of the Tibetan Plateau, Schoenbohm et al. (2004) calculated the Red River incised ~1400 m in the regional low-relief landscape from the paleoprofiles of a series of perched tributaries above the Red River. Since the paleoprofile of the Red River is estimated at 1500 m and considering that it has risen from 0–100 m, sea level and present day elevation respectively, they deduced a value of 1400–1500 m for surface uplift in the Red River region (Yunnan Province of China).

The second method to derive an amount of rock uplift is based on paleomarkers of the river profile such as river terraces. The strong assumption is that rock uplift is balanced by river incision (e.g., Burbank et al., 1996). However, such assumption is difficult to demonstrate in most cases, and because river incision is not only a response to rock uplift, then

this method has to be validated by other data. For example, climate can be responsible for incision in the piedmont leading to a fall of the base level, which results in an upstream propagation of incision in the mountainous area without any change in rock uplift (e.g., Carretier and Lucazeau, 2005). Upstream integration of drainage areas by river network growth also leads to deep incisions in the downstream parts of a longitudinal profile (e.g., Carretier et al., 2009; Vassallo et al., 2007). In both cases paleoriver profiles will overestimate rock uplift.

#### 5.6.2.2 Paleoaltimetry from Sedimentology

To understand the continental tectonic processes responsible for surface uplift, and to understand how the feedbacks between such tectonic processes and climate and erosion processes modify the surface uplift, the appropriate paleoaltimetric methods need to be used. As pointed out by Clark (2007), a need exists to assess the paleo-mean elevation of region, not only the local paleoelevation. This comes from the fact that, although an increase in local elevations, local relief or drainage basin relief can be associated to some rock uplift, it does not necessarily indicate a surface uplift (an increase of the mean elevation) (Molnar and England, 1990).

##### *5.6.2.2.1 Paleoaltimetry from marine sediments*

The easiest way to infer rock uplift is from the elevation of the youngest shallow marine sediments preserved in the studied region (including eustasy). The choice of mapping the youngest strata instead of an older strata preserved everywhere has the advantage to minimize the underestimation of rock uplift when the upper limit of the marine unit is partially eroded (e.g., Pederson et al., 2002). Any localized incision or spatially homogenous erosion into these marine sediments implies that a fraction of the rock uplift is to be attributed to the erosionally driven isostatic rebound. As a consequence the deduced rock uplift does not match the necessarily lower surface uplift. An important constraint for any tectonic model of plateau uplift can be deduced from the surface uplift rate. However, the ratio between the elevation and the age of the youngest shallow marine sediments only gives a minimum estimate of the mean rock uplift rate since a time-lag can exist between the depositional age and the subsequent rock uplift. In the following the authors show two examples of surface uplift deduced from marine strata.

In the Colorado Plateau, the Late Cretaceous landscape reconstruction represents the last known time surface elevation. Based on the widespread distribution of the Late Cretaceous shallow-marine and coastal sediments, Roy et al. (2009) estimated the Colorado Plateau underwent ~1.9 km of rock uplift using data from the previous work of Pederson et al. (2002) and taking into account that the Late Cretaceous sea level was 200 to 250 m higher than today. Roy et al. (2009) estimated ~0.5 km of net erosion (erosion minus sedimentation) during the Cenozoic, taking into account the amount of erosion of the Late Cretaceous marine sediments and the amount of preserved younger continental deposits and volcanic rocks. To the rock uplift associated with erosional-unloading, Roy et al. (2009) added the flexural response of the plateau to the tectonic unloading at the plateau margins where extension took place during the Cenozoic (Basin and Range and Rio Grande Rift). They obtained ~0.5–0.6 km and ~1 km of rock uplift associated with crustal unloading (erosion and extension) at the center of the plateau and at the edges, respectively. They deduced that >1.6 km of the remaining mean rock/surface uplift must be explained by tectonic processes that occurred during the Cenozoic. In summary, widespread evidence of sea level or slightly below sea level paleoelevations are very useful where preserved to deduce rock and surface uplift.

The Andes were also at sea level during the Cretaceous such that the surface uplift of the Altiplano must have been later (e.g., Hoke and Garzione, 2008). In contrast, on the southern Tibetan Plateau, Fielding (1996) deduced 5 km of surface uplift from Cretaceous marine limestone deposited in the Lhasa block (Hennig, 1915; Norin, 1946). As Fielding (1996) noticed, it is difficult to generalize the paleoelevation of an extensive region like the Tibetan Plateau from just a small part of it, given that Tibet results from the accretion of several crustal blocks and volcanic arcs associated with oceanic subduction under the southern margin of Asia before the collision. If the Andes are a contemporary analog of what Tibet was like before the collision between India and Asia, then mean elevations were probably well above the sea level, at least in some part of it (Fielding, 1996). Consequently, the 5 km surface uplift since the Cretaceous (Fielding, 1996) might be an overestimation when applied to the whole of Tibet.

##### *5.6.2.2.2 Paleoaltimetry from paleohorizontality of lacustrine sediments*

Some shallow lake deposits form in flat regions where they can be used to deduce differential rock uplift. Changes in elevation between deposits of the same age and of the same facies that cannot be accounted for by any variation in depositional depth indicate relative rock uplift. South of the Eastern Moroccan Atlas belts and plateau, the remnants of the lower Pliocene shallow lacustrine sedimentation closer to the Atlas lie at ~1200 m asl and the more distant at ~600 m asl. The ~600 m difference of elevation have been inferred by Babault et al. (2008) as a postdepositional tilting to the south indicating up to ~600 m of relative rock uplift of the southern margin of the Atlas since the early Pliocene. If the lake deposits are assumed to have not undergone subsidence and the elevation of the lower deposits is considered to have remained the same, such estimate corresponds to minimum rock uplift.

##### *5.6.2.2.3 Paleoaltimetry from paleoslopes: Large-scale patterns of deposition*

Postdepositional changes in slope can also be determined from fluvial sediments or erosional landforms.

Since slopes in braided rivers are generally less than 1.14° (Paola and Mohrig, 1996) then greater slopes can be used to deduce a tilt of such depositional surfaces. Moreover, paleoslopes can be back calculated in order to quantify more accurately the amount of tilting. The method is based on the assumption that the basal shear stress at bankfull stage has to be higher than the critical shear stress required to transport the coarsest clast (Paola and Mohrig, 1996). The paleoslope is

then derived from measuring the median clast size in channel scours and the depth of such ancient channels of preserved coarse-grained braided rivers. Errors from this method come from the underestimation of the paleodepth resulting in an overestimation of the paleoslope by 30 – 40%, and from the underestimation of the surface grain size leading to an underestimation of the paleoslope by 30 – 40%. Paola and Mohrig (1996) compared estimated values of slopes from their formula to the actual slopes of modern braided rivers and they show that the error in the estimated slopes is about a factor of 2.

McMillan et al. (2002) have shown that the paleoslopes to the east of the Rocky Mountains piedmont, estimated using the method of Paola and Mohrig (1996), ranged between ~0.006° to ~0.06° during the Miocene–Pliocene and that they have been subsequently increased up to ~0.6°. The Great Plains are connected to the Rocky Mountains that are themselves connected to the south to the Colorado Plateau and defined the Rocky Mountain orogenic plateau (McMillan et al., 2006). As a consequence, the regional rock uplift associated with the tilt to the east observed in the Great Plains over 250 km has then been used to infer 680 m (410–815 m) of regional rock uplift that affected the whole Rocky Mountain orogenic plateau (McMillan et al., 2002).

The same concept has been roughly applied to the western flank of the Western Cordillera in the Andes of Chile. Based on the models of Stanistreet and McCarthy (1993), the depositional slope of the Oligocene–Miocene braided fluvial fan that mantle the Paleozoic basement of the Precordillera of northern Chile, in the western flank of the Altiplano have been assumed to be less than 1°. Today these piedmont sediment dips varies between 2° and 4° to the West and such westward tilts have been used to infer a post-10 Ma rock uplift of the Western Cordillera (Mortimer, 1973; Riquelme et al., 2003) ranging between 500 and 1400 m (Farías et al., 2005).

#### 5.6.2.2.4 Grain size distribution in piedmont sedimentation

If it is assumed that an increase in rock uplift of the upstream mountainous areas induce both a change in the sedimentary flux that enters the basins from the rivers draining the rim of a plateau and the slope of the streams, then a change in facies can be expected from fined-grained sediments to clasts and boulders as well as higher sedimentation rates. However, erosion and transport also depend on water discharge, which is subject to changes throughout the history of plateau building in response to regional or global climate changes (e.g., Blackstone, 1975; Frostick and Reid, 1989). Consequently the relation between grain size and rock uplift is not straightforward (e.g., Molnar and England, 1990) and overall, the method does not allow any quantification of either rock uplift or surface uplift.

A change in depositional facies in the northwestern Tibetan Plateau and southern margin of the Tarim basin is interpreted as a response to a main rock and surface uplift of the Kunlun Mountains with respect to the Tarim basin (Zheng et al., 2000). The shift from distal alluvial fan or flood-plain environments to proximal debris-flow accumulation is associated with an increase in sedimentation rate from an average ~0.15 mm $yr^{-1}$ to 1.4 mm $yr^{-1}$, as well as growth strata (Zheng et al., 2000). Such association of increase in grain size, as well as sedimentation rate can be interpreted as the evidence for the main rock/surface uplift of the northwestern Tibetan Plateau (Zheng et al., 2000).

### 5.6.2.3 Paleoaltimetry Data Based on Paleobotany

Three methods that analyze plant physiognomy have been proposed to infer paleoaltimetry. Two of them use floras (1) to estimate temperature then divided by lapse rate (the rate of temperature change with elevation) to give an elevation, and (2) to estimate enthalpy that is combined with gravitational acceleration to deduce an elevation. The third method uses stomatal frequency in leaves to deduce changes in $CO_2$ partial pressure, which is a function of elevation.

Within the first method, paleotemperatures from fossil floras, three fundamentally different approaches are used (see Meyer, 2007, for a review). The first two are based on the climatic distribution of nearest living relatives (or the floristic method), and on the correlation of plant physiognomic characters with climate. The third differs by the way the lapse rates can be utilized to derive a paleoelevation. Most of the current methods use the plant physiognomic method rather than the nearest living relatives, which is believed to be less accurate. Following the work of Bailey and Sinnott (1916) that demonstrate that leaf margins correlate with climate in modern floras, the plant morphological characters used in the physiognomic method include leaf size and the presence or absence of teeth. An extensive database called the Climate-Leaf Analysis Multivariate Program (Wolfe, 1993, 1995; Wolfe and Spicer, 1999) relates many physiognomic characters of leaves from modern forests to climate variables (e.g., untoothed leaf margins correlate to warm mean annual temperature and large leaf size correlates to high levels of moisture). The main results of the Climate-Leaf Analysis Multivariate Program is that the mean annual temperature is the most accurate climatic parameter estimated ($1\sigma$ error $\leq 1$ °C). Giving that temperature change varies with elevation, continentality, and the effect of broad uplifted land surfaces, three different lapse rates exist depending on the spatial scale considered with values ranging between 3 °C $km^{-1}$ in the regional (between the coast and the continental interior of a continent) lapse rate method (Wolfe, 1992a), 5.5 °C $km^{-1}$ in the global mean terrestrial lapse rate (e.g., Axelrod, 1966), and 3.64 to 8.11 °C $km^{-1}$ in the local lapse rate method (e.g., Meyer, 1992). Almost the double of palaeoelevation estimate can be derived from the regional instead of the global lapse rate, highlighting the major impact lapse rate has on the paleoelevation calculations.

Global climate changes through time imply that the mean temperature at a given altitude does not remain constant. As a consequence, paleotemperature estimates at a given locality must be compared to paleotemperature estimates at sea level for isochronous floras. The late Eocene Florissant flora of central Colorado is a good candidate to estimate the error of the different methodologies employed to deduce paleotemperature from fossil floras and paleoatlimetry from lapse rates methods since it has been studied by many workers using one or more of these methods (Meyer, 2007). Excluding low elevation estimates (455 m) derived from the global

lapse rate method (Axelrod, 1998) the estimates of paleoelevation range between 1900–3200 m (Meyer, 1992) and 1900–2300 m (Gregory, 1994; Gregory and Chase, 1992; Gregory and McIntosh, 1996) for the local lapse rate method and values of 2900 m asl (Wolfe, 1992b) and 4133 m asl (Wolfe, 1994) are obtained using the regional lapse rate method. All these studies lead to a high to very high paleoelevation range of $3000 \pm 1100$ m asl. In the second method, paleoelevation from fossil leaves is obtained from the moist static energy, $h$ ($J\,Kg^{-1}$) (Forest, 2007; Forest et al., 1995, 1999). In the mean annual temperature method, present lapse rates are transferred to past climate with no meteorologically sound physical basis and such empirical lapse-rates with large spatial variations (Meyer, 1992; Wolfe, 1992a) are used to infer paleoelevation leading to estimates that can vary by a factor of two. Unlike the mean annual temperature method, the aim of the moist static energy method is to quantify a variable with a theoretically and by observation, well-constrained behavior with altitude and longitude. At mid-latitudes the mean flow of the atmosphere is from west to east. Since moist static energy is conserved along air masses it is also generally constant across a region with longitude. Finally, moist static energy is constrained by thermodynamics such that

$$h = c_p' T + L_v q + gZ,$$

where $c_p'$ is the specific heat capacity at constant pressure of moist air, $T$ is the temperature (in K), $L_v$ is the latent heat of vaporization for water, $q$ is the specific humidity, $g$ is the gravitational acceleration, $Z$ is altitude, and

$$H = c_p' T + L_v q,$$

where $H$ is moist enthalpy.

Assuming that $h$ is invariant within the same latitudinal band, if we can estimate the enthalpy at sea level and at a site of unknown elevation $Z$ for a particular latitude, then such elevation is given by (Forest, 2007; Forest et al., 1995, 1999)

$$Z = \frac{H_{\text{sealevel}} - H_z}{g}.$$

Both enthalpy estimates are derived from fossil leaf assemblage with the Climate-Leaf Analysis Multivariate Program. The total expected error in this method comes from two sources of error (Forest, 2007; Forest et al., 1999): (1) from the standard deviation from zonal invariance (the longitudinal variability) of $h$ (yielding a minimum estimate of the error in altitude of 460 m); and (2) from the uncertainty in predicting mean annual enthalpy from fossil leaf physiognomy (yielding 560 m of uncertainty in altitude). Forest et al. (2007, 1999) estimated the paleoelevation difference between two isochronous fossil assemblage sites is $\pm 910$ m assuming that the expected errors apply to past.

Recently, Peppe et al. (2010) argued that many sources of large potential error are related to this method. Specifically, they demonstrated a significant bias toward underestimation of leaf area in the Climate-Leaf Analysis Multivariate Program data set affecting all predicted climatic variables such as enthalpy, leading to an uncertainty in mean annual enthalpy higher than that predicted by Forest et al. (1999). Errors in paleoelevation estimates when the leaf size bias is included are $\pm 2000$ m or more. Peppe et al. (2010) concluded that among others, this bias affects previously published paleoelevations inferred by this method and that such paleoelevations are unlikely to be accurate either in magnitude or estimated error (e.g., Forest et al., 1995; Gregory-Wodzicki, 1997; Spicer et al., 2003; Wolfe et al., 1997, 1998).

The third method is based on the stomatal frequency change over altitudinal gradients (Kouwenberg et al., 2007; McElwain, 2004). Atmospheric pressure decreases with altitude and is shown to depend on the molecular weight of air, elevation, acceleration due to gravity, the gas constant and mean July temperature (Jones, 1992). $CO_2$ partial pressure is a fraction of the atmospheric pressure that does not vary with altitude (Gale, 1972). The globally averaged atmospheric pressure at sea level has not changed significantly over the Cenozoic and the available estimates of molar volume of $CO_2$ at sea level are sufficiently accurate for the Cenozoic. Consequently, the $CO_2$ partial pressure at any elevation is a function of the $CO_2$ partial pressure at sea-level and the atmospheric pressure divided by a constant (Beerling and Royer, 2002; McElwain, 2004; McElwain et al., 2002). McElwain (2004) shows an inverse relationships between stomatal density of plant leaves and the $CO_2$ partial pressure, converting the stomatal density into a potential tool to infer paleoaltimetry, independent of ecological or local climatic variability. This is true for many species but not all. Therefore the sensitivity of the selected fossil leaves needs to be tested as well as the response limit to high or low $CO_2$ partial pressure due to morphological and physiological constraints (Kouwenberg et al., 2007). This method applies to extant floras since stomatal density of modern leaves of same or close to the fossil species need to be calibrated to $CO_2$ partial pressure or elevation (Kouwenberg et al., 2007). McElwain (2004) obtained a $\pm 300$ m of average error. However, Kouwenberg et al. (2007) highlighted other types of errors such as the light intensity-related uncertainties due to mixture of sun and shade leaves and varying for different species, and from uncertainties in exact sea-level $CO_2$ concentrations. For the species studied by McElwain (2004) and Kouwenberg et al. (2007) estimated errors related to the light intensity give error ranges of 162 and 558 m whereas errors introduced in estimating sea-level $CO_2$ from proxy data when sea-level $CO_2$ estimates on the same species are not available, hypothetically range between $\pm 450$ m and $\pm 1200$ m and could increase to $\pm 1400$ m (Kouwenberg et al., 2007). When the uncertainty in sea-level $CO_2$ estimates is high, such method is not better than the others based on paleobotany, whereas it is the best one when sea-level $CO_2$ estimates from proxies are accurate or modern low-elevation leaf of extant species available (Kouwenberg et al., 2007).

In summary, the paleoelevations inferred in the Rocky Mountain orogenic plateau from paleobotanic methods indicate the plateau was already high in the late Eocene but the accuracy of such estimates are low, more than $\pm 1100$ m, and the many factors that influence the character of the flora prevent a reliable estimation of the accuracy of the paleoelevation. The new paleoaltimetric method based on stomatal frequency and stomatal index may be a good alternative in the

particular cases where the uncertainty in sea-level $CO_2$ estimates is low.

In the case of the Altiplano–Puna plateau of the Andes, paleoelevation estimates from fossil floras (nearest-living-relative and foliar-physiognomy methods) now lying at 4000 to 4300 m asl argue for low elevations at 1000 m asl in the early Miocene (25 to 19 Ma) and ranging from 0 m to 2800 m asl in the mid Miocene ($\sim$20 to $\sim$10 Ma) but with large uncertainties ranging from $\pm$1200 to $\pm$2000 m (see Gregory-Wodzicki, 2000 for a review).

#### 5.6.2.4 Paleoaltimetry Data Based on Stable Isotopes

##### 5.6.2.4.1 Paleoaltimetry data based on the stable isotopic records ($\delta^{18}O$ and $\delta^{2}H$) of carbonates derived from meteoric and surface waters

Empirical and theoretical approaches have used the $\delta^{18}O$ and the $\delta^{2}H$ to deduce paleoelevation estimates. The condensation of water vapor driven by the ascension of regional winds along orographic obstacles creates a fractionation of H and O in atmospheric water vapor, rainfall, and snowfall. At the equilibrium water-vapor transformation, heavy isotopes ($^{18}O$ and $^{2}H$ (D)) are removed from water vapor because they form stronger bonds than those formed by lighter isotopes ($^{16}O$ and $^{1}H$) which are more likely to break and to remain in the gas phase. Consequently, rainfall is enriched in heavy isotopes, whereas continuing rising air is depleted in heavy isotopes and the observation of decreasing in $\delta^{18}O$ and $\delta^{2}H$ values in rainfall as elevation increases has been used as a proxy for paleoelevations.

Rowley et al. (2001) and Rowley and Garzione (2007) have presented a theory that tracks the change in oxygen isotopic composition of precipitation based on the equilibrium fractionation during Rayleigh distillation coupled with the thermodynamics of atmospheric ascent and water vapor condensation. In their model, however, the complex processes involved in the conversion from condensate to precipitation and its influence on isotopic compositions is based on an empirical relationship (based on data from the Alps). They show that low-elevation temperature primarily controls the vertical distribution of condensation whereas low-elevation relative humidity only results in a small contribution. The low-elevation temperature, especially, and to a lesser degree the relative humidity, consequently control the vertical distribution of the difference in isotopic composition ($\Delta(\delta^{18}O)$) between a low, preferably near sea level, composition of meteoric water and a potentially elevated sample of meteoric water. Their model fits well with the modern vertical profiles of $\delta^{18}O$ in precipitation (Rowley and Garzione, 2007). Hence, they theoretically demonstrate that $\Delta(\delta^{18}O)$ can be used as a measure of elevation with a greater accuracy of the modeled elevations at higher elevations, and a general tendency of the modeled elevations to be underestimated. Where the low-elevation temperature and the relative humidity of local climate is used, instead of global means, the model is also more accurate (Rowley and Garzione, 2007).

Studies that track paleoelevation changes through geological times generally use carbonates derived from surface of ground waters that integrate precipitation waters. The quantity of precipitation varies along months and seasons with precipitations of different isotopic compositions. It explains why the mean isotopic composition at any given station is precipitation amount-weighted. Streams also spatially integrate precipitation above the sample site with isotopic compositions that vary with elevation. But the frequency of elevations within a catchment (the hypsometry) is not a linear function and must be computed individually. Furthermore, the amount of precipitation also varies as a function of elevation (Anders et al., 2006; Rowley and Garzione, 2007). Consequently, the isotopic compositions of surface water reflect the amount of precipitation falling as a function of elevation on that hypsometry: the precipitation amount-weighted hypsometric mean elevation of Rowley and Garzione (2007). An important conclusion is that the isotopic lapse rate of precipitation and that determined by surface waters are expected to be different (Rowley and Garzione, 2007).

In the following, important advantages, restrictions and uncertainties inherent of the methods, and highlighted by Rowley and Garzione (2007), are briefly summarized.

First, since the resulting paleoelevation corresponds to the precipitation amount-weighted hypsometric mean elevation, it does not give any information on the distribution of drainage basin elevations and particularly on the maximum elevations. For that reason estimates of paleoelevations from low-elevation samples of fluvial origin taken in foreland basins cannot discriminate between plateau-like topographies and rugged mountains, both implying different tectonic implications. Intermontane basins at higher elevations are then considered to be better targets to reduce the effects of the hypsometric and elevation dependence (e.g., Garzione et al., 2006; Ghosh et al., 2006b).

Second, past climates were globally warmer than today leading to a shallower isotopic lapse rate, which means that the use of modern isotopic lapse rate underestimates paleoelevations in the cases past-climates were really warmer.

Third, evaporation of precipitation in the atmosphere before reaching the ground or in stream waters results in $^{18}O$ enrichment relative to $^{2}H$ when plotted against the Global Meteoritic Water Line. Data from regions where evaporation occurs do not fit the model of Rowley et al. (2001), or Rowley and Garzione (2007). Although sedimentary carbonates reflect as well as stream waters various sources with hypsometric and elevation-dependent precipitation amount effects as potentially evaporation effects, paleosol carbonates have the advantage to reflect rainfall that directly infiltrates through the soil making them potentially better proxies for local rainfall composition estimates.

Fourth, although isotopic compositions of precipitation may be highly variable at short time scales, the low values of carbonate sedimentation rates imply that samples integrate isotopic compositions at least over thousands of years and maybe tens of thousands of years. This is an advantage to deduce the long-term variation of $\Delta$ ($\delta^{18}O$) and the associated changes of elevations.

Fifth, the isotopic composition of carbonates is different, however, from that of surface waters from which they precipitate, with an additional fractionation of oxygen isotopes that depend on the temperature ($\sim -1\%$ each $5\,^{\circ}C$).

Consequently, the assumption of a given paleotemperature when the carbonate formed adds a significant uncertainty for calculations of paleoelevations. Mean annual temperature can, for example, be deduced from the Climate-Leaf Analysis Multivariate Program (Wolfe, 1993, 1995; Wolfe and Spicer, 1999). However, it may neither correspond to the temperature of formation of paleosol carbonates since they are associated with evaporation events that only occur during the dry season, or during the growing season when evapotranspiration rates are highest (Cerling and Quade, 1993; Liu et al., 1996), nor the temperature of formation of lacustrine carbonates since they form during the summer when the evaporation rates are highest and the carbonate solubility is lowest (e.g., Duston et al., 1986; Effler and Johnson, 1987). The recently published carbonate thermometer based on $^{13}C$-$^{18}O$ bonds is however a good alternative to deduce the mean temperature of carbonate formation and finally, knowing $\delta^{18}O$ of carbonates, to calculate the $\delta^{18}O$ of meteoric water from which they form. Rowley and Garzione (2007) also pointed out that diagenesis can also alter $\delta^{18}O$ of carbonates where temperature of recrystallization exceeds 40 °C, leading to useless carbonates for paleoelevation estimates. In summary, the uncertainties in this method come from various sources like the low-elevation temperature used in modeled $\delta^{18}O$ of meteoric waters, the dispersion of the data used to deduce empirical isotopic lapse rates, and the temperature of carbonate precipitation (see Rowley and Garzione, 2007 for more details), and are estimated to range between $\pm 400$ to $\pm 500$ m ($1\sigma$ errors) at paleoelevations higher than 4000 m asl to $\pm 1000$ m at paleoelevations lower than 500 m asl (errors are deduced from bootstrap simulations in both the Andes and the Himalaya/Tibet). However, other errors come from global or local climate changes, as well as from the evaporation of surface waters, but their impact on the accuracy of paleoelevation estimates is not easy to quantify (Rowley and Garzione, 2007).

#### 5.6.2.4.2 Paleoaltimetry data based on the abundance of $^{18}O^{13}C^{16}O$ ($\Delta_{47}$): The 'carbonate clumped' isotope paleothermometer

Recently a new technique has been developed to estimate paleoelevations using a new paleothermometer: the 'clumped-isotope' $\Delta_{47}$ (Ghosh et al., 2006a). The ionic group $^{13}C^{18}O^{16}O_2^{-2}$ is a multiply substituted isotopolog in carbonate minerals. The two heavy isotopes make it to have lower zero-point energies than its isotopically 'normal' and singly substituted relatives ($^{12}C^{16}O_3$, $CO_3$, $COO_2$, and $COO_2$). A direct consequence is that rare isotopes are clumped by a thermodynamic driving force creating bonds with each other instead of being randomly dispersed throughout the mineral lattice. The abundance of multiply substituted molecules increases with decreasing temperature (Wang et al., 2004). The abundance of $^{13}C^{18}O^{16}O$ (mass 47) in $CO_2$ produced by digesting a carbonate mineral in phosphoric acid has been shown to be proportional to the abundance of $^{13}C^{18}O^{16}O^{-2}$ in carbonates (Ghosh et al., 2006a). It is hence possible to measure the $\delta^{18}O$, $\delta^{13}C$, and abundance of $\Delta_{47}$ isotopologs (mostly $^{13}C^{18}O^{16}O$) in the product $CO_2$ (e.g., Ghosh et al., 2006b). The abundance of $^{13}C^{18}O^{16}O$ (mass 47) is measured relative to $^{16}O^{12}C\ ^{16}O$ (mass 44) and called $R^{47}$. $R^{47}$ is normalized by the $R^{47}_{random}$ and called:

$$\Delta_{47} = (R^{47}_{measured}/R^{47}_{random} - 1) \times 1000),$$

with $R^{47}_{random}$ calculated from the random distribution of heavy isotopes in the sample based on the measured $\delta^{18}O$, $\delta^{13}C$ values (Eiler and Schauble, 2004). The temperature-dependant enrichment in $^{13}C^{18}O^{16}O$ has been calibrated using synthetic calcites precipitated under a temperature range of 1 °C to 50 °C, representative of surface conditions (Ghosh et al., 2006a) leading to a relation between the new paleothermometer $\Delta_{47}$ and the temperature ($T$ in °K) of carbonate precipitation in nature:

$$\Delta_{47} = 0.0592 \times 10^6 \times T^{-2} - 0.02.$$

This new paleothermometer is particularly useful since it allows paleoelevations to be obtained in three ways (Ghosh et al., 2006b; Quade et al., 2007; Rowley, 2007). Firstly obtained paleotemperature can be compared to the measured temperature lapse rate to deduce paeloelevations, especially in arid regions where $\delta^{18}O$ and $\delta^{2}H$ techniques cannot be applied due to evaporation of precipitation before reaching the ground. The second way to use the $\Delta_{47}$ and the associated paleotemperature is to deduce the isotopic composition of meteoric water from which carbonate precipitates, since the $\delta^{18}O$ of carbonate is known and can be used to compare such values to the altitude dependence of $\delta^{18}O$ (Garzione et al., 2006). The third way to obtain paleoelevations is to sample a vertical transect to obtain the modern mean annual and mean summer surface temperature as a function of the modern annual weighted mean $\delta^{18}O$. The same two variables are obtained from the $\Delta_{47}$ and can be compared to the expected values estimated from the modern vertical transect (Ghosh et al., 2006b). The similarity in slope in these two dimensions between sampled data and the modern mean annual trend is shown to reflect primarily the change in elevation (which is the strength of this method) and not a change in the global climate or latitude or changes in the season of formation of soil carbonates (although these second-order effects must be corrected) (Ghosh et al., 2006b). The modern meteoric water $\delta^{18}O$ values and surface temperatures vary with season during the year and soil carbonates may grow during different seasons leading to an offset from the modern mean annual trend (meteoric waters $\delta^{18}O$ vs. temperatures). At each elevation, the seasonal variation of meteoric waters $\delta^{18}O$ versus temperatures is shown to be a series of lines almost perpendicular to the modern mean annual trend in the graph of meteoric waters $\delta^{18}O$ versus temperatures (cf. **Figure 1** of Ghosh et al., 2006b). Linking seasonal extreme values with the mean annual trend for corresponding altitudes allows the generation of lines of constant altitude (isohypse) from which paleoelevations can be derived.

The uncertainties linked to the $\Delta_{47}$ method are significantly lower than most of any other method. Ghosh et al. (2006b) presented values of paleoelevations for the Bolivian Altiplano from the Late Miocene to Pliocene of $-200 \pm 200$ m between

11.4 and 10.3 Ma, 2500 ± 500 m between 7.6 and 7.3 Ma, and 3500 ± 400 m between 6.7 and 5.8 Ma.

This method is based on the assumption that atmospheric circulation patterns have not changed significantly in the past 10 to 15 Ma at the latitude of the Andes (Ghosh et al., 2006b). Any change in climate and atmospheric circulations would however modify the moisture supply, the amount of rain that falls before the clouds reach the studied orogen and consequently the $\delta^{18}O$ values (Ghosh et al., 2006b; Poulsen et al., 2010). Poulsen et al. (2010) used a global circulation model that tracked the water vapor and rainfall isotopic composition in space and time. Poulsen et al. (2010) also showed that surface uplift of the Atliplano results in spatially heterogeneous variations in the amounts of precipitations over the Andes, with positive or negative variations. They showed that the decrease in rainfall $\delta^{18}O$ is not systematic with surface uplift.

Here the authors present only two examples from the paper of Poulsen et al. (2010) to illustrate their results. First, as surface uplift increases, precipitation $\delta^{18}O$ also increases in the eastern flanks of the central Andes where moisture supply coming from the enriched $\delta^{18}O$ of the Amazon Basin is enhanced as a consequence of intensification and a shift to the west toward the Andes of the South American low-level jetstream. Second, modifications of the South American low-level jet also lead to large increases in precipitation in the northern central Andes and consequently to a substantial decrease in meteoric water $\delta^{18}O$ due to amount effects (the $\delta^{18}O$ of airmasses is correlated to rainfall rates). Poulsen et al.'s (2010) model shows that isotopic lapse rates can change through time from low to high isotopic lapse rates, leading to an underestimation of paleoelevations and consequently an overestimation of a recent surface uplift if modern isotopic lapse rates are applied to past $\delta^{18}O$ values to estimate paleoelevations. Poulsen et al. (2010) concluded that the depletion in meteoric water $\delta^{18}O$ preserved in Miocene soil carbonates of the central Andes (Ghosh et al., 2006b) partially explains an increase in mean elevations. The remaining part reflects the initiation and the intensification of convective rainfall induced by orographic lifting of water vapor, which is in turn enhanced by climate change (atmospheric circulation changes in wind directions and speeds) and obviously by surface uplift (Poulsen et al., 2010).

#### 5.6.2.5 Paleoaltimetry Data Based on Paleoatmospheric Pressure from Basalt Vesicularity

Atmospheric pressure is simply the mass of air above a given level, and the mass of air above a given level decreases with elevation as well as the density of molecules that constitute our atmosphere. Consequently air pressure decreases with elevation and it does so at a standard atmospheric lapse rate of $\sim 100$ mb km$^{-1}$ in the lower atmosphere. During the Cenozoic atmospheric pressure at sea level probably did not change significantly. Since the atmosphere composition did not evolve significantly, the standard atmospheric lapse rate can be considered constant. Everyone knows from weather forecast maps that surface atmospheric pressures vary spatially, with anticyclonic centers of high pressure and cyclonic centers of low pressure. Such meteorologic features move horizontally at daily to season timescales as a function of insolation, a spatial distribution also influenced by the landmass distribution and the oceanic circulations. Since landmass distribution varies at the geological timescale one can also expect variations in the spatial distribution of highs and lows at the geological time scale. However, modern surface atmospheric pressure changes range between $\sim 970$ mb in deep lows (hurricane) to $\sim 1040$ mb in strong highs at sea level, leading to maximum modern climate-driven variations on the order of $\sim 70$ mb between highs and lows, a value reduced to a most likely 30 mb by Sahagian et al. (2002b). As a consequence, a change in topographic elevation of 3 km will result in a mean surface air pressure decrease of 300 mb leading to a signal 10-fold higher than that of a likely climate-driven maximum change in air pressure. Since the standard atmospheric lapse rate is constant through time (during at least the Cenozoic) and known, a measure of a past surface air pressure is a direct measure of paleoelevation independent of long term climate changes.

The pressure near the surface of a lava flow is mostly the atmospheric pressure whereas at the bottom of a lava flow the pressure is the sum of the hydrostatic pressure that the column of lava exerts, plus the atmospheric pressure. Hence, the difference in internal pressure in bubbles at the base and top of a lava flow depends on atmospheric pressure and lava flow thickness (Sahagian et al., 1989, 2002a; Sahagian and Maus, 1994; Sahagian et al., 2002b). Because lava flow thickness is easy to measure in the field, the size of bubbles in vesicular basalts records the paleoatmospheric pressure, the variation of which can be interpreted in terms of elevation changes, assuming a known air pressure lapse rate (Sahagian and Proussevitch, 2007; Sahagian et al., 2002a, and references herein). The measurement of vesicle size in 2.5 cm core samples is realized using numerical analysis techniques (Proussevitch and Sahagian, 2001; Proussevitch et al., 2007) of slice images obtained by X-ray computed tomography (Ketcham and Carlson, 2001).

The uncertainties associated with the method are $\pm 400$ m ($\sigma$) based on elevation of modern Hawaiian lavas used to validate the method with more accurate results with multiple sampling. The accuracy of the technique asserted by another approach, including errors from the measurements of vesicle size and lava flow thickness, and the use of average sea-level barometric pressure is $\pm 410$ m agreeing with the standard deviation approach (Sahagian et al., 2002a).

This method has been applied to unravel the uplift history of the Colorado Plateau (Sahagian et al., 2002a). Studied lavas were emplaced between 800 and 2000 m regardless of the age suggesting that basalts were erupted in all parts of the Colorado Plateau since 25 Ma (Sahagian et al., 2002a). This means the plateau was not flat during the past 25 Ma with a relief of at least 1200 m and a mean elevation higher than 800 m. Sahagian et al. (2002a) obtained a rock uplift rate of 40 m Ma$^{-1}$ between 25 and 5 Ma (800 m of rock uplift), and an acceleration to 220 m Ma$^{-1}$ since 5 Ma (1100 m of rock uplift).

#### 5.6.2.6 Paleoaltimetry Data Based on Cosmogenic Nuclides

Cosmogenic nuclide production rates increase with elevation above sea level (e.g., Lal and Peters, 1967). As such, this might

be used to determine a paleoaltimetry (e.g., Blard et al., 1995, 2005; Dunai, 2010; Gosse and Phillips, 2001; Libarkin et al., 2002; Riihimaki and Libarkin, 2007; Schäfer et al., 1999; Van der Wateren and Dunai, 2001). First, the exposure history of a sample must be well constrained to derive a paleoelevation or an average uplift rate from its cosmogenic nuclide concentration. Two methods have been used and summarized by Riihimaki and Libarkin (2007) and Dunai (2010).

The simplest one consists of determining the paleoelevation of a dated volcanic flow. The lava flow sampled must have been preserved from erosion and unshielded by sediments during the time of exposure, which must be known accurately. Duration of exposure can be deduced where the sampled lava flow has been buried under a more recent, sufficiently thick and also dated lava flow that prevents further cosmogenic nuclides from being produced (Blard et al., 2005). Dividing the paleoelevation estimate by the age of the overlying lava gives a mean rock uplift rate since the end of exposure. True rock uplift rate may be higher if the uplift event lasted less than the time passed since the emplacement of the overlying lava flow. Uncertainties come from the analytical methods of both cosmogenic nuclide concentration and dating method used to constrain the lava ages, and from the uncertainties in the depth-history of a sample and duration of exposure (Riihimaki and Libarkin, 2007). In order to be able to measure a paleoelevation, the duration of exposure must exceed tens of thousands years and in some cases up to several hundred thousand years (Dunai, 2010). The depth history of a sample is the primary source of uncertainties. Riihimaki and Libarkin (2007) illustrated clearly that the high density contrast between atmosphere and rocks makes a 0.5 m uncertainty in depth equivalent to more than 1000 m of error in altitude.

The only way to deduce complex exposure history where a sedimentary layer may have once capped the sample site is to perform depth profiles and to analyze the exposure history by multiple nuclides (Riihimaki et al., 2006). At best paleoelevation will not be more accurate than $\sim$200 m at a low paleoelevation to $\sim$500 m at a high paleoelevation (Riihimaki and Libarkin, 2007). This is a minimum range of error because this estimate does not include any uncertainty in the depth of the sample due to erosion or burying (Riihimaki and Libarkin, 2007), but Blard et al. (2005) argued that the cosmogenic $^{3}$He paleoaltimeter can potentially reach resolutions better than $\sim$1000 m. However, this method has been seldom used for dating probably due to the usually poorly constrained depth history of potential targets. The second method is a test for recent rapid uplift (Brook et al., 1995; Brown et al., 1991). Brook et al. (1995) have shown that high concentration of $^{10}$Be in poorly dated glacial deposits of the Dry Valleys in Antarctica suggest that they were deposited at their current high elevation, which deny any recent high (0.43–1 mm yr$^{-1}$) rock uplift rate as previously proposed. However, the method did not allow the discarding of an alternative explanation in which the glacial sediments are older and that they have been raised, with a moderate uplift rate of 0.2 mm yr$^{-1}$, for example, allowing enough exposure time to produce the high concentration of cosmogenic nuclides.

#### 5.6.2.7 Cooling-History and Erosion Rates as a Proxy for Rock or Surface Uplift

Cooling-ages can be deduced from thermochronologic data (e.g., Reiners, 2007, and references herein). A cooling-age defines a specific temperature (or range of temperatures) during cooling history of a sample. Cooling-history $T(t)$ can also be tracked by thermochronological data. Moreover, a thermal model of the crust allows converting temperatures into depth and cooling histories that can be transformed into exhumation histories (erosional denudation or tectonic exhumation in normal fault footwalls). Thermochronologic techniques and interpretations relevant to uplifts and topographic changes can be found in Reviews in Mineralogy and Geochemistry (Reiners and Ehlers, 2005).

First, thermochronology describes the cooling of rocks (exhumation when temperatures are converted into depth): the movement of rocks relative to Earth's free cooling surface, which may raise or decrease in elevation through time. Consequently, thermochronology alone neither provides estimates of paleoelevation, nor of rock and surface uplift. Second, the cooling-ages do not directly relate to changes in mean elevation or mean local relief and changes in erosion rates (e.g., Reiners, 2007, and references herein). For that reason, in most cases, it is the spatial changes in cooling-ages or cooling-histories that are used to unravel the topographic evolution, that is, the changes in local relief. Third, thermochronologic data allow amounts of mean elevation change or rock uplift to be estimated only when combined with geologic data. Fourth, channel incision and erosion on coupled hillslopes can reflect transient response to tectonically driven rock uplift (e.g., Whipple and Tucker, 1999). But it can also reflect transient response to climatically driven changes in sediment supply and fluvial discharge (Molnar and England, 1990). Provided prior sufficient thickening of the crust, moderate to high mean elevations are supported by a crustal root. Rock uplift in thickened settings is then the sum of the tectonic rock uplift and the erosionally driven rock uplift (e.g., Whipple, 2009).

##### 5.6.2.7.1 *Vertical profiles of thermochronological data combined with other lines of evidence as a proxy for rock and surface uplift*

Age-elevation relationships in a vertical profile show a normal correlation where erosion rates and rock uplift rates are uniform and the slope of this relation is the erosion rate. Provided additional geologic information on paleoelevation is available (e.g., stratigraphic) and assuming a geothermal gradient, vertical profiles of thermochronologic cooling-dates can be used to deduce rock-uplift and surface-uplift rates even if direct paleoelevation markers like marine sediments are missing (e.g., Ducea et al., 2003). In the Santa Lucia Mountains of California (US), the last major transition from submarine to subaerial sedimentation occurred at approximately 4 Ma. Ducea et al. (2003) deduced the topography was at sea level at 4 Ma. Assuming a geothermal gradient of 25 °C km$^{-1}$, a mean surface temperature of 10 °C and the (U-Th)/He closure isotherm for apatite at 76 °C, they deduced the closure depth in the Santa Lucia Mountains of California (US) at 2640 m below the sea level at 4 Ma. The current elevation (800 m) of the 4 Ma closure depth (deduced from the vertical

profile) plus the paleoelevation of the closure depth at 4 Ma (−2640 m) led to ~3440 m of rock uplift since then (0.86 mm $yr^{-1}$). The next step consisted of using the acquired estimates of erosion rates (0.66 mm $yr^{-1}$) from the vertical profile (0.35 mm $yr^{-1}$ for the period 4–2.3 Ma and ~0.9 mm $yr^{-1}$ since 2.3 Ma) to calculate the corresponding surface uplift (rock uplift minus erosion rates) (Molnar and England, 1990). Ducea et al. (2003) deduced both the rock uplift (0.86 mm $yr^{-1}$) and the surface uplift (0.2 mm $yr^{-1}$) from denudation rates and stratigraphic data. Such an approach however makes the assumption that erosion rates are uniform in space, at least at the scale of mean elevation, that is, 1000 $km^2$ (at the same spatial scale than that of the crust, see Section 5.6.1.1).

#### 5.6.2.7.2 Horizontal profiles of thermochronological data combined with other lines of evidence as a proxy for rock/surface uplift

Spatially extensive sampling over horizontal distances is more useful to constrain the local relief evolution rather than rock/surface uplift evolution (e.g., Reiners, 2007, and references herein). A paleorelief (paleo local-relief) for a specific location gives a minimum estimate of paleoelevation above sea level. But both the distribution of the paleorelief within the landscape and the history of change in base level must be known to convert a local relief change in a mean elevation change (Clark, 2007), a geodynamically more grounded measure of elevations. As long as there is no direct relationship between mean elevation or local relief and erosion rates there is no direct relation between mean elevation and local relief. In settings like high plateaus (e.g., Tibet, Altiplano), low-relief in the internally drained regions dominates whereas mean elevations are the highest in the world. Clark (2007) stressed that local relief is expected to increase during a fall in base level without an increase in mean elevation. The low local-relief of the high plateaus will undoubtedly increase when it is integrated into the drainage network draining the edges of the plateaus down to the sea without a need for the mean elevation to increase if any geodynamic process that could account for it occurs in the meantime.

The crustal thermal field is composed of deep isotherms ($T > 100\ ^{\circ}C$) parallel to the long topographic wavelengths (or mean elevations). Lower isotherms progressively fold toward the shallow depths where isotherms closely fit to the short-wavelength topography (local relief). The perturbation depth of the disturbance is shown numerically to be a strong function of the short wavelength of the topography, but it is weakly dependent on its amplitude (Braun, 2002a, b, 2003; Braun et al., 2006; Reiners et al., 2003). However, additional geologic information is here also needed since any thermal perturbation can also result from thrust kinematics and from changes in erosion rates and rock uplift rates (e.g., Braun, 2005; Brewer and Burbank, 2006; Ehlers et al., 2005; Huntington et al., 2007). Many studies used the influence of topography on cooling-ages or cooling-histories to demonstrate local relief changes through time in orogens (Braun, 2002a; Clark et al., 2005a, b; Densmore et al., 2007; Ehlers et al., 2006; House et al., 2001; Mancktelow and Grasemann, 1997; Reiners et al., 2006; Stock et al., 2006; Stockli, 2006; Stüwe et al., 1994). Because warping of isotherms is higher for the lowest temperature thermochronometers, local relief changes will be best evidenced by the lowest thermochronometers (see Valla et al., 2010).

In the Sierra Nevada of California, House et al. (1998, 2001) have shown using a constant-elevation sample transect parallel to the orogen that the apatite helium cooling-ages for the closure temperature of 68–75 °C are roughly anticorrelated with modern valleys and ridges transverse to the range. They interpret this spatial correlation as the evidence for a long-wavelength ($\lambda = 70$ km) relief of $1500 \pm 500$ m higher in the Late Cretaceous–early Tertiary than today. They also correlated the local relief to a mean elevation higher than 3000 m asl by analogy with the modern Andes. Clark et al. (2005b) showed that such an analogy is misleading and they combined the results on local relief obtained from thermochronologic data with geomorphic data allowing them to argue for a range elevation of only 1500 m asl during the same time. This highlights the constant need from other lines of evidence to better interpret thermochronologic data in terms of paleotopography.

Braun (2002a) showed that decreasing or increasing local relief can modify the age-elevation relation in vertical profiles leading to, respectively, steeper or shallower slopes of the linear regressions than the actual erosion rate. Braun (2002a, b, 2005) defined a method of unraveling the transient state of landscape evolution, that is, whether local relief increases or decreases through time. It is based on an analysis of the age-elevation relationship over a continuous three dimensional spectrum of topographic wavelengths. The main assumptions are constant geothermal gradient, steady landforms, and no horizontal advection of rock (Braun, 2002b). When applied to the Sierra Nevada of California, Braun's (2002a) approach leads to the same conclusion of House et al.'s (1998, 2001), that is, a local relief decrease since the Late Cretaceous. However, it does not define the mean elevation change, which is critical in the understanding of high plateaus.

The lithosphere flexural strength controls the isostatic-flexural rebound to erosion and consequently potentially controls the spatial distribution of thermochronologic data. In the postorogenic evolution of an orogen, a greater reduction in topographic relief (at shorter and longer wavelengths, 12 and 150 km, respectively, for the case of the Dabie Shan, China) has a similar effect on the spatial distribution of the thermochronologic ages as does a thinner lithosphere (Braun and Robert, 2005). In their study of the postorogenic decay of the Dabie Shan and following the spectral method of Braun (2002a, b, 2005), Braun and Robert (2005) confirmed that a low elastic thickness and flexural isostatic rebound can explain the recent ages in the center of the orogen without any need for a recent (Cenozoic) tectonic event and associated surface uplift.

#### 5.6.2.7.3 Incision rates obtained from thermochronological data combined with other lines of evidence as a proxy for uplift

Local relief history can also be unraveled by measuring depth in incision evolution of a canyon where it is incised within a smooth and mainly uneroded paleolandscape. Under particular conditions local relief (canyon depth) can be used as a proxy for rock uplift and surface uplift. First, depth in incision is limited by rock uplift. The incision response time to rock uplift is controlled by a geomorphic response time that can

reach several million years (e.g., Hoke et al., 2007; Schildgen et al., 2010; Schlunegger et al., 2006). Second, the thermal response to changes in the shape of Earth free cooling surface is likely to lag ~1 Ma (e.g., Schildgen et al., 2007). As a consequence the incision amounts and rates inferred from cooling-histories give a minimum rock uplift amount and rate (Schildgen et al., 2007). Only if climate is steady or becomes drier during the period of incision, rock uplift and the resulting incision can be interpreted as tectonics in origin, and they are accompanied with surface uplift (e.g., Schildgen et al., 2007).

Incision history can be deduced from dating methods such as low-temperature thermochronology of samples collected in vertical profiles or collected along valley at river level. K/Ar or Ar/Ar dates of tuffs or lava flows preserved above the current river level are also used to deduce mean incision rates since their formation (e.g., Thouret et al., 2007). But thermochronology is not a unique technique. Cosmogenic nuclide dates of terraces also give values of mean incision since the abandonment of a terrace. Cosmogenic nuclide techniques, however, generally allow dating of surfaces for the last tens of thousands to hundreds of thousands years, rarely up to a few million or tens million years (e.g., Dunai et al., 2005).

In the western slopes of the Peruvian Altiplano, Schildgen et al. (2007) have deduced from samples collected along a valley at river level and their He ages, a minimum of 2.4 km of erosion between 9 and 2.3 Ma in the Cotahuasi-Ocoña Canyon, a canyon of up to 3 km depth. They interpret it as the evidence for rock uplift of tectonic origin since climate shifted to drier conditions in the meantime (e.g., Ehlers and Poulsen, 2009; Gaupp et al., 1999; Hartley, 2003; Rech et al., 2006). Rock uplift can then be converted to surface uplift since erosion is restricted to canyon incision into a well preserved paleosurface older than 14–16 Ma.

At the eastern margin of the Tibetan Plateau, Kirby et al. (2002) and Clark et al. (2005a) showed in age-elevation relations a break in slope at ~5–12 Ma and 9–13 Ma, respectively. They interpreted the recent (late Miocene or early Pliocene) rapid incision of rivers within a widespread relict landscape, with mean elevations now above 1000 m asl and up to 3000 m asl, slowly eroding since the Jurassic as evidence for eastward plateau growth, that is, surface uplift.

On the Colorado Plateau, in the upper reaches of the Grand Canyon, Flowers et al. (2008) determined cooling-histories similar during the Early- to mid-Tertiary in samples now separated by 1500 m in both elevation and stratigraphic position. They interpret it as evidence for a proto-Grand Canyon that was ~1 km deep, implying a minimum rock uplift of 1 km before mid-Tertiary and that the watershed of the Grand Canyon already lay at high elevation by that time.

### 5.6.3 Tectonic Mechanisms and Associated Surface Uplift Rates for Plateau Uplift, Regional Warping, and Subsidence

Uplift of Earth's surface expresses the isostatic response to the thickness variation of the lithosphere resting on the asthenosphere (e.g., Fleitout and Froidevaux, 1982), as well as the differential buoyancy of the convective mantle resulting in 'dynamic topography' (e.g., Hager et al., 1985). So, whatever the tectonic model envisioned to explain uplift, including the case of dynamic topography, it implies a change of density at depth. Density changes in the lithosphere may be achieved in two ways: (1) changing rock densities; and (2) changing the respective thickness of the crust and the mantle, more precisely thickening the crust and thinning the lithosphere mantle. Changing rock densities requires changing temperature such as increasing temperature induces decreasing density, increasing buoyancy forces and eventually surface uplift. Rocks of the mantle lithosphere are much denser than the rocks of the crust and the mantle lithosphere is much thicker than the crust. Therefore, temperature increase in the lithospheric mantle will be much more efficient to Earth's surface uplift than it does in the crust. The boundary between lithosphere and asthenosphere is of thermal nature, so thinning of the mantle lithosphere can be achieved either by mechanical processes or a temperature increase. Crustal thickening requires mechanical processes, even if magma underplating from underlying mantle can be considered as 'thermal' thickening regarding the role of temperature in magma production. For a normal geothermal gradient, the shear strength of the crust is much lower than that of the lithospheric upper mantle, and crustal thickening is easier than lithosphere mantle thinning, considering mechanical processes. Finally, there are multiple ways to change density at depth in the lithosphere, which results in numerous models for plateau surface uplift. The line of argument for plateau uplift has its symmetrical thinking for subsidence: decreasing temperature will induce increasing rocks density, decreasing buoyancy and plateau subsidence, and thickening of the mantle lithosphere as well, and so on.

Discussing exhaustively the numerous tectonic models that have been proposed to explain the uplift of large areas at Earth surface is beyond the scope of this chapter. First, we must remember that we are dealing with plateaus as we recall the definition in the first section, that is, large areas with flat topography. We must also remember that two types of hypotheses sustain the interpretation of such features at Earth's surface: the acquirement of the flat topography precedes uplift; and smoothing of topography results from the interaction of surface processes (erosion/sedimentation) with tectonics during uplift.

The question arises as to what kind of data allow us to discern between the effective mechanisms that are proposed to explain plateau uplift. We can group together these increasingly numerous models into three types: (1) crustal thickening as the driving mechanism; (2) uplift due to the thinning of the mantle lithosphere; and (3) the role of the deep convective mantle as the cause of uplift and referring to 'dynamic' uplift.

Crustal thickening and thinning of the mantle lithosphere may be achieved either by homogeneous or heterogeneous deformation. Of course, end-member models imply hybrid models. Symmetrical end-members models, that is, crustal thinning and mantle lithosphere thickening, either by homogeneous or heterogeneous deformation, exist to explain subsidence.

Crustal thickening can be induced either by: (1) crustal shortening beneath the uplifting plateau (e.g., Argand, 1924; Bird, 1978; Dewey and Burke, 1973; Froidevaux and Ricard, 1987); (2) by lateral flow of ductile crust from immediately adjacent thickened area (e.g., Bird, 1991; Zhao and Morgan, 1987); (3) by crustal underplating of material coming from the continental margin and tectonically eroded by the subducting plate (e.g., Baby et al., 1997; Schmitz, 1994); and (4) by magmatic addition (Gotberg et al., 2010; Kono et al., 1988; Thorpe et al., 1981) but to a much smaller contribution than shortening and, mid and lower crustal flow (e.g., Baby et al., 1997; Francis and Hawkesworth, 1994; Giese et al., 1999; Sheffels, 1990). Crustal thickening by thrust faults, that is, involving strain localization, corresponds to a heterogeneous deformation mode. Crustal shortening by homogeneous deformation will require homogeneous ductile rheology, which implies a high geothermal gradient. As heterogeneous deformation is likely to produce strong topographic gradients and relief roughness at Earth's surface, mass redistribution by erosion/sedimentation process is needed to maintain a flat topography. Lateral flow of ductile crust may be assimilated to a homogeneous deformation mode. In this case, flat topography may exist long before uplift, unlike the previous case where syn- or late uplift sedimentation will be inevitably observed at the plateau surface.

Thinning of the mantle lithosphere may develop in two ways. First as mentioned above, the thermal boundary between lithosphere and asthenosphere migrates upward as the geothermal gradient increases. Mantle plumes may generate such processes resulting in surface uplift (e.g., Eaton, 2008; Teixell et al., 2005). Second, the lithosphere mantle, which is colder and denser than the underlying asthenosphere mantle, may be removed from the buoyant crust and sink into the asthenosphere. Whether such lithospheric mantle removal is considered to result from progressive peeling away during continental collision, or more or less sudden foundering by convective removal after lithosphere thickening, it is named lithosphere delamination (Bird, 1978) or detachment (e.g., Houseman et al., 1981).

The term 'dynamic uplift' is often used when Earth's mantle, including the lithospheric mantle, is suspected of being involved in surface uplift processes, but strictly speaking it does not imply a thinning of the mantle lithosphere. Dynamic topography refers to vertical stress generated by the deep convective mantle that results in subsidence or uplift of Earth's surface (e.g., Gurnis, 1993; Hager et al., 1985; Lithgow-Bertelloni and Silver, 1998).

Most interpretations of uplifted plateaus appeal to hybrid models, that is, a more or less complex combination of the different processes discussed above. For the same object, different contradictory processes, in that they result in a conflicting uplift history, are invoked. For example, as crustal thickening is related to plate convergence, the rate of surface uplift controlled by this process must match the rate of plate convergence and it implies a gradual growth of the plateau (e.g., Liu-Zeng et al., 2008; Tapponnier et al., 2001). Sudden detachment of a lithospheric root should generate faster uplift and plateau uplift as a whole (e.g., Garzione et al., 2006; Molnar et al., 1993).

To illustrate the complexity of this problem, the authors provide the following, but not exhaustive, interpretations

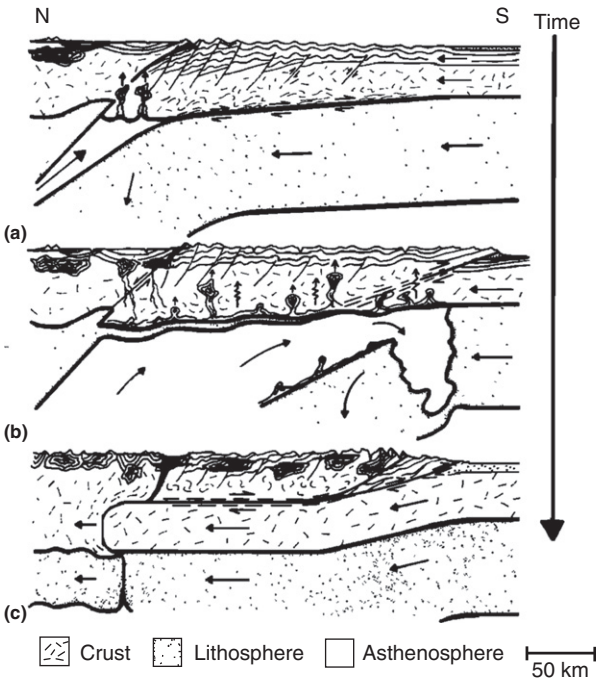


**Figure 11** Himalaya-Tibet tectonic history involving crustal thickening and delamination of the mantle lithosphere first proposed by Bird, P., 1978. Initiation of intracontinental subduction in the Himalaya. Journal of Geophysical Research 83, 4975–4987.

that have been proposed for the surface uplift of the Tibetan, Altiplano, and Colorado plateaus:

1. For the Tibetan Plateau (**Figure 11**): crustal thickening by localized deformation (Dewey and Burke, 1973; Tapponnier et al., 2001) or by lateral flow of ductile crust (Clark and Royden, 2000), crustal thickening and lithosphere delamination (Bird, 1978), homogeneous deformation of the whole lithosphere and consecutive detachment of the mantle lithospheric root (England and Houseman, 1988; Houseman et al., 1981; Molnar et al., 1993).
2. For the Altiplano (for an exhaustive review of mechanisms see Barnes and Ehlers, 2009): crustal thickening by lateral flow of ductile crust (Husson and Sempere, 2003), crustal thickening and detachment of the mantle lithosphere (Garzione et al., 2006), crustal thickening, magma underplating, and thinning of the mantle lithosphere (Allmendinger et al., 1997).
3. For the Colorado Plateau: crustal thickening (McQuarrie and Chase, 2000), delamination of the lithospheric mantle (Bird, 1979), lateral flow of ductile crust (Bird, 1991), thinning of the lithosphere mantle due to mantle plume (Eaton, 1987) or Laramide subduction (Spencer, 1996), or by warming the lithosphere (Roy et al., 2004), dynamic uplift (Liu and Gurnis, 2010; Moucha et al., 2009).

### 5.6.4 Plateau Uplift and Global Climate Change

Uplift of Earth's surface as a cause of climate change goes back at least to Dana (1856) who argued, through geomorphologic

and tectonic analysis, that the Paleozoic Appalachians had been rejuvenated during the Late Cenozoic. A few decades later, Chamberlin (1899) postulated that the simultaneous occurrence of orogens and ice ages in Earth's history was not a coincidence but a causal relation: enhanced chemical weathering of aluminosilicate minerals, consecutive to intense erosion of rocks in mountain belts, subtracts $CO_2$ from the atmosphere resulting in decreasing atmospheric greenhouse effect and global cooling (e.g., Raymo, 1991; Raymo and Ruddiman, 1992). As the authors are concerned with high continental plateaus, erosion in such areas is weak by definition, and this process will be limited. The primary physical effects of plateau surface uplift are changes in the atmospheric circulations that are induced by the presence of an elevated surface at cooler upper levels in the atmosphere. This may result in increasing erosion and chemical weathering and eventually in climate change. The authors will not discuss here this indirect consequence of plateau surface uplift that is largely debated elsewhere (e.g., Ruddiman, 1997).

Plateau uplift has three main effects on climate (Ruddiman and Prell, 1997): (1) lapse-rate cooling of high-elevation surfaces; (2) perturbation of jet stream meanders; and (3) creation and intensification of monsoon circulations.

The main present-day high plateaus arose during the Late Cenozoic, a period of progressive cooling of Earth's climate that culminates in the Late Neogene. So, it is difficult, indeed even impossible, to determine the influence of a distinctive plateau on global climate change during this period. Most of works recognize the primary influence of the Tibetan plateau because of its extent and elevation, which are far greater than the other plateaus, and because of its particular latitudinal position as well (Raymo and Ruddiman, 1992).

Lapse-rate cooling, that is, the atmospheric cooling with increasing elevation ($6.5\ ^{\circ}C\ km^{-1}$), refers to the fact that it causes the high plateaus to be much colder than the nearby plains. This is especially the case in winter because temperatures are further lowered by snow cover, through albedo-temperature feedback. Depending on the extent and the height of the plateau, and its latitudinal position, this effect may result in nucleating continental ice sheets and global cooling (Birchfield and Wertman, 1983).

The second effect concerns the increase in amplitude of the meanders of the subtropical jet stream, as most high plateaus are lying in lower middle latitudes. Uplifting plateaus create obstacles to the west-to-east flow that results in the diversion into a broad poleward meander around the obstacles, and eventually large meanders develop upstream and downstream from the high plateaus (e.g., Kutzbach et al., 1989; Rind and Chandler, 1991; Ruddiman and Kutzbach, 1991; Ruddiman et al., 1989).

The third direct effect of plateau uplift is the intensification, and even the creation, of seasonal monsoon circulation (Molnar et al., 1993; Ruddiman and Prell, 1997). The symmetrical Hadley cells describe the atmospheric circulation in a general west-to-east flow between equatorial and mid-latitudes. Warm moist air rises in the intertropical convergence zone. Condensation and precipitation release latent heat that causes this now drier air to rise in the troposphere, then to flow poleward. At approximately 30° N and S latitudes, it flows east and sinks causing a high pressure area at the surface. Because of adiabatic heating, this air dries further as evidenced by the pervasive occurrence of deserts at this latitude. The uplift of a high plateau such as the Tibetan Plateau at this latitude has two effects. First, the general west-to-east flow is altered, so that the high pressure zone at latitude 30° is displaced northward and a low pressure zone develops aloft in northern India in the summer monsoon. Consequently, the summer winds originate in the Arabian Sea moving to India, and the eastern Himalaya receive increasing moisture owing to the barrier erected by the plateau (orographic effect). Second, the presence of the 'hot' Tibet in summer causes air to rise near and above the plateau and to flow toward the equator. This creates a cell with a reverse sense of rotation compared to the Hadley cell, that is, air is drawn from equatorial areas and ascent above the plateau, producing the Indian summer monsoon, characterized by moisture-bearing winds at surface blowing from the southwest (from the sea) to the northeast (to the continent).

In the case of southeast Asia, this perturbation of the general circulation of the atmosphere due to the Tibet uplift, which originates from lithosphere dynamics, is considered to have a strong impact on Earth's climate, although timing of uplift and of related climate change are still strongly debated (e.g., Dupont-Nivet et al., 2007; Molnar et al., 2006; Rowley and Currie, 2006). The question remains open and is best summarized by Molnar et al. (1993) who finally asked the question: "Did convective removal of the lower lithosphere beneath the Tibetan Plateau force a rapid uplift at approximately 8 Ma that created a heat source sufficient to strengthen the monsoon, which in turn increased precipitation and weathering in the Himalaya, causing sufficient extraction of $CO_2$ from the atmosphere to induce global cooling?"

### 5.6.5 Conclusion

Most of interpretations of uplifted plateaus appeal to models with a more or less complex combination of the different tectonic processes discussed above. Such a situation underscores the urgent need to obtain more pertinent and clear records of the surface uplift and subsidence history of present-day and past plateaus, respectively, and to come back to the difficulty of determining paleoaltitudes and structures at depth.

## Acknowledgments

This review was conducted with support from the MINISTERIO DE CIENCIA E INNOVACIÓN (CGL2006-07226 y CGL2010-15416). An anonymous reviewer helped clarify aspects of the manuscript. The authors also thank Lewis Owen for comments and corrections that improved the manuscript.

## References

Abbott, L.D., Silver, E.A., Anderson, R.S., et al., 1997. Measurement of tectonic surface uplift rate in a young collisional mountain belt. Nature 385, 501–507.

Al-Lazki, A., Eric, I., Dogan, S., Muawia, S., Niyazi, B., Randa, M., T., 2004. Pn tomographic imaging of mantle lid velocity and anisotropy at the junction of the Arabian, Eurasian, and African plates. Geophysical Journal International 158, 1024–1040.

Allmendinger, R.W., Jordan, T.E., Kay, S.M., Isacks, B.L., 1997. The evolution of the Altiplano–Puna Plateau of the Central Andes. Annual Review of Earth and Planetary Sciences 25, 139–174.

Amante, C., Eakins, B.W., 2009. ETOPO1 1 Arc-minute global relief model: procedures, data sources and analysis. In: Memorandum, N.T. (Ed.), National Geophysical Data Center, Marine Geology and Geophysics Division, Boulder, CO, 19 pp.

Anders, A.M., Roe, G.H., Hallet, B., Montgomery, D.R., Finnegan, N.J., Putkonen, J., 2006. Spatial patterns of precipitation and topography in the Himalaya. Geological Society of America Special Papers 398, 39–53.

Argand, E., 1924. La Tectonique de l'Asie. Compte-rendu du 13e Congrès Géologique International, Bruxelles, pp. 171–372.

Armijo, R., Tapponnier, P., Mercier, J.L., Han, T.-L., 1986. Quaternary extension in southern Tiber; field observations and tectonic implications. Journal of Geophysical Research 91, 13,803–13,872.

Atalay, I., Koçman, A., 1979. Kuzeydoğu Anadolu'nun jeotektonik ve morfotektonik evriminin ana çizgileri. Jeomorfoloji Dergisi 8, 41–75.

Axelrod, D.I., 1966. A method for determining the altitudes of Tertiary floras. The Palaeobotanist 14, 144–171.

Axelrod, D.I., 1998. The Oligocene Haynes Creek flora of eastern Idaho. University of California Publications in Geological Sciences 143, 99.

Ayalew, L., Yamagishi, H., 2004. Slope failures in the Blue Nile basin, as seen from landscape evolution perspective. Cosmogenic isotopes in geomorphology 57, 95–116.

Ayele, A., Stuart, G., Kendall, J.-M., 2004. Insights into rifting from shear wave splitting and receiver functions: an example from Ethiopia. Geophysical Journal International 157, 354–362.

Babault, J., Bonnet, S., Crave, A., Van Den Driessche, J., 2005a. Influence of piedmont sedimentation on erosion dynamics of an uplifting landscape: an experimental approach. Geology 33, 301–304. http://dx.doi.org/10.1130/G21095.1.

Babault, J., Bonnet, S., Van Den Driessche, J., Crave, A., 2007. High elevation of low-relief surfaces in mountain belts: does it equate to postorogenic surface uplift? Terra Nova 19, 272–277.

Babault, J., Teixell, A., Arboleya, M.L., Charroud, M., 2008. A Late Cenozoic age for long–wavelength surface uplift of the Atlas Mountains of Morocco. Terra Nova 20, 102–107. http://dx.doi.org/10.1111/j.1365-3121.2008.00794.x.

Babault, J., Van Den Driessche, J., Bonnet, S., Castelltort, S., Crave, A., 2005b. Origin of the highly elevated Pyrenean peneplain. Tectonics 24, TC2010. http://dx.doi.org/10.1029/2004TC001697.

Baby, P., Rochat, P., Mascle, G., Herail, G., 1997. Neogene shortening contribution to crustal thickening in the back arc of the Central Andes. Geology 25, 883–886.

Bai, D., Unsworth, M.J., Meju, M.A., et al., 2010. Crustal deformation of the eastern Tibetan plateau revealed by magnetotelluric imaging. Nature Geosci. 3, 358–362.

Bailey, I.W., Sinnott, E.W., 1916. The climatic distribution of certain types of Angiosperm leaves. American Journal of Botany 3, 24–39.

Barke, R., Lamb, S., 2006. Late Cenozoic uplift of the Eastern Cordillera, Bolivian Andes. Earth and Planetary Science Letters 249, 350–367.

Barnes, J.B., Ehlers, T.A., 2009. End member models for Andean Plateau uplift. Earth–Science Reviews 97, 105–132.

Bastow, I.D., Nyblade, A.A., Stuart, G.W., Rooney, T.O., Benoit, M.H., 2008. Upper mantle seismic structure beneath the Ethiopian hot spot: rifting at the edge of the African low-velocity anomaly. Geochemistry Geophysics Geosystems 9, Q12022.

Beaumont, C., Jamieson, R.A., Nguyen, M.H., Medvedev, S., 2004. Crustal channel flows: 1. Numerical models with applications to the tectonics of the Himalayan–Tibetan orogen. Journal of Geophysical Research 109, B06406.

Baumont, D., Paul, A., Zandt, G., Beck, S.L., Pedersen, H., 2002. Lithospheric structure of the central Andes based on surface wave dispersion. Journal of Geophysical Research–Solid Earth, 107.

Beck, S.L., Zandt, G., 2002. The nature of orogenic crust in the central Andes. Journal of Geophysical Research 107, 2230.

Beck, S.L., Zandt, G., Myers, S.C., Wallace, T.C., Silver, P.G., Drake, L., 1996. Crustal-thickness variations in the central Andes. Geology 24, 407–410.

Becq-Giraudon, J.F., Montenat, C., Van Den Driessche, J., 1996. Hercynian high-altitude phenomena in the French Massif Central: tectonic implications. Palaeogeography, Palaeoclimatology, Palaeoecology 122, 227–241.

Becq-Giraudon, J.F., Van Den Driessche, J., 1994. Depots periglaciaires dans le Stephano-Autunien du Massif Central; temoin de l'effondrement gravitaire d'un haut plateau hercynien. Comptes Rendus de l'Academie des Sciences, Serie II. Sciences de la Terre et des Planetes 318, 675–682.

Beerling, D.J., Royer, D.L., 2002. Fossil plants as indicators of the phanerozoic global carbon cycle. Annual Review of Earth and Planetary Sciences 30, 527–556.

Best, M.G., Barr, D.L., Christiansen, E.H., Gromme, S., Deino, A.L., Tingey, D.G., 2009. The Great Basin Altiplano during the middle Cenozoic ignimbrite flareup: insights from volcanic rocks. International Geology Review 51, 589–633.

Birchfield, G.E., Wertman, J., 1983. Topography, albedo-temperature feedback, and climate sensitivity. Science 219, 284–285.

Bird, P., 1978. Initiation of intracontinental subduction in the Himalaya. Journal of Geophysical Research 83, 4975–4987.

Bird, P., 1979. Continental delamination and the Colorado Plateau. Journal of Geophysical Research 84, 7561–7571.

Bird, P., 1988. Formation of the Rocky Mountains, Western United States: a continuum computer model. Science 239, 1501–1507.

Bird, P., 1991. Lateral extrusion of lower crust from under high topography, in the isostatic limit. Journal of Geophysical Research 96, 10,275–10,286.

Blackstone, D.L., 1975. Late cretaceous and cenozoic history of laramie basin region, Southeast Wyoming. Geological Society of America Memoirs 144, 249–279.

Blard, P.-H., Lavé, J., Pik, R., Quidelleur, X., Bourlès, D., Kieffer, G., 2005. Fossil cosmogenic $^{3}$He record from K-Ar dated basaltic flows of Mount Etna volcano (Sicily, 38°N): evaluation of a new paleoaltimeter. Earth and Planetary Science Letters 236, 613–631.

Braun, J., 2002a. Estimating exhumation rate and relief evolution by spectral analysis of age– elevation datasets. Terra Nova 14, 210–214.

Braun, J., 2002b. Quantifying the effect of recent relief changes on age-elevation relationships. Earth and Planetary Science Letters 200, 331–343.

Braun, J., 2003. Pecube: a new finite-element code to solve the 3D heat transport equation including the effects of a time-varying, finite amplitude surface topography. Computers & Geosciences 29, 787–794.

Braun, J., 2005. Quantitative constraints on the rate of landform evolution derived from low-temperature thermochronology. Reviews in Mineralogy and Geochemistry 58, 351–374.

Braun, J., Robert, X., 2005. Constraints on the rate of post-orogenic erosional decay from low-temperature thermochronological data: application to the Dabie Shan, China. Earth Surface Processes and Landforms 30, 1203–1225.

Braun, J., van der Beek, P., Batt, G., 2006. Quantitative Thermochronology: Numerical Methods for the Interpretation of Thermochronological Data. Cambridge University Press, Cambridge.

Brewer, I.D., Burbank, D.W., 2006. Thermal and kinematic modeling of bedrock and detrital cooling ages in the central Himalaya. Journal of Geophysical Research 111, B09409.

Brook, E.J., Brown, E.T., Kurz, M.D., Ackert, R.P., Raisbeck, G.M., and Yiou, F., 1995.Constraints on age, erosion, and uplift of Neogene glacial deposits in the Transantarctic Mountains determined from in situ cosmogenic 10Be and 26Al. Geology 23, 1063-1066.

Brown, E.T., Edmond, J.M., Raisbeck, G.M., Yiou, F., Kurz, M.D., Brook, E.J., 1991. Examination of surface exposure ages of Antarctic moraines using in situ produced 10Be and 26Al. Geochimica et Cosmochimica Acta 55, 2269–2283.

Buck, W.R., 1991. Modes of continental lithospheric extension. Journal of Geophysical Research 96, 20161–20178.

Burbank, D.W., Leland, J., Fielding, E., Anderson, R.S., Brozovic, N., Reid, M.R., Duncan, C., 1996. Bedrock incision, rock uplift, and threshold hillslopes in the northwestern Himalayas. Nature 379, 505–510.

Cahill, T., Isacks, B.L., 1992. Seismicity and shape of the subducted Nazca Plate. Journal of Geophysical Research 97, 17503–17529.

Carretier, S., Lucazeau, F., 2005. How does alluvial sedimentation at range fronts modify the erosional dynamics of mountain catchments? Basin Research 17, 361–381.

Carretier, S., Poisson, B., Vassallo, R., Pepin, E., Farias, M., 2009. Tectonic interpretation of transient stage erosion rates at different spatial scales in an uplifting block. Journal of Geophysical Research 114, F02003.

Casas-Sainz, A.M., Cortes-Gracia, A.L., 2002. Cenozoic landscape development within the central Iberian Chain, Spain. Cosmogenic Isotopes in Geomorphology 44, 19–46.

Castelltort, S., Simpson, G., 2006. River spacing and drainage network growth in widening mountain ranges. Basin Research 18, 267–276.

Cerling, T.E., Quade, J., 1993. Stable carbon and oxygen isotopes in soil carbonates. In: Swart, P., Lohmann, K.C., McKenzie, J.A., Savin, S. (Eds.),

Continental Indicators of Climate. American Geophysical Union, Jackson Hole, WY, pp. 217–231.
Chamberlin, T.C., 1899. An attempt to frame a working hypothesis of the cause of glacial periods on an atmospheric basis. Journal of Geology, 545–584.
Chorowicz, J., Collet, B., Bonavia, F.F., Mohr, P., Parrot, J.F., Korme, T., 1998. The Tana Basin, Ethiopia; intra-plateau uplift, rifting and subsidence. Tectonophysics 295, 351–367.
Clark, M.K., 2007. The significance of paleotopography. Reviews in Mineralogy and Geochemistry 66, 1–21.
Clark, M.K., House, M.A., Royden, L.H., Whipple, K.X., Burchfiel, B.C., Zhang, X., Tang, W., 2005a. Late Cenozoic uplift of southeastern Tibet. Geology 33, 525–528.
Clark, M.K., Maheo, G., Saleeby, J., Farley, K.A., 2005b. The nonequilibrium landscape of the southern Sierra Nevada, California. GSA Today 15, 4–10.
Clark, M.K., Royden, L.H., 2000. Topographic ooze: building the eastern margin of Tibet by lower crustal flow. Geology 28, 703–706.
Clark, M.K., Royden, L.H., Whipple, K.X., Burchfiel, B.C., Zhang, X., Tang, W., 2006. Use of a regional, relict landscape to measure vertical deformation of the eastern Tibetan Plateau. Journal of Geophysical Research 111, F03002.
Clark, M.K., Schoenbohm, L.M., Royden, L.H., et al., 2004. Surface uplift, tectonics, and erosion of eastern Tibet from large-scale drainage patterns. Tectonics 23, TC1006. doi:10.1029/2002TC001402.
Coffin, M.F., 1992. Emplacement and subsidence of Indian Ocean plateaus and submarine ridges. Geophysical Monograph 70, 115–125.
Coney, P.J., Harms, T.A., 1984. Cordilleran metamorphic core complexes: Cenozoic extensional relics of Mesozoic compression. Geology 12, 550–554.
Cox, K.G., 1989. The role of mantle plumes in the development of continental drainage patterns. Nature (London) 342, 873–877.
Dana, J.D., 1856. On American geological history; address before the American Association for the Advancement of Science, August, 1855. American Journal of Science and Arts 22, 305–334.
Das, T., Nolet, G., 1998. Crustal thickness map of the western United States by partitioned waveform inversion. Journal of Geophysical Research 103, 30021–30038.
Davis, W.M., 1899. The geographical cycle. Geographical Journal 14, 481–504.
Debayle, E., Lévêque, J.-J., Cara, M., 2001. Seismic evidence for a deeply rooted low-velocity anomaly in the upper mantle beneath the northeastern Afro/Arabian continent. Earth and Planetary Science Letters 193, 423–436.
DeCelles, P.G., Robinson, D.M., Zandt, G., 2002. Implications of shortening in the Himalayan fold-thrust belt for uplift of the Tibetan Plateau. Tectonics 21, 1062.
Densmore, M.S., Ehlers, T.A., Woodsworth, G.J., 2007. Effect of Alpine glaciation on thermochronometer age-elevation profiles. Geophysical Research Letters 34, L02502.
Detrick, R.S., Sclater, J.G., Thiede, J., 1977. The subsidence of aseismic ridges. Earth and Planetary Science Letters 34, 185–196.
Dewey, J.F., Burke, K.C.A., 1973. Tibetan, Variscan, and Precambrian basement reactivation: products of continental collision. The Journal of Geology 81, 683–692.
Dickinson, W.R., Snyder, W.S., 1978. Plate tectonics of the Laramide Orogeny. Memoir – Geological Society of America, 355–366.
Dorbath, C., Granet, M., 1996. Local earthquake tomography of the Altiplano and the Eastern Cordillera of northern Bolivia. Tectonophysics 259, 117–136.
Douglass, J., Meek, N., Dorn, R.I., Schmeeckle, M.W., 2009. A criteria-based methodology for determining the mechanism of transverse drainage development, with application to the southwestern US. Geological Society of America Bulletin 121, 586–598.
Ducea, M., House, M.A., Kidder, S., 2003. Late Cenozoic denudation and uplift rates in the Santa Lucia Mountains, California. Geology 31, 139–142.
Dugda, M.T., Nyblade, A.A., Julia, J., 2007. Thin lithosphere beneath the Ethiopian plateau revealed by a joint inversion of rayleigh wave group velocities and receiver functions. Journal of Geophysical Research 112, B08305.
Dugda, M.T., Nyblade, A.A., Julia, J., Langston, C.A., Ammon, C.J., Simiyu, S., 2005. Crustal structure in Ethiopia and Kenya from receiver function analysis: implications for rift development in eastern Africa. Journal of Geophysical Research 110, B01303.
Dunai, T.J., 2010. Cosmogenic Nuclides Principles, Concepts and Applications in the Earth Surface Sciences. Cambridge University Press, New York.
Dunai, T.J., Lopez, G.A.G., Juez-Larre, J., 2005. Oligocene-Miocene age of aridity in the Atacama Desert revealed by exposure dating of erosion-sensitive landforms. Geology 33, 321–324.
Duncan, C., Masek, J., Fielding, E., 2003. How steep are the Himalaya? Characteristics and implications of along-strike topographic variations. Geology 31, 75–78.
Dupont-Nivet, G., Krijgsman, W., Langereis, C.G., Abels, H.A., Dai, S., Fang, X., 2007. Tibetan plateau aridification linked to global cooling at the Eocene–Oligocene transition. Nature 445, 635–638.
Duston, N., Owen, R., Wilkinson, B., 1986. Water chemistry and sedimentological observations in Littlefield Lake, Michigan: implications for lacustrine marl deposition. Environmental Geology 8, 229–236.
Dziewonski, A.M., 1984. Mapping the Lower Mantle: determination of lateral heterogeneity in P velocity up to degree and order 6. Journal of Geophysical Research 89, 5929–5952.
Eaton, G.P., 1987. Topography and Origin of the Southern Rocky Mountains and Alvarado Ridge. Geological Society, London, Special Publications 28, 355–369.
Eaton, G.P., 2008. Epeirogeny in the southern Rocky Mountains region: evidence and origin. Geosphere 4, 764–784.
Ebinger, C.J., Bechtel, T.D., Forsyth, D.W., Bowin, C.O., 1989. Effective elastic plate thickness beneath the East African and Afar plateaus and dynamic compensation of the uplifts. Journal of Geophysical Research 94, 2883–2901.
Effler, S.W., Johnson, D.L., 1987. Calcium carbonate precipitation and turbidity measurements in Otisco Lake, New York. Journal of the American Water Resources Association 23, 73–79.
Ehlers, T.A., Chaudhri, T., Kumar, S., et al., 2005. Computational tools for low-temperature thermochronometer interpretation. Reviews in Mineralogy and Geochemistry 58, 589–622.
Ehlers, T.A., Farley, K.A., Rusmore, M.E., Woodsworth, G.J., 2006. Apatite (U-Th)/He signal of large-magnitude accelerated glacial erosion, southwest British Columbia. Geology 34, 765–768.
Ehlers, T.A., Poulsen, C.J., 2009. Influence of Andean uplift on climate and paleoaltimetry estimates. Earth and Planetary Science Letters 281, 238–248.
Eiler, J.M., Schauble, E., 2004. $^{8}O^{13}C^{16}O$ in Earth's atmosphere. Geochimica et Cosmochimica Acta 68, 4767–4777.
England, P., Houseman, G.A., 1989. Extension during continental convergence, with application to the Tibetan Plateau. Journal of Geophysical Research 94, 17,561–17,579.
England, P., Molnar, P., 1990. Surface uplift, uplift of rocks, and exhumation of rocks. Geology 18, 1173–1177.
England, P.C., Houseman, G.A., 1988. The mechanics of the Tibetan Plateau. The Evolution of Passive Continental Margins in the Light of Recent Deep Drilling Results 326, 301–320.
Epis, R.C., Chapin, C.E., 1975. Geomorphic and tectonic implications of the post-Laramide Late Eocene erosion surface in the Southern Rocky Mountains. Geological Society of America Memoirs 144, 45–74.
Farías, M., Charrier, R., Comte, D., Martinod, J., Herail, G., 2005. Late Cenozoic deformation and uplift of the western flank of the Altiplano; evidence from the depositional, tectonic, and geomorphologic evolution and shallow seismic activity (northern Chile at 19 degrees 30′S). Tectonics 24, TC4001. http://dx.doi.org/10.1029/2004TC001667.
Fielding, E., Isacks, B., Barazangi, M., Duncan, C., 1994. How flat is Tibet? Geology 22, 163–167.
Fielding, E.J., 1996. Tibet uplift and erosion. Tectonphysics 260, 55–84.
Fleitout, L., Froidevaux, C., 1982. Tectonics and topography for a lithosphere containing density heterogeneities. Tectonics 1, 21–56.
Flint, J.J., 1974. Stream gradient as a function of order, magnitude, and discharge. Water Resource Research 10, 969–973.
Flowers, R.M., Wernicke, B.P., Farley, K.A., 2008. Unroofing, incision, and uplift history of the southwestern Colorado Plateau from apatite (U-Th)/He thermochronometry. Geological Society of America Bulletin 120, 571–587.
Forest, C.E., 2007. Paleoaltimetry: a review of thermodynamic methods. Reviews in Mineralogy and Geochemistry 66, 173–193.
Forest, C.E., Molnar, P., Emanuel, K.A., 1995. Palaeoaltimetry from energy conservation principles. Nature 374, 347–350.
Forest, C.E., Wolfe, J.A., Molnar, P., Emanuel, K.A., 1999. Paleoaltimetry incorporating atmospheric physics and botanical estimates of paleoclimate. Geological Society of America Bulletin 111, 497–511.
Francis, P.W., Hawkesworth, C.J., 1994. Late Cenozoic rates of magmatic activity in the Central Andes and their relationships to continental crust formation and thickening. Journal of the Geological Society 151, 845–854.
Froidevaux, C., Ricard, Y., 1987. Tectonic evolution of high plateaus. Tectonophysics 134, 227–238.
Fromm, R., Zandt, G., Beck, S.L., 2004. Crustal thickness beneath the Andes and Sierras Pampeanas at 30° S inferred from Pn apparent phase velocities. Geophysical Research Letters 31, L06625.
Frostick, L.E., Reid, I.A.N., 1989. Climatic versus tectonic controls of fan sequences: lessons from the Dead Sea, Israel. Journal of the Geological Society 146, 527–538.

Fukao, Y., Yamamoto, A., Kono, M., 1989. Gravity anomaly across the Peruvian Andes. Journal of Geophysical Research 94, 3867–3890.
Gale, J., 1972. Availability of carbon dioxide for photosynthesis at high altitudes: theoretical considerations. Ecology 53, 494–497.
Gani, N., Gani, M., Abdelsalam, M., 2007. Blue Nile incision on the Ethiopian Plateau: pulsed plateau growth, Pliocene uplift, and hominin evolution. GSA Today 17, 4–11.
Garzione, C.N., 2008. Surface uplift of Tibet and Cenozoic global cooling. Geology 36, 1003–1004.
Garzione, C.N., Hoke, G.D., Libarkin, J.C., et al., 2008. Rise of the Andes. Science 320, 1304–1307.
Garzione, C.N., Molnar, P., Libarkin, J.C., MacFadden, B.J., 2006. Rapid late Miocene rise of the Bolivian Altiplano: evidence for removal of mantle lithosphere. Earth and Planetary Science Letters 241, 543–556.
Gaupp, R., Kött, A., Wörner, G., 1999. Palaeoclimatic implications of Mio-Pliocene sedimentation in the high-altitude intra-arc Lauca Basin of northern Chile. Palaeogeography, Palaeoclimatology, Palaeoecology 151, 79–100.
Gephart, J.W., 1994. Topography and subduction geometry in the central Andes: clues to the mechanics of a noncollisional orogen. Journal of Geophysical Research 99, 12279–12288.
Ghosh, P., Adkins, J., Affek, H., et al., 2006a. $^{13}C$-$^{18}O$ bonds in carbonate minerals: a new kind of paleothermometer. Geochimica et Cosmochimica Acta 70, 1439–1456.
Ghosh, P., Garzione, C.N., Eiler, J.M., 2006b. Rapid uplift of the Altiplano revealed through $^{13}C$-$^{18}O$ bonds in paleosol carbonates. Science 311, 511–515.
Giese, P., Scheuber, E., Schilling, F., Schmitz, M., Wigger, P., 1999. Crustal thickening processes in the Central Andes and the different natures of the Moho-discontinuity. Journal of South American Earth Sciences 12, 201–220.
Gök, R., Michael, E.P., Ekrem, Z., 2007. Lithospheric structure of the continent–continent collision zone: eastern Turkey. Geophysical Journal International 169, 1079–1088.
Gök, R., Sandvol, E., Türkelli, N., Seber, D., Barazangi, M., 2003. Sn attenuation in the Anatolian and Iranian plateau and surrounding regions. Geophysical Research Letters 30, 8042.
Gosse, J.C., Phillips, F.M., 2001. Terrestrial in situ cosmogenic nuclides: theory and application. Quaternary Science Reviews 20, 1475–1560.
Gotberg, N., McQuarrie, N., Caillaux, V.C., 2010. Comparison of crustal thickening budget and shortening estimates in southern Peru (12–14° S): implications for mass balance and rotations in the "Bolivian orocline". Geological Society of America Bulletin 122, 727–742.
Götze, H.J., Lahmeyer, B., Schmidt, S., Strunk, S., 1994. The lithospheric structure of the Central Andes (20–25S) as inferred from quantitative interpretation of regional gravity. In: Reutter, K., Scheuber, E., Wigger, P. (Eds.), Tectonics of the Southern Central Andes: Structure and Evolution of an Active Continental Margin. Springer-Verlag, Berlin, pp. 23–48.
Gregory, K.M., 1994. Paleoclimate and paleoelevation of the 35 Ma Florissant flora, Front Range, Colorado. Palaeoclimates 1, 23–57.
Gregory, K.M., Chase, C.G., 1992. Tectonic significance of paleobotanically estimated climate and altitude of the late Eocene erosion surface, Colorado. Geology 20, 581–585.
Gregory, K.M., Chase, C.G., 1994. Tectonic and climatic significance of a late Eocene low-relief, high-level geomorphic surface, Colorado. Journal of Geophysical Research 99, 20,141–20,160.
Gregory, K.M., McIntosh, W.C., 1996. Paleoclimate and paleoelevation of the Oligocene Pitch-Pinnacle flora, Sawatch Range, Colorado. Geological Society of America Bulletin 108, 545–561.
Gregory-Wodzicki, K.M., 1997. The late Eocene House Range flora, Sevier Desert, Utah; paleoclimate and paleoelevation. Palaios 12, 552–567.
Gregory-Wodzicki, K.M., 2000. Uplift history of the Central and Northern Andes: a review. Geological Society of America Bulletin 112, 1091–1105.
Griot, D.-A., Montagner, J.-P., Tapponnier, P., 1998. Phase velocity structure from Rayleigh and Love waves in Tibet and its neighboring regions. Journal of Geophysical Research 103, 21215–21232.
Gurnis, M., 1993. Phanerozoic marine inundation of continents driven by dynamic topography above subducting slabs. Nature 364, 589–593.
Gurnis, M., Mitrovica, J.X., Ritsema, J., van Heijst, H.-J., 2000. Constraining mantle density structure using geological evidence of surface uplift rates; the case of the African Superplume. Geochemistry, Geophysics, Geosystems 1(7), 1020. http://dx.doi.org/10.1029/1999GC000035.
Gurnis, M., Mueller, R.D., Moresi, L., 1998. Cretaceous vertical motion of Australia and the Australian-Antarctic discordance. Science 279, 1499–1504.
Hack, J.T., 1957. Studies of longitudinal stream profiles in Virginia and Maryland. United States Geological Survey Professional Paper 294, 45–94.
Hager, B.H., Clayton, R.W., Richards, M.A., Comer, R.P., Dziewonski, A.M., 1985. Lower mantle heterogeneity, dynamic topography and the geoid. Nature 313, 541–545.
Haines, S.S., Klemperer, S.L., Brown, L., et al., 2003. INDEPTH III seismic data: from surface observations to deep crustal processes in Tibet. Tectonics 22, 1001.
Harrison, T.M., Copeland, P., Kidd, W.S.F., Yin, A., 1992. Raising Tibet. Science 255, 1663–1670.
Hartley, A., 2003. Andean uplift and climate change. Journal of the Geological Society 160, 7–10.
Heit, B., Yuan, X.H., Bianchi, M., Sodoudi, F., Kind, R., 2008. Crustal thickness estimation beneath the southern central Andes at 30° S and 36° S from S wave receiver function analysis. Geophysical Journal International 174, 249–254.
Hennig, A., 1915. Zur Petrographie und geologie von Sudwest Tibet. In: Hedin, S. (Ed.), Southern Tibet. Norstedt, Stockholm, 220 pp.
Hirn, A., Lepine, J.-C., Jobert, G., et al., 1984a. Crustal structure and variability of the Himalayan border of Tibet. Nature (London) 307, 23–25.
Hirn, A., Nercessian, A., Sapin, M., et al., 1984b. Lhasa Block and bordering sutures; a continuation of a 500-km Moho traverse through Tibet. Nature (London) 307, 25–27.
Hodges, K.V., Wobus, C., Ruhl, K., Schildgen, T., Whipple, K., 2004. Quaternary deformation, river steepening, and heavy precipitation at the front of the Higher Himalayan ranges. Earth and Planetary Science Letters 220, 379–389.
Hofmann, C., Courtillot, V., Feraud, G., Rochette, P., Yirgu, G., Ketefo, E., Pik, R., 1997. Timing of the Ethiopian flood basalt event and implications for plume birth and global change. Nature 389, 838–841.
Hoke, G.D., Garzione, C.N., 2008. Paleosurfaces, paleoelevation, and the mechanisms for the late Miocene topographic development of the Altiplano plateau. Earth and Planetary Science Letters 271, 192–201.
Hoke, G.D., Garzione, C.N., Araneo, D.C., Latorre, C., Strecker, M.R., Williams, K.J., 2009. The stable isotope altimeter: do Quaternary pedogenic carbonates predict modern elevations? Geology 37, 1015–1018.
Hoke, G.D., Isacks, B.L., Jordan, T.E., Blanco, N., Tomlinson, A.J., Ramezani, J., 2007. Geomorphic evidence for post-10 Ma uplift of the western flank of the central Andes 8°30′-22° S. Tectonics 26, TC5021.
Hoke, L., Hilton, D.R., Lamb, S.H., Hammerschmidt, K., Friedrichsen, H., 1994. 3He evidence for a wide zone of active mantle melting beneath the Central Andes. Earth and Planetary Science Letters 128, 341–355.
Holt, W.E., Wallace, T.C., 1990. Crustal thickness and upper mantle velocities in the Tibetan plateau region from the inversion of regional Pnl waveforms: evidence for a thick upper mantle lid beneath Southern Tibet. Journal of Geophysical Research 95, 12499–12525.
Horton, B.K., 1999. Erosional control on the geometry and kinematics of thrust belt development in the Central Andes. Tectonics 18, 1292–1304.
House, M.A., Wernicke, B.P., Farley, K.A., 1998. Dating topography of the Sierra Nevada, California, using apatite (U-Th)/He ages. Nature 396, 66–69.
House, M.A., Wernicke, B.P., Farley, K.A., 2001. Paleo-Geomorphology of the Sierra Nevada, California, from (U-TH) /He Ages in Apatite. American Journal of Science 301, 77–102.
Houseman, G.A., McKenzie, D.P., Molnar, P., 1981. Convective instability of a thickened boundary layer and its relevance for the thermal evolution of continental convergent belts. Journal of Geophysical Research 86, 6115–6132.
Howard, A.D., Kerby, G., 1983. Channel changes in badlands. GSA Bulletin 94, 739–752.
Huerta, A.D., Nyblade, A.A., Reusch, A.M., 2009. Mantle transition zone structure beneath Kenya and Tanzania: more evidence for a deep-seated thermal upwelling in the mantle. Geophysical Journal International 177, 1249–1255.
Hunt, C.B., 1956. Cenozoic geology of the Colorado Plateau. U.S. Geological Survey Professional Paper 279, 99.
Huntington, K.W., Ehlers, T.A., Hodges, K.V., Whipp, Jr. D.M., 2007. Topography, exhumation pathway, age uncertainties, and the interpretation of thermochronometer data. Tectonics 26, TC4012.
Husson, L., Sempere, T., 2003. Thickening the Altiplano crust by gravity-driven crustal channel flow. Geophysical Research Letters 30, 1243.
Isacks, B.L., 1988. Uplift of the Central Andean plateau and bending of the Bolivian Orocline. Journal of Geophysical Research 93, 3211–3231.
James, D.E., Fouch, M.J., 2002. Formation and evolution of Archaean cratons; insights from Southern Africa. Coastal tectonics 199, 1–26.
Jarvis, A., Reuter, H.I., Nelson, A., Guevara, E., 2008. Hole-filled SRTM for the globe Version 4. Available from the CGIAR-CSI SRTM 90 m: http://srtm.csi.cgiar.org.

Johnson, M.R.W., 2002. Shortening budgets and the role of continental subduction during the India–Asia collision. Earth-Science Reviews 59, 101–123.

Jones, H., 1992. Plants and Microclimate: A Quantitative Approach to Environmental Plant Physiology. Cambridge University Press, New York, 456 pp.

Kennan, L., 2000. Large-scale geomorphology of the Andes; interrelationships of tectonics, magmatism and climate. In: Summerfield, M.A. (Ed.), Geomorphology and Global Tectonics. Wiley, Chichester, pp. 167–199.

Kennan, L., Lamb, S.H., Hoke, L., 1997. High altitude palaeosurfaces in the Bolivian Andes: evidence for late Cenozoic surface uplift. In: Widdowson, M. (Ed.), Palaeosurfaces: Recognition, Reconstruction, and Interpretation. Geological Society of London Special Publications, Bath, UK, pp. 307–324.

Keskin, M., 2003. Magma generation by slab steepening and breakoff beneath a subduction-accretion complex: an alternative model for collision-related volcanism in Eastern Anatolia. Turkey. Geophysical Research Letters 30, 8046.

Ketcham, R.A., Carlson, W.D., 2001. Acquisition, optimization, and interpretation of X-ray computed tomographic imagery: applications to the geosciences. Computers & Geosciences 27, 381–400.

Kind, R., Yuan, X., Saul, J., et al., 2002. Seismic images of Crust and Upper Mantle beneath Tibet: evidence for Eurasian Plate subduction. Science 298, 1219–1221.

King, L.C., 1953. Canons of landscape evolution. Geological Society of America Bulletin 64, 721–752.

Kirby, E., Reiners, P.W., Krol, M.A., et al., 2002. Late Cenozoic evolution of the eastern margin of the Tibetan Plateau: inferences from 40Ar/39Ar and (U-Th)/He thermochronology. Tectonics 21, 1001.

Kirby, E., Whipple, K.X., Tang, W., Chen, Z., 2003. Distribution of active rock uplift along the eastern margin of the Tibetan Plateau: inferences from bedrock channel longitudinal profiles. Journal of Geophysical Research 108, 2217.

Kono, M., Fukao, Y., Yamamoto, A., 1988. Mountain building in the Central Andes. Rock Magnetism and Paleogeophysics 15, 73–80.

Kono, M., Fukao, Y., Yamamoto, A., 1989. Mountain Building in the Central Andes. Journal of Geophysical Research 94, 3891–3905.

Kosarev, G., Kind, R., Sobolev, S.V., Yuan, X., Hanka, W., Oreshin, S., 1999. Seismic evidence for a detached Indian lithospheric Mantle beneath Tibet. Science 283, 1306–1309.

Koulakov, I., Sobolev, S.V., Asch, G., 2006. P- and S-velocity images of the lithosphere–asthenosphere system in the Central Andes from local-source tomographic inversion. Geophysical Journal International 167, 106–126.

Kouwenberg, L.L.R., Kurschner, W.M., McElwain, J.C., 2007. Stomatal frequency change over altitudinal gradients: prospects for paleoaltimetry. Reviews in Mineralogy and Geochemistry 66, 215–241.

Kutzbach, J.E., Guetter, P.J., Ruddiman, W.F., Prell, W.L., 1989. Sensitivity of climate to Late Cenozoic uplift in southern Asia and the American West: numerical experiments. Journal of Geophysical Research 94, 18393–18407.

Lal, D., Peters, B., 1967. Cosmic-Ray Produced Radioactivity on the Earth, Handbook of Physics 46. Springer-Verlag, Berlin, pp. 551–662.

Lamb, S., Hoke, L., 1997. Origin of the high plateau in the Central Andes, Bolivia, South America. Tectonics 16, 623–649.

Lamb, S., Hoke, L., Kennan, L., Dewey, J., 1997. Cenozoic evolution of the Central Andes in Bolivia and northern Chile. Coastal Tectonics 121, 237–264.

Leonard, E.M., 2002. Geomorphic and tectonic forcing of late Cenozoic warping of the Colorado piedmont. Geology 30, 595–598.

Li, C., van der Hilst, R.D., Meltzer, A.S., Engdahl, E.R., 2008. Subduction of the Indian lithosphere beneath the Tibetan Plateau and Burma. Earth and Planetary Science Letters 274, 157–168.

Li, S., Mooney, W.D., 1998. Crustal structure of China from deep seismic sounding profiles. Tectonophysics 288, 105–113.

Libarkin, J.C., Quade, J., Chase, C.G., Poths, J., McIntosh, W., 2002. Measurement of ancient cosmogenic 21Ne in quartz from the 28 Ma Fish Canyon Tuff, Colorado. Chemical Geology 186, 199–213.

Lithgow-Bertelloni, C., Silver, P.G., 1998. Dynamic topography, plate driving forces and the African superswell. Nature (London) 395, 269–272.

Liu, B., Phillips, F.M., Campbell, A.R., 1996. Stable carbon and oxygen isotopes of pedogenic carbonates, Ajo Mountains, southern Arizona: implications for paleoenvironmental change. Palaeogeography, Palaeoclimatology, Palaeoecology 124, 233–246.

Liu, L., Gurnis, M., 2010. Dynamic subsidence and uplift of the Colorado Plateau. Geology 38, 663–666.

Liu-Zeng, J., Tapponnier, P., Gaudemer, Y., Ding, L., 2008. Quantifying landscape differences across the Tibetan plateau: implications for topographic relief evolution. Journal of Geophysical Research 113, F04018.

Mackenzie, G.D., Thybo, H., Maguire, P.K.H., 2005. Crustal velocity structure across the Main Ethiopian Rift: results from two-dimensional wide-angle seismic modeling. Geophysical Journal International 162, 994–1006.

Maggi, A., Priestley, K., 2005. Surface waveform tomography of the Turkish-Iranian plateau. Geophysical Journal International 160, 1068–1080.

Mancktelow, N.S., Grasemann, B., 1997. Time-dependent effects of heat advection and topography on cooling histories during erosion. Tectonophysics 270, 167–195.

Masek, J.G., Isacks, B.L., Gubbels, T.L., Fielding, E.J., 1994. Erosion and tectonics at the margins of continental plateaus. Journal of Geophysical Research 99, 13,941–13,956.

McElwain, J.C., 2004. Climate-independent paleoaltimetry using stomatal density in fossil leaves as a proxy for $CO_2$ partial pressure. Geology 32, 1017–1020.

McElwain, J.C., Mayle, F.E., Beerling, D.J., 2002. Stomatal evidence for a decline in atmospheric $CO_2$ concentration during the Younger Dryas stadial: a comparison with Antarctic ice core records. Journal of Quaternary Science 17, 21–29.

McGlashan, N., Brown, L., Kay, S., 2008. Crustal thickness in the central Andes from teleseismically recorded depth phase precursors. Geophysical Journal International 175, 1013–1022.

McMillan, M.E., Angevine, C.L., Heller, P.L., 2002. Postdepositional tilt of the Miocene–Pliocene Ogallala Group on the western Great Plains: evidence of late Cenozoic uplift of the Rocky Mountains. Geology 30, 63–66.

McMillan, M.E., Heller, P.L., Wing, S.L., 2006. History and causes of post-Laramide relief in the Rocky Mountain orogenic plateau. Geological Society of America Bulletin 118, 393–405.

McNamara, D.E., Owens, T.J., Walter, W.R., 1995. Observations of regional phase propagation across the Tibetan Plateau. Journal of Geophysical Research 100, 22,215–22,229.

McNamara, D.E., Walter, W.R., Owens, T.J., Ammon, C.J., 1997. Upper mantle velocity structure beneath the Tibetan Plateau from Pn travel time tomography. Journal of Geophysical Research 102, 493–505.

McQuarrie, N., Chase, C.G., 2000. Raising the Colorado Plateau. Geology 28, 91–94.

Menard, G., Molnar, P., 1988. Collapse of a Hercynian Tibetan Plateau into a late Palaeozoic European Basin and Range province. Nature 334, 235–237.

Meyer, H.W., 1992. Lapse rates and other variables applied to estimating paleoaltitudes from fossil floras. Palaeogeography, Palaeoclimatology, Palaeoecology 99, 71–99.

Meyer, H.W., 2007. A Review of paleotemperature lapse rate methods for estimating paleoelevation from fossil floras. Reviews in Mineralogy and Geochemistry 66, 155–171.

Molnar, P., 2005. Mio-pliocene growth of the Tibetan Plateau and evolution of East Asian climate. Palaeontologia Electronica 8(1), 2A:23 pp.

Molnar, P., England, P., 1990. Late Cenozoic uplift of mountain ranges and global climate change: chicken or egg? Nature 346, 29–34.

Molnar, P., England, P., Martinod, J., 1993. Mantle dynamics, uplift of the Tibetan Plateau, and the Indian monsoon. Reviews of Geophysics 31, 357–396.

Molnar, P., Houseman, G.A., England, P.C., 2006. Palaeo-altimetry of Tibet. Nature 444, E4.

Molnar, P., Tapponnier, P., 1978. Active tectonics of Tibet. Journal of Geophysical Research 83, 5361–5375.

Montgomery, D.R., Gran, K.B., 2001. Downstream variations in the width of bedrock channels. Water Resource Research 37, 1841–1846.

Moore, A., Blenkinsop, T., 2002. The role of mantle plumes in the development of continental-scale drainage patterns: the southern African example revisited. South African Journal of Geology 105, 353–360.

Mortimer, C., 1973. The Cenozoic history of the southern Atacama Desert, Chile. Journal of the Geological Society 129, 505–526.

Moucha, R., Forte, A.M., Rowley, D.B., Mitrovica, J.X., Simmons, N.A., Grand, S.P., 2009. Deep mantle forces and the uplift of the Colorado Plateau. Geophysical Research Letters 36, L19310.

Myers, S.C., Beck, S., Zandt, G., Wallace, T., 1998. Lithospheric-scale structure across the Bolivian Andes from tomographic images of velocity and attenuation for P and S waves. Journal of Geophysical Research 103, 21233–21252.

Nábělek, J., Hetenyi, G., Vergne, J., et al., 2009. Underplating in the Himalaya-Tibet Collision Zone Revealed by the Hi-CLIMB Experiment. Science 325, 1371–1374.

Nelson, K.D., Zhao, W., Brown, L.D., et al., 1996. Partially molten middle crust beneath southern Tibet; synthesis of Project INDEPTH results. Science 274, 1684–1688.

Neuendorf, K.K.E., Mehl, Jr. J.P., Jackson, J.A., 2005. Glossary of Geology. Alexandria, Virginia, 779 pp.

Nguuri, T.K., Gore, J., James, D.E., et al., 2001. Crustal structure beneath southern Africa and its implications for the formation and evolution of the Kaapvaal and Zimbabwe cratons. Geophysical Research Letters 28, 2501–2504.

Ni, J., Barazangi, M., 1983. High-frequency seismic wave propagation beneath the Indian Shield, Himalayan Arc, Tibetan Plateau and surrounding regions; high uppermost mantle velocities and efficient Sn propagation beneath Tibet. Geophysical Journal of the Royal Astronomical Society 72, 665–689.

Nicoll, K., 2010. Landscape development within a young collision zone; implications for post-Tethyan evolution of the upper Tigris River system in southeastern Turkey. International Geology Review 52, 404–422.

Norin, E., 1946. Geological explorations in western Tibet. In: Hedin, S. (Ed.), Reports from the Scientific Expedition to the Northwestern Provinces of China Under the Leadership of Dr. Sven Hedin. Tryckeri Aktiebolaget, Thule, Stockholm, 214.

Nyblade, A.A., Owens, T.J., Gurrola, H., Ritsema, J., Langston, C.A., 2000. Seismic evidence for a deep upper mantle thermal anomaly beneath east Africa. Geology 28, 599–602.

Nyblade, A.A., Pollack, H.N., Jones, D.L., Podmore, F., Mushayandebvu, M., 1990. Terrestrial heat flow in East and southern Africa. Journal of Geophysical Research 95, 17371–17384.

Nyblade, A.A., Robinson, S.W., 1994. The African superswell. Geophysical Research Letters 21, 765–768.

Ollier, C.D., 1981. Tectonics and Landforms. Longman, London and New York, 324 pp.

Ollier, C.D., 1985. Morphotectonics of passive continental margins: introduction. Zeitschrift für Geomorphologie, Supplementbände 54, 1–9.

Ollier, C.D., Marker, M.E., 1985. The great escarpment of southern Africa. Zeitschrift fuer Geomorphologie Supplementband 54, 37–56.

Olson, P., Nam, I.S., 1986. Formation of seafloor swells by mantle plumes. Journal of Geophysical Research 91, 7181–7191.

Owens, T.J., Zandt, G., 1997. Implications of crustal property variations for models of Tibetan plateau evolution. Nature 387, 37–43.

Paola, C., Mohrig, D., 1996. Palaeohydraulics revisited: palaeoslope estimation in coarse-grained braided rivers. Basin Research 8, 243–254.

Park, Y., Nyblade, A.A., 2006. P-wave tomography reveals a westward dipping low velocity zone beneath the Kenya Rift. Geophysical Research Letters 33, L07311.

Pearce, J.A., Bender, J.F., De Long, S.E., et al., 1990. Genesis of collision volcanism in Eastern Anatolia, Turkey. Journal of Volcanology and Geothermal Research 44, 189–229.

Pederson, J.L., Mackley, R.D., Eddleman, J.L., 2002. Colorado Plateau uplift and erosion evaluated using GIS. GSA Today 12, 4–10.

Peppe, D.J., Royer, D.L., Wilf, P., Kowalski, E.A., 2010. Quantification of large uncertainties in fossil leaf paleoaltimetry. Tectonics 29, TC3015.

Pik, R., Marty, B., Carignan, J., Lave, J., 2003. Stability of the upper Nile drainage network (Ethiopia) deduced from (U-Th)/He thermochronometry; implications for uplift and erosion of the Afar Plume dome. Earth and Planetary Science Letters 215, 73–88.

Poulsen, C.J., Ehlers, T.A., Insel, N., 2010. Onset of convective rainfall during gradual late Miocene rise of the Central Andes. Science 328, 490–493.

Powell, J.W., 1875. Exploration of the Colorado River of the West and its Tributaries. Publisher unknown, Washington, DC.

Press, F., Siever, R., Grotzinger, J., Jordan, T.H., 2004. Understanding Earth. W. H. Freeman and Company, New York, NY.

Proussevitch, A.A., Sahagian, D.L., 2001. Recognition and separation of discrete objects within complex 3D voxelized structures. Computers & Geosciences 27, 441–454.

Proussevitch, A.A., Sahagian, D.L., Carlson, W.D., 2007. Statistical analysis of bubble and crystal size distributions: Application to Colorado Plateau basalts. Journal of Volcanology and Geothermal Research 164, 112–126.

Quade, J., Garzione, C., Eiler, J., 2007. Paleoelevation Reconstruction using Pedogenic Carbonates. Reviews in Mineralogy and Geochemistry 66, 53–87.

Raymo, M.E., 1991. Geochemical evidence supporting chamberlin,T.,C. theory of glaciation. Geology 19, 344–347.

Raymo, M.E., Ruddiman, W.F., 1992. Tectonic forcing of late Cenozoic climate. Nature (London) 359, 117–122.

Rech, J.A., Currie, B.S., Michalski, G., Cowan, A.M., 2006. Neogene climate change and uplift in the Atacama Desert, Chile. Geology 34, 761–764.

Reiners, P.W., 2007. Thermochronologic approaches to paleotopography. Reviews in Mineralogy and Geochemistry 66, 243–267.

Reiners, P.W., Ehlers, T.A., 2005. Low-Temperature Thermochronology; Techniques, Interpretations, and Applications. Mineralogical Society of America, Alexandria Virginia, 622 pp.

Reiners, P.W., McPhillips, D., Brandon, M.T., Mulch, A., Chamberlain, C.P., 2006. Thermochronologic approaches to paleotopography. Geochimica et Cosmochimica Acta 70, A525.

Reiners, P.W., Zhou, Z., Ehlers, T.A., Xu, C., Brandon, M.T., Donelick, R.A., Nicolescu, S., 2003. Postorogenic evolution of the Dabie Shan, eastern China, from (U-Th)/He and fission-track thermochronology. American Journal of Science 303, 489–518.

Rigby, J.K., 1977. Southern Colorado Plateau, K/H Geology Field Guide Studies. Kendall/Hunt Pub. Co., Dubuque, Iowa, pp. 148.

Riihimaki, C.A., Anderson, R.S., Safran, E.B., Dethier, D.P., Finkel, R.C., Bierman, P.R., 2006. Longevity and progressive abandonment of the Rocky Flats surface, Front Range, Colorado. Cosmogenic Isotopes in Geomorphology 78, 265–278.

Riihimaki, C.A., Libarkin, J.C., 2007. Terrestrial cosmogenic nuclides as paleoaltimetric proxies. Reviews in Mineralogy and Geochemistry 66, 269–278.

Rind, D., Chandler, M., 1991. Increased ocean heat transports and warmer climate. Journal of Geophysical Research 96, 7437–7461.

Riquelme, R., Martinod, J., Herail, G., Darrozes, J., Charrier, R., 2003. A geomorphological approach to determining the Neogene to Recent tectonic deformation in the Coastal Cordillera of northern Chile (Atacama). Tectonophysics 361, 255–275.

Ritsema, J., Heijst, H.J.V, Woodhouse, J.H., 1999. Complex shear wave velocity structure imaged beneath Africa and Iceland. Science 286, 1925–1928.

Ritsema, J., Nyblade, A.A., Owens, T.J., Langston, C.A., VanDecar, J.C., 1998. Upper mantle seismic velocity structure beneath Tanzania, east Africa: implications for the stability of cratonic lithosphere. Journal of Geophysical Research 103, 21201–21213.

Ritsema, J., van Heijst, H., 2000. New seismic model of the upper mantle beneath Africa. Geology 28, 63–66.

Roberge, J., Wallace, P.J., White, R.V., Coffin, M.F., 2005. Anomalous uplift and subsidence of the Ontong Java Plateau inferred from $CO_2$ contents of submarine basaltic glasses. Geology 33, 501–504.

Rowley, D.B., 2007. Stable isotope-based paleoaltimetry: theory and validation. Reviews in Mineralogy and Geochemistry 66, 23–52.

Rowley, D.B., Currie, B.S., 2006. Palaeo-altimetry of the late Eocene to Miocene Lunpola basin, central Tibet. Nature 439, 677–681.

Rowley, D.B., Garzione, C.N., 2007. Stable isotope-based paleoaltimetry. Annual Review of Earth and Planetary Sciences 35, 463–508.

Rowley, D.B., Pierrehumbert, R.T., Currie, B.S., 2001. A new approach to stable isotope-based paleoaltimetry: implications for paleoaltimetry and paleohypsometry of the High Himalaya since the Late Miocene. Earth and Planetary Science Letters 188, 253–268.

Roy, M., Jordan, T.H., Pederson, J., 2009. Colorado Plateau magmatism and uplift by warming of heterogeneous lithosphere. Nature (London) 459, 978–982.

Roy, M., Kelley, S., Pazzaglia, F., Cather, S., House, M., 2004. Middle Tertiary buoyancy modification and its relationship to rock exhumation, cooling, and subsequent extension at the eastern margin of the Colorado Plateau. Geology 32, 925–928.

Ruddiman, W.F., 1997. Tectonic Uplift and Climate Change. Plenum Press, New York, NY.

Ruddiman, W.F., Kutzbach, J.E., 1991. Plateau uplift and climatic change. Scientific American 264(66–72), 74–75.

Ruddiman, W.F., Prell, W.L., 1997. Introduction to the Uplift-Climate Connection. Plenum Press, New York, NY.

Ruddiman, W.F., Prell, W.L., Raymo, M.E., 1989. Late Cenozoic Uplift in Southern Asia and the American West: Rationale for General Circulation Modeling Experiments. Journal of Geophysical Research 94, 18379–18391.

Sahagian, D., Proussevitch, A., 2007. Paleoelevation measurement on the basis of vesicular basalts. Reviews in Mineralogy and Geochemistry 66, 195–213.

Sahagian, D., Proussevitch, A., Carlson, W., 2002a. Timing of Colorado Plateau uplift: initial constraints from vesicular basalt-derived paleoelevations. Geology 30, 807–810.

Sahagian, D.L., Anderson, A.T., Ward, B., 1989. Bubble coalescence in basalt flows: comparison of a numerical model with natural examples. Bulletin of Volcanology 52, 49–56.

Sahagian, D.L., Maus, J.E., 1994. Basalt vesicularity as a measure of atmospheric pressure and palaeoelevation. Nature 372, 449–451.

Sahagian, D.L., Proussevitch, A.A., Carlson, W.D., 2002b. Analysis of vesicular basalts and lava emplacement processes for application as a paleobarometer/paleoaltimeter. The Journal of Geology 110, 671–685.

Schäfer, J.M., Ivy-Ochs, S., Wieler, R., Leya, I., Baur, H., Denton, G.H., Schlüchter, C., 1999. Cosmogenic noble gas studies in the oldest landscape on earth: surface exposure ages of the Dry Valleys, Antarctica. Earth and Planetary Science Letters 167, 215–226.

Schildgen, T.F., Balco, G., Shuster, D.L., 2010. Canyon incision and knickpoint propagation recorded by apatite 4He/3He thermochronometry. Earth and Planetary Science Letters 293, 377–387.

Schildgen, T.F., Hodges, K.V., Whipple, K.X., Reiners, P.W., Pringle, M.S., 2007. Uplift of the western margin of the Andean plateau revealed from canyon incision history, southern Peru. Geology 35, 523–526.

Schlunegger, F., Zeilinger, G., Kounov, A., Kober, F., Hüsser, B., 2006. Scale of relief growth in the forearc of the Andes of Northern Chile (Arica latitude, 18° S). Terra Nova 18, 217–223.

Schmitz, M., 1994. A balanced model of the southern Central Andes. Tectonics 13, 484–492.

Schoenbohm, L.M., Whipple, K.X., Burchfiel, B.C., Chen, L., 2004. Geomorphic constraints on surface uplift, exhumation, and plateau growth in the Red River region, Yunnan Province, China. Geological Society of America Bulletin 116, 895–909.

Schulte-Pelkum, V., Monsalve, G., Sheehan, A., Pandey, M.R., Sapkota, S., Bilham, R., Wu, F., 2005. Imaging the Indian subcontinent beneath the Himalaya. Nature (London) 435, 1222–1225.

Şengör, A.M.C., Ozeren, M.S., Keskin, M., Sakinc, M., Ozbakir, A.D., Kayan, I., 2008. Eastern Turkish high plateau as a small turkic-type orogen; implications for postcollisional crust-forming processes in turkic-type orogens. Earth-Science Reviews 90, 1–48.

Servant, M., Sempere, T., Argollo, J., Bernat, M., Feraud, G., Lo Bello, P., 1989. Morphogenese et soulevement de la Cordillere Orientale des Andes de Bolivie au Cenozoique. Comptes Rendus de l'Academie des Sciences, Série 2(309), 416–422.

Sheffels, B.M., 1990. Lower bound on the amount of crustal shortening, in the central Bolivian Andes. Geology 18, 812–815.

Shi, D., Zhao, W., Brown, L., et al., 2004. Detection of southward intracontinental subduction of Tibetan lithosphere along the Bangong–Nujiang suture by P-to-S converted waves. Geology 32, 209–212.

Simmons, N.A., Forte, A.M., Grand, S.P., 2007. Thermochemical structure and dynamics of the African superplume. Geophysical Research Letters 34, L02301.

Sine, C.R., Wilson, D., Gao, W., Grand, S.P., Aster, R., Ni, J., Baldridge, W.S., 2008. Mantle structure beneath the western edge of the Colorado Plateau. Geophysical Research Letters 35, L10303.

Snyder, N.P., Whipple, K.X., Tucker, G.E., Merritts, D.J., 2000. Landscape response to tectonic forcing: digital elevation model analysis of stream profiles in the Mendocino triple junction region, northern California. Geological Society of America Bulletin 112, 1250–1263.

Sobel, E.R., Hilley, G.E., Strecker, M.R., 2003. Formation of internally drained contractional basins by aridity-limited bedrock incision. Journal of Geophysical Research 108, 2344.

Sonder, L.J., England, P.C., 1989. Effects of a temperature-dependent rheology on large-scale continental extension. Journal of Geophysical Research 94, 7603–7619.

Sonder, L.J., Jones, C.H., 1999. Western United States extension: how the west was widened. Annual Review of Earth and Planetary Sciences 27, 417–462.

Spencer, J.E., 1996. Uplift of the Colorado Plateau due to lithosphere attenuation during Laramide low-angle subduction. Journal of Geophysical Research 101, 13,595–13,609.

Spicer, R.A., Harris, N.B.W., Widdowson, M., et al., 2003. Constant elevation of southern Tibet over the past 15 million years. Nature 421, 622–624.

Stanistreet, I.G., McCarthy, T.S., 1993. The Okavango fan and the classification of subaerial fan systems. Sedimentary Geology 85, 115–133.

Stark, C.P., Stewart, J., Ebinger, C.J., 2003. Wavelet transform mapping of effective elastic thickness and plate loading: Validation using synthetic data and application to the study of southern African tectonics. Journal of Geophysical Research 108, 2558.

Stock, G.M., Ehlers, T.A., Farley, K.A., 2006. Where does sediment come from? Quantifying catchment erosion with detrital apatite (U-Th)/He thermochronometry. Geology 34, 725–728.

Stockli, D.F., 2006. Thermochronometric constraints on paleoaltimetry and paleotopography – case studies from the Colorado Plateau, Tibet, and Labrador. Geochimica et Cosmochimica Acta 70, A617.

Strecker, M.R., Alonso, R.N., Bookhagen, B., Carrapa, B., Hilley, G.E., Sobel, E.R., Trauth, M.H., 2007. Tectonics and climate of the southern Central Andes. Annual Review of Earth and Planetary Sciences 35, 747–787.

Stüwe, K., White, L., Brown, R., 1994. The influence of eroding topography on steady-state isotherms. Application to fission track analysis. Earth and Planetary Science Letters 124, 63–74.

Summerfield, M.A., 1991. Global Geomorphology. Prentice Hall Longman/Wiley, London/New York.

Sutherland, R., Spasojevic, S., Gurnis, M., 2010. Mantle upwelling after Gondwana subduction death explains anomalous topography and subsidence histories of eastern New Zealand and West Antarctica. Geology 38, 155–158.

Swenson, J.L., Beck, S.L., Zandt, G., 2000. Crustal structure of the Altiplano from broadband regional waveform modeling: Implications for the composition of thick continental crust. Journal of Geophysical Research 105, 607–621.

Tabatabai Mir, S., Bergman, E., Gheitanchi, M.R., 2008. 3-Dimensional upper mantle velocity structure for Iranian Plateau revealed by Pn and Sn tomography. Journal of the Earth and Space Physics 33, 13–24.

Tapponnier, P., Zhiqin, X., Roger, F., Meyer, B., Arnaud, N., Wittlinger, G., Jingsui, Y., 2001. Oblique stepwise rise and growth of the Tibet Plateau. Science 294, 1671–1677.

Teixell, A., Ayarza, P., Zeyen, H., Fernandez, M., Arboleya, M.-L., 2005. Effects of mantle upwelling in a compressional setting: the Atlas Mountains of Morocco. Terra Nova 17, 456–461.

ten Brink, U., Stern, T., 1992. Rift flank uplifts and Hinterland Basins: comparison of the transantarctic mountains with the great escarpment of southern Africa. Journal of Geophysical Research 97, 569–585.

Thorpe, R.S., Francis, P.W., Harmon, R.S., Anonymous., 1981. Andean andesites and crustal growth. The Evolution of Passive Continental Margins in the Light of Recent Deep Drilling Results 301, 305–320.

Thouret, J.C., Wörner, G., Gunnell, Y., Singer, B., Zhang, X., Souriot, T., 2007. Geochronologic and stratigraphic constraints on canyon incision and Miocene uplift of the Central Andes in Peru. Earth and Planetary Science Letters 263, 151–166.

Tilmann, F., Ni, J., Team, I.I.S., 2003. Seismic imaging of the downwelling Indian lithosphere beneath Central Tibet. Science 300, 1424–1427.

Turkelli, N., Sandvol, E., Zor, E., et al., 2003. Seismogenic zones in Eastern Turkey. Geophysical Research Letters 30, 8039.

Turner, S., Hawkesworth, C., Liu, J., Rogers, N., Kelley, S., van Calsteren, P., 1993. Timing of Tibetan uplift constrained by analysis of volcanic rocks. Nature (London) 364, 50–54.

Valla, P.G., Herman, F., van der Beek, P.A., Braun, J., 2010. Inversion of thermochronological age-elevation profiles to extract independent estimates of denudation and relief history – I: Theory and conceptual model. Earth and Planetary Science Letters 295, 511–522.

Van der Wateren, F.M., Dunai, T.J., 2001. Late Neogene passive margin denudation history – cosmogenic isotope measurements from the central Namib desert. Global and Planetary Change 30, 271–307.

Vandervoort, D.S., Jordan, T.E., Zeitler, P.K., Alonso, R.N., 1995. Chronology of internal drainage development and uplift, southern Puna plateau, Argentine central Andes. Geology 23, 145–148.

Vassallo, R., Ritz, J.F., Braucher, R., et al., 2007. Transpressional tectonics and stream terraces of the Gobi-Altay, Mongolia. Tectonics 26, TC5013.

Wang, X., Ni, J.F., Aster, R., et al., 2008. Shear-wave splitting and mantle flow beneath the Colorado Plateau and Its boundary with the Great Basin. Bulletin of the Seismological Society of America 98, 2526–2532.

Wang, Z., Schauble, E.A., Eiler, J.M., 2004. Equilibrium thermodynamics of multiply substituted isotopologues of molecular gases. Geochimica et Cosmochimica Acta 68, 4779–4797.

Wdowinski, S., Bock, Y., 1994. The evolution of deformation and topography of high elevated plateaus 2. Application to the central Andes. Journal of Geophysical Research 99, 7121–7130.

Weeraratne, D.S., Forsyth, D.W., Fischer, K.M., Nyblade, A.A., 2003. Evidence for an upper mantle plume beneath the Tanzanian craton from Rayleigh wave tomography. Journal of Geophysical Research 108, 2427.

Wernicke, B.P., Christiansen, R.L., England, P.C., Sonder, L.J., 1987. Tectonomagmatic evolution of Cenozoic extension in the North American Cordillera. Coastal tectonics 28, 203–221.

West, M., Ni, J., Baldridge, W.S., Wilson, D., Aster, R., Gao, W., Grand, S., 2004. Crust and upper mantle shear wave structure of the southwest United States:

Implications for rifting and support for high elevation. Journal of Geophysical Research 109, B03309.
Whipple, K.X., 2001. Fluvial landscape response time: how plausible is steady-state denudation? American Journal of Science 301, 313–325.
Whipple, K.X., 2004. Bedrock rivers and the geomorphology of active orogens. Annual Review of Earth and Planetary Sciences 32, 151–185.
Whipple, K.X., 2009. The influence of climate on the tectonic evolution of mountain belts. Nature Geosci 2, 97–104.
Whipple, K.X., Tucker, G.E., 1999. Dynamics of the stream-power river incision model: implications for height limits of mountain ranges, landscape response timescales, and research needs. Journal of Geophysical Research 104, 17,661–17,674.
Whitman, D., Isacks, B.L., Chatelain, J.-L., Chiu, J.-M., Perez, A., 1992. Attenuation of high-frequency seismic waves beneath the Central Andean Plateau. Journal of Geophysical Research 97, 19929–19947.
Whitman, D., Isacks, B.L., Kay, S.M., 1996. Lithospheric structure and along-strike segmentation of the Central Andean Plateau; seismic Q, magmatism, flexure, topography and tectonics. Tectonophysics 259, 29–40.
Whittaker, A.C., Cowie, P.A., Attal, M., Tucker, G.E., Roberts, G.P., 2007. Bedrock channel adjustment to tectonic forcing: implications for predicting river incision rates. Geology 35, 103–106.
Widdowson, M., 1997. The geomorphological and geological importance of palaeosurfaces. Coastal Tectonics 120, 1–12.
Wigger, P., Baldzuhn, S., Giese, P., et al., 1994. Variations of the Crustal structure of the southern Central Andes deduced from seismic refraction investigations. In: Reuter, H.J., Scheuber, E., Wigger, P.J. (Eds.), Tectonics of the Southern Central Andes: Structure and Evolution of an Active Continental Margin. Springer, Berlin, pp. 23–48.
Wilson, D., Aster, R., Ni, J., et al., 2005. Imaging the seismic structure of the crust and upper mantle beneath the Great Plains, Rio Grande Rift, and Colorado Plateau using receiver functions. Journal of Geophysical Research 110, B05306.
Wittlinger, G., Masson, F., Poupinet, G., et al., 1996. Seismic tomography of northern Tibet and Kunlun; evidence for crustal blocks and mantle velocity contrasts. Earth and Planetary Science Letters 139, 263–279.
Wittlinger, G., Vergne, J., Tapponnier, P., et al., 2004. Teleseismic imaging of subducting lithosphere and Moho offsets beneath western Tibet. Earth and Planetary Science Letters 221, 117–130.
Wobus, C., Whipple, K.X., Kirby, E., et al. , 2006.Tectonics from topography; procedures, promise, and pitfalls. Special Paper – Geological Society of America 398, pp. 55–74.
Wobus, C.W., Hodges, K.V., Whipple, K.X., 2003. Has focused denudation sustained active thrusting at the Himalayan topographic front? Geology 31, 861–864.
Wolfe, J.A., 1992a. An analysis of present-day terrestrial lapse rates in the western conterminous United States and their significance to paleoaltitudinal estimates. U. S. Geological Survey Bulletin B 1964, 35.
Wolfe, J.A., 1992b. Climatic, floristic, and vegetational changes near the Eocene/Oligocene boundary. In: Prothero, D.R., Berggren, W.A. (Eds.), Eocene-Oligocene Climatic and Biotic Evolution. Princeton University Press, Princeton, pp. 421–436.
Wolfe, J.A., 1993. A method of obtaining climatic parameters from fossil leaf assemblages. U. S. Geological Survey Bulletin 2040, 1–71.
Wolfe, J.A., 1994. Tertiary climatic changes at middle latitudes of western North America. Palaeogeography, Palaeoclimatology, Palaeoecology 108, 195–205.
Wolfe, J.A., 1995. Paleoclimatic estimates from tertiary leaf assemblages. Annual Review of Earth and Planetary Sciences 23, 119–142.
Wolfe, J.A., Forest, C.E., Molnar, P., 1998. Paleobotanical evidence of Eocene and Oligocene paleoaltitudes in midlatitude western North America. Geological Society of America Bulletin 110, 664–678. http://dx.doi.org/10.1130/0016–7606.
Wolfe, J.A., Schorn, H.E., Forest, C.E., Molnar, P., 1997. Paleobotanical evidence for high altitudes in Nevada during the Miocene. Science 276, 1672–1675.
Wolfe, J.A., Spicer, R.A., 1999. Fossil leaf character states; multivariate analyses. In: Jones, T.P., Rowe, N.P. (Eds.), Fossil Plants and Spores; Modern Techniques. Geological Society, London, UK, pp. 233–239.
Xu, L., Rondenay, S., van der Hilst, R.D., 2007. Structure of the crust beneath the southeastern Tibetan Plateau from teleseismic receiver functions. Physics of the Earth and Planetary Interiors 165, 176–193.
Yao, H., Beghein, C., van der Hilst, R.D., 2008. Surface wave array tomography in SE Tibet from ambient seismic noise and two-station analysis – II. Crustal and upper-mantle structure. Geophysical Journal International 173, 205–219.
Yilmaz, Y., Güner, Y., Saroglu, F., 1998. Geology of the quaternary volcanic centers of the east Anatolia. Journal of Volcanology and Geothermal Research 85, 173–210.
Yuan, X., Sobolev, S.V., Kind, R., 2002. Moho topography in the central Andes and its geodynamic implications. Earth and Planetary Science Letters 199, 389–402.
Yuan, X., Sobolev, S.V., Kind, R., et al., 2000. Subduction and collision processes in the Central Andes constrained by converted seismic phases. Nature 408, 958–961.
Zandt, G., Myers, S.C., Wallace, T.C., 1995. Crust and mantle structure across the Basin and Range-Colorado Plateau boundary at 37° N latitude and implications for Cenozoic extensional mechanism. Journal of Geophysical Research 100, 10529–10548.
Zhao, W.-L., Morgan, W.J., 1987. Injection of Indian crust into Tibetan lower crust: a two-dimensional finite element model study. Tectonics 6, 489–504.
Zheng, H., Powell, C.M., Zhou, Z., Dong, G., J., 2000. Pliocene uplift of the northern Tibetan Plateau. Geology 28, 715–718.
Zhu, L., Owens, T.J., Randall, G.E., 1995. Lateral variation in crustal structure of the northern Tibetan Plateau inferred from teleseismic receiver functions. Bulletin of the Seismological Society of America 85, 1531–1540.
Zor, E., 2008. Tomographic evidence of slab detachment beneath eastern Turkey and the Caucasus. Geophysical Journal International 175, 1273–1282.
Zor, E., Sandvol, E., Gürbüz, C., Türkelli, N., Seber, D., Barazangi, M., 2003. The crustal structure of the East Anatolian plateau (Turkey) from receiver functions. Geophysical Research Letters 30, 8044.

## Biographical Sketch

Julien Babault is a lecturer in Earth Surface Processes in the Department of Geology, Universitat Autònoma de Barcelona, Spain. He holds an MSc degree in Geology, and a PhD in Geology from the Department of Géosciences Rennes, Université de Rennes 1. His research interest include mountain belts dynamics of erosion at continental scale and dynamics of river network using field examples (Pyrenees, High Atlas of Morocco, Eastern Cordillera of Colombia in the Andes), quantification of erosion rates and rock/surface uplift rates, and experimental modeling.

Jean Van Den Driessche is a professor of Geology at the University of Rennes1. He has a PhD from the University of Montpellier and completed a State thesis in tectonics at the University Denis Diderot of Paris and the Institute of Earth Physics of Paris. His teaching and research concern tectonics, lithosphere mechanics and dynamics of continental erosion.

# Shortening, structural relief and drainage evolution in inverted rifts: insights from the Atlas Mountains, the Eastern Cordillera of Colombia and the Pyrenees

JULIEN BABAULT[1], ANTONIO TEIXELL[1]*, LUCÍA STRUTH[1], JEAN VAN DEN DRIESSCHE[2], MARÍA LUISA ARBOLEYA[2] & ELISEO TESÓN[3]

[1]*Departament de Geologia, Universitat Autònoma de Barcelona, 08193 Bellaterra (Barcelona), Spain*

[2]*Géosciences Rennes, Université de Rennes 1, Campus de Beaulieu, Rennes, France*

[3]*Instituto Colombiano del Petróleo-Ecopetrol, km 7 Via a Piedecuesta, Bucaramanga, Colombia*

**Corresponding author (e-mail: antonio.teixell@uab.es)*

**Abstract:** The Atlas, Eastern Cordillera and Pyrenees are thick-skinned thrust-fold belts formed by tectonic inversion of rift basins in continental settings. A comparison of shortening between them shows a gradation from 20–25% in the central High Atlas, to 25–30% in the Eastern Cordillera, and *c.* 40% in the Pyrenees. Accordingly, there is a structural variation from interior zones with low structural relief and isolated basement massifs in the first two cases, to an axial culmination of stacked basement thrust sheets in the Pyrenees. This results in marked topographic and drainage variation: the High Atlas and Eastern Cordillera contain axial plateaus dominated by structure-controlled longitudinal rivers and orogen flanks with slope-controlled transverse rivers, whereas the Pyrenees show a two-sided wedge profile dominated by transverse rivers. In spite of singularities exhibited by each orogen, we propose that this spatial variation can be understood as reflecting different degrees of evolution in mountain building. Rapidly incising, transverse rivers are capturing earlier longitudinal streams of the Atlas and Eastern Cordillera, thus reducing their axial plateaux, which will eventually disappear into a transverse-dominated drainage. This pattern of landscape evolution may be characteristic of inversion orogens as they develop from initial stages of inversion to full accretion.

The Atlas Mountains, the Eastern Cordillera of Colombia and the Pyrenees are typical examples of thrust-fold belts formed by tectonic inversion of former continental rifts. Rift inversion is a common modality of compressional deformation in intraplate regions, in addition to other mechanisms characteristic of craton deformation such as lithospheric folding or upthrusting of isolated basement massifs (e.g. Ziegler *et al.* 1998). Inverted rifts typically show a lesser amount of orogenic shortening than collisional mountain belts at plate-boundaries because they lack powerful slab-pull forces by a subducting oceanic plate, and are driven by far-field stresses instead.

In spite of the singularities in structural style exhibited by each case, we aim to illustrate that the studied inverted rifts possess some common characteristics in terms of topography and drainage evolution, and at least two of them demonstrably differ from self-similar, growing wedge models commonly envisaged for collisional belts. Hovius (1996) remarked that many actively uplifting mountain belts around the world have simple drainage patterns transverse to their main structural trend. On the other hand, Babault *et al.* (2012) show that in the High Atlas hinterland, the drainage is longitudinal and inherited from an early stage of fluvial organization controlled by the tectonic structures developed during upper crustal folding and thrusting. Amplification of regional slope perpendicular to the tectonic trend in the western High Atlas by continued crustal shortening and thickening triggered a new organization of the drainage system towards the regional slope, thus recording an evolution from longitudinal to transverse-dominated drainage that may represent a common mechanism of fluvial network development in mountain belts where lithospheric convergence progressively increases the regional slopes.

In this paper, we first review and synthesize the structural features of each of the three mountain belts (largely based on earlier works; Figs 1–3), showing that they represent different amounts of deformation and cumulative shortening, and then make a comparison of their drainage network, which we propose defines a consistent pattern of drainage gradation from longitudinal- to transverse-dominated.

*From*: Nemčok, M., Mora, A. & Cosgrove, J. W. (eds) *Thick-Skin-Dominated Orogens: From Initial Inversion to Full Accretion*. Geological Society, London, Special Publications, **377**, http://dx.doi.org/10.1144/SP377.14 

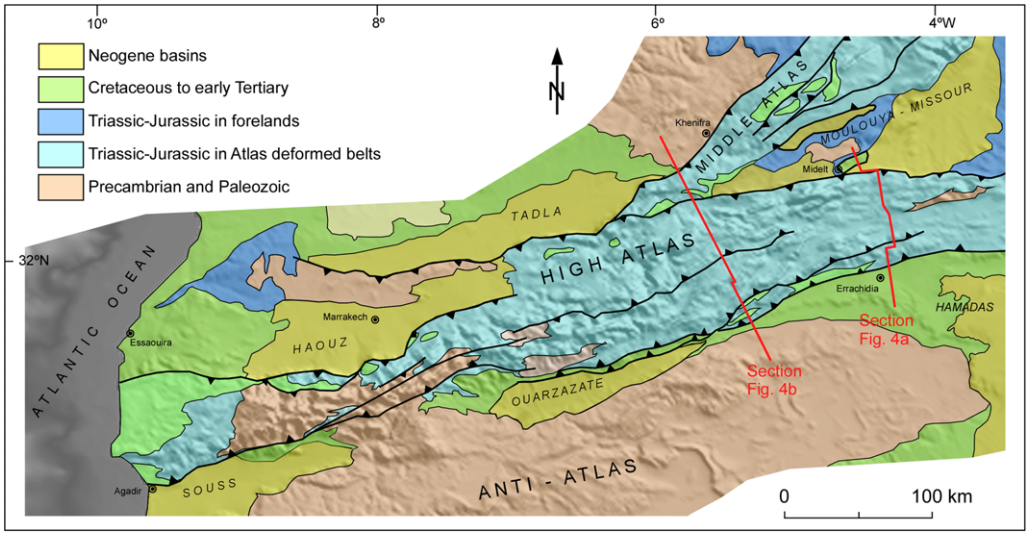


**Fig. 1.** Tectonic sketch map of the Moroccan High Atlas Mountains, indicating the lines of section of Figure 4a, b.

## The High Atlas

The Atlas Mountains of Morocco formed during the Cenozoic in the interior of the African plate but in close association with the Europe–Africa convergence (Mattauer *et al.* 1977). They consist of two thrust-fold belts (the NE-trending Middle Atlas and the ENE-trending High Atlas), and a wide arch with modest post-Palaeozoic deformation (the Anti-Atlas; Fig. 1). The High and Middle Atlas belts were created by the tectonic inversion of pre-existing extensional/transtensional basins of Triassic–Jurassic age (Mattauer *et al.* 1977; Beauchamp 1988; Warme 1988; Frizon de Lamotte *et al.* 2000; Gomez *et al.* 2000; Piqué *et al.* 2002; Teixell *et al.* 2003; Arboleya *et al.* 2004), whereas the Anti-Atlas, lying originally outside of the rift basins, conforms to a large (100 km-scale or lithospheric-scale) domal fold cut by minor faults (Guimerà *et al.* 2011).

We will focus this review on the High Atlas, a 50–120 km wide belt of thrusts and folds deforming a thick succession of sedimentary rocks, dominantly Jurassic in age. The structural style of compressive deformation is mainly thick-skinned (Frizon de Lamotte *et al.* 2000; Teixell *et al.* 2003), whereas in the southern part of the central High Atlas there is a belt of south-verging detached folds and thrusts (Laville *et al.* 1977; Beauchamp *et al.* 1999; Tesón 2009). This is related to salt or other favourable weak layers in the area. Salt diapirs formed during the earlier extensional episode are occasionally observed (Teixell *et al.* 2003; Michard *et al.* 2011; Fig. 4).

The cross-sections of Figure 4a, b illustrate the characteristic structural style of the central High Atlas. Compressional deformation is heterogeneously distributed: narrow deformation bands constituted by anticlines or thrust faults are commonly separated by broad synclines or tabular plateaux. Variations in Mesozoic stratigraphy and thickness across many thrust faults attest to their origin as synsedimentary extensional faults. The trend of the main individual thrusts and folds is NE–SW, slightly oblique to the general orientation of the High Atlas belt (Fig. 1), and whose inheritance argues for oblique rifting during the Jurassic (El Kochri & Chorowicz 1995; Arboleya *et al.* 2004). Consistent with the original dip of the Mesozoic basin-bordering faults, the present High Atlas is a doubly verging chain, in which a strongly exhumed internal zone cannot be defined as in other orogenic belts. In fact, owing to the moderate degree of inversion, in much of the interior of the chain, basement is at lower structural elevation than in the peripheral forelands (Fig. 4a, b). In the central High Atlas there is an axial plateau-like structure (e.g. Fig. 4b), where the topographic surface is at an elevation of ca. 2000 m. Hence, most of the total orogenic shortening across the High Atlas is concentrated in its northern and southern margins (e.g. Benammi *et al.* 2001; Tesón 2009). In addition to thrusting, buckle folding (not necessarily fault-related) is also common in the High Atlas. These folds, even if tight, may involve basement rocks (e.g. as observed at the basement massif SE of Midelt, Fig. 1). Section construction resulted in less line-length shortening in basement than

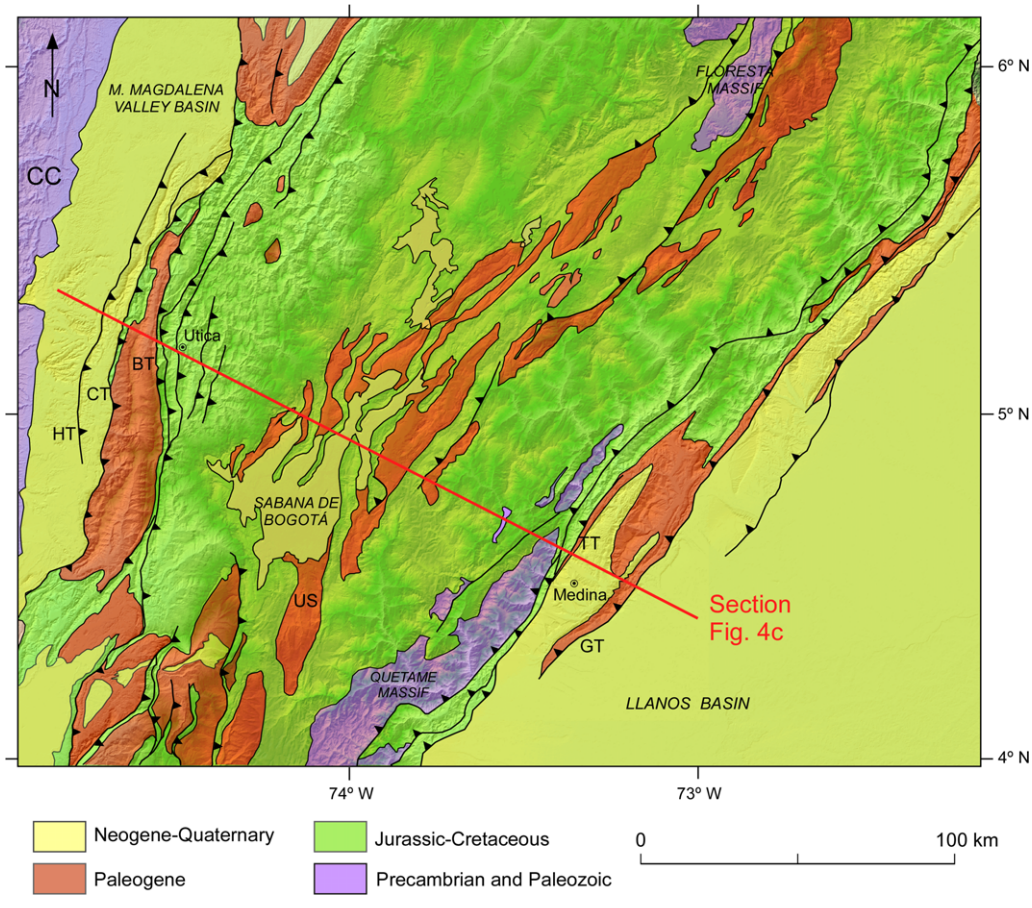


**Fig. 2.** Tectonic sketch map of the Eastern Cordillera of Colombia. This map is a synthesis of Toro *et al.* (2004), Parra *et al.* (2009b) and unpublished maps by ICP-Ecopetrol. Indicated is the line of section of Figure 4c. CC, Central Cordillera; HT, Honda thrust; CT, Cambao thrust; BT, Bituima thrust; US, Usme syncline; TT, Tesalia thrust; GT, Guaicáramo thrust.

in the post-Palaeozoic cover (Teixell *et al.* 2003); additional shortening mechanisms such as homogeneous flattening or underthrusting must have occurred in the former. In spite of these difficulties, total orogenic shortening from the restoration of post-palaeozoic layers in the central High Atlas has been estimated as 24% for the eastern section of Figure 4a and 18% for the western section of Figure 4b (Teixell *et al.* 2003). Total shortening still decreases further to the west, in spite of higher topographic elevations and wide exposure of basement in the western High Atlas, a fact not completely understood yet.

### *Timing of deformation and surface uplift*

The Cretaceous post-rift conditions in the Atlas domain gave way to the initiation of compressional deformation in the latest Cretaceous or earliest Cenozoic. Adjacent to the present-day High Atlas is a discontinuous system of foreland basins filled with Neogene deposits (the Souss, Ouarzazate, Haouz–Tadla and Moulouya–Missour basins; Fig. 1). Cenozoic sediments provide timing of the rift inversion process from tectonics–sedimentation relationships, although there have been marked discrepancies among different authors that have faced the subject (e.g. Laville *et al.* 1977; Fraissinet *et al.* 1988; Görler *et al.* 1988; Frizon de Lamotte *et al.* 2000). For the main deformation episode we follow the recent attributions by Tesón & Teixell (2008) and Tesón *et al.* (2010), which combine field observations with magnetostratigraphy.

The earliest indications of folding are provided by the uppermost Cretaceous to Eocene inliers within the High Atlas or the southern thrust front.

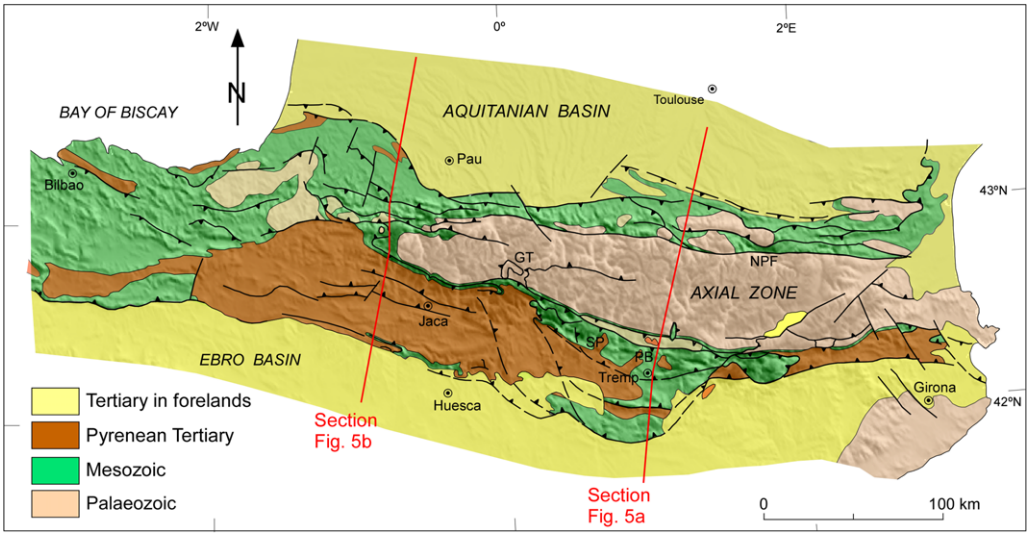


**Fig. 3.** Tectonic sketch map of the Pyrenees (after Teixell 1996) indicating the lines of section of Figure 5. NPF, North Pyrenean fault; GT, Gavarnie thrust; PB, Pobla and Senterada basins; SP, Sis palaeovalley.

They occasionally display angular and progressive unconformities (Laville *et al.* 1977; Froitzheim *et al.* 1988; Tesón 2009), indicating that contractional deformation has been initiated in this time. However, the sparse occurrences and degree of development of the unconformities indicate that this deformation was very limited, consisting of isolated fold ridges of local extent (occasionally salt-related) growing within the post-rift basin. The palaeogeography of the correlative subtabular limestone deposits of Paleocene to mid Eocene age still does not conform to a foreland basin system (Herbig & Trappe 1994; Tesón & Teixell 2008). Above the limestone, fluvial–alluvial red shales, sandstones and microconglomerates of mid to late Eocene age, occurring only in the southern frontal thrust belt of the High Atlas, have been interpreted as the first foreland basin deposits (El Harfi *et al.* 1996; Frizon de Lamotte *et al.* 2000; Tesón & Teixell 2008). It must be pointed out, however, that synsedimentary deformation structures have never been observed in these deposits, and that fission-track studies have failed to detect contemporaneous exhumation in the High Atlas hinterland. Still, provenance from an eroding High Atlas seems probable (Tesón 2009); microconglomerates are composed dominantly of recycled pebbles from lower Cretaceous red beds (i.e. approximately the youngest deposits of the Mesozoic Atlas basins), attesting to moderate deformation and exhumation prevailing during the entire Eocene.

The best record for the age of main thrusting in the Atlas comes from the Ouarzazate Basin (Fig. 1) and the marginal thrust belt adjacent to it. The main infill of the basin (Ait Kandoula fm) has been recently dated as Middle to Late Miocene (Tesón *et al.* 2010). This formation rests unconformably over selected thrusts and folds, whereas it is affected by others (Fraissinet *et al.* 1988; Tesón & Teixell 2008). Hence, main thrusting must have initiated sometime within a generalized sedimentary hiatus below the Ait Kandoula Formation (Oligocene to early Miocene), and has continued at similar rate until the Quaternary (Sébrier *et al.* 2006; Arboleya *et al.* 2008; Pastor 2008). Apatite fission track ages of 9–25 Ma recorded in the High Atlas of Marrakech (Missenard *et al.* 2008; Balestrieri *et al.* 2009) and thermal modelling in the central High Atlas (Barbero *et al.* 2007) are compatible with the Neogene age of main thrusting. Shortening and crustal thickening since late Eocene times, probably with relatively faster rates since the Miocene, has led to surface uplift in the Atlas.

However, an enigmatic feature of the Atlas region as a whole, which has received the attention of many geoscientists, is its high topographic elevation compared with the modest values of shortening and crustal thickening. An inverse correlation between shortening and elevation along the central High Atlas belt indicates that crustal thickening does not fully explain the observed topography and suggests a mantle-sourced, thermal contribution to uplift (Teixell *et al.* 2003), which is corroborated by geophysical data and modelling (Seber *et al.* 1996; Ayarza *et al.* 2005; Teixell *et al.* 2005; Zeyen *et al.* 2005; Missenard *et al.* 2006). While

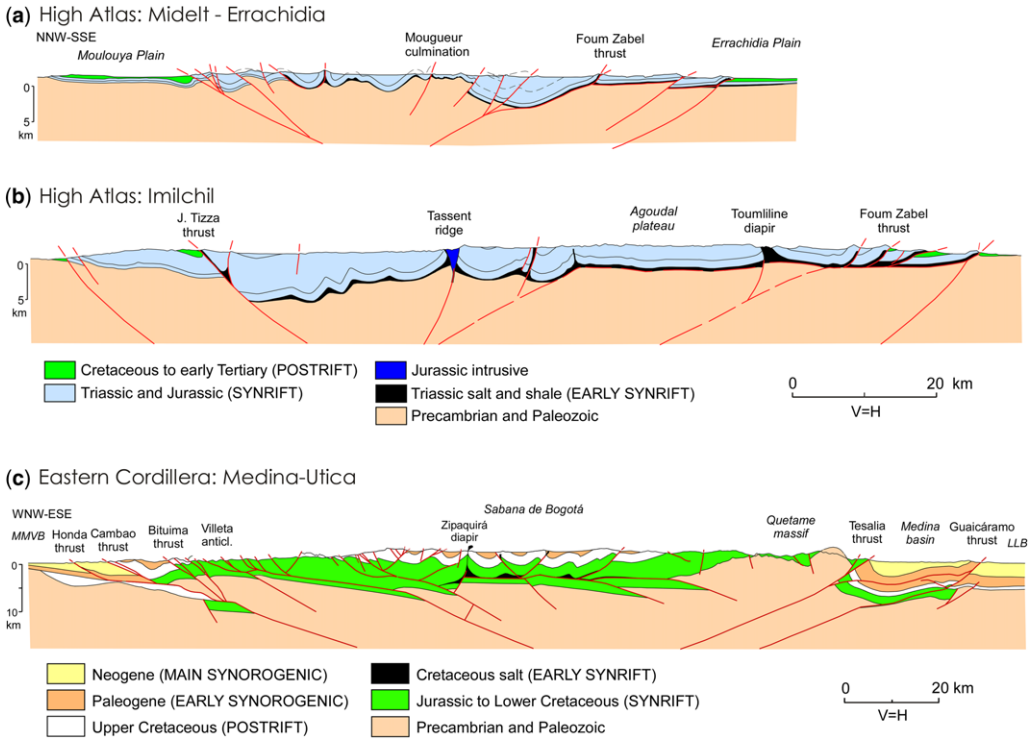


**Fig. 4.** Structural cross-sections across the High Atlas and the Eastern Cordillera of Colombia. (**a**, **b**) Sections across the eastern and central High Atlas (from Teixell *et al.* 2003). These sections are based on field data and were modified from the original according to gravity modelling by Ayarza *et al.* 2005 (see location in Fig. 1). Although largely eroded, the Cretaceous sediments probably formed a tabular body that covered the entire Atlas domain, representing post-rift conditions. (**c**) Simplified structural cross-section of the Eastern Cordillera of Colombia, approximately through the latitude of Bogotá (see location in Fig. 2). This section was constructed on the basis of maps, seismic profiles and structural data provided by ICP-Ecopetrol. The deep structure of the Sabana de Bogotá region is conjectural as it is poorly imaged in the seismic profiles. The lower–upper Cretaceous boundary is taken for the sake of convenience at the top of the Une and Hiló formations. MMVB, Middle Magdalena Valley basin; LLB, Llanos basin.

crustal thickness is moderate (only locally reaching values *c*. 40 km, Wigger *et al.* 1992; Ayarza *et al.* 2005), models show a prominent lithospheric thinning that accounts not only for the high topography at long wavelengths but also for the poor preservation of foreland basins (note that much of the High Atlas lacks peripheral foredeeps or they are very shallow; Figs 1 & 4a, b), and for the occurrence of Cenozoic alkaline magmatism contemporaneous to compression (see a review in Teixell *et al.* 2005).

The timing of long-wavelength surface uplift related to the mantle structure has been indirectly inferred from the chronology of associated magmatic events (last 15 Ma for the later phase; Teixell *et al.* 2005; Missenard *et al.* 2006), and from stratigraphic palaeoelevation markers (1000 m in the past 5 Ma at *c.* 0.2 mm $a^{-1}$; Babault *et al.* 2008). The reasons for the thinned lithosphere in a region that has been subject to compression during much of the Cenozoic remain unresolved.

## The Eastern Cordillera of Colombia

The Eastern Cordillera is the easternmost branch of the northern Andes of Colombia. It is a NNE-trending, 110–200 km wide thrust-fold belt that is separated from the subduction/magmatic complexes of the Western and Central Cordilleras by an intervening depression, the Middle Magdalena Valley Basin. The Eastern Cordillera appears now as a doubly verging thrust system formed during the Cenozoic by the inversion of a Mesozoic back-arc rift (Colletta *et al.* 1990; Cooper *et al.* 1995; Mora *et al.* 2006).

Uplift of the Eastern Cordillera was related to transmission of stresses to the South American

plate by the accretion of arcs in the northwestern Andes, and was associated with subsidence in the adjacent foreland basins of the Middle Magdalena Valley and the Llanos (Fig. 2). The general structure of the Cordillera has long been reported by cross-sections that illustrate diverse conceptions of its structural style (Campbell & Burgl 1965; Julivert 1970; Colletta *et al.* 1990; Dengo & Covey 1993; Cooper *et al.* 1995; Roeder & Chamberlain 1995; Restrepo-Pace *et al.* 2004; Cortés *et al.* 2006; Mora *et al.* 2008; Tesón *et al.*, this volume, in press; Toro *et al.* 2004). There are conflicting views regarding the role of low-angle thrusting and the magnitude of associated translations, from thin-skinned interpretations (Dengo & Covey 1993; Roeder & Chamberlain 1995) to thick-skinned models dominated by basement-involved, inverted extensional faults (see a review in Tesón *et al.*, this volume, in press). Rifting history of the Eastern Cordillera dates back to the Triassic–Jurassic for a first phase, and to the early Cretaceous for a main phase when a graben system roughly coincident with the present Cordillera was developed (Etayo *et al.* 1976; Cooper *et al.* 1995; Sarmiento-Rojas 2001 and references therein). Post-rift deposits accumulated from the late Albian through the late Cretaceous. Triassic–Jurassic rift deposits are areally restricted and consist mainly of terrestrial red beds, whereas widespread lower Cretaceous sediments (up to 5 km thick) are dominantly marine, including alternating sandstone and shale formations in the eastern flank of the Cordillera, and mainly deeper-water shales in the west, with turbiditic formations at the base. The upper Cretaceous of the Sabana de Bogotá area still includes marine shales and sandstones; the first terrestrial deposits indicative of an overfilled basin appear in the late Maastrichtian–Paleocene.

The structure of the Eastern Cordillera is illustrated by a cross-section through its central segment near the latitude of Bogotá (Fig. 4c). Clear structural and geomorphic variations can be seen in this cross-section: from steep orogen flanks of high relief dominated by outward-verging thrust systems to the axial plateau of the Sabana de Bogotá, which is characterized by relatively open and symmetric folds with minor thrust displacements (see also Julivert 1970; Mora *et al.* 2008).

As observed in the case of the High Atlas, thrust deformation is concentrated along the former rift margins. The thrust belts at the flanks of the Eastern Cordillera are asymmetric with regard to deformation intensity, topography and morphology, and magnitude and age of exhumation (Mora *et al.* 2008). The eastern margin shows clear evidence of thick-skinned deformation in the Quetame basement massif (Figs 2 & 4c). This massif was uplifted by a major, west-dipping thrust (Tesalia Fault), formed by inversion of a formerly extensional fault. Extensional faults, inverted or not, are common around the massif (Mora *et al.* 2006). In front of the Quetame massif, the Guaicáramo thrust sheet carries a reduced Cretaceous succession and the Cenozoic Medina Basin (Parra *et al.* 2009a, 2010), and is separated from the autochthonous Llanos foreland basin by another thrust derived from the inversion of a graben margin. The western flank of the Eastern Cordillera shows less structural relief; basement is not exposed but previous authors, on the basis of stratigraphic variations, reported inverted extensional faults defining major thrust units (Salina, Bituima, Cambao thrusts; Gomez *et al.* 2003; Restrepo-Pace *et al.* 2004; Cortés *et al.* 2006). Thin-skinned thrusts do occur, either in the lowermost Cretaceous successions of the Villeta anticlinorium (Cortés *et al.* 2006) or within the Cenozoic succession of the proximal Middle Magdalena Valley foreland (Honda thrust sheet, Fig. 4c).

The interior of the Eastern Cordillera at the Sabana de Bogotá keeps a rather homogeneous structural elevation as defined by fold envelopes (Fig. 4c). The Sabana preserves Palaeogene sediments (mainly terrestrial), largely eroded in the orogen flanks. The deep structure of the Sabana de Bogotá is poorly constrained owing to a constant exposure level and poor imaging in seismic reflection data. The Floresta basement massif located 150 km northwards along-strike (Fig. 2) indicates that basement faults may exist at depth, although fold geometry at the Sabana suggests a detachment in the lower part of the Cretaceous succession. Depth-to-detachment calculations tentatively indicate that such detachment level might be some 4 km below the surface of the Sabana. A salt formation sourcing the Zipaquirá and Nemocón diapirs and many other salt occurrences throughout the Sabana (McLaughlin 1972) is thought to have accumulated at the level of the earliest Cretaceous Macanal or Fómeque formations (Lopez *et al.* 1988). This is approximately the position of our estimated detachment level in the subsurface, and accordingly we interpret the Sabana as a salt-detached fold belt of the style represented in Figure 4c. That salt tectonics may have played an important role in the Sabana folding is also suggested by the exposed fold geometries. Systematic limb overturning in many anticlines (e.g. Julivert 1963, 1970) may represent diapir-margin deformation similar to that described in well-documented salt provinces (e.g. Giles & Lawton 2002; Rowan *et al.* 2003); folds may have originated as salt walls, later squeezed during continuous shortening, so the salt formation has been removed from most of them (although its existence at depth is suggested by the brine springs reported in Campbell & Burgl 1965 and McLaughlin 1972). Synclinal topographic depressions in

the Sabana de Bogotá were eventually filled during the late Neogene and Quaternary with fluviolacustrine deposits (Tilata and Sabana formations, Julivert 1963, Andriessen *et al.* 1993; Torres *et al.* 2005), which smoothed the relief of the plateau.

Estimates of total orogenic shortening in the Eastern Cordillera have been published in several papers (see Toro *et al.* 2004 and Tesón *et al.*, this volume, in press for a review). On one hand, dominantly thin-skinned interpretations have come up with magnitudes from 150 to 200 km (Dengo & Covey 1993; Roeder & Chamberlain 1995). On the other, thick-skinned models arrived at shortening magnitudes of *c.* 70–100 km, which is about 25–30% of the original length (Colletta *et al.* 1990; Toro *et al.* 2004; Tesón *et al.*, in volume, in press). We favour the later values, appreciating the structural style displayed in the above-cited publications and a preliminary estimate of line lengths in Figure 4c.

### *Timing of deformation and surface uplift*

Many studies indicated a main Andean phase starting in the mid Miocene and continuing into recent times as the principal episode of mountain building in the Eastern Cordillera of Colombia, which was the locus of the more or less disrupted foreland basin of the Central Cordillera before that time (e.g. Dengo & Covey 1993; Cooper *et al.* 1995; Hoorn *et al.* 1995; Toro *et al.* 2004; Bayona *et al.* 2008; Horton *et al.* 2010). Increasing evidence for Palaeogene deformation indicating that the former Eastern Cordillera Basin was far from stable and was strongly compartmentalized includes: (1) a regional mid Eocene unconformity in the Middle Magdalena Valley and western foothills (Gomez *et al.* 2003; Restrepo-Pace *et al.* 2004; Parra *et al.* 2012); (2) growth stratal geometries in the Palaeogene of the western foothills and of the Sabana de Bogotá (Julivert 1963; Gomez *et al.* 2003, 2005); and (3) flexural modelling of the Paleocene–Eocene formations of the Cordillera interior (Sarmiento-Rojas 2001; Bayona *et al.* 2008). These were relatively mild deformations in the former rift basin that did not prevent connection between the Central Cordillera and the Llanos foreland, although they controlled significantly the sedimentary thicknesses of the Paleocene–Eocene formations, their palaeogeography and palaeocurrents, which locally flowed NE parallel to the growing folds (Gomez *et al.* 2005). Fold limb rotation and overturning in the Sabana de Bogotá is a persistent and long-lived feature recorded by uppermost Cretaceous to lower Oligocene growth strata (Julivert 1963; Gomez *et al.* 2005). Neogene main emergence of the major thrust faults that characterize the Cordillera flanks attest to strong basin-margin inversion that had probably commenced already in the late Oligocene to early Miocene, as recently indicated by subsidence and exhumation analysis (Parra *et al.* 2009*a*, *b*; Mora *et al.* 2010) and detrital sediment provenance. Detrital zircon geochronology studies reveal a recycling of the Palaeogene Sabana sediments into the Carbonera Formation of the Medina and Llanos basins during this time (Horton *et al.* 2010). The Eastern Cordillera developed into an effective topographic barrier that separated the Central Cordillera from the Llanos Basin at least before mid to late Miocene times, when detrital zircons of Meso-Cenozoic age (which indicate a Central Cordillera provenance or recycling of Cenozoic clastic rocks of the Eastern Cordillera) disappear in the stratigraphic succession of the eastern foothills (Horton *et al.* 2010). The contemporaneous conglomeratic fluxes of the Honda and Guayabo formations into the Middle Magdalena Valley and Llanos basins may be the expression of these uplift events (Hoorn *et al.* 1995; Gomez *et al.* 2003).

The late Neogene fluviolacustrine deposits of the Sabana de Bogotá contain palaeoflora which has been compared with the range of temperature tolerance for modern taxa presumed to be their nearest living relatives. Using this method, Van der Hammen *et al.* (1973) and Hooghiemstra *et al.* (2006) inferred low altitudes until the late Miocene, and a rapid surface uplift of *c.* 1500 $\pm$ 500 m between 6 and 3 Ma ago, a period in which the Sabana de Bogotà (*c.* 5000 km$^2$) experienced sedimentary aggradation. However, following Gregory-Wodzicki (2000), the error margins may be significantly larger ($\pm$1500 m), which implies that the proposed palaeoelevation changes may not be reliably resolved by the nearest living relatives method. Therefore, we cannot discard that the Eastern Cordillera has experienced continuous thickening and surface uplift since the onset of mountain building.

The record of ongoing shortening to recent times is provided by the strong deformation of the Honda and Guayabo formations in the most external thrust sheets of the Cordillera, also in agreement with very young apatite fission track ages in the Quetame massif (*c.* 3 Ma and younger) that attest strong exhumation in the Cordillera margins in the latest Neogene and Quaternary (Mora *et al.* 2008).

## The Pyrenees

The Pyrenees formed in late Cretaceous to Cenozoic times as a result of convergence between the Iberian and European continental masses, which closed a rift basin located in between. The Pyrenean continental crust was severely attenuated during Mesozoic rifting, to a point where peridotites of the

upper mantle were exhumed to the rift-basin floor according to recent interpretations (Jammes *et al.* 2009; Lagabrielle *et al.* 2010), although oceanic crust did not form in the segment now separating France from the Iberian peninsula (Fig. 3). As such, the central and eastern Pyrenees can be considered an inverted rift much like the Atlas or Eastern Cordillera, but with greater amounts of extension and subsequent contraction.

Rifting in the Pyrenees commenced in the Permian–Triassic, with the main phase of extension during the early Cretaceous, when an east–west-trending basin system, approximately spatially coincident with the present mountain belt, was defined (e.g. Puigdefàbregas & Souquet 1986; Vergés & García Senz 2001). Upper Cretaceous sediments are laterally extensive and could be viewed as post-rift deposits, although extensional faulting was locally still under way. The Mesozoic basins were strongly inverted during the Pyrenean orogeny, in association with rapid subsidence in adjacent foreland basins, the proximal parts of which were deformed and incorporated in the thrust system. Hence, much of the southern Pyrenees are built by deformed Cenozoic sedimentary rocks that provide an unique record of the timing and kinematics of the thrust-fold belt (e.g. Séguret 1972; Labaume *et al.* 1985; Puigdefàbregas *et al.* 1986, 1992; Martínez *et al.* 1988; Mutti *et al.* 1988; Vergés & Muñoz 1990; Burbank *et al.* 1992; Teixell 1996; Millán *et al.* 2000; Teixell & Muñoz 2000).

Recognition of the structure of the Pyrenees started approximately a century ago, and has benefitted from the deep seismic profiling of the ECORS programme. Complete cross-sections based on extensive field geology and inferences from seismic profiles (along the section trace or projected) include Muñoz (1992), Vergés *et al.* (1995) and Teixell (1998). The cross-sections of Figure 5 illustrate the structure of the central Pyrenees, showing a north-verging thrust belt in the northern part (the North Pyrenean Zone) with very thick Cretaceous successions corresponding to the axis of the previous rift or transtensional basin. Localized high-temperature metamorphism of mid Cretaceous age attests to severe crustal thinning and high heat flow. The North Pyrenean belt shows a thick-skinned style with thrust faults that usually involve the Hercynian basement and that have been formed by the inversion of Cretaceous normal faults (Peybernès & Souquet 1984). Additionally, local detachments and diapirism sourced in Triassic salt are common (Canérot *et al.* 2005; Lagabrielle *et al.* 2010).

A southern, wider part of the Pyrenees is characterized by south-verging thrusting and includes the Axial Zone, a stack of basement-involved thrust

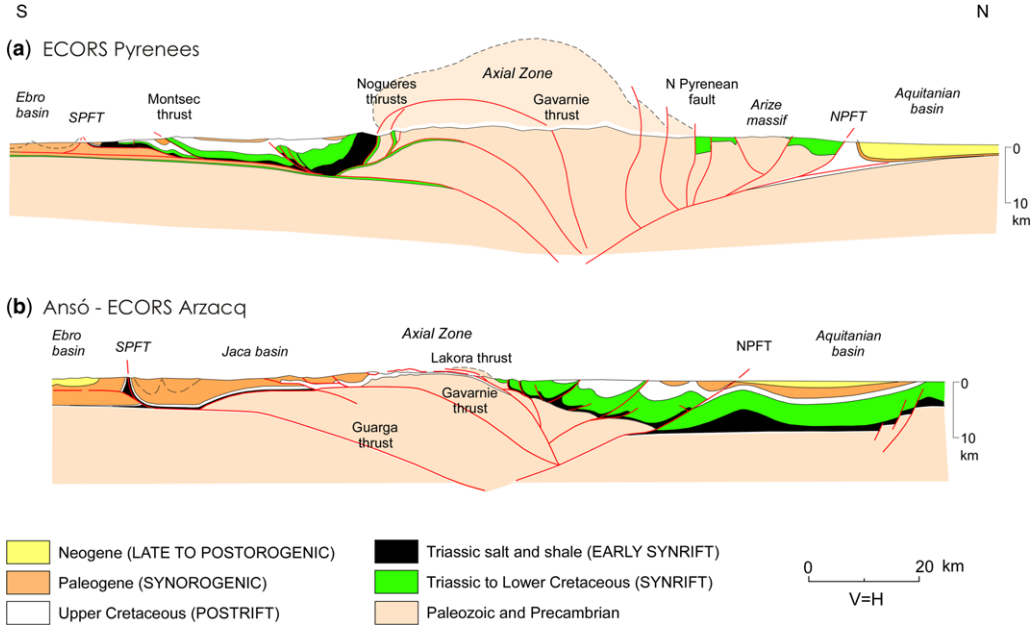


**Fig. 5.** Cross-sections of the central Pyrenees following the trace of (**a**) the ECORS-Pyrenees (simplified after Muñoz 1992) and (**b**) the ECORS-Arzacq (simplified after Teixell 1998) seismic profiles. The sections are based on field data combined with commercial and deep (ECORS) seismic profiles.

sheets that forms the core of the chain, and a detached imbricate fan in front of it (South Pyrenean Zone; Fig. 5). Hence the Pyrenees differ from the central High Atlas and the Eastern Cordillera in the occurrence of an axial massif with high structural relief (and high topographic relief as well). The massif consists of large antiformal stack in the Eastern Pyrenees and in the eastern Central Pyrenees (Fig. 5a), whereas to the west the basement thrust sheets exhibit a lesser degree of overlap and structural relief decreases (although a central culmination can still be defined; Figs 3 & 5b). Much of the South Pyrenean Zone shows a major detachment in Triassic salt (and local diapirism), although there are marked variations along-strike. Cretaceous successions are thick beneath the Tremp Basin (on top of the Montsec thrust in Fig. 5a), as the main thrust sheets there derive from the inverted basin, whereas in the Jaca Basin transect the southern Pyrenees contain only a reduced upper Cretaceous succession accumulated out of the early Cretaceous deep basin trough. Large basement thrusts as the Gavarnie and Guarga are thus shortcut thrusts from the basin margin existing to the north (Fig. 5b). All this is because the original southern margin of the rift basin was not linear, but formed salients and re-entrants, a geometry that resulted in the frequent lateral thrust ramps of the present-day Pyrenees (Fig. 3).

Total shortening for the ECORS-Pyrenees section of Figure 5a has been estimated as *c.* 100 km (Roure *et al.* 1989) or 150–165 km (Muñoz 1992; Beaumont *et al.* 2000). For the narrower, west-central Pyrenees (Fig. 5b), shortening was estimated as *c.* 80 km (Teixell 1998). In both transects the percentage shortening across the mountain chain is probably not less than 40%.

### *Timing of deformation and surface uplift*

Our present knowledge of the timing of the Pyrenean mountain building is mainly based in the South Pyrenean and Axial zones, where there are larger datasets on tectonics–sedimentation relationships and thermochronology. The beginning of Pyrenean contraction was in the late Cretaceous (late Santonian), on the basis of growth folding in the northernmost Bóixols thrust sheet of the southern Pyrenees, which derives from the inversion of a lower Cretaceous fault system (Garrido-Megías & Ríos 1972). Late Cretaceous to early Cenozoic limited contraction has been postulated for the North Pyrenean Basin as well. Later, during the Palaeogene, the Pyrenees experienced a broad piggy-back sequence of imbrication where the main thrust units were defined (e.g. Cámara & Klimowitz 1985; Labaume *et al.* 1985; Vergés & Muñoz 1990; Teixell 1998; Beaumont *et al.* 2000). Recent accounts for the end of the orogenic activity in the Pyrenees place it in the Burdigalian (*c.* 18–16 Ma ago), on the basis of tectonics–sedimentation relationships in the south Pyrenean thrust front and fission-track thermochronology in the Axial Zone (Millán *et al.* 2000; Jolivet *et al.* 2007).

Orogenic growth of the Pyrenees has been synthesized by Sinclair *et al.* (2005) in an early history of fault inversion and frontal accretion, followed by an accelerated growth of the Axial Zone antiformal stack by underplating. The correlation between the ages of the main cover imbricate thrusts, well constrained from syntectonic sediments, and the ages of the basement thrusts of the Axial Zone duplex is a major challenge. Recent attempts to unravel the timing of the Axial Zone are based on fission track thermochronology. A southward propagation of exhumation is recorded in the ECORS-Pyrenees transect (Fig. 5a), with: (1) rapid cooling of the northern Axial Zone and North Pyrenean massifs initiating at 50 Ma; (2) granitic plutons of the central Axial Zone providing ages of rapid exhumation of *c.* 30–32 Ma; and (3) cooling ages of 20 Ma in the southernmost Axial Zone (Fitzgerald *et al.* 1999; Sinclair *et al.* 2005; Metcalf *et al.* 2009). Closer to the transect of Figure 5b, the major Gavarnie thrust sheet has provided late Eocene–early Oligocene apatite fission track ages (Jolivet *et al.* 2007) consistent with tectonics–sedimentation relationships observed further south in the Jaca Basin (Teixell 1996). The main emergence of thrust systems at the Pyrenean mountain fronts started in this epoch, contemporaneous with major structural relief creation in the southern Axial Zone. In the early Miocene, convergence and surface uplift ended.

## Tectonics and macroscale drainage development

The High Atlas, the Eastern Cordillera and the Pyrenees exhibit drainage organization features in parallel with the structural characteristics described. In the central High Atlas and in the Bogotá segment of the Eastern Cordillera, shortening is concentrated along the former rift margins, and the orogen interiors consist of less deformed plateau-like areas with a homogeneous structural relief (Figs 4 & 6a, b). On the other hand, the Pyrenees, with a greater magnitude of orogenic shortening, have developed an axial culmination with high structural relief and also strong regional topographic slopes (Figs 5 & 6c). The differences in the amount of shortening between these three mountain belts may allow a spatial comparison to be used as a proxy for the analysis of drainage evolution in growing inversion orogens. Current climates in

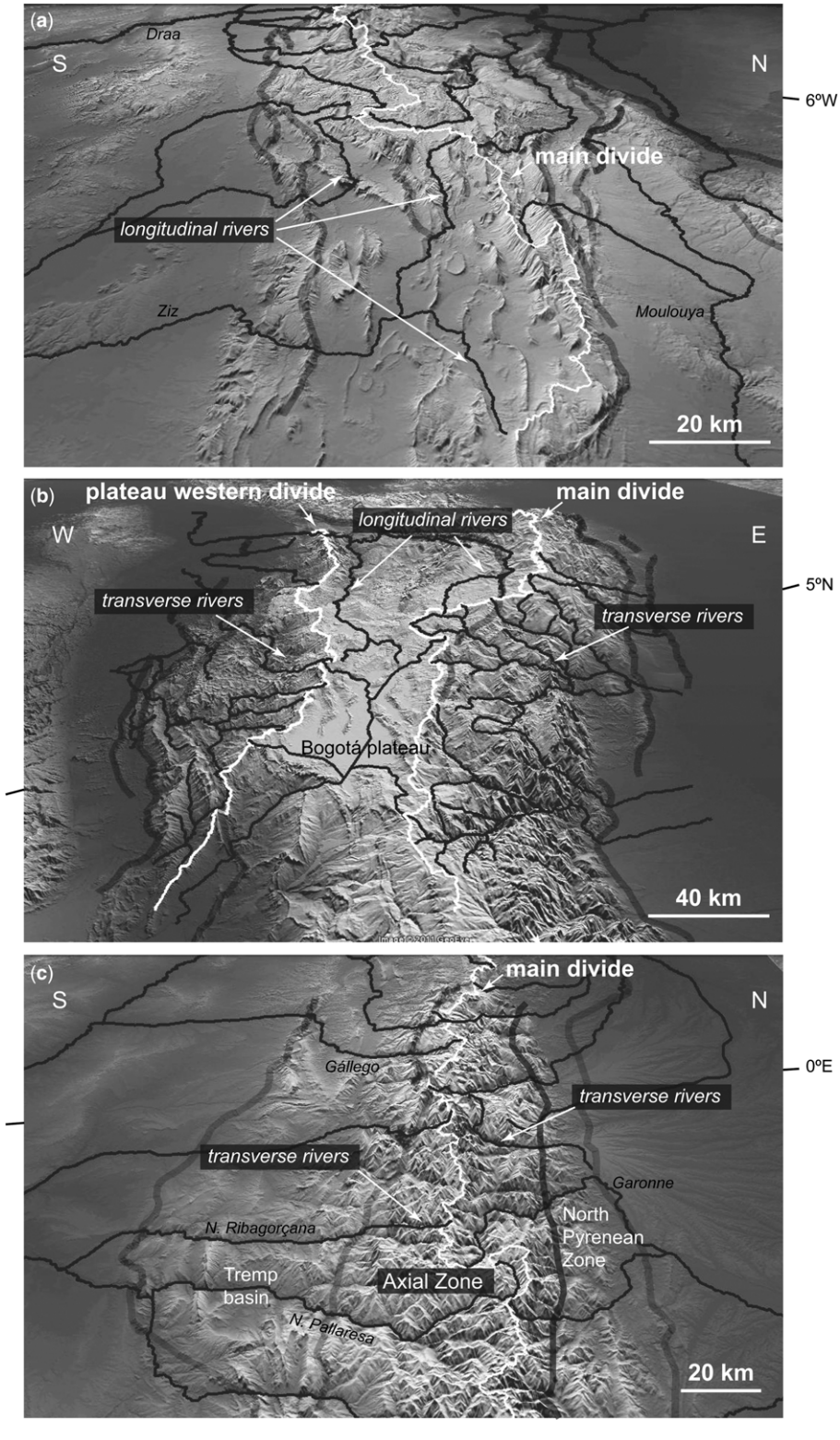

these orogens encompassed semi-arid in the eastern High Atlas to temperate and humid in the Pyrenees and tropical in the Eastern Cordillera. In these mountainous regions, past climates are less known than in their adjacent foreland basins, but if present climates held in the past, these differences may have played a role in shaping the topography. In what follows we show that the large-scale patterns of drainage organization in the three mountain belts are consistent with their respective regional slopes, and then are most probably due to tectonic shortening, crustal thickening and surface uplift.

The fluvial drainage of the High Atlas is characterized by abundant reaches that flow longitudinally, that is, parallel to the structural grain, in the orogen interior (Fig. 6a). Transverse rivers are more common in the orogen flanks, near the northern and southern mountain fronts. Most longitudinal rivers flow along synclines in relatively soft sediments (Jurassic shales), and often cut across thrusts or antiformal ridges (constituted by lower Liassic resistant carbonates) at structural depressions along fold axes. A similar pattern is observed in the Eastern Cordillera, where longitudinal rivers in valleys of relatively low local relief flow along the Sabana de Bogotá plateau and the areas located to the north along-strike (Fig. 6b). Valleys in the Sabana de Bogotá also occupy synclinal depressions containing Cenozoic sediments between anticlinal ridges constituted by resistant upper Cretaceous sandstone. The flanks of the Eastern Cordillera are characterized by deeply incised transverse rivers (Fig. 6b), with local relief stronger than in the High Atlas, consistently with the greater bulk shortening and higher regional slope of the former. On the other hand, the Axial Zone of the Pyrenees is characterized by a well-developed transverse drainage (Fig. 6c).

Observations in the High Atlas suggest that the longitudinal drainage predates the development of transverse rivers in the orogen flanks (Babault *et al.* 2007, 2012). Remnants of low-relief longitudinal valleys are occasionally seen perched at high altitude, and captures of longitudinal streams by transverse streams are common, especially towards the western, more elevated High Atlas. In the plateau of the Eastern Cordillera, longitudinal rivers also have a protracted history, dating back to Palaeogene times. For this period, palaeogeographic reconstructions indicate sediment dispersal strongly controlled by emerging tectonic structures in the basin (Gomez *et al.* 2005). Since the Eastern Cordillera became a topographic barrier in Miocene times, the amounts of erosion in the plateau have been very low. By contrast, the Cordillera flanks are characterized by very active recent erosion, yielding young apatite fission track ages frequently younger than Miocene (Mora *et al.* 2008). Again, stream capture of the gently sloping longitudinal rivers in the plateau by the steep and incising transverse rivers in the flanks is common. Headward erosion in the transverse rivers and captures are expressed by wind gaps and depressions in the main drainage divides bordering the Sabana de Bogotá (Struth 2011; Struth *et al.* 2012). This geomorphologic evidence indicates that drainage divides migrate towards the centre of the plateau and that drainage areas of transverse rivers in the flanks increase at the same time (Struth *et al.* 2012).

The timing relationships described above argue for a process of drainage reorganization, from longitudinal-dominated to transverse-dominated, occurring alike in these two orogens of moderate tectonic inversion. Absolute chronologies are not available for the Atlas case, although low-relief, structure-controlled drainage can be envisaged at least for the late Eocene times, when earliest indications of growth of structural highs go in parallel with little exhumation (no fission track cooling records) and with the unroofing of only the highest levels of the preorogenic sedimentary cover (Tesón 2009; Tesón *et al.* 2010). Babault *et al.* (2012) suggest that the increased tectonic thickening and surface uplift in later times incremented potential energy on both sides of the deformed western High Atlas, and enhanced the fluvial erosion in short transverse rivers (Fig. 7). Record of the progressive development of the transverse network might be first indicated by the mid Miocene Ait Kandoula alluvial fans in the Ouarzazate Basin (El Harfi *et al.* 1996; Tesón 2009), and by contemporaneous fission track cooling ages in the western High Atlas (Missenard *et al.* 2008; Balestrieri *et al.* 2009).

In the Eastern Cordillera, growth strata in Palaeogene sediments along the detachment folds of the Bogotá area, together with palaeocurrents, indicate that longitudinal drainage dominated at least the present-day interior of the Cordillera during the early stages of inversion (Paleocene to early Oligocene; Gomez *et al.* 2005). Pliocene and Quaternary fluviolacustrine aggradation in the Sabana de Bogotá (Andriessen *et al.* 1993; Torres *et al.* 2005; Hooghiemstra *et al.* 2006) argue for a low-relief uplifting plateau, possibly internally

**Fig. 6.** Oblique views showing shaded topography and drainage network of (**a**) the eastern and central High Atlas, (**b**) the central Eastern Cordillera and (**c**) the central Pyrenees. These images are based on the digital elevation model SRTM90 draped onto Google Earth. Thick grey lines indicate main tectonic boundaries.

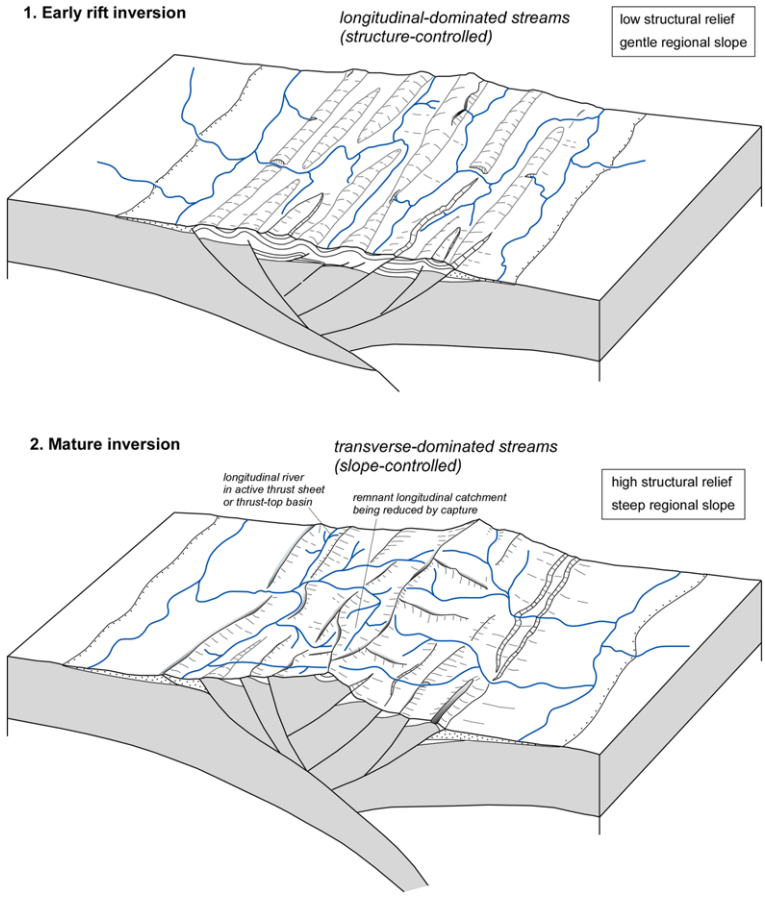


**Fig. 7.** Two-stage sketch model for the evolution of the drainage network in the Atlas Mountains of Morocco, modified after Babault *et al.* (2012), which can be of general application to inversion orogens which experience progressive increase of tectonic thickening and regional topographic slope.

drained or with limited connectivity (as observed today; Fig. 6c). As in the High Atlas, it can be envisaged that the inversion of the Cordillera during the Neogene increased the mean elevation and, in its flanks, the regional slopes, favouring the development of an actively incising transverse drainage. In addition, the main mechanism of transverse river development was probably headward erosion, as evidenced by stream captures (Struth *et al.* 2012). As the plateau area is reduced by piracy and the transverse rivers increase their catchments, an increase in terrigenous influx into the foreland basins is expected. This process may have influenced the coarse accumulations of the late middle Miocene Honda and Guayabo formations in both sides of the Eastern Cordillera.

Evidence for a previous longitudinal drainage has not been reported in the area now occupied by the Axial Zone in the Pyrenees. Certainly, and before grading to transverse from mid Eocene times, longitudinal sediment routing has extensively been reported for the south Pyrenean foreland basin and thrust-top basins, especially in their early stages (e.g. Nijman & Nio 1975; Marzo *et al.* 1988; Barnolas *et al.* 1991; Puigdefàbregas *et al.* 1992; Whitchurch *et al.* 2011 and references therein). This is not surprising as longitudinal rivers have been elsewhere described as characteristic of external parts of growing mountain belts (e.g. Oberlander 1985; Koons 1995; Burbank 1992; Jackson *et al.* 1996, Humphrey & Konrad 2000; van der Beek *et al.* 2002; Ramsey *et al.* 2008). However, for comparison with what is observed in the High Atlas and Eastern Cordillera, what is relevant here is to determine whether a longitudinal drainage ever existed in the growing Pyrenean orogen, that is, the hinterland (the Pyrenean Axial Zone). This possibility has never been addressed before.

As mentioned above, compelling evidence for an early longitudinal drainage in the Axial Zone is not currently available, but a few provenance observations in the southern Pyrenees lead us to contend that it cannot be ruled out. A detrital zircon U–Pb geochronological study (Whitchurch *et al.* 2011) shows that the upper Cretaceous and Paleocene sediments in the Tremp Basin (Fig. 6) contain zircons with Cadomian crystallization ages. Plutons formed during the Cadomian orogeny are only present in the Eastern Pyrenees and in the northern flank. Whitchurch *et al.* (2011) interpret these detrital ages as evidence for an Eastern-Pyrenean provenance. Since palaeocurrents are to the west in these strata, the authors implicitly assume that sediment was transported by transverse rivers from the hinterland of the Eastern Pyrenees to the southern foredeep, and from the eastern foredeep to the central foredeep, parallel to the strike of the orogen. Alternatively, we cannot discard the possibility that part of the longitudinal transport from the Eastern to the Central Pyrenees occurred in the hinterland (the growing mountain belt) and was eventually transported by a transverse river in the eastern part of the Tremp Basin. The stacking of basement units in the Axial Zone resulted in the cannibalization, in the Central Pyrenees, of the northern (proximal) margin of the late Cretaceous to Paleocene foredeep before 40 Ma (Beamud *et al.* 2011), and consequently neither of these two sediment routing possibilities can be demonstrated with the current knowledge. The same reasoning could be applied to younger deposits preserved in the wedge-top basins of the Central Pyrenees, the Pobla and Senterada Basins at the southern margin of the Axial Zone, where north-derived, Oligocene-age proximal fan sediments (*c.* 30–25 Ma, Beamud *et al.* 2011) also show a clear Cadomian detrital zircon signal.

At present, the Noguera Pallaresa River and its tributaries drain the Axial Zone (Fig. 6), incising the Pobla and Senterada basins. However, there are no outcrops of Cadomian rocks in their catchments, which means that the Oligocene catchment of the palaeo-Noguera Pallaresa River had a greater extent or that higher structural levels that supplied the Pobla and Senterada basins contained Cadomian sources that are now completely eroded. Oligocene conglomerates of the Sis palaeovalley (Beamud *et al.* 2011), located only *c.* 20 km west, do not show a Cadomian signal, indicating that the higher structural levels of the central Pyrenean Axial Zone, now eroded, were lacking Cadomian plutons or earlier sedimentary deposits (Palaeozoic or Mesozoic) with that signal. Consequently, we may suggest that the upstream parts of the palaeo-Noguera Pallaresa River, previously draining the Eastern Pyrenees, where the Cadomian plutons are located, have been captured after the deposition of the sediments stored in the Pobla and Senterada basins. On the other hand, it is considered unlikely that the palaeo-Noguera Pallaresa River was draining the North Pyrenean zone, north of the North Pyrenean Fault, during the Oligocene (Beamud *et al.* 2011).

In summary, transverse rivers have been described in the internal part of most of the Cenozoic orogens (Hovius 1996). Structural evidence coupled with indications of drainage reorganization in the western High Atlas (Babault *et al.* 2012) and the Eastern Cordillera of Colombia (Struth *et al.* 2012) suggest that these inversion orogens evolved from early stages of orogenic growth dominated by structure-controlled longitudinal rivers in its inner parts, and as deformation was accumulated and the regional slope increased, the drainage evolved into a regional slope-controlled, transverse network (Fig. 7). The case of the Pyrenees may be consistent with this pattern of evolution, as this orogen, in a more advanced stage of tectonic accretion, shows a double-wedge topographic pattern and a drainage network almost completely dominated by transverse rivers, as observed in most of the Cenozoic linear mountain belts considered by Hovius (1996).

## Conclusions

The High Atlas, the Eastern Cordillera of Colombia and the Pyrenees share in common their origin from rift basins, where contractional deformation of continental crust, even if severely attenuated in the rifting stage, was not driven by oceanic slab pull forces. A prominent deformation style is thick-skinned thrust faulting, either derived from the reactivation of early extensional faults, or newly formed as large-scale shortcuts in their footwalls. However, while thick-skinned thrusting is effectively a primary mechanism in the inverted rifts described, weak levels in the syn-rift sedimentary infill (salt, overpressured rocks) have enabled decoupling between basement and cover, and the formation of localized detachment folds or imbricate thrust systems.

Variations in structural geometry between the sections selected reflect different magnitudes of total shortening accumulated, increasing from the High Atlas (20–25%) to the Eastern Cordillera (25–30%) and the Pyrenees (*c.* 40%). The High Atlas and Eastern Cordillera show shortening largely concentrated at the outer flanks, which coincide with the former rift basin margins. Greater thrust translations in the Eastern Cordillera result in high-relief basement massifs in the eastern flank, whereas much of the central and eastern High Atlas lack basement culminations (basement

is at a rather homogeneous elevation), with a few exceptions (Fig. 1). In both orogens the axial regions are high-elevation plateaus with comparatively less deformation and structural relief. Accordingly, much of the exhumation is concentrated in the orogen flanks, especially in the case of the Eastern Cordillera. In contrast, the Pyrenees can be viewed as more mature inversion orogen where a central high-relief culmination of stacked basement thrust sheets occupies the core. This central core (the so-called Axial Zone), which transfers thrust displacement to the mountain fronts via décollement levels in the sedimentary cover, concentrated the greatest exhumation in the Pyrenees.

Convergence in the Pyrenees ceased in the early Miocene, whereas it is still active in the Eastern Cordillera and the Atlas, which experienced major periods of mountain building during the Neogene. In spite of this difference, timing relationships revealed by tectonics–sedimentation relationships and thermochronology indicate a common pattern of evolution. This pattern consists in an early stage of shallow and distributed deformation of the rift basin fill (folding and localized thrusting, with low structural relief), followed by strong inversion and rock uplift concentrated at the basin margins in later stages, with large basement-involved faults causing higher structural relief and high topographic elevations. This is particularly clear in the case of the Eastern Cordillera, while it seems likely in the east-central High Atlas as well. In the west-central Pyrenees, an episode of major rock uplift by shortcut thrusting at the southern basin margin (beginning in the late Eocene) can also be differentiated. We conclude in a mechanism of rift inversion by which initially rift interiors deform in a distributed way, and evolve to a point where strong deformation is concentrated in weaker faults at the rift margins (inverted or newly formed according to the specific mechanical conditions, e.g. Hilley *et al.* 2005), giving way to the episode when the prominent mountain topography is acquired.

Observations from the western High Atlas (Babault *et al.* 2012) showed that, as this inverted rift evolved from the initial deformation stages to the full accretion, a parallel evolution of the fluvial drainage network was triggered. The axial, plateau-like regions existing in the High Atlas and Eastern Cordillera are dominated by old longitudinal valleys, whereas the orogen flanks are commonly characterized by strongly incised transverse rivers. Transverse rivers are dynamically enlarging their catchments at the expense of longitudinal rivers, by mechanisms of headward extension and stream capture (Babault *et al.* 2012; Struth *et al.* 2012). The Pyrenees show a two-sided wedge profile with a high-relief Axial Zone and transverse rivers dominating in both sides of the main drainage divide. Applying the longitudinal-to-transverse scheme, deduced from the High Atlas and the Eastern Cordillera, to the hinterland of the Pyrenees (Axial Zone) gives an alternative explanation for unexpected provenance features, which would be indicative of the former existence of longitudinal river reaches. Hence, spatial variations between the different orogens might be taken as a hint to temporal variations, arguing for a common pattern where in the early, mild stages of inversion a longitudinal fluvial network controlled by local structures is established, and as shortening and mean elevation are accumulated, the system reorganizes into a regional slope-controlled network of prevailing transverse rivers.

Incisive comments by two anonymous referees and by J. C. Ramírez substantially helped to improve the manuscript. A.T. acknowledges A. Mora and the Instituto Colombiano del Petróleo-Ecopetrol for providing maps and additional information which formed the basis for section construction of Figure 4c. This section was constructed with the software *Move*, provided by Midland Valley through the ASI. Financial support was provided by Spanish projects CGL2010-15416, Consolider-Ingenio CDS2006-00041 (TopoIberia) and CGL2007-66431-CO2-01 (TopoMed). Finally, we would like to thank A. Mora and M. Nemčok for organizing stimulating discussions at the Barichara meeting and for encouragement to prepare this review paper.

## References

Andriessen, P. A. M., Helmens, K. F., Hooghiemstra, H., Riezebos, P. A. & Van der Hammen, T. 1993. Pliocene-Pleistocene chronology of the sediments of the basin of Bogotá, Eastern Cordillera. *Quaternary Science Reviews*, **12**, 483–501.

Arboleya, M. L., Teixell, A., Charroud, M. & Julivert, M. 2004. A structural transect through the High and Middle Atlas of Morocco. *Journal of African Earth Sciences*, **39**, 319–327.

Arboleya, M. L., Babault, J., Owen, L., Teixell, A. & Finkel, R. C. 2008. Timing and nature of Quaternary fluvial incision in the Ouarzazate foreland basin, Morocco. *Journal of the Geological Society, London*, **165**, 1059–1073.

Ayarza, P., Alvarez-Lobato, F., Teixell, A., Arboleya, M. L., Tesón, E., Julivert, M. & Charroud, M. 2005. Crustal structure under the central High Atlas Mountains (Morocco) from geological and gravity data. *Tectonophysics*, **400**, 67–84.

Babault, J., Van Den Driessche, J., Crave, A. & Teixell, A. 2007. High Atlas morphology: insight from the drainage pattern. *Abstract book, 3rd Meeting of the International Lithosphere Program – Task Force Sedimentary Basins*, Marrakech.

Babault, J., Teixell, A., Arboleya, M. L. & Charroud, M. 2008. A Late Cenozoic age for long-wavelength surface uplift of the Atlas Mountains of Morocco. *Terra Nova*, **20**, 102–107.

Babault, J., Van Den Driessche, J. & Teixell, A. 2012. Longitudinal to transverse drainage network evolution in the High Atlas (Morocco): the role of tectonics. *Tectonics*, **31**, TC4020, doi: 10.1029/2011TC003105.

Balestrieri, M. L., Moratti, G., Bigazzi, G. & Algouti, A. 2009. Neogene exhumation of the Marrakech High Atlas (Morocco) recorded by apatite fission-track analysis. *Terra Nova*, **21**, 75–82.

Barbero, L., Teixell, A., Arboleya, M. L., Del Río, P., Reiners, P. W. & Bougadir, B. 2007. Jurassic-to-present thermal history of the Central High Atlas (Morocco) assed by low-temperature thermochronology. *Terra Nova*, **19**, 58–64.

Barnolas, A., Samsó, J. M., Teixell, A., Tosquella, J. & Zamorano, M. 1991. *Evolución sedimentaria entre la cuenca Graus-Tremp y la cuenca de Jaca-Pamplona*. Libro-Guía Excursión 1, I Congreso del Grupo Español del Terciario, Vic. Grafiques Emegé, Barcelona.

Bayona, G., Cortés, M., Jaramillo, C., Ojeda, G., Aristizabal, J. J. & Reyes-Harker, A. 2008. An integrated analysis of an orogen-sedimentary basin pair: latest Cretaceous–Cenozoic evolution of the linked Eastern Cordillera orogen and the Llanos foreland basin of Colombia. *Geological Society of America Bulletin*, **120**, 1171–1197.

Beamud, E., Muñoz, J. A., Fitzgerald, P. G., Baldwin, S. L., Garcés, M., Cabrera, L. & Metcalf, J. R. 2011. Magnetostratigraphy and detrital apatite fission track thermochronology in syntectonic conglomerates: constraints on the exhumation of the South-Central Pyrenees. *Basin Research*, **23**, 309–331.

Beauchamp, J. 1988. Triassic sedimentation and rifting in the High Atlas (Morocco). *In*: Mainspeizer, W. (ed.) *Triassic–Jurassic rifting. Continental Breakup and the Origin of the Atlantic Ocean and Passive Margins*. Elsevier, Amsterdam, 477–497.

Beauchamp, W., Allmendinger, R. W., Barazangi, M., Demnati, A., El Alji, M. & Dahmani, M. 1999. Inversion tectonics and the evolution of the High Atlas Mountains, Morocco, based on a geological–geophysical transect. *Tectonics*, **18**, 163–184.

Beaumont, C., Muñoz, J. A., Hamilton, J. & Fullsack, P. 2000. Factors controlling the Alpine evolution of the Central Pyrenees inferred from a comparison of observations and geodynamical models. *Journal of Geophysical Research*, **105**, 8121–8145.

Benammi, M., Toto, E. & Chakiri, S. 2001. Les chevauchements frontaux du Haut Atlas central marocain: styles structuraux et taux de raccourcissement différentiel entre les versants nord et sud. *Comptes Rendus de l'Academie des Sciences*, **333**, 241–247.

Burbank, D. W. 1992. Causes of recent Himalayan uplift deduced from deposited patterns in the Ganges basin. *Nature*, **357**, 680–683.

Burbank, D. W., Vergés, J., Muñoz, J. A. & Bentham, P. 1992. Coeval hindward- and forward-imbricating thrusting in the south-central Pyrenees, Spain: timing and rates of shortening and deposition. *Geological Society of America Bulletin*, **104**, 3–17.

Cámara, P. & Klimowitz, J. 1985. Interpretación geodinámica de la vertiente centro-occidental surpirenaica (Cuencas de Jaca-Tremp). *Estudios Geológicos*, **41**, 391–404.

Campbell, C. J. & Burgl, H. 1965. Section though the Eastern Cordillera of Colombia, South America. *Geological Society of America Bulletin*, **76**, 567–590.

Canérot, J., Hudec, M. R. & Rockenbauch, K. 2005. Mesozoic diapirism in the Pyrenean orogen: salt tectonics on a transform plate boundary. *Association of Petroleum Geologists Bulletin*, **89**, 211–229.

Colletta, B., Hebrard, F., Letouzey, J., Werner, P. & Rudkiewicz, J.-L. 1990. Tectonic style and crustal structure of the Eastern Cordillera (Colombia) from a balanced cross-section. *In*: Letouzey, J. (ed.) *Petroleum and Tectonics in Mobile Belts*. Technip, Paris, 81–100.

Cooper, M. A., Addison, F. T. *et al.* 1995. Basin development and tectonic history of the Llanos Basin, Eastern Cordillera, and Middle Magdalena Valley, Colombia. *American Association of Petroleum Geologists Bulletin*, **79**, 1421–1443.

Cortés, M., Colletta, B. & Angelier, J. 2006. Structure and tectonics of the central segment of the Eastern Cordillera of Colombia. *Journal of South American Earth Sciences*, **21**, 437–465.

Dengo, C. A. & Covey, M. C. 1993. Structure of the Eastern Cordillera of Colombia: implications for trap styles and regional tectonics. *American Association of Petroleum Geologists Bulletin*, **77**, 1315–1337.

El Harfi, A., Lang, J. & Salomon, J. 1996. Le remplissage continental cénozoique du bassin d'avant-pays de Ouarzazate; implications sur l'évolution géodynamique du Haut-Atlas central (Maroc). *Comptes Rendus de l'Academie des Sciences*, **323**, 623–630.

El Kochri, A. & Chorowicz, J. 1995. Oblique extension in the Jurassic trough of the central and eastern High Atlas (Morocco). *Canadian Journal of Earth Sciences*, **33**, 84–92.

Etayo, F., Renzoni, G. & Barrero, D. 1976. Memoria del Primer Congreso Colombiano de Geologia. *Imprenta Nacional de Bogotá, Bogotá*, **1**, 217–252.

Fitzgerald, P. G., Muñoz, J. A., Coney, P. J. & Baldwin, S. L. 1999. Asymmetric exhumation across the Pyrenean orogen: implications for the tectonic evolution of a collisional orogen. *Earth Planetary Science Letters*, **173**, 157–170.

Fraissinet, C. E., Zouine, M., Morel, J.-L., Poisson, A., Andrieux, J. & Faure-Muret, A. 1988. Structural evolution of the southern and northern central High Atlas in Paleogene and Mio-Pliocene times. *In*: Jacobshagen, V. (ed.) *The Atlas System of Morocco*. Springer, New York, 273–291.

Frizon de Lamotte, D., Saint Bezar, B., Bracène, E. & Mercier, E. 2000. The two main steps of the Atlas building and geodynamics of the western Mediterranean. *Tectonics*, **19**, 740–761.

Froitzheim, N., Stets, N. & Wurster, P. 1988. Aspects of western High Atlas tectonics. *In*: Jacobshagen, V. (ed.) *The Atlas System of Morocco*. Springer, New York, 219–244.

Garrido-Megías, A. & Ríos, L. M. 1972. Síntesis geológica del Secundario y Terciario entre los ríos Cinca y Segre (Pirineo Central de la vertiente surpirenaica, provincias de Huesca y Lérida). *Boletín Geológico y Minero*, **83**, 1–47.

GILES, K. A. & LAWTON, T. F. 2002. Halokinetic sequence stratigraphy adjacent to the El Papalote diapir, northeastern Mexico. *American Association of Petroleum Geologists Bulletin*, **86**, 823–840.

GOMEZ, F., BEAUCHAMP, W. & BARAZANGI, M. 2000. Role of Atlas Mountains (northwest Africa) within the African-Eurasian plate-boundary zone. *Geology*, **28**, 775–778.

GOMEZ, E., JORDAN, T. E., ALLMENDIGER, R. W., HEGARTY, K., KELLEY, S. & HEIZLER, M. 2003. Controls on architecture of the Late Cretaceous to Cenozoic southern Middle Magdalena Valley Basin, Colombia. *Geological Society of America Bulletin*, **115**, 131–147.

GOMEZ, E., JORDAN, T. E., ALLMENDINGER, R. W. & CARDOZO, N. 2005. Development of the Colombian foreland-basin system as a consequence of diachronous exhumation of the northern Andes. *Geological Society of America Bulletin*, **117**, 1272–1292.

GÖRLER, K., HELMDACH, F.-F. *ET AL.* 1988. The uplift of the Central Atlas as deduced from Neogene continental sediments of the Ouarzazate province, Morocco. *In*: JACOBSHAGEN, V. (ed.) *The Atlas System of Morocco*. Springer, New York, 361–404.

GREGORY-WODZICKI, K. M. 2000. Uplift history of the Central and Northern Andes: a review. *Geological Society of America Bulletin*, **112**, 1091–1105.

GUIMERÀ, J., ARBOLEYA, M. L. & TEIXELL, A. 2011. Structural control on present-day topography of a basement massif: the Central and Eastern Anti-Atlas (Morocco). *Geologica Acta*, **9**, 55–65.

HERBIG, H. G. & TRAPPE, J. 1994. Stratigraphy of the Subatlas Group (Maastrichtian–Middle Eocene, Morocco). *Newsletters on Stratigraphy*, **30**, 125–165.

HILLEY, G. E., BLISNIUK, M. M. & STRECKER, M. R. 2005. Mechanics and erosion of basement-cored uplift provinces. *Journal of Geophysical Research*, **110**, B12409, doi: 10.1029/2005JB003704.

HOOGHIEMSTRA, H., WIJNINGA, V. M. & CLEEF, A. M. 2006. The paleobotanical record of Colombia: implications for biogeography and biodiversity. *Annals of the Missouri Botanical Garden*, **93**, 297–325.

HOORN, C., GUERRERO, J., SARMIENTO, G. A. & LORENTE, M. A. 1995. Andean tectonics as a cause for changing drainage patterns in Miocene northern South America. *Geology*, **23**, 237–240.

HORTON, B. K., SAYLOR, J. E., NIE, J., MORA, A., PARRA, M., REYES-HARKER, A. & STOCKLI, D. F. 2010. Linking sedimentation in the northern Andes to basement configuration, Mesozoic extension, and Cenozoic shortening: evidence from detrital zircon U–Pb ages, Eastern Cordillera, Colombia. *Geological Society of America Bulletin*, **122**, 1423–1442.

HOVIUS, N. 1996. Regular spacing of drainage outlets from linear mountain belts. *Basin Research*, **8**, 29–44.

HUMPHREY, N. F. & KONRAD, S. K. 2000. River incision or diversion in response to bedrock uplift. *Geology*, **28**, 43–46.

JACKSON, J., NORRIS, R. & YOUNGSON, J. 1996. Structural evolution of active fault and fold systems in central Otago, New Zealand: evidence revealed by drainage patterns. *Journal of Structural Geology*, **18**, 217–234.

JAMMES, S., MANATSCHAL, G., LAVIER, L. & MASINI, E. 2009. Tectono-sedimentary evolution related to extreme crustal thinning ahead of a propagating ocean: the example of the western Pyrenees. *Tectonics*, **28**, TC4012, doi: 10.1029/2008TC002406.

JOLIVET, M., LABAUME, P., MONIÉ, P., BRUNEL, M., ARNAUD, N. & CAMPANI, M. 2007. Thermochronology constraints for the propagation sequence of the south-Pyrenean basement thrust system (France-Spain). *Tectonics*, **26**, doi: 10.1029/2006TC002080.

JULIVERT, M. 1963. Los rasgos tectónicos de la región de la Sabana de Bogotá y los mecanismos de la formación de las estructuras. *Boletin de Geología Universidad Industrial Santander*, **13–14**, 5–102.

JULIVERT, M. 1970. Cover and basement tectonics in the Cordillera Oriental of Colombia, South America, and a comparison with some other folded chains. *Geological Society of America Bulletin*, **81**, 3623–3646.

KOONS, P. O. 1995. Modeling the topographic evolution of collisional belts. *Annual Reviews of Earth and Planetary Sciences*, **23**, 375–408.

LABAUME, P., SÉGURET, M. & SEYVE, C. 1985. Evolution of a turbiditic foreland basin and analogy with an accretionary prism: example of the Eocene South-Pyrenean basin. *Tectonics*, **4**, 661–685.

LAGABRIELLE, Y., LABAUME, P. & DE SAINT BLANQUAT, M. 2010. Mantle exhumation, crustal denudation, and gravity tectonics during Cretaceous rifting in the Pyrenean realm (SW Europe): insights from the geological setting of the lherzolite bodies. *Tectonics*, **29**, TC4012, doi: 10.1029/2009TC002588.

LAVILLE, E., LESAGE, J. L. & SÉGURET, M. 1977. Géometrie, cinématique (dynamique) de la tectonique atlasique sur le versant sud du Haut Atlas marocain. Aperçu sur les tectoniques hercyniennes et tardi-hercyniennes. *Bulletin Société Géologique France*, **19**, 527–539.

LOPEZ, C., BRICEÑO, A. & BUITRAGO, J. 1988. Edad y origen de los diapiros de sal de la Sabana de Bogotá. *III Simposio Bolivariano Exploración Petrolera en las Cuencas Subandinas*, Bogotá.

MARTÍNEZ, A., VERGÉS, J. & MUÑOZ, J. A. 1988. Secuencias de propagación del sistema de cabalgamientos de la terminación oriental del manto del Pedraforca y relación con los conglomerados sinorogénicos. *Acta Geológica Hispánica*, **23**, 119–128.

MARZO, M., NIJMAN, W. & PUIGDEFÀBREGAS, C. 1988. Architecture of the Castissent fluvial sheet sandstones, Eocene, South Pyrenees, Spain. *Sedimentology*, **35**, 719–738.

MATTAUER, M., TAPPONIER, P. & PROUST, F. 1977. Sur les mécanismes de formation des chaines intracontinentales. L'exemple des chaines atlasiques du Maroc. *Bulletin Société Géologique France*, **19**, 521–526.

MCLAUGHLIN, D. H. 1972. Evaporite deposits of Bogotá area, Cordillera Oriental, Colombia. *American Association of Petroleum Geologists Bulletin*, **56**, 2240–2259.

METCALF, J. R., FITZGERALD, P. G., BALDWIN, S. & MUÑOZ, J. A. 2009. Thermochronology of a convergent orogen: constraints on the timing of thrust faulting and subsequent exhumation of the Maladeta pluton in the Central Pyrenean Axial Zone. *Earth Planetary Science Letters*, **287**, 488–503.

MICHARD, A., IBOUH, H. & CHARRIÈRE, A. 2011. Syncline-topped anticlinal ridges from the High

Atlas: a Moroccan conundrum, and inspiring structures from the Syrian Arc, Israel. *Terra Nova*, **23**, 314–323.

Millán, H., Pueyo, E. L., Aurell, M., Aguado, A., Oliva, B., Martinez Peña, M. B. & Pocoví, A. 2000. Actividad tectónica registrada en los depósitos terciarios del frente meridional del Pirineo central. *Revista de la Sociedad Geológica de España*, **13**, 279–300.

Missenard, Y., Zeyen, H., Frizon de Lamotte, D., Leturmy, P., Petit, C., Sébrier, M. & Saddiqi, O. 2006. Crustal versus asthenospheric origin of relief of the Atlas Mountains of Morocco. *Journal of Geophysical Research*, **111**, B3, doi: 10.1029/2005JB003708.

Missenard, Y., Saddiqi, O., Barbarand, J., Leturmy, P., Ruiz, G., El Haimer, F. & Frizon de Lamotte, D. 2008. Cenozoic denudation in the Marrakech High Atlas, Morocco; insight from apatite fission-track thermochronology. *Terra Nova*, **20**, 221–228.

Mora, A., Parra, M., Strecker, M. R., Kammer, A., Dimaté, C. & Rodríguez, F. 2006. Cenozoic contractional reactivation of Mesozoic extensional structures in the Eastern Cordillera of Colombia. *Tectonics*, **25**, TC2010, doi: 10.1029/2005TC001854.

Mora, A., Parra, M., Strecker, M. R., Sobel, E. R., Hooghiemstra, H., Torres, V. & Vallejo-Jaramillo, J. 2008. Climatic forcing of asymmetric orogenic evolution in the Eastern Cordillera of Colombia. *Geological Society of America Bulletin*, **120**, 930–949.

Mora, A., Horton, B. K. *et al.* 2010. Migration of Cenozoic deformation in the Eastern Cordillera of Colombia interpreted from fission track results and structural relationships: implications for petroleum systems. *American Association of Petroleum Geologists Bulletin*, **94**, 1543–1580.

Muñoz, J. A. 1992. Evolution of a continental collision belt: ECORS-Pyrenees crustal balanced cross-section. *In*: McClay, K. R. (ed.) *Thrust Tectonics*. Chapman and Hall, London, 235–246.

Mutti, E., Séguret, M. & Sgavetti, M. 1988. Sedimentation and deformation in the Tertiary sequences of the southern Pyrenees. *Field Trip Guidebook 7, AAPG Mediterranean Basins Conference*, Nice.

Nijman, W. J. & Nio, S. D. 1975. The Eocene Montañana delta (Tremp-Graus Basin, Southern Pyrenees). *In*: Rosell, J. & Puigdefàbregas, C. (eds) *Sedimentary Evolution of the Paleogene South Pyrenean Basin, Excursion Guidebook 19, IXth International Sedimentology Congress*, Nice.

Oberlander, T. M. 1985. Origin of drainage transverse to structures in orogens. *Binghamton Symposia in Geomorphology, International Series*, **15**, 155–182.

Parra, M., Mora, A. *et al.* 2009*a*. Orogenic wedge advance in the northern Andes: evidence from the Oligocene–Miocene sedimentary record of the Medina Basin, Eastern Cordillera, Colombia. *Geological Society of America Bulletin*, **121**, 780–800.

Parra, M., Mora, A., Sobel, E. R., Strecker, M. R. & González, R. 2009*b*. Episodic orogenic front migration in the northern Andes: constraints from low-temperature thermochronology in the Eastern Cordillera, Colombia. *Tectonics*, **28**, TC4004, doi: 10.1029/2008TC002423.

Parra, M., Mora, A., Jaramillo, C., Torres, V., Zeilinger, G. & Strecker, M. R. 2010. Tectonic controls on Cenozoic foreland basin development in the northeastern Andes, Colombia. *Basin Research*, **22**, 874–903.

Parra, M., Mora, A., Lopez, C., Rojas, L. E. & Horton, B. K. 2012. Detecting earliest shortening and deformation advance in thrust belt hinterlands: example from the Colombian Andes. *Geology*, **40**, 175–178.

Pastor, A. 2008. *Tectónica reciente al S del Alto Atlas de Marruecos (Valles de Izerki-Toundout, Cuenca de Ouarzazate)*. MSc thesis, Universitat Autònoma de Barcelona.

Peybernès, B. & Souquet, P. 1984. Basement blocks and tecto-sedimentary evolution in the Pyrenees during Mesozoic times. *Geological Magazine*, **121**, 397–405.

Piqué, A., Tricart, P., Guiraud, R., Laville, E., Bouaziz, S., Amrhar, M. & Ait Ouali, R. 2002. The Mesozoic–Cenozoic Atlas belt (North Africa): an overview. *Geodinamica Acta*, **15**, 185–208.

Puigdefàbregas, C. & Souquet, P. 1986. Tecto-sedimentary cycles and depositional sequences of the Mesozoic and Tertiary from the Pyrenees. *Tectonophysics*, **129**, 173–203.

Puigdefàbregas, C., Muñoz, J. A. & Marzo, M. 1986. Thrust belt development in the eastern Pyrenees and related depositional sequences in the southern foreland basin. *In*: Allen, P. A. & Homewood, P. (eds) *Foreland Basins*. International Association of Sedimentologists, Special Publications, 8, 229–246.

Puigdefàbregas, C., Muñoz, J. A. & Vergés, J. 1992. Thrusting and foreland basin evolution in the Southern Pyrenees. *In*: McClay, K. R. (ed.) *Thrust Tectonics*. Chapman and Hall, London, 247–254.

Ramsey, L. A., Walker, R. T. & Jackson, J. 2008. Fold evolution and drainage development in the Zagros Mountains of Fars Province, SE Iran. *Basin Research*, **20**, 23–48.

Restrepo-Pace, P. A., Colmenares, F., Higuera, C. & Mayorga, M. 2004. A fold-and-thrust belt along the western flank of the Eastern Cordillera of Colombia. Style, kinematics, and timing constraints derived from seismic data and detailed surface mapping. *In*: McClay, K. R. (ed.) *Thrust Tectonics and Hydrocarbon Systems*. American Association of Petroleum Geologists, Tulsa, OK, Memoirs, 82, 598–613.

Roeder, D. & Chamberlain, R. L. 1995. Eastern Cordillera of Colombia: Jurassic–Neogene evolution. *In*: Tankard, A. J., Suarez-Soruco, R. & Welsink, H. J. (eds) *Petroleum Basins of South America*. American Association of Petroleum Geologists, Tulsa, OK, Memoirs, 62, 633–645.

Roure, F., Choukroune, P. *et al.* 1989. ECORS Deep Seismic data and data and balanced cross-sections: geometric constraints on the evolution of the Pyrenees. *Tectonics*, **8**, 41–50.

Rowan, M. G., Lawton, T. F., Giles, K. A. & Ratliff, R. A. 2003. Near-salt deformation in La Popa basin, Mexico, and the northern Gulf of Mexico: a general model for passive diapirism. *American Association of Petroleum Geologists Bulletin*, **87**, 733–756.

Sarmiento-Rojas, L. F. 2001. *Mesozoic Rifting and Cenozoic Basin Inversion History of the Eastern Cordillera, Colombian Andes*. PhD thesis, Vrije Universiteit.

SEBER, D., BARAZANGI, M., TADILI, B. A., RAMDANI, M., IBENBRAHIM, A. & BEN SARI, D. 1996. Three dimensional upper mantle structure beneath the intraplate Atlas and interplate Rif mountains of Morocco. *Journal of Geophysical Research*, **101**, 3125–3138.

SÉBRIER, M., SIAME, L., ZOUINE, E. M., WINTER, T., MISSENARD, Y. & LETURMY, P. 2006. Active tectonics in the Moroccan High Atlas. *Comptes Rendus Géosciences*, **338**, 65–79.

SÉGURET, M. 1972. *Etude tectonique des nappes et séries décollées de la partie centrale du versant sud des Pyrénées. Caractère synsédimentaire, rôle de la compression et de la gravité*. Thèse doctorale, Publ. USTELA, Montpellier, Série Géologie structurale 2.

SINCLAIR, H. D., GIBSON, M., NAYLOR, M. & MORRIS, R. G. 2005. Asymmetric growth of the Pyrenees revealed through measurement and modeling of orogenic fluxes. *American Journal of Science*, **305**, 369–406.

STRUTH, L. 2011. *Interacciones entre la tectónica y la red de drenaje: la Cordillera Oriental de Colombia*. MSc thesis, Universitat Autònoma de Barcelona.

STRUTH, L., BABAULT, J. & TEIXELL, A. 2012. Tectónica y evolución de la red de drenaje en la Cordillera Oriental del Colombia. *Geotemas*, **13**, 4.

TEIXELL, A. 1996. The Ansó transect of the southern Pyrenees: basement and cover thrust geometries. *Journal of the Geological Society, London*, **153**, 301–310.

TEIXELL, A. 1998. Crustal structure and orogenic material budget in the west-central Pyrenees. *Tectonics*, **17**, 395–406.

TEIXELL, A. & MUÑOZ, J. A. 2000. Evolución tectonosedimentaria del Pirineo meridional durante el Terciario: una síntesis basada en la transversal del río Noguera Ribagorçana. *Revista de la Sociedad Geológica de España*, **13**, 251–264.

TEIXELL, A., ARBOLEYA, M. L., JULIVERT, M. & CHARROUD, M. 2003. Tectonic shortening and topography in the Central High Atlas (Morocco). *Tectonics*, **22**, 1051, doi: 10.1029/2002TC001460.

TEIXELL, A., AYARZA, P., ZEYEN, H., FERNÁNDEZ, M. & ARBOLEYA, M. L. 2005. Effects of mantle upwelling in a compressional setting: the Atlas Mountains of Morocco. *Terra Nova*, **17**, 456–461.

TESÓN, E. 2009. *Estructura y cronología de la deformación en el borde Sur del Alto Atlas de Marruecos a partir del registro tectono-sedimentario de la cuenca de antepaís de Ouarzazate*. PhD thesis, Universitat Autònoma de Barcelona.

TESÓN, E. & TEIXELL, A. 2008. Sequence of thrusting and syntectonic sedimentation in the eastern Sub-Atlas thrust belt (Dades and Mgoun valleys, Morocco). *International Journal of Earth Sciences*, **97**, 103–113.

TESÓN, E., PUEYO, E. L., TEIXELL, A., BARNOLAS, A., AGUSTÍ, J. & FURIÓ, M. 2010. Magnetostratigraphy of the Ouarzazate Basin: implications for the timing of deformation and mountain building in the High Atlas Mountains of Morocco. *Geodinamica Acta*, **23**, 151–165.

TESÓN, E., MORA, A. *ET AL.* In press. Relationship of Mesozoic graben development, stress, shortening magnitude, and structural style in the Eastern Cordillera of the Colombian Andes. *In*: MORA, A., NEMČOK, M. & COSGROVE, J. (eds) *Thick-Skin-Dominated Orogens: From Initial Inversion to Full Accretion*, Geological Society, London, Special Publications, **377**, http://dx.doi.org/10.1144/SP377.10

TORO, J., ROURE, F., BORDAS-LE FLOCH, N., LE CORNEC-LANCE, S. & SASSI, W. 2004. Thermal and kinematic evolution of the Eastern Cordillera fold-and-thrust belt, Colombia. *In*: SWENNEN, R., ROURE, F. & GRANATH, J. W. (eds) *Deformation, Fluid Flow, and Reservoir Appraisal in Foreland Fold and ThrustBelts*. American Association of Petroleum Geologists, Tulsa, OK, Hedberg Series, **1**, 79–115.

TORRES, V., VANDENBERGHE, J. & HOOGHIEMSTRA, H. 2005. An environmental reconstruction of the sediment infill of the Bogotá basin (Colombia) during the last 3 million years from abiotic and biotic proxies. *Palaeogeography, Palaeoclimatology, Palaeoecology*, **226**, 127–148.

VAN DER BEEK, P., CHAMPEL, B. & MUGNIER, J.-L. 2002. Control of detachment dip on drainage development in regions of active fault-propagation folding. *Geology*, **30**, 471–474.

VAN DER HAMMEN, T., WERNER, J. H. & VAN DOMMELEN, H. 1973. Palynological record of the upheaval of the northern Andes: a study of the Pliocene and Lower Quaternary of the Colombian Eastern Cordillera and the early evolution of its High-Andean biota. *Review of Palaeobotany and Palynology*, **16**, 1–42.

VERGÉS, J. & GARCÍA SENZ, J. M. 2001. Mesozoic evolution and Cainozoic inversion of the Pyrenean rift. *In*: ZIEGLER, P. A., CAVAZZA, W., ROBERTSON, A. H. F. & CRASQUIN-SOLEAU, S. (eds) *Peri-Tethys Memoir 6: Peri-Tethyan Rift/Wrench Basins and Passive Margins*. Mémoires du Museum National d'Histoire Naturelle, **186**, 187–212.

VERGÉS, J. & MUÑOZ, J. A. 1990. Thrust sequences in the southern central Pyrenees. *Bulletin Société Géologique France*, **6**, 265–271.

VERGÉS, J., MILLÁN, H. *ET AL.* 1995. Eastern Pyrenees and related foreland basins: pre-, syn- and post-collisional crustal-scale cross-sections. *Marine and Petroleum Geology*, **12**, 893–915.

WARME, J. E. 1988. Jurassic carbonate facies of the central and eastern High Atlas rift, Morocco. *In*: JACOBSHAGEN, V. (ed.) *The Atlas System of Morocco*. Springer, New York, 169–199.

WHITCHURCH, A. L., CARTER, A., SINCLAIR, H. D., DULLER, R. A., WHITTAKER, A. C. & ALLEN, P. A. 2011. Sediment routing system evolution within a diachronously uplifting orogen: insights from detrital zircon thermochronological analyses from the South-Central Pyrenees. *American Journal of Science*, **311**, 442–482.

WIGGER, P., ASCH, G., GIESE, P., HEINSOHN, W.-D., EL ALAMI, S. O. & RAMDANI, F. 1992. Crustal structure along a traverse across the Middle and High Atlas mountains derived from seismic refraction studies. *Geologische Rundschau*, **81**, 237–248.

ZEYEN, H., AYARZA, P., FERNÁNDEZ, M. & RIMI, A. 2005. Lithospheric structure under the western African-European plate boundary: a transect across the Atlas Mountains and the Gulf of Cadiz. *Tectonics*, **24**, TC2001, doi: 10.1029/2004TC001639.

ZIEGLER, P. A., VAN WESS, J.-D. & CLOETINGH, S. 1998. Mechanical controls of collision-related compressional intraplate deformation. *Tectonophysics*, **300**, 103–129.

Tectonophysics xxx (2015) xxx–xxx

Contents lists available at ScienceDirect

Tectonophysics

journal homepage: www.elsevier.com/locate/tecto

# Extracting dynamic topography from river profiles and cosmogenic nuclide geochronology in the Middle Atlas and the High Plateaus of Morocco

Alvar Pastor [a,*], Julien Babault [a], Lewis A. Owen [b], Antonio Teixell [a], María-Luisa Arboleya [a]

[a] Departament de Geologia, Universitat Autònoma de Barcelona, E-08193 Bellaterra, Spain
[b] Department of Geology, University of Cincinnati, Cincinnati, OH 45221, USA

ARTICLE INFO

*Article history:*
Received 23 September 2014
Received in revised form 20 May 2015
Accepted 2 June 2015
Available online xxxx

*Keywords:*
Atlas Mountains
River profile
Knickpoint
Cosmogenic dating
Active tectonics
Dynamic topography

ABSTRACT

The Moulouya river system has intensely eroded the Arhbalou, Missour, and Guercif Neogene foreland basins in northeastern Morocco, having changed from net aggradation during the Miocene–early Pliocene to net incision punctuated by alluvial fan deposition at late Pliocene or early Quaternary time. This region as a whole has experienced mantle-driven, surface uplift (dynamic topography) since the late Cenozoic, being locally affected by uplift due to crustal shortening and thickening of the Middle Atlas too. Knickpoints located along the major streams of the Moulouya fluvial network, appear on both the undeformed margins of the Missour and Guercif foreland basins (High Plateaus), as well as along the thrust mountain front of the southern Middle Atlas, where they reach heights of 800–1000 m. 500–550 m of the knickpoint vertical incision might be explained by long-wavelength mantle-driven dynamic surface uplift, whereas the remaining 450–500 m in the southern Middle Atlas front and 200–300 m in the northeastern Middle Atlas front seem to be thrust-related uplift of the Jebel Bou Naceur. Be-10 terrestrial cosmogenic nuclides have been used to date two Quaternary river terraces in the Chegg Ard valley at 62 ± 14 ka and 411 ± 55 ka. The dated terraces allow the incision rates associated with the frontal structures of the Middle Atlas to be estimated at ~0.3 mm $yr^{-1}$. Furthermore, these ages have served to evaluate mantle-driven regional surface uplift since the middle Pleistocene in the central Missour basin, yielding values of ~0.1–0.2 mm $yr^{-1}$.



## 1. Introduction

The Atlas Mountains of Morocco and the surrounding plains underwent long-wavelength surface uplift caused by thermal mantle-driven buoyancy since the late Cenozoic (Anahnah et al., 2011; Babault et al., 2008; Teixell et al., 2003, 2005; Zeyen et al., 2005). Deformation of drainage networks and geomorphic indexes suggest that surface uplift is still active (e.g., Barbero et al., 2011; Barcos et al., 2014). This mantle-driven surface uplift is superimposed onto the tectonic effect of the thickened crust of the High and Middle Atlas produced by thrusting since the Paleogene. Although tectonic shortening is moderate in the Atlas thrust belts, deformation registered in Quaternary alluvial deposits at the southern fronts of the High and Middle Atlas indicates that thrusting is still active (Delcaillau et al., 2008; Laville et al., 2007; Pastor et al., 2012; Sébrier et al., 2006). Within this framework, the landscape of the foreland of the High and Middle Atlas (Arhbalou, Missour, and Guercif basins; Fig. 1), changed from net aggradation to erosion and fluvial incision in late Pliocene or Quaternary time (Bouazza et al., 2009). The Moulouya river system currently drains these basins, its headwaters being located in the flanking reliefs of the Middle Atlas, the High Atlas, and the High Plateaus (Fig. 1a). The Arhbalou, Missour, and Guercif basins are only deformed in the proximity of the High and Middle Atlas thrust fronts (Fig. 1b), and, together with the flanking mountain belts, provide a useful natural laboratory to examine the triggers of landscape change and, in particular, to evaluate the sources of surface uplift.

This work presents a tectonic and geomorphic study on the Arhbalou, Missour and southern Guercif basins, as well as on their eastern and western margins, featuring an analysis of stream profiles in the upper Moulouya river drainage network. The river profiles reveal the systematic presence of large knickpoints or knickzones on tributaries draining both flanks of the Moulouya river system, i.e., the folded Middle Atlas and the undeformed High Plateaus, enabling a discussion on the origin of knickpoints as due to large-scale surface uplift. We present the first $^{10}$Be terrestrial cosmogenic nuclide (TCN) dating of Quaternary deposits within the Missour basin, allowing the determination of fluvial incision rates since the Middle Pleistocene, which, in turn, can be converted to surface uplift rates. Combined with the geomorphic analysis, the geochronological data allow us to assess the relative role of different driving-mechanisms of surface uplift in the landscape evolution of the

* Corresponding author. Tel.: +34 569 93830679.
*E-mail address:* alvarpastorc@gmail.com (A. Pastor).

http://dx.doi.org/10.1016/j.tecto.2015.06.007
0040-1951/

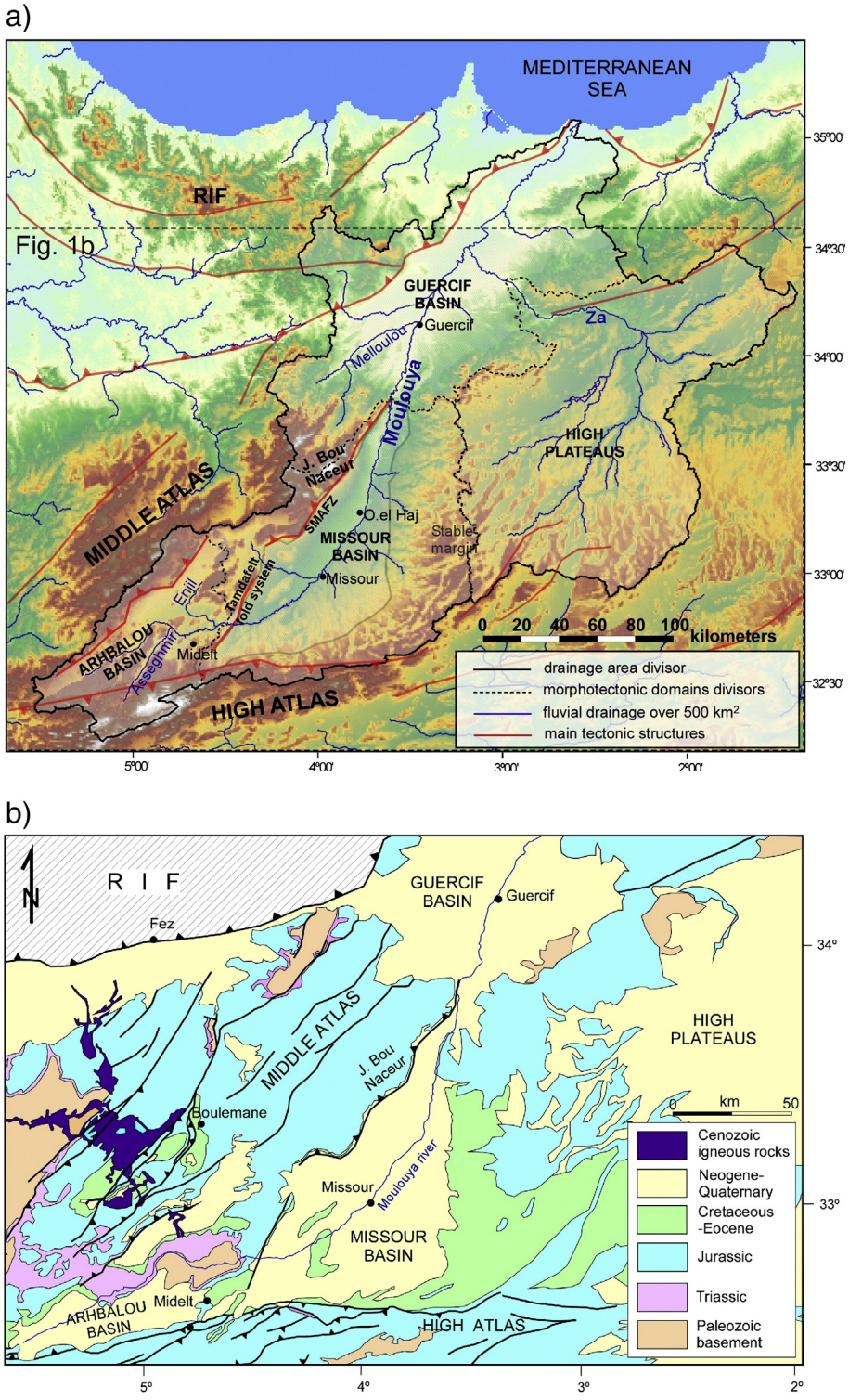


**Fig. 1.** a) Digital elevation model (DEM SRTM90) of northeastern Morocco, with the main morphotectonic features and the Moulouya drainage basin. SMAFZ, Southern Middle Atlas frontal zone. b) Geological map of part of the area shown in panel a.

northeastern Atlas region. Other studies elsewhere attempted to retrieve magnitudes of mantle-driven uplift from geomorphic indicators (e.g., Nereson et al., 2013; Paul et al., 2014; Schildgen et al., 2012). This study intends to discriminate for the first time the amount and rate of river incision directly related to tectonic deformation from those associated with the large-scale mantle-driven dynamic topography.

## 2. Regional setting

The Moulouya river (~650 km-long) is, after the Nile, the second largest river in North Africa that drains to the Mediterranean Sea (Fig. 1a). From headwaters to outlet, the Moulouya river flows across the Arhbalou, Missour, and Guercif Neogene foreland basins, draining an area of ~74,000 km$^2$, that includes the High Plateaus in the east,

Please cite this article as: Pastor, A., et al., Extracting dynamic topography from river profiles and cosmogenic nuclide geochronology in the Middle Atlas and the High Plateaus of Morocco, Tectonophysics (2015), http://dx.doi.org/10.1016/j.tecto.2015.06.007

the High Atlas in the south, the Middle Atlas towards the west, and the eastern Rif in the north-west, to eventually enter the Mediterranean sea near Nador in northern Morocco. The Moulouya river begins at 2000 m.a.s.l. at the junction of the Middle and High Atlas, which is the drainage divide between rivers flowing to the Atlantic and to the Mediterranean. The course of the Moulouya river is at least twice the distance from its headwaters to the Atlantic. For that reason, slopes are steeper on the Atlantic Atlas side, where headward eroding rivers threaten to capture the upper part of the Moulouya catchment.

The geologic evolution of the Arhbalou and Missour sedimentary basins is related to the thrust loading of the Cenozoic High and Middle Atlas orogenic belts (Arboleya et al., 2004; Beauchamp et al., 1996), whereas the Guercif basin has been influenced by the Rif orogen (Gomez et al., 2000). These three basins are mostly filled with Miocene alluvial and lacustrine sediments. The sedimentary record has been described in detail by Bernini et al. (1999, 2000), Gomez et al. (2000), Krijgsman et al. (1999), Krijgsman and Langereis (2000) and Sani et al. (2000) for the Guercif basin, by Beauchamp et al. (1996) and Ellouz et al. (2003) for the Missour basin, and by Dutour (1983) for the Arhbalou basin. Bouazza et al. (2009) proposed that sedimentation in the Guercif basin ended at early Quaternary time when the basin probably have changed from endorheic to externally drained, connecting the Moulouya river to the Mediterranean Sea.

The Middle Atlas is a NE-trending, basement-involved thrust belt that derives from the inversion of a Triassic–Jurassic rift, with a relatively simple structure and a modest amount of total orogenic shortening (<10%, Gomez et al., 1998; Arboleya et al., 2004). The southern Middle Atlas front defines the western margin of the Missour basin (Fig. 1b). The mountain front coincides with the foot of the Jebel Bou Naceur, where Jurassic rocks of the Middle Atlas overthrust Tertiary and Quaternary fanglomerates at the foot of Jebel Bou Naceur range (jebel is Moroccan for mountain) (Fig. 1b). The Jebel Bou Naceur is a mountain ridge with a maximum elevation of 3356 m.a.s.l., rising ~2500 m above the Moulouya basin, which is limited by a southeastern facing topographic scarp that Delcaillau et al. (2008) interpreted as an active fault zone. The Neogene–Quaternary basin fill onlaps the undeformed Jurassic bedrock of the High Plateaus on the eastern margin of the Missour basin. Plio–Pleistocene lacustrine deposits overlap much of the Jurassic carbonates of the High Plateaus. The timing of initial thrusting at Jebel Bou Naceur is unknown, but according to Laville et al. (2007), the thrust system was active during the Neogene, when Mesozoic rocks were thrust over fluvial rocks of the Bou Irhardaiene Formation. Paleomagnetic data reported by Krijgsman and Langereis (2000) suggest that the deposit of the Bou Irhardaiene Formation lasted till the lower Pliocene (Zanclean). Thrust-related folding occurs in the northwestern margin of the basin and deforms the Bou Irhardaiene Formation and Quaternary alluvial gravels; the gravels are unconformable in some places (Delcaillau et al., 2008).

The mean elevation of the Middle Atlas mountains (between 1500 and 2000 m) contrasts with its crustal thickness, recently determined in ca. 32 km by a wide-angle seismic survey (Ayarza et al., 2014). The relatively thin crust suggests a modest degree of crustal thickening, which is consistent with the amount of observed shortening, and provides support to the view that the crust is not isostatically equilibrated at crustal level. To explain this discrepancy, the subcrustal structure was investigated by means of potential-field modeling, which indicated that the lithosphere was thin (<90 km) under the Middle Atlas mountains and the Arhbalou–Missour basins (Fullea et al., 2010; Teixell et al., 2005; Zeyen et al., 2005), an inference recently confirmed by seismological data (Miller and Becker, 2014; Palomeras et al., 2014). Hence, surface uplift of the Atlas region is divided into two components: a component of crustal isostasy related to (modest) thickness variations of the crust during the Atlas orogeny, and a component related to changes in mantle buoyancy, probably due to an asthenospheric upwelling (which was described as dynamic topography by Teixell et al., 2005, and Sun et al., 2014). The first component is circumscribed to the High and Middle Atlas deformed belts, whereas the second is of longer wavelength and affects also the peripheral Arhbalou and Missour basins. On the basis of unconformable, Messinian-age marine deposits at high altitude, Babault et al. (2008) estimated the magnitude of post-Miocene mantle-driven rock uplift in the Middle Atlas is ~1000 m. Furthermore, geomorphic indexes from the lower Moulouya river led Barcos et al. (2014) to suggest that this component of uplift is still active.

## 3. Methods

### 3.1. Knickpoints and paleoprofile reconstruction

The river profiles shown in this paper are based on the Digital Elevation Model (DEM) with 90 m of pixel resolution provided by the Shuttle Radar Topography Mission (SRMT) from the National Aeronautics and Space Administration (NASA).

The term knickpoint describes an abrupt change in river gradient, which creates a local convexity in the generally concave-up idealized graded stream longitudinal profile (Whipple and Tucker, 1999). The term knickzone is used when the convex segment of the river longitudinal profile persists along some kilometers. In our analysis, we consider the present-day position of knickpoint as due to an incision wave related to base level fall by comparing the current longitudinal profile with a reconstructed past hypothetical ideal longitudinal profile (paleoprofile). Therefore, we use paleo-longitudinal river profiles as a proxy for surface uplift. A paleo-longitudinal river profile can be determined for the segment located upstream of a knickpoint by using the equation proposed by Hoke et al. (2007). This approach implies that knickpoint separates an unmodified upstream segment from a downstream one that adapts its slope to the new boundary conditions imposed by the base level fall (Bishop, 2007; Whipple and Tucker, 1999). It is also assumed that the upstream segment (headwater from the knickpoint) was equilibrated to the conditions prior to the base-level fall. Under these assumptions, the empirical power–law gradient–area relationship (Flint, 1974; Howard and Kerby, 1983) together with the relationship between downstream distance, *x*, and cumulative drainage area (Hack, 1957), can be used to reconstruct a paleo-longitudinal river profile from the equation (Whipple, 2001; Whipple and Tucker, 1999):

$$\mathbf{z(X) = k_s k_a^{-\theta}(1-h\theta)^{-1}\left(L^{1-h\theta}-x^{1-h\theta}\right)+z(L)} \quad \mathbf{h\ \theta\neq 1;\quad x_c \le x \le L;} \tag{1}$$

where z(X) is the elevation z at a distance X from drainage divide, L is the distance from the outlet to the drainage divide, $x_c$ is the distance from the divide at which fluvial processes become dominant over hillslope processes, $k_s$ is the steepness index, θ is the concavity index, $k_a$ is Hack's (1957) coefficient and h is Hack's (1957) exponent. The difference in elevation between the paleo profile and the present-day downstream segment at the outlet gives the knickpoint height. We have reconstructed the unmodified upstream segment profile (inherited from the old boundary conditions), which allowed us to obtain values for $k_s$ and θ, and used these values to the downstream segment, affected by the new boundary conditions.

### 3.2. Surface dating

We have dated two alluvial fan/terrace surfaces (T1 and T2) in the Chegg Ard valley, which traverses the Middle Atlas and the eastern Missour basin. The surfaces dated in this study were mostly composed of pebbles, cobbles, and occasional small boulders limestone and dolostone. However, there are also minor amounts of sandstone and phyllite cobbles. We selected cobbles of sandstone and phyllite for $^{10}$Be TCN dating. The sampled surfaces are flat and extensive, and unaffected by topographic shielding. Samples were collected from sites far enough from hill slopes as to minimize material gained from upper

Please cite this article as: Pastor, A., et al., Extracting dynamic topography from river profiles and cosmogenic nuclide geochronology in the Middle Atlas and the High Plateaus of Morocco, Tectonophysics (2015), http://dx.doi.org/10.1016/j.tecto.2015.06.007

**Table 1**
Sample numbers, descriptions, locations, $^{10}$Be data, and $^{10}$Be ages for surfaces in the Chegg Ard valley.

| Sample number | Surface | Lithology | Class size Height/width/length (cm) | Sample thickness (cm) | Latitude (°N) | Longitude (°E) | Altitude[1] (m.a.s.l) | Topographic correction | $^{10}$Be concentration[2] (atoms/g $SiO_2$ $\times 10^4$) | Age Time independent Lal (1991)/Stone (2000)[3,4] (ka) | Age Desilets and Zreda (2003), Desilets et al. (2006)[5] (ka) | Age Dunai (2001)[5] (ka) | Age Lifton et al. (2005)[5] (ka) | Age Time dependent Lal (1991)/Stone (2000)[5] (ka) | Age Time dependent Lal (1991)/Stone (2000)[5] applying 1.4 m/Ma erosion (ka) |
|---|---|---|---|---|---|---|---|---|---|---|---|---|---|---|---|
| M908 | T1a | Quartzite | 12/8/5 | 5 | 33.36906667 | −3.880783333 | 1144 | 1 | 383 ± 8 | 473.6 ± 47.8 (11.5) | 464.5 ± 62.7 | 447.2 ± 59.8 | 444.4 ± 50.2 | 424.1 ± 41.1 | n/a |
| M909 | T1a | Sandstone | 35-long | 5 | 33.36913333 | −3.88035 | 1140 | 1 | 351 ± 11 | 431.8 ± 44.4 (14.9) | 421.9 ± 57.3 | 404.5 ± 54.4 | 401.5 ± 45.9 | 385.5 ± 38.2 | n/a |
| M910 | T1a | Sandstone | 17/11/8 | 5 | 33.36906667 | −3.88035 | 1143 | 1 | 351 ± 9 | 430.7 ± 43.6 (12.7) | 420.5 ± 56.5 | 403.2 ± 53.8 | 400.3 ± 45.2 | 384.5 ± 37.5 | n/a |
| M911 | T1a | Sandstone | 15/8/5 | 5 | 33.36893333 | −3.879966667 | 1145 | 1 | 464 ± 13 | 590.6 ± 62.6 (18.9) | 573.3 ± 80.4 | 553.1 ± 76.8 | 549.8 ± 46.7 | 528.5 ± 53.6 | n/a |
| M912 | T1a | Sandstone | 10/8/05 | 5 | 33.36965 | −3.879683333 | 1147 | 1 | 355 ± 11 | 435.0 ± 44.8 (15.0) | 425.2 ± 57.7 | 407.3 ± 54.8 | 404.4 ± 46.3 | 388.1 ± 38.4 | n/a |
| M913 | T1a | Sandstone | 15/10/5 | 5 | 33.36973333 | −3.87945 | 1147 | 1 | 364 ± 12 | 446.4 ± 46.3 (16.0) | 437.4 ± 59.7 | 419.6 ± 56.8 | 416.2 ± 48.0 | 397.8 ± 39.7 | n/a |
| M915 | Tlb | Sandstone | 14/10/5 | 5 | 33.37775 | −3.896533333 | 1208 | 1 | 392 ± 11 | 463.0 ± 47.5 (14.5) | 451.4 ± 61.4 | 434.5 ± 58.5 | 431.1 ± 49.3 | 412.3 ± 40.6 | n/a |
| M916 | Tlb | Sandstone | 17/10/6 | 6 | 33.37796667 | −3.897616667 | 1212 | 1 | 363 ± 9 | 427.0 ± 43.1 (12.3) | 413.4 ± 55.4 | 397.4 ± 52.8 | 394.4 ± 44.4 | 380.3 ± 36.9 | n/a |
| M917 | Tlb | Sandstone | 11/7/05 | 5 | 33.37855 | −3.897766667 | 1211 | 0.8542 | 345 ± 8 | 474.4 ± 48.3 (12.9) | 462.7 ± 62.7 | 445.9 ± 59.9 | 442.6 ± 50.3 | 424.1 ± 41.4 | n/a |
| M918 | Tlb | Sandstone | 15/11/5 | 5 | 33.37838333 | −3.89695 | 1209 | 1 | 316 ± 10 | 363.5 ± 36.8 (12.4) | 348.1 ± 46.4 | 335.4 ± 44.3 | 332.5 ± 37.4 | 320.9 ± 31.3 | n/a |

| | | | | | | | | | | | | | | |
|---|---|---|---|---|---|---|---|---|---|---|---|---|---|---|
| M919 | Tlb | Sandstone | 11/9/04 | 4 | 33.37893333 | −3.898333333 | 1214 | 1 | 451 ± 15 | 534.1 ± 56.9 (20.4) | 521.0 ± 72.9 | 501.3 ± 69.5 | 498.1 ± 58.8 | 478.6 ± 49.0 | n/a |
| | | | | | | | | | | | | | Average | **411 ± 55** | |
| M920 | T2a | Sandstone | 17/13/6 | 6 | 33.39696667 | −3.905066667 | 1134 | 1 | 45 ± 2 | 50.8 ± 5.3 (2.7) | 49.8 ± 6.5 | 48.6 ± 6.3 | 47.8 ± 5.4 | 45.7 ± 4.6 | 48.5 ± 5.1 |
| M921 | T2a | Sandstone | 13/7/4 | 4 | 33.39696667 | −3.905083333 | 1135 | 1 | 73 ± 2 | 81.5 ± 7.5 (1.9) | 80.9 ± 9.9 | 78.6 ± 9.6 | 77.8 ± 8.0 | 74.3 ± 6.6 | 81.7 ± 8.1 |
| M922 | T2a | Sandstone | 13/8/6 | 6 | 33.39696667 | −3.905 | 1135 | 1 | 51 ± 3 | 57.3 ± 5.8 (2.9) | 57.1 ± 7.4 | 55.6 ± 7.2 | 54.7 ± 6.1 | 51.9 ± 5.2 | 55.8 ± 5.9 |
| M923 | T2a | Sandstone | 15/12/7 | 7 | 33.39673333 | −3.905066667 | 1134 | 1 | 59 ± 3 | 67.5 ± 6.8 (3.2) | 67.0 ± 8.7 | 65.4 ± 8.4 | 64.7 ± 7.2 | 61.8 ± 6.1 | 66.6 ± 7.1 |
| M924 | T2a | Sandstone | 9/7/06 | 7 | 33.3967 | −3.9048 | 1135 | 1 | 69 ± 5 | 79.3 ± 9.5 (6.4) | 78.6 ± 11.4 | 76.4 ± 11.0 | 75.6 ± 9.7 | 72.3 ± 8.5 | 79.2 ± 10.3 |
| M925 | T2a | Sandstone | 12/8/05 | 5 | 33.39643333 | −3.90445 | 1134 | 1 | 42 ± 10 | 47.0 ± 12.0 (11.2) | 46.0 ± 12.3 | 45.1 ± 12.0 | 44.4 ± 11.5 | 42.6 ± 10.8 | 44.8 ± 12.0 |
| M926 | T2b | Siltstone | 26/18/7 | 7 | 33.35616667 | −3.856266667 | 1018 | 0.8542 | 236 ± 10 | 368.5 ± 39.3 (17.5) | 360.2 ± 49.6 | 345.8 ± 47.2 | 343.6 ± 40.4 | 327.8 ± 33.8 | 671.5 ± 193.2 |
| M927 | T2b | Phyllite | 7/7/07 | 7 | 33.35606667 | −3.856516667 | 1021 | 1 | 92 ± 3 | 116.4 ± 11.3 (4.5) | 113.7 ± 14.5 | 110.7 ± 14.0 | 109.7 ± 11.9 | 105.1 ± 10.0 | 119.7 ± 13.2 |
| M928 | T2b | Sandstone | 20/7/7 | 7 | 33.35596667 | −3.857266667 | 1022 | 1 | 48 ± 2 | 59.8 ± 5.8 (2.5) | 60.2 ± 7.6 | 58.7 ± 7.4 | 57.9 ± 6.3 | 54.6 ± 5.2 | 58.8 ± 6.0 |
| M929 | T2b | Sandstone | 20/10/4 | 4 | 33.35536667 | −3.855733333 | 1016 | 1 | 17 ± 1 | 21.1 ± 2.1 (1.0) | 22.7 ± 2.8 | 22.4 ± 2.9 | 22.1 ± 2.4 | 20.4 ± 2.0 | 20.9 ± 2.1 |
| M930 | T2b | Sandstone | 18/8/5 | 5 | 33.35615 | −3.857966667 | 1021 | 1 | 69 ± 3 | 84.5 ± 8.2 (3.3) | 84.6 ± 10.7 | 82.2 ± 10.4 | 81.4 ± 8.8 | 77.3 ± 7.3 | 85.3 ± 9.0 |
| M932 | T2b | Sandstone | 16/8/6 | 6 | 33.35588333 | −3.853433333 | 1012 | 1 | 19 ± 2 | 22.7 ± 2.7 (1.9) | 24.3 ± 3.5 | 24.0 ± 3.5 | 23.7 ± 3.1 | 22.0 ± 2.6 | 22.5 ± 2.7 |
| | | | | | | | | | | | | | Average[6] | **52 ± 20** | |

[1] Altitudes were determined using a handheld GPS with an uncertainty of ±30 m.
[2] Six blanks were measured with $^{10}Be/^{9}Be$ ratio = $4.24 \pm 2.3 \times 10^{-14}$.
[3] Ages were determined using a rock density of 2.75 g/cm$^3$ and 07KNSTD standard. Uncertainties include analytical and production rate/scale model uncertainties.
[4] Uncertainty includes analytical and production rates and uncertainty in parenthesis is only analytical.
[5] Samples M926 and M927 were not included in average.

levels. We also selected sampling sites with little evidence of erosion, generally in areas with well-developed rock varnish. The sampled cobble was 5–10 cm-tall and 10–20 cm in diameter (Table 1).

Samples were prepared at the TCN Geochronology Laboratories of the University of Cincinnati. About 500 g of each sample was crushed and sieved to obtain 250–500 μm fraction, from which quartz was separated using the methods of Kohl and Nishiizumi (1992). Be carrier was added to each sample, and by means of an ion exchange chromatography technique, Be was separated, purified and precipitated as $Be(OH)_2$ at a pH 7. The $Be(OH)_2$ gel was calcinated by ignition at 750 °C for 5 min in quartz crucibles. The resultant BeO was mixed with Nb powder and loaded into steel targets. $^{10}Be/^{9}Be$ ratios were measured with accelerator mass spectrometry at the Purdue Rare Isotope Measurement Laboratory of the Purdue University. Isotope ratios were compared with ICN Pharmaceutical Incorporated $^{10}Be$ and NIST (National Institute Standard of Technology) standards prepared by K. Nishiizumi.

Ages were calculated with CRONUS-Earth online calculator Version 2.2, applying appropriate $^{10}Be$ standardizations (Balco et al., 2008) with a sea-level high latitude (SLHL) production rate of 4.49 ± 0.39 $^{10}Be$ atoms $g^{-1}$ of quartz $yr^{-1}$, a $^{10}Be$ half-life of $1.36 \times 10^6$ years (Nishiizumi et al., 2007) and a rock density of 2.75 g $cm^{-3}$ at zero-erosion rate.

There is currently much debate regarding the appropriate scaling models and geomagnetic corrections to calculate surface exposure ages from TCN production (e.g., Pigati and Lifton 2004; Staiger et al. 2007; Balco et al., 2008). We present ages for all scaling models, but choose those of Lal (1991) and Stone (2000) in our discussion (Table 1). However, we are aware that other scaling models would produce ages that may be up to 10% older (Table 1).

### 3.3. Quantifying fluvial incision and deformation rates

Incised fluvial surfaces allow fluvial incision rates (I) to be estimated by using the age (A) and height (h) of the surface with respect to the present-day position of the river channel, such that $I = h/A$ (e.g., Burbank and Anderson, 2001). In this work, the absolute elevation of terrace surfaces (h) as obtained from the SRTM90 DEM, whose precision is optimal when measuring surfaces with slopes < 10% (Gorokhovich et al., 2006). The accuracy decreases when measuring the absolute elevation of surfaces narrower than 180 m, as occurs in some parts of the river channel and locally in terraces. In these cases, the elevation data have been contrasted with field measurements obtained with a conventional altimeter. Although absolute elevation values requires frequent calibration (according to atmospheric conditions), in our analysis we do not use absolute elevation data, but elevation difference between terrace surfaces and present-day river channel. Thus, altimeter accuracy is approximately 1 m when the elevation of two surfaces is measured in a short time lapse. Relative structural uplift has been calculated by comparing the relative elevation of a geomorphic surface with respect to the present-day river channel at both sides of a tectonic flexure, thus assuming that the original surface sloped at a gradient similar to today's stream.

## 4. River profiles and knickpoint analysis

### 4.1. Moulouya river

The Moulouya river profile is not the typical concave up shaped denoting equilibrium, but it shows a series of knickpoints. The upper reach of the Moulouya river flows over its own alluvial deposits through a wide valley, presenting a surprisingly gentle gradient of 0.16° along 50 km, after which slope abruptly increases (gradient > 0.3°) for about 10 km defining a 80 m-high knickpoint (Fig. 2b). The knickpoint coincides with scarcely erodible Paleozoic granitic bedrock. Downstream, the Moulouya river flows again over alluvial deposits and shows its gentle slope until its confluence with the Asseghmir river. The Asseghmir river drains ~1350 $km^2$ of the northern flank of the High Atlas, representing a third of the total drainage area of the Moulouya river downstream of their confluence. The Asseghmir river has a knickpoint of similar characteristics to those on the Moulouya river (Fig. 2a), though located in the northern flank of the High Atlas Mountains at an elevation ~300 m higher than in the Moulouya river. From the tributary junction, the Moulouya river flows east for almost 50 km across Jurassic limestone, granite and slate of the Aouli Massif, showing a steeper gradient of 0.38° until it reaches the Tamdafelt fold system (Figs. 1 and 2a). This steeper segment defines a knickzone that is 300–400 m-high (Fig. 2b). The Enjil river joins the Moulouya downstream this knickzone, also depicting a knickzone, located close to the confluence (Fig. 2a).

Downstream from the Tamdafelt fold system (Fig. 1), the Moulouya river flows along the Missour sedimentary basin where its gradient becomes gentle again, averaging 0.14° for >150 km. A slight increase in gradient occurs again at the boundary between the Missour and Guercif basins, where the river cuts Jurassic dolostones, but the gradient becomes gentler in the Guercif basin, averaging 0.12° until the outlet. Along the Missour and Guercif basins, the Moulouya river joins tributaries, that drain both the High Plateaus and the Middle Atlas (Jebel Bou Naceur), the most important one being the Za river.

### 4.2. Streams draining the High Plateaus

The western edge of the High Plateaus is drained by tributaries of the Moulouya, which have significant knickzones (red reaches in Fig. 3). Fig. 4a shows the profiles of the Moulouya river and its tributaries, all shearing the same distance to the Mediterranean outlet. All profiles have gentler slopes in their upper courses (generally <0.2°), with an abrupt slope increase along their middle courses, and progressively gentler slopes downstream. The gentle gradient of the upper segments suggests that little channel incision has occurred upstream of the knickpoints, and therefore these upper course gradients can be interpreted as inherited from the Missour basin paleosurface. In this case, the lateral correlation of these gentle gradients allows us to delineate a paleosurface reaching 500–550 m above the present Moulouya river (Fig. 4a). The knickpoints for the Fajane and Kaddou tributaries, draining the High Plateaus into the Missour basin, are 500 and 550 m-high, respectively (Fig. 4b and c). The Za river is the main tributary of the Moulouya river, draining ~20,000 $km^2$ of the High Plateaus to the lower Guercif basin. The upper Za course is ~300 km-long into the Plio–Pleistocene fluvial deposits of the High Plateaus, with entrenchments of ~100 m close to the knickzone. The gradient of the upper course is 0.15°, while downstream, the gradient increases to 0.33° for almost 80 km at the eastern edge of the Guercif basin that is composed of Jurassic carbonates and shows a 400–450 m-high knickzone (Fig. 4d). Considering an average entrenchment of 100 m for the Za river into the Guercif basin, the total height of this knickpoint is 500–550 m.

### 4.3. Streams draining the Jebel Bou Naceur

The Chegg Ard, El Mansoor, El Berd and Timrhout rivers drain the southeastern Jebel Bou Naceur into the Missour and Guercif basins (Fig. 3). The Chegg Ard has a catchment area of ~240 $km^2$ upstream the Missour basin, showing an impressive 1000 m-high knickpoint (Fig. 5a), located at approximately the contact between Toarcian marls and overlying Bathonian–Callovian sandstone (Charroud, 2002). The upper course of the Chegg Ard river flows for ~10 km on a wide valley (Fig. 5b), where the channel is slightly entrenched and has a gradient of 1.3°. Downstream, channel gradient abruptly increases to 3.1° and is deeply entrenched. Finally, the Chegg Ard river has an average gradient of 0.9° from the knickpoint to the confluence with the Moulouya river.

Tributary streams that flow parallel to the structural grain of the Middle Atlas drain the eastern edge of the Jebel Bou Naceur. These tributaries converge downstream to become the Melloulou river, which, in

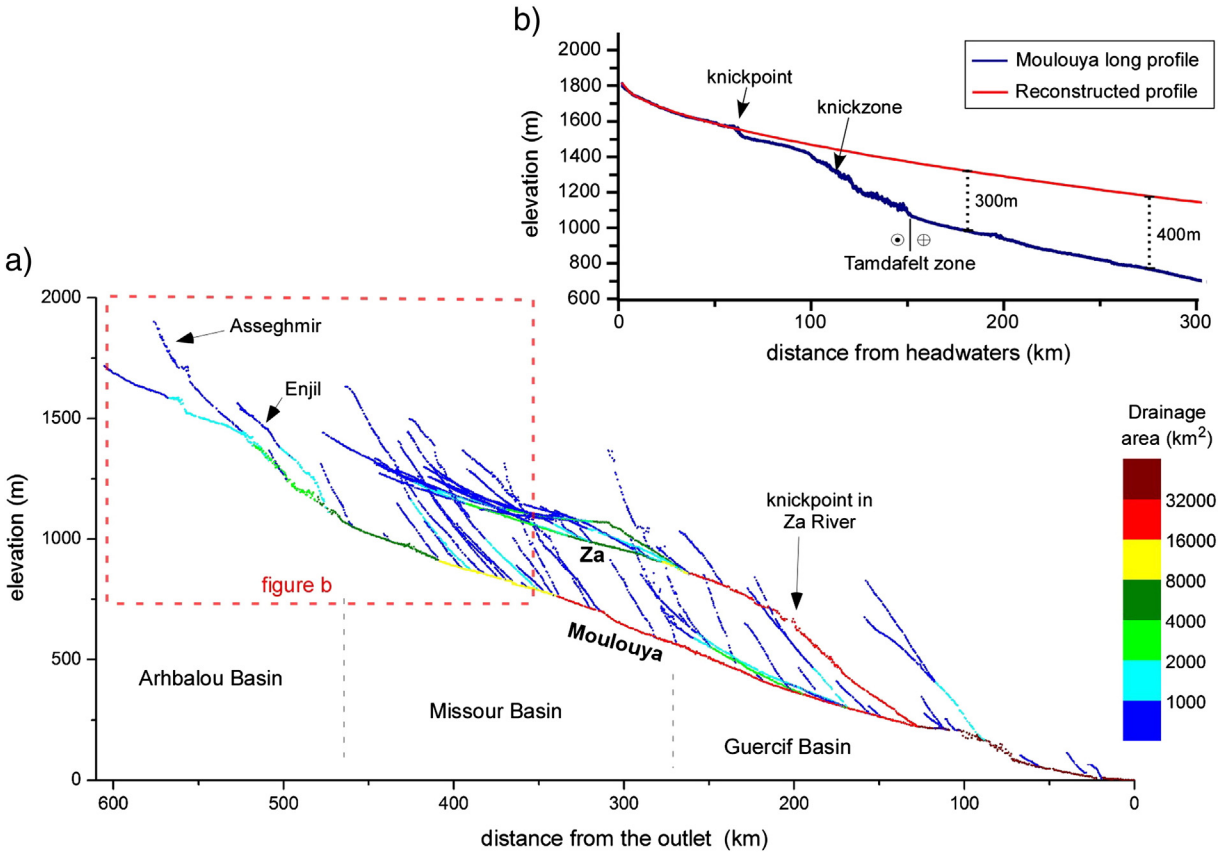


**Fig. 2.** a) Profiles of the Moulouya river system from headwaters to the Mediterranean. The color bar indicates the area of the upstream drainage area. b) Profile of the Moulouya river in the Arhbalou and Missour basins, showing a knickzone located 100–150 km from the headwaters. The reconstructed profile (using $K_s = 21$ and $\theta = 0.24$) shows a difference in elevation of 300–400 m with respect to the current river channel.

turn, joins the Moulouya river in the central Guercif basin. Tributaries of the Melloulou river include the El Mansoor, El Berd and Timrhout rivers, which have large knickpoints in their mountainous courses with heights of 700–800 m (Fig. 5c and d). The channel of the Timrhout river has been blocked by a rock-slide to form a lake (Gualta Tamda; Fig. 5e). The location of the rock-slide coincides with the upper segment of an 800 m-high knickpoint, thus suggesting that slope instability may have been partially triggered by rapid fluvial incision.

## 5. Quaternary fluvial surfaces in the lower Chegg Ard valley

Alluvial fan surfaces and fluvial terraces along the Chegg Ard, the main river draining the Jebel Bou Naceur to the Missour basin, were selected for dating because they preserve a good record of fluvial deposits and exhibit signs of recent deformation related to folds associated with the southern Middle Atlas thrust front (Fig. 6) (Delcaillau et al., 2008; Laville et al., 2007). Four sets of fluvial deposits and abandoned alluvial fan surfaces were mapped along the Chegg Ard valley, which we have named T1 (oldest) to T4 (youngest) (Figs. 6 and 7).

The T1 is an extensive alluvial fan surface, which has a radial length of ~12 km with its apex located near the mountain front, at the boundary between the Middle Atlas Mesozoic carbonate rocks and the Tertiary clastic deposits of the Missour basin. This alluvial fan surface is entrenched by the Chegg Ard channel to a depth of 135–185 m. The surface is defined by 1–5 m thick fanglomerate level, which conformably overlies Tertiary conglomerates of the Bou Irhardaiene Formation. The T1 fanglomerate is composed of cobbles and boulders that become smaller downstream. Locally, in the upper areas of the abandoned alluvial fan, old longitudinal bars composed of >50 cm-diameter imbricated boulders are observed, suggesting of a highly energetic depositional environment. The clasts mainly comprise carbonate rocks. The T1 surface also shows well-developed pedogenic carbonate cement (Stage V of Gile et al., 1981). The alluvial fan is almost completely eroded southward of the frontal monocline fold (FMF; Fig. 6), being restricted to small patches in the forelimb. Stratified conglomerates abutting the forelimb of the FMF, which are unconformable on the Bou Irhardaiene Formation conglomerates, may be the sole distal remnants of T1 at the foot of the FMF. The presence of embedded deposits suggests a relative base level drop, and we assume that remnants of T1 had to be formed above the T2, at least 35 m above the present-day channel height.

The abandoned fluvial and alluvial surface T2 is present in three locations along the Chegg Ard valley (Fig. 6b). The main exposure occurs south of the FMF, where it forms a large lobe of an alluvial fan that extends for 14 km until it reaches the Moulouya river (T2b). Other remnants are present as river terraces in the cores of the FMF and the Beni Aioun anticline (T2c and T2a; Figs. 6a and 7a). The T2 deposits have the same general characteristics as T1, but the average size of the clasts is smaller, rarely reaching >20 cm in diameter. T2 usually shows moderate pedogenic carbonate development (carbonate morphology stages III–IV of Gile et al., 1981). The T3 and T4 deposits are well preserved south of the FMF, displaying similar features to T2, though carbonate cement is less developed. T3 is composed of decimeter-size clasts, some of them reaching 30 cm in diameter, whereas T4 has smaller clasts (rarely reaching 15 cm in diameter).

## 6. $^{10}$Be terrestrial cosmogenic nuclide results

### 6.1. Erosion rate estimates

TCN concentrations can be used to estimate steady-state erosion rates (erosional equilibrium; Lal, 1991). Thus, samples with higher TCN concentrations provide lower limits on erosion rates. We have

Please cite this article as: Pastor, A., et al., Extracting dynamic topography from river profiles and cosmogenic nuclide geochronology in the Middle Atlas and the High Plateaus of Morocco, Tectonophysics (2015), http://dx.doi.org/10.1016/j.tecto.2015.06.007

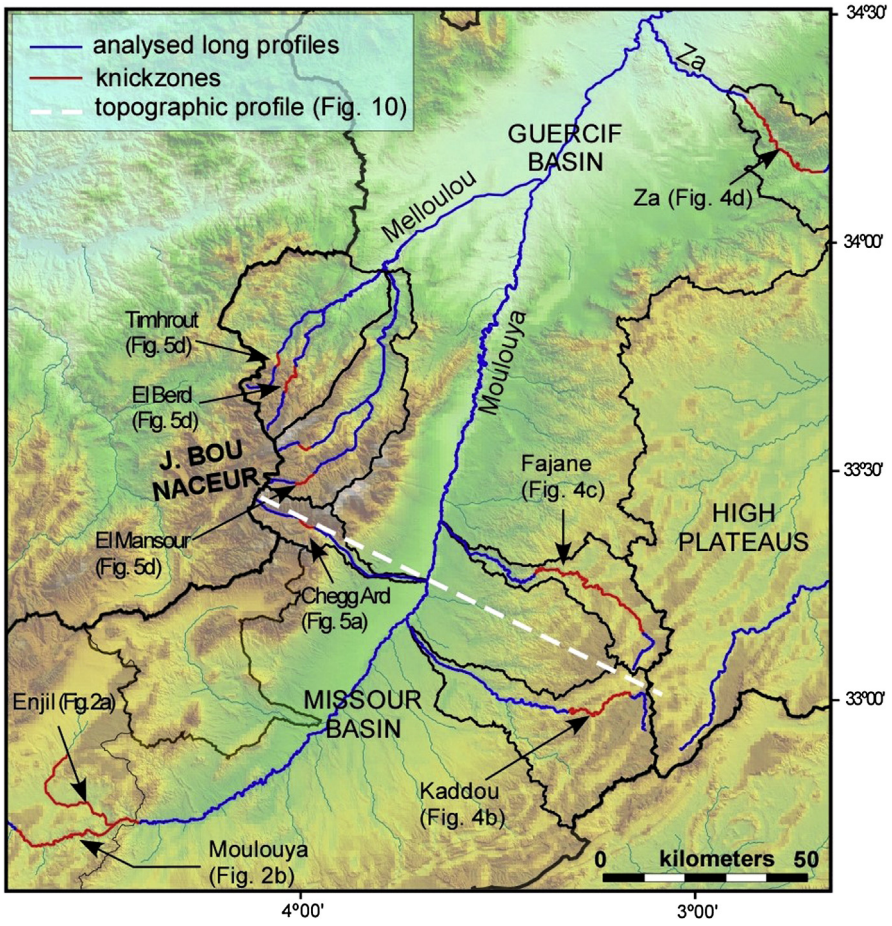


**Fig. 3.** Digital elevation model (DEM SRTM90) for the Missour and Guercif basins (central segment of the Moulouya river). The river courses analyzed in this study are highlighted. The dashed white line marks the location of the topographic profile shown in Fig. 10.

used $^{10}$Be concentrations in the clasts for T1 samples (except M918, which yielded an age significantly younger than the other ones) to estimate erosion rates by using the method of Lal (1991). This provides a minimum erosion-rate estimate because we preferentially selected clasts that appeared more resistant to erosion, most of them still preserving rounded fluvial shapes and an absence of notable weathering features, such as exfoliated surfaces, pitting, or granular disintegration. Moreover, T1 surface is strongly cemented, thus increasing its resistance to erosion. The ten oldest ages of surface clasts provide a mean erosion rate of 1.4 ± 0.2 m Ma$^{-1}$, which is in good agreement with those obtained in climatically similar settings (e.g., Matmon et al., 2009; Portenga and Bierman, 2011), as discussed by Arboleya et al. (2008) in their study on terrace dating in the Ouarzazate basin.

### 6.2. Terrace ages in the Chegg Ard Valley

Sampled boulders may retain a signal of prior exposure with inherited TCNs, which result in ages that are older than the surface being dated (Anderson et al., 1996; Hancock et al., 1999). Intense weathering or exhumation of clasts may result in lower concentrations of TCNs, which, in turn, would underestimate the age of the surface. Collecting multiple samples from each terrace and looking for potential outliers, that is, exposure ages that fall significantly outside the mean value (>2 σ) of all the ages obtained for a given landform, can help to identify the problem of derived and/or weathered/exhumed boulders. We have used the erosion rates estimates based on the oldest ten ages of surface clasts (as described in the previous sub-section) as a test to assess the likely effects of erosion on the samples used to define the surface ages. For samples having an erosion rate of 1.4 m Ma$^{-1}$, a calculated age of 10 ka would underestimate the true age by a ~1%, an age of 50 ka by ~5%, an age of 100 ka by ~10%, and an age of 300 ka by ~50%. Given the uncertainties in defining the erosion rate, we have plot all our ages with zero erosion, but also present them in Table 1 for an erosion rate of 1.4 m Ma$^{-1}$, which places an upper limit on the possible ages.

Terrace T1 has been dated by using 11 samples from two different localities (T1a and T1b in Fig. 6), which yield ages from 321 to 528 ka (Fig. 8), with a mean age of 411 ± 55 ka (uncertainty = 1 σ). The sampled clasts of sandstone and phyllite were carefully selected from the surface, mainly composed of carbonate rocks. Since the sampled clasts were well rounded, retaining their original shape, we argue that they have not undergone significant weathering. Twelve samples were dated on T2 terrace at two different localities (T2a and T2b in Figs. 6 and 7a), yielding ages between 20 and 327 ka (Fig. 8). Samples M926 (327.8 ± 33.8 ka) and M927 (105.1 ± 10.0 ka) are considered outliers since they are >2 σ older than the mean age of the rest of the population. The presence of conglomerate clasts at locality T2b reworked from T1 or from the Bou Irhardaiene Formation supports the view that M926 and M927 have been derived from an older surface. Omitting the ages of M926 and M927, the T2 terrace has a mean age 52 ± 20 ka (uncertainty = 1 σ). Two other samples, M929 and M932, fall outside the mean value (>2 σ) with ages of 20.4 ± 10.0 ka and 22.0 ± 2.6 ka. We recognize that these younger age samples might have been exhumed, although we cannot prove this assumption. Omitting the ages of M929 and M932 too, the T2 terrace has a mean age 62.6 ± 14.1 ka

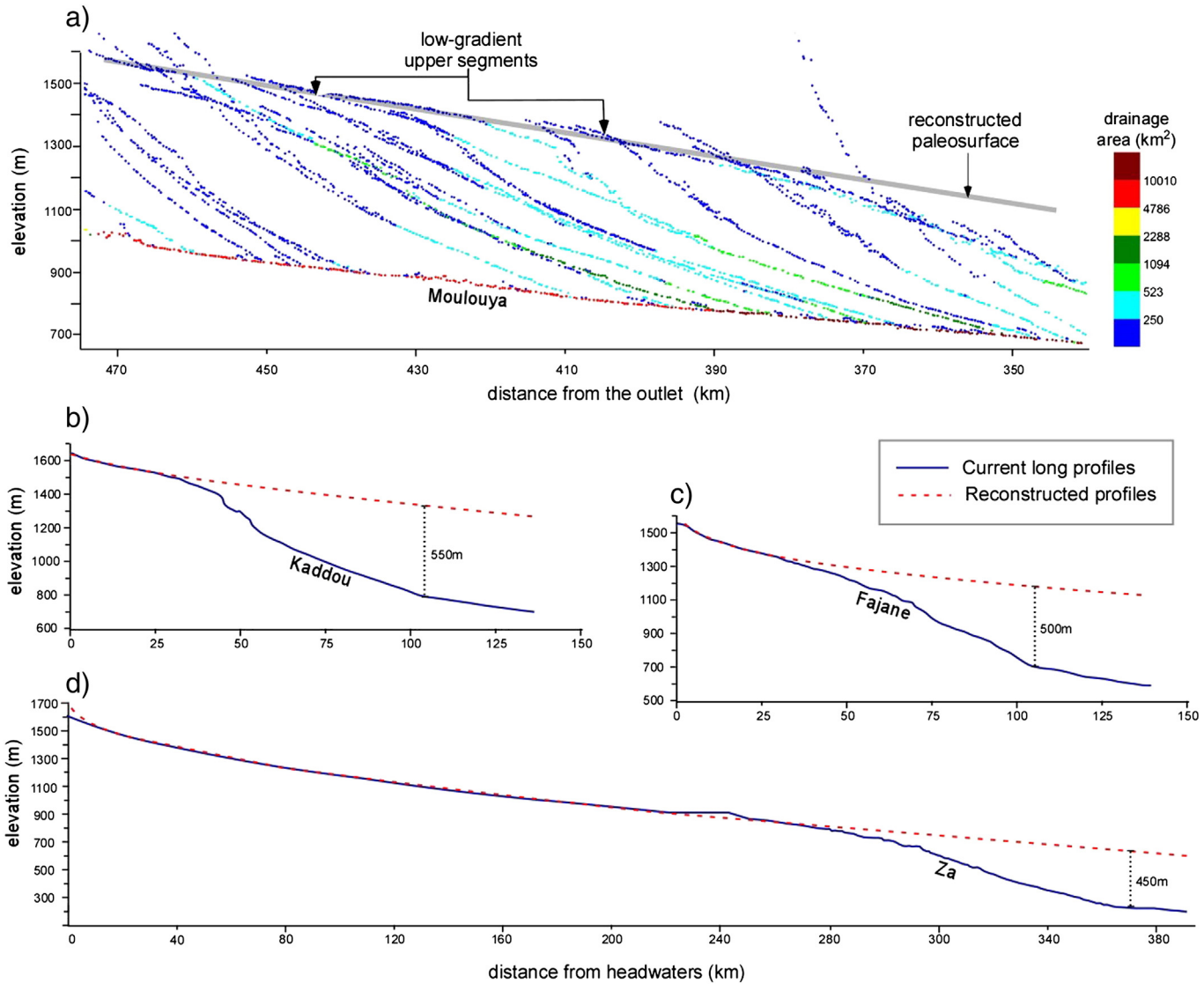


**Fig. 4.** (a) Profiles for the Moulouya river and its tributaries with drainage areas over 50 km$^2$ projected on the same plane. Most of the tributaries draining the stable margin of the Missour basin exhibit anomalously low gradients in their upper courses and similar knickzones. The prolongation of these upper courses allows reconstructing the basin paleosurface, which was 500–550 m above the current Moulouya river channel. (b) Profile of the Kaddou river (see location in Fig. 3) draining the stable margin of the Missour basin; red dashed line shows the reconstructed paleoprofile (using $K_s = 13$ and $\theta = 0.19$) that reaches 550 m over the current Moulouya river. (c) Profile of the Fajane river (see location in Fig. 3); red dashed line shows the reconstructed paleoprofile with $K_s = 83$ and $\theta = 0.40$; this paleoprofile reaches 500 m over the Moulouya river channel. (d) Profile of the Za river (see location in Fig. 3) draining the High Plateaus to the Guercif basin; red dashed line shows the reconstructed paleoprofile using $K_s = 34$ and $\theta = 0.26$, which reaches 450 m over the Moulouya river channel. (For interpretation of the references to color in this figure legend, the reader is referred to the web version of this article.)

(uncertainty = 1 σ). In the following we will use the older mean value for the age of T2 (62 ± 14 ka).

### 6.3. Tectonic uplift and incision rates

The dated T1 and T2 terraces are incised by the Chegg Ard river in different places along the Chegg Ard Valley, where incision can be measured in both the tectonically uplifted area of the basin margin and the central Missour basin. The FMF and Beni Aioun anticline (Fig. 6) have deformed the upper segments of terraces T1 and T2. The FMF is the frontal-most structure of the Middle Atlas, being located ~12 km downstream from the mountain front. This SE-vergent fold trends SW–NE and shows an almost horizontal backlimb and a subvertical forelimb, whereas the Beni Aioun anticline (BAA in Fig. 6) is a gentle anticline located between the mountain front and the FMF.

Immediately northwards of the FMF in the tectonically uplifted fold limb, T1 surface is 133 ± 3 m above the current river channel (Fig. 9). T1 is also tilted by the Beni Aioun anticline and reaches 182 ± 5 m above the current river channel near the mountain front (Fig. 9). Thus, incision rates measured from T1 in the tectonically uplifted area range from 0.32 ± 0.04 to 0.44 ± 0.06 mm yr$^{-1}$ (Fig. 9). The difference between these rates is ~0.1 mm yr$^{-1}$, and is likely due to the local uplift generated by the Beni Aioun anticline.

Surface T2 is not continuously preserved along the Chegg Ard valley and shows very little deformation, though its elevation with respect to the current river channel significantly varies along the valley. Thus, T2 is present in the cores of FMF and Beni Aioun anticline, being at ~51 to 55 m above the present-day channel respectively (T2c and T2a in Figs. 6b and 7a; Fig. 9). T2 also forms the alluvial fan located downstream from the FMF, being incised ~16 ± 3 m in the distal course and 32 ± 3 m in its upper one (T2b in Figs. 6b and 7a; Fig. 9). The

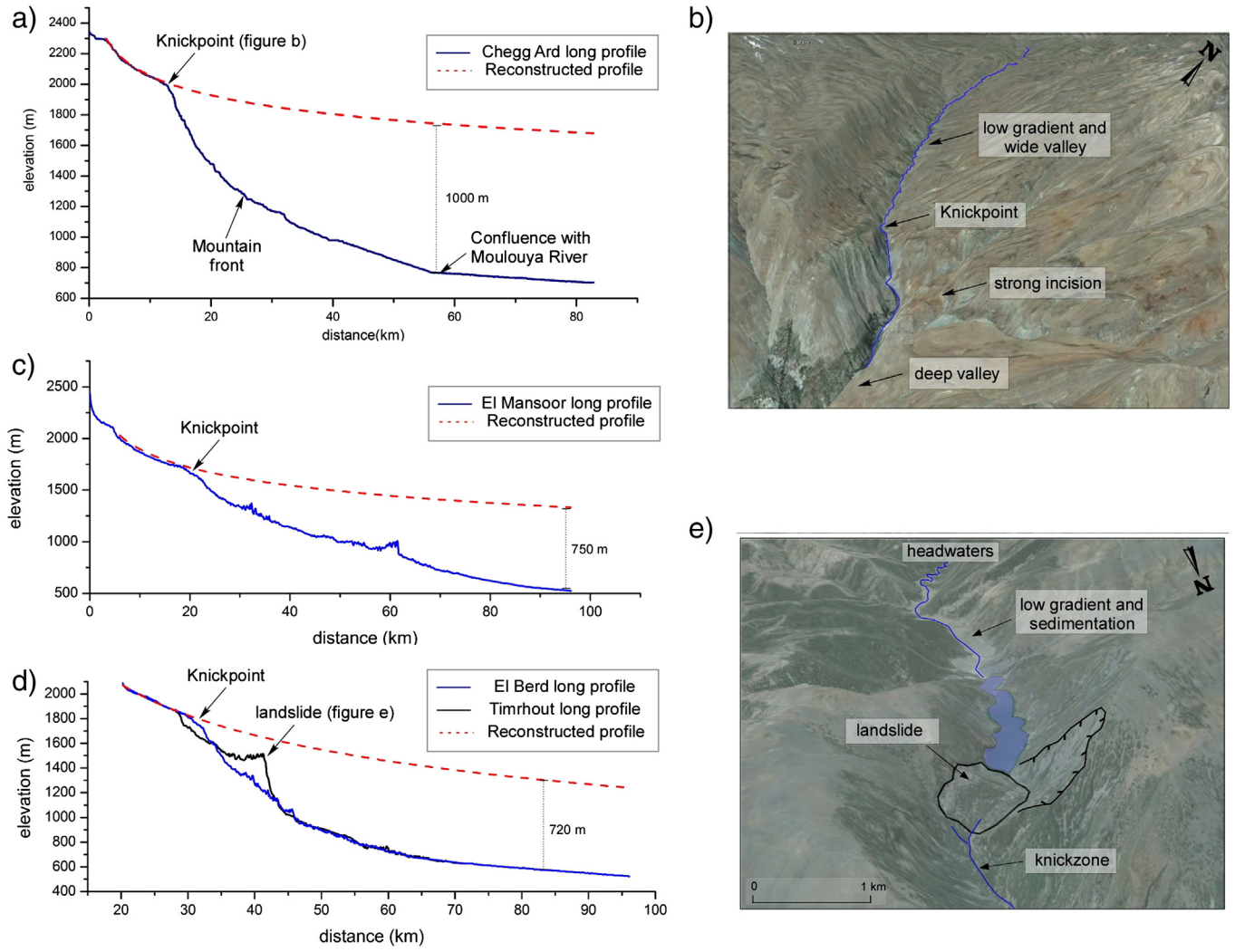


**Fig. 5.** (a) Profile of the Chegg Ard river (see location in Fig. 3), which drains the Jebel Bou Naceur to the Missour basin. Red dashed line shows a reconstructed paleoprofile (using $K_s = 680$ and $\theta = 0.62$) that reaches 1000 m over the current Moulouya river channel. (b) Satellite image from Google Earth of the mountainous course of the Chegg Ard river. Upstream the channel flows along a wide valley; downwards the profile exhibits a large knickpoint, downstream from which the channel is deeply incised. (c) Profile of the El Mansoor river (see location in Fig. 3), which drain the Jebel Bou Naceur to the Guercif basin. Red dashed line shows a reconstructed paleoprofile (using $K_s = 950$ and $\theta = 0.62$) that reaches 750 m over the current Moulouya river channel. (d) Profile of the El Berd and Timrhout rivers (see location in Fig. 3), which drain the Jebel Bou Naceur to the Guercif basin. Red dashed line shows a reconstructed paleoprofile (using $K_s = 5722$ and $\theta = 0.75$) that reaches 7200 m over the current Moulouya river channel. (e) Satellite image from Google Earth showing the mountainous course of the Timrhout river blocked by a rock-slide, that created an abrupt knickpoint and the lake Gualta Tamda. (For interpretation of the references to color in this figure legend, the reader is referred to the web version of this article.)

difference between these incision values, with higher incision in the apex and lower incision in distal parts of the fan, is probably mostly due to the difference in gradient between the steeper slope of the incised alluvial fan and the gentler slope of the contemporary river. Considering an age of 62 ± 14 ka for T2, we calculate incision rates that range from 0.28 ± 0.12 mm $yr^{-1}$ in the distal alluvial fan surface to 0.55 ± 0.17 mm $yr^{-1}$ in the fan apex (Fig. 9). T2c, in the core of the FMF is uplifted ~19 m with respect to the proximal parts of T2b, located 500 m downstream (Fig. 9). This difference in elevation corresponds to tectonic uplift related to the FMF since the abandonment of T2, which yields an average rate of ~0.3–0.4 mm $yr^{-1}$. Such a rate is comparable to those recorded for the past 250 ka in the deformed terraces of the proximal Ouarzazate basin in the foreland of the High Atlas (Pastor et al., 2012).

The incision rate calculated for terrace T1 at the backlimb of the FMF is 0.32 ± 0.04 mm $yr^{-1}$, which is significantly lower than that obtained from T2c and T2a (0.93 ± 0.26 mm $yr^{-1}$ and 0.88 ± 0.25 mm $yr^{-1}$ respectively; Fig. 9). We suggest that the more recentmost rates (calculated from T2) are probably overestimated because of the terrace formation cycle of incision/aggradation has not been completed (aggradation of the newest riverbed terrace), as Arboleya et al. (2008) documented in the Ouarzazate basin. Therefore, the longer-term incision rates are likely more representative of tectonic uplift than recentmost ones, the latter being significantly higher due to climatic factors.

## 7. Discussion

### 7.1. Knickpoints, surface uplift and erosion in the Moulouya catchment

The analysis of river profiles reveals the systematic presence of large knickpoints or knickzones in the Moulouya river and its main tributaries. The formation and upstream retreat of knickpoints is typically understood as the dominant mode of channel adjustment in response to either regional or local perturbations due to one or more of the following triggering factors: regional surface uplift (e.g., Burbank and Anderson, 2001; Lavé and Avouac, 2001; Quezada et al., 2010; Wobus

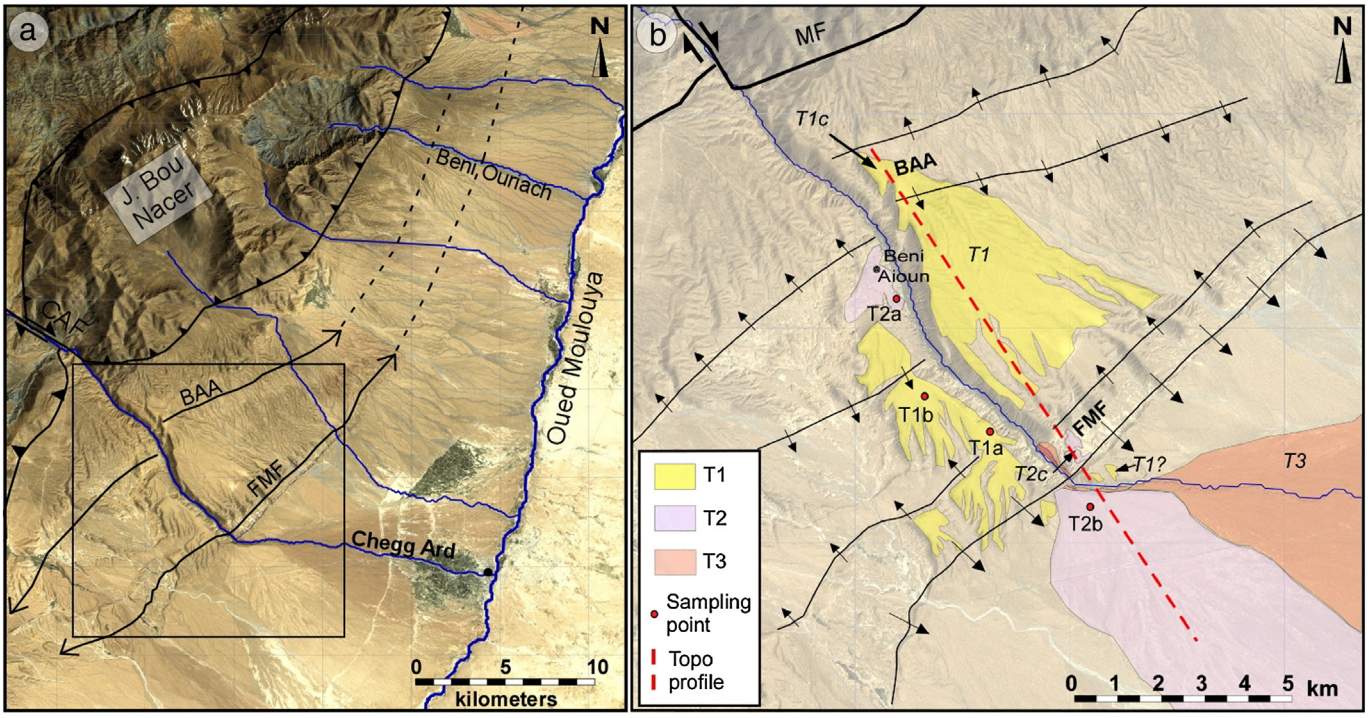


**Fig. 6.** (a) Google Earth image of the central Missour basin and the Jebel Bou Naceur with the main geologic structures and rivers. (b) Close-up of the Chegg Ard valley showing the mapping of fluvial deposits and landforms, tectonic flexures, sample location, and the trace of the profile in Fig. 9 (red dashed line). CAF — Chegg Arg fault; MF — mountain front; BAA — Beni Aioun anticline; FMF — Frontal monocline. (For interpretation of the references to color in this figure legend, the reader is referred to the web version of this article.)

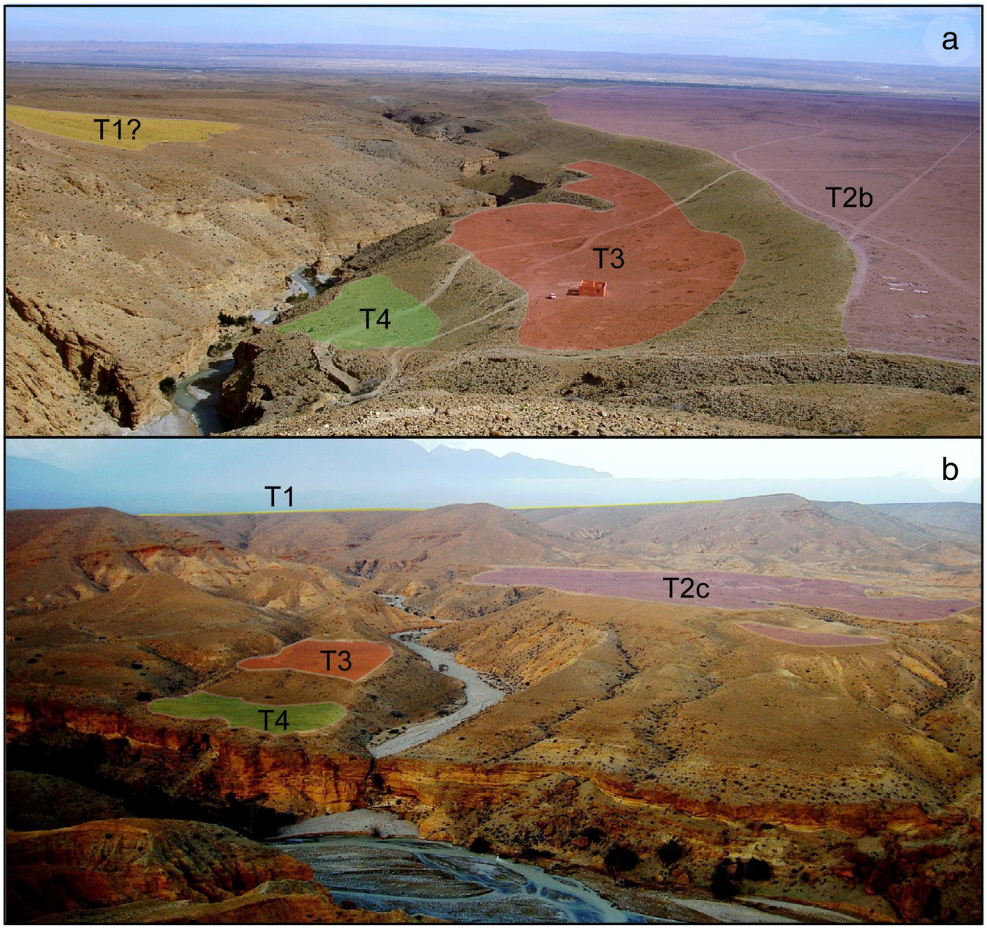


**Fig. 7.** Views of terrace levels at the western side of the Chegg Ard from the fold crest of the Frontal monocline. (a) View to the SE where alluvial fan surfaces T2 and T3 dominate. (b) View to the NE showing terrace T1 in the background and T2, T3 and T4 preserved in the core of the Frontal monocline.

Please cite this article as: Pastor, A., et al., Extracting dynamic topography from river profiles and cosmogenic nuclide geochronology in the Middle Atlas and the High Plateaus of Morocco, Tectonophysics (2015), http://dx.doi.org/10.1016/j.tecto.2015.06.007

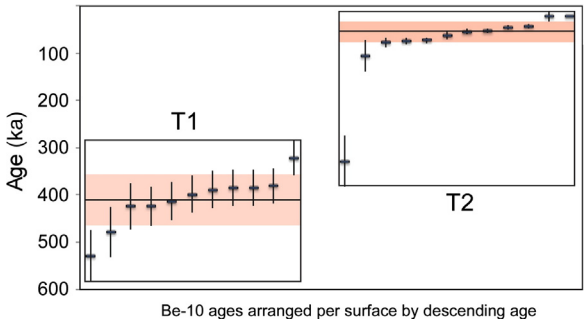


**Fig. 8.** Be-10 TCN ages for terrace levels T1 and T2. The horizontal black line and gray band are the mean and 1 σ values for each surface.

et al., 2006), localized structural surface uplift (e.g., Burbank et al., 1996), regional base level drop (e.g., Begin et al., 1981; Snyder et al., 2002; Bishop et al., 2005; Crosby and Whipple, 2006), local base level fall directly caused by stream piracy (e.g., García, 2006) and differential erosion caused by lithological contrast (e.g., Goldrick and Bishop, 2007). Other causes may be associated with inherited relief features due to glacial erosion and/or landsliding (e.g., Benda and Dunne, 1997; Korup, 2006; Lancaster and Grant, 2006). Knickpoints in the upper Moulouya catchment near the Middle Atlas front were interpreted by Laville et al. (2007) and Delcaillau et al., (2008) as related to recent thrust deformation, without discussing the potential role of regional uplift and base level drop. Similarly, Boulton et al. (2014) has interpreted existing knickpoints in the southern High Atlas mountain front, as entirely related to active faults.

The knickpoints in the Missour and Guercif basins are situated on tributaries draining both sides of the Moulouya river, from the stable High Plateaus to the active Middle Atlas, and must therefore be explained by a regional-scale process. This regional-scale process is most likely the adaptation of the fluvial network to the mantle-driven, long-wavelength uplift. This uplift remains active in the region (Barbero et al., 2011; Barcos et al., 2014) and has produced a maximum surface uplift of ~1000 m at a rate ranging from 0.17 to 0.22 mm $yr^{-1}$ since at least the earliest Pliocene (Babault et al., 2008). The Missour basin was still accumulating sediments (Bou Irhardaiene Formation) at early Pliocene time, after the mantle-related uplift has started. The change from internal to external drainage in the basin probably occurred when its surface was raised at a significant elevation and had accumulated potential energy enough as to be capture by a former Moulouya river with its base level located in the Mediterranean. The capture of an endorheic basin likely triggers faster erosion rates during the first stages, which, in turn, may have caused the development of a knickpoint that propagated upwards along the entire fluvial network, until its present position at the contact between the Neogene basin fill and the Jurassic carbonate bedrock of the basin margins.

The analysis of river profiles shows that the height of knickpoints differs in the High Plateaus margin with respect to the Middle Atlas thrust front, where knickpoints present larger vertical drop. Knickpoints in rivers draining the eastern margin of the Missour basin (adjacent to the High Plateaus), where there are no active tectonic structures, are 500–550 m-high at the junction with the Moulouya river (Fig. 4). This is consistent with the presence of lacustrine deposits preserved in the eastern margin of the Missour basin at ~550 m above the present-day Moulouya river channel (labeled Q6 in the 1/100,000 geological map of Hassi el Ahmar and attributed to the Villafranchian -indetermined upper Pliocene; Choubert, 1964), which we interpret as the maximum elevation reached by the basin fill before erosion started.

The Moulouya river has a knickzone with a vertical drop of 300–400 m located at the boundary between the Arhbalou and Missour basins. Laville et al. (2007) related this knickzone to active deformation in the Tamdafelt fold system, located just at the base of the knickzone. However, the knickzone as a whole coincides with the contact between the easily erodible sediments of the Missour basin and Jurassic carbonates/Paleozoic basement rocks. Alternatively, we propose that the knickzone is related to uplift that affected the entire drainage basin, which caused upstream knickpoint propagation until the river lost its erosive capacity at the lithological boundary. The knickzone in the Moulouya river is 150–250 m lower than in its tributaries draining the High Plateaus. Within the middle of the Arhbalou basin (upstream of the Moulouya's knickzone), the Gara of Midelt is a 100 m-high butte composed of Neogene sediments, thus providing a minimum estimate of the elevation of the basin fill, and supporting the role of active erosion in landscape evolution.

### 7.2. Thrust surface uplift of the Jebel Bou Naceur

The main rivers draining the Jebel Bou Naceur to the Missour and Guercif basins show knickzones with higher difference in elevation than those measured in tributaries draining the High Plateaus. Laville et al. (2007) and Delcaillau et al. (2008) analyzed Quaternary deposits and knickpoints along major streams in the southern flank of the Middle Atlas, and interpreted them as related to recent thrust tectonic deformation, though they did neither quantify deformation rates nor discuss the potential role of regional uplift. The impressive 1000 m-high knickzone

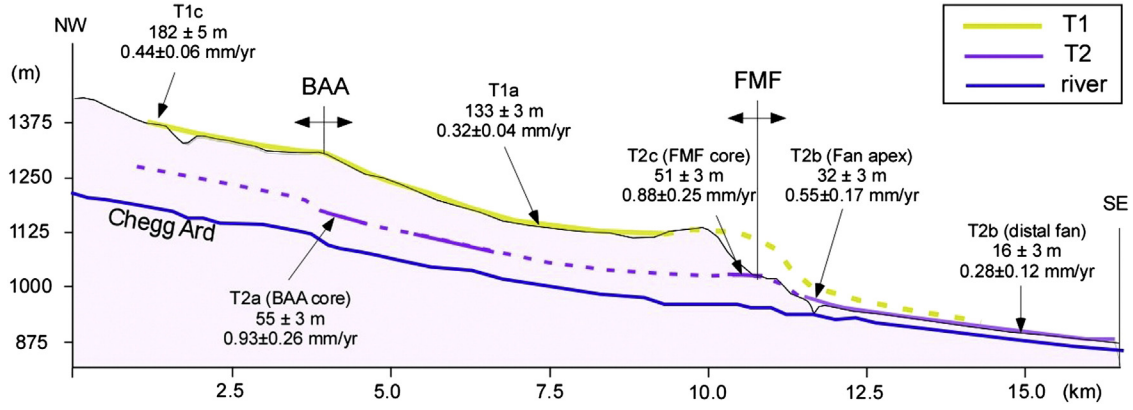


**Fig. 9.** Topographic profile traced parallel to the Chegg Ard river along its eastern margin (see Fig. 6b for location). Surfaces T1 and T2 are projected in the same plane, in continuous line where preserved, and dashed line were inferred. The figure shows the difference in elevation of terraces T1 and T2 with respect to the active Chegg Ard channel at both sides of the tectonic structures. Incision rates in mm/yr are also shown along the profile.

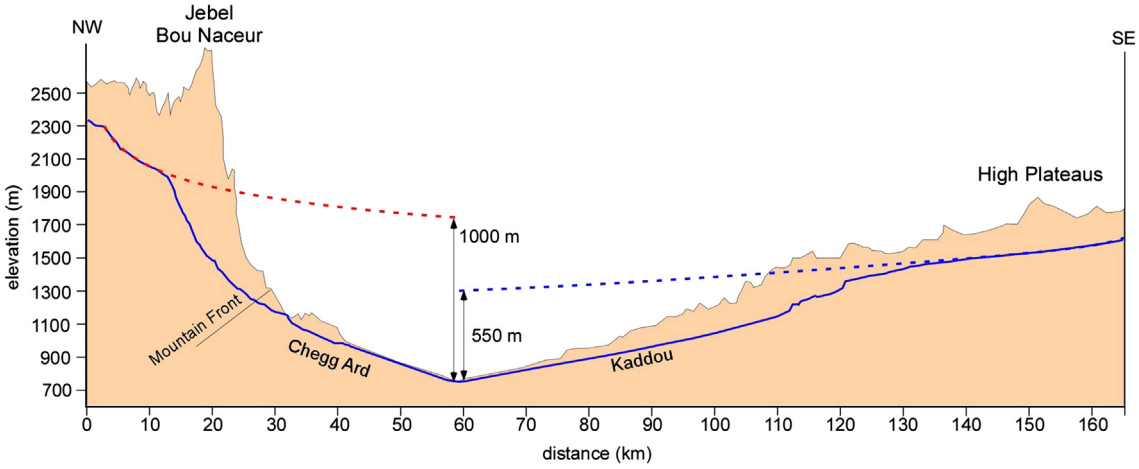


**Fig. 10.** Topographic profile across the Missour basin and its margins from the Jebel Bou Naceur to the High Plateaus (see Fig. 3 for location), with the longitudinal profiles of the Chegg Ard and Kaddou rivers projected in the same plane. The knickzone of the Kaddou river is 550 m-high and is related to the regional-scale surface uplift affecting the entire fluvial network. The difference in elevation between the Chegg Ard river and Kaddou river knickzones (450 m) is probably due to local (thrust-related) recent surface uplift of the Jebel Bou Naceur.

of the Chegg Ard river (Fig. 5a) was interpreted exclusively as a result of recent out-of-sequence thrusting by these authors.

The El Mansoor, El Berd and Timrhout tributaries drain the eastern Jebel Bou Naceur to the Guercif basin (Fig. 3) and have 700–800 m-high knickzones (Fig. 5c and d). We propose that in the same way as in tributaries draining the High Plateaus, 500–550 m of the total height of these knickzones is due to regional-scale uplift, whereas the remaining 450–500 m in the central Southern Middle Atlas frontal zone (Fig. 10) and 200–300 m in the eastern edge of the Jebel Bou Naceur can be explained by the localized (thrust-related) uplift of the Middle Atlas associated with its frontal structures. In the Chegg Ard valley, signs of tectonic deformation in Quaternary alluvial deposits attest the active structures emerging within the Missour basin. Delcaillau et al. (2008) proposed small knickpoints within the Missour basin and relate them to active structures too. We argue that knickpoint preservation is rare within the basin where streams flow over easily erodible sediments. Instead, knickpoints retreat upstream until they reach more resistant rock types at the basin margin. Resistant rocks are more difficult for the streams to erode, and therefore, knickpoints become knickzones that remain at the lithological boundary for some time, progressively increasing in height. Hence, neither the current location nor the elevation of knickzones along the Moulouya fluvial network can be simply related to active thrust deformation as suggested by Delcaillau et al. (2008).

### *7.3. Regional (mantle-driven) versus local (thrust-related) surface uplift rates*

Our TCN dating of T1 and T2 terraces allows us to calculate incision rates at different points along the Chegg Ard valley. Moreover, the two obtained ages (T2: 62 ± 14 ka and T1: 411 ± 55 ka) enable us to examine incision rates at different time spans, particularly for the area affected by surface uplift due to the FMF. Incision rates measured in the upper Chegg Ard valley must result from combined mantle-driven surface uplift and structural surface uplift produced by the frontal structures of the Middle Atlas, named the FMF and the Beni Aioun anticline, which affect both T1 and T2 surfaces. For the lower reach of the Chegg Ard, downstream from the frontal active structures, we argue that estimated incision rates are rather valid for the Moulouya river, which constitute the base level for the Middle Atlas tributaries. Thus, these rates can be taken as a proxy for the recent surface uplift rates related to dynamic topography within the Moulouya drainage basin, i.e., they represent the large-scale regional surface uplift due to buoyancy changes in the mantle not directly related to crustal tectonic shortening (e.g., Coblentz and Karlstrom, 2011; Nereson et al., 2013 for terminology).

Average regional surface uplift rates since the latest Miocene or earliest Pliocene were estimated in the northern Middle Atlas by Babault et al. (2008) at ~0.2 mm $yr^{-1}$, on the basis of elevated Messinian marine deposits, scarcely eroded and lying at 1200 m.a.s.l. in the Skoura area, only 65 km WNW of our study area. The marine Messinian deposits dated by Krijgsman and Langereis (2000) in the center of the Guercif basin are significantly lower, at 450–650 m.a.s.l., and the resulting surface uplift rate here is of ~0.1 mm $yr^{-1}$. Hence, we retain the value of 0.1–0.2 mm $yr^{-1}$ based on Messinian shallow marine deposits as an average long-term surface uplift in the study area during the late Pleistocene. The incision rate of 0.28 ± 0.12 mm $yr^{-1}$ at the distal part of T2b in the Missour basin is of the same order of magnitude, or slightly greater than this average long-term surface uplift (Babault et al., 2008). Nevertheless, as discussed above, T2-based rates might be slight overestimations of the true values.

We argue that entrenchment of the lower Chegg Ard river since ~411 ka is keeping pace with the rising dynamic topography at a rate of ~0.1–0.2 mm $yr^{-1}$. Under this assumption, the fluvial incision rate calculated for T1c near the Jebel Bou Naceur mountain front at 0.44 ± 0.06 mm $yr^{-1}$ (Fig. 9) can be divided into ~0.1–0.2 mm $yr^{-1}$ of regional surface uplift plus ~0.3 mm $yr^{-1}$ of thrust-related surface uplift.

The combined geomorphic analysis of river profiles and the incision rates presented above provide inferences on the recent tectonic and erosional history of the Missour basin. We have showed that the Chegg Ard river profile exhibits a knickpoint with a height of 1000 m, 500–550 m of which might be explained by mantle-driven (regional) surface uplift and the remaining 450–500 m by upthrusting of the Jebel Bou Naceur (Fig. 10). However, our geochronological data suggest that since the Middle Pleistocene the rate of local structural surface uplift has been greater than that of regional surface uplift. Our calculations imply a local structural surface uplift rate of ~0.3 mm $yr^{-1}$ since the Middle Pleistocene within the Missour basin close to the mountain front in association with the two frontal structures. We cannot discard however the possibility that other active structures are present in the mountain area, but, as a first approximation, we retain the minimum rate of 0.3 mm $yr^{-1}$, and at such a rate, the 450–500 m height of the knickzone related to thrust activity would have been produced in 1.2–1.5 Ma.

The capture of the Missour basin generated a knickpoint that propagated upwards along the entire Moulouya catchment until its present-day location at the lithological contrasts along the basin margins. Favoring this view, terrace T1 is the oldest Pleistocene deposit, being characterized by larger clasts that suggest a very high-energy transportational/depositional setting, which, in turn, might be related to the arrival of the knickpoint to the mountain front. The thick alluvial

deposits reported by Bouazza et al. (2009) in the outlet of two gorges incised by the Za and Moulouya rivers in Beni Snassen and Horts Chain may have had a similar origin. Alternatively, the formation of T2 could be climatically controlled, as suggested by Arboleya et al. (2008) for the extensive Quaternary fanglomerates of similar age in the Ouarzazate basin, or due to pulses in the FMF as suggested by Delcaillau et al. (2008).

## 8. Conclusions

The geomorphic analysis of the Moulouya drainage network within the Missour basin and adjacent highlands (Middle Atlas and High Plateaus) reveals the existence of knickpoints or knickzones along most streams. The knickpoints are located in the rivers draining the tectonically active margin of the Middle Atlas, as well as in those draining the tectonically quiescent High Plateaus. The systematic presence of knickpoints attests adjustment of the fluvial network due to regional (long-wavelength) surface uplift of mantle origin (dynamic topography), which resulted in the Missour basin changing from dominantly aggradational to erosional in the late Pliocene or early Quaternary. Geomorphic evidence shows that the knickpoints related to regional surface uplift propagated upstream along the Moulouya river and its tributaries. The height of knickpoints along the rivers draining the undeformed (High Plateaus) margin indicates that 500–550 m of sediments have been eroded in the central parts of the Neogene Missour and Guercif basins. In contrast, rivers draining the tectonically active margin of the Middle Atlas (Jebel Bou Naceur) show 800–1000 m-high knickpoints. From the undeformed margin, it can be inferred that 500–550 m of this height might be explained by regional dynamic surface uplift, whereas the remaining 450–500 m in the central part of the southern Middle Atlas Front and the 200–300 m in the northeastern edge of the Middle Atlas might be related to thrust uplift of the Jebel Bou Naceur (Fig. 10).

Two Quaternary deformed river terraces in the Chegg Ard valley have been dated at 62 ± 14 ka and 411 ± 55 ka. Dated river terraces allow incision rates to be calculated. This in turn, can be related to the combined surface uplift triggered by both the Middle Atlas structures emerging within the basin, and by large-scale mantle buoyancy since the Middle Pleistocene. Moreover, from terrace deformation we estimate surface uplift along the foreland folds to be ~0.3 mm $yr^{-1}$. This discriminates localized uplift from the background large-scale surface uplift of ~0.1–0.2 mm $yr^{-1}$ in the central part of the Missour basin

## Acknowledgments

This research was supported by Spanish projects CGL2010-15416 and CGL2007-66431-CO2-01 (TOPOMED), and Consolider-Ingenio2010 CSD2006-00041 (TOPOIBERIA). Mohammed Charroud is thanked for early guidance to the field area. The comments by J.V. Pérez-Peña, an anonymous reviewer, and the editor A. Azor helped substantially to improve the original manuscript.

## References

Anahnah, F., Galindo-Zaldivar, J., Chalouan, A., Pedrera, A., Ruano, P., Pous, J., Heise, W., Ruiz-Constan, A., Benmakhlouf, M., Lopez-Garrido, A.C., Ahmamou, M., Sanz de Galdeano, C., Arzate, J., Ibarra, P., Gonzalez-Castillo, L., Bouregba, N., Corbo, F., Asensio, E., 2011. Deep resistivity cross section of the intraplate Atlas Mountains (NW Africa): new evidence of anomalous mantle and related Quaternary volcanism. Tectonics 30, 1–9.

Anderson, R.S., Repka, J.L., Dick, G.S., 1996. Explicit treatment of inheritance in dating depositional surfaces using in situ $^{10}$Be and $^{26}$Al. Geology 24, 47–51.

Arboleya, M.L., Teixell, A., Charroud, M., Julivert, M., 2004. A structural transect through the High and Middle Atlas of Morocco. J. Afr. Earth Sci. 39, 319–327.

Arboleya, M.-L., Babault, J., Owen, L.A., Teixell, A., Finkel, R.C., 2008. Timing and nature of fluvial incision in the Ouarzazate foreland basin, Morocco. J. Geol. Soc. Lond. 165, 1059–1073.

Ayarza, P., Carbonell, R., Teixell, A., Palomeras, I., Martí, D., Kchikach, M., Levander, A., Gallart, J., Arboleya, M.L., Alcalde, J., Fernàndez, M., Charroud, M., Amrhar, M., 2014. Crustal thickness and velocity structure across the Moroccan Atlas from long offset wide-angle reflection seismic data: the SIMA experiment. Geochem. Geophys. Geosyst. 15, 1698–1717.

Babault, J., Teixell, A., Arboleya, M.L., Charroud, M., 2008. A Late Cenozoic age for long-wavelength surface uplift of the Atlas Mountains of Morocco. Terra Nova 20, 102–107.

Balco, G., Stone, J.O., Lifton, N.A., Dunai, T.J., 2008. A complete and easily accessible means of calculating surface exposure ages or erosion rates from $^{10}$Be and $^{26}$Al measurements. Quat. Geochronol. 8, 174–195.

Barbero, L., Jabaloy, A., Gómez-Ortiz, D., Pérez-Peña, J.V., Rodríguez-Peces, M.J., Tejero, R., Estupiñán, J., Azdimousa, A., Vázquez, M., Asebriy, L., 2011. Evidence for surface uplift of the Atlas Mountains and the surrounding peripheral plateaux: combining apatite fission track results and geomorphic indicators in the Western Moroccan Meseta (Coastal Variscan Paleozoic Basement). Tectonophysics 502, 90–104.

Barcos, L., Jabaloy, A., Azdimousa, A., Asebriy, L., Gómez-Ortiz, D., Rodríguez-Peces, M.J., Tejero, R., Pérez-Peña, J.V., 2014. Study of relief changes related to active doming in the eastern Moroccan Rif (Morocco) using geomorphological indices. J. Afr. Earth Sci. 100, 493–509.

Beauchamp, W., Barazangi, M., Demnati, A., El Alji, M., 1996. Intracontinental rifting and inversion: Missour Basin and Atlas Mountains, Morocco. AAPG Bull. 80, 1459–1482.

Begin, Z.e.B., Meyer, D.F., Schumm, S.A., 1981. Development of longitudinal profiles of alluvial channels in response to base-level lowering. Earth Surf. Process. Landf. 6, 49–68.

Benda, L., Dunne, T., 1997. Stochastic forcing of sediment routing and storage in channel networks. Water Resour. Res. 33, 2865–2880.

Bernini, M., Boccaletti, M., Gelatti, R., Moratti, G., Papani, G., El Mokhtari, J., 1999. Tectonics and sedimentation in the Taza-Guercif basin, northern Morocco: implications for the Neogene evolution of the Rif-Middle Atlas orogenic system. J. Pet. Geol. 22, 115–128.

Bernini, M., Boccaletti, M., Moratti, G., Papani, G., 2000. Structural development of the Taza-Guercif Basin as a constraint for the Middle Atlas Shear Zone tectonic evolution. Mar. Pet. Geol. 17, 391–408.

Bishop, P., 2007. Long-term landscape evolution: linking tectonics and surface processes. Earth Surf. Process. Landf. 32, 329–365.

Bishop, P., Hoey, T.B., Jansen, J.D., Artza, I.L., 2005. Knickpoint recession rate and catchment area: the case of uplifted rivers in Eastern Scotland. Earth Surf. Process. Landf. 30, 767–778.

Bouazza, A., AïtBrahim, L., Dugué, O., Laville, E., Delcaillau, B., Cattaneo, G., Charroud, M., de Luca, P., 2009. Changements Sédimentaires dans les Bassins Néogènes de Taourirt et Guercif (Maroc Oriental): Recherche de l'épisode d'érosion Messinienne. Eur. J. Sci. Res. 28, 317–327.

Boulton, S.J., Stokes, M., Mather, A.E., 2014. Transient fluvial incision as an indicator of active faulting and Plio-Quaternary uplift of the Moroccan High Atlas. Tectonophysics 633, 16–33.

Burbank, D.W., Anderson, R.S., 2001. Tectonic Geomorphology. Blackwell Science, Malden (274 pp.).

Burbank, D.W., Leland, J., Fielding, E., Anderson, R.S., Brozovic, N., Reid, M.R., Duncan, C., 1996. Bedrock incision, rock uplift and threshold hillslopes in the northwestern Himalaya. Nature 379, 505–510.

Charroud, A., 2002. Evolution geodynamique des hauts plateaux (Maroc) et de leurs bordures du Mesozoique au Cenozoique (Thèse 3è Cycle), Université Sidi Mohamed Ben Abdellah, Fes (314 pp.).

Choubert, M.G., 1964. Carte géologique du Maroc, sheet NI-30-IX-2: Hassi el Ahmar. Service Géologique du Maroc, Notes et Mémoires. Ministère de l'Énergie et des Mines, Direction de la Géologie, Rabat.

Coblentz, D., Karlstrom, K.E., 2011. Tectonic geomorphometrics of the western United States: speculations on the surface expression of upper mantle processes. Geochem. Geophys. Geosyst. 12, Q11002. http://dx.doi.org/10.1029/2011GC003579.

Crosby, B.T., Whipple, K.X., 2006. Knickpoint initiation and distribution within fluvial networks: 236 waterfalls in the Waipaoa River, North Island, New Zealand. Geomorphology 82 (1–2), 16–38.

Delcaillau, B., Laville, E., Carozza, J.-M., Dugué, O., Charroud, M., Amrhar, M., 2008. Morphotectonic evolution of the Jebel Bou Naceur in the South Middle Atlas Fault Zone (Morocco). Compt. Rendus Geosci. 339, 553–561.

Desilets, D., Zreda, M., 2003. Spatial and temporal distribution of secondary cosmicray nucleon intensities and applications to in-situ cosmogenic dating. Earth Planet. Sci. Lett. 206, 21–42.

Desilets, D., Zreda, M., Prabu, T., 2006. Extended scaling factors for in situ cosmogenic nuclides: new measurements at low latitude. Earth Planet. Sci. Lett. 246, 265–276.

Dutour, A., 1983. Etude géomorphologique de la partie occidentale de la Haute Moulouya (Maroc) (Thèse 3è Cycle), Poitiers (361 pp.).

Dunai, T., 2001. Influence of secular variation of the magnetic field on production rates of in situ produced cosmogenic nuclides. Earth Planet. Sci. Lett. 193, 197–212.

Ellouz, N., Patriat, M., Gaulier, J.-M., Bouatmani, R., Sabounji, S., 2003. From rifting to Alpine inversion: Mesozoic and Cenozoic subsidence history of some Moroccan basins. Sediment. Geol. 156, 185–212.

Flint, J.J., 1974. Stream gradient as a function of order, magnitude, and discharge. Water Resour. Res. 10 (5), 969–973.

Fullea, J., Fernàndez, M., Afonso, J.C., Vergés, J., Zeyen, H., 2010. The structure and evolution of the lithosphere–asthenosphere boundary beneath the Atlantic–Mediterranean Transition Region. Lithos 120, 74–95.

García, A.F., 2006. Thresholds of strath genesis deduced from a landscape response to stream piracy by Pancho Rico Creek in the Coast Ranges of central California. Am. J. Sci. 306, 655–681.

Gile, L.H., Hawley, J.W., Grossman, R.B., 1981. Soils and geomorphology in the Basin and Range area of southern New Mexico — guidebook to the Desert Project. New Mex. Bur. Min. Mineral Resour. Mem. 39 (222 pp.).

Gorokhovich, Y., Voustianiouk, A., 2006. Accuracy assessment of the processed SRTMbased elevation data by CGIAR using field data from USA and Thailand and its relation to the terrain characteristics. Remote Sens. Environ. 104, 409–415.
Goldrick, G., Bishop, P., 2007. Regional analysis of bedrock stream long profiles: evaluation of Hack's SL form, and formulation and assessment of an alternative (the DS form). Earth Surf. Process. Landf. 32, 649–671.
Gomez, F., Allmendinger, R., Barazangi, M., Er-Raji, A., Dahmani, M., 1998. Crustal shortening and vertical strain partitioning in the Middle Atlas mountains of Morocco. Tectonics 17, 520–533.
Gomez, F., Barazangi, M., Demnati, A., 2000. Structure and evolution of the Neogene Guercif Basin at the junction of the Middle Atlas Mountains and the Rif Thrust Belt, Morocco. AAPG Bull. 84, 1340–1364.
Hack, J.T., 1957. Studies of longitudinal stream profiles in Virginia and Maryland. U. S. Geol. Surv. Prof. Pap. 294 (B), 45–94.
Hancock, G.S., Anderson, R.S., Chadwick, O.A., Finkel, R.C., 1999. Dating fluvial terraces with $^{10}$Be and $^{26}$Al profiles: application to the Wind River, Wyoming. Geomorphology 27, 41–60.
Hoke, G.D., Isacks, B.L., Jordan, T.E., Blanco, N., Tomlinson, A.J., Ramezani, J., 2007. Geomorphic evidence for post-10 Ma uplift of the western flank of the central Andes. Tectonics 26. http://dx.doi.org/10.1029/2006TC002082.
Howard, A.D., Kerby, G., 1983. Channel changes in badlands. Geol. Soc. Am. Bull. 94 (6), 739–752.
Kohl, C.P., Nishiizumi, K., 1992. Chemical isolation of quartz for measurement of in situ-produced cosmogenic nuclides. Geochim. Cosmochim. Acta 56, 3583–3587.
Korup, O., 2006. Rock-slope failure and the river long profile. Geology 34, 45–48.
Krijgsman, W., Langereis, C.G., 2000. Magnetostratigraphy of the Zobzit and Koudiat Zarga sections (Taza-Guercif Basin, Morocco); implications for the evolution of the Rifian Corridor. Mar. Pet. Geol. 17, 359–371.
Krijgsman, W., Langereis, C.G., Zachariasse, W.J., Boccaletti, M., Moratti, G., Gelati, R., Iaccarino, S., Papani, G., Villa, G., 1999. Late Neogene evolution of the Taza-Guercif Basin (Rifian Corridor, Morocco) and implications for the Messinian salinity crisis. Mar. Geol. 153, 147–160.
Lal, D., 1991. Cosmic ray labeling of erosion surfaces: in situ nuclide production rates and erosion models. Earth Planet. Sci. Lett. 104, 429–439.
Lancaster, S.T., Grant, G.E., 2006. Debris dams and the relief of headwater streams. Geomorphology 82, 84–97.
Lavé, J., Avouac, J.P., 2001. Fluvial incision and tectonic uplift across the Himalayas of central Nepal. J. Geophys. Res. 106, 26561–26591.
Laville, E., Delcaillau, B., Charroud, M., Dugué, O., AitBrahim, L., Cattaneo, G., Deluca, P., Bouazza, A., 2007. The Plio-Pleistocene evolution of the Southern Middle Atlas Fault Zone (SMAFZ) front of Morocco. Int. J. Earth Sci. 96, 497–515.
Lifton, N., Bieber, J., Clem, J., Duldig, M., Evenson, P., Humble, J., Pyle, R., 2005. Addressing solar modulation and long-term uncertainties in scaling secondary cosmic rays for in situ cosmogenic nuclide applications. Earth Planet. Sci. Lett. 239, 140–161.
Matmon, A., Simhai, O., Amit, R., Haviv, I., Porat, N., McDonald, E., Benedetti, L., Finkel, R., 2009. Desert pavement-coated surfaces in extreme desert presents the longest-lived landforms on Earth. Geol. Soc. Am. Bull. 121, 688–697.
Miller, M.S., Becker, T.W., 2014. Reactivated lithospheric-scale discontinuities localize dynamic uplift of the Moroccan Atlas Mountains. Geology 42, 35–38.
Nereson, A., Stroud, J., Karlstrom, K., Heizler, M., McIntosh, W., 2013. Dynamic topography of the western Great Plains: geomorphic and $^{40}$Ar/$^{39}$Ar evidence for mantle-driven uplift associated with the Jemez lineament of NE New Mexico and SE Colorado. Geosphere 9, 521–545.
Nishiizumi, K., Imamura, M., Caffee, M.W., Southon, J.R., Finkel, R.C., McAninch, J., 2007. Absolute calibration of Be-10 AMS standards. Nuclear Instruments and Methods in Physics Research. Section B: Beam Interactions with Materials and Atoms 258, 403–413.
Palomeras, I., Thurner, S., Levander, A., Liu, K., Villaseñor, A., Carbonell, R., Harnafi, M., 2014. Finite-frequency Rayleigh wave tomography of the western Mediterranean: mapping its lithospheric structure. Geochem. Geophys. Geosyst. 15, 140–160.
Pastor, A., Teixell, A., Arboleya, M.L., 2012. Rates of Quaternary deformation in the Ouarzazate Basin (Southern Atlas Front, Morocco). Ann. Geophys. 55, 1003–1016.
Paul, J., Roberts, G., White, N., 2014. The African landscape through space and time. Tectonics 33, 898–935.
Portenga, E.W., Bierman, P.R., 2011. Understanding Earth's eroding surface with $^{10}$Be. Geol. Today 21, 4–10.
Pigati, J.S., Lifton, N.A., 2004. Geomagnetic effects on time-integrated cosmogenic nuclide production with emphasis on in situ 14C and 10Be. Earth Planet. Sci. Lett. 226, 193–205.
Quezada, J., Cerda, J.L., Jensen, A., 2010. Efectos de la tectónica y el clima en la configuración morfológica del relieve costero del norte de Chile. Andean Geol. 37, 78–109.
Sani, F., Zizi, M., Bally, A.W., 2000. The Neogene–Quaternary evolution of the Guercif Basin (Morocco) reconstructed from seismic line interpretation. Mar. Pet. Geol. 17, 343–357.
Schildgen, T.F., Cosentino, D., Bookhagen, B., Niedermann, S., Yıldırım, C., Echtler, H., Wittmann, H., Strecker, M.R., 2012. Multi-phased uplift of the southern margin of the Central Anatolian Plateau, Turkey: a record of tectonic and upper mantle processes. Earth Planet. Sci. Lett. 317–318, 85–95.
Sébrier, M., Siame, L., Zouine, E.M., Winter, T., Missenard, Y., Leturmy, P., 2006. Active tectonics in the Moroccan High Atlas. Compt. Rendus Geosci. 338, 65–79.
Snyder, N.P., Whipple, K.X., Tucker, G.E., Merritts, D.J., 2002. Interactions between onshore bedrock-channel incision and nearshore wave-base erosion forced by eustasy and tectonics. Basin Res. 14, 105–127.
Staiger, J., Gosse, J., Toracinta, R., Oglesby, B., Fastook, J., Johnson, J.V., 2007. Atmospheric scaling of cosmogenic nuclide production: climate effect. J. Geophys. Res. 112, B02205.
Stone, J.O., 2000. Air pressure and cosmogenic isotope production. J. Geophys. Res. 105, 23753–23759.
Sun, D., Miller, M.S., Holt, A.F., Becker, T.W., 2014. Hot upwelling conduit beneath the Atlas Mountains, Morocco. Geophys. Res. Lett. 41, 8037–8044.
Teixell, A., Arboleya, M.L., Julivert, M., Charroud, M., 2003. Tectonic shortening and topography in the central High Atlas (Morocco). Tectonics 22. http://dx.doi.org/10.1029/2002TC001460.
Teixell, A., Ayarza, P., Zeyen, H., Fernandez, M., Arboleya, M.L., 2005. Effects of mantle upwelling in a compressional setting: the Atlas Mountains of Morocco. Terra Nova 17, 456–461.
Whipple, K.X., 2001. Fluvial landscape response time: how plausible is steady-state denudation? Am. J. Sci. 301, 313–325.
Whipple, K.X., Tucker, G.E., 1999. Dynamics of the stream-power river incision model: implications for height limits of mountain ranges, landscape response timescales, and research needs. J. Geophys. Res. 104 (B8), 17,661–17,674.
Wobus, C., Whipple, K.X., Kirby, E., Snyder, N., Johnson, J., Spyropolou, K., Crosby, B., Sheehan, D., 2006. Tectonics from topography; procedures, promise, and pitfalls. Geol. Soc. Am. Spec. Pap. 398, 55–74.
Zeyen, H., Ayarza, P., Fernàndez, M., Rimi, A., 2005. Lithospheric structure under the western African–European plate boundary: a transect across the Atlas Mountains and the Gulf of Cadiz. Tectonics 24. http://dx.doi.org/10.1029/2004TC001639.

Please cite this article as: Pastor, A., et al., Extracting dynamic topography from river profiles and cosmogenic nuclide geochronology in the Middle Atlas and the High Plateaus of Morocco, Tectonophysics (2015), http://dx.doi.org/10.1016/j.tecto.2015.06.007

# Drainage network evolution and patterns of sedimentation in an experimental wedge

Marc Viaplana-Muzas[a], Julien Babault[a] , Stéphane Dominguez[b] , Jean Van Den Driessche[c], Xavier Legrand[d]

[a] Departament de Geologia, Universitat Autònoma de Barcelona,08193 Bellaterra (Barcelona), Spain.

marc.via.mu@gmail.com, julien.babault@uab.es

[b] Géosciences Montpellier, Université Montpellier II, F-34095, France.

dominguez@gm.univ-montp2.fr

[c] Géosciences Rennes, Université de Rennes 1, Campus de Beaulieu, Rennes, France.

jean.van-den-driessche@univ-rennes1.fr

[d] Petronas CariGali, Twin Tower KLCC, 50088, Kuala Lumpur, Malaysia.

legrand.xavier@petronas.com.my

## Abstract

*In fold and thrust belts drainage organization and patterns of sedimentation depend conceptually on the ability or not for preexisting reaches to incise uplifting thrust sheets. In this study we investigate experimentally the dynamics of drainage network in a wedge submitted to shortening and erosion. It allows us to reproduce and to monitor the interactions between tectonics, erosion and sedimentation during the development of up to five successive thrust sheets. In the experiments channels adjust to uplift rate by both increasing their slope and narrowing their channels as it is observed in nature. The series of experiments shows that the proportion of persistent preexisting transverse channels increases with the ratio of rainfall over shortening rates. The experiments confirm the view that the competition between discharge and tectonic uplift controls along-strike variations in sediment flux in sedimentary basins by controlling the drainage organization. If the transverse channels draining a wedge are not diverted, a line-source dispersal system develops in front of the active structure. If channels are diverted in the backlimb of the frontal structure it results in point-sourced depositional systems separated by areas fed only by small channels developing in the front of the wedge. Fans accumulated in front of the active structures reveal two stages of sedimentation, one of progradation, while the frontal structure is active and a second one of valley backfilling and thrust sealing during internal deformation of the wedge.The experiments also suggest that spatial variations in rock uplift rate along a thrust front may be evidenced by minimum-discharge variations of persistent transverse channels.*

Keywords:experimental modeling, accretionary wedge, drainage network organization, river diversion, sedimentation patterns, source-to-sink.

# 1 Introduction

The drainage network at the Earth's surface exerts a first order control on the relief dynamics and the erosion of mountain belts. Beyond its role in shaping the topography,the drainage network is a main controlling factor of the coupling between surface processes and deep crustal deformation, as well as of the relations between tectonics and climate variations, and the sedimentary record in basins. During mountain building, the drainage network development involves river diversions and captures at different scales(e.g. Babault et al., 2012; Castelltort et al., 2012; Giletycz et al., 2015)resulting in rapid changes in sediment routing and spatial distribution of erosion. Indeed, in response to folding or thrusting, transverse rivers are commonly diverted into longitudinal reaches, parallel to the structures, that gather into greater rivers, which maintain gorges through growing structures (e.g. Burbank et al., 1999; Burbank and Vergés, 1994; Jackson et al., 1996; Jolley et al., 1990; Oberlander, 1985; Talling et al., 1995). By controlling the spacing between outlets, drainage diversion may eventually control the loci of sediment supply and the stratigraphic architecture in foreland-basins (Gupta, 1997; Horton and DeCelles, 2001; Tucker and Slingerland, 1996). Conceptually, the ability or not for preexisting reaches to incise uplifting structures controls the number of diversions, and by extension drainage organization, a view confirmed by numerical models (Champel et al., 2002; Humphrey and Konrad, 2000; Koons, 1994; Koons, 1995; Sobel et al., 2003; Tomkin and Braun, 1999; van der Beek et al., 2002). In particular, numerical models, where deformation is reduced to uplift and advection over a thrust, show that the proportion of persistent preexisting transverse channels scales with the ratio of precipitation over shortening rate (Champel et al., 2002; Tomkin and Braun, 1999). Alternatively, it has been proposed that aggradation in the backlimb of emergent thrusts also helps transverse rivers to balance uplift rates allowing them to maintain their course instead of being diverted (Humphrey and Konrad, 2000), or that axial slopes, controlled by the dip of the décollement layer where the thrusts are rooted, may divert preexisting transverse channels before they reach the uplifts (Champel et al., 2002; van der Beek et al., 2002).

In this study we investigate experimentally how the interaction between drainage network and deformation controls along-strike variations in sediment flux in wedges submitted to shortening and erosion. We first investigate the similarities of behavior (geometries and kinematics) between experimental and natural channels evolving under uplifting conditions. We examine the differences in both the drainage organization and along-strike variations in sediment accumulations as a function of the ratio of rainfall rate over shortening rate. We determine the factors that control (1) the capacity for channels to incise uplifting structures and (2) the patterns of sedimentation that resulted from the drainage organization.

# 2 Method

## 2.1 Setup

The experimental set-up used in this study is adaptedfrom the setup used by Graveleau and Dominguez, (2008) and Graveleau et al., (2011). The deformation device dimensions are 80 x 150 cm and are constituted by a basal film pulled beneath a static buttress. The film is overlaid by the analogue material that models the upper part of the crust. Shortening induces material deformation and generates an accretionary wedge composed of imbricated thrusts. The rainfall system is composed by sprinklers that deliver water micro-droplets over the model. Sprinklers deliver water micro-droplets in sequences of 10 seconds with rain and 3 seconds without rain in order to improve channel incision processes.During the 3 seconds without rain, slope erosion processes are mostly inhibited whereas in the river network, water, collected by the channel catchments during the 10 seconds rain phase, continues to flow for a while (a few seconds up to tens of seconds depending on the length of the considered channel). During the dry time period, channel incision is then enhanced generating a more incised topography and favoring fluvial and alluvial terrace formation. This protocol was implemented to limit channel widening induced by the high river flow dynamics. Droplet size is small enough (diameter $\leq$ 100 μm) to reduce rain-splash effect and potential surface craterization. Rainfall in the experiment allows water runoff to generate both diffusive erosion processes on hillslopes and incision/lateral erosion in channelsbut it does not intend to simulate real water droplets(Graveleau et al., 2015). Spatial variation of rainfall rates due to air convection induced by water supply from sprinklers have been measured to be minor (<10%on average).

The analogue material is composed of three different materials: glass microbeads, silica powder and plastic powder (PVC). To obtain experiments with thrusts spaced enough to avoid the burying of thrust backlimbs by fans, we adjust the composition of material mixtures, the thickness of the material and layering of different materials. As mentioned above, aggradation in the backlimb of an uplifting thrust helps transverse rivers to balance uplift rates.Two different analogue material mixtures were derived and deposited in two layers in the sand-box. The upper layer is the material submitted to erosion and it is made up with 46% of glass microbeads, 30% of silica powder and 24% of plastic powder (PVC) plus some graphite (<1%) necessary for photo-correlations (material IV). This mixture is slightly different to the material IV used in Graveleau et al.(2008), Graveleau et al.(2011) and Strack et al., (2011). The lower layer is made of 50% of glass microbeads and 50% of PVC. We performed several tests and we found empirically that a total thickness of 55 mm made by a basal layer of 5 mm of glass microbeads (décollement layer), overlaid by 45 mm of the analog materials plus a thin layer (5 mm) of glass microbeads within the upper mixture results in 14-cm-spaced thrust sheets (Fig. 1). The thin layer of glass microbeads within the upper mixture allows slip to occur within the material IV

resulting in foldingat the surface above the ramps, as in nature. The deformation style reproduces well an accretionary wedge pattern made of individualized in-sequence thrust faults dipping toward the buttress.The material IV submitted to erosion has enough cohesion for valleys and crests to develop but not too high for basal shear stress applied by the fluid on the riverbed to exceed the thresholds for detachment and transport.

Digital Elevation Models (DEM) are acquired by an optical measurement bench composed by high resolution cameras coupled to a laser interferometer.This device acquires digital topographies at a 3D resolution close to 0.2 mm. It requires stops in both shortening and rainfall systems during 30-45 minutes to dry the uppermost 1-2 mm of the model surface and avoid bright laser points that could affect DEM resolution. Photograph cameras allow us to document the dynamical evolution of the relief by video movies and image correlation analyses(Graveleau and Dominguez, 2008). Finally, the model is cut in serial cross-sections in order to study the 3D geometry of thrusts and syntectonic deposits.

In this work we present eight experiments run under shortening rates ranging from 4 cm/h to 100 cm/h, of which six were submitted to a precipitation rate of 9 mm/h (named A1 to A6) and the other two to a precipitation rate of 18 mm/h (named B1 and B2).

## 2.2 Analysis of the accretionary wedges

Most of the deformation in the experimental wedges occurs by frontal accretion due to forward propagation of the thrust sequence as observed classically in experiments (e.g. Davis et al., 1983). Two domains can be differentiated in the experimental wedges. The prowedge, located in the frontal part of the wedge, and formed by forethrusts and the retrowedge located in the rear of the wedge and formed by backthrusts. Prowedge slope is ruled by the Coulomb wedge theory (Davis et al., 1983) and depends on the internal friction of the material, the basal friction and the dip angle of the décollement level (flat in our experiments). The spacing between thrusts and the dip of the thrusts also depends on the basal friction and on the total thickness of the layer but also on the mechanical resistance (cohesion) of the layer. We measured prowedge slopes, spacing between thrusts in the external part of the prowedge, when a new thrust appears, and we measured the dip of the thrusts to check if the rheology of the bulk material was equivalent in all the experiments.

## 2.3 Scaling

Experimental modeling is ruled by a set of geometric, kinematic and dynamic similarity criteria that imply, respectively, proportionality of length, time and forces between nature and model(Hubbert, 1951; Paola et al., 2009). Applying these similarity criteria to the Mohr-Coulomb equation and neglecting inertial forces, leads to the expression:

$$C_o^* = \rho^* \cdot L^* \quad (1)$$

where $C_o^*$, $\rho^*$ and $L^*$ are the ratios between model and nature for cohesion, density and length, respectively. We calculated the cohesion of the erodible material using a modified Hubbert-type set-up, following the methodology described in Graveleau et al. (2011). This device measures frictional properties of water-saturated granular materials. It consists of two aluminum rings, 8 cm in internal diameter and 50 $cm^2$ in horizontal cross-sectional area, which contain the granular material sample. The lower ring, 3 cm deep, is fixed on a mobile plateau controlled by a stepping motor. The upper ring is fixed on a rigid pendulum that rests on a force gauge. Its internal surface is covered with a low friction material (Teflon) to reduce sidewall friction. Between both rings there is a gap of 0.1 mm filled with low viscosity grease to prevent water and material from escaping. When the lower ring moves, material inside the ring is sheared and the upper ring presses the force gauge. We performed several tests with increasing normal loads to measure normal and tangential stress couples at failure and to deduce a yield locus. Displacement and force gauge data are recorded and allow for the generation of a Mohr-Coulomb failure envelope. Best fit to the data gives a slope equal to the coefficient of internal friction ($\mu$) and an extrapolated cohesion ($C_o$). Results for our mixture, material IV (matIV), for stable friction, are $\mu$ = 0.67 ($\phi_{matIV}$ = 35º) and cohesion of $C_o$ = 610 Pa for stabilized water saturation of 21-22 % (Fig.2).Cohesion in natural rocks ranges between $10^7$ Pa for sandstone or granite and $10^8$ Pa for marble and limestone(Schellart, 2000), hence the cohesion ratio $C_o$* ranges between $6.1 \cdot 10^{-5}$- $6.1 \cdot 10^{-6}$. Considering the bulk density of matIV ($\rho_{matIV}$=1600 $kg.m^{-3}$) and natural rocks (between 2000 $kg.m^{-3}$ for sandstone and 2800 $kg.m^{-3}$ for granite), the density ratio $\rho$* ranges between 0.57 and 0.80. According to equation (1)$L^*$ is $1 \cdot 10^{-5}$- $8 \cdot 10^{-6}$, that is, 1 cm in the experiments equals ~0.1 kmto~1km in nature.

## 2.4 Analysis of the digital topographies

### 2.4.1 Quantification of the stream power erosion law in the experiments

We searched for relationships between metrics of the topography in the framework of the stream power theory for understanding and quantifying the landscape evolution and the drainage evolution in response to external perturbations.We analyzed the relationship between the steepness indices (a metric based on slope-area plots), the relative uplift rates as defined in

Babault et al. (2005), the upstream velocity of propagation of knickpoints, the channel widths and the drainage areas of steady-state reaches identified within the channels that cross uplifting thrust sheets. The stream power theory assumes that fluvial erosion is a power law function of the drainage area, *A*, and the channel slope, *S*, (Howard and Kerby, 1983). Stream power erosion laws have the form:

$$\frac{dz}{dt} = U - f(Q_s) \cdot K \cdot \frac{A^m}{W} \cdot S^n \quad (2)$$

where the rate of change of elevation, *z*, with time, t, depends on the imposed uplift rate, U, and on a power law function of drainage area, *A* (as a proxy for catchment discharge), channel width, *W*, and downstream channel slope, *S*. The exponents*m* and *n*are positive, $f(Q_s)$ describes the tool and cover effects of sediment supply and it is often taken to be equal to 1. In the experiments, uplifts induce waves of incision and knickpoints that propagate upstream indicating conditions close to the detachment-limited model of incision(Cowie et al., 2008; Whipple and Tucker, 2002). We consider that there is no effect of $Q_s$on erosion efficiency in the experiments and $f(Q_s)$ equals 1. *K* is a parameter describing erosional efficiency. Channel width(*W)*, may be described as a power law function of *A* (and is often taken to scale with $\sqrt{A}$)(Montgomery and Gran, 2001; Schellart, 2000; Whittaker et al., 2007a), in which case its effect can be subsumed into exponent *m* and coefficient *K*(Attal et al., 2008; Whipple and Tucker, 1999). However, it has been shown in a few settings that in response to an incrementof the uplift rate, incision rate can be increased by the narrowing of channels in order to increase the stream power(e.g. Amos and Burbank, 2007; Finnegan et al., 2005; Whittaker and Boulton, 2012; Whittaker et al., 2007a, 2007b).

At steady-state, by definition the channel erosion rate is equal to the uplift rate of rock (*E* = *U*), and the steady-state channel gradient ($S_e$) can be found by solving equation (2) for slope under this condition(Howard, 1980):

$$S_e = \left(\frac{WU}{K}\right)^{\frac{1}{n}} \cdot A^{-\frac{m}{n}} \quad (3)$$

The m/n ratio is predicted to depend only on the rate of increase of water discharge and channel width with drainage area(Whipple and Tucker, 1999), with a typical value of ~½ in nature. The exponents *m* and *n* reflect the mechanics of the dominant incision process, or combination of processes(Whipple, 2004). Equation (3) has the same form of Flint's law that relates the channel slope, *S*, to drainage area, *A*, with the normalized channel steepness index, $k_{sn}$, and concavity, $\theta$(we used a reference concavity equal to 0.5 in this study):

$$S = k_{sn} \cdot A^{-\theta}, \quad (4)$$

Steady-state channels adjust to increasing uplift rate by increasing their slope (normalized channel steepness index,$k_{sn}$)(Bookhagen and Strecker, 2012; DiBiase et al., 2010; Gudmundsdottir et al., 2013; Kirby and Ouimet, 2011; Kirby and Whipple, 2012; Ouimet et al., 2009; Perron and Royden, 2013; Wobus et al., 2005) and/or by narrowing their width, which

concentrates runoff and increases the stream power(Amos and Burbank, 2007; Finnegan et al., 2005; Whittaker et al., 2007a). The stream power erosion law predicts at steady-state that the relation between the erosion/uplift rate,the normalized steepness index and channel width depends on parameter *n*:

$$U = \frac{K}{W} \cdot {k_{sn}}^{n} \quad (5)$$

If channel width scales with drainage areas then equation (5) can be rewritten as:

$$U = K \cdot {k_{sn}}^{n} \quad (6)$$

We calculated the steepness indices and we measured the channel width of the steady-state reaches to understandthe way channels adjust to uplift rates.*K* is constant inthe series of experiments run under the same rainfall rate. We estimated the parameter *n* using equation (5).

The family of stream power models also predicts equation (2) takes the form of a nonlinear kinematic wave of erosion in response to external perturbation(Rosenbloom and Anderson, 1994; Royden et al., 2000; Whipple, 2001; Whipple and Tucker, 1999) and can be rewritten as:

$$\frac{\partial z}{\partial t} = -\frac{K}{W} \cdot A^{m} \cdot S^{n-1} \left|\frac{\partial h}{\partial x}\right|, \ \frac{\partial h}{\partial x} < 0 \quad (7)$$

where

$$C = \Psi_K \cdot A^{m} \cdot S^{n-1}, \text{with} \qquad \Psi_K = \frac{K}{W} \quad (8)$$

*C*is the wave celerity which has been used to represent knickpoint retreat rate(e.g. Berlin and Anderson, 2007; Bishop et al., 2005; Crosby and Whipple, 2006; Loget and Van Den Driessche, 2009; Parker and Anderson, 1977; Tucker and Whipple, 2002; Whipple and Tucker, 2002; Whittaker et al., 2008; Whittaker and Boulton, 2012; Wobus et al., 2006a; Wobus et al., 2006b)and$\Psi_K$ embeds lithological and width effects. Field evidence shows that knickpoint migration rates scalewith drainage area(e.g. Berlin and Anderson, 2007; Bishop et al., 2005; Crosby and Whipple, 2006; Loget and Van Den Driessche, 2009; Parker and Anderson, 1977)and equation (8) reduces to:

$$C = \Psi_A \cdot A^{m} \quad (9)$$

*m* is shown to be equal to 0.5 and $\Psi_A$ is a coefficient of retreat efficiency ($L^{(1-2\ h)}T^{-1}$). This relationship implies that the upstream drainage area is the predominant parameter on knickpoint migration, with regard to lithology(e.g. Berlin and Anderson, 2007; Bishop and Cowell, 1997; Bishop et al., 2005; Loget and Van Den Driessche, 2009). We first estimated the parameter *m* using equation (9), we also studied the width effect on parameter *m*using a simplified version of equation (8) relating thevariables *C*, *A* and *W*:

$$C = \Psi_{AW} \cdot \frac{A^{m}}{W} \quad (10)$$

where $\Psi_{AW}$ is the product $K \cdot S^{n-1}$ with a dimension depending on *m*.

The width (*W*)and the distance of knickpoint propagation used to calculate *C* have been measured using the GridVisual program (P. Davy, University of Rennes 1, http://terrasse.geosciences.univ-rennes1.fr/?p=1). In all the experiments we observed that the ramp dips vary at depth, with a constant dip from the trace of the thrust up to a distance of ≤ 8-10 cm. Beyond this distance the ramp flattens before rooting to the décollement layer of glass microbeads. In order to study the controls on*W*, $k_{sn}$ and knickpoints propagation velocities (*C*) at a given uplift rate, we restricted the study of knickpoints to the first 8-10 cm from the trace of the thrust where uplift rates can be considered spatially uniform. Mean channel widths, *W*, in uplifting thrusts sheets have been calculated from three measures spaced by ~4-5 cm and located in the hanging wall of the thrust between fan apexes and knickpoints.$k_{sn}$of each pixel in the channels located in the uplifting thrust sheets have been calculated using GridVisual and they have been averaged for comparison to uplift rates. Knickpoint location corresponds to the point where channel local slopes increase downstream. The distance over which a knickpoint has propagated has been measured between the knickpoints and the point where a thrust startsto emerge. Repeated measures indicate typical error values of 1 mm. This error has been used to derive an error of the values of the knickpoint propagation velocities (*C*).

### 2.4.2 Quantification of erosion and uplift

To estimate the amounts of erosion and uplift rates in the experiments we subtractedthe eroded topography from reconstructed initial topographies. The initial topographies are derived by the highest values surrounding a given pixel and measured within a rectangular-moving window. The width of the window, parallel to the transverse-channel width, is determined by the widest valleys and it has been set to 80 mm from the experiment A1. The length, parallel to the transverse channels, has been set to 1 mm to take into account the folding of the initial topography.The uplift rates we calculated are relative uplift rates as defined in Babault et al. (2005). We divided the change of elevation above the apex of the fans deposited in front of the structuresby the time spanof uplift.

### 2.4.3 Quantification ofthe proportion of deviations

We calculate the proportion of persistent antecedent channels,*R*, defined as the ratio between the number of transverse streams cutting through the uplifted ridge and the initial number of streams(Champel et al., 2002):

$$R = \frac{N_p}{N_{ch}} \quad (11)$$

The variable *R* varies between 0 (all rivers deflected) and 1 (all rivers cut through the growing ridge). The initial number of channels has been obtained by counting the number of incisions on the surface of a thrust sheet, when it appears. This number may beaffected by processes that

merge initial channels during the growth of a structure, as valley widenning, and by deviations not controlled by the growing frontal structure but by backthrusts in the backlimb. Fan aggradation in the backlimb also helps transverse streams to maintain their course instead of being diverted (Humphrey and Konrad, 2000). The variable *R* measured in this study strictly reflects the processes of deviation by uplift.

#### 2.4.4 Quantification of sedimentation rates

By sprinkling tinted analogue material we added time markers on the surface of the fans at the foot of the thrust sheets. Because these color layers would alter the acquisition of digital elevation models from the surface of the experiments, they were sprinkled after the digitalization of the surface. After drying, the experiments are cut and these timelines are used to calculate the sedimentation rates from the cross-sections of the fans.

# 3 Results

## 3.1 Style of deformation

We do not observe structural differences between the models. In the series, the mean slopes of the prowedge ($\alpha$) range between 8º and 11º,thrust dips ($\phi$) range between 20º and 30º with a mean dip of 24±2˚ and the spacing between thrust sheets is ~ 14±2 cm (Figs. 3C, 3D and 3E). These results indicate that the rheology of the material (internal friction and basal friction) is almost constant in all the models and that the pattern of deformationin the series is not influenced by the two orders of magnitude of shortening rates we applied. Experiment results also reveal that erosion has no effect on the pattern of deformation under the rates of shortening and precipitation we applied.

When a new thrust appears, it is accompanied by a small amplitude fold located above the ramp (Fig. 4A). The maximum structural offset on the thrusts is ~10 cm, most of it being completed in the initial stage of activity of a structure in the external part of the wedge. Once a new structure appears the older ones remain only weakly active. Since thrust dips are almost constant in the series of models, uplift rate is ruled by shortening rate. The faster the shortening rates, the faster the uplift rates. In most experiments we observed small thrusts rooted in the intermediate layer of glass microbeads that break the surface (offset ~1 cm). Less often we observed back thrusts with displacement <1 cm. These secondary structures have little influence on the uplift rates of the external structures.

### 3.2 Surface processes

In the experiments, we observe channel incision by runoff, sapping and landslide.As described in previous experiments(Graveleau et al., 2011), the high rate of precipitation (9 and 18 mm/h)we apply leads to the formation of apermanent sheet flow in the external and flat areas of the model, the thickness of which ranges between 0.5mm and 1 mm. When a new structure emerges in the external part of the wedgethe resulting slopemakes the water to converge, and channels to formleading to the onset of incision of the erodible material (Figs.4A and 4B). The small channelsrapidly grow and they attain 0.5-1 mm in depth and 2-5 mm in width (Fig.4C). Ongoing shortening and uplift trigger retreating incision on the structure and a wave of incision migrates to the backlimb of the fold-thrust, i.e.toward the inner part of the wedge (Figs. 4D, 4E and 4F).Not all of the initial channels (antecedent)succeed to cutin afold-thrust (see animation 1). We discuss in detail in the next section the controls of such behavior. Qualitatively, we observe that transverse channels with faster velocities of knickpoint retreat achieve to cross-cut the uplifting thrust sheets and we refer to them as persistent transverse channels. The number of these persistent transverse channels decreases when shortening rates increase resulting in drainage networks dominated by longitudinal reaches (Fig. 5).Lateral erosion in the channels generates terraces, which is common in such kind of experiments (Graveleau and Dominguez, 2008), and widens the valleys. The wideningof these valleys may eventually merge adjacent channels.The products of erosion are transported over a small distance that is a function of the nature of the grain. Most of the composite material (Silica Powder, PVC, Glass microbeads) accumulates at the foot of the thrust sheets, forming centimeter-scale fans by avulsion (Fig. 4D). A small fraction of the eroded products, the smaller and lighter grains of the mixture (mostly PVC), covers the flat undeformed part of the models up to15 cm to 20 cm away from the frontal structure (Fig. 4A),and another small fraction in suspension leavesthe model (<1%).

In the headwaters of the channels we observe that drainage expansion is achieved by sapping of the upper millimeter of the erodible material (Figs.6A and 6B). These results imply that erosion by groundwater flow is very limited. Landslidesmay also occur in the external limb of the compressive structures, usually in areas preserved from channelincision. A landslidecan start when the slope of the external limb becomes steeper than 20º. Normal fault scarps first appear, immediatelyfollowed by mass movement involving areas of 2×2 cm, as observed in experiment A4 (Figs.4E and 4F) and up to 20×5 cm as in experiment A6 (Figs.6C and 6D). As expected landslides aremore common at high shortening rates when the ratio between uplift and surface erosion rates reach a limit allowing the topography to attain and exceed its equilibrium slope.

The accretion of new structures in the wedge tilts the abovethrust sheetstoward the inner part (Fig. 3A), decreasing the local slopes of the topographythus inhibiting erosion. Below a threshold slope of c.a. 3˚,the cohesion of theerodiblematerial strongly decreases the erosion rate. In all the experiments we observe preserved, non-eroded surfaces. The extent of these surfaces is higher in the experiments run at ahigh shortening rate (Figs.6C and 6D).We also observe that drainage areas in the prism shrink through time, because shortening is not only accommodated by the external thrusts,but also by minor thrust reactivations within the wedge that induceunderthrusting. In experiment A6, the distance between thrusts 2 and 3 decreases from 13 cm to 10 cm after 12 cm of shortening (Figs.4B and 4F). At the scale of the whole prowedge, underthrusting results in a ~20% decrease in drainage areas.

### 3.3 Amounts of erosion and erosion rates

For a given precipitation rate (9 mm/h), the mean volumes of channel erosion,achieved during the activity of the external thrust sheets,show that the amount of erosion in valleys is five to twelve fold higher in the experiments running under shortening rates between 4 cm/h and 20 cm/h, compared to experiments at higher shortening rates(Fig.7A). However, volumes mobilized by landslidesarethree to four times higher at shortening rates higher than 10 cm/h.These resultsindicate that in all these experiments, surface mass balance is dominated by channel erosion and transport at shortening ratesequal to or lower than 9 cm/h (Fig.7A),and it is dominated by landslides at high shortening rates (A4 and A5).

Steady-state is never achieved at the scale of the active thrust sheets and erosion ratesare roughly one eighth of relative uplift rate (Fig.7B), far from equilibrium as evidenced from the flat surfaces preserved from erosion and from the continuing increase in elevation of the active thrust sheets. However, the channels crossing an active thrust sheet as in figure 4D do adapt to the relative uplift rates. We can see that the wave of incision propagates upstream toward the inner parts of the uplifting topography, being limited in its upstream part by a knickpoint (Fig. 8). Downstream of a knickpoint the incision rate balances the relative uplift rate, indicating that this portion of a channel is at steady-state.

### 3.4 Scaling erosion law with steady-state reaches

We measured the width of the steady-state channel reaches once the knickpoints have propagated in the hanging wall of the thrusts, as in figure 8C, in the series of experiments run under a precipitation rate of 9 mm/h. In thisseries, relative uplift rates vary from ~0.1 mm/minin experiment A1 up to ~2.6 mm/min inexperiment A6. Uplift rates are balanced by incision rates

in the persistent transverse channels. In all the experiments we observe that the relationship between $W$ and $A$ follows a power law:

$$W = W_n A^b, \quad (12)$$

where $W_n$is a reference width measurenamed width coefficient following Whittaker and Boulton (2012). Best fits are obtained for $b$=0.2. Channel widths narrow in responseto uplift rateas predicted by the stream power theory (Equation 5).The channel width coefficientdecreasesby a factor of three over one order of magnitude of uplift rate (Fig. 9).

Equation (3) also predicts that channels at steady-state are expected to steepen with increasing uplift rate. In particular, the stream power theory predicts that the exponent on the slope, parameter n, controls the nonlinearity between uplift rates,$U$, and normalized steepness indices,$k_{sn}$ (Equation 6). Even if there is some dispersion in the data at high uplift rates, we observe a positive relation between$k_{sn}$and uplift rates, which is non-linear (Fig. 10A) in the series of experiments run under a precipitation rate of 9 mm/h:

$$U \propto {k_{sn}}^{p'} \quad (13)$$

where best fit of exponent $p'$is 2. However, we know that channels also adjust to uplift rate by narrowing. Combining the adjustment of channel steepness and width to uplift rate we obtain:

$$U \propto \frac{1}{W} \cdot {k_{sn}}^{p} \quad (14)$$

withexponent$p$=1.5±0.2 (Fig. 10B).Using both approaches we observe a non-linear relationship between channel steepness indices and uplift rates. The combination of a threshold for incision and a non-uniform distribution of discharge eventscould explain a non-linear relationship between channel steepness and erosion rate at steady-state (DiBiase and Whipple, 2011; Lague et al., 2005; Snyder et al., 2003b; Tucker, 2004). If true in the experiments, it would imply thatthe exponent $p$ may not be equal to the parameter $n$ in the erosion law (Equation 2). However, in the experiments rainfall rate is constantand runoff distribution events are rather uniform,implying that they should not affect erosion rates. On the other hand, downstream of the retreating knickpoints, the transverse reaches are at steady-state (Fig.8C), indicating that the threshold for incision is overcome.This suggests that the slope exponent $n$ is higher than 1 and taking into account the width effect we infer$n$ = 1.5±0.2.

As predicted by the stream power theory (Equation 9) we obtain, in the series of experiments run under precipitation rates of 9 mm/h and 18mm/h, a power law relation between the velocity of knickpoint retreat, C, and the drainage area, A with $m$ = 0.4. We observe that the knickpoint retreat rates are higher at higher uplift rates(Fig. 11A) as observed in nature(e.g. Loget and Van Den Driessche, 2009; Weissel and Seidl, 1998; Whittaker and Boulton, 2012) and,as predicted by the stream power theory for values of $n$>1 (Whipple and Tucker, 1999). This finding is consistent with the value of $n$ recovered from the uplift rate, steepness index and width relationship.Taking into account the width effect (Equation 10), we infer$m$= 0.8±0.2, a

slightly highervalue, in the series A of experiments run under a precipitation rate of 9 mm/h(Fig. 11B).In the experimentB1run under a rainfall rate two times higher (18 mm/h), rates of knickpoint retreats are higherfor a given drainage area when compared to the experiment A1 run under 9 mm/h of rainfall. We also observe that smaller catchments managed to incise the uplifts (Fig. 11A).

### 3.5 Patterns of drainage network and sedimentation

During the emergence of a fold-thrust not all the preexisting-transverse channels (antecedent) (Fig.12A) succeed to cut through an uplifting thrust sheet, some antecedent channels are defeated (Fig.12B). In the model A1 at low shortening rate, most of the preexisting channels maintained their course through the emerged thrust sheet and these channels are referred to as persistent antecedent channels. In the model A2, some antecedent-transverse channels are defeated, and the discharge they lose is diverted into longitudinal channels located in the backlimb of the thrust sheets. As a consequence, the downstream part of a defeated channel that has lostits upstream area eventually drainsonly the forelimbs of the active thrusts(Fig. 12).The channels crossing an active thrust sheet adapt to the uplift rates, and if knickpoints retreat fast enough through the uplifting structure the antecedent transverse channels persist.We have shown that knickpoint retreat depends on drainage area or discharge (Fig.11A). The drainage area of a persistent channel is either initially large enough or it increases when adjacent diverted channels merge with it.

In the experiment A1, that is, at low uplift rates,75% of the antecedent channels manage to incise the uplifting thrust sheets and the 25% remaining are diverted into longitudinal reaches developed in the backlimb of the fold-thrusts (Fig. 5). At higherrates of uplift and under the same precipitation rate,<35% of the antecedent channels are persistent.As expected in the frame of the above-outlined conceptual model, the proportion of persistent antecedent channels decreases with shortening rate, i.e., with uplift rate (Fig.13A). We also observe that the proportion of persistent preexisting transverse channels, R, does not scale linearly with the ratio of precipitation over shortening rate:

$$R \propto \frac{Rainfall\ \ rate}{shortening\ \ rate}^{0.65\pm0.2} \quad (15)$$

At high R values diversions are sparse and the spacing between outlets of transverse persistent channels is low. Lower values of R mean that the spacing is higher. By controlling the spacing between the outlets of the transverse channels, the magnitude of the uplift rates also control the dispersal of the products of erosion in front of the active thrust. Low spacing between outlets leads to a line-source dispersal system where fans grow by lateral avulsion and finally coalesce in a bajada-like piedmont (Fig. 14A).Some fans are fed by larger drainage areas while most of them are small-scale fans fed by small channels that drain the external limb of the

454 next to last thrust sheet and the active frontal thrust sheet (Fig. 14B). At higher values of
455 spacing between outlets, a point-sourced depositional system develops and the reduced number
456 of fans may not merge. Large catchments feed large prograding fans that may locally bury the
457 backlimb of the active thrust sheet (Figs. 14C and14D). We also see in figure 14 that the
458 oldsedimentary zoneshave been incorporated into the prism as wedge-top basins (highlighted in
459 red in Fig. 14). Although the process of wedge widening implies the incorporation of channels
460 into larger integrated networks, we do not observe anincrease of sediment outflux, which results
461 from a limitation of the experimental setup. The bulk of erosion in all the experiments comes
462 mostly from the active external thrust sheet and in minor proportion from the next to last thrust
463 sheets. Thrust sheets are back tilted when incorporated into the wedge, resulting in the decrease
464 of channel steepness below the critical slope where erosion is strongly reduced (threshold slope
465 of c.a. 3º).
466 In the experiment A1, the thickness of sediments accumulated in front of the thrust 5at
467 t=160 min has reached~1.5 cm and in cross-section the area covered by sediments is 480
468 $mm^2$(Fig. 15A). In the experiment A4, the area of sedimentation in cross-section reached 460
469 $mm^2$ (at the same stage asFig. 15B), i.e., the volume of sediment accumulated in front of an
470 active thrustis more or less the same whatever the shortening rate. This is explained by the fact
471 that sediments shed by persistent channels come mainly from the erosion of the external thrust
472 sheets during thrust activity and that the geometries of the valleys of the persistent channels are
473 very similar in all the series of experiments. The volumes of sediment in experiments A1 and
474 A4 have been accumulated during ~160 min and ~55 min, respectively, leading to
475 sedimentation rates much higher in the experiment evolving under the higher shortening rate
476 (Fig. 16).
477 We observe in all the experiments two sequences of aggradation. In the first one the growth
478 of the prograding fans is evidenced by downlaps while in the second stage a thin layer of
479 sediments seals the thrust that has become inactive (Fig. 15B). The second sequenceis almost
480 not visible inthe cross-section of the experiment A1(Fig. 15A) because the trace of the cross-
481 section is slightly oblique to the bottom of the valley where sediments were accumulated.
482 Backtilting, in the backlimb of the youngestthrust sheets, triggers erosion of the distal parts of
483 the wedge-top basins, resulting in an unconformity between the first and the second sequence.
484 Once a basin is incorporated within the wedge deformation eventually folds both sequences and
485 the thin second sequence may be totally eroded.
486

# 4 Discussion

## 4.1 Dynamics of the erosion in the experimental models and comparison to numerical models

We infer from uplift rates, incision rates and metrics of the topography that erosion in the persistent transverse channels scales nonlinearly to slope and drainage area (discharge):

$$E = K \cdot \frac{A^{0.8\pm0.2}}{W} \cdot S^{1.5\pm0.2} \quad (16)$$

The inferred exponents *m* and *n* are different to findings from other experiments undertaken at Geosciences Montpellier where*m* = *n* = 1(Graveleau et al., 2011; Strak et al., 2011). These differences likely reflect different material proportions in the mixture, since the basic materials used in the above cited experiments and in this study are the same. An exponent on the slope*n* higher than one is consistent with the high degree of knickpoint preservation. Knickpointsshould gradually become smoother with time following the stream power theoryif *n* would beless than 1 (Tucker and Whipple, 2002). The relationship between faster knickpoint celerity and large uplift rates (Fig. 11) is also explainable if *n*> 1 (Eq. 10), taking into account that the channels steepen under higher uplift rates (Fig.10). We obtain $\Psi_{AW} \propto U^{0.5\pm0.1}$ supporting *n* = 1.5 inferred from the scaling of $k_{sn}$ with *W* and *U*.It is a higher value than inferred in studies from rates of erosion or uplift that shows that *n* vary between *n* = 1 in the Siwalik Hills, Nepal(Wobus et al., 2006a)and in Hawaii(Ferrier et al., 2013),and *n*< 1 for the same Siwalik Hills(Kirby and Whipple, 2001).Recent theoretical and field studies demonstrated a nonlinear dependence between steepness indices and erosion rates with an exponent *n* > 1 that can be explained by thresholds in the process of erosion combined to rainfall and runoff variability(DiBiase and Whipple, 2011; Finnegan, 2013; Lague, 2014). In our experiments the discharge in the persistent-transverse channels is by definition largely higher than the threshold for erosion and we do not observe temporal variations in flow velocity in these channels indicating that a threshold cannot account for the high value of *n*. The inferred high value is however consistent with some studies that inferred *n*> 1.3 in Turkey and Italy (Whittaker and Boulton, 2012) and with theoretical estimations inferring *n*to vary from 1.05 to 1.45(Attal et al., 2008). Although *m* is generally believed to be close to 0.5(e.g. Berlin and Anderson, 2007; Bishop and Cowell, 1997; Bishop et al., 2005; Loget and Van Den Driessche, 2009) we found *m* = 0.8±0.2. The experiments also show a dependence of channel width*W* to drainage area and uplift rate that implies that a simple scaling of *W* with drainage area*A* is not correct and that the experimental channels adjust to uplift rate by both increasing their slope and narrowing their width as it is observed in nature(Duvall et al., 2004; Lavé and Avouac, 2001; Snyder et al., 2003a; Turowski et al., 2009; Whittaker and Boulton, 2012; Whittaker et al., 2007a; Yanites and Tucker, 2010). The propagation of a knickpoint during the uplift of a thrust suggests that the

erosion model in the experiments is not a transport-limited model (e.g., Whipple and Tucker, 2002) except maybe in the areas of sedimentation.The model that best characterizes the areas under erosion in the experiments is a detachment-limited model or a hybrid model including transport capacity of channels(Whipple and Tucker, 2002). Our results indicate that the experimental models have geometric and kinematic similarities to what is observed in natural landscapes even if rigorous scaling is not feasibleforthese types of experiments(see discussions in Bonnet, 2009; Lague et al., 2003; Paola et al., 2009).

In the models experiencing the higher shortening rates (A5 and A6), the time for runoff-driven erosion to incise the forelimb of the uplifting thrust sheets is too short, leaving the slopes preserved from incision and submitted to generalized mass wasting. Even in dry land context, extensive non-eroded surfaces are usually not so preservedindicating that these high shortening rate experiments represent an end-member. The preservation of flatsurfaces from erosion isinherent to this kind of models, which are composed of cohesive materials that satisfy the mechanical properties for large fold-thrust to develop,in return inhibiting erosion below slopes of ~3º. However, in the models run under the slower rates of convergence, most of the erosion is achieved by runoff (Fig.6A) and the topographies dissected by channels show valleys, channels, terraces, and other features found in natural landscapes.

Until now, the influence of uplift on drainage diversion has been studied by the use of kinematic numerical models, where deformation isreduced to uplift and advection over a thrust (e.g. Champel et al., 2002; Humphrey and Konrad, 2000; Tomkin and Braun, 1999; van der Beek et al., 2002).In this study, we consider an accretionary wedge system thatallows us to reproduce and to monitor the dynamics of drainage network, erosion and sedimentation patterns,above and during the development of up to five successive thrust sheets.Onset of thrusting and spacing between thrust sheetsemerge naturally from the experiment.The deformation is controlled by the mechanical properties of the experimental material and the setup (layering and thicknesses). Except at very high rates of shortening,surface processes in the experimental models are dominated by runoff-erosion, transport (advection) and sedimentation (see also Graveleau et al., 2011 and Strak et al., 2011). In particular, this experimental setup allows investigating the effects of shortening and rainfall rates on drainage organization and sediment dispersal unlike 3D numerical studies of thrust wedges implementing 2D diffusive surface process(Ruh et al., 2013). Recently a study coupling 3D mechanical and surface process model(Collignon et al., 2014)has shown that where folds grow (thrust are not modeled) they all deviate the main channels resulting in a longitudinal-dominated network. To date no specific treatment of the controlling factors on drainage network evolution and sedimentation pattern in wedges has been done using a coupled 3D mechanical/surface process model.

## 4.2 Controls on spacing of persistent transverse channels

In fold-and-thrust belts drainage organization depends conceptually on the capability for preexisting reaches to incise or not uplifting thrust sheets(Jackson et al., 1996). Progradation of fans in wedge top-like basins potentially makes aggradation in the backlimb of emergent thrusts to balance uplift ratesallowingtransverse rivers to maintain theircourse instead of being diverted(Humphrey and Konrad, 2000). We designed our sand-box experiments in order forthe spacing between thrusts to be large enough (14 cm) to avoid the burying of the backlimbs (Fig.4). When a fold-thrust emerges, it propagates laterally and an axial slope parallel to the structure and perpendicular to the regional slope may be created in the backlimb. Like frontal uplift, this axial slope has, if large enough, the potential to divert preexisting transverse channels. Axial slopes are controlled by the ratio of the lateral to frontal propagation rate and by the dip of the décollement layer where the thrusts are rooted(Champel et al., 2002; van der Beek et al., 2002). In our experiments the basal décollement is flat, and when lateral growth occurs, the lateral propagation rates are 10 to 100 times higher than the convergence rates, both elements preventing the development of channel diversion by the growthof axial slopes (seefigure4B). The setup we used allows studying the influence of the rate of uplifting thrust sheet alone on channel diversion. The series of experiments shows that the proportion of persistent preexisting transverse channels, R, does not scale linearly with the ratio of precipitation over shortening rate (Fig. 13B). It has been shown numerically that thisratio scales linearly with the ratio of precipitation over shortening rateif the law of erosion is linearly proportional to the drainage area and to the slope (Champel et al., 2002; Tomkin and Braun, 1999; van der Beek et al., 2002). The scaling ofthe erosion law suggests erosionis not linearly dependent on drainage area and slope, which seems to be confirmed by the non-linear behavior of the number of diversions in response to uplift.We observe that the minimum drainage area of the persistent transverse channels increases with the rate of shortening and that it decreases under wetter conditions (Fig.11A). It means that the minimum discharge needed to overcome a new uplifting thrust sheet increases with uplift rate. Figure 17 shows that the minimum discharge increases slightly exponentially with uplift rate. Theoretically, at steady-state, discharge is proportional to uplift rate raised to the power of $1/m$. Our data follow this relation using $m$=0.8 ($1/m$=1.25). This relation ultimately controls the spacing of persistent transverse channels.

As mentioned above, it is generallyaccepted that the spacing of persistent antecedent rivers depends on the competition between stream power and uplift(Gupta, 1997; Jackson et al., 1996; Tomkin and Braun, 1999), although aggradation in the backlimb and the décollement dip of a thrust may complicate this simple relation(Champel et al., 2002; Humphrey and Konrad, 2000;

van der Beek et al., 2002).At the scale of an orogen, lithology does not appear to control the diversion of rivers(Gupta, 1997). Consequently, if lateral variations in drainage deflection are neither controlled by thrust geometry (décollement dip) nor by substantial changes in lithology,spatial variations in rock uplift rate along a thrust front may be evidenced by minimum-discharge variations of persistent transverse channels.

### 4.3 Controls on sediment dispersal

The drainage organization is an additional control on sedimentary flux to sedimentary basins. If the transverse channels draining the wedge are not diverted, a line-source dispersal system develops in front of the active structure. The merger of drainage basins results in point-sourced depositional systems separated by areas fed only by small channels developing in the external limb of the active thrust sheet. We reproduce similar sediment patternthat occurs at the Himalayan and Andean fronts(Gupta, 1997; Horton and DeCelles, 2001). The experiments confirm the view that the competition between discharge and tectonic uplift controls along-strike variations in sediment flux in sedimentary basins by controlling drainage organization(Tucker and Slingerland, 1994). The magnitude of drainage reorganization should modulate the magnitude of stratigraphic architecture variations along strike. However, we do not observe significant larger volumes of sediments in front of larger drainage basins with respect to smaller ones of the same experiments as it is observed in nature. This is an experimental limit due to the inhibition of erosion in the interior of the prism.Italso prevents the lateral expansion of drainage network in the interior of the prism, which is believed to maintain the spacing ratio of outlets (half mountain width over outlet spacing) during orogen widening(Horton and DeCelles, 2001; Hovius, 1996). In the experiments this ratio is not honored because it can only increase during widening of the prism.Once a thrust becomes inactive, it is incorporated, with its associated basin, into the prism, and minor erosion and bypass dominate. Because the spacing between thrusts is the same at different convergence rates, the time of activity of the external thrusts is lower at higher rates of shortening. This explains why the total amount of sediments delivered for different convergence rates (two orders of magnitude) does not vary although we show higher rates of sedimentation and erosion under higher rates of shortening (Fig. 16).

### 4.4 Prism widening

In all modelsthe spatial extent of the wedge-top basins, as well as the distance between the traces of the thrusts, both shrink through time indicating that the internal structural units are slightly underthrusted with ongoing shortening.As in previous studies we observe that the

growth of a prism fluctuates between periods of frontal accretion and internal thickening(e.g. Gutscher et al., 1996; Hoth et al., 2006; Konstantinovskaia and Malavieille, 2005; Naylor and Sinclair, 2007; Naylor et al., 2005; Simpson, 2006). Detail cross-sections of fans accumulated in front of a thrust sheet not yet active reveal two stages of sedimentation, one of progradation and a second one of backfilling and sealing of the thrust (Fig. 15B). We suggest that this two-phase sedimentary infill may be used as a marker for the transition between frontal accretion and internal growth in orogenic wedges.A proposed timescale for the activity of external thrust is 0.1-5 Myr(Naylor and Sinclair, 2007).In between periods of frontal accretion, the ratio of drainage area lost during internal growth represents ~20% of a thrust sheet initial area sincethe thrust emerged. The fluctuation between periods of frontal accretion and internal thickening, as well asdrainage area shrinking,may modulate the sedimentary flux at these timescales in foreland basins.

It is interesting to note that local slopes created by folding and faulting develop since the initial stages of tectonic growth of a wedge, and that this structurally-controlled relief is incorporated within a wedge during widening. Local slopes may divert runoff in directions perpendicular to the regional slope and create longitudinal-dominated drainage networks. Therefore tectonic-related relief may influence the long-term drainage network organization not only in the external part of an orogen but also in its interior. This can occur during the inversion of a rift (Babault et al., 2012) or during widening of a wedge by forward propagation and incorporation of thrust sheets as in the experiments.

## 5 Conclusions

Our results suggest that the rule of erosion in the experimental models has many similarities to what is observed in natural landscape. We infer from uplift rates, incision rates and metrics of the topography that erosion scales nonlinearly to slope and drainage area. We found for the exponents on the slope ($n$) and on the drainage ($m$) the respective values of 1.5±0.2 and 0.8±0.2. The experimental channels adjust to uplift rate by both increasing their slope and narrowing their channels as it is observed in nature above active faults.

Drainage pattern in fold-and-thrust belts depends on the capability for antecedent reaches to incise or not the uplifting thrust sheets. We observe that the minimum drainage area for transverse channels to incise the uplifting structure increases with the rate of shortening and decreases under wetter conditions, suggesting that discharge is the controlling factor. Indeed, a minimum discharge exists for a new uplifting thrust sheet to be overcome and it increases exponentially with uplift rate. This minimum discharge ultimately controls the spacing of persistent transverse channels. Consequently, if lateral variations in drainage deflection are neither controlled by thrust geometry (décollement dip) nor by substantial changes in lithology

as shown in previous studies, then the spatial variations in rock uplift rate along a thrust front could be evidenced by studying minimum-discharge variations of persistent transverse channels.

The experiments confirm the view that competing discharge and tectonic uplift control drainage pattern resulting in along-strike variations of sediment flux in sedimentary basins. When the transverse channels that drain a wedge are not diverted, a line-source dispersal system develops in front of the active thrust sheet. The merger of drainage basins in the backlimb of the frontal thrust sheet results in point-sourced depositional systems separated by areas fed by small channels that develop in the external limb.

Detail cross-sections of fans accumulated in front of a thrust sheet that became inactive reveal two stages of sedimentation, one of progradation and a second one of backfilling and sealing of the thrust. We suggest that this two-phase sedimentary infill may be used as a marker for the transition between frontal accretion and internal growth in orogenic wedges.

## Acknowledgments

Financial support was provided to J. Babault by REPSOL, for M. Viaplana-Muzas PhD grant, and they also benefited from Spanish national projects (CGL2010-1516 and CONSOLIDER-Ingenio CSD2006-00041). We thank C. Romano from Géosciences Montpellier for technical assistance and we thank J. Malavieille for helpful discussions. Thanks to M. González, C. Díaz and E. Álvarez de Buergo for discussions on preliminary results of this work. We thank the editor Rob Govers, Kosuke Ueda and one anonymous reviewer for their constructive comments and suggestions that have contributed to the improvement of the manuscript.

## References

Amos, C.B., Burbank, D.W., 2007. Channel width response to differential uplift. Journal of Geophysical Research: Earth Surface 112, F02010.

Attal, M., Tucker, G.E., Whittaker, A.C., Cowie, P.A., Roberts, G.P., 2008. Modeling fluvial incision and transient landscape evolution: Influence of dynamic channel adjustment. J. Geophys. Res.-Earth Surf. 113, 16.

Babault, J., Bonnet, S., Crave, A., Van Den Driessche, J., 2005. Influence of piedmont sedimentation on erosion dynamics of an uplifting landscape: An experimental approach. Geology 33, 301-304, doi: 310.1130/G21095.21091.

Babault, J., Van Den Driessche, J., Teixell, A., 2012. Longitudinal to transverse drainage network evolution in the High Atlas (Morocco): The role of tectonics. Tectonics 31, TC4020.

Berlin, M.M., Anderson, R.S., 2007. Modeling of knickpoint retreat on the Roan Plateau, western Colorado. Journal of Geophysical Research: Earth Surface 112, F03S06.

Bishop, P., Cowell, P., 1997. Lithological and Drainage Network Determinants of the Character of Drowned, Embayed Coastlines. The Journal of Geology 105, 685-700.

Bishop, P., Hoey, T.B., Jansen, J.D., Artza, I.L., 2005. Knickpoint recession rate and catchment area: the case of uplifted rivers in Eastern Scotland. Earth Surface Processes and Landforms 30, 767-778.
Bonnet, S., 2009. Shrinking and splitting of drainage basins in orogenic landscapes from the migration of the main drainage divide. Nature Geoscience 2, 897-897.
Bookhagen, B., Strecker, M.R., 2012. Spatiotemporal trends in erosion rates across a pronounced rainfall gradient: Examples from the southern Central Andes. Earth and Planetary Science Letters 327–328, 97-110.
Burbank, McLean, Bullen, Abdrakhmatov, Miller, 1999. Partitioning of intermontane basins by thrust-related folding, Tien Shan, Kyrgyzstan. Basin Research 11, 75-92.
Burbank, D.W., Vergés, J., 1994. Reconstruction of topography and related depositional systems during active thrusting. Journal of Geophysical Research: Solid Earth 99, 20281-20297.
Castelltort, S., Goren, L., Willett, S.D., Champagnac, J.-D., Herman, F., Braun, J., 2012. River drainage patterns in the New Zealand Alps primarily controlled by plate tectonic strain. Nature Geosci 5, 744-748.
Champel, B., van der Beek, P., Mugnier, J.-L., Leturmy, P., 2002. Growth and lateral propagation of fault-related folds in the Siwaliks of western Nepal; rates, mechanisms, and geomorphic signature. Journal of Geophysical Research 107.
Collignon, M., Kaus, B., May, D., Fernandez, N., 2014. Influences of surface processes on fold growth during 3-D detachment folding. Geochemistry, Geophysics, Geosystems 15, 3281-3303.
Cowie, P.A., Whittaker, A.C., Attal, M., Roberts, G., Tucker, G.E., Ganas, A., 2008. New constraints on sediment-flux–dependent river incision: Implications for extracting tectonic signals from river profiles. Geology 36, 535-538.
Crosby, B.T., Whipple, K.X., 2006. Knickpoint initiation and distribution within fluvial networks: 236 waterfalls in the Waipaoa River, North Island, New Zealand. Geomorphology 82, 16-38.
Davis, D., Suppe, J., Dahlen, F.A., 1983. Mechanics of fold-and-thrust belts and accretionary wedges. Journal of Geophysical Research: Solid Earth 88, 1153-1172.
DiBiase, R.A., Whipple, K.X., 2011. The influence of erosion thresholds and runoff variability on the relationships among topography, climate, and erosion rate. Journal of Geophysical Research: Earth Surface 116, F04036.
DiBiase, R.A., Whipple, K.X., Heimsath, A.M., Ouimet, W.B., 2010. Landscape form and millennial erosion rates in the San Gabriel Mountains, CA. Earth and Planetary Science Letters 289, 134-144.
Duvall, A., Kirby, E., Burbank, D., 2004. Tectonic and lithologic controls on bedrock channel profiles and processes in coastal California. Journal of Geophysical Research: Earth Surface 109, F03002.
Ferrier, K.L., Huppert, K.L., Perron, J.T., 2013. Climatic control of bedrock river incision. Nature 496, 206-209.
Finnegan, N., 2013. Interpretation and downstream correlation of bedrock river terrace treads created from propagating knickpoints. Journal of Geophysical Research: Earth Surface 118, 54-64.
Finnegan, N.J., Roe, G., Montgomery, D.R., Hallet, B., 2005. Controls on the channel width of rivers: Implications for modeling fluvial incision of bedrock. Geology 33, 229-232.
Giletycz, S., Loget, N., Chang, C.P., Mouthereau, F., 2015. Transient fluvial landscape and preservation of low-relief terrains in an emerging orogen: Example from Hengchun Peninsula, Taiwan. Geomorphology 231, 169-181.
Graveleau, F., Dominguez, S., 2008. Analogue modelling of the interaction between tectonics, erosion and sedimentation in foreland thrust belts. Comptes Rendus. Geoscience 340, 324-333.
Graveleau, F., Hurtrez, J.E., Dominguez, S., Malavieille, J., 2011. A new experimental material for modeling relief dynamics and interactions between tectonics and surface processes. Tectonophysics 513, 68-87.
Graveleau, F., Strak, V., Dominguez, S., Malavieille, J., Chatton, M., Manighetti, I., Petit, C., 2015. Experimental modelling of tectonics–erosion–sedimentation interactions in compressional, extensional, and strike–slip settings. Geomorphology.

759 Gudmundsdottir, M.H., Blisniuk, K., Ebert, Y., Levine, N.M., Rood, D.H., Wilson, A., Hilley,
760 G.E., 2013. Restraining bend tectonics in the Santa Cruz Mountains, California, imaged using
761 10Be concentrations in river sands. Geology 41, 843-846.
762 Gupta, S., 1997. Himalayan drainage patterns and the origin of fluvial megafans in the Ganges
763 foreland basin. Geology 25, 11-14.
764 Gutscher, M.-A., Kukowski, N., Malavieille, J., Lallemand, S., 1996. Cyclical behavior of thrust
765 wedges: Insights from high basal friction sandbox experiments. Geology 24, 135-138.
766 Horton, B.K., DeCelles, P.G., 2001. Modern and ancient fluvial megafans in the foreland basin
767 system of the central Andes, southern Bolivia: implications for drainage network evolution in
768 fold-thrust belts. Basin Research 13, 43-63.
769 Hoth, S., Adam, J., Kukowski, N., Oncken, O., 2006. Influence of erosion on the kinematics of
770 bivergent orogens: Results from scaled sandbox simulations. Geological Society of America
771 Special Papers 398, 201-225.
772 Hovius, N., 1996. Regular spacing of drainage outlets from linear mountain belts. Basin
773 Research 8, 29-44.
774 Howard, A.D., 1980. Thresholds in river regimes. Thresholds in geomorphology, 227-258.
775 Howard, A.D., Kerby, G., 1983. Channel changes in badlands. GSA Bull. 94, 739-752.
776 Hubbert, M.K., 1951. Mechanical basis for certain familiar geologic structures. Geological
777 Society of America Bulletin 62, 355-372.
778 Humphrey, N.F., Konrad, S.K., 2000. River incision or diversion in response to bedrock uplift.
779 Geology 28, 43-46.
780 Jackson, J., Norris, R., Youngson, J., Wojtal, S.F., 1996. The structural evolution of active fault
781 and fold systems in central Otago, New Zealand; evidence revealed by drainage patterns.
782 Journal of Structural Geology 18, 217-234.
783 Jolley, E., Turner, P., Williams, G., Hartley, A., Flint, S., 1990. Sedimentological response of an
784 alluvial system to Neogene thrust tectonics, Atacama Desert, northern Chile. Journal of the
785 Geological Society 147, 769-784.
786 Kirby, E., Ouimet, W., 2011. Tectonic geomorphology along the eastern margin of Tibet:
787 insights into the pattern and processes of active deformation adjacent to the Sichuan Basin.
788 Geological Society, London, Special Publications 353, 165-188.
789 Kirby, E., Whipple, K., 2001. Quantifying differential rock-uplift rates via stream profile
790 analysis. Geology 29, 415-418.
791 Kirby, E., Whipple, K.X., 2012. Expression of active tectonics in erosional landscapes. Journal
792 of Structural Geology 44, 54-75.
793 Konstantinovskaia, E., Malavieille, J., 2005. Erosion and exhumation in accretionary orogens:
794 Experimental and geological approaches. Geochem. Geophys. Geosyst. 6, Q02006.
795 Koons, P.O., 1994. Three-dimensional critical wedges: Tectonics and topography in oblique
796 collisional orogens. Journal of Geophysical Research: Solid Earth 99, 12301-12315.
797 Koons, P.O., 1995. Modeling the topographic evolution of collisional belts. Annual Review of
798 Earth and Planetary Sciences 23, 375-408.
799 Lague, D., 2014. The stream power river incision model: evidence, theory and beyond. Earth
800 Surface Processes and Landforms 39, 38-61.
801 Lague, D., Crave, A., Davy, P., 2003. Laboratory experiments simulating the geomorphic
802 response to tectonic uplift. Journal of geophysical research 108, 2008,
803 doi:2010.1029/2002JB001785.
804 Lague, D., Hovius, N., Davy, P., 2005. Discharge, discharge variability, and the bedrock
805 channel profile. Journal of Geophysical Research: Earth Surface 110, F04006.
806 Lavé, J., Avouac, J.P., 2001. Fluvial incision and tectonic uplift across the Himalayas of central
807 Nepal. Journal of Geophysical Research: Solid Earth 106, 26561-26591.
808 Loget, N., Van Den Driessche, J., 2009. Wave train model for knickpoint migration.
809 Geomorphology 106, 376-382.
810 Montgomery, D.R., Gran, K.B., 2001. Downstream variations in the width of bedrock channels.
811 Water Resour. Res. 37, 1841-1846.
812 Naylor, M., Sinclair, H.D., 2007. Punctuated thrust deformation in the context of doubly vergent
813 thrust wedges: Implications for the localization of uplift and exhumation. Geology 35, 559-562.

814 Naylor, M., Sinclair, H.D., Willett, S., Cowie, P.A., 2005. A discrete element model for
815 orogenesis and accretionary wedge growth. Journal of Geophysical Research: Solid Earth 110,
816 B12403.
817 Oberlander, T.M., 1985. Origin of drainage transverse to structures in orogens. Binghamton
818 Symposia in Geomorphology: International Series 15, 155-182.
819 Ouimet, W.B., Whipple, K.X., Granger, D.E., 2009. Beyond threshold hillslopes: Channel
820 adjustment to base-level fall in tectonically active mountain ranges. Geology 37, 579-582.
821 Paola, C., Straub, K., Mohrig, D., Reinhardt, L., 2009. The "unreasonable effectiveness" of
822 stratigraphic and geomorphic experiments. Earth-Science Reviews 97, 1-43.
823 Parker, G., Anderson, A.G., 1977. Basic principles of river hydraulics. Journal of the Hydraulics
824 Division 103.
825 Perron, J.T., Royden, L., 2013. An integral approach to bedrock river profile analysis. Earth
826 Surface Processes and Landforms 38, 570-576.
827 Rosenbloom, N.A., Anderson, R.S., 1994. Hillslope and channel evolution in a marine terraced
828 landscape, Santa Cruz, California. Journal of Geophysical Research: Solid Earth 99, 14013-
829 14029.
830 Royden, L., Clark, M., Whipple, K., 2000. Evolution of river elevation profiles by bedrock
831 incision: Analytical solutions for transient river profiles related to changing uplift and
832 precipitation rates. Eos Trans. AGU 81, 48.
833 Ruh, J.B., Gerya, T., Burg, J.-P., 2013. High-resolution 3D numerical modeling of thrust
834 wedges: Influence of décollement strength on transfer zones. Geochemistry, Geophysics,
835 Geosystems, n/a-n/a.
836 Schellart, W.P., 2000. Shear test results for cohesion and friction coefficients for different
837 granular materials: scaling implications for their usage in analogue modelling. Tectonophysics
838 324, 1-16.
839 Simpson, G.D.H., 2006. Modelling interactions between fold–thrust belt deformation, foreland
840 flexure and surface mass transport. Basin Research 18, 125-143.
841 Snyder, N.P., Whipple, K.X., Tucker, G.E., Merritts, D.J., 2003a. Importance of a stochastic
842 distribution of floods and erosion thresholds in the bedrock river incision problem. Journal of
843 Geophysical Research: Solid Earth 108, 2117.
844 Snyder, N.P., Whipple, K.X., Tucker, G.E., Merritts, D.J., 2003b. Channel response to tectonic
845 forcing: field analysis of stream morphology and hydrology in the Mendocino triple junction
846 region, northern California. Geomorphology 53, 97-127.
847 Sobel, E.R., Hilley, G.E., Strecker, M.R., 2003. Formation of internally drained contractional
848 basins by aridity-limited bedrock incision. Journal of Geophysical Research 108, 2344.
849 Strak, V., Dominguez, S., Petit, C., Meyer, B., Loget, N., 2011. Interaction between normal
850 fault slip and erosion on relief evolution: Insights from experimental modelling. Tectonophysics
851 513, 1-19.
852 Talling, P.J., Lawton, T.F., Burbank, D.W., Hobbs, R.S., 1995. Evolution of latest Cretaceous–
853 Eocene nonmarine deposystems in the Axhandle piggyback basin of central Utah. Geological
854 Society of America Bulletin 107, 297-315.
855 Tomkin, J.H., Braun, J., 1999. Simple models of drainage reorganisation on a tectonically active
856 ridge system. New Zealand Journal of Geology and Geophysics 42, 1-10.
857 Tucker, G.E., 2004. Drainage basin sensitivity to tectonic and climatic forcing; implications of a
858 stochastic model for the role of entrainment and erosion thresholds. Earth Surface Processes and
859 Landforms 29, 185-205.
860 Tucker, G.E., Slingerland, R., 1994. Erosional dynamics, flexural isostasy, and long-lived
861 escarpments: a numerical modeling study. Journal of Geophysical Research 99, 12,229-212,243.
862 Tucker, G.E., Slingerland, R., 1996. Predicting sediment flux from fold and thrust belts. Basin
863 Research 8, 329-349.
864 Tucker, G.E., Whipple, K.X., 2002. Topographic outcomes predicted by stream erosion models:
865 Sensitivity analysis and intermodel comparison. Journal of Geophysical Research: Solid Earth
866 107, 2179.

Turowski, J.M., Lague, D., Hovius, N., 2009. Response of bedrock channel width to tectonic forcing: Insights from a numerical model, theoretical considerations, and comparison with field data. Journal of Geophysical Research: Earth Surface 114, F03016.
van der Beek, P., Champel, B., Mugnier, J.-L., 2002. Control of detachment dip on drainage development in regions of active fault-propagation folding. Geology 30, 471-474.
Weissel, J.K., Seidl, M.A., 1998. Inland Propagation of Erosional Escarpments and River Profile Evolution Across the Southeast Australian Passive Continental Margin, Rivers Over Rock: Fluvial Processes in Bedrock Channels. American Geophysical Union, pp. 189-206.
Whipple, K.X., 2001. Fluvial Landscape Response Time: How Plausible Is Steady-State Denudation? Am J Sci 301, 313-325.
Whipple, K.X., 2004. Bedrock rivers and the geomorphology of active orogens. Annual Review of Earth and Planetary Sciences 32, 151-185.
Whipple, K.X., Tucker, G.E., 1999. Dynamics of the stream-power river incision model: Implications for height limits of mountain ranges, landscape response timescales, and research needs. Journal of Geophysical Research 104, 17,661-617,674.
Whipple, K.X., Tucker, G.E., 2002. Implications of sediment-flux-dependent river incision models for landscape evolution. Journal-of-geophysical-research 107, ETG3.1-ETG3.20.
Whittaker, A.C., Attal, M., Cowie, P.A., Tucker, G.E., Roberts, G., 2008. Decoding temporal and spatial patterns of fault uplift using transient river long profiles. Geomorphology 100, 506-526.
Whittaker, A.C., Boulton, S.J., 2012. Tectonic and climatic controls on knickpoint retreat rates and landscape response times. Journal of Geophysical Research: Earth Surface 117, F02024.
Whittaker, A.C., Cowie, P.A., Attal, M., Tucker, G.E., Roberts, G.P., 2007a. Bedrock channel adjustment to tectonic forcing: Implications for predicting river incision rates. Geology 35, 103-106.
Whittaker, A.C., Cowie, P.A., Attal, M., Tucker, G.E., Roberts, G.P., 2007b. Contrasting transient and steady-state rivers crossing active normal faults: new field observations from the Central Apennines, Italy. Basin Research 19, 529-556.
Wobus, C., Heimsath, A., Whipple, K., Hodges, K., 2005. Active out-of-sequence thrust faulting in the central Nepalese Himalaya. Nature 434, 1008-1011.
Wobus, C., Whipple, K.X., Kirby, E., Snyder, N., Johnson, J., Spyropolou, K., Crosby, B., Sheehan, D., 2006a. Tectonics from topography; procedures, promise, and pitfalls. Special Paper - Geological Society of America 398, 55-74.
Wobus, C.W., Crosby, B.T., Whipple, K.X., 2006b. Hanging valleys in fluvial systems; controls on occurrence and implications for landscape evolution. Journal of Geophysical Research 111.
Yanites, B.J., Tucker, G.E., 2010. Controls and limits on bedrock channel geometry. Journal of Geophysical Research: Earth Surface 115, F04019.

916
917
918
919

## 920 Figures and captions:

921

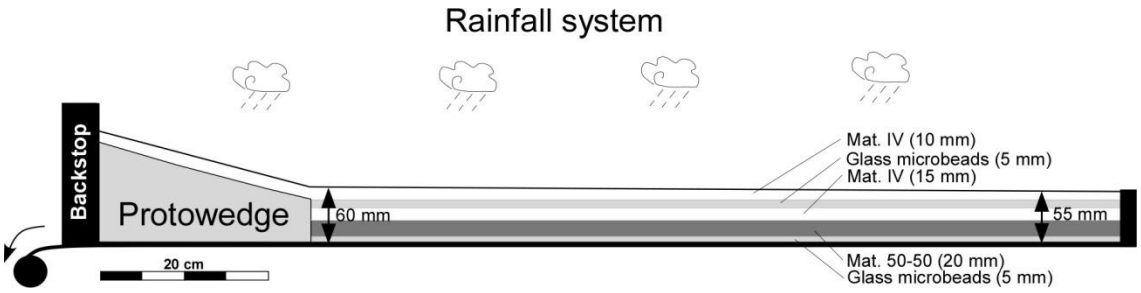


922

923 ***Figure 1.*** *Scheme of the experimental setup. We imposed a slope of 0.5º at the surface of the models in order to*
924 *enhance runoff connectivity. The initial thickness of the layered material is 60 mm close to the protowedge and 55*
925 *mm in the distal part.*

926

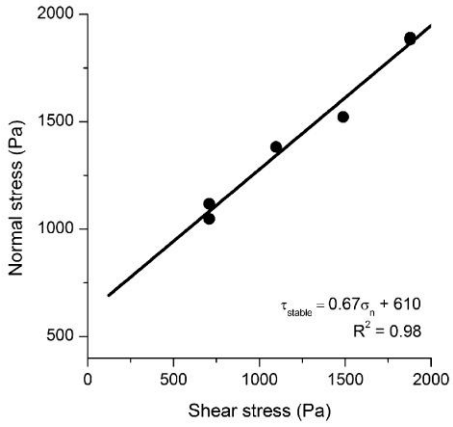


927

928 ***Figure 2.*** *Mohr–Coulomb envelope (stable friction measurements) for failure of the erodible mixture (material IV)*
929 *used in our experiments.*

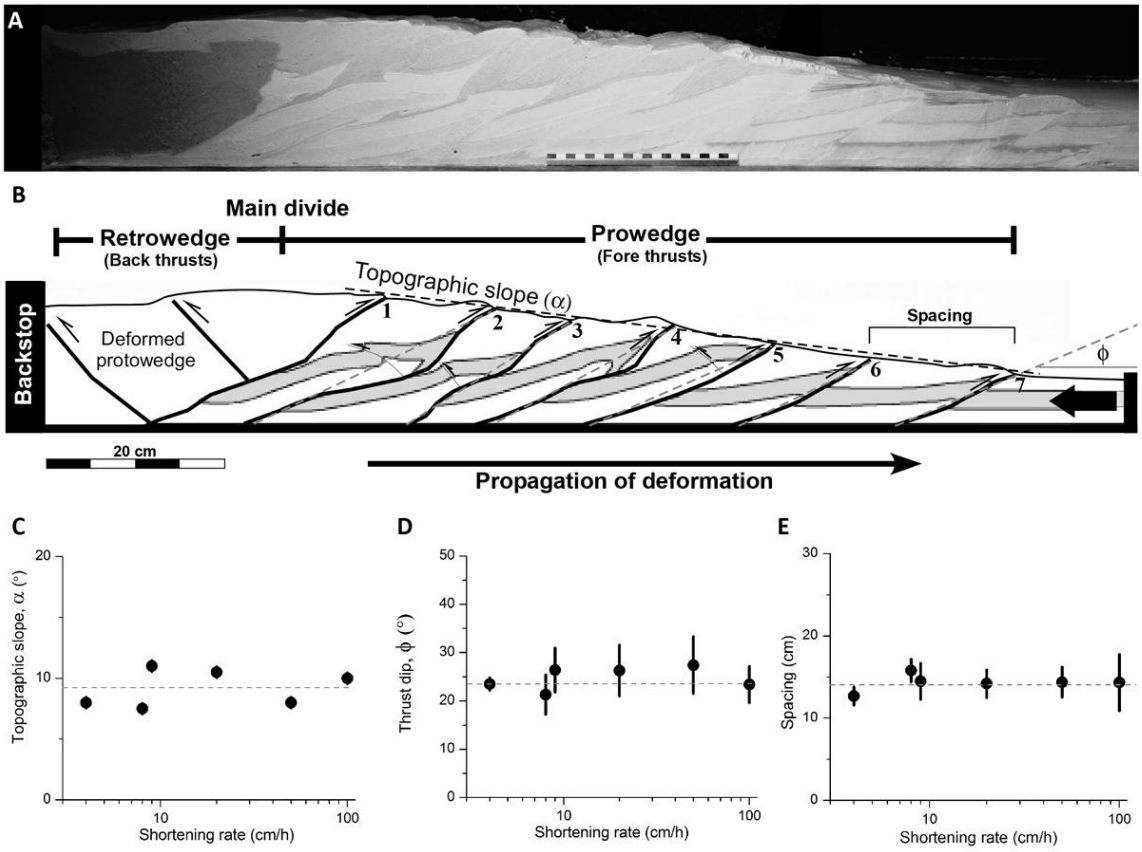


***Figure 3.*** *(A) Cross-section of the model A4 after 1 m of shortening. (B) Interpretation showing the main thrusts. For all the experiments we calculated the topographic mean slopes (α) of the prowedges (C), the thrust dips (ϕ) measured between the root and the tip of the thrust (dashed grey lines in B) (D) and the thrust spacing measured in the external part when a new thrust emerges (E).*

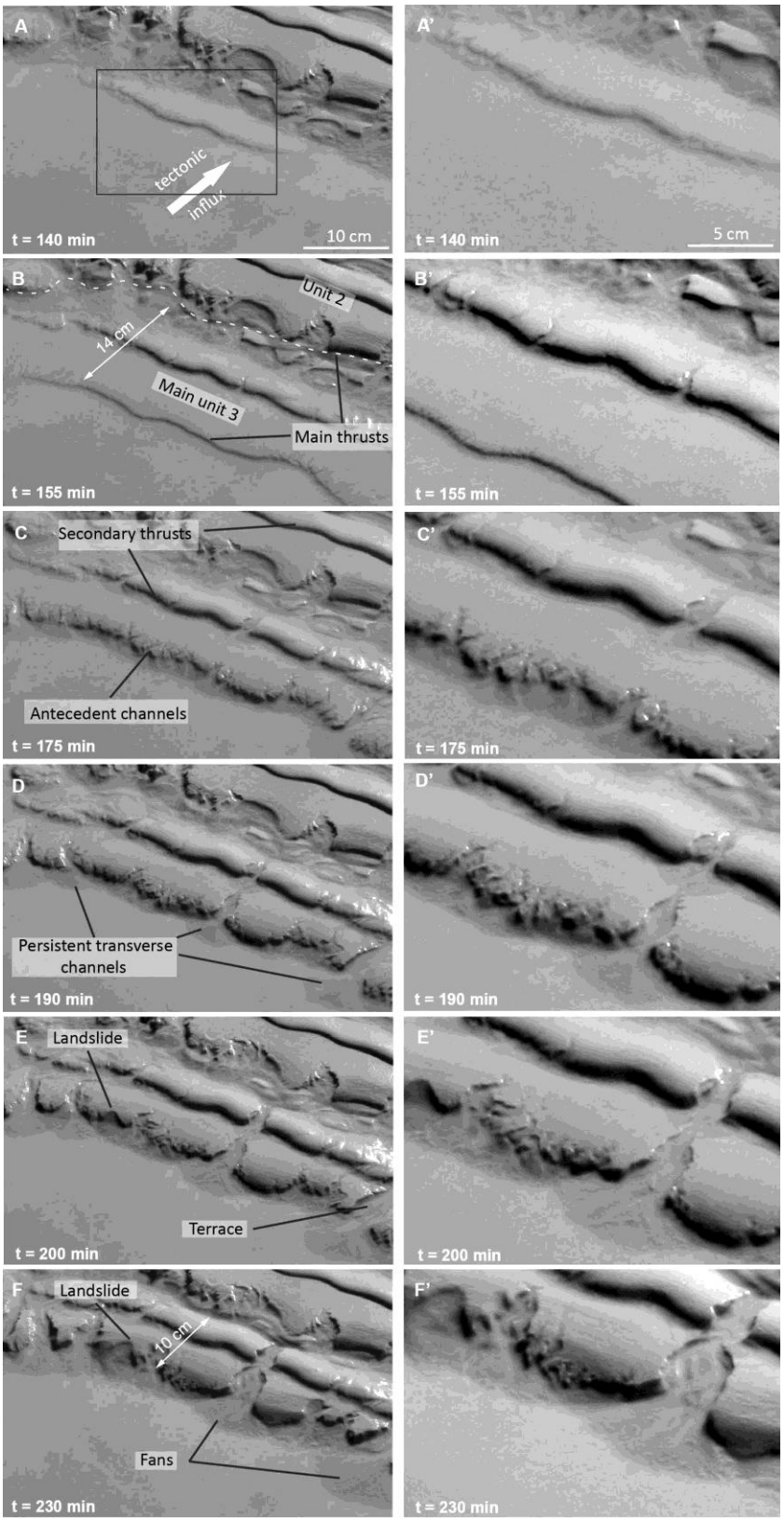


***Figure 4.*** *Photos of the experiment, A2, from t=140 min, (A), before thrust 3 emerges, to t=230 min (F) when the third thrust sheet has totally emerged (animation 1 add in supplementary data). The amount of shortening between (A) and (F) is 12 cm.*

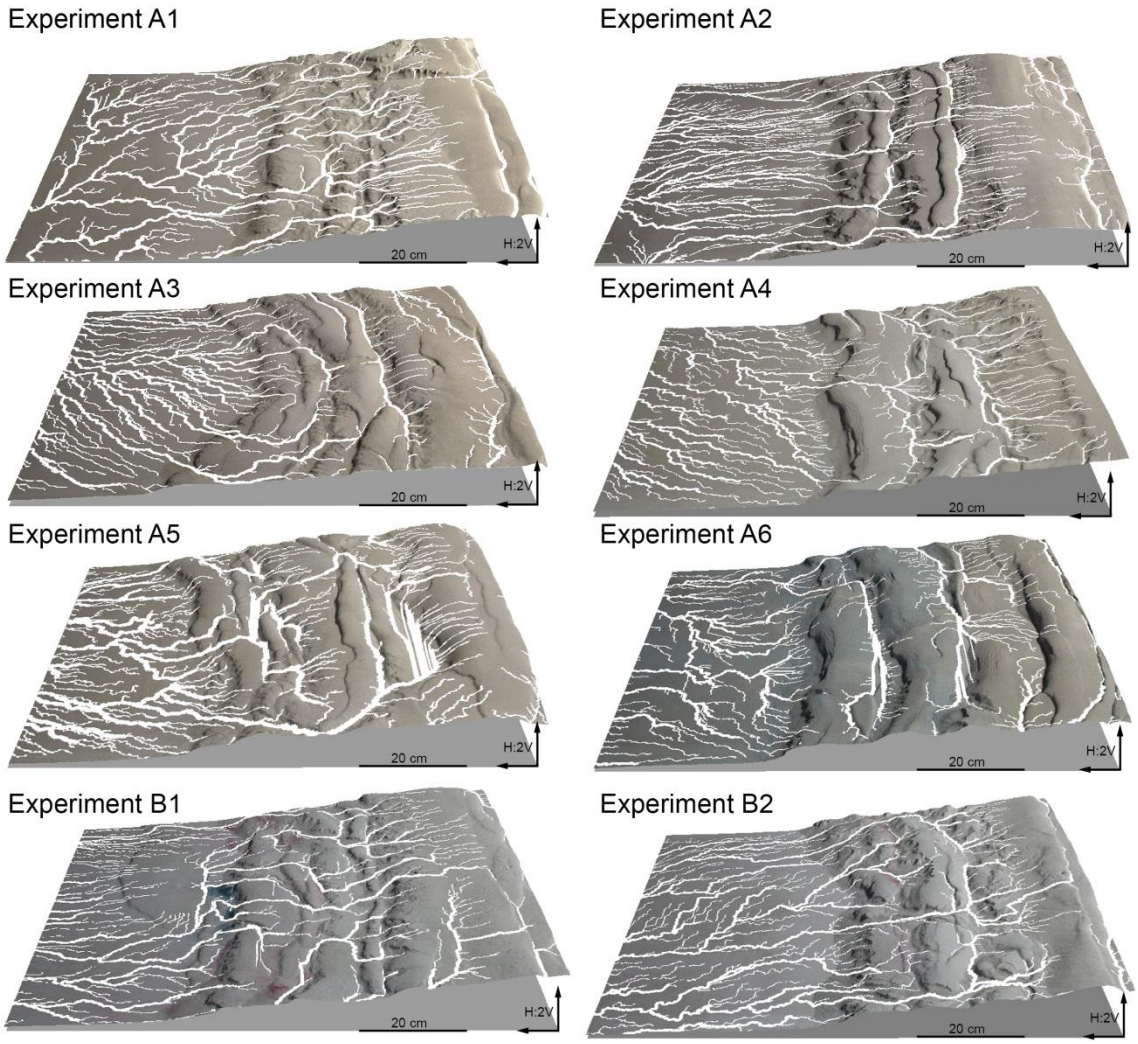


***Figure 5.*** *3D views of all the models after the third thrust activity( the photographs are overlapped on the DEM). The drainage network is superimposed in white. The models run under 9 mm/h of rainfall rate in the A series with the shortening rate ranging between 4-100 cm/h (A1: 4 cm/h; A2: 8 cm/h; A3: 9 cm/h; A4: 20 cm/h; A5: 50 cm/h; A6: 100 cm/h). In the models run under 18 mm/h of rainfall rate, the B series, the shortening rate varied between 8 cm/h (B1) and 18 cm/h (B2).*

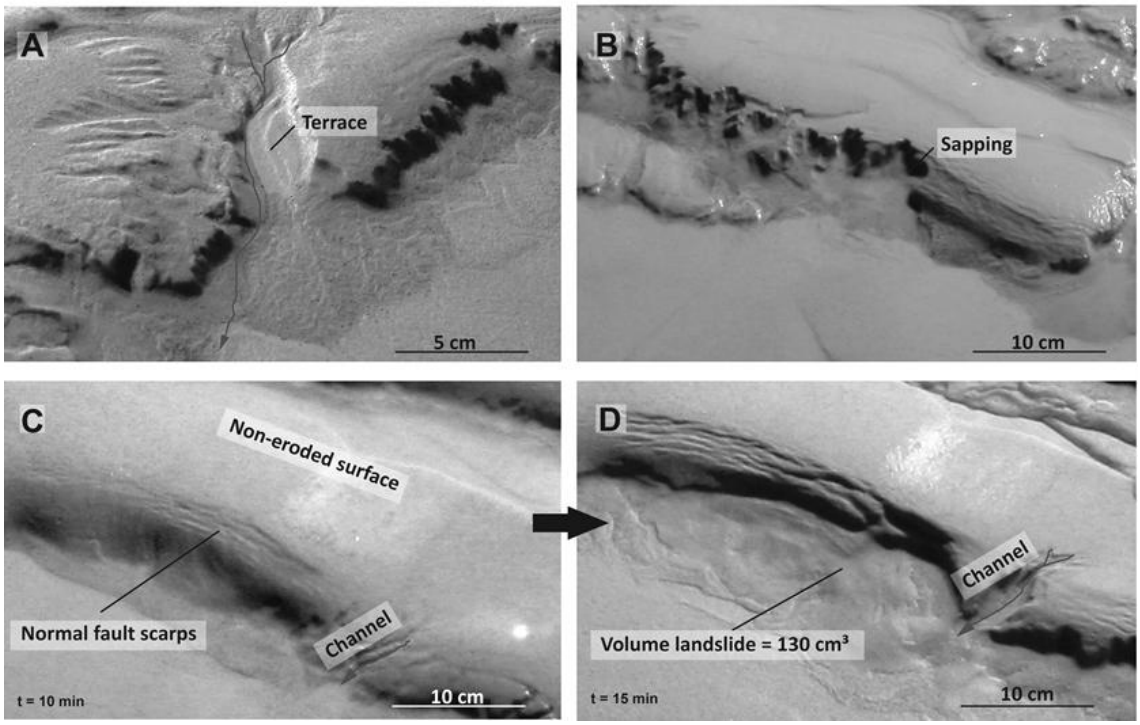


***Figure 6.*** *Detail pictures of the principal surface processes active in experiments (A). Detail of a channel crossing the fourth thrust sheet in the experiment A4 at t= 350 min. Note the formation of a terrace in the right part of the channel and the alluvial fan located in the channel outlet. (B) Detail of sapping in the external part of the second thrust sheet of the experiment B2 at t=70 min. (C) and (D) Evolution of a landslide in the experiment A6, from t=10 min to t=15min, situated in the external part of the third thrust sheet.*

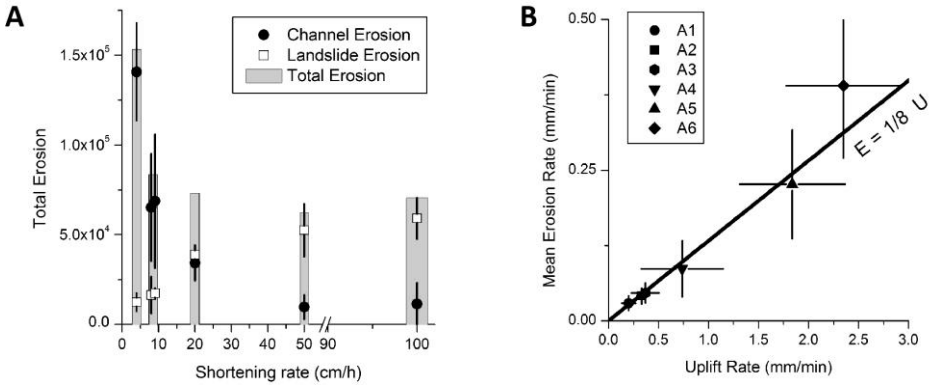


***Figure 7.*** *(A) Mean amounts and standard deviations of erosion of the frontal thrust sheets, during their activity, calculated for experiments run under 9 mm/h of precipitation rates. (Dots) Erosion done by persistent channels and small channels developed on the forelimb of the fold-thrust. (White squares) Erosion done by landslides those develop in the forelimbs of the thrusts. (B) Mean erosion rates and standard deviations calculated from channel-driven amounts of erosion (dots in A) against uplift rate (landslide-derived erosion not included):* $E \cong \frac{1}{8} U$.

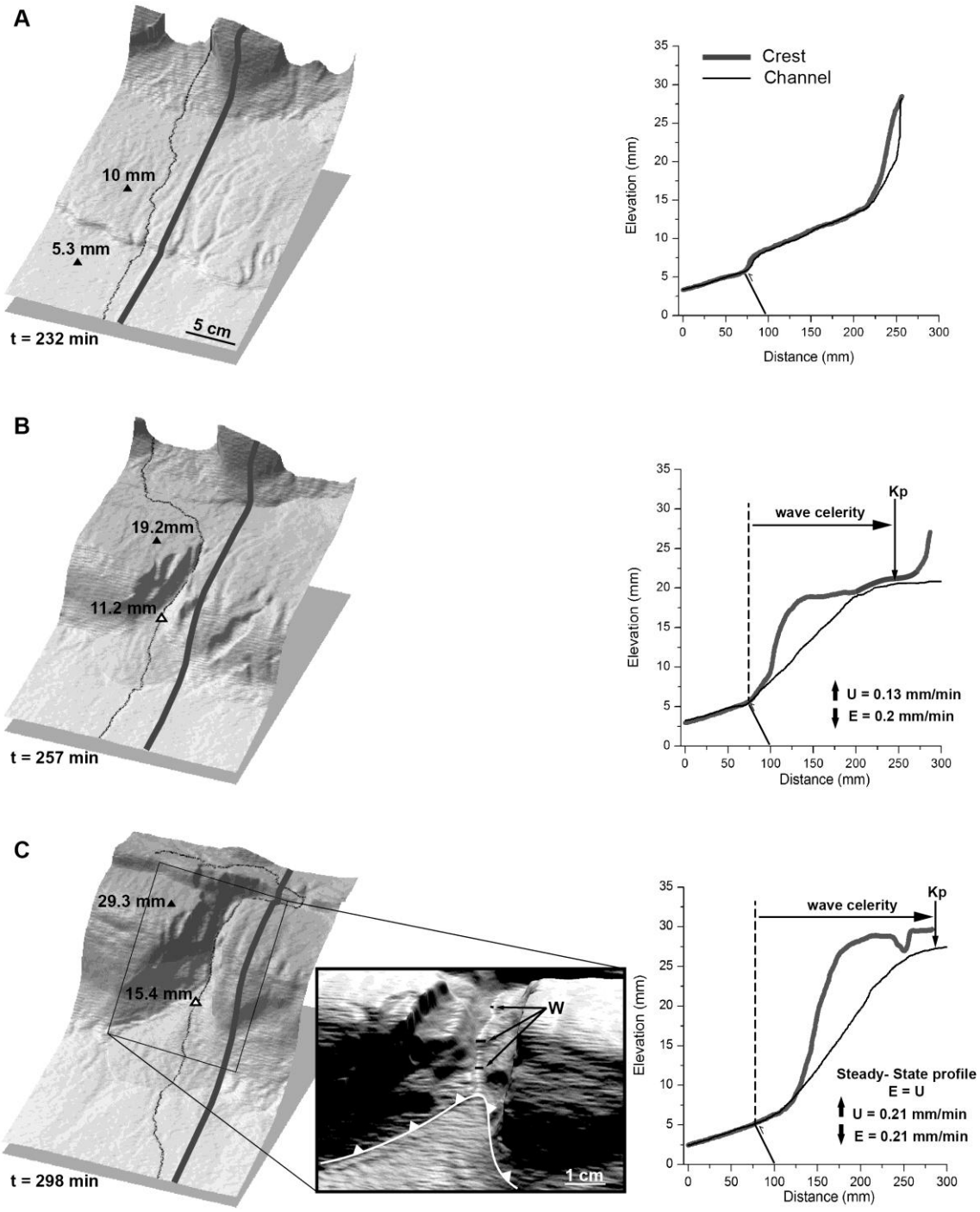


***Figure 8.*** *(Left) 3D detail views of a persistent-channel incision during thrust activity (experiment A2). (Right) Crest and channel topographic profiles (traces superimposed on 3D views) showing the formation of a knickpoint (Kp), when the third thrust sheet starts to emerge at t=232 min (A). The knickpoint migrates upstream (B) until the fourth thrust sheet starts to emerge (C). At this moment channel erosion rate (E) balances relative uplift rate (U), 0.21 mm/min, indicating that this portion of the channel is at steady-state. The inset illustrates where the width of channels, W, has been measured along the channel. The length of the channel in this figure is 6 cm long.*

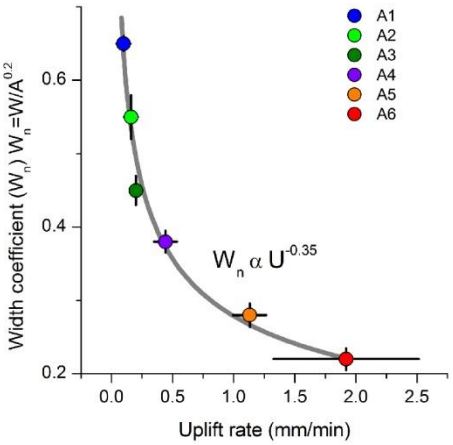


***Figure 9:*** *Channel width coefficient, $W_n$ (channel width normalized for drainage area), of persistent transverse channels against mean relative uplift rate (error bars are standard deviation, 1σ), in the series of experiments run under a precipitation rate of 9 mm/h. (Black line) Best fit using a non-linear regression: $W_n = 0.3 \cdot U^{-0.35}$.*

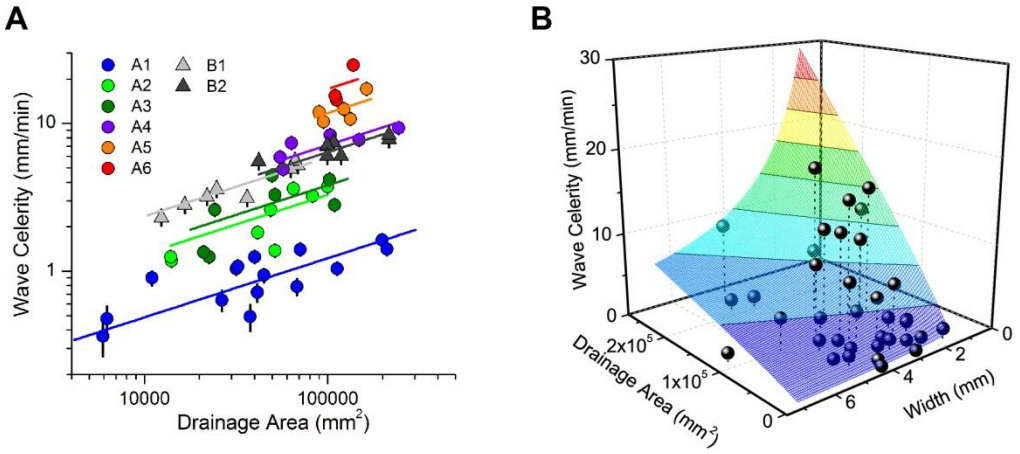


***Figure 10:*** *(A) Normalized steepness index ($k_{sn}$) of the persistent antecedent channels against uplift rates, (Series A). The equation that best fits is $U=k_{sn}^2$. (B) Graphic combining the adjustment of channel steepness and width to uplift rate.*

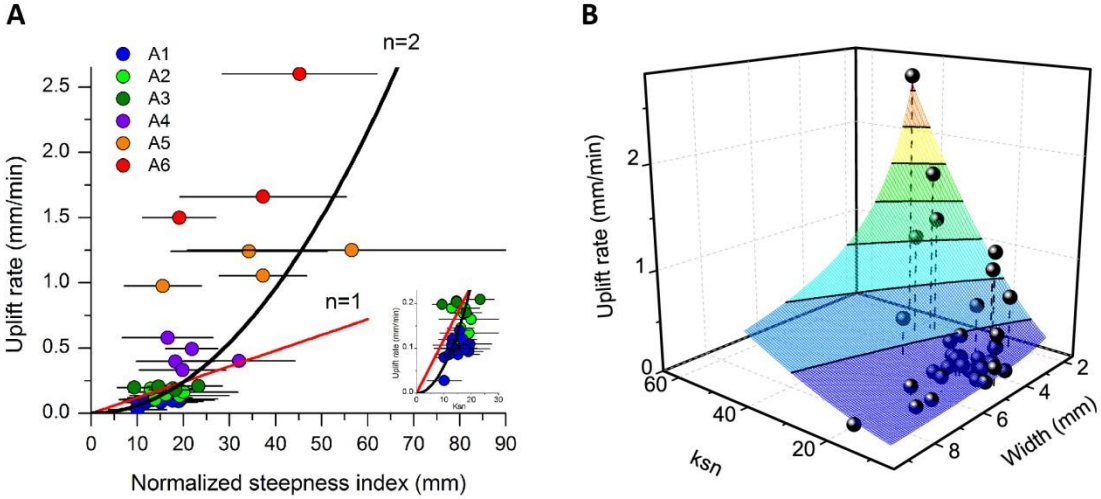


***Figure 11:****(A) Knickpoint wave celerity of the antecedent persistent channels against drainage area best fit using eq. (9): $C = \Psi_A \cdot A^{0.4}$. Error bars come from the error in measuring the amount of knickpoint propagation, typically <1*

*mm. (B) Knickpoint wave celerity as a function of drainage area and channels width, in the series of experiments ran under a precipitation rate of 9 mm/h, best fit using eq. (10):* $C = \Psi_{AW} \frac{A^{0.8}}{W}$

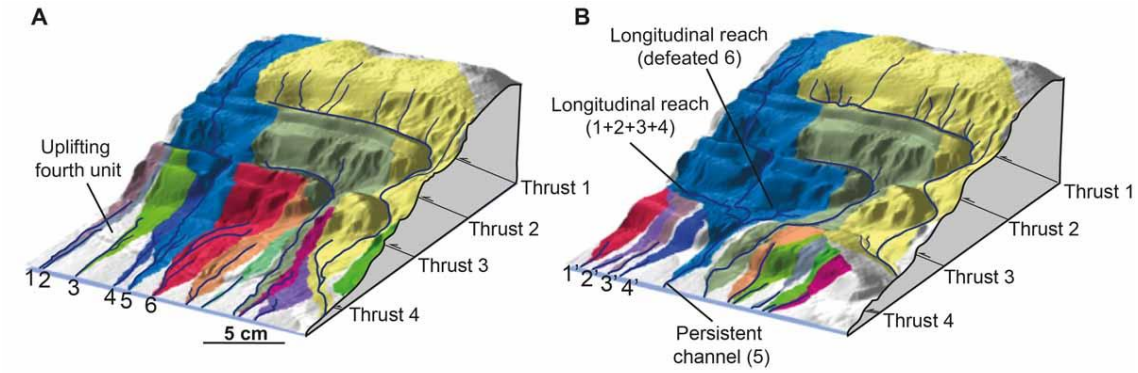


***Figure 12:*** *Drainage areas of the catchments draining the emerging thrust sheet 4 of experiment A2 (rainfall 9 mm/h) at t=232 min (A) and at t=298 min (B). The channels 1 to 6 are pre-existing transverse channels. The antecedent channel 5 managed to cut through the uplifting thrust sheet 4 (persistent channel). Channels 1', 2', 3' and 4' are the downstream parts of the small catchments 1, 2, 3 and 4 that lost their upstream drainage area by diversion above the thrust sheet the 4 (defeated channels). Their upstream drainage areas are gathered together in the longitudinal reach of channel 5 in the backlimb of the active thrust 4.*

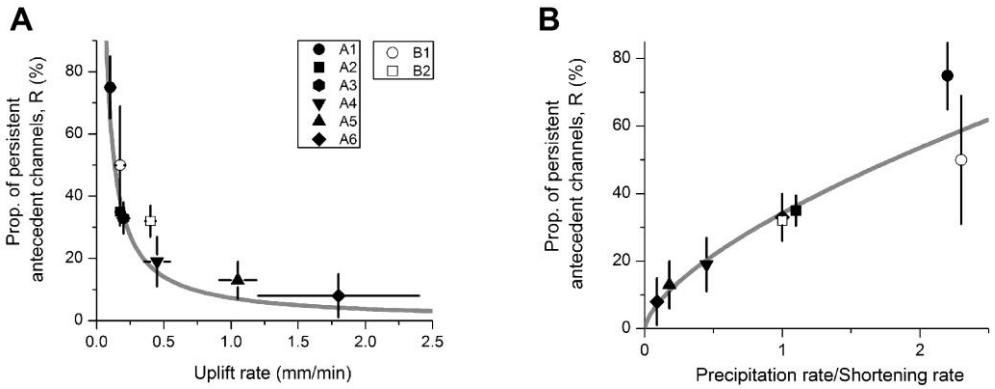


***Figure 13:*** *(A) Proportion of persistent transverse channels against uplift rates. Note the decrease of the proportion of persistent transverse channels with the increase of the uplift rate in both series of experiments run under different rainfall rates. We obtained a good fit ($R^2$=98 %) using a power law regression $R=7.3 \cdot U^{-0.95}$. (B) Proportion of persistent antecedent channels against precipitation over shortening rate (labels are the same as in (A)). We obtained a good fit ($R^2$=98 %) using a power law regression $R=35 \cdot (Prec./Short.)^{0.65}$.*

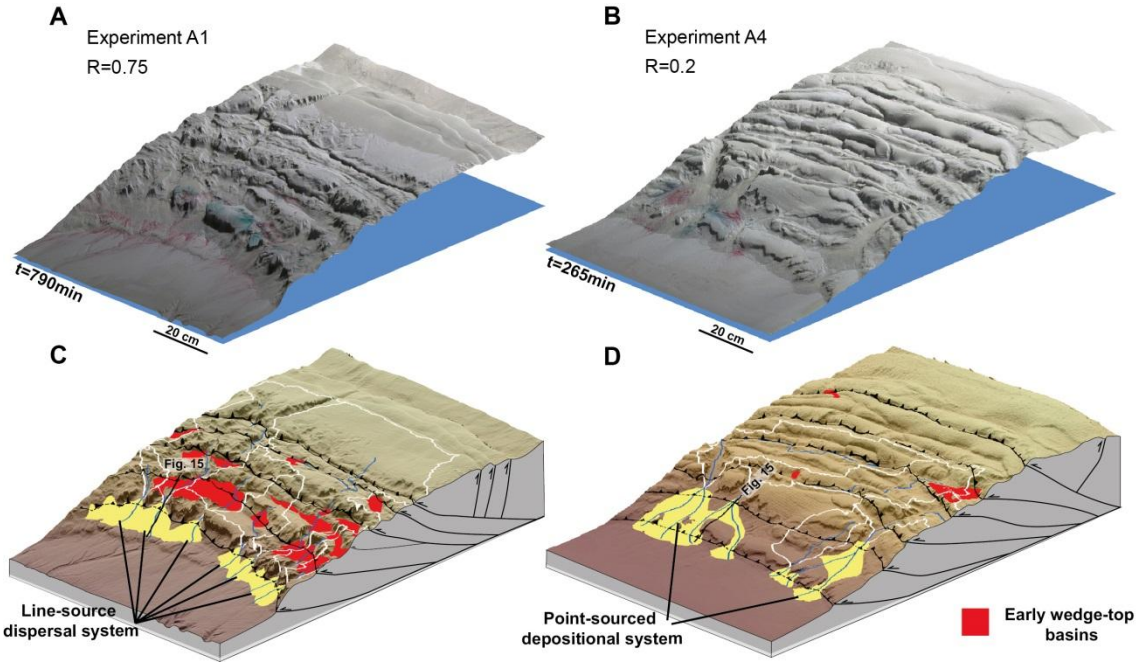


***Figure 14:*** *Patterns of sedimentation in two experiments run under low (A) and high (B) shortening rates (rainfall is 9 mm/h). (C) Experiment A1, the high proportion of persistent transverse channels (R=75%) results in a line-source dispersal system. (D) Experiment A4, the low proportion of persistent transverse channels (R=20%) results in 2 large point-sourced depositional systems plus some small fan systems.*

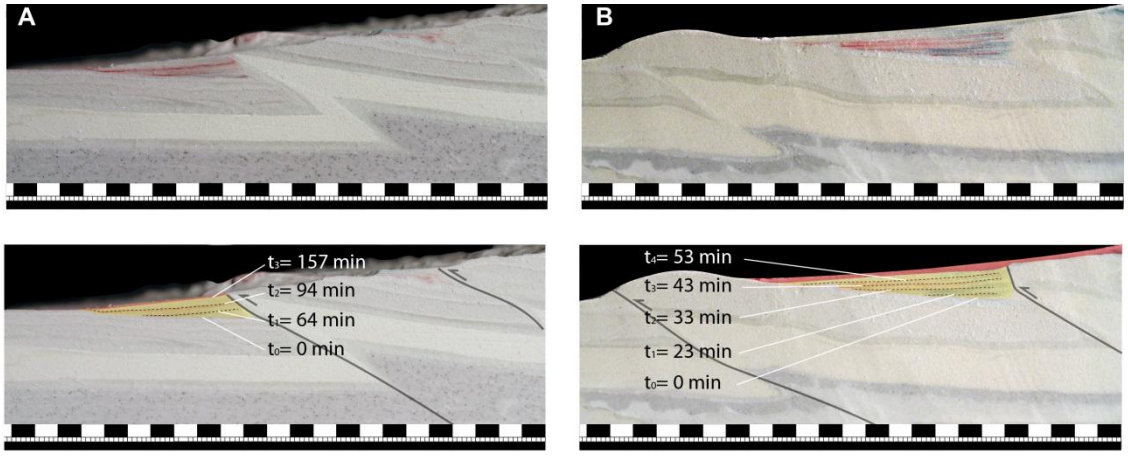


***Figure 15:*** *(A) Detail cross-section of the sedimentation zone in front of thrust 4 in the model A1. (B) Detail cross section of the sedimentation zone in front of thrust 5 in the model A4. Photos are interpreted below and the traces of the cross sections are located in figure 14. The areas of the sedimentation zones in yellow accumulated during thrust activity and the deposits in red accumulated after thrust activity. Note that the second sequence of sediments (in red) seals the inverse faults.*

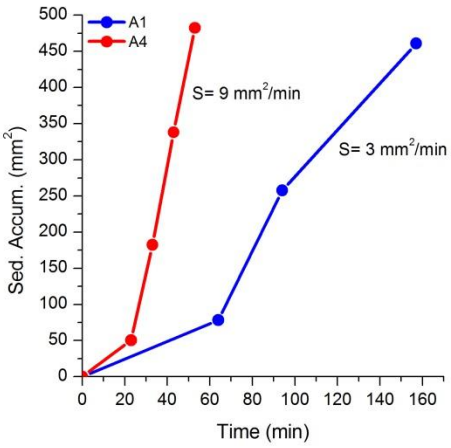


***Figure 16:*** *Mean rates of aggradation (S) calculated from the area of sedimentation measured in the cross-sections presented in figure 15.*

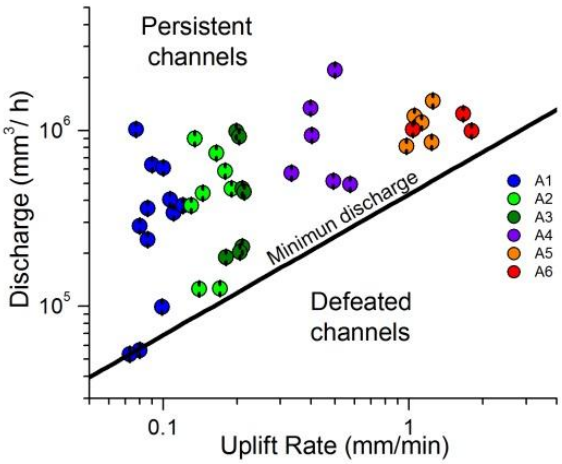


***Figure 17:*** *Discharge of persistent transverse channels against uplift rate. Note that the minimum discharge needed to overcome a new uplifting thrust sheet increases with uplift rate. This minimum discharge increases slightly exponentially with uplift rate:* $Q_w \alpha\ U^{1/m}$ *with m=0.8.*

# Drainage reorganization during mountain building in the river system of the Eastern Cordillera of the Colombian Andes

Lucía Struth[1‡], Julien Babault[1], Antonio Teixell[1]

[1] Departament de Geologia, Universitat Autònoma de Barcelona, 08193 Bellaterra (Barcelona), Spain.

+34935811035/+34935811263, Lucia.Struth@gmail.com

[‡] Corresponding author

ABSTRACT

The Eastern Cordillera of Colombia is a thick-skinned thrust-fold belt that is characterized by two topographic domains: 1) the axial zone, a high altitude plateau (the Sabana de Bogotá, 2500 m asl) with low local relief and dominated by longitudinal rivers, and 2) the Cordillera flanks, where local relief exceeds 1000 m and transverse rivers dominate. On the basis of an analysis of digital topography and river parameters combined with a review of paleodrainage data, we show that the accumulation of shortening and crustal thickening during the Andean orogeny triggered a process of fluvial reorganization in the Cordillera. Due to a progressive increase of the regional slope, the drainage network evolves from longitudinal to transverse-dominated, a process that is still active at present. This study provides the idea of progressive divide migration towards the inner part of the mountain belt, by which the area of the Sabana de Bogotá plateau is decreasing,
the flanks increase in area, and ultimately transverse rivers will probably dominate the drainage of the Cordillera.

*Keywords*: Drainage network; Fluvial capture; Drainage evolution; Eastern Cordillera of Colombia.

## 1. Introduction

In the internal, thickened and uplifting parts of the orogens, rivers are expected to follow the regional slope and flow perpendicular to the structural trend of mountain ranges, a pattern always matched by numerical models of continental-scale surface processes (e.g. Koons, 1995; Kooi and Beaumont, 1996; Willett et al., 2001; Goren et al., 2014). However, during mountain building, active folds and thrusts can deviate rivers from the regional slope (e.g. Van der Beek et al., 2002). Conceptually, the ability or not of preexisting reaches to incise uplifting structures controls the number of diversions, and by extension it determines the drainage organization, a phenomenon confirmed by modeling (Koons, 1994, 1995; Tomkin and Braun, 1999; Humphrey and Konrad, 2000; Champel, 2002; Van der Beek et al., 2002; Sobel et al., 2003). Additional factors as bedrock lithology determine spatial changes in strength and erodibility, and climate may control changes in weathering and discharge.

Babault et al. (2012) showed in the High Atlas Mountains of Morocco (a thrust-fold belt formed by tectonic inversion of a continental rift) an evolution from early fold-and-fault-controlled longitudinal rivers to a transverse-dominated drainage network during mountain building and crustal thickening in response to a progressive increase in regional slope. This may be a common transient mechanism of fluvial network evolution in mountain belts (Babault et al., 2013).

A fluvial capture implies changes in flow direction, that is, the flow/discharge of the captured drainage basin (victim) is deviated towards the neighbor captor basin with higher erosion potential, due to either higher local precipitation, erodibility and/or slope (e.g. Brookfield, 1998). Unlike models that show progressive divide migration and small-scale capture events during mountain building (Willett et al., 2001; Pelletier, 2004; Bonnet, 2009; Castelltort et al., 2012; Perron et al., 2012; Goren et al., 2014), the model of evolution from longitudinal- to transverse-dominated drainage network implies captures of large longitudinal drainages and substantial modifications of sedimentary outflux into adjacent basins, potentially influencing clastic systems and petroleum reservoirs. Captures of longitudinal rivers by transverse rivers are episodic and initially localized, whereas the

integrated long-term effect of the episodic capture events may be a major drainage reorganization as discussed in this work.

The aim of this study is to characterize the fluvial network and the drainage dynamics in the central segment of the Eastern Cordillera of the Colombian Andes, as a case for drainage reorganization. Like the High Atlas, the Eastern Cordillera of Colombia is an example of a thrust-fold belt formed by the inversion of a former continental rift, and shows similarities in the fluvial network, with a high-elevation axial area dominated by low-energy longitudinal rivers, and flanking belts of high-relief transverse valleys debouching into the forelands. By means of field observations, morphometric analysis, and a review of published palaeodrainage data, we first document that a longitudinal- to transverse-pattern of fluvial evolution also applies to the Eastern Cordillera, and then discuss a main mechanism which may have enhanced drainage reorganization (and captures), together with the potential implications for the downstream basin sediment supply.

## 2. Regional setting

### *2.1. Geological setting*

The northern Andes in Colombia are divided into three belts: the Western, the Central and the Eastern Cordilleras. While the Western and Central Cordilleras are mainly composed of crystalline rocks, including Precambrian to Paleozoic basement and Mesozoic intrusives and ophiolites, the Eastern Cordillera is an inverted continental rift constituted by a thick sequence of Mesozoic and Cenozoic sedimentary rocks (Julivert, 1970; Colleta et al., 1990; Cooper et al., 1995) (Fig. 1A).

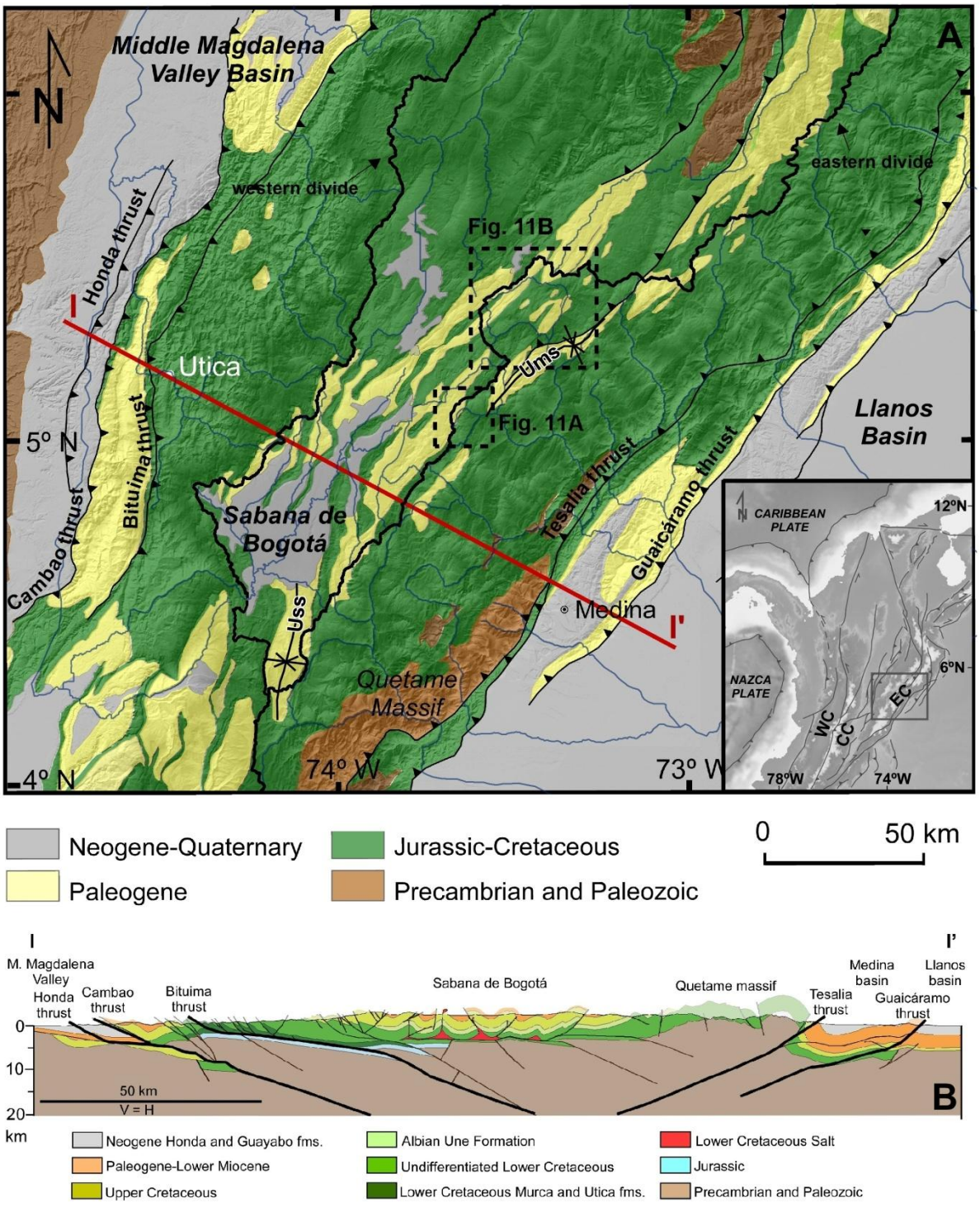


**Fig. 1.** *(A) Geological sketch map of the study area in the Eastern Cordillera of Colombia. Thick black lines represent the western and eastern drainage divides and thin blue lines correspond to the river network (modified from* Babault et al., 2013*). Inset shows a map of the northern Andes showing the location of the Eastern (EC), Central (CC) and Western (WC) Cordilleras of Colombia. (B) Structural cross section of the central part of the Eastern*

84 *Cordillera (location in Fig.1A). The main thrust faults in thick black lines are from west to*
85 *east the Honda, Cambao, Bituima, Tesalia (here including the Servitá-Lengupá and Tesalia*
86 *ss. faults) and Guaicáramo thrusts (modified from* Teixell et al., 2015*)*

87 The Eastern Cordillera is a doubly-verging thrust system (Fig.1B) with a long
88 convergence history, but whose main episode of shortening and thickening began during
89 the Miocene as a response to the accretion of the Panama arc against the western margin
90 of Colombia (Duque-Caro, 1990; Kellogg and Vega, 1995; Rolon et al., 2004; Taboada et
91 al., 2000). Many of the thrust faults observed are derived from the reactivation of former
92 extensional faults of early Cretaceous age, belonging to the main episode of rifting in a
93 back-arc tectonic setting (Cooper et al., 1995; Mora et al., 2006, 2008; Tesón et al., 2013).
94 Since the mid-late Miocene, no major fault activity is recorded in the central or axial part of
95 the orogen; the main deformation was concentrated in the flanks (Mora et al., 2008;
96 Hermeston and Nemcok, 2013; Teixell et al., 2015). Evidence for active faulting along the
97 foothill thrust system, composed by the Servitá-Lengupá, Tesalia, Guaicáramo and Yopal
98 thrusts, is provided by deformed terraces and fault scarps in Quaternary alluvial deposits
99 (Taboada et al., 2000; Mora et al., 2010; Hermeston and Nemcok, 2013; Veloza et al.,
100 2015).

101 From a topographic point of view (Fig. 2), the Eastern Cordillera can be divided into: 1) a
102 plateau area of approximately 4300 $km^2$ at high altitude (~2500 m) in the axial zone, called
103 the Sabana de Bogotá, and 2) the Cordillera flanks and foothills, where deep incisions
104 locally exceed 1000 m (e.g. middle-lower part of the Guayuriba river). The boundary
105 between the plateau and the flanks is defined by two main drainage divides.

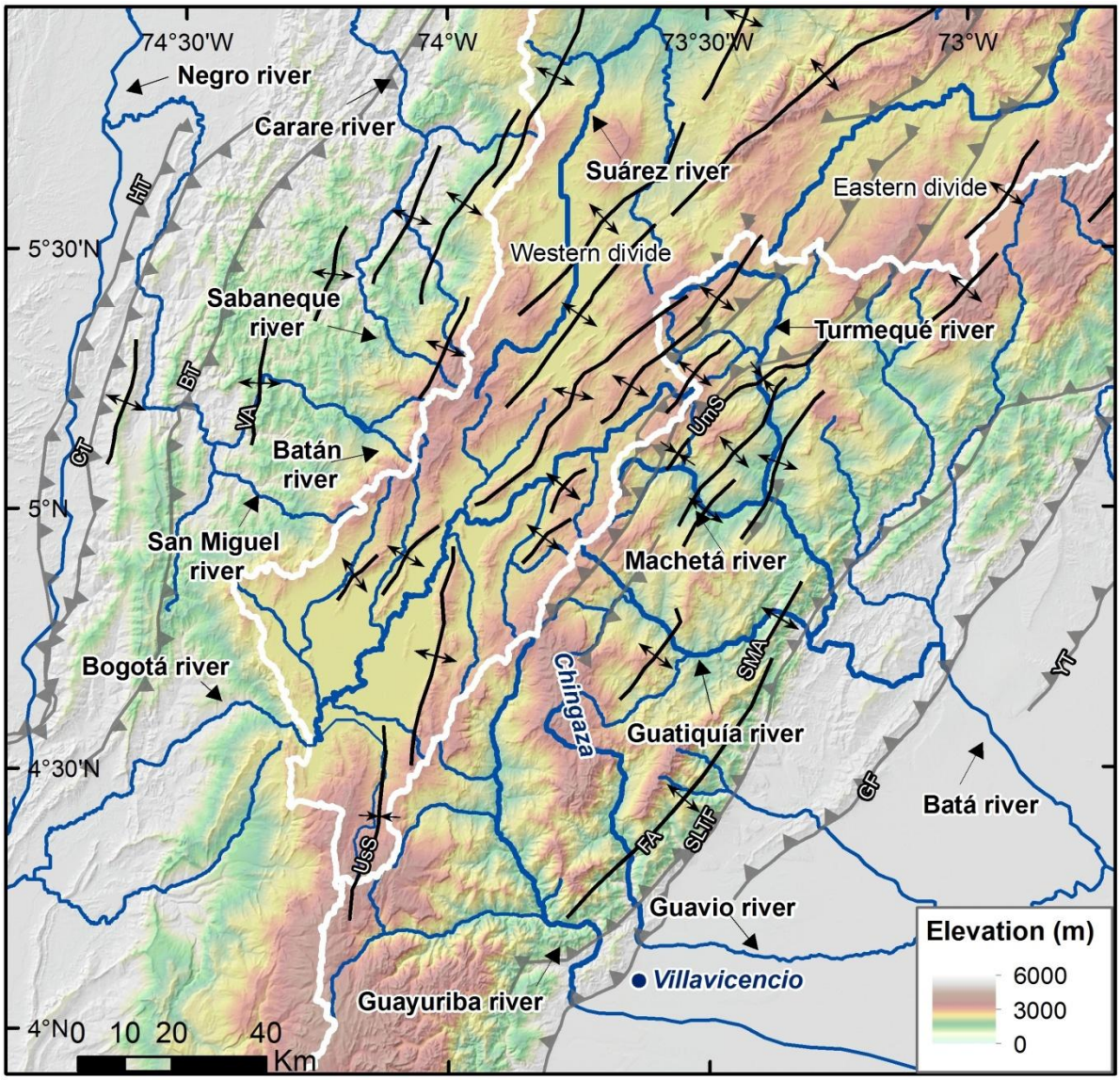


106

107 ***Fig. 2.*** *Main tectonic elements and rivers of the central part of Eastern Cordillera*
108 *superimposed over digital topography. Thick white lines represent the western and eastern*
109 *drainage divides between the axial plateau and flanks, and rivers are in blue (the main*
110 *rivers highlighted by thicker lines). Grey barbed lines represent the main thrusts, and black*
111 *lines represent the main folds. Rivers in the Sabana de Bogotá run parallel to the main folds*
112 *and rivers located in the flanks are transverse to the main tectonic structures. SLTF:*
113 *Servitá-Lengupá, Tesalia faults, GF: Guaicáramo fault; YT: Yopal thrust, FA: Farallones*
114 *anticline, SMA: Santa Maria anticline, VA: Villeta anticlinorium, BT: Bituima thrust, CT:*
115 *Cambao thrust, HT: Honda thrust, UsS: Usme syncline, UmS: Umbita syncline.*

116 The Sabana de Bogotá is dominated by Cenozoic sandstone and shale formations with
117 upper Cretaceous sandstone outcrops in anticlinal cores (Fig.1). The flanks of the Cordillera
118 are characterized by lower and upper Cretaceous sandstone and shale formations and
119 isolated Precambrian to Paleozoic basement massifs. Despite of the basement outcrops,
120 there is no overall difference in bedrock strength between the Sabana de Bogotá and the
121 flanks, as both are dominated at the surface by sandstone and shale formations. The
122 Eastern Cordillera is flanked on both sides by foreland basins dominated by Neogene and
123 Quaternary alluvial deposits that correspond to the Middle Magdalena Valley Basin in the
124 West and the Llanos Basin in the East, at elevations of ~200-300 m.a.s.l.

125 Most of the tectonic shortening of the Eastern Cordillera is concentrated in the orogen
126 flanks, especially in the eastern margin (Fig. 1B). In the eastern thrust belt, basement rocks
127 are uplifted by thick-skinned thrust faults and exposed at the surface in the rugged
128 Quetame massif (Toro et al., 2004; Mora et al., 2006, 2008). The western thrust belt does
129 not expose basement to the surface, but is still characterized by large thrust displacements
130 (Gómez et al., 2003; Restrepo-Pace et al., 2004; Cortés et al., 2006). In contrast, the
131 interior of the Eastern Cordillera is constituted by the simple fold belt of the Sabana de
132 Bogotá (Figs. 1A, B) with low, rather homogeneous structural relief and without major
133 thrusting (e.g. Julivert, 1963; Mora et al., 2008; Teixell et al., 2015). As a whole, the Eastern
134 Cordillera was mostly uplifted by the major thrusts on the mountain flanks of the belt (Fig.
135 1B).

136 The amount of orogenic shortening in the Cordillera is still in debate and depends on the
137 mode of thrusting adopted and on the role of the pre-orogenic extensional faults. Values of
138 150-200 km (up to 50%) of shortening have been calculated in thin-skinned models (e.g.
139 Dengo and Covey, 1993; Roeder and Chamberlain, 1995), whereas smaller values of 70-
140 100 km (25-30%) are reported in thick-skinned models (e.g. Colletta et al., 1990; Cooper et
141 al., 1995; Tesón et al., 2013; Teixell et al., 2015).

## 2.2. *Fluvial drainage in the Eastern Cordillera*

Rivers in the Sabana de Bogotá run approximately NNE-SSW, parallel to fold axes, and preferentially located in synclines (Fig. 2). Synclinal valleys are wide and flat, and ridges in between correspond to anticline cores (Fig.3A). The main river draining the plateau is the Bogotá River, which ultimately incises into the western flank and drains to the Magdalena river. The Bogotá River when draining in the plateau approximately lengths 220 km, and its tributaries flow to the SSW, parallel to the structural trend (Fig.2). Rivers in the Sabana typically show a general meandering pattern (Fig.3C), gentle slopes and low runoff velocity, in accordance with the smooth topography.

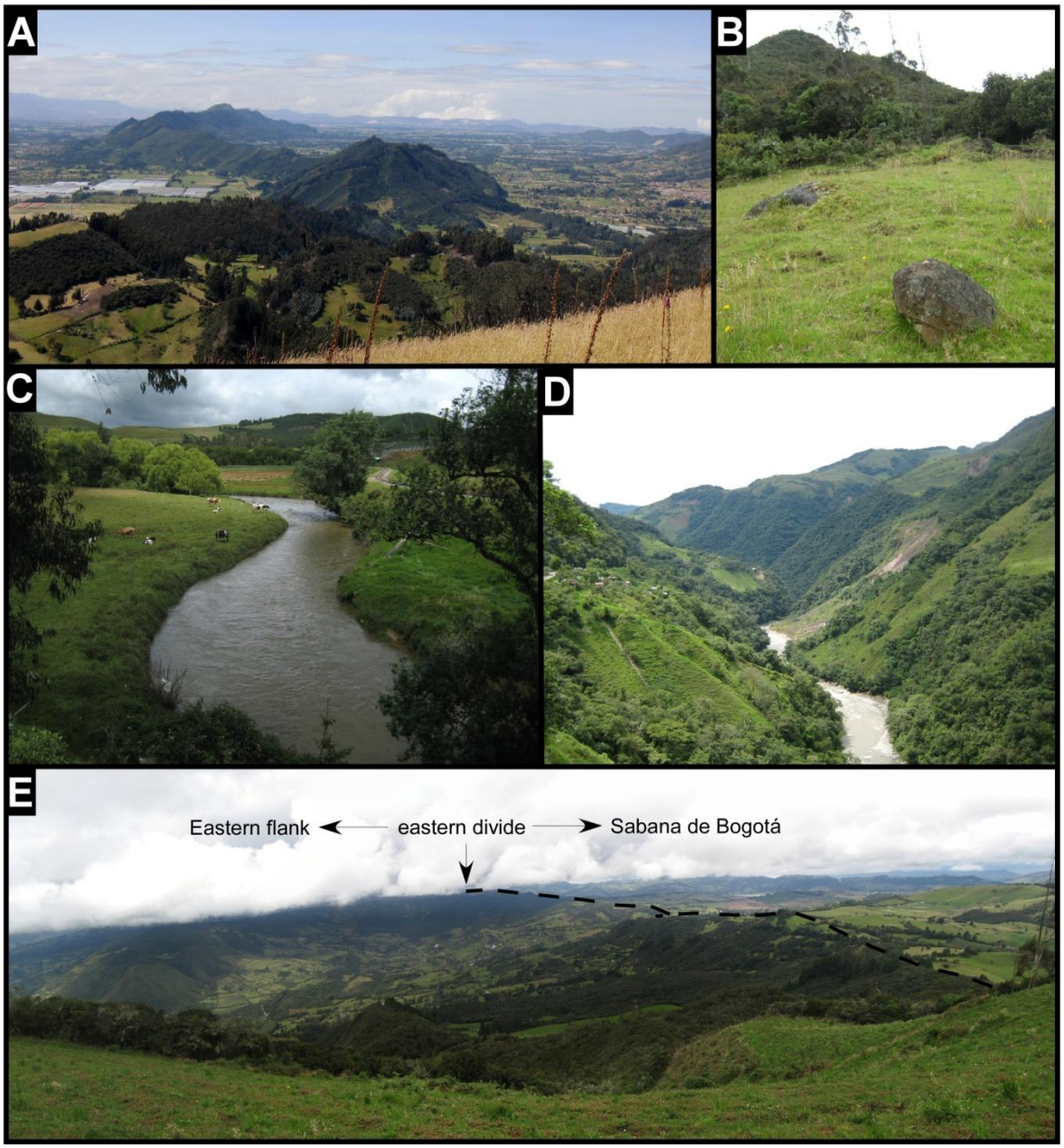


***Fig. 3.*** *(A) Field photograph of the Sabana de Bogotá showing the sandstone anticlinal ridge of the Chía range (middle) and low slopes in adjacent synclinal areas. (B) Rock boulders product of a rockfall located on the eastern divide of the Cordillera, in the Machetá river capture zone (location in Fig. 9). (C) View of the longitudinal river Bogotá flowing in the plateau. (D) View of the transverse river Guayuriba in the eastern flank of the Cordillera with greater slopes and local relief, and common landslides in the hillslopes linked to the high slope angles. (E) Field image of the two topographic domains of the Eastern*

*Cordillera: the Sabana de Bogotá and the upstream part of the Machetá transverse river in the eastern flank (field of view 4 km, view to the south).*

In the eastern flank of the Cordillera the main rivers from south to north are Guayuriba (Fig. 3D), Guatiquía, Guavio and Batá rivers, draining to the Orinoco River in the Llanos basin. These rivers range between 70-170 km long in the flank and flow perpendicular to the structural grain, i.e. transverse to the trend of the Eastern Cordillera.

In the western flank of the Eastern Cordillera the main rivers are the Río Negro and Minero-Carare draining to the Magdalena River at the Middle Magdalena Valley (108±46 m of elevation in this region). These rivers are 150 and 110 km long respectively, and flow mainly in an E-W direction, transverse to the general trend of the Cordillera and perpendicular to the main tectonic structures (Fig. 2). However, they also show sharp changes in flow direction with longitudinal reaches separated by transverse reaches in the medium and lower part of the western flank, displaying a gridiron-like drainage organization which is common in fold-and-thrust belts (e.g. Gupta, 1997).

### 2.2.1. Paleogene drainage in the Eastern Cordillera from paleocurrent data

Paleocurrent and sediment provenance data of the early Cenozoic deposits of the Eastern Cordillera indicate a western and southwestern sediment source, and a drainage network controlled by emerging folds and thrust sheets following a regional slope to the NNE (Laverde et al., 1989; Cooper et al., 1995; Diaz and Serrano, 2001; Gómez et al., 2005a; Bayona et al., 2008; Horton et al., 2010; Nie et al., 2010, Saylor et al., 2011; Bande et al., 2012; Nie et al., 2012; Caballero et al., 2013; Silva et al., 2013).

In Paleocene-Early Eocene times, there was an longitudinal drainage pattern (Fig.4), parallel to the structural grain (Brown et al., 1991; Gómez et al., 2005b, 2005c; Bayona, 2008; Bayona et al., 2008; Saylor et al., 2011; Mora et al., 2013; Silva et al., 2013). Paleocene fluvial sediments in the Sabana de Bogotá region record paleocurrents to the NNE (Laverde et al., 1989; Bayona, 2008; Bayona et al., 2008; Saylor et al., 2011).

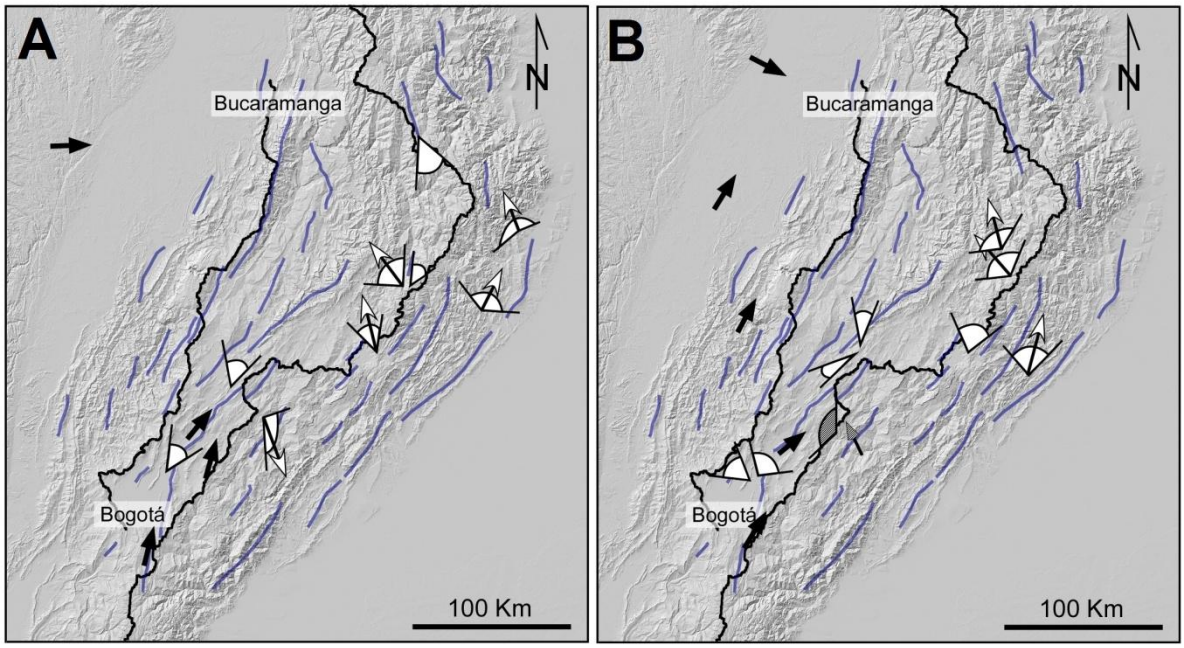


***Fig. 4.*** Summary of paleocurrent data from Paleocene (A) to Eocene (B) in the Eastern Cordillera compiled from Gómez et al. (2005b) (black arrows); Bayona et al. (2008) (white arrows) and Bayona (2008) (line filled arrows).

The Late Eocene-Oligocene still records a mean northward drainage in the current Sabana de Bogotá area and in the Magdalena Valley (Diaz and Serrano, 2001; Gómez et al., 2005a; Silva et al., 2013). In the late Oligocene-mid Miocene interval important changes occurred in the Middle Magdalena Valley Basin (MMVB): due to deformation in the northern part of the basin, the base level start to rise and forced rivers to divert toward the Llanos Basin across the Eastern Cordillera (Gómez et al., 2005a,b). During the late mid and late Miocene, the MMVB paleodrainage returned to the north in relation with continued rising of the Cordillera. In the eastern foreland of the Cordillera, a transverse, eastward paleocurrent direction is observed in the entire Miocene succession (Parra et al., 2010).

## ***2.3.*** *Summary of climate features*

Climate can be a major control on the evolution of drainage network (e.g. Schumm, 1979; Bull, 1991; Whitfield and Harvey, 2012). A mean annual precipitation map (Fig.5) was

compiled for the years 1998-2009 using TRMM data (Bookhagen and Strecker, 2008) following the methodology of Bookhagen and Burbank (2010).

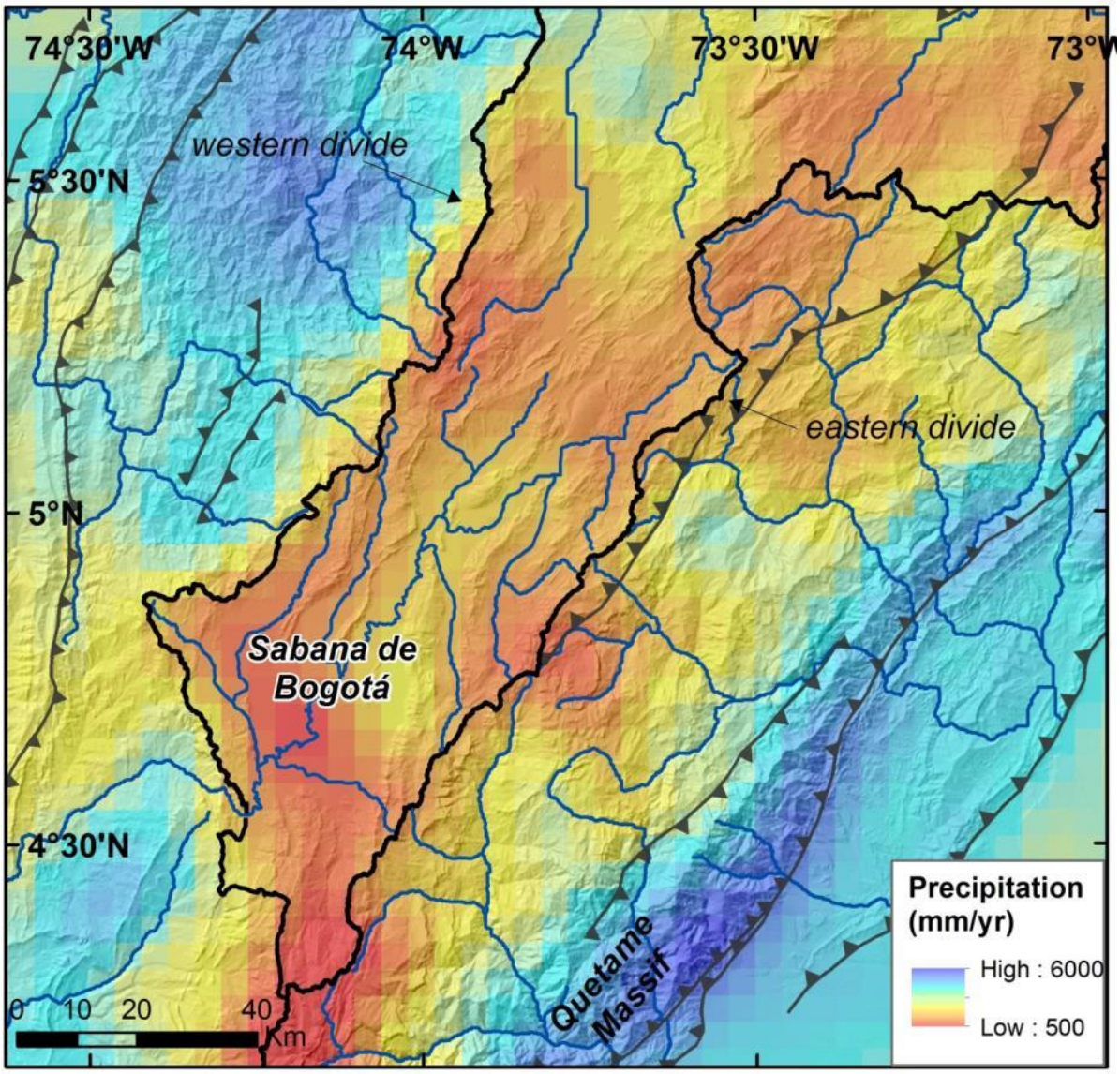


***Fig. 5.*** *Precipitation map of the Eastern Cordillera of Colombia compiled for the years 1998-2009 (after* Bookhagen and Strecker, 2008*).*

The map shows a strong gradient of precipitation in the vicinity of the western divide, by which rainfall increases markedly in the western flank of the Cordillera. In contrast, a similar gradient is not observed across the eastern divide, as the distribution of annual precipitation is approximately homogeneous in the plateau and upper eastern flank. Precipitation is higher in the eastern foothills and Quetame Massif.

In the Sabana de Bogotá there is sparse record of glaciation during the last 50 kyr, at altitudes higher than 3500 m (Helmens, 1988, 1990; Helmens and Kuhry, 1995; Helmens et al., 1997). On the basis of moraine deposits, glaciers are described as a very small and poorly developed valley glaciers or ice caps, ranging from 0.5 to 8 $km^2$, and were deglaciated at ca. 12.5 ka (Helmens, 2004). U-shaped valley forms have never been reported (Mark and Helmens, 2005).

## ***2.4.*** *Summary of the deformation and uplift history of the Eastern Cordillera*

During the late Cretaceous and the early Tertiary, the Eastern Cordillera was the foreland basin system of the Central Cordillera (Cooper et al., 1995; Gómez et al., 2005a). Progressive growth of the Eastern Cordillera structures since the late Maastrichtian or early Paleogene disrupted and compartmentalized the foreland basin, and ultimately subdivided it into the Magdalena Valley and the Llanos basins (Gómez et al., 2003; Parra et al., 2009; Horton et al., 2010; Mora et al., 2013).

Based on subsidence and exhumation analysis (Parra et al., 2009a, 2009b; Mora et al., 2010) and detrital sediment provenance (Horton et al., 2010), the main emergence of the major thrust faults in the flanks of the Eastern Cordillera started during late Oligocene to early Miocene times. The disappearance of Meso-Cenozoic detrital zircons (which indicate a Central Cordillera provenance) in the eastern foothills (Horton et al., 2010), indicates that the Eastern Cordillera had already become an effective topographic barrier that separated the Central Cordillera from the Llanos basin by the mid-late Miocene. This is marked by a contemporaneous conglomeratic influx of the Honda and Guayabo formations (upper Miocene to Pliocene) into the Middle Magdalena Valley and Llanos basins (Hoorn et al., 1995; Gómez et al., 2003; Parra et al., 2009a).

After a sedimentary hiatus that comprises most of the Oligocene and Miocene, the Sabana de Bogotá accumulated ca. 600 m of fluvio-lacustrine deposits (Tilatá and Sabana formations, Julivert, 1963; Andriessen et al., 1993; Torres et al., 2005), which partially filled

synclinal depressions and contributed to smooth the relief of the plateau as we see it today. In spite of this, Van der Hammen et al. (1973) and Hooghiemstra et al. (2006) inferred low altitudes for the Sabana until the late Miocene and a rapid surface uplift of 1500 ± 500 m between 6 and 3 Ma ago, based on the palynological content of the late Neogene deposits using the nearest living relatives method. However, these data may not be reliable enough because Gregory-Wodzicki (2000) reported errors in paleoaltimetry estimates for the Andes of ±1500 m, implying that the proposed paleoelevation changes of the Sabana de Bogotá may not be accurately resolved by the nearest living relatives method. For this reason, a continuous crustal thickening and surface uplift since the onset of mountain building is not discarded (Babault et al 2013), as shortening was accumulating in a progressive way (e.g., Moreno et al., 2013; Teixell et al., 2015) and explains the current high elevation of the Eastern Cordillera.

## 3. Digital topographic analysis

Comparison of the paleodrainage data summarized above and the present-day fluvial network of the Eastern Cordillera of Colombia suggests that drainage has experienced a process of reorganization over geologic time. We undertook an analysis of the spatial distribution of the local and mean slopes, of the drainage network organization, and of the longitudinal profiles of the main rivers of the Cordillera with the aim of characterizing the river dynamics and the signal of reorganization in the current network. According to Bishop (1995), drainage rearrangement in mountain belts can be produced by beheading during progressive divide migration and by discrete events of capture, which are mechanisms of drainage expansion that result from headward erosion (Fig.6A) The beheading process results in the non-preservation of early drainages, and thus capture elbows (sharp changes in the river channel direction) and wind gaps (dry valleys with fluvial deposits) in the divide are not preserved. However, low-elevation zones (anomalous depressions) in the topographic profile of a divide may be the topographic expression of the migration of a divide originally located at the crest and later reaching the bottom of an adjacent valley, as

reproduced in numerical models (e.g. Willett et al., 2001). Stream capture (piracy) can be identified by distinctive geomorphic features (e.g. Fig.6B). These include the preservation of the early lines of the drainage network, elbows and knickpoints (Small, 1978; Bishop, 1995). Elbows and knickpoints cannot be used separately as diagnostic for captures because changes in rock uplift and river diversion may also produce them. Other features potentially indicating capture events are hanging depressions (wind gaps) or discrete jumps (or reentrants) of a drainage divide, but they are seldom preserved in rapidly eroding settings like active orogenic belts (e.g. Clark et al., 2004; Prince et al., 2011; Brocard et al., 2012). Wind gaps correspond to segments of captured rivers where water does no longer flow, and show a width that is impossible to relate with the actual basin drainage area upstream (suggesting that they were created in past times with larger drainage areas). Stratigraphic evidence for captures include abandoned river terrace tracts and the existence of fluvial sediments with larger grain size than the current channel can transport or with lithologies linked to source areas that are now disconnected from the basin.

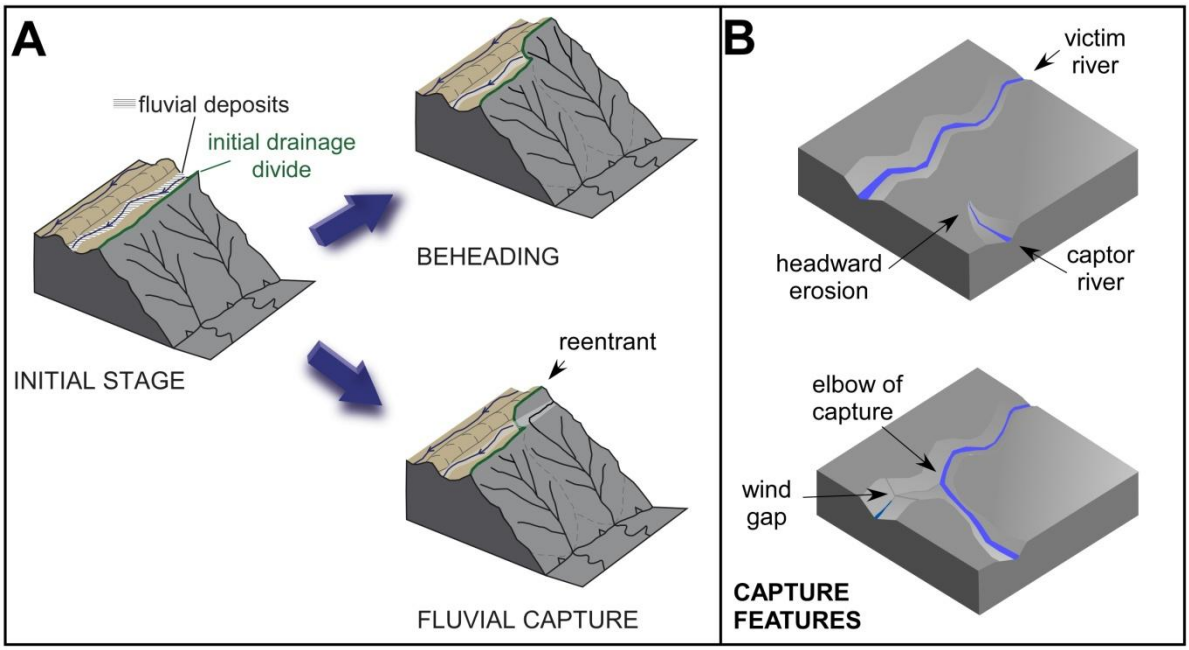


***Fig.6.*** *(A) Diagram showing the process of beheading and fluvial capture from the same initial stage. (B) Fluvial capture processes preserve the initial drainage lines and produce elbows and fluvial deposits in the divide (wind gap). These features do not occur in beheading.*

## *3.1. Methods*

In this study we analyzed the topography in the search of geomorphologic evidence for divide migration and captures as previously mentioned. Beheading and stream captures occur if disequilibrium of erosion exists between two catchments. We highlighted potential disequilibrium of erosion by quantifying morphological differences between the axial plateau of the Sabana de Bogotá and the steep Cordillera flanks between latitudes 5º30'N and 4º10'N (Fig.2). We used the 90 m resolution digital elevation model (DEM) SRTM90v4 (Jarvis et al., 2008) in the analysis. However, in areas where the fluvial channel is narrow (<90 m), the SRTM90 DEM leads to overestimated elevations in gorges, providing wrong data for river parameter extraction. Such errors were corrected using elevations from Instituto Geográfico Agustín Codazzi (IGAC) 1:100,000 topographic maps and then modifying the raster elevation matrix (DEM) pixel by pixel. Morphometric analysis and calculation of the geomorphologic parameters described in the following sections was carried out by using the D8 flow routine (eight-flow direction matrix, O'Callaghan and Mark, 1984; Tarboton, 1997; Mudd et al., 2014).

We compared the current drainage network geometry with the regional slope obtained by calculating the local slopes of the mean elevations. The mean elevations have been calculated with a moving window of 30 km of diameter. We compared the frequencies of elevations, the local slopes and the channel slopes between the plateau and the western and eastern flanks of the Cordillera to highlight their topographic difference. In the supplementary data we provide longitudinal river profiles of the main rivers draining the Sabana de Bogotá and the Cordillera flanks.

River erosion depends at least on bedrock erodibility, water flow and slope (e.g. Howard and Kerby, 1983). Analysis of slope-area relationships is often used to reveal spatial trends of erosion and/or rock uplift in channel networks by the mean of the channel steepness index or Ksn (e.g. Kirby and Whipple, 2001; Kirby, 2003; Snyder et al., 2003; Wobus et al., 2006; DiBiase et al., 2010). However, scatters in local slope data in regions of noisy and low-resolution DEM such as the Eastern Cordillera prevent accurate estimates of

normalized channel steepnesses. Therefore, for the measurement of the normalized channel slopes we preferred an alternative methodology, the $\chi$ (chi) gradient (Mx) approach, where the river profile elevation (instead of the slope data) is the dependent variable which is plotted against the integral of the drainage area ($\chi$) as the independent variable, giving more accurate results (Perron and Royden, 2013; Mudd et al., 2014). The value of the channel slope in chi-elevation space (Mx) depends on the concavity, and we determined the best concavity with AICc-collinearity tests and chi-plots following the method developed by Mudd et al. (2014). Assuming that rock uplift is balanced by erosion (steady-state condition), and that uplift, erosion and erodibility are constant in time and space, the stream power theory predicts that river profile will have a linear chi plot and Mx is proportional to erosion rates (Royden and Perron, 2013; Mudd et al., 2014). However, transient states where uplift rates change spatially or temporally can lead to piecewise (stepped) channel profiles. In this case, we used the collinearity test to identify the concavity (m/n ratio) for each river basin that best collapses the tributaries in chi-plots (Mudd et al., 2014).

We generated topographic elevation profiles of the eastern and western main divides, and we calculated their mean elevation using an adjacent-averaging smoothing method (over 900 km and 550 km distance for the eastern and western divide respectively). Smoothing with the adjacent-averaging method calculates the average of elevations around each point and replaces the actual elevation of the point with the average value. The location of the divide depressions (low-elevation segments) was compared with the geometry and characteristics of the current drainage network. A fluvial capture leaves depressed zones or gaps in the drainage divide where water does not actually flow (wind gaps). These depressed zones can have fluvial sediments relict of the old fluvial drainage network.

### ***3.2.*** *Analysis and Results*

338 The differentiation between the topographic domains of the Eastern Cordillera is evidenced
339 by the results of the morphometric analysis. A first differentiation is based on
340 hypsometric and slope frequency curves (Fig.7). The plateau region shows a high
341 frequency in elevation around 2500 m, corresponding to the average elevation of the
342 Sabana plains (Fig.7B and D). This region is also characterized by a high frequency (21%)
343 of slopes of less than 3° and secondary maxima close to 8º (14%) (Fig. 7C). On the other
344 hand, the flanks of the Cordillera show a wider range of elevation. The eastern flank shows
345 the highest frequency values close to 2300 m, whereas in the western flank they are close
346 to 1300 m. The Cordillera flanks also show a higher local relief, with local slopes greater
347 than 10º. Greater local slope values (>30º) are located in the external parts of the flanks
348 coinciding with the frontal fold-thrust structures (Servitá, Lengupá and Tesalia faults and
349 Farallones anticline in the eastern flank, Bituima fault and Villeta anticlinorium in the
350 western flank; Fig.2).

351 The Sabana de Bogotá plateau shows a short range of elevation, giving a high frequency in
352 2500 m. The Cordillera flanks are characterized by a wider range of elevation values.

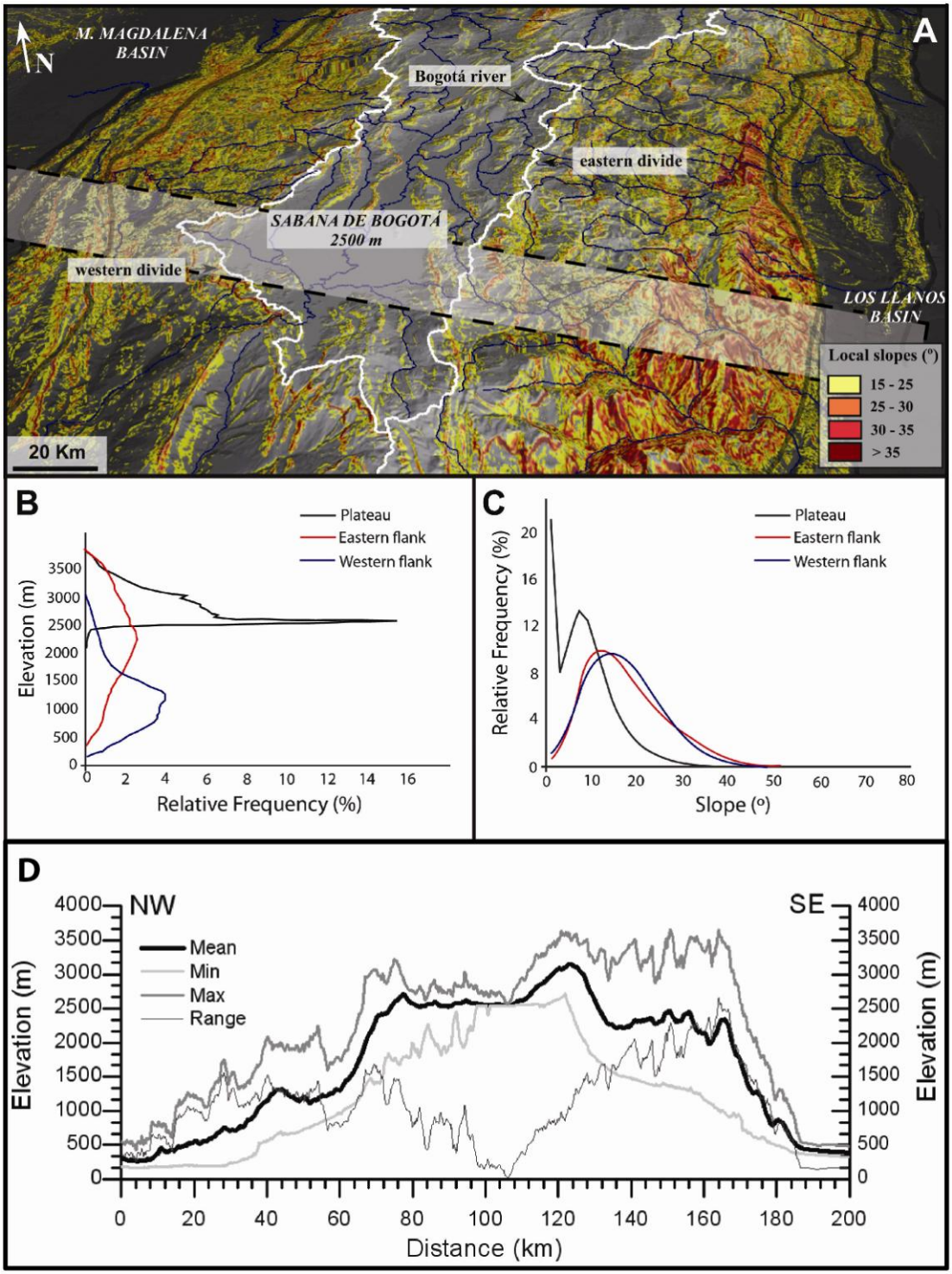


353

354 ***Fig. 7.*** *(A) Oblique view of the Eastern Cordillera indicating local slopes (in colors). The*
355 *transparent white band indicates the location of the 30 km swath used for the elevation*
356 *profiles in D. (B) Plot of the relative frequency of elevations that characterize each*
357 *topographic domain defined for the Eastern Cordillera. (C) Plot of relative frequency of*
358 *slopes in each domain. (D) Orogen-transverse topographic profiles of the Eastern Cordillera*

*along the swath indicated in A, including maximum, minimum and mean elevations and the elevation range (difference between maximum and minimum).*

The contrast between the plateau and the eastern flank is illustrated in Fig. 8, where we plot the long profile of the Guayuriba River in the eastern flank and the profile of the Siecha-Bogotá River in the plateau, including the projections of lateral divides and local relief for each one. The plateau area, represented in Fig. 8 by the Siecha-Bogotá river, is characterized by a low-elevation lateral divide and a very low local relief (500 m maximum). In contrast, the Guayuriba basin, in the eastern flank, is characterized by a higher-elevation lateral divide, as well as by a greater local relief (up to 2750 m).

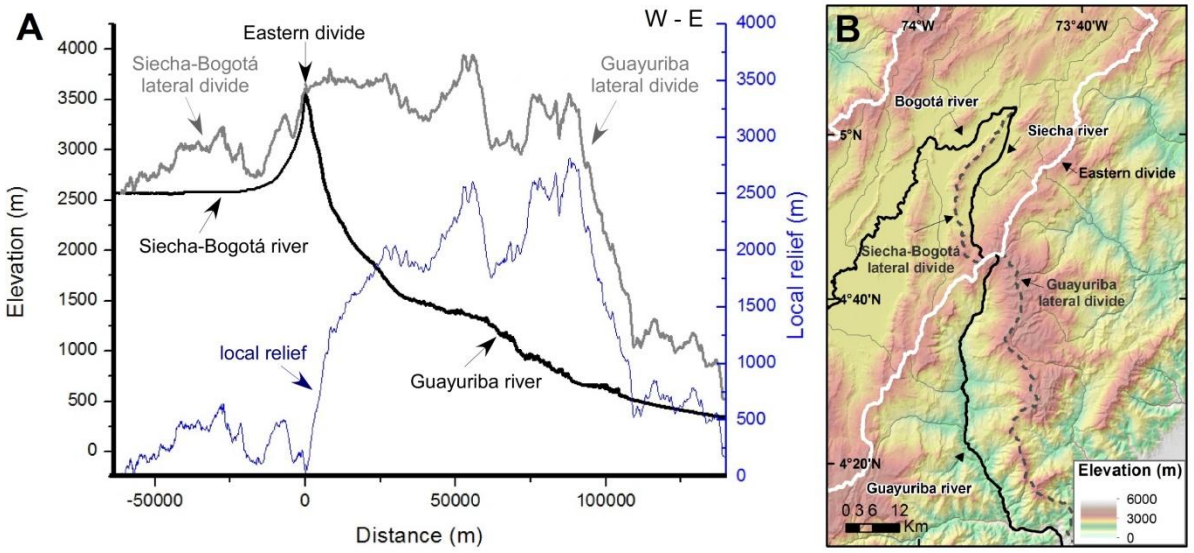


***Fig. 8.*** *(A) Longitudinal profiles of the Siecha-Bogotá (Sabana de Bogotá plateau) and Guayuriba (eastern flank) Rivers, compared with a projection of their lateral divides and the local relief (difference between maximum and minimum elevations) between rivers and divide ridges. (B) Location map of the rivers and divides shown in A.*

Mean regional slopes in the Eastern Cordillera illustrate that the Sabana de Bogotá plateau is characterized by a very low mean regional slope of 1º (Fig.9) and rivers follow the main structures longitudinally. Rivers in the eastern flank follow the regional slope, that is, to the east. The eastern flank shows greater mean slope values than the plateau, which

becomes greatest in the lower part of the flank (mean values of 2.5º and, 4.5º respectively) (Fig. 9). The western flank shows high values of regional slope (mean value of 4.5º), immediately west of the western divide where the main rivers are also transverse.

Significant variations in channel slope (expressed by Mx, the slope in chi-elevation plots) are not only observed between the Sabana and the flanks. Relevant variations in channel slope occur either along the same river or between different rivers in each domain (see supplementary data, SD1). The Mx values were calculated in function of the best concavity for all the basins analyzed. We found a 0.45 concavity as the best value based on the AICc-collinearity test and chi-plots (see supplementary data, SD2 and SD3).

The map distribution of the Mx index of major rivers (Fig. 9) shows generally low values (Mx=0-3) in the plateau area, coinciding with the lower regional slope and consistently with the results of digital analysis of local slopes and with field observations: rivers in the plateau show a meandering morphology (Fig.3C) as well as lower slope and runoff velocity than those in the flanks (Fig.3D). The eastern flank shows Mx average values between 5-12, with peaks of 20-27. The greatest values are located in areas of recent tectonic uplift (e.g. Farallones and Santa Maria anticlines in the eastern flank; Mora et al., 2008), or in rivers with a drastic slope increase where they leave high-elevation, low-relief upstream areas like the Chingaza region (see Fig.2). Mx values in the higher parts of the western flank (bordering the divide), where rivers are transverse, range around 5-12, and the Mx values decrease in the lower part of the flank where rivers are longitudinal (Mx=1-4).

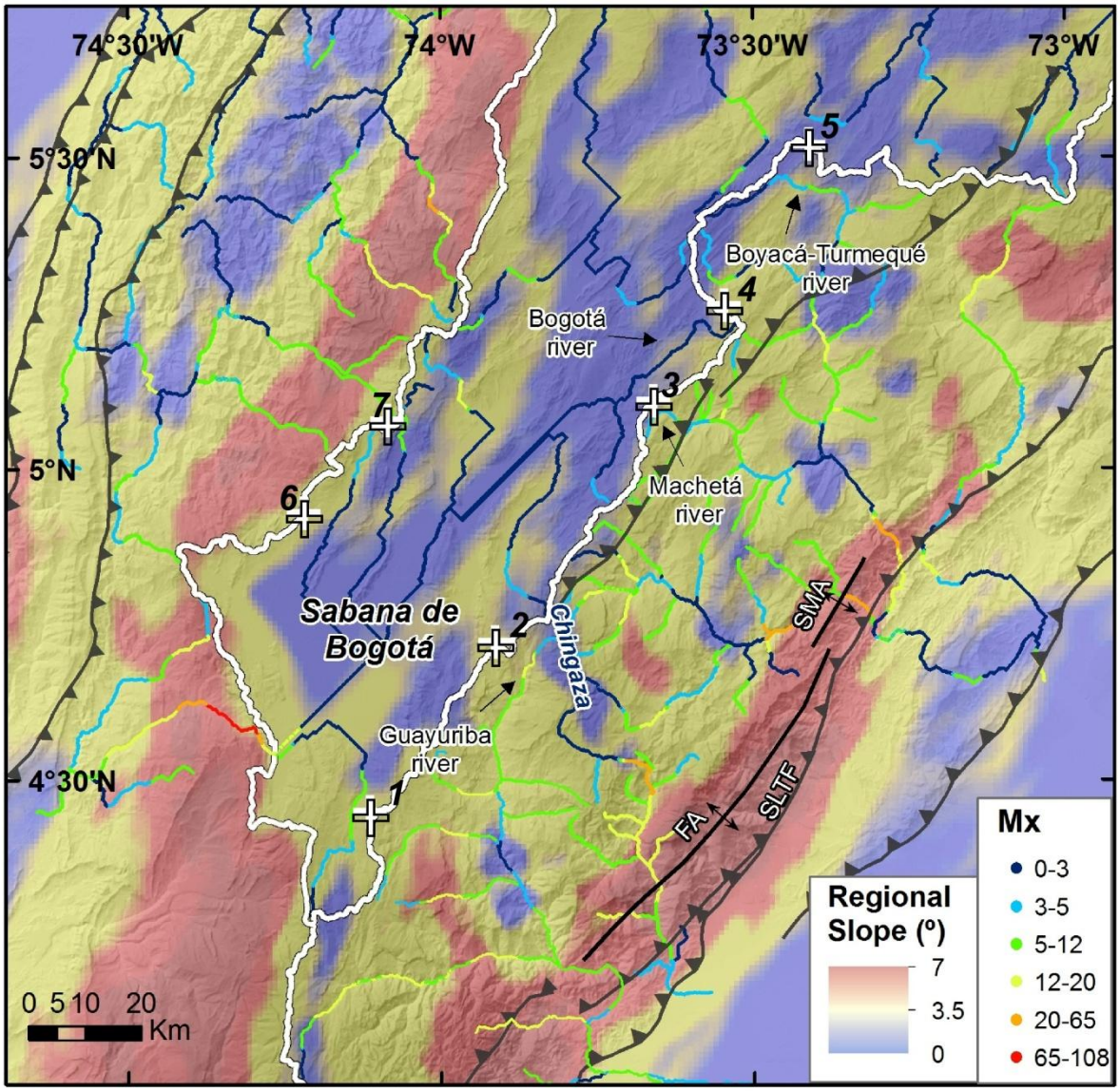


397

398 ***Fig. 9.*** *Map of Mx (slope in chi-elevation plots) values for the analyzed rivers and regional*
399 *slope (º) calculated with a mobile window of 30 km of diameter. The eastern and western*
400 *divides are indicated by white lines. Note low Mx values in the Sabana de Bogotá and high*
401 *values in the flanks of the Cordillera. Depressions in the divide ridges are indicated by white*
402 *crosses and labeled with numbers from 1 to 7 (see text for discussion). FA: Farallones*
403 *anticline, SMA: Santa Maria anticline, SLTF: Servitá-Lengupá-Tesalia fault.*

404 Topographic profiles of the two drainage divides separating the axial plateau of the
405 Sabana de Bogotá from the eastern and western flanks (Fig. 10) show a series of
406 depressions (low-elevation segments in the divide) several hundreds m deep below the

407 average elevation of the divide ridges. Depressions usually coincide with reentrants of the
408 divide trace into the plateau (Fig. 9 and Fig. 10), i.e. segments of the divide that diverge
409 from the main orientation and project towards the axial plateau of the orogen.

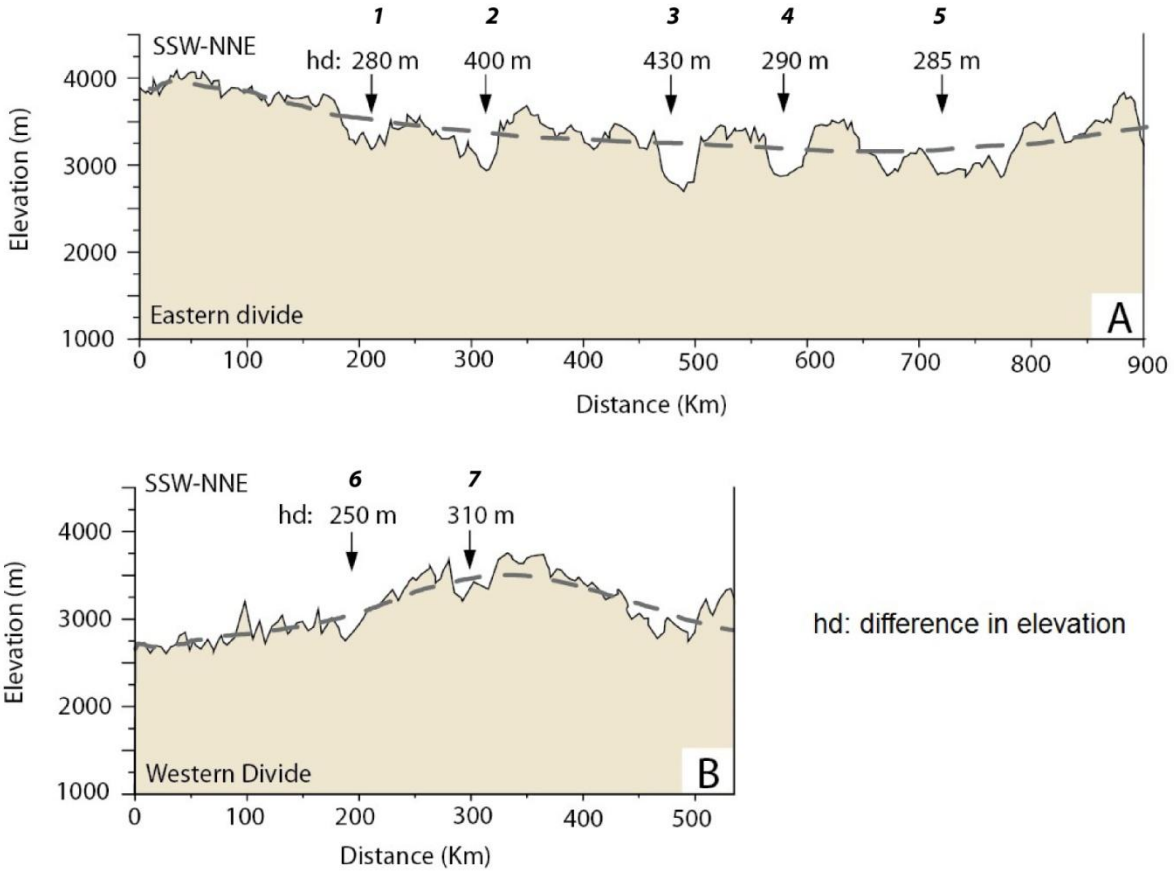


410

411 ***Fig. 10.*** *Profiles of the eastern (A) and western (B) drainage divides that bound the Sabana*
412 *de Bogotá plateau showing the location of depressions (numbers in italic refer to Fig.9).*
413 *Additionally, we indicate the difference in elevation between the lower part of the divide*
414 *(depressed area) and the mean elevation of the divide (dashed line).*

415 An illustrative example of a divide depression is observed between the Machetá and
416 Bogotá Rivers (see Fig. 2 for location). In the headwater of the east-flowing Machetá River
417 the elevation low in the divide (2700 m) rises only 50 m above the longitudinal river in the
418 Sabana (2750 m) (Fig. 11A). Local slopes are higher to the east of the divide (15°) than to
419 the west in the plateau (5°) (Fig.3E). Further north, the depression in the eastern divide
420 between the Boyacá-Turmequé and Bogotá Rivers is only 80 m above the later (Fig. 11B).

421 As in the case of Machetá River, local slopes are higher to the east (20º) than in the plateau
422 (10º). In addition, the Mx of rivers is higher in the flanks than in the plateau (Fig.9), in
423 agreement with the distribution of local slopes. The depressions are associated with elbow
424 geometries with knickpoints in the downstream part of the longitudinal reach in the flank
425 rivers, and we do not observe spatial correlations with the trace of active faults nor with
426 easily erodible bedrock lithologies (Fig. 11C and D). Neither these areas correspond to
427 zones of fold plunge (which could in principle provide low resistance to incision and favor
428 capture localization). This lack of correlation between divide depressions or re-entrants and
429 tectonic structures or specific lithologies is observed all along the eastern and western
430 divides of the Eastern Cordillera.

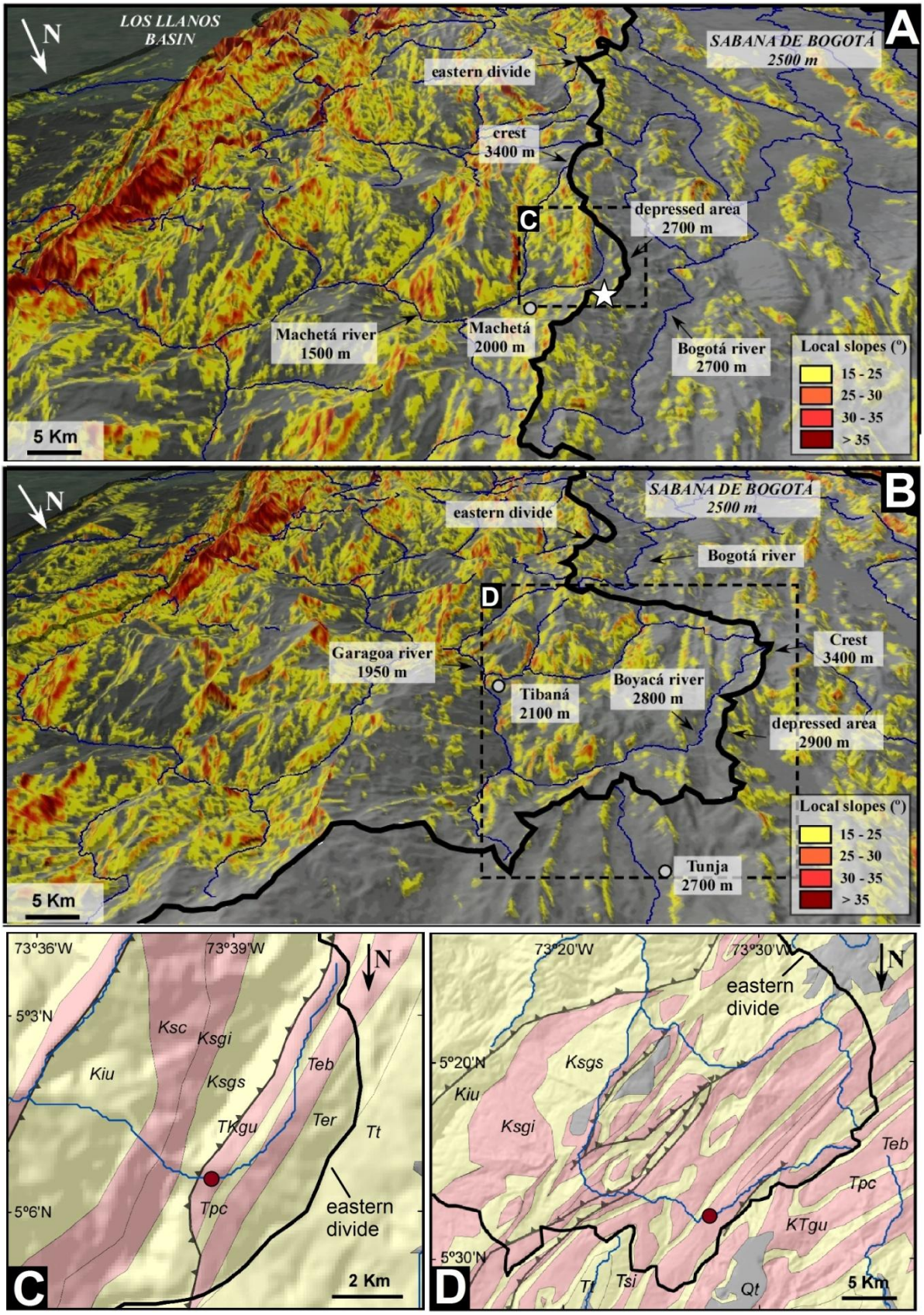


***Fig. 11.*** *Local slope and lithology distribution at the Eastern Cordillera of Colombia. Note that they are oriented with North to the bottom of the page for a better appreciation of the*

*topography and drainage. (A) Oblique view showing local slopes in the Eastern Cordillera. A reentrant in the divide associated to a depressed area is indicated in Fig. 9 and 10, testifying processes of fluvial capture with a difference in elevation of 430 m between the mean altitude of the divide and the bottom of the depression. The occurrence of rounded rockfall deposits (Fig.3B) is marked by a white star (see text for discussion). (B) Oblique view indicating local slopes in the plateau and in the upstream part of the Boyacá-Turmequé transverse river. The reentrant area is indicated in Fig. 9 and corresponds to a depression in the elevation profile of the divide (see Fig. 10), with a difference in elevation of 285 and 290 m. (C and D) Lithologic maps of the depressed divide in A and B, respectively, showing no lithologic or tectonic control on the divide depression and on its trace. Red polygons are shale formations and yellow polygons sandstone formations. The red circle shows the location of a knickpoint. Cretaceous and Tertiary sandstone formations: Kiu (Une Fm), Ksgs (Guadalupe Superior Fm), Tpc (Cacho Fm), Ter (Regadera Fm), Tt (Tilatá Fm), Tsi (Socha inferior Fm). Cretaceous and Tertiary shale formations: Ksc (Chipaque Fm), Ksgi (Guadalupe Inferior Fm), KTgu (Guaduas Fm), Teb (Bogotá Fm) (modified from Toro et al., 2004; Parra et al., 2009b, Mora et al., 2010 and unpublished maps by ICP-Ecopetrol).*

### ***3.3.*** *River capture and evidence for drainage divide migration*

At present, the main rivers flowing in the Sabana de Bogotá plateau are longitudinal and follow synclines constituted by Cenozoic strata, mostly terrestrial in origin. In the Cordillera flanks, the main rivers are transverse to the chain and they are deeply incised across Cretaceous and Paleogene folded series. As summarized above, during Paleocene-Oligocene times the drainage network was controlled by the emerging folds and thrusts and followed a gentle regional slope to the NNE (Gómez et al., 2005a, Silva et al., 2013).

Incised transverse rivers that cut across the Paleogene folded series in the eastern flank evidence a strong contrast between the current flow drainage organization and the paleodrainage deduced from the Paleogene strata. The northern flow direction from

palaeocurrent data in these Paleogene series are now incised by an eastern transverse flow. This is the case of the Tertiary Umbita and Usme synclines (Fig.1). The Usme syncline, with a N-S orientation parallel to the mean trend of the orogen, records an Oligocene paleoflow in the same direction. Nevertheless, part of this syncline has been captured by a river of the eastern flank and now drains to the east, which indicates a migration of the main eastern divide toward the inner part of the Cordillera (the plateau) after the Oligocene. The Umbita syncline records a western flow in Paleocene times (see location in Fig.1 and Fig.4). This syncline is actually in the eastern flank and dominated by a transverse drainage flowing to the east (Fig.11A and C). Paleogene strata are not preserved in the western flank of the Cordillera, and this line of evidence cannot be applied.

Captures usually leave gaps/depressions in drainage divides (e.g. Bishop, 1995). The topographic profiles of the main divides of the Eastern Cordillera show low-elevation tracts (Fig. 9 and 10). These depressed tracts coincide with map-view reentrants of the divide trace toward the plateau, suggesting a drainage area transfer from the plateau to the Cordillera flanks, as explained above. In addition, elbows with knickpoints at or above the elbow can be observed in these areas (see Fig. 11C, D), and the channel slope map (Mx values) (Fig. 9) also illustrates a strong topographic contrast across the main divides separating the Sabana plateau from its flanks. On the other hand, rounded rockfall deposits are locally found on the eastern divide into the Sabana plateau (Fig. 3B, 11A), where none of the current debris flow corridors observed in the slopes of the surrounding peaks lead to the rockfall deposit. This suggests that the missing crest that fed these boulders must have been eroded away indicating divide migration toward the plateau.

On the assumption that erosion balances the local base level fall, the Mx value relates to the ratio between erosion rate and erodibility (Royden and Perron, 2013; Mudd et al., 2014). Therefore, the high Mx values observed in the Eastern Cordillera flanks suggest greater erosion rates than in the plateau. This may have favored the progressive divide migration toward the plateau and captures of longitudinal rivers previously flowing in the

plateau by expanding transverse rivers in the flanks, thus providing an explanation for the contrast between the Eocene paleodrainage organization recorded in the Usme and Umbita synclines, and the current river network. We observe the same distribution of local slopes and channel slopes (Mx) between the western flank and the axial plateau, suggesting a similar migration in the western divide toward the centre of the Eastern Cordillera.

In summary, the depressions in the main divides, the occurrence in the flanks of knickpoints in the upstream parts of the longitudinal river profiles (e.g. Chingaza area), the existence of rock landslides with no source near the divide (Fig. 3B and 11), the observation of elbows in the rivers of the eastern flank with knickpoints upstream, and the contrast between the local slopes and the channel slopes of the main rivers support the view that the drainage network of the Eastern Cordillera reorganizes by progressive divide migration toward the inner part of the chain and by discrete events of capture. This is in agreement with the reorganization inferred from the contrast between the palaeocurrent data of the geological record and the present-day drainage network. The case of the Umbita and Usme synclines (where youngest strata are Oligocene in age), indicates that in those areas such reorganization did not start before the Miocene. As the main divides converge toward the centre of the Eastern Cordillera, and given the scarcity of Cenozoic strata in the Eastern Cordillera flanks, we cannot rule out that reorganization may have started earlier in the external parts of the eastern and western flanks.

## 4. Causes and implications of drainage reorganization

### *4.1. Mechanism causing drainage reorganization*

Our observations suggest that the drainage network in the Eastern Cordillera evolves from longitudinal-dominated to transverse-dominated, with rivers turning into the direction of the regional slope. The steep transverse rivers must have higher rates of incision than the gentle longitudinal rivers in the plateau to expand their catchment. At least four potential mechanisms that could explain differential erosion between the plateau rivers and rivers in the flanks can be considered.

First, a gradient of precipitation perpendicular to the trend of an orogen can result in divide migration towards the dry side, as has been observed in numerical models (e.g. Willett, 1999; Bonnet, 2009). Figure 5 shows the annual precipitation for the period 1998-2009 in the Eastern Cordillera, where no precipitation gradient is observed across the eastern main divide. On the basis of evidence as stable isotope geochemistry from fossil and present-day growth bands in mollusks, from palynology and from macroscopic paleoflora, Mora et al. (2008) suggested that the influence of the erosion processes by global climate change was negligible since the Pliocene in the region. The precipitation pattern appears to have remained similar at least since middle Miocene time (Mora et al., 2008 and references herein), coinciding with the early topographic growth causing the topographic asymmetry of the orogen (Mora et al., 2008). Moreover, an eastward gradient in moisture could not explain the similar contrast of morphology between the western flank and the plateau. Therefore, the reorganization of longitudinal to transverse drainage may not be attributed to an asymmetric precipitation pattern across the eastern divide.

Second, erodibility differences associated with lithological changes can explain spatial variations in erosion rates (e.g. Safran et al., 2005), and can produce local changes in the organization of drainage. In the Eastern Cordillera of Colombia, the depressions along the main divides are not located on less-resistant lithologies, and they occur indistinctly over shale or sandstone formations, from which we can conclude that the reorganization of the drainage is not controlled by lithology.

Third, in some mountain settings at mid-latitudes, different intensity of glacial erosion by valley or cirque glaciers may produce a divide migration toward the hillslopes receiving less insolation (Brocklehurst and Whipple, 2002). The Eastern Cordillera of Colombia is close to the equator so that the reorganization of drainage cannot be controlled by glacial erosion since eastern and western slopes receive the same amount of insolation. Indeed, it is unlikely that the small and poorly developed valley glaciers deduced for the Eastern Cordillera during the Quaternary (Helmens, 2004) contributed to an important difference in

542 erosion between the flanks and the plateau, especially in view of the abundant fluvial
543 geomorphologic features that point for drainage reorganization.

544 Fourth, longitudinal drainage largely coincides with areas where the regional slopes are
545 low, whereas transverse rivers are related to higher regional slopes. The marked slope
546 contrast between the flanks and the plateau appears to be the sole factor responsible for
547 the higher erosional activity on the flanks. Consequently, we propose that the
548 reorganization of the drainage network in the Eastern Cordillera is the result of increased
549 regional slope. We interpret that the regional slope increase was acquired during orogenic
550 shortening and crustal thickening of the mountain belt. The slope contrast between the axial
551 plateau and the flanks associated with orogenic building promotes fluvial capture of the
552 initial longitudinal drainage area by the transverse drainage system. The longitudinal-to-
553 transverse drainage evolution thus deduced may represent a transient stage in mountain
554 building, as previously discussed for High Atlas mountains of Morocco by Babault et al.
555 (2012, 2013). Moreover, the occurrence of precipitations in the eastern flank will enhance
556 the eastern divide migration towards the central part of the Cordillera.

557 The dynamics of drainage network described here is currently active in the Eastern
558 Cordillera, and we can expect future captures to occur in areas where steep transverse
559 rivers flow close to low-gradient longitudinal rivers located in the plateau, especially if they
560 are separated by a low-elevation stretch of the main divide. As an illustrative example, the
561 Batán river in the western flank threatens to capture the Frío river in the Plateau (zone 7 in
562 Fig. 9).

### 563 ***4.2.*** *Implications for sediment supply into the adjacent basins*

564 Changes in the sediment supply, sedimentation rate and detrital composition are often
565 considered to be caused by climatic and/or tectonic variations (e.g. Molnar and England,
566 1990; Stokes et al., 2002; Allen, 2008). Drainage reorganization can exert, alternatively, a
567 control on the sedimentation rates (e.g. Mather, 2000; Stokes et al., 2002; Prince et al.,
568 2011; Antón et al., 2012; Willett et al., 2014). Capture processes involve sudden changes in

569 the drainage areas of the captor river and of the victim river. The captor river gains drainage
570 area and therefore the erosion rate increases connecting an elevated catchment to a lower
571 base level. The remnant drainage basin, the victim, experiences an erosion rate decrease
572 as it loses headwaters and drainage area. These variations must affect the clastic fluxes at
573 the outlets, then modifying the spatial and temporal localization of the proximal clastic
574 bodies at the toe of the thrust front. Therefore, with the reorganization of the drainage
575 network in the Eastern Cordillera related to the increase of the regional slope, the
576 transverse rivers located in the flanks increased their drainage areas against the rivers
577 located in the Sabana. In this way, the erosion of the captured areas may have enhanced
578 sedimentation rates in the Llanos and Magdalena basins.

579 Previous works interpreted the distribution of maximum sediment thickness of the late
580 Oligocene to Miocene Carbonera to Guayabo formations (which are coarse-clastic foreland
581 basin deposits derived from the Eastern Cordillera) as associated with the orogenic loads
582 (Parra et al., 2009a, 2009b; Hermeston and Nemcok, 2013; Jimenez et al., 2013). We
583 propose that the migration of the orogenic load is not the only mechanism to explain
584 sedimentation rate increases, coarse-clastic inputs and depocenter migration in the basins
585 adjacent to the Eastern Cordillera. The process of fluvial drainage reorganization in the
586 source areas of the mountain belt may have exerted an additional control.

587

588 ## 5. Conclusions

589 The Eastern Cordillera of Colombia presents a clear differentiation into two topographic
590 domains: an axial plateau dominated by gentle longitudinal rivers, with low local relief and
591 local slopes, and the flanks with high local relief and slope dominated by steep transverse
592 rivers. These domains are separated by two main drainage divides in the eastern and
593 western sides of the Sabana de Bogotá plateau.

594 In the eastern flank of the Cordillera the change in flow direction between the Paleogene
595 palaeodrainage towards the NNE, parallel to the early tectonic structures, and the current

drainage toward the SE, incising across folded Paleogene strata near the eastern divide, argues for drainage reorganization. This work highlights the convenience of morphological analysis to characterize a drainage reorganization and supports models of evolution of relief in mountain belts. Morphometric analysis and field observations show depressions and map-view reentrants in the main divides, debris flow deposits with no source near the divide, elbows with knickpoints upstream, and an evident contrast of the local and river slopes across the divides. This evidence indicates that the drainage network reorganizes by progressive divide migration toward the inner part of the chain by discrete events of capture.

We interpret that fluvial reorganization from longitudinal to transverse-dominated drainage in the Eastern Cordillera was triggered by the increase of the orogen regional slope by the progressive accumulation of crustal shortening and thickening. This pattern of drainage evolution is comparable to the drainage evolution described in other orogenic belts as the Moroccan High Atlas. The evolution from longitudinal to transverse drainage in the Eastern Cordillera of Colombia may lead to a progressive area reduction and eventually a disappearance of the high plateau of the Sabana de Bogotá.

## Acknowledgments

This work was financed by Spanish MINECO project CGL2010-15416. L. Struth was supported by a FPI PhD grant (BES-2011-050262) from MECD (Spain). We acknowledge Andrés Mora, Andrés Valencia, Eliseo Tesón and Maria Luisa Arboleya for assistance and discussion during field work. Logistic support was generously provided by the ICP-Ecopetrol. We thank the three reviewers of the manuscript for incisive and instructive comments which helped to significally improve the original text and figures. .

## References

622 Allen, P. A. ,2008. From landscapes into geological history. Nature, 451, 274–276.
623 http://doi.org/10.1038/nature06586

624 Andriessen, P. A. M., Helmens, K. F., Hooghiemstra, H., Riezebos, P. A., Van der Hammen, T. ,1993.
625 Absolute chronology of the Pliocene-Quaternary sediment sequence of the Bogota area,
626 Colombia. Quaternary Science Reviews, 12, 483–501. http://doi.org/10.1016/0277-
627 3791(93)90066-U

628 Antón, L., Rodés, A., De Vicente, G., Pallàs, R., Garcia-Castellanos, D., Stuart, F. M. Braucher, R.,
629 Bourlès, D. ,2012. Quantification of fluvial incision in the Duero Basin (NW Iberia) from
630 longitudinal profile analysis and terrestrial cosmogenic nuclide concentrations.
631 Geomorphology, 165-166, 50–61. http://doi.org/10.1016/j.geomorph.2011.12.036

632 Babault, J., Teixell, A., Struth, L., Driessche, J. Van Den, Arboleya, M., Tesón, E. ,2013. Shortening,
633 structural relief and drainage evolution in inverted rifts: insights from the Atlas Mountains,
634 the Eastern Cordillera of Colombia and the Pyrenees. Geological Society of London, Special
635 Publications, 377, 141–158. http://doi.org/10.1144/SP377.14

636 Babault, J., Van Den Driessche, J., Teixell, A. ,2012. Longitudinal to transverse drainage network
637 evolution in the High Atlas (Morocco): The role of tectonics. Tectonics, 31.
638 http://doi.org/10.1029/2011TC003015

639 Bande, A., Horton, B. K., Ramírez, J. C., Mora, A., Parra, M., Stockli, D. F. ,2012. Clastic deposition,
640 provenance, and sequence of Andean thrusting in the frontal Eastern Cordillera and Llanos
641 foreland basin of Colombia. Bulletin of the Geological Society of America, 124, 59–76.
642 http://doi.org/10.1130/B30412.1

643 Bayona, G. ,2008. Geocronología, termocronología, bioestratigrafía y procedencia de unidades
644 paleógenas en la zona axial de la Cordillera Oriental; Aportes al modelamiento del sistema
645 petrolífero en las cuencas adyacentes. ICP-Ecopetrol report.

646 Bayona, G., Cortés, M., Jaramillo, C., Ojeda, G., Aristizabal, J. J., Reyes-Harker, A. ,2008. An
647 integrated analysis of an orogen-sedimentary basin pair: Latest Cretaceous-Cenozoic
648 evolution of the linked Eastern Cordillera orogen and the Llanos foreland basin of Colombia.
649 Bulletin of the Geological Society of America, 120, 1171–1197.
650 http://doi.org/10.1130/B26187.1

651 Bishop, P. ,1995. Drainage rearrangement by river capture, beheading and diversion. Progress in
652 Physical Geography, 19, 449–473. http://doi.org/10.1177/030913339501900402

653 Bonnet, S. ,2009. Shrinking and splitting of drainage basins in orogenic landscapes from the
654 migration of the main drainage divide. Nature Geoscience, 2, 766–771.
655 http://doi.org/10.1038/ngeo666

656 Bookhagen, B., Burbank, D. W. ,2010. Toward a complete Himalayan hydrological budget:
657 Spatiotemporal distribution of snowmelt and rainfall and their impact on river discharge.
658 Journal of Geophysical Research: Earth Surface, 115, 1–25.
659 http://doi.org/10.1029/2009JF001426

660 Bookhagen, B., Strecker, M. R. ,2008. Orographic barriers, high-resolution TRMM rainfall, and relief
661 variations along the eastern Andes. Geophysical Research Letters, 35, 1–6.
662 http://doi.org/10.1029/2007GL032011

663 Brocard, G., Willenbring, J., Suski, B., Audra, P., Authemayou, C., Cosenza-Muralles, B., Moran-Ical,
664 S., Demory, F., Rochette, P., Vennemann, T., Holliger, K., Teyssier, C. ,2012. Rate and
665 processes of river network rearrangement during incipient faulting: The case of the Cahabon
666 River, Guatemala. American Journal of Science, 312, 449–507.
667 http://doi.org/10.2475/05.2012.01

668 Brocklehurst, S. H., Whipple, K. X. ,2002. Glacial erosion and relief production in the Eastern Sierra
669 Nevada, California. Geomorphology, 42, 1–24. http://doi.org/10.1016/S0169-555X(01)00069-
670 1

671 Brookfield, M. E. ,1998. Evolution of the great river systems of southern Asia during the Cenozoic
672 India-Asia collision: Rivers draining southwards. Geomorphology, 22, 285–312.
673 http://doi.org/10.1016/j.geomorph.2008.01.003

674 Brown, E. T., Edmond, J. M., Raisbeck, G. M., Yiou, F., Kurz, M. D., Brook, E. J. ,1991. Examination of
675 surface exposure ages of Antarctic moraines using in situ produced 10Be and 26Al.
676 Geochimica et Cosmochimica Acta. http://doi.org/10.1016/0016-7037(91)90103-C

677 Bull, W. B. ,1991. Geomorphic Responses to Climatic Change. Oxford University Press: New York.

678 Caballero, V., Mora, A., Quintero, I., Blanco, V., Parra, M., Rojas, L. E., Lopez, C., Sanchez, N.,
679 Horton, B.K. Stockli, S., Duddy, I. ,2013. Tectonic controls on sedimentation in an
680 intermontane hinterland basin adjacent to inversion structures: the Nuevo Mundo syncline,
681 Middle Magdalena Valley, Colombia. Geological Society, London, Special Publications, 377,
682 315–342. http://doi.org/10.1144/SP377.12

683 Castelltort, S., Goren, L., Willett, S. D., Champagnac, J.D., Herman, F., Braun, J. ,2012. River
684 drainage patterns in the New Zealand Alps primarily controlled by plate tectonic strain.
685 Nature Geoscience, 5, 744–748. http://doi.org/10.1038/ngeo1582

686 Champel, B. ,2002. Growth and lateral propagation of fault-related folds in the Siwaliks of western
687 Nepal: Rates, mechanisms, and geomorphic signature. Journal of Geophysical Research, 107.
688 http://doi.org/10.1029/2001JB000578

689 Clark, M. K., Schoenbohm, L. M., Royden, L. H., Whipple, K. X., Burchfiel, B. C., Zhang, X., Tang, W.,
690 Wang, E., Chen, L. ,2004. Surface uplift, tectonics, and erosion of eastern Tibet from large-
691 scale drainage patterns. Tectonics, 23, TX1006. doi:10.1029/2002TC001402

692 Colletta, B., Hebrard, F., Letouzey, J., Werner, P., Rudkiewicz, J.R. ,1990. Tectonic style and crustal
693 structure of the Eastern Cordillera (Colombia) from a balanced cross-section. Petroleum and
694 Tectonics in Mobile Belts, 81–100.

695 Cooper, M. a, Addison, F. T., Alvares, R., Hayward, A B., Howe, S., Pulham, A J., Taborda, A. ,1995.
696 Basin development and tectonic history of the Llanos basin, Colombia. Petroleum Basins of
697 South America. AAPG. Memoir No. 62, 10, 659–666.

698 Cortés, M., Colletta, B., Angelier, J. ,2006. Structure and tectonics of the central segment of the
699 Eastern Cordillera of Colombia. Journal of South American Earth Sciences, 21, 437–465.
700 http://doi.org/10.1016/j.jsames.2006.07.004

701 Dengo, C. A., Covey, M. C. ,1993. Structure of the Eastern Cordillera of Colombia: Implications for
702 trap styles and regional tectonics. American Association of Petroleum Geologists Bulletin, 77,
703 1315–1337.

704 Diaz, L., Serrano, M. ,2001. Observaciones sobre el Terciario del Piedemonte. Reporte Presentado a
705 Occidental de Colombia Por Ariana Ltda.

706 Dibiase, R. A., Whipple, K. X., Heimsath, A. M., Ouimet, W. B. ,2010. Landscape form and millennial
707 erosion rates in the San Gabriel Mountains , CA. Earth and Planetary Science Letters, 289,
708 134–144. http://doi.org/10.1016/j.epsl.2009.10.036

709 Duque-Caro, H. ,1990. Neogene stratigraphy, paleoceanography and paleobiogeography in
710 northwest South America and the evolution of the Panama Seaway. Palae, 77, 203–234.

711 Gómez, E., Jordan, T. E., Allmendinger, R. W., Cardozo, N. ,2005a. Development of the Colombian
712 foreland-basin system as a consequence of diachronous exhumation of the northern Andes.
713 Geological Society of America Bulletin, 117, 1272. http://doi.org/10.1130/B25456.1

714 Gómez, E., Jordan, T. E., Allmendinger, R. W., Cardozo, N. ,2005b. Development of the Colombian
715 foreland-basin system as a consequence of diachronous exhumation of the northern Andes.
716 Bulletin of the Geological Society of America, 117, 1272–1292.
717 http://doi.org/10.1130/B25456.1

718 Gómez, E., Jordan, T. E., Allmendinger, R. W., Hegarty, K., Kelley, S. ,2005c. Syntectonic Cenozoic
719 sedimentation in the northern middle Magdalena Valley Basin of Colombia and implications
720 for exhumation of the Northern Andes. Bulletin of the Geological Society of America, 117,
721 547–569. http://doi.org/10.1130/B25454.1

722 Gómez, E., Jordan, T. E., Allmendinger, R. W., Hegarty, K., Kelley, S., Heizler, M. ,2003. Controls on
723 architecture of the Late Cretaceous to Cenozoic southern Middle Magdalena Valley Basin,
724 Colombia. GSA Bulletin, 131–147. http://doi.org/10.1130/0016-
725 7606(2003)115<0131:COAOTL>2.0.CO;2

726 Goren, L., Fox, M., Willett, S. D. ,2014. Tectonics from fluvial topography using formal linear
727 inversion: Theory and applications to the Inyo Mountains, California. Journal of Geophysical
728 Research: Earth Surface, n/a–n/a. http://doi.org/10.1002/2014JF003079

729 Gregory-Wodzicki, K. M. ,2000. Uplift history of the Central and Northern Andes: A review.
730 Geological Society of America Bulletin, 112, 1091–1105. http://doi.org/10.1130/0016-
731 7606(2000)112<1091:uhotca>2.0.co;2

732 Gupta, S. ,1997. Himalayan drainage patterns and the origin of fluvial megafans in the Ganges
733 foreland basin. Geology, 25, 11–14.

734 Helmens, K.F., 2004. The Quaternary glacial record of the Colombian Andes. In: Ehlers, J; Gibbard P
735 L (eds), Quaternary Glaciations-extent and chronology, Part III: South America, Asia, Africa,
736 Australasia, Antarctica. Developments in Quaternary Science, 2c, 115–134.

737 Helmens, K.F., Rutter, N.W., Kuhry, P., 1997. Glacier fluctuations in the eastern Andes of Colombia
738 (South America) during the past 45,000 radiocarbon years. Quaternary International 38-9,
739 39–48.

740 Helmens, K.F., Kuhry, P., 1995. Glacier fluctuations and vegetation change associated with Late
741 Quaternary climatic oscillations in the area of Bogotá, Colombia. Quat. South America
742 Antarctica Peninsula, 9, 117–140.

743 Helmens, K.F., 1990. Neogene-Quaternary Geology in the high plain of Bogotá, Eastern Cordillera,
744 Colombia (stratigraphy, paleoenvironments and landscape evolution). Dissertas Botanicae,
745 163, pp 202.

746 Helmens, K.F., 1988. Late Pleistocene glacial sequence in the area of the high plain of Bogotá
747 (Eastern Cordillera, Colombia). Palaeogeogr. Palaeoclimatol. Palaeoecol. 67, 263–283.

748 Hermeston, S., Nemcok, M. ,2013. Thick-skin orogen-foreland interactions and their controlling
749 factors, Northern Andes of Colombia. Geological Society, London, Special Publications, 377,
750 443–471. http://doi.org/10.1144/SP377.16

751 Hooghiemstra, H., Wijninga, V. M., Cleef, A. M. ,2006. The paleobotanical record of Colombia:
752 implications for biogeography and biodiversity. Annals of Missouri Botanical Garden, 93,
753 297–325.

754 Hoorn, C., Guerrero, J., Sarmiento, G.A., Lorente, M. A. ,1995. Andean tectonics as a cause for
755 changing drainage patterns in Miocene northern South America. Geology, 23, 237–240.
756 http://doi.org/10.1130/0091-7613(1995)023<0237:ATAACF>2.3.CO;2

757 Horton, B. K., Saylor, J. E., Nie, J., Mora, A., Parra, M., Reyes-Harker, A., Stockli, D. F. ,2010. Linking
758 sedimentation in the northern Andes to basement configuration, Mesozoic extension, and
759 Cenozoic shortening: Evidence from detrital zircon U-Pb ages, Eastern Cordillera, Colombia.
760 Bulletin of the Geological Society of America, 122, 1423–1442.
761 http://doi.org/10.1130/B30118.1

762 Howard, A.D., Kerby, G., 1983. Channel changes in badlands. Geological Society of America Bulletin,
763 94, 739-752.

764 Humphrey, N. F., Konrad, S. K. ,2000. River incision or diversion in response to bedrock uplift.
765 Geology, 28, 43–46. http://doi.org/10.1130/0091-7613(2000)028<0043:RIODIR>2.3.CO;2

766 Jarvis, A., Reuter, H. I., Nelson, A., Guevara, E. ,2008. Hole-filled SRTM for the globe. Version 4.
767 http://srtm.csi.cgiar.org.

768 Jimenez, L., Mora, A., Casallas, W., Silva, A., Teson, E., Tamara, J., Namson, J., Higuera-Diaz, I.C.,
769 Lasso, A., Stockli, D. ,2013. Segmentation and growth of foothill thrust-belts adjacent to

770 inverted grabens: the case of the Colombian Llanos foothills. Geological Society, London,
771 Special Publications, 377, 189–220. http://doi.org/10.1144/SP377.11

772 Julivert, M. ,1963. Los rasgos tectónicos de la región de la Sabana de Bogotá y los mecanismos de la
773 formación de las estructuras. Boletín de Geología Universidad Industrial Santander, 13-14, 5–
774 102.

775 Julivert, M. ,1970. Cover and Basement Tectonics in the Cordillera Oriental of Colombia, South
776 America, and a Comparison with Some Other Folded Chains. Geological Society of America
777 Bulletin, 81, 3623–3646.

778 Kellogg, J. N., Vega, V. ,1995. Tectonic development of Panama, Costa Rica, and the Colombian
779 Andes: Constraints from global positioning system geodetic studies and gravity. Geologic and
780 Tectonic Development of the Caribbean Plate Boundary in Southern Central America.
781 http://doi.org/10.1130/SPE295-p75

782 Kirby, E. ,2003. Distribution of active rock uplift along the eastern margin of the Tibetan Plateau:
783 Inferences from bedrock channel longitudinal profiles. Journal of Geophysical Research, 108,
784 2217. http://doi.org/10.1029/2001JB000861

785 Kirby, E., Whipple, K. ,2001. Quantifying differential rock-uplift rates via stream profile analysis.
786 Geology, 6, 415–418.

787 Kooi, H., Beaumont, C. ,1996. Large-scale geomorphology: Classical concepts reconciled and
788 integrated with contemporary ideas via a surface processes model. Journal of Geophysical
789 Research, 101, 3361. http://doi.org/10.1029/95JB01861

790 Koons, P. O. ,1994. Three-dimensional critical wedges: Tectonics and topography in oblique
791 collisional orogens. Journal of Geophysical Research, 99, 12301–12315.
792 http://doi.org/10.1029/94JB00611

793 Koons, P. O. ,1995. Modeling the topographic evolution of collisional belts. Annual Review of Earth
794 and Planetary Sciences, 23, 375–408.

795 Laverde, F. E., Segall, M. P., Allen, R. B., Ressetar, R. ,1989. Recognition of an ancient fluvial system
796 in the Upper Magdalena Valley, Colombia. In Programme and Abstracts of the IV
797 International Conference on Fluvial Sedimentology (Barcelona), p. 165.

798 Mark, B.G., Helmens, K.F., 2005. Reconstruction of glacier equilibrium-line altitudes for the Last
799 Glacial Maximum on the High Plain of Bogota, Eastern Cordillera, Colombia: Climatic and
800 topographic implications. J. Quat. Sci. 20, 789–800. doi:10.1002/jqs.974

801 Mather, A. E. ,2000. Adjustment of a drainage network to capture induced base-level change: an
802 example from the Sorbas Basin, SE Spain. Geomorphology, 34, 271–289.
803 http://doi.org/10.1016/S0169-555X(00)00013-1

804 Molnar, P., England, P. ,1990. Late Cenozoic uplift of mountain ranges and global climatic change:
805 chicken or egg? Nature, 346, 29–34.

Mora, A., Reyes-Harker, a., Rodriguez, G., Teson, E., Ramirez-Arias, J. C., Parra, M., Caballero, V., Mora, J.P., Quintero, I., Valencia, V., Ibanez, M., Horton, B..K, Stockli, D. F. ,2013. Inversion tectonics under increasing rates of shortening and sedimentation: Cenozoic example from the Eastern Cordillera of Colombia. Geological Society, London, Special Publications, 377, 411–442. http://doi.org/10.1144/SP377.6

Mora, A., Horton, B. K., Mesa, A., Rubiano, J., Ketcham, R. A., Parra, M., Blanco, V., Garcia, D., Stockli, D. F. ,2010. Migration of cenozoic deformation in the eastern cordillera of colombia interpreted from fission track results and structural relationships: Implications for petroleum systems. AAPG Bulletin, 94, 1543–1580. http://doi.org/10.1306/01051009111

Mora, A., Parra, M., Strecker, M. R., Kammer, A., Dimaté, C., Rodríguez, F. ,2006. Cenozoic contractional reactivation of Mesozoic extensional structures in the Eastern Cordillera of Colombia. Tectonics, 25, 1–19. http://doi.org/10.1029/2005TC001854

Mora, A., Parra, M., Strecker, M. R., Sobel, E. R., Hooghiemstra, H., Torres, V., Jaramillo, J. V. ,2008. Climatic forcing of asymmetric orogenic evolution in the Eastern Cordillera of Colombia. Bulletin of the Geological Society of America, 120, 930–949. http://doi.org/10.1130/B26186.1

Moreno, N., Silva, A., Mora, A., Tesón, E., Quintero, I., Rojas, L.E., Lopez, C., Blanco, V., Castellanos, J., Sanchez, J., Osorio, L., Namson, J., Stockli, D., Casallas, W., 2013. Interaction between thin- and-thick-skinned tectonics in the foothill areas of an inverted graben. The Middle Magdalena Foothill belt. Geol. Soc. London, Spec. Publ. 377, 221-255. Doi:10.1144/SP377.18

Mudd, S. M., Attal, M., Milodowski, D. T., Grieve, S. W. D., Valters, D. A. ,2014. A statistical framework to quantify spatial variation in channel gradients using the integral method of channel profile analysis. Journal of Geophysical Research: Earth Surface, 119, 138–152. http://doi.org/10.1002/2013JF002981

Nie, J., Horton, B. K., Mora, A., Saylor, J. E., Housh, T. B., Rubiano, J., Naranjo, J. ,2010. Tracking exhumation of Andean ranges bounding the Middle Magdalena Valley Basin, Colombia. Geology, 38, 451–454. http://doi.org/10.1130/G30775.1

Nie, J., Horton, B. K., Saylor, J. E., Mora, A., Mange, M., Garzione, C. N., Basu, A., Moreno, C.J., Caballero, V., Parra, M. ,2012. Integrated provenance analysis of a convergent retroarc foreland system: U-Pb ages, heavy minerals, Nd isotopes, and sandstone compositions of the Middle Magdalena Valley basin, northern Andes, Colombia. Earth-Science Reviews, 110, 111–126. http://doi.org/10.1016/j.earscirev.2011.11.002

O'Callaghan, J. F., Mark, D. M. ,1984. The extraction of drainage networks from digital elevation data. Computer Vision, Graphics, and Image Processing, 28, 323–344.

Parra, M., Mora, A., Jaramillo, C., Strecker, M. R., Sobel, E. R., Quiroz, L., Rueda, M., Torres, V. ,2009. Orogenic wedge advance in the northern Andes: Evidence from the Oligocene-Miocene sedimentary record of the Medina Basin, Eastern Cordillera, Colombia. Bulletin of the Geological Society of America, 121, 780–800. http://doi.org/10.1130/B26257.1

844 Parra, M., Mora, A., Jaramillo, C., Torres, V., Zeilinger, G., Strecker, M. R. ,2010. Tectonic controls
845 on Cenozoic foreland basin development in the north-eastern Andes, Colombia. Basin
846 Research, 22, 874–903. http://doi.org/10.1111/j.1365-2117.2009.00459.x

847 Parra, M., Mora, A., Sobel, E. R., Strecker, M. R., González, R. ,2009. Episodic orogenic front
848 migration in the northern Andes: Constraints from low-temperature thermochronology in the
849 Eastern Cordillera, Colombia. Tectonics, 28. http://doi.org/10.1029/2008TC002423

850 Pelletier, J. D. ,2004. Persistent drainage migration in a numerical landscape evolution model.
851 Geophysical Research Letters, 31, L20501. http://doi.org/10.1029/2004GL020802

852 Perron, J. T., Richardson, P. W., Ferrier, K. L., Lapôtre, M. ,2012. The root of branching river
853 networks. Nature, 492, 100–103. http://doi.org/10.1038/nature11672

854 Perron, J. T., Royden, L. ,2013. An integral approach to bedrock river profile analysis. Earth Surface
855 Processes and Landforms, 38, 570–576. http://doi.org/10.1002/esp.3302

856 Prince, P. S., Spotila, J. A., Henika, W. S. ,2011. Stream capture as driver of transient landscape
857 evolution in a tectonically quiescent setting. Geology, 39, 823–826.
858 http://doi.org/10.1130/G32008.1

859 Restrepo-Pace, P. A., Colmenares, F., Higuera, C., Mayorga, M. ,2004. A Fold-and-thrust belt along
860 the western flank of the Eastern Cordillera of Colombia—Style, kinematics, and timing
861 constraints derived from seismic data and detailed surface mapping. Thrust Tectonics and
862 Hydrocarbon Systems, 598–613.

863 Roeder, D., Chamberlain, R. L. ,1995. Eastern Cordillera of Colombia: Jurassic–Neogene crustal
864 evolution. In A. J. Tankard, S. R. Suarez, and H. J. Welsink, Eds., Petroleum Basins of
865 SouthAmerica:AAPG Memoir 62, 633–645.

866 Rolon, L. F., Toro, J., Wilson, T., ,2004. Structural Geometry of the Jura-Cretaceous Rift of the
867 Middle Magdalena Valley Basin – Colombia.

868 Royden, L., Taylor Perron, J. ,2013. Solutions of the stream power equation and application to the
869 evolution of river longitudinal profiles. Journal of Geophysical Research: Earth Surface, 118,
870 497–518. http://doi.org/10.1002/jgrf.20031

871 Safran, E. B., Bierman, P. R., Aalto, R., Dunne, T., Whipple, K. X., Caffee, M. ,2005. Erosion rates
872 driven by channel network incision in the Bolivian Andes. Earth Surface Processes and
873 Landforms, 30, 1007–1024. http://doi.org/10.1002/esp.1259

874 Saylor, J. E., Horton, B. K., Nie, J., Corredor, J., Mora, A. ,2011. Evaluating foreland basin
875 partitioning in the northern Andes using Cenozoic fill of the Floresta basin, Eastern Cordillera,
876 Colombia. Basin Research, 23, 377–402. http://doi.org/10.1111/j.1365-2117.2010.00493.x

877 Schumm, S. A. ,1979. Geomorphic Thresholds: the concept and its application. Transaction of the
878 Institute of British Geographers, 4, 485–515.

879 Silva, a., Mora, a., Caballero, V., Rodriguez, G., Ruiz, C., Moreno, N., Parra, M., Ramirez-Arias, J.C.,
880 Ibanez, M., Quintero, I. ,2013. Basin compartmentalization and drainage evolution during rift

881 inversion: evidence from the Eastern Cordillera of Colombia. Geological Society, London,
882 Special Publications, 377, 369–409. http://doi.org/10.1144/SP377.15

883 Small, R. J. ,1978. The study of landforms (2nd edn). Cambridge: Cambridge University Press.

884 Snyder, N. P., Whipple, K. X., Tucker, G. E., Merritts, D. J. ,2003. Channel response to tectonic
885 forcing: field analysis of stream morphology and hydrology in the Mendocino triple junction
886 region, northern California. Geomorphology, 53, 97–127. http://doi.org/10.1016/S0169-
887 555X(02)00349-5

888 Sobel, E. R., Hilley, G. E., Strecker, M. R. ,2003. Formation of internally drained contractional basins
889 by aridity-limited bedrock incision. Journal of Geophysical Research: Solid Earth, 108.
890 http://doi.org/10.1029/2002JB001883

891 Stokes, M., Mather, a. E., Harvey, a. M. ,2002. Quantification of river-capture-induced base-level
892 changes and landscape development, Sorbas Basin, SE Spain. Geological Society, London,
893 Special Publications, 191, 23–35. http://doi.org/10.1144/GSL.SP.2002.191.01.03

894 Taboada, A., Rivera, L. A., Fuenzalida, A., Cisternas, A., Philip, H., Bijwaard, H., Olaya, J., Rivera, C.
895 ,2000. Geodynamics of the northern Andes: Subductions and intracontinental deformation
896 (Colombia). Tectonics, 19, 787–813. http://doi.org/10.1029/2000TC900004

897 Tarboton, D. G. ,1997. A new method of determination of flow directions and upslope areas in grid
898 digital elevation models. Water Resources Research, 33, 309–319.

899 Teixell, A., Tesón, E., Ruiz, J.C., Mora, A. ,2015. The structure of an inverted back-arc rift : insights
900 from a transect across the Eastern Cordillera of Colombia near Bogotá. , in C. Bartolini, and P.
901 Mann, eds. Petroleum Geology and Hydrocarbon Potential of Colombia Caribbean Margin:
902 AAPG Memoir, 108, in press.

903 Tesón, E., Mora, A., Silva, A., Namson, J., Teixell, A., Castellanos, J., Casallas, W., Julivert, M., Taylor,
904 M., Ibanez-Mejia, M., Valencia, V. A. ,2013. Relationship of Mesozoic graben development,
905 stress, shortening magnitude, and structural style in the Eastern Cordillera of the Colombian
906 Andes. Geological Society, London, Special Publications, 377, 257–283.
907 http://doi.org/10.1144/SP377.10

908 Tomkin, J. H., Braun, J. ,1999. Simple models of drainage reorganisation on a tectonically active
909 ridge system. New Zealand Journal of Geology & Geophysics, 42, 1–10.

910 Toro, J., Virginia, W., Cornec-lance, S. Le, Malmaison, R., Sassi, W., Floch, NB., 2004. Thermal and
911 Kinematic Evolution of the Eastern Cordillera Fold and Thrust Belt, Colombia. Am. Assoc. Pet.
912 Geol. 1, 79-115. Doi:10.1306/1025687H13114

913 Torres, V., Vandenberghe, J., Hooghiemstra, H. ,2005. An environmental reconstruction of the
914 sediment infill of the Bogotá basin (Colombia) during the last 3 million years from abiotic and
915 biotic proxies. Palaeogeography, Palaeoclimatology, Palaeoecology, 226, 127–148.
916 http://doi.org/10.1016/j.palaeo.2005.05.005

Van der Beek, P., Champel, B., Mugnier, J. L. ,2002. Control of detachment dip on drainage development in regions of active fault-propagation folding. Geology, 30, 471–474. http://doi.org/10.1130/0091-7613(2002)030<0471:CODDOD>2.0.CO;2

Van der Hammen, T., Werner, J. H., van Dommelen, H. ,1973. Palynological record of the upheaval of the Northern Andes: A study of the pliocene and lower quaternary of the Colombian Eastern Cordillera and the early evolution of its high-Andean biota. Review of Palaeobotany and Palynology, 16, 1–122. http://doi.org/10.1016/0034-6667(73)90031-6

Veloza, G., Taylor, M., Mora, a., Gosse, J. ,2015. Active mountain building along the eastern Colombian Subandes: A folding history from deformed terraces across the Tame anticline, Llanos Basin. Geological Society of America Bulletin, 1–19. http://doi.org/10.1130/B31168.1

Whitfield, E., Harvey, A. M. ,2012. Interaction between the controls on fluvial system development: Tectonics, climate, base level and river capture - Rio Alias, Southeast Spain. Earth Surface Processes and Landforms, 37, 1387–1397. http://doi.org/10.1002/esp.3247

Willett, S. D. ,1999. Orogeny and orography: The effects of erosion on the structure of mountain belts. Journal of Geophysical Research, 104, 28957. http://doi.org/10.1029/1999JB900248

Willett, S. D., McCoy, S. W., Perron, J. T., Goren, L., Chen, C.-Y. ,2014. Dynamic reorganization of river basins. Science (New York, N.Y.), 343, 1248765. http://doi.org/10.1126/science.1248765

Willett, S. D., Slingerland, R., Hovius, N. ,2001. Uplift, shortening, and steady state topography in active mountain belts. Am. J. Sci, 301, 455–485.

Wobus, C., Whipple, K. X., Snyder, N., Johnson, J., Sheehan, D. ,2006. Tectonics from topography : Procedures , promise , and pitfalls, 2398, 55–74. http://doi.org/10.1130/2006.2398(04).

# PENEPLANATION AND DEEP DYNAMICS OF THE PYRENEES

Gemma V. Bosch[1,2*], Jean Van Den Driessche[1], Julien Babault[3], Alexandra Robert[4], Alberto Carballo[5], Christian Le Carlier, Nicolas Loget[6], Caroline Prognon[2,7], Robert Wyns[2], Thierry Baudin[2]

[1]Geosciences Rennes, Université Rennes 1 /CNRS, UMR 6118, 35042 Rennes cedex (France)

[2]BRGM, 45100 Orléans, France

[3]Departament de Geologia, Universitat Autònoma de Barcelona, 08193 Bellaterra (Barcelona), Spain

[4]Géosciences Environnement Toulouse, Université Paul Sabatier/CNRS, UMR 5563/IRD, ER 234, 31400 Toulouse

[5]Institut de Ciènces de la Terra Jaume Almera, CSIC, Barcelona, E-08028, Spain

[6]Institut des Sciences de la Terre de Paris (ISTeP), Université Pierre et Marie Curie/CNRS, UMR 7193 75005 Paris (France)

[7]Institut des Sciences de la Terre d'Orléans, Université d'Orléans/CNRS, UMR 7327, 45071 Orléans cedex 2 (France)

[*] Corresponding author

Address: UMR 6118 Géosciences Rennes, B.15 - Off.127 / Campus de Beaulieu, 35042 / Rennes Cedex (France)

Tél: (+33)2 23 23 67 83

E-mail: gemmav.bosch@gmail.com

## ABSTRACT

The morphology of the Pyrenees is characterized by the presence of high-elevation, low-relief surfaces. The origin of these Lower Miocene surfaces is still debated. Two major interpretations have been proposed, both admitting that theses surfaces are remnants of a single composite planation surface recently dissected, but they differ on their origin. The first interpretation considers that this surface corresponds to a peneplain developed near sea-level before the late Miocene, subsequently uplifted and dissected. The present-day Pyrenees is therefore supposed to rise from the late Miocene. The second proposes that the rise of the efficient base level of the chain induced the progressive inhibition of erosion and the smoothing of the relief before the late Miocene, resulting in highly elevated peneplain. According to this later interpretation, high- elevation, low-relief surfaces do not equate to post-orogenic uplift. We test these two interpretations by investigating, among other considerations, the relation between the altitude of these planation surface remnants and the deep structure of the chain. We find that (1) the isostatic compensation of the dissected Pyrenean planation surface by crustal thickening and (2) the absence of thinning of the lithosphere mantle below the chain favor the second interpretation.



**KEYWORDS**: Pyrenees, erosion, peneplanation, Moho, isostasy, lithosphere


## INTRODUCTION

Moving plate tectonics and deep mantle dynamics create uplift and subsidence of the Earth's surface whereas Earth's surface processes, namely erosion, transport and sedimentation, tend

to counteract these positive and negative vertical movements. Uplift (or subsidence) has two origins: isostasy that is controlled by the difference between crustal and mantle densities, and dynamic topography that is controlled by mantle dynamics. Wavelength and elevation changes for local isostasy are respectively of several tens to hundreds km and up to several km, whereas for dynamic topography they are typically of several hundred to thousand km, and several hundred m up to 1 km respectively (e. g., Braun 2010). Whether or not surface uplift equates to rock uplift depends on whether or not erosion is active (England and Molnar, 1990). As surface uplift is controlled by crust and/or mantle dynamics, the resulting elevation change must be considered in terms of mean elevation at a minimum area of a thousand of km² (e. g. England and Molnar , 1990). In a general way, crustal thickening causes surface uplift. The growth of a mountain belt by crustal thickening requires a rate of erosion much lower than the rate of rock uplift. Increasing erosion rate up to equate to rock uplift rate will result in dynamic equilibrium once the mountain belt has risen. Crustal thinning will result in surface lowering that can be partially compensated by sedimentation and/or by concomitant thinning of the lithospheric mantle. Extreme thinning of the continental lithosphere inevitably causes surface lowering below sea level. Only thinning of the lithospheric mantle and its concomitant replacement by less dense asthenospheric mantle can produce surface uplift when crustal thickness is kept constant. So, any attempt to determine the evolution of the topography requires investigating both Earth's surface and deep processes at the origin of the relief (e.g. Casas-Sainz and de Vicente, 2009, Molnar et al. 2015). The Pyrenees is an emblematic example: how their topography has changed over time and what were the deep processes involved is highly debated.

The Pyrenees are classically described as an intracontinental orogen that results from the inversion of a continental rift during the convergence between Eurasia and Africa (Choukroune et al., 1990; Munoz, 1992). Beyond the considerable debate that is currently

concerned with the width of this rift that developed during the Cretaceous and resulted in mantle exhumation (Jammes et al., 2009; Lagabrielle et al. 2010), no doubt exits that crustal thickening was at the origin of the Pyrenees uplift during Eocene and Oligocene times. Indeed the Moho beneath the central Pyrenees reaches a depth of about 50 km (Choukroune et al., 1990, Chevrot et al., 2014).

The “Pyrenees” geographic and geomorphologic appellations differ from the Pyrenean orogen (“tectonic” Pyrenees). The Pyrenean orogen extends from the Cantabric Range in northwestern Spain to the west, to Provence in southeastern France to the east. The initial chain was about 1000 km long, whereas the geomorphologic Pyrenees are only 400 km long. The disappearance of the Pyrenean orogen below the Mediterranean is due to the tectonic collapse of the former during considerable Oligocene to Aquitanian crustal and lithospheric thinning in the Gulf of Lion margin and subsequent oceanic accretion in the NW Mediterranean (Séranne et al., 1995). This event succeeds the continental rifting that developed in Western Europe from the Oligocene. It also affected the easternmost part of the geomorphologic Pyrenees. We refer hereafter the geomorphologic Pyrenees to the Pyrenees.

## THE HIGH-ELEVATION, LOW-REFIEF EROSIONAL SURFACES OF THE PYRENEES

The most striking feature of the Pyrenean morphology is the occurrence at high elevation of low-relief erosional surfaces, which are considered as remnants of a single composite planation surface recently dissected ( de Sitter, 1952; Kleinsmiede, 1960; Zandvliet, 1960; Calvet, 1996; Babault et al., 2005). This planation surface erodes the Pyrenean tectonic structures and is locally overlapped by Upper Miocene continental deposits

in the Val d'Aran and Cerdagne, providing an upper limit age for its development (de Sitter, 1953; Jelgersma, 1957; Cabrera et al. 1988; Roca, 1996; Ortuño et al., 2008, 2013). The high-elevation, low-relief surfaces form smooth reliefs paradoxically situated at crest zones up to ~2800m asl in the Axial Zone of the Pyrenees (figure 1). They occur irrespective of lithology, mainly granitic rocks and micaschists. Typically, the slope along these surfaces does not exceed 20º. Depending on their altitude in the chain, they are more or less disrupted by glacial erosion. Within the high-elevation, low-relief surfaces, glacial erosion produces excavation surfaces, easily identifiable by their concave-up geometry, their steep slopes and their marked roughness. To reconstruct the Pyrenean planation surface we analyzed and mapped several remnants of this surface and we used bibliography data to compile a regional map (Kleinsmiede, 1960; Zandvliet, 1960; Calvet, 1996; Babault et al., 2005; Ortuno et al., 2008). Then we used an automatic method of landform classification called TPI (Topographic position index; Weiss, 2001; Jenness et al., 2006) to map these remnants across the Axial Zone of the Pyrenees.

The Weiss method uses digital elevations models to measure the difference between the elevation of each cell and the mean elevation with a variable radius of calculation. The variation of the radius, the TPI type and the slope permit to distinguish different landforms in the landscape. We use 25 m resolution DEMs from the French, the Spanish and the Andorran Geographical Institutes, allowing to detect areas down to 500 m². TPI type, TPI radius and slope were determined from surfaces previously mapped by field investigations. Concave-up landforms related to Quaternary glacial erosion were distinguished from Lower Miocene erosional surface using a TPI radius minimized to 100 m. The applied methodology results in a more consistent and regular limit between the remnants of the planation surface and glacial landforms than using traditional interpretative mapping (figure 1). We then verify on the field

the existence of the surfaces identified by the Weiss method, that were not previously mapped.

The figure 2a shows the pervasive occurrence of the remnants of the Pyrenean planation surface in the Axial Zone. Hypothesing that these surfaces are the remnants of a single paleosurface of planation, we tentatively restore this latter by interpolating the neighboring remnants (figure 2b). The resulting surface is gently undulating with a mean elevation of about 2400 m. Local relief does not exceed 300 m (figure 2c). This surface can therefore be described as an uplifted peneplain (Davis, 1899; King, 1953). Note that the mean elevation of the restored planation surface is some hundred meters higher than mean elevation of the present-day topography. The difference in altitude between the restored planation surface and the present-day mean topography of the Pyrenees is explained by the isostatic rebound due to the dissection of the former (Babault et al., 2005). This difference in altitude stems from the fact that our restoration ignores the isostatic rebound consecutive to recent dissection of the planation surface (Babault et al. 2005).

## MOHO DEPTH AND DEEP STRUCTURES OF THE PYRENEES

First works on the Moho depth below the Pyrenees (Daignières et al. 1982, Choukroune et al. 1989; Souriau and Granet, 1995; Vacher and Souriau, 2001) have revealed the presence of a crustal root that corresponds to the thickening of the Iberian crust during the incipient subduction of the Iberian lithosphere below the European lithosphere. Recent studies coupling receiver functions and local tomography investigation have provided more accurate images of both the crustal and lithospheric structures below the Pyrenees (Chevrot et al. 2014).

In order to compare independently geophysical approaches for the calculus of the depths of the Moho and of the base of the lithosphere, we present a new geophysical modeling using topographic data and geoid anomaly together with thermal analysis in a 1D approach (Fullea et al., 2007; Robert et al. in press). Topographic and bathymetric data are extracted from the ETOPO1 database (Amante and Eakins, 2009) and the geoid anomaly from EGM2008 global model (Pavlis et al., 2008). In order to avoid the sub-lithospheric density variations, we filtered the geoid so that the signal corresponding to the lower spherical harmonics until degree and order 10 is ruled out. Our modeling approach assumes that (1) local isostasy is verified, considering a depth of compensation of 300 km, and (2) the system is in thermal equilibrium. It also considers a four-layered density model composed of atmosphere/sea water, crust, lithospheric and asthenospheric mantle. The crustal density linearly increases with depth, and the density of the lithospheric mantle is temperature dependent.

The figure 3 shows three models involving variable crustal densities (table 1). We compare the Moho depths with the dataset from Chevrot et al., (2014) that involves recent receiver functions data and reflection-refraction profiles from France and Spain (see references in Chevrot et al., 2014). We perform a new interpolation of the Moho surface from the Chevrot et al.'s dataset, using the 3D GOCAD modeler (Mallet, 2002).

This interpolation reveals the main pattern of the Moho surface, avoiding short wavelength variations (figure 3). The three models are in agreement with the Moho depth determined from the dataset of Chevrot et al. (2014). We observe that the mean elevation of the Pyrenees is generally compensated by crustal thickening, so that the variation of elevation across the chain matches that of the Moho depth. Similarly, the base of the lithosphere parallels the Moho surface, and does not show any anomalous thickening or thinning that could affect the mean elevation of the chain.

In the easternmost Pyrenees, the Moho and the lithosphere-asthenosphere boundary rises progressively whereas the mean elevation of the chain decreases. Lithospheric thinning increases offshore in relation with the opening of the Gulf of Lion (e.g. Séranne, 1999). In this area, there is a misfit between our models and the data set of Chevrot et al. (2014) that does not exceed 5 km. Whether this misfit has to be related to the error inherent to both methods (Gomez-Ortiz et al., 2011, Molnar et al. 2015) remains to determine. Our density model for the crust is probably not fully pertinent is this area where the thick Neogene sedimentary cover makes the mean crustal density lower than in the rest of the Pyrenees. To what extent this affects the results of our modeling is to evaluate. Further investigation, especially 2D and 3D modelling, is needed to improve the fit (work in progress).

## DISCUSSION

The above considerations about the “Pyrenees” appellations highlight the prominent part played by isostasy on the surface expression of the Pyrenean orogen as whole. We argue here that isostasy, and not mantle dynamics, is responsible for the occurrence of low relief erosional surfaces at high elevation in the Pyrenees.

Low-relief erosional surfaces are considered to be produced by long-term erosional processes that result in the peneplanation near sea level of earlier reliefs such as mountain belts (Davis, 1899). Thus low-relief surfaces at high elevation at the Earth surface are classically interpreted as a result of a surface uplift (e. g. Davis, 1899, de Sitter, 1952, Chorley et al., 1973, Gregory and Chase, 1994; Philipps, 2002, Farias et al., 2008, Hetzel et al., 2011). Uplift generates relief rejuvenation so that these surfaces appear as relics of a dissected peneplain. Mantle dynamics is required to trigger surface uplift because these relics appear

rather flat and not deformed, while considerable crustal thickening would inevitably induced their folding and faulting. A major consequence of such an interpretation is the absence of crustal root together with an extreme thinning of the lithospheric mantle below these surfaces (figure 4). In the eastern Pyrenees a similar interpretation involving a near 2000 m post-orogenic uplift has been proposed for the high altitude of these low relief surfaces (e.g. de Sitter, 1952; Gunnell et al., 2008).

The present preliminary results show that these surfaces are ubiquitous in the Pyrenees. Their interpolation at the scale of the chain suggests that they are remnants of a single, gently undulating planation surface. The altitude variation of the later follows that of the present-day mean topography, which appears to be in isostatic equilibrium. We do not find any crustal overcompensation of the elevation of the chain as previously suggested (Vacher and Souriou, 2001) nor anomalous thinning of the mantle lithosphere to explain the altitude of the planation surface in the eastern Pyrenees (Gunnell et al. 2008). Our results therefore contradict the hypothesis of peneplanation near sea-level, and subsequent uplift due to mantle dynamics.

Additionally, the present-day level of erosion in the central and eastern Pyrenees also disagrees with the hypothesis of peneplanation near sea-level. The peneplanation of an initial mountain belt with a mean altitude of 2000 m asl, would require to remove by erosion a crustal thickness of about 12 km. The rocks exposed along the peneplanation surface would therefore show a metamorphic imprint corresponding to a minimum burial of 12 km. The Hercynian basement in both the central and eastern Pyrenees show a remarkable similar metamorphic zonation (e. g. Carreras and Capella, 1994), which reveals a similar level of erosion. To our knowledge, there is presently no data to support a differential 12 km crustal thickening during Pyrenean tectonics between the central and eastern Pyrenees. So in the easternmost Pyrenees thinning of the crust is not achieved by greater erosion resulting in

225 downwearing and peneplanation as previously suggested (Gunnell et al. 2008) but from Upper
226 Oligocene to Lower Miocene extensional tectonics (Séranne, 1999).

227 We conclude that the high-elevation, low-relief surfaces of the Pyrenees are the
228 remnants of the single planation surface. This surface formed at high elevation in response to
229 the progressive inhibition of erosion, as shown by thermochronological data (Fitzegerald et al.
230 1999, Gibson et al. 2007, Gunnell et al., 2009) and the concomitant sediment aggradation
231 along the Pyrenean piedmonts during the mountain growth from the late Eocene to the early
232 Miocene (Babault et al. 2005, 2007). This process allowed the preservation of a thick crustal
233 root below the Pyrenees (figure 4). Reactivation of fluvial incision and glacial erosion is
234 responsible for the removal of thick detrital sediment accumulation and the dissection of the
235 initial planation surface into disseminated remnants as observed today (Babault et al. 2005).
236 According to the Molnar and England's model (1990), if any post-tectonic uplift of the
237 planation surface did occur in the Pyrenees, it was caused by isostatic rebound consecutive to
238 erosion and did not exceed 400 m (Babault et al., 2005). Whether relief rejuvenation occurs
239 during the Plio-Quaternary climate change or from the early Miocene onwards (e.g. Coney et
240 al. 1996; Babault et al., 2005, 2006, Garcia-Castellanos et al., 2003, Fillon and van der Beek,
241 2012) is still a matter of debate and behind the scoop of the present study.
242
243
244 **CONCLUSION**
245
246 Remnants of planation surfaces at high elevation are ubiquitous in the Pyrenean Axial Zone.
247 First attempt to interpolate these remnants suggests that they correspond to a single planation
248 surface that was completed before the late Miocene and later dissected. The presence of a
249 crustal root together with the absence of lithospheric mantle thinning below the Axial Zone

precludes any peneplanation near sea-level before the late Miocene and subsequent uplift triggered by mantle dynamics as classically proposed to explain such planation surface remnants at high elevation. Rather, it favors a process of erosion inhibition at high altitude, a process probably undervalued in many other mountain belts where remnants of planation surfaces are observed.


## ACKNOWLEDGEMENTS

We are grateful to the BRGM (Bureau de Recherches Géologiques et Minières) for funding the Gemma V. Bosch PhD thesis (Project RGF, Référentiel Géologique de la France). We wish to thank constructive thorough reviews by Antonio Casas-Sainz and Michel Séranne. Annabelle Bernard is thanked for field assistance.


## REFERENCES


Amante, C., Eakins, B.W., 2009. ETOPO1 1 arc-minute global relief model: Procedures, data sources and analysis. NOAA Tech. Memo. NESDIS NGDC 24, 19 pp.

Babault, J., Bonnet, S., Van Den Driessche, J., Crave, A., 2007. High elevation of low-relief surfaces in mountain belts: does it equate to post-orogenic surface uplift? Terra Nova 19, 272–277. doi:10.1111/j.1365-3121.2007.00746.x

Babault, J., Loget, N., Van Den Driessche, J., Castelltort, S., Bonnet, S., Davy, P., 2006. Did the Ebro basin connect to the Mediterranean before the Messinian salinity crisis? Geomorphology 81, 155–165. doi:10.1016/j.geomorph.2006.04.004

Babault, J., Van Den Driessche, J., Bonnet, S., Castelltort, S., Crave, A., 2005. Origin of the highly elevated Pyrenean peneplain. Tectonics 24, n/a–n/a. doi:10.1029/2004TC001697

Braun, J., 2010. The many surface expression of mantle dynamics. Nature Geoscience, 3, 825-833.

Calvet, M., 1996. Morphogenèse d'une Montagne Méditerranéenne: Les Pyrenées Orientales (Editions BRGM). Université de Perpignan, Paris.

Carreras,J., Capella, I., 1994. Tectonic levels in the Paleozoic basement of the Pyrenees: a review and a new interpretation. J Struct. Geol., 16, 1509-1524.

Casas-Sainz, A.M., de Vicente, G., 2009. On the tectonic origin of Iberian topography. Tectonophysics 474, 214–235. doi:10.1016/j.tecto.2009.01.030

Chevrot, S., Villaseñor, A., Sylvander, M., Benahmed, S., Beucler, E., Cougoulat, G., Delmas, P., de Saint Blanquat, M., Diaz, J., Gallart, J., Grimaud, F., Lagabrielle, Y., Manatschal, G., Mocquet, A., Pauchet, H., Paul, A., Péquegnat, C., Quillard, O., Roussel, S., Ruiz, M., Wolyniec, D., 2014. High-resolution imaging of the Pyrenees and Massif Central from the data of the PYROPE and IBERARRAY portable array deployments. J. Geophys. Res. Solid Earth 119, 6399–6420. doi:10.1002/2014JB010953

Chorley, R.J., Beckinsale, R.P., Dunn, A.J., 1973. The hystory of the study of landforms or the development of geomorphology, Meuthuen and Co. ed. London.

Choukroune, P., ECORS Team, 1989. The ECORS Pyrenean deep seismic profile reflection data and the overall structure of an orogenic belt. Tectonics 8, 23–39.

Choukroune, P., Roure, F., Pinet, B., ECORS PYRENEES TEAM, 1990. Main results of the ECORS Pyrenees profile. Tectonophysics 173, 411 – 423.

Clauser, C., Huenges, E., 1995. Thermal conductivity of Rocks and Minerals, in: Rocks Physics and Phase Relations: A Handbook of Physical Constants. pp. 105–126.

Coney, P.J., Muñoz, J.A., McClay, K.R., Evenchick, C.A., 1996. Syntectonic burial and post-tectonic exhumation of the southern Pyrenees foreland fold–thrust belt. J. Geol. Soc. 153, 9–16.

Daignières, M., Gallart, J., Banda, E., Hirn, A., 1982. Implications of the seismic structure for the orogenic evolution of the Pyrenean Range. Earth Planet. Sci. Lett. 57, 88–100.

Davis, W.M., 1899. The geographical cycle. Geogr. J. 14, 481–504.

De Sitter, L.U., 1953. Note préliminaire sur la géologie du Val d'Aran. Leidse Geol. Meded. 18, 272–280.

De Sitter, L.U., 1952. Pliocene uplift of Tertiary mountain chains. Am. J. Sci. 297–307.

England, P., Molnar, P., 1990. Surface uplift, uplift of rocks, and exhumation of rocks. Geology 18, 1173–1177.

Farías, M., Charrier, R., Carretier, S., Martinod, J., Fock, A., Campbell, D., Cáceres, J., Comte, D., 2008. Late Miocene high and rapid surface uplift and its erosional response in the Andes of central Chile (33°-35°S): Uplift and erosion in central Chile Andes. Tectonics 27, doi:10.1029/2006TC002046

Fernàndez, M., Marzán, I., Correia, A., Ramalho, E., 1998. Heat flow, heat production, and lithospheric thermal regime in the Iberian Peninsula. Tectonophysics 291, 29–53.

317 Fillon, C., van der Beek, P., 2012. Post-orogenic evolution of the southern Pyrenees:
318 constraints from inverse thermo-kinematic modelling of low-temperature thermochronology
319 data. Basin Res. 24, 418–436. doi:10.1111/j.1365-2117.2011.00533.x

320 Fitzgerald, P.G., Muñoz, J.A., Coney, P.J., Baldwin, S.L., 1999. Asymmetric exhumation
321 across the Pyrenean orogen: implications for the tectonic evolution of a collisional orogen.
322 Earth Planet. Sci. Lett. 173, 157–170.

323 Fullea, J., Fernàndez, M., Zeyen, H., Vergés, J., 2007. A rapid method to map the crustal and
324 lithospheric thickness using elevation, geoid anomaly and thermal analysis. Application to the
325 Gibraltar Arc System, Atlas Mountains and adjacent zones. Tectonophysics 430, 97–117.
326 doi:10.1016/j.tecto.2006.11.003

327 García-Castellanos, D., Vergés, J., Gaspar-Escribano, J., Cloetingh, S., 2003. Interplay
328 between tectonics, climate, and fluvial transport during the Cenozoic evolution of the Ebro
329 Basin (NE Iberia). J. Geophys. Res. Solid Earth 108, n/a–n/a. doi:10.1029/2002JB002073

330 Gibson, M., Sinclair, H.D., Lynn, G.J., Stuart, F.M., 2007. Late- to post-orogenic exhumation
331 of the Central Pyrenees revealed through combined thermochronological data and modelling.
332 Basin Res. 19, 323–334. doi:10.1111/j.1365-2117.2007.00333.x

333 Gómez-Ortiz, D., Agarwal, B.N.P., Tejero, R., Ruiz, J., 2011. Crustal structue from gravity
334 signatures in the Iberian Peninsula. Geol. Soc. Am. Bull. 123, 1247–1257.

335 Gregory, K.M., Chase, C.G., 1994. Tectonic and climatic significance of a late Eocene low-
336 relief, high-level geomorphic surface, Colorado. J. Geophys. Res. 99, 141–160.

Gunnell, Y., Zeyen, H., Calvet, M., 2008. Geophysical evidence of a missing lithospheric root beneath the Eastern Pyrenees: Consequences for post-orogenic uplift and associated geomorphic signatures. Earth Planet. Sci. Lett. 276, 302–313. doi:10.1016/j.epsl.2008.09.031

Gunnell, Y., Calvet, M., Brichau, S., Carter, A., Aguilar, J. P., Zehyen, H., 2009. Low long-term erosion rates in high-energy mountain belts: Insights from thermo- and biochronology in the Eastern Pyrenees. Earth and Planetary Sciences Letters, 278, 208-218.

Hetzel, R., Dunkl, I., Haider, V., Strobl, M., von Eynatten, H., Ding, L., Frei, D., 2011. Peneplain formation in southern Tibet predates the India-Asia collision and plateau uplift. Geology 39, 983–986.

Jammes, S., Manatschal, G., Lavier, L., Masini, E., 2009. Tectonosedimentary evolution related to extreme crustal thinning ahead of a propagating ocean: Example of the western Pyrenees: Extreme crustal thinning in the Pyrenees. Tectonics 28, doi:10.1029/2008TC002406

Jenness, J., Brost, B., Beier, P., 2013. Land Facet Corridor Designer.

Kleinsmiede, W.F.J., 1960. Geology of the Valle de Arán (Central Pyrenees). Leidse Geol. Meded. 25, 129–245.

King, L. C., 1953. Canons and landscape evolution. Geol. Soc. Am. Bull., 64, 721-754.

Lagabrielle, Y., Labaume, P., de Saint Blanquat, M., 2010. Mantle exhumation, crustal denudation, and gravity tectonics during Cretaceous rifting in the Pyrenean realm (SW Europe): Insights from the geological setting of the lherzolite bodies. Tectonics 29, n/a–n/a. doi:10.1029/2009TC002588

Mallet, J.L., 2002. Geomodeling. Applied Geostatistics. Oxford University Press, New York, NY, 624 p.

Molnar, P., England, P., Jones, C. H., 2015. Mantle dynamics, isostasy and the support of high terrain. J. Geophys. Res., Solid Earth, 120, doi:10.1002/2014JB011724.

Muñoz, J.A., 1992. Evolution of a continental collision belt: ECORSPyrenees crustal balanced cross-section., in: Thrust Tectonics. Mc Clay, K.R., Chapman & Hall, London, pp. 235–246.

Ortuño, M., Martí, A., Martín-Closas, C., Jiménez-Moreno, G., Martinetto, E., Santanach, P., 2013. Palaeoenvironments of the Late Miocene Prüedo Basin: implications for the uplift of the Central Pyrenees. J. Geol. Soc. 170, 79–92.

Ortuño, M., Queralt, P., Martí, A., Ledo, J., Masana, E., Perea, H., Santanach, P., 2008. The North Maladeta Fault (Spanish Central Pyrenees) as the Vielha 1923 earthquake seismic source: Recent activity revealed by geomorphological and geophysical research. Tectonophysics 453, 246–262. doi:10.1016/j.tecto.2007.06.016

Parsons, B., Sclater, J.G., 1977. An analysis of the variations of ocean floor bathimetry and heath flow with age. J. Geophys. Res. 82, 803–827.

Pavlis, N.K., Holmes, S.A., Kenyon, S.C., Factor, J.K., 2008. An earth gravitational model to degree 2160: EGM2008. Presented at the Abstracts European Geosciences Union, General Assembly 2008, Vienna.

382 Phillips, J.D., 2002. Erosion, isostatic response, and the missing peneplains. Geomorphology
383 45, 225–241.

384 Robert, A., Fernàndez M., Jiménez-Munt I., Vergés J. (in press). "Lithospheric structures in
385 Central Eurasia derived from elevation, geoid anomaly and a thermal analysis", *Geological*
386 *Society of London, Special Publications*.
387
388 Seranne, M., 1999. The Gulf of Lion continental margin (NW Mediterranean) revisited by
389 IBS: an overview. Geol. Soc. Lond. Spec. Publ. 156, 15–36.
390 doi:10.1144/GSL.SP.1999.156.01.03

391 Souriau, A., Granet, M., 1995. A tomographic study of the lithosphere beneath the Pyrenees
392 from local and teleseismic data. J. Geophys. Res. 1000, 117–134.

393 Vacher, P., Souriau, A., 2001. A three-dimensional model of the Pyrenean deep structure
394 based on gravity modelling, seismic images and petrological constraints. Geophys. J. Int. 145,
395 460–470.

396 Weiss, A.D., 2001. Topographic Position and Landforms Analysis. Poster.

397 Zandvliet, J., 1960. The geology of the upper Salat and Pallaresa valleys, Central Pyrenees,
398 France/Spain. Leidse Geol. Meded. 25, 1–127.

399

**TABLE 1**. Parameters used in the 1D modeling using topographic data and geoid anomaly together with thermal analysis

Kc and Km: thermal conductivity for the crust and the mantle, respectively; Ts: temperature at the Earth' surface; Ta: temperature at the base of the lithosphere; α: coefficient of thermal expansion; $H_0$: Crustal surface heat production. (After Parsons and Sclater, 1977; Clauser and Huenges 1995; Fernàndez et al., 1998; Robert et al., in press).

## FIGURE CAPTIONS

**Figure 1**. Examples of high-elevation, low-relief surfaces in the Axial Zone of the Pyrenees. Field examples (left) and corresponding topographic maps (right) (location on Figure 2). Top: Pla d'Envalira (Andorra) (2500m asl); middle: Pla de Boldis (Cardos Valley) (2500m asl); dashed lines: ECORS profiles; bottom: Pla de Prüedo (Val d'Aran) (2000 m). These surfaces have been previously mapped by Kleismiede (1960), Zandvliet (1960), Calvet (1996) and Ortuño et al. (2008). The present contours (in red) have been determined using the TPI method.

**Figure 2**. The planation surface of the Pyrenees.

A. top: Map of the different remnants of the Pyrenean planation surface; A. bottom: Map of the planation surface obtained by the interpolation of neighboring remnants using GOCAD 3D modeler. B: east-west and north-south profiles (red) of the restored planation surface.

425 **Figure 3**. 3D superposition of topography, Moho and LAB in the Axial Zone of the Pyrenees.

426

427 A (left): Superposition of the three surfaces (topography, Moho and LAB) (see text for further
428 explanation). A (right): Topography and Moho surfaces. The figure shows the comparison
429 between the Moho surface interpolated from Chevrot et al.'s dataset (red) and three Moho
430 surfaces and the corresponding LAB surfaces (green) resulting from the 1D gravity modeling
431 using different three crustal densities (see table 1 for parameters).

432

433 B. E-W and N-S profiles of the three surfaces (topography, Moho and LAB). Red line
434 corresponds to mean elevation. Orange line is the Moho profile from Chevrot et al. dataset
435 (the margin of error (± 5 km) is shown). Green lines are the profiles of the Moho and the
436 corresponding LAB resulting from the 1D gravity modeling.

437

438

439 **Figure 4**. Two end-member conceptual models for the explanation of high elevation, low
440 relief erosional surfaces.

441

442 A. Model 1 considers planation near sea-level, then uplift triggered by mantle dynamics and
443 relief rejuvenation. Note the absence of crustal root below the dissected peneplain.
444 B. Model 2 considers planation at high elevation due to erosion inhibition emphasized by
445 thick piedmont sedimentation and the persistence of a crustal root below the high-elevated
446 planation surface.

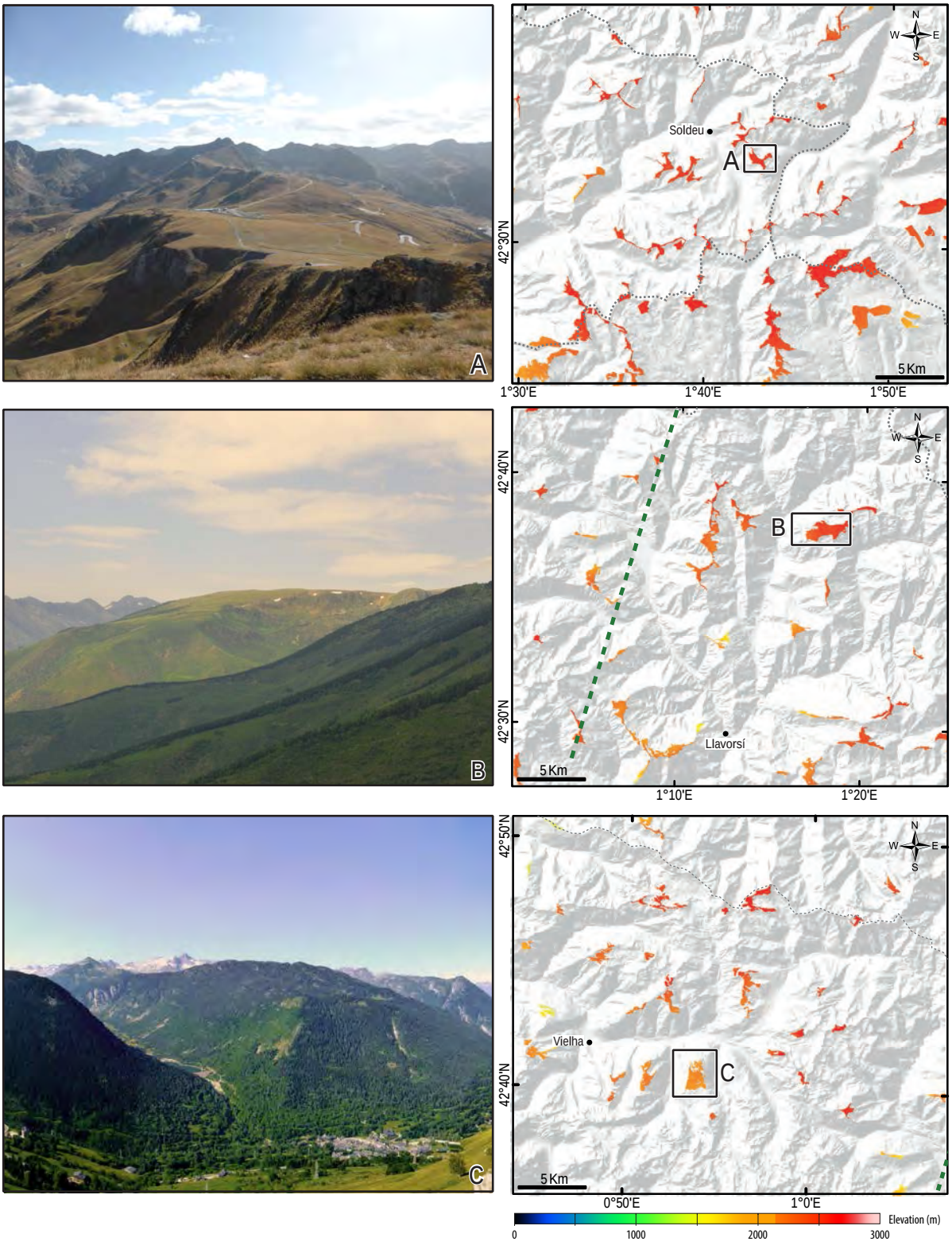
A
B
C
N
W
E
S
Soldeu
A
42°30'N
1°30'E
1°40'E
1°50'E
5 Km
B
42°40'N
42°30'N
Llavorsí
1°10'E
1°20'E
42°50'N
42°40'N
Vielha
C
0°50'E
1°0'E
Elevation (m)
0
1000
2000
3000

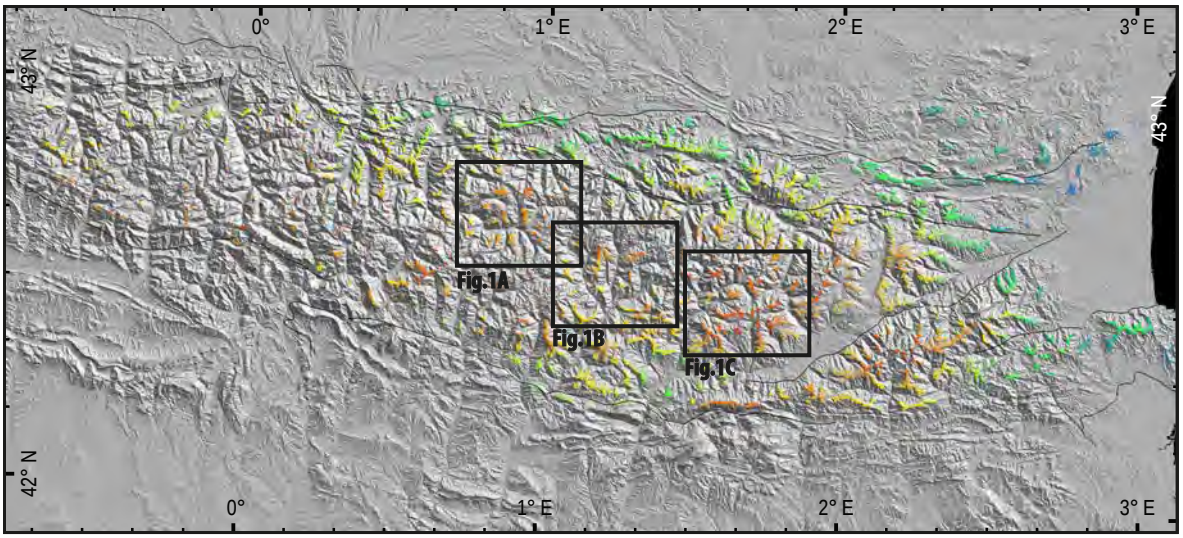


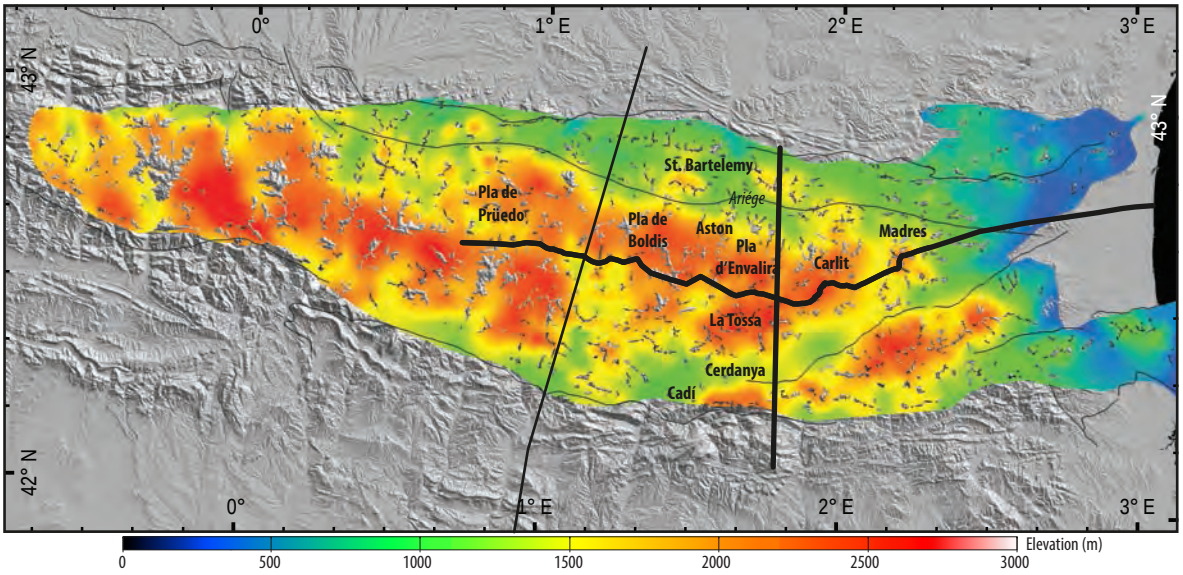


## Est - West profile

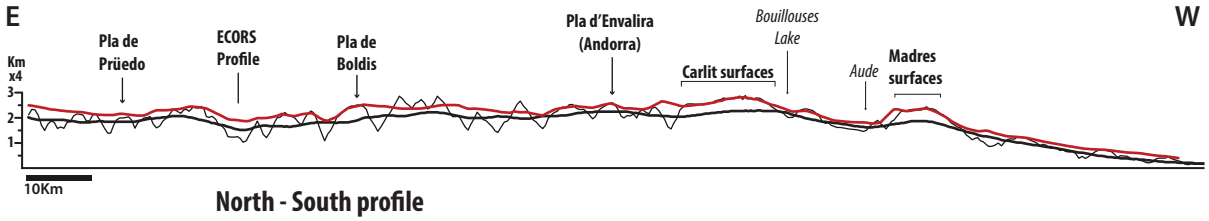


## North - South profile

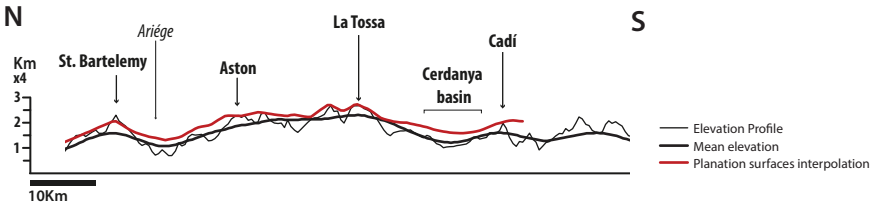

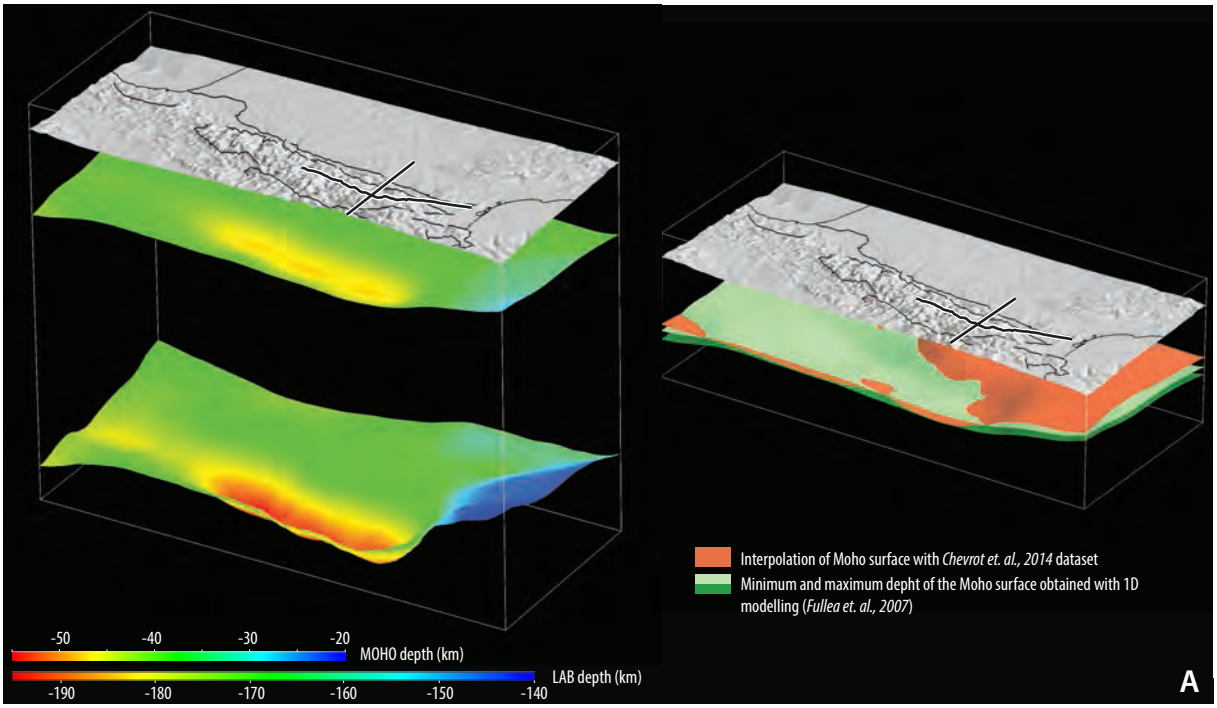
-50
-40
-30
-20
MOHO depth (km)
-190
-180
-170
-160
-150
-140
LAB depth (km)
Interpolation of Moho surface with Chevrot et. al., 2014 dataset
Minimum and maximum depht of the Moho surface obtained with 1D modelling (Fullea et. al., 2007)
A

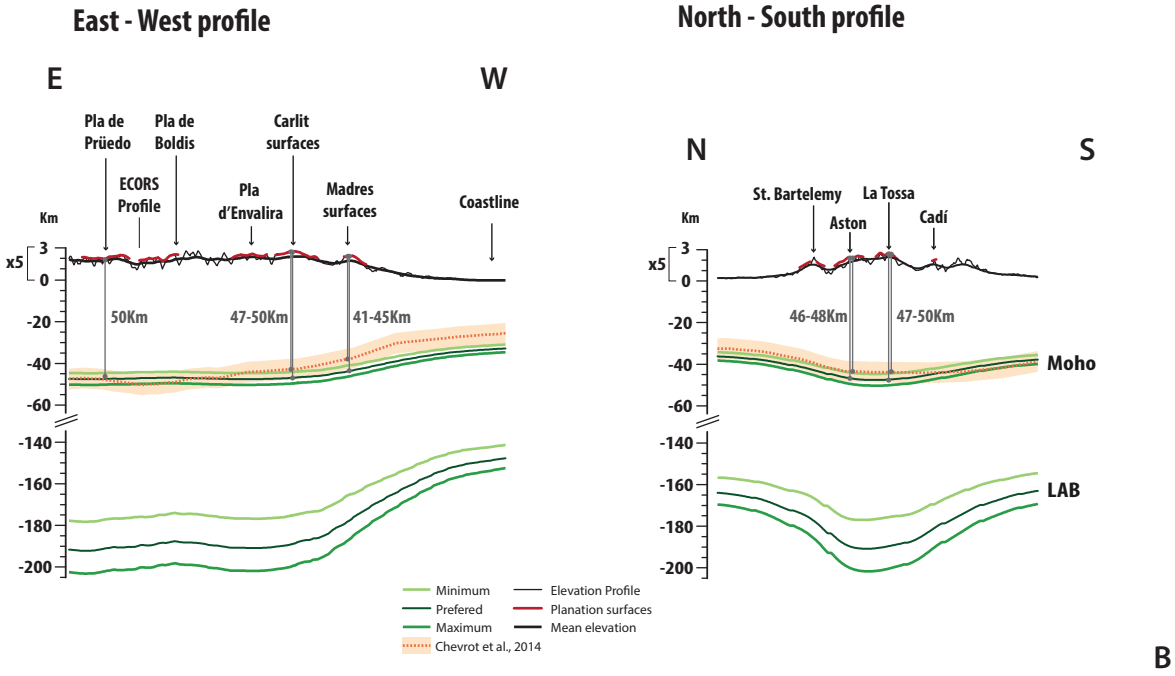
East - West profile
E
W
Pla de Prüedo
ECORS Profile
Pla de Boldis
Pla d'Envalira
Carlit surfaces
Madres surfaces
Coastline
Km
x5
3
0
-20
-40
-60
-140
-160
-180
-200
50Km
47-50Km
41-45Km
North - South profile
N
S
St. Bartelemy
Aston
La Tossa
Cadí
46-48Km
47-50Km
Moho
LAB
Minimum
Prefered
Maximum
Chevrot et al., 2014
Elevation Profile
Planation surfaces
Mean elevation
B

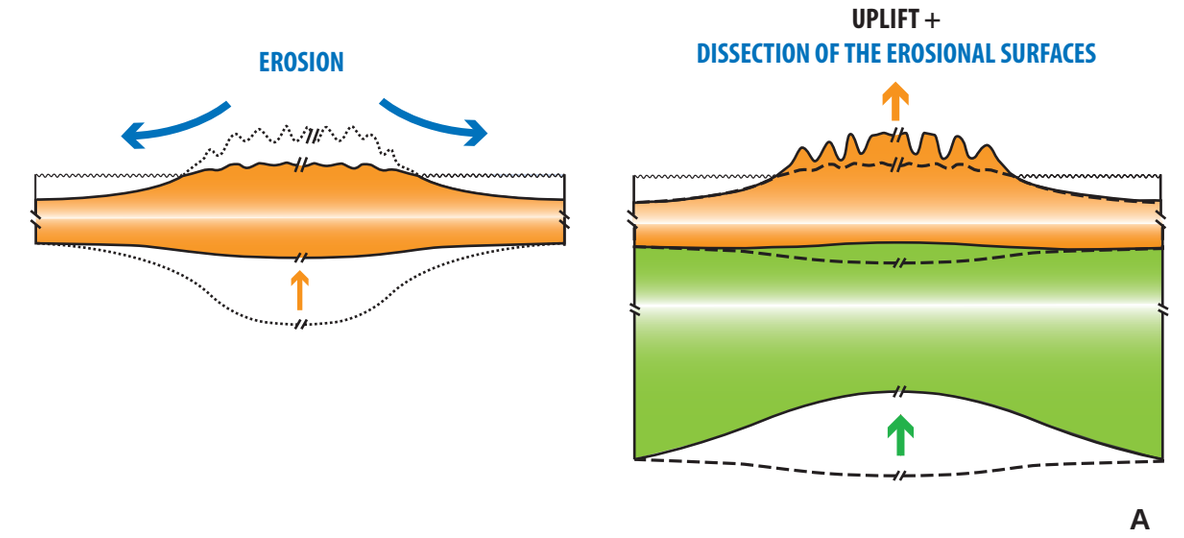
EROSION
UPLIFT +
DISSECTION OF THE EROSIONAL SURFACES
A

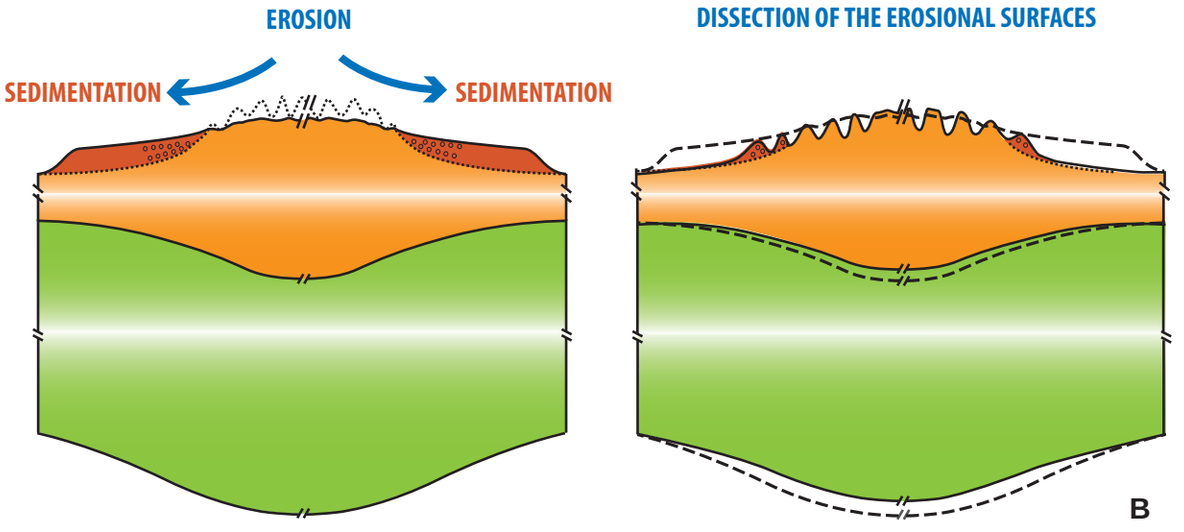
EROSION
SEDIMENTATION
SEDIMENTATION
DISSECTION OF THE EROSIONAL SURFACES
B